Chemical Profiling of Endophytic and Marine-Organism-Derived Microorganisms from Diverse Egyptian Ecosystems

by

Jack Peter Robinson

A thesis submitted in partial fulfilment for the requirements for the degree of Doctor of Philosophy MA (by Research) Doctor of Philosophy at the University of Central Lancashire

September 2025

RESEARCH STUDENT DECLARATION FORM

Type of Award _____PhD_____

School _____Pharmacy and biomedical_____

Sections marked * delete as appropriate

1. Concurrent registration for two or more academic awards

I declare that while registered as a candidate for the research degree, I have not been a registered candidate or enrolled student for another award of the University or other academic or professional institution

_____

_____

2. Material submitted for another award

I declare that no material contained in the thesis has been used in any other submission for an academic award and is solely my own work

_____

_____

3. Collaboration

Where a candidate's research programme is part of a collaborative project, the thesis must indicate in addition clearly the candidate's individual contribution and the extent of the collaboration. Please state below:

_____

4. Use of a Proof-reader

No proof-reading service was used in the compilation of this thesis.

Signature of Candidate _____

Jack Robinson

_____

Print name: __Jack Peter Robinson_____

Acknowledgements

First and foremost, I would like to express my gratitude to the University of Central Lancashire (UCLan) in Preston and the National Research Centre (NRC) in Cairo for providing me with the opportunity and resources to pursue my PhD in natural product chemistry. I owe my deepest thanks to my primary supervisor, Dr. Jioji Tabudravu, whose unwavering support and encouragement, even on my most stressful days, pushed me to become the best natural product chemist I could be. Your wisdom not only guided me in making sound decisions within my research but also shaped my personal growth and resilience. I am also immensely grateful to my secondary supervisors. Dr. Artur Witkowski, thank you for your patience and expertise in helping me navigate the intricate world of statistical analysis and its applications in advancing research within our field. Dr. Ahmed Shalabi, not only do I owe you for making my trip to Egypt, not only memorable, but deeply enjoyable. I deeply appreciate your guidance through the microbiological processes critical to sample preprocessing before the chemistry work could begin. A big thanks also to Arvin Moser and Dr. Jioji Tabudravu for their assistance and work on the ACD structure elucidation. A special thank you to Dr. Will Stockburn and Prof. Harry Eccles—your invaluable advice and guidance throughout my journey have profoundly shaped my path in chemistry, and for that, I am deeply grateful. To the laboratory technicians—Tamara, Blake, Ameera, and Kate—thank you for generously sharing your expertise and helping me master the analytical instruments necessary for my research. Your guidance has been indispensable. I would also like to extend my thanks to the natural product research team: Shubam, Abdi, Jamie, Nat, Khalid, and Marwa. Your camaraderie, shared experiences, and encouragement have made my journey as a natural product chemist both fulfilling and enjoyable. Beyond the university, I am grateful to my friends who have shown endless patience and understanding of my commitments. Your support has made the challenges of this journey far more manageable. Finally, I would like to thank my family—my Mum, Dad, Grandma Janice, Grandad Peter, Grandma Dorine, Grandad John, Jodie, Amber, and Char. Your unwavering love, support, and financial generosity made this achievement possible. I am forever indebted to you all for believing in me and standing by my side every step of the way.

Table of Contents

List of Tables

List of Figures

VLC was carried out using silica gel 70-230 mesh (Loba Chemie, particle size: d10 75-95 µm, d50 125-

Introduction

Natural product chemistry has been a long-standing source of novel pharmaceuticals, with a vast pool of bioactive natural products produced by organisms in nature, particularly from plants, fungi, bacteria and marine organisms. Within these biotic pools, endophytic microorganisms residing inside plant tissues, as well as symbiotic microorganisms residing inside marine organisms, have become increasingly important sources for the production of novel natural products active against disease targets.[1] Thus, the exploration of these microorganisms for the production of novel natural products has become increasingly important, with respect to solving some of the pressing global health issues today, such as Alzheimer's, cancer, and to the emerging antibiotic resistance epidemic.[2]

Alzheimer's disease is a progressive, neurodegenerative disorder associated with the accumulation of the proteins beta-amyloid and phosphorylated tau in the brain.[3] It is a major cause of suffering for individuals, families and healthcare systems across the globe. There is an urgent unmet need for new forms of treatment for Alzheimer's disease as the available drugs for treating the disease only treat symptoms. Similarly, cancer continues to be a major cause of illness and death across the globe, and conventional treatments, such as radiotherapy and chemotherapy, often cause serious side effects and are prone to developing resistance to cancer-cell death.[4] Meanwhile, the problem of antibiotic-resistant microbes remains an increasing threat to modern medicine, raising the serious risk that existing antibiotics may become obsolete and highlighting the need for new antibiotics and antimicrobial treatments.[5]

Endophytic microorganisms and marine organisms and their associated symbiotic microorganisms are some promising leads as sources of new bioactive natural products with therapeutic activity against Alzheimer's disease, cancer, and drug-resistant pathogenic organisms.[6] These microorganisms reside in biologically isolated niches and have evolved multiple biosynthetic pathways to produce distinct chemical natural products with bioactivities against these specific drug targets. The host-symbiont interaction gives rise to massive chemical diversity and gives us the potential to find chemicals by structure and mechanism that are not in our collection of natural products so far.[6] This work proposes to discover new natural products as therapeutic candidates against Alzheimer's disease, cancer, and infection-causing diseases. Utilising modern natural product discovery techniques including isolation, purification, structural elucidation, and biological evaluation, this research aims to discover new bioactive drug lead molecules for potential future therapeutic development. Adopting interdisciplinary approaches bridging chemistry, microbiology and pharmacology, this research aims to contribute to the field of natural product drug discovery with potential for future development to treat critical unmet medical needs.

Abstract

Endophytic microorganisms hold immense promise as sources of diverse and potentially bioactive compounds, making them a focal point of investigation in natural product research. In this study, natural products have been explored from symbiotic fungi and bacteria isolated from organisms collected from three distinct collection sites in Egypt. The Orman Garden in Giza, the soda lakes of Wadi Natrun, and the coral reefs of Hurghada, representing ecologically diverse habitats rich in microbial diversity. The strains collected and cultured have most likely never been screened against disease targets and so have high potential to harbour novel bioactive natural products that have yet to be studied. A total of 31 samples were collected from these sites, yielding 87 microbial isolates: 12 isolates from Orman Garden, 45 from Wadi Natrum, and 30 from Hurghada. The microbial extracts obtained have been biologically evaluated against microbial, biofilm and acetylcholinesterase targets, with a large proportion of the samples exhibiting high inhibitory activities, indicative of potential bioactive natural products. Following bioassays, the most biologically active extracts were then fractionated using various chromatographic techniques, guided by biological evaluation each step of the process, dereplication performed using LC-HRMS, and bioactive compounds isolated using HPLC. Following purification, structure elucidation was conducted using high-resolution mass spectrometry (LC-HRMS). Chemical profiling was further aided by use of Global Natural Products Social Molecular Networking (GNPS) platform, alongside one-dimensional (1D) and two-dimensional (2D) nuclear magnetic resonance (NMR) techniques. Three compounds from the antibiofilm, and two compounds from the anti-acetylcholinesterase active fractions have been isolated and structures fully characterised using mass spectrometry and NMR, and confirmed by computer assisted structure elucidation (CASE).

1. Literature Review

1.1 Endophytes

Endophytic microorganisms are found within the tissues of host plants and inhabit the intra- and intercellular regions of the host tissues, however, not causing disease to the host plant. There is a mutual benefit to be had to both host plant and endophytic fungi as they can promote plant growth, help combat pathogens and improve resistance to abiotic stress.[7] Endophytes, due to evolving besides their co-companion plant hosts, are known to produce metabolites similar to the metabolites produced by the plant, and so choosing endophytic fungi from plants already known to have therapeutic value has the potential to be a very rich source of future pharmaceuticals. The host plant also provides a home for the endophyte and the endophyte providing a diverse range of secondary metabolites.[8] These metabolites may be beneficial to the plant host in protecting it from disease as some metabolites may have antimicrobial properties.[9] Endophytic fungi-mediated biosynthesis of well-known metabolites includes several notable examples. Cytosporone B (1.1) isolated from *Cytospora* sp. has been observed to exhibit antimicrobial[10] and anti-inflammatory properties[11], and Ambuic acid (1.2), isolated from *Pestalotiopsis* sp. has shown antibacterial (quorum sensing inhibitor) properties[12], with the potential to inhibit biofilm production in bacteria. Codinaeopsin (1.3), isolated from *Vochysia* endophytes, has shown antimalarial properties (antiplasmodial activity) against *Plasmodium falciparum*.[13] Examples of secondary metabolites isolated from endophytic bacteria used in medicine include Fusaricidin (1.4), isolated from the endophytic bacteria species *Paenibacillus polymyxa*, found in various plants, has shown potent antibacterial activity against a variety of Gram-positive bacteria, and antifungal activity against plant fungal pathogens.[14] Examples of secondary metabolites isolated from endophytic actinomyces include, the antibiotic streptomycin (1.5), produced by *Streptomyces griseus*, actinomycin D (1.6) used to treat various cancers, isolated from *Streptomyces sp*, and antifungal agents such as nystatin (1.7) and amphotericin B (1.8), used to treat candidiasis and aspergillosis[15], and also the immunosuppressive agent cyclosporin A (1.9), isolated from *Tolypocladium inflatum,* used to treat autoimmune diseases and organ rejection post-transplant[16]. Endophytes have been identified in nearly 300,000 plant species, where they are known to dwell in almost every organ (the root, stem, leaf, flower, fruit, and seed) of the host plant; almost all of them produce bioactive metabolites but only a few of these microorganisms have been studied, showing the vast potential endophyte secondary metabolites hold in the search for novel biologically active agents.[6]

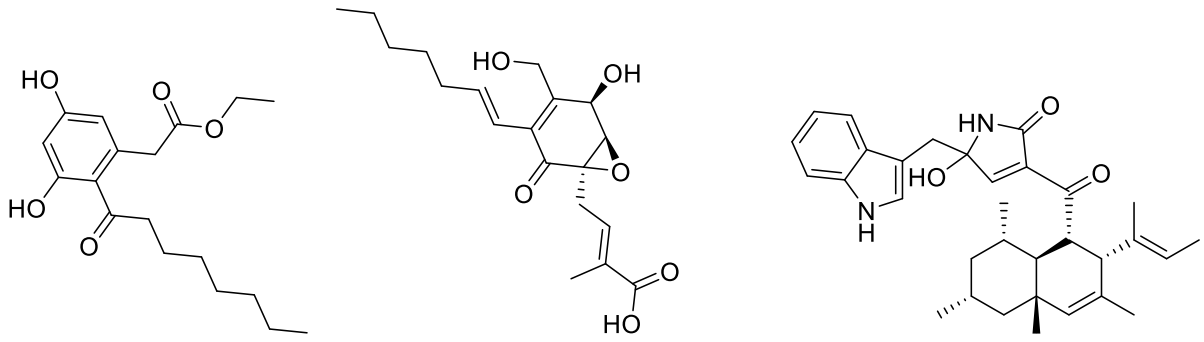

1.1 1.2 1.3

Figure 1.1.1. Examples of known natural product drugs isolated from endophytic fungi. Cytosporone B (1.1), Ambuic acid (1.2) and Codinaeospin (1.3).

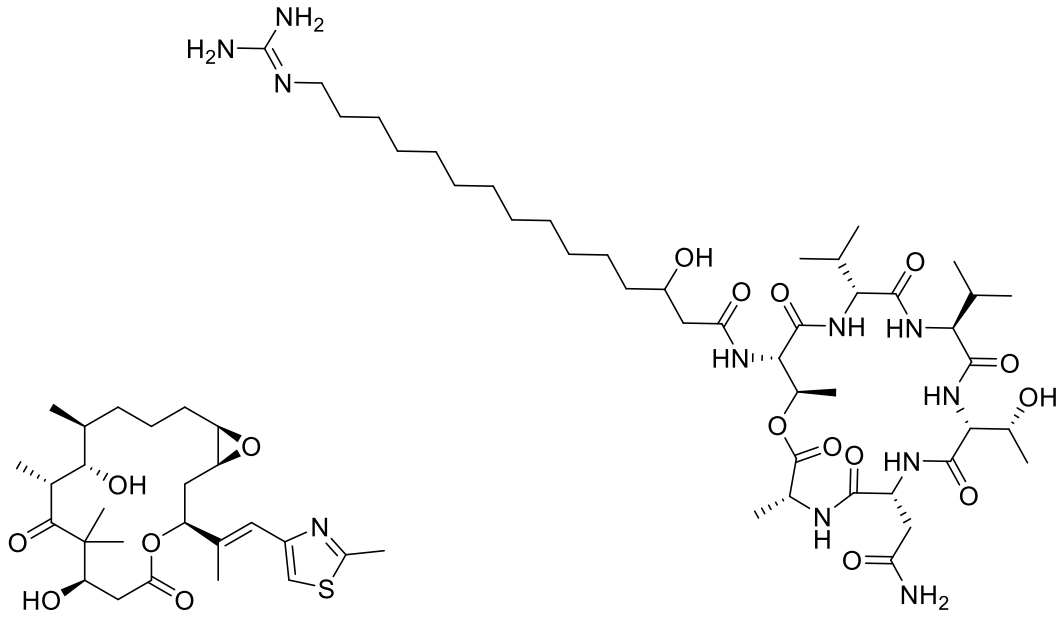

1.4 1.5

Figure 1.1.2. Examples of known natural product drugs isolated from endophytic bacteria. Epothilone (1.4) and Fusaricidin (1.5).

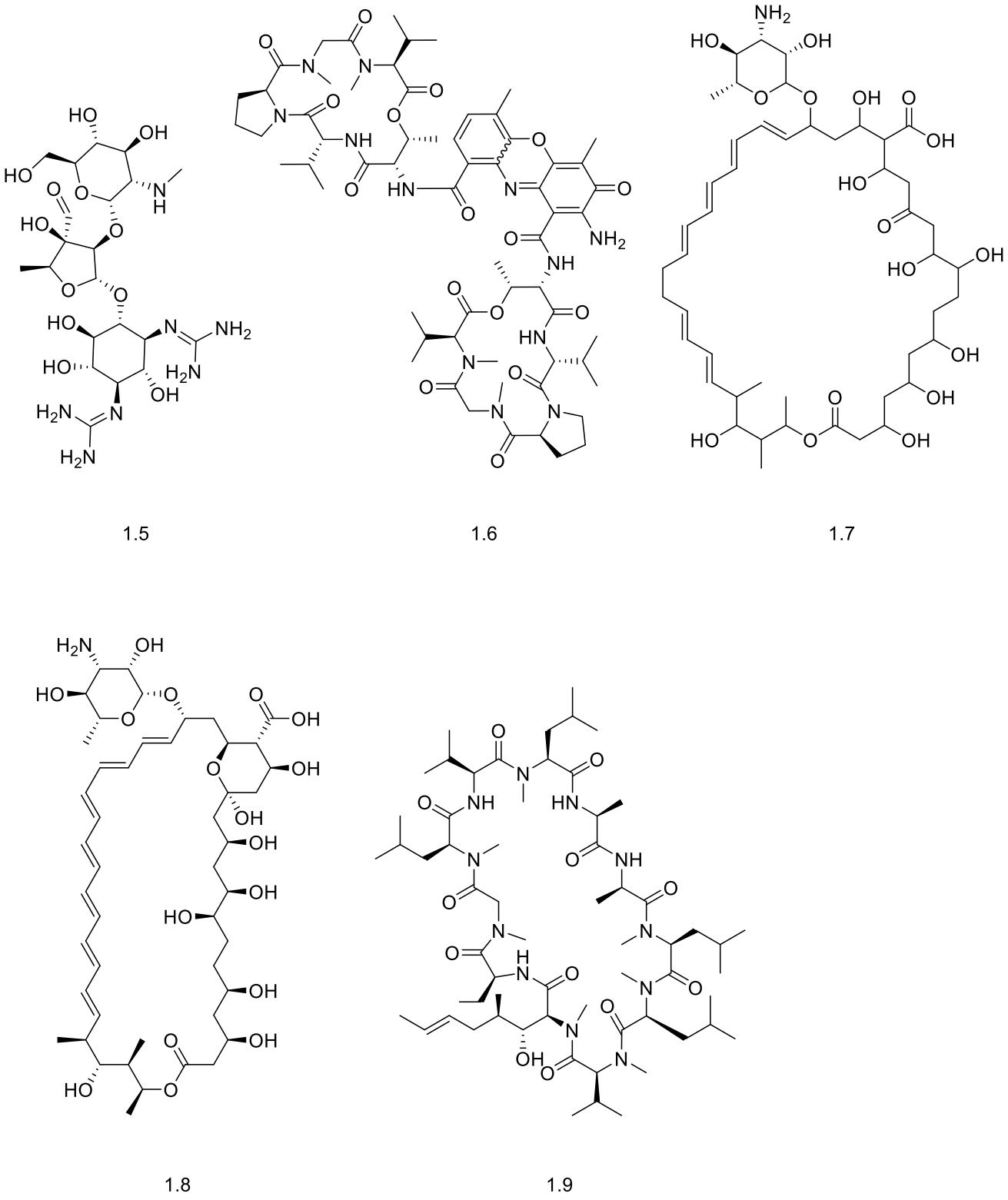

Figure 1.1.3. Examples of known natural product drugs isolated from endophytic actinomycetes. Streptomycin (1.5), actinomycin D (1.6), nystatin (1.7), amphotericin B (1.8) and cyclosporin A (1.9).

1.1.1 The marine habitat and endophytes

Marine ecosystems and marine endophytes have, in the past few decades, played a crucial role in the exploration for novel biologically active compounds, making substantial contributions to the domains of various scientific fields, including drug development and biotechnology. The marine environment is such a significant source of novel natural products because marine ecosystems, encompassing oceans, seas, and coral reefs, host an exceptionally wide array of species. The presence of many biological species offers a wide range of genetic and chemical diversity, which can potentially lead to the identification of new and unique natural products. Anti-cancer properties have been observed in a multitude of natural products derived from marine sources. Compounds such as cytarabine (1.10) and Discodermolide (1.11), which are obtained from a Caribbean sponge,[17] with both processing strong antitubulin properties against tumours, and nucleoside analogues that have shown strong antiviral activity.[18] Trabectedin (1.12), which is derived from a sea squirt,[19] has played a substantial role in the advancement of cancer therapy. Many marine organisms have also been found to produce natural products that possess antimicrobial properties. An example is halymecin F (1.13), isolated from the endophytic fungi from the red alga *Halimeda incrassata*, which has been observed to exhibit potent antimicrobial activity against a range of pathogenic bacteria, including multidrug-resistant strains.[20] Marine endophytes are microorganisms that reside intracellularly within the tissues of marine flora. These symbiotic relationships often result in the production of bioactive natural products as part of the host-microbe interaction. Many marine endophytes, particularly bacteria and fungi, have been discovered to synthesise unexplored bioactive compounds. These microorganisms are an untapped source of potentially biologically active natural products. A number of bioactive natural products that were previously identified in the marine environment were attributed to the host organism, however, subsequent study indicates that many of these natural products may really originate from the symbiotic endophytes residing within the host. The quantity of newly discovered bioactive natural compounds derived from the marine ecosystem is continuously expanding. Marine fungi use marine macro-organisms such as sponges, sea cucumbers, soft corals and algae as hosts, and are a substantial reservoir of chemical diversity. For example in 1992, just 15 metabolites had been extracted from marine fungi,[21] but by 2002, 270 metabolites had been characterised.[22] From 2000 to 2005, researchers found 100 new marine fungus compounds. The number of detected metabolites increased further between 2006 and 2010, with an additional 690 being characterised.[23] The promise of discovering pharmacologically active metabolites within the field of marine fungi and other marine endophytes is incredibly exciting for natural product discovery.

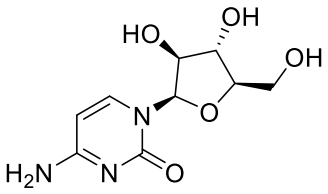

1.10

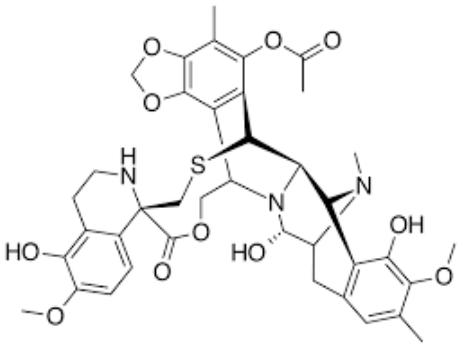

1.11

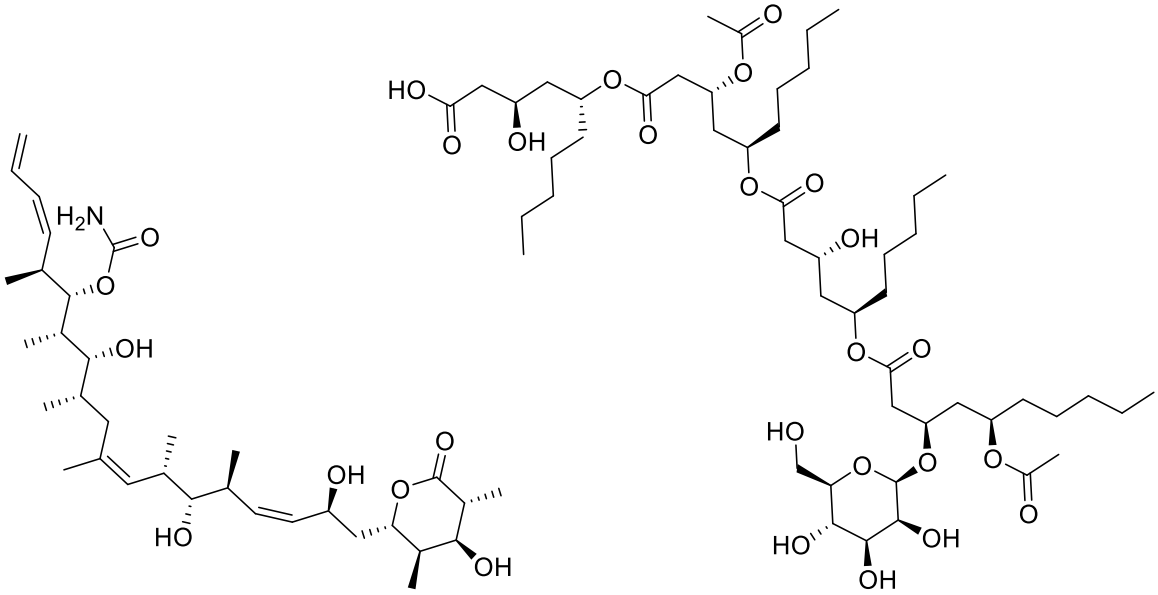

1.12 1.13

Figure 1.1.1. Examples of known natural product drugs isolated from marine-derived microorganisms. Cytarabine (1.10), trabectedin (1.11), discodermolide (1.12), and halymecin F (1.13).

1.1.2 Anticancer agents from endophytes

Cancer is one of the greatest health challenges worldwide, as the second greatest cause of death by disease. It is the most prevalent disease by frequency of occurrence; every year, about 15 million people succumb to it and this incidence keeps rising.[4] Current cancer therapies include radiation, surgery and chemotherapy, but these general strategies are often limited by their adverse effects on the lungs, liver, kidney and other important organs of the body.[24] Multidrug resistance is another obstacle to effective treatment of cancer progression.[25] For this reason, we need new and less toxic treatment options. Endophytes found inside plants are a reservoir of natural bioactive substances of diverse properties. Generally, in comparison to their synthetic counter parts, natural products are less likely to be toxic, and offer a better option because they have benefits including the suppression of multidrug resistance.[26] Examples of anticancer agents from entophytes: In **Figure 1.1.2.1** we see the

chemical structure of paclitaxel or Taxol (1.14), one of the most-used anticancer drugs known today, derived originally from the Pacific yew tree. Paclitaxel slows down the growth of tumours, blocking the dissociation of microtubules from the cell to avoid proliferation. Based on this mechanism, in 2024, paclitaxel has been given a non-conditional marketing authorisation in the UK for the treatment of ovarian, breast, lung, bladder, prostate, melanoma, oesophageal and Kaposi's sarcoma cancers.[27] Taxol is extracted from bark of *Taxus brevifolia*, the most prolific of the three, and also the slowest growing among them.[28] For scaled-up production, Taxol has been semi-synthesised from an abundant precursor, 10-Deacetylbaccatin III, found in the pines of the European yew tree (Taxus baccata taxanes).[29] Taxol has now been discovered from different endophytes inhabiting a variety of yew trees, including the endophyte *Taxomyces andreanae*.[30] Camptothecin (1.15) is an alkaloid derived from the wood of the Chinese *Camptotheca acuminata* Decaisne (Nyssaceae).[31] Many endophytes are able to synthesize camptothecins, including *A niger*.[32] Camptothecin and derivatives such as 10-hydroxycamptothecin can be used for synthesis of the most effective anticancer curative agents, such as topotecan (1.16) and irinotecan (1.17).[33] They are used in the treatment of a wide range of cancers, such as ovarian, breast, and prostate cancers, lymphoma, and leukaemia. Other anticancer agents: Vinblastine (1.18), vincristine (1.19), podophyllotoxin (1.20) and its derivatives are currently on the market, and are used in the treatment of a wide range of cancers, including the same cancers as Taxol, as shown above.[34]

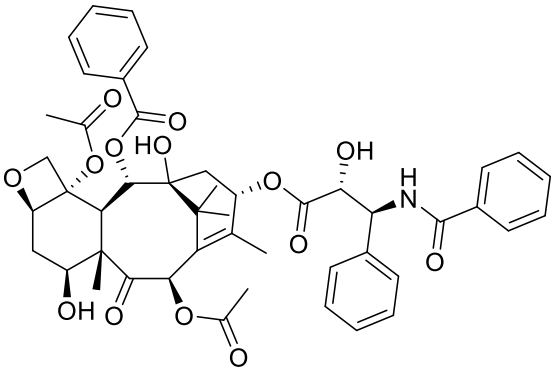

1.14

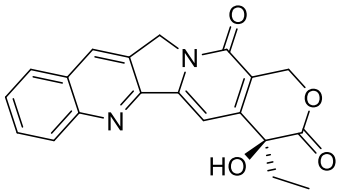

1.15

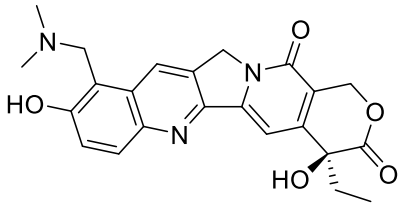

1.16

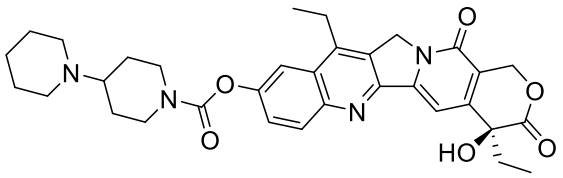

1.17

Figure 1.1.2.1. Examples of known anticancer agents isolated from endophytes. Taxol (1.14),[30] Camptothecin (1.15).[31] Other prominent cancer agents derived from endophytes include Topotecan (1.16),[33] and Irinotecan (1.17).[33]

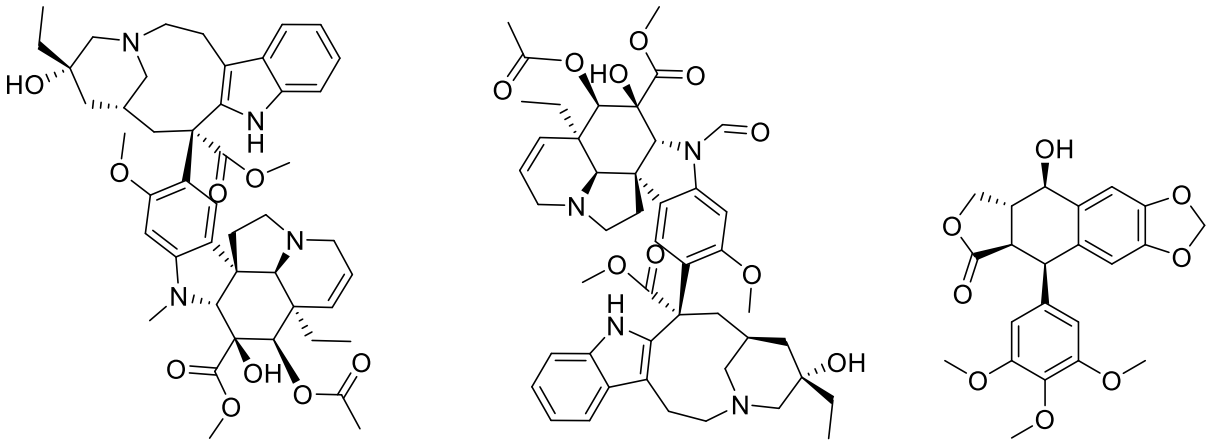

1.18 1.19 1.20

Figure 1.2.2.2. Examples of known anticancer agents isolated from endophytes. Vinblastine (1.18), vincristine (1.19) and Podophyllotoxin (1.20).

1.1.3 Antimicrobials from endophytes

Antimicrobial resistance (AMR) is one of the greatest medical threats of the 21st century. In 2019, according to statistics provided by the World Health Organization (WHO), bacterial AMR was directly responsible for 1.27 million deaths and caused or contributed to 4.95 million deaths in the same year. The amount of death if it's left unchecked could, by 2050, be as high as more than 10 million people per year, taking over cancer as the leading cause of death. In addition to human toll, the annual economic burden could reach tens to hundreds of billions of USD annually.[35] A plethora of antimicrobial metabolites produced by them offered promising antimicrobial prospects to treat infectious diseases and promising innovation to tackle AMR. Pestalotiopsin A (1.21), a metabolite isolated from an endophytic fungus *Pestalotiopsis microspora* contains a significant antifungal activity against pathogenic fungi such as *Candida albicans*, a common pathogen for fungal infection.[36] Hirsutellide A (1.22) produced by an endophytic fungi *Hirsutella sp.* shows high antifungal activity against dermatophyte fungi such as the fungi *Trichophyton* and *Microsporum*, the common culprit of superficial fungal infections on skin and nails.[37] Xanthocillin (1.23) and Griseofulvin (1.24), two antimicrobial metabolites from *Penicillium* endophytes of plants, showed significant antibacterial activity against bacterial pathogens, such as methicillin-resistant *Staphylococcus aureus* (MRSA).[38] Cytosporone E (1.25), other than having anti-cancer activity, was isolated from the endophytic fungi *Cytospora sp.* which was found to have high antibacterial activity against infections caused by MRSA.[39] These examples underscore the profound impact of endophyte-derived antimicrobials in shaping the future of antimicrobial therapy and combating the global burden of drug resistance in infectious diseases.

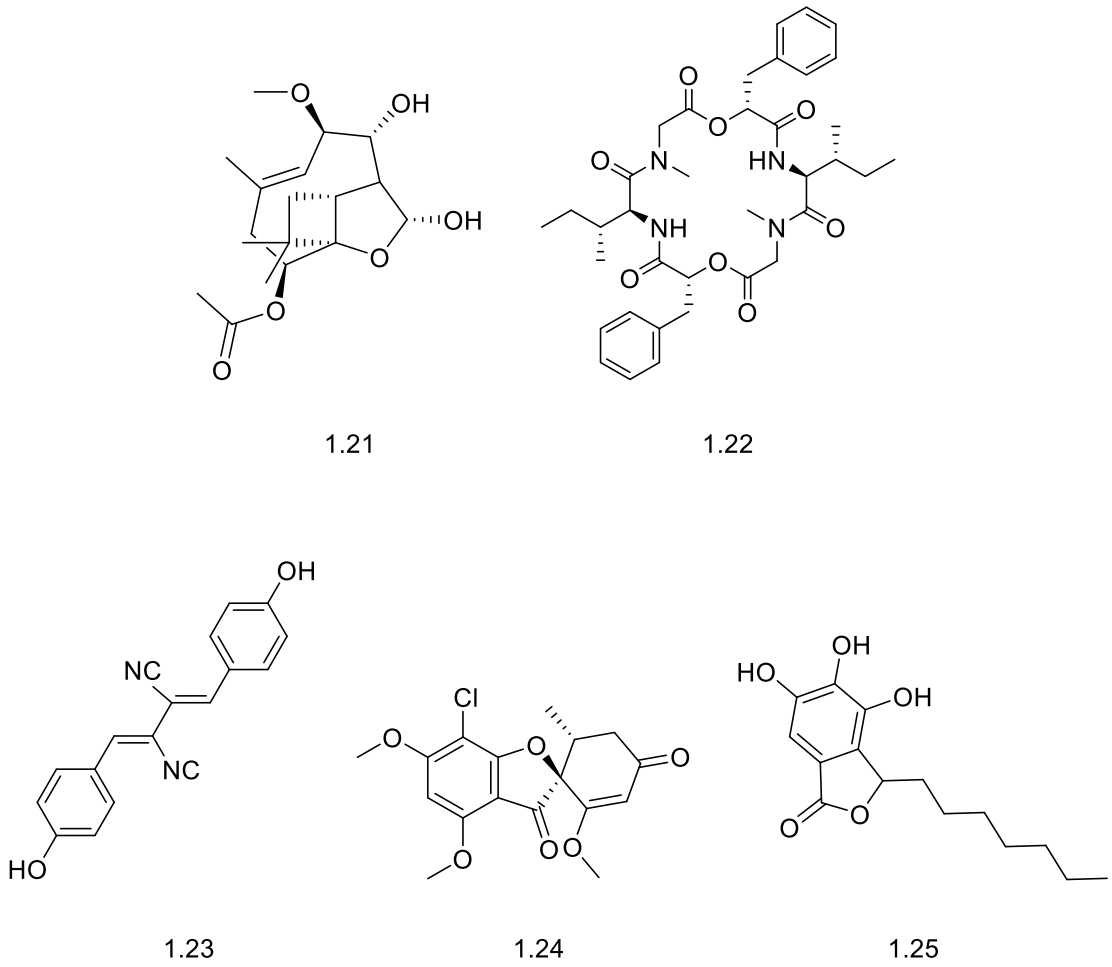

Figure 1.1.3.1. Examples of known antimicrobial agents isolated from endophytes. Pestalotiopsin A (1.21), Hirsutellide A (1.22), Xanthocillin (1.23), Griseofulvin (1.24) and Cytosporone E (1.25).

1.1.4 Anti-Alzheimer's agents from endophytes

Alzheimer's disease (AD) is the most common form of dementia, contributing to 50-70 per cent of cases, which places it as the leading cause of dementia worldwide. The accumulation of beta-amyloid and phosphorylated tau proteins, along with nerve cell degeneration, are considered primary contributors to the development and progression of AD.[40] As our population ages, the incidence of AD will rise dramatically. The World Health Organization projects a threefold increase in the number of people with dementia, including those with AD, by 2050.[41] Age is the major risk factor for AD. Incidences of dementia range from 5.0 % to 13.1 % among those over 65 years of age and those over 85 years of age have an incidence of 33.2 %. Mortality rates due to AD accelerate with age. Mortality among those >65 years increases by 33-51 % and among those >80 years, an additional 78 % mortality was found.[40] Currently approved drugs to treat AD include, Memantine (1.26) is a glutamate receptor antagonist used for moderate to severe dementia in AD[42]. Donepezil (1.27) is a reversible acetylcholinesterase inhibitor, acting with both competitive and non-competitive action, that can help improve memory, attention and focus in people with mild to moderate AD.[43] Rivastigmine (1.28) is a reversible non-competitive inhibitor of acetylcholinesterase used in the treatment of AD.[44] Tacrine (1.29) is a centrally acting acetylcholinesterase inhibitor and an indirect cholinergic agonist used in the

treatment of AD.[45] Huperzine A (1.30), isolated from *Huperzia serrata*, shows acetylcholinesterase inhibitory activity, with endophytic fungi isolated from the same plant now known to produce similar metabolites with similar activities.[46] However, these drugs only treat symptoms of AD, providing only a modestly effective reduction in disease progression. There exists little clinicopathological correlation between symptoms and actual disease progression in those treated with relatively novel medications (acetylcholinesterase inhibitors and N-methyl-D-aspartate (NMDA) antagonists).[3,47,48] The selective acetylcholinesterase inhibitors, such as donepezil, are deemed to be recommended treatments for symptom management of AD. However, the optimal dose of these drugs is debated, and their medical efficacy only provides modest benefits that are time-limited for 20-26 weeks. Reliable published observations regarding the actual outcomes of AD clinical trials and the consideration of published trials that were never published have not shown any substantial efficacy of drug candidates tested for improving physical and mental health.[49]

Between 2002 and 2022, 468 different types of natural products derived from endophytic fungi have been identified with anti-Alzheimer's-related activities, with various assays used, including cholinesterase inhibition, anti-amyloidogenic, anti-tau aggregation, antioxidant and neuroprotective, and anti-neuroinflammatory assays.[50] The chemical groups of these natural products include alkaloids, peptides, polyketides, terpenoids and steroids.[50] In effect, this reveals the rich diversity of endophytic fungi and their capability of producing bioactive compounds that can be used for AD research and therapy. Among the identified anti-Alzheimer's-related activities of the metabolites are those that inhibit key enzymes involved in the pathology of AD. For example, inhibition of acetylcholinesterase and butyrylcholinesterase, which are normally associated with cholinergic neurotransmission disruption in AD, has been investigated extensively. Inhibition of these cholinesterase enzymes will restore the cholinergic function that is lost in AD.[50] Further, endophytic fungi metabolites exhibit neuroprotective activities that safeguard neurons from the neurotoxic nature of AD pathology. In effect, endophytic fungi metabolites could mitigate neuronal injury, enhance the survival of neurons, and promote synaptic plasticity, which helps to preserve cognitive function in AD.[50] Another activity of these natural products from endophytes are the inhibition of β-site amyloid precursor protein-cleaving enzyme 1 (BACE1). BACE1 is a critical enzyme involved in the processing of a protein called amyloid-β peptides that aggregate to form senile plaques; a neuropathological hallmark of AD. Inhibition of BACE1 indicates its potential to block the production of amyloid-β peptides and mitigate neuronal toxicity in AD.[50] Furthermore, many of the metabolites possess potent antioxidant activities. Oxidative stress is a key feature of AD pathogenesis. Inhibition and mitigation of oxidative stress via these endophytic fungi metabolites prevent ROS-induced damage and promote neuronal integrity, which helps to maintain cognitive function in AD.[50] Endophytic fungal metabolites from strains L10Q37 and LQ2F02 isolated from *Huperzia serrata* showed activity against neurodegenerative disease targets, including acetylcholinesterase inhibition (AChEI). Interestingly, these AChEI-active metabolites were isolated from both host plants and microbial cells of *Huperzia serrata*, suggesting that the plant host and its endophytic symbionts must collaborate reciprocally to produce most active bioactive compounds. This indicated that several endophytic fungi inhabiting *Huperzia serrata* have the potential to produce novel therapeutic lead compounds for AD, and possibly other neurodegenerative diseases as well.[46] One bioactive natural product isolated from the *Huperzia serrata* plant is Huperzine A (1.30), which shows acetylcholinesterase inhibitory activity, with endophytic fungi isolated from the same plant now known to produce similar metabolites with similar activities.[46] These endophytic fungal leads could be crucial in developing innovative drug treatments

for AD, as the current treatments are chiefly limited to symptomatic management.

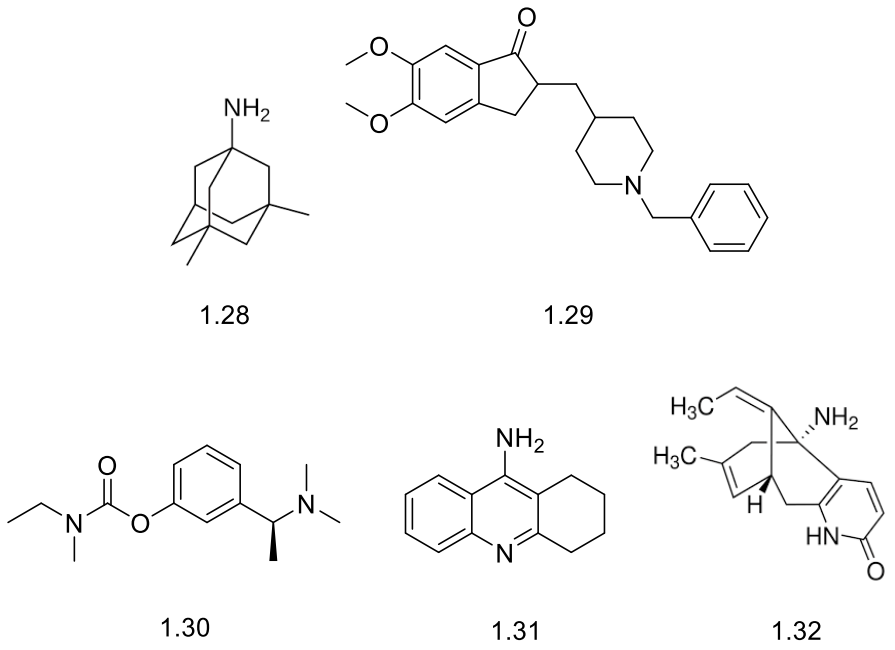

Figure 1.1.4.1. Examples of known antiAlzheimer's agents isolated from endophytes. Memantine (1.26), Donepezil (1.27), Rivastigmine (1.28), Tacrine (1.29), and Huperzine A (1.30).

1.2 Isolation of natural products

Drug discovery from natural products is a well-established area of research with a systematic procedure consisting of following steps: sampling, extraction, fractionation, biological evaluation, purification and structural elucidation. Sample collection and extraction: samples can be collected in fresh or dried form from a variety of natural sources, including plants, fungi, bacteria and marine organisms. After collecting samples, they are subjected to extraction processes for isolating biologically active compounds. Usually, extraction solvents are chosen according to the chemical nature of extractable compounds; generally, solvents are selected based on their polarities. Drug-like molecules usually fall within a specific polarity range. They need to balance water solubility and membrane permeability. If a compound is too polar, it may dissolve well in blood but struggle to cross lipid membranes. If it's too non-polar, it may have poor solubility and bioavailability. Ideal drug candidates have moderate polarity, which lets them move through both watery and lipid environments efficiently. This balance is shown in Lipinski's Rule of Five. The rule provides guidelines on molecular weight, hydrogen bonding, and lipophilicity (logP) to ensure good oral absorption. Moderate polarity also helps with effective drug-target binding through both polar interactions, like hydrogen bonds, and hydrophobic contacts. This balance promotes better pharmacokinetic properties, including absorption, distribution, metabolism, and excretion. Fractionation: After extraction process, crude extract is separated and concentrated into compounds possessing similar properties such as polarities or molecular sizes. Usually, fractionation methods are low-resolution methods such as liquid-liquid extraction (LLE), column chromatography (CC), solid phase extraction

(SPE) systems, vacuum liquid chromatography (VLC), flash chromatography (FC), size exclusion chromatography (SEC) and droplet counter-current chromatography (DCC). Isolation and purification: Final isolation is carried out via high-performance liquid chromatography (HPLC) in combination with UV and photodiode array (DAD). HPLC is generally used for isolation of pure compounds from complex samples, and generally separation of compounds is carried out according to their chemical properties such as polarity and size. Biological assays: Biological assays are performed throughout the full process to help guild the procedure towards compounds that are biologically active towards a specific disease target. Molecular structural elucidation: After isolating pure compounds showing bioactivities, their structures are elucidated by using nuclear magnetic resonance (NMR) spectroscopy, mass spectrometry (MS) and infrared (IR) spectroscopy. This technique provides chemical compositions and configurations to characterise and identify drug candidates and indicates if the isolated natural products are previously known or novel.[51]

1.2.1 Liquid-liquid extraction

Liquid-liquid extraction (LLE) is commonly utilized in natural product chemistry for the separation and purification of bioactive chemicals from structurally complicated mixtures, characterised by the differential solubility of molecules in two immiscible solvents such as an organic solvent and an aqueous solvent. The LLE approach is based on the selective separation of target molecules upon the choice of solvents with different polarity for the two phases. Once the sample is vigorously mixed with the solvent system, the two phases are left to separate, and the desired chemicals are extracted into one of the phases depending on their affinity for each solvent. The suspension is left to allow the two phases to settle, so the desired categories of chemicals can be extracted into the phase where they are the most affined to, according to the partition coefficient of the chemicals. The extracts of each fraction are then dried using solvent evaporation methods, such as rotary evaporation. Liquid-liquid extraction (LLE) enjoys its prevalence in the field of natural product chemistry owing to the valuable adaptability of the technique, promising efficiency with processing large volume of samples, and the ability to harmoniously compliment and with diverse complementary methods. It is instrumental in the isolation of the bioactive chemicals with medicinal potential from structurally complex natural matrices.[52]

1.2.2 Vacuum liquid chromatography (VLC)

Vacuum Liquid Chromatography (VLC) is suitable for larger amounts of purifying extracts or fractions over 1 gram in size. Here, silica gel is compressed under vacuum pressure, forming a solid cake. The sample is adsorbed onto a tiny amount of silica gel using appropriate organic solvents, mainly methanol (MeOH) or ethyl acetate (EtOAc). After the solvent evaporates, the sample mixture is placed at the top of the column. The sample mixture is then introduced at the top of the column by employing appropriate organic solvents, especially non-polar ones, such as n-hexane or dichloromethane (DCM), which have a narrow range of polarity, thus fit good starting points for chromatographic separation. They should be followed by polar solvents, such as ethyl acetate (EtOAc), or methanol (MeOH). So, successive fractions are collected in a step gradient elution mode: from least polar to most polar. The pressure through the column is due to a pump exerting a vacuum, thus forcing flow through the silica

gel and separating compounds based on their polarity and affinity to the silica surface. VLC allows for the separation of pure substances from complex mixtures, thereby facilitating downstream analysis and characterization.[53] Some of the limitations associated with VLC include: Lower Resolution compared to other chromatographic techniques like High-Performance Liquid Chromatography (HPLC). This can lead to the co-elution of compounds and the less efficient separation of complex mixtures. Achieving consistent and reproducible results can be difficult, especially when dealing with complex natural product mixtures. Some natural products may be sensitive to the vacuum conditions, or the solvents used, leading to degradation or transformation of the compounds. Some compounds may irreversibly adsorb to the silica stationary phase, leading to sample loss.[53]

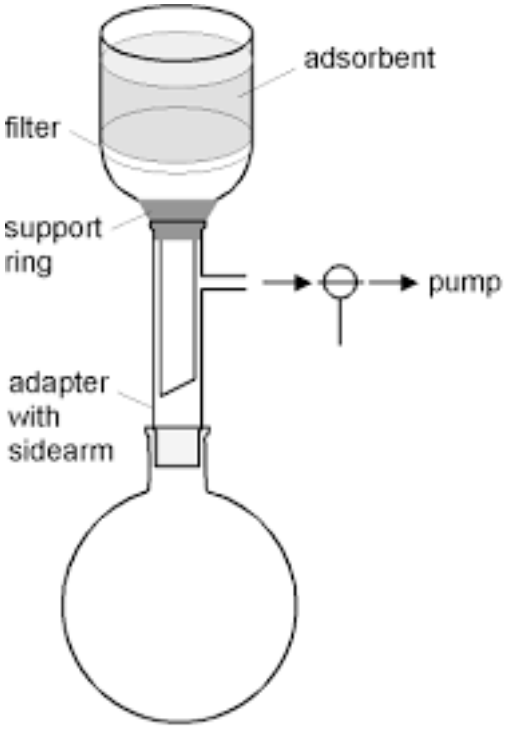

Figure 1.2.2.1. Equipment used in vacuum liquid chromatography (VLC).

1.2.3 Size exclusion chromatography

Size exclusion chromatography (SEC) is a chromatographic technique of separating compounds based on their differences in molecular sizes. The stationary phase used in SEC comprises porous beads, so the matrix functions as a molecular sieve. Fractions are separated during passage as smaller molecules enter the pores of these beads, while medium- and large-size molecules flow around them and elute first. The size of the column and the solvent system used depend on the size and solubility of the fraction under study. Natural products are separated using a variety of solvent systems based on their polarity characteristics and solubility. Polar and non-polar solvent systems include methanol, ethanol, acetone, chloroform, ethyl acetate and hexane, either alone or in combinations in different ratios.[54] Size Exclusion Chromatography (SEC) has emerged as an indispensable technique for natural product chemistry. The technique offers a mechanistically straightforward and highly efficient method for resolving molecules based on their size. Natural products are notoriously diverse and highly complex mixtures of chemical compounds, but SEC is especially suited for the purification of large molecules

(such as proteins, polysaccharides and nucleic acids) from solid-phase mixtures that often accompany the isolation processes from living organisms. Over 300,000 natural products have been identified, showing a wide range of sizes and polarities.[55] Most bioactive natural compounds have molecular weights between 200–1500 Da, with drug-like ones typically around 300–600 Da.[56] Their polarity spans a broad range, from very polar (e.g. glycosides, logP < 0) to non-polar (e.g. terpenoids, logP > 4), though many fall in a moderate logP range of 0–3, ideal for drug development.[57] SEC shows high sample recovery and is amenable for a diverse array of sample types. Its non-destructive instrumental approach makes it ideal for preparative uses that precede analytically focused investigations. Last, but not least, its capability to desalinate and remove small derivations from sample solutions is particularly valuable for the purification and subsequent analytical investigation of natural products that are prone to degradation or contain contaminants that hinder their purification or analysis.[54] Limitations involved in SEC include: SEC columns are designed to work within specific molecular weight ranges. Molecules outside this range may not be effectively separated, limiting the technique's applicability. Molecules smaller than the exclusion limit will elute together, and molecules larger than the inclusion limit will also elute together, leading to low size-resolution, potentially resulting in poor resolution for these size extremes. SEC columns typically have a lower sample load capacity compared to other chromatographic techniques. Overloading the column can lead to poor separation and column damage. SEC assumes that molecules do not interact with the stationary phase, only with the pore structure. However, some molecules may interact non-specifically with the LH-20 Sephadex column stationary phase, leading to skewed results. SEC can be slower compared to other chromatographic techniques, as it relies on the diffusion of molecules through the column matrix. Natural product extracts often contain particulate matter that can clog the column, leading to increased back pressure and potential damage to the column. Some natural products are sensitive to the conditions used in SEC, such as changes in pH or the presence of certain solvents, leading to degradation or transformation during separation.[54]

1.2.4 Thin layer chromatography (TLC)

Thin layer chromatography (TLC) can function as an analytical tool in resolving natural products as it is helpful in the evaluation of separations achieved during the various chromatographic steps of a purification workflow. TLC acts as a rapid and economical means of monitoring separations of chromatographic processes at any scale in real-time. The results obtained are easily visualised and can direct future work during the final purification of natural products, providing insights into the degree of compound separation, impurities observed or closely eluting compounds, and the optimal conditions required for subsequent chromatographic separations. Furthermore, TLC can serve as a tool for semi-quantitative analysis by estimating the concentrations of the compounds within the sample and calculating their Rf values.[58] However, separation by TLC is generally not sufficient for isolating complex mixtures and compounds present in low concentration. The resolution is low, leading to co-migrating spots that renders the identification of closely related compounds challenging. The technique offers little, if any, quantitative accuracy. Owing to its insufficient sensitivity compared with high performance liquid chromatography (HPLC), the analysis of minor components is not straightforward. In most cases, differentiation of spots from the chromatograms depends on staining with destructive reagents that do not allow further analysis of the separated compounds. Additionally, its suitability for preparative applications is unlikely to elevate it from being a useful qualitative tool for laboratory support. TLC is not efficient enough for large-scale separations and is not adequate for

many tasks (such as those requiring sensitive quantitative analysis, column-to-column repeatability, selected missed peaks and more) in advanced natural product analysis, unlike the newer improved chromatographic techniques. TLC use remains limited and is best suited for cheaper, faster, and simpler qualitative analysis.[58] Even so, TLC plays a crucial role in guiding chromatographic purification strategies for natural products, integration with other chromatic techniques ensures the isolation of pure compounds with desired properties for further characterization and biological evaluation.[58]

1.2.5 High-performance liquid chromatography

In any case, HPLC is an essential tool for resolving natural products because of its outstanding resolving power to separate highly complex mixtures into single components in a highly efficient manner. In natural product chemistry, HPLC is often used to fractionate crude extracts of natural origin, such as plants, microbes, or marine organisms. Fractionation by HPLC is based on differences in physicochemical properties, such as polarity, size, charge or a combination of these parameters between structural analogues that are closely related to each other. Using different chromatographic columns, HPLC can allow chemists to separate components from the natural extract according to their chromatographic behaviour. Elution of the target molecules occurs when they interact with a mobile phase that can be selectively altered both in composition and flow rate, and adjusted for the separation conditions based on the specific physicochemical properties of the target molecules. Using HPLC, chemists can separate the pure natural products of interest starting from raw extracts or fractions previously separated from the extract by low-resolution chromatographic separations. To do this, the chemist can use detection methods such as ultraviolet-visible spectroscopy (UV-VIS) and mass spectrometry (MS) to monitor in real-time the compounds eluting from the column, allowing the chemist to quickly and accurately isolate bioactive compounds. The purity and structural integrity of the isolated natural product are necessary to determine its structure using the same techniques used for the crude extract, such as NMR, and to determine the intensity of the biological activity and the pharmacological mechanism using the general methods present in medicinal chemistry. HPLC used in this way is essential for getting pure compounds from the original natural extract, allowing a characterisation investigation for natural products and the subsequent discovery of medicinal natural products.[59] While HPLC is widely used in natural product chemistry, it has several limitations. One major drawback is peak overlap. This is especially true when analysing complex extracts with similar compounds, which can make it hard to identify and separate them accurately.[60] Additionally, HPLC often lacks quantification without suitable calibration standards. This makes it tough to determine exact concentrations.[61] Furthermore, many natural products do not have strong chromophores. This limits their detection by typical UV detectors and requires using other methods, such as MS or derivatization, to improve sensitivity.[62]

1.3 Structure elucidation and dereplication

1.3.1 Dereplication in Natural Product Chemistry

Chemical dereplication is the use of various spectroscopic and chromatographic techniques, alongside

databases, to identify previously isolated compounds present within an extract matrix during the early stages of screening and analysis. It can be used to quickly identify known interfering compounds such as fatty acids or known, previously isolated, compounds from literature or that are associated with the extract in question. The main goal of dereplication is to avoid the unnecessary re-isolation and re-characterization of previously identified substances, thus saving time and resources in the search for novel bioactive compounds. This issue is deep and widespread due to the recurrence of natural products across diverse organisms and the often subtle differences between known and novel compounds. Effective dereplication not only accelerates the discovery of new bioactive molecules but also improves efficiency in screening and isolation workflows, making it an essential practice in modern drug discovery. Dereplication can also be used to home-in on fractions or extracts with known or suspected activity due to a known compound, prioritizing those fractions to streamline the chemical isolation process. [63] This can massively reduce the time and workload taken to isolate compounds of value, making the search for biological activity in natural products a more attractive route of drug discovery.

The first step is the initial screening. To quickly identify known compounds in an initial screening of extracts from natural sources such as plants, micro-organisms or marine organisms, dereplication is usually carried out by primarily by automated high-throughput MS, with NMR used sparingly due to the peak overlap of complex matrices. The second step is comparison with databases. Spectral data acquired by these two techniques in this initial screening are subsequently compared with large libraries of known natural products containing their spectra, including molecular weights, fragmentation patterns and chemical shifts. The third step is chromatographic profiling. Separation techniques such as HPLC or LC-MS are then used to analyse each extract into its individual components. The chromatographic profiles of these separated compounds are compared against those of known standards or reference databases, with the retention times matched against MS mass spectral data. The fourth step is the exclusion of redundancy. Expanding the database using tandem MS is more resource-intensive, however it provides more accurate results The known compounds are thus excluded at an early stage and can be filtered out of the overall process, enabling researchers to focus only on novel compounds that possess new activities. The fifth step is to determine their structure. For compounds that can't be matched to any particular known entries, subsequent spectral analysis using advanced spectroscopic, or MS techniques are carried out to determine their structure. In this manner, resources are directed towards the discovery of truly novel compounds. The sixth step is to enhance the efficiency of resource allocation Since known compounds are identified and excluded early in the process, this helps in optimising the efficiency of resource allocation and allows researchers to concentrate on novel but possibly more promising candidates.

1.3.2 Structure elucidation strategy

After obtaining pure compounds, the process of determining their structure involves using a combination of procedures that work together to ultimately confirm the chemical structure. High resolution mass spectrometry (HRMS) is employed as the initial step to determine the precise molecular mass of a compound. This enables the identification of the most probable molecular formula for each compound, hence narrowing down the range of potential molecular formulas for the

molecular ion. Determining a molecular formula from a molecular weight can be difficult. Many different formulas can have the same or similar masses, especially at higher molecular weights. Low-resolution data, adduct formation, and uncertainty about which elements are present make the process even more complicated. High-resolution mass spectrometry (HRMS) helps narrow down the options, but interpreting the results correctly is still crucial. Tools like ChemCalc, Sirius, GNPS, and instrument-specific software such as Bruker SmartFormula, Agilent MassHunter or ACD labs Spectrus help by combining accurate mass, isotope patterns, and fragmentation data to predict and rank possible formulas. FT-IR spectroscopy can be utilised to determine the functional groups present in the compound present by analysing their distinct infrared absorption peaks.[64] Diverse nuclear magnetic resonance (NMR) techniques provide extensive information regarding the chemical composition, atom connectivity, and spatial layout of functional groups inside a molecule. 1D ^{1}H and ^{13}C NMR spectroscopy can determine the number of protons and carbons present in a compound and provide information about their chemical environments. These 1D NMR techniques are used in conjunction with various 2D techniques, such as, COSY, HSQC, HMBC, NOESY and ROESY. ^{1}H-^{1}H COSY is employed to establish correlations between protons. It facilitates the identification of vicinal hydrogen pairs that are linked together by 2-4 bonds ($^{2\text{-}4}J_{HH}$), and assists in determining spin systems. HSQC NMR establishes a heteronuclear correlation between the chemical shifts of ^{1}H and ^{13}C atoms, thereby revealing the connectivity between protons and carbon atoms that are intimately connected to each other. HMBC spectroscopy establishes heteronuclear correlations between ^{1}H and ^{13}C or ^{15}N nuclei that are usually distanced by 2 to 3, but occasionally 4, chemical bonds. It is particularly useful for locating quaternary carbons without directly attached protons and aids in joining disparate fragments or spin systems to form the overall carbon skeleton. Additionally, HMBC pinpoints the exact attachment sites of side chains or branches, identifies substitution patterns in aromatic or ring systems, and elucidates the connectivity of functional groups. When combined with COSY and HSQC, this makes it an effective tool for assembling entire molecular structures. Nuclear Overhauser Effect spectroscopy (NOESY or ROESY) provides information on the coupling of ^{1}H atoms through space (within a range of ≤5Å), hence revealing the stereochemical configuration of these atoms in relation to one another.[65] Polarimetry using optical rotation, and circular dichroism (CD) are essential techniques for verifying the absolute configuration of stereocentres in chemical structures, thereby completing the full chemical structure.[66]

1.3.3 Mass spectrometry

Mass spectrometry (MS) is a pivotal analytical technique in natural product chemistry, playing a central role in elucidating molecular structures. MS facilitates the determination of the molecular mass and structural characteristics of natural products by ionising and fragmenting molecules into ions, which are then separated based on their mass-to-charge ratio. In structure elucidation, MS is often coupled with other analytical techniques, such as liquid chromatography (LC-MS) or gas chromatography (GC-MS), to enhance its capabilities. The mass analysers Orbitrap, Time-of-Flight (TOF), and Fourier Transform (FT), represent the pinnacle of MS technology for high-throughput screening of natural products. These advanced instruments enable the comparison of exact masses and the fragments they produce with known, previously isolated compounds, utilizing fragmentation patterns, akin to fingerprints, for rapid dereplication of natural product structures. By analysing the mass spectra generated from the fragmentation of natural product molecules, researchers can deduce

valuable information about the elemental composition, connectivity of atoms, and presence of specific functional groups within the compound. Additionally, MS can provide insights into the presence of isotopic patterns, characteristic fragment ions, and other spectral features that aid in the determination of structural motifs and stereochemistry. High-resolution MS instruments further enhance the accuracy and precision of structural elucidation by resolving closely related mass peaks and providing more detailed information about the composition and arrangement of atoms within the molecule. Overall, MS is an indispensable tool in natural product chemistry, enabling researchers to unravel the intricate structures of bioactive compounds derived from diverse natural sources.[64]

1.3.4 Nuclear magnetic resonance spectroscopy (NMR)

NMR (nuclear magnetic resonance) spectroscopy is the backbone of the dereplication of natural products, because it provides necessary spectroscopic structural information in both qualitative and quantitative terms to chemists, and it works under non-destructive conditions. It is informative about the spatial relationship between its elementary atoms and the connectivity of their functional groups, allowing chemists to distinguish between known compounds and 'look-alike' compounds with the same or very similar masses. This helps to prevent a redundant effort in the dereplication process. But, the most informative characteristic of NMR is its spectral similarity libraries for structural elucidation, a system widely accepted by scientists and applied to all natural products, from the very simple to complex compounds such as macrolides, terpenoids, polyketides, and peptides. NMR enables us to compare the spectra of targeted compounds with similar compounds already identified in the public databases, such as the Spectral Database for Organic Compounds (SDBS), which contains a wide range of spectral data, including NMR, MS, IR, and UV-Vis; the Biological Magnetic Resonance Data Bank (BMRB), which focusses on biomolecules and provides detailed NMR parameters; and NMRShiftDB, a community-driven database that offers experimental and predicted ^{1}H and ^{13}C chemical shifts for organic compounds. Annotated NMR spectra for thousands of metabolites are also available in the Human Metabolome Database (HMDB). Structure and some NMR data are included in COCONUT, a sizable collection of open natural products. Although they require subscriptions, commercial options such as ACD/NMR DB, ChemSpider, and Reaxys offer more comprehensive datasets and integrated literature references.. Increased magnetic fields and cryoprobes used by NMR instruments enable many of these advancements, resulting in faster, more sensitive, and higher-resolution NMR spectra. The information gathered from these hyphenated methods (LC-NMR-MS) adds to and complements each other, making it easier and faster to identify and characterise the compounds present.[67]

1.3.5 Circular dichroism and polarimetry

CD spectroscopy and rotary polarimetry are commonly used to prove the presence and specify the configuration of stereocentres in the structure elucidation of natural products. Circular Dichroism (CD) spectroscopy is especially useful in determining the absolute configuration of chiral molecules by measuring how optically active compounds differentially absorb left- and right-circularly polarized light, resulting in a CD spectrum that is characteristic of the stereochemistry. If the experimental CD spectrum is compared to known reference compounds, theoretical predictions (ex. TD-DFT

calculations), and empirical methods (ex. the octant rule or the exciton chirality method), one can assign the R or S configuration of stereocenters. This method is very advantageous for studying natural products and small chiral molecules with chromophores located adjacent to the chiral center, and it provides a solution phase alternative to X-ray crystallography when there is no other alternative. CD spectra of natural products reveal the presence of specific functional groups and stereocentres, and their absolute configurations. Another method is to use rotary polarimetry, in which the rotation of linearly polarised light by achiral molecules is used to determine the specific rotation of the optically active compounds, giving quantitative information about the chirality of a molecule. CD spectroscopy and rotary polarimetry are complementary techniques for determining the stereochemistry of molecular structures.[66]

1.3.6 Databases

The availability and calibre of natural product databases or strain libraries have a significant impact on the capacity of a dereplication method to quickly identify recognised compounds. Over the past 20 years, numerous commercial or open-access databases of low molecular weight metabolites have been created. The more thorough databases include the Dictionary of Natural Products (DNP) with over 260,000 molecular structures, MarinLit with about 48,000 molecular structures derived from marine organisms, the ACD/Labs NMR and ACD/Spectrus databases with structural and spectral data of tens of thousands of synthetic and natural compounds, and the UCSD Natural Products Database (RSC) with a sizable collection of microorganism and marine organism natural products. Databases are an instrumental tool in the quick and efficient dereplication of unknown compounds can all be used to speed up the dereplication process to streamline the discovery of bioactive new or novel natural products. Databases can assist in accelerating natural product research, mainly through rapid dereplication, the process of determining whether a compound is known or potentially novel. By publicly assessing and matching experimental data (such as high-resolution mass spectrometry (HRMS), mass spectrometry and tandem mass spectrometry (MS/MS) fragmentation patterns, NMR spectra, UV profiles, or IR spectra) with curated libraries, you can quickly identify and correlate features, like molecular weight, isotopic patterns, and functional groups, to known compounds. For efficiency, it is beneficial to utilize multiple databases when working with natural products (e.g., GNPS for MS/MS, NMRShiftDB or SDBS for NMR, HMDB for metabolite profiling) and to apply methods such as structure-based or spectrum-based searches, or software that supports fully or semi-automated matching. When used effectively, these invaluable resources not only help avoid re-isolating known compounds but also enhance your understanding, allowing you to select extracts to prioritize and analyse more strategically.

68

1.0.1 Computer-Aided Structure Elucidation (CASE)

The structure of chemical compounds is solved by using computational tools in Computer-Aided Structure Elucidation (CASE). These programs are used by researchers to deduce molecular structures from spectroscopic data and to determine the most likely molecular architecture. Over time, the adoption of CASE tools has grown steadily within the scientific community.[69] For example, the Logic

for Structure Determination (LSD) software (available at www.univ-reims.fr/LSD) was able to identify compounds that had not been entered into a database. This was accomplished through the combination of chromatographic fractionation, 13C NMR data clustering, and computational database searching. However, the ACD Labs Structure Elucidator is another very popular CASE tool, based on a database of over 300 000 validated compounds to solve structures quickly. The major benefit of the CASE systems is their rapidness and the fact that they can help save time and work.[69] They also have the ability to process both NMR and MS data at the same time, thus improving the reliability of the structural elucidation. The amount of spectroscopic data required for a CASE analysis is the minimum of 1D 1H-NMR, 1D 13C-NMR, HSQC and HMBC spectra. In addition, FTIR and Raman spectroscopy can be involved in the process. The structural elucidation workflow begins with the input of the spectroscopic data into the software. The program then combines the data and produces a Molecular Connectivity Diagram (MCD). The MCD is then used to computationally derive molecular structures, using both database information and computational logic.[69]

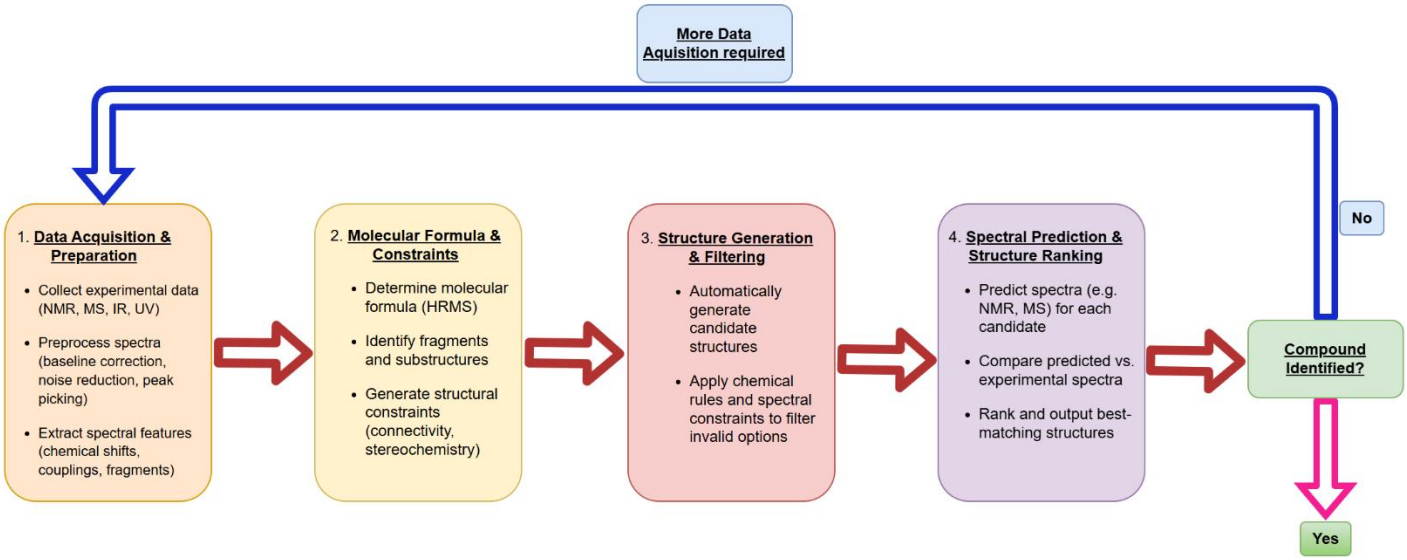

Figure 1.3.6.1. Flowchart showing the main steps in CASE.

1.3.7 Molecular Networking

Molecular networking is a powerful computational method used in natural products chemistry. It allows visualisation and organisation of tandem mass spectrometry (MS/MS) data, allowing researchers to analyse structural relationships of metabolites. The molecular networking methods can be particularly useful for dereplication, prioritizing novel compounds, or for the discovery of analogues that exist in complex mixtures of bioactive compounds. Data repositories or platforms like GNPS (Global Natural Products Social Molecular Networking) provide access to extensive public databases with tens of thousands of curated spectra and spectra from users in the community, which can be useful for comparative metabolomics. For natural products chemists, this means that unknown compounds can be contextualized into known chemical families, speeding structural elucidation and decreasing redundancy in isolation efforts.[70] A major obstacle in the search for novel,

pharmaceutically significant, natural products is the time it takes for identification, isolation, structure elucidation and biological testing of such compounds from complex biological organisms. The use of GNPS can quickly identify and compare HRMS fragmentation data with known compounds within its molecular network database, which lets researchers know if the compound is of potential value, bioactive or novel, without even separating it from the sample matrix, maximising the efficiency of the dereplication process. Even simple organisms can produce a very large number of different secondary metabolites, that may take an excessive amount of time to separate. Using chemical similarity, MS/MS data, alongside databases of known compounds and their fragmentation patterns, molecular networking can be used to identify known compounds to significantly reduce the time taken to identify and elucidate structures of unknown ones making the process quicker and efficient. In this project molecular networks will be used to cluster and visualise MS data to increase the efficiency of the full dereplication process for the metabolites isolated. Alongside traditional chemical dereplication techniques, molecular networking can be an invaluable tool to efficiently streamline the dereplication process.[71] Functionally, molecular networking utilises covariance in fragmentation patterns to identify spectra similarities. Each node in a molecular network represents one MS/ MS spectrum, and an edge between nodes indicates a level of similarity, usually modelled or scored by cosine. Clusters that are formed in a molecular network often represent chemical families that can shed light on similar or related structures (and biosynthetic pathways). This method is also developmentally more functional than conventional dereplication practices that employ exact mass matching or library matching, as the inclusion of fragmentation renders molecular networking more robust for finding analogues or modified metabolites. Unlike NMR analysis of isolated compounds, molecular networking can be performed directly on crude extracts, which allows the use of untargeted, high-throughput methods for understanding chemical diversity. This feature makes molecular networking an exceptionally efficient tool for natural products research and metabolome mining.[72]

1.3.8 Metabolomics

Metabolomics, sometimes referred to as chemometrics or multivariate statistical analysis applied to biochemical data, has a substantial impact on natural product research. This methodology entails the utilisation of mathematical and statistical techniques to derive significant insights from intricate biological and chemical datasets. Biochemometric analysis is used to identify trends in metabolomic data obtained from natural products. It aids in differentiating between various samples, recognising changes in metabolite profiles, and identifying compounds linked to specific biological functions. Statistical analysis, such as Principal Component Analysis (PCA), may be carried out on HRMS data of natural product mixtures to promptly detect any natural compounds of interest. By employing chemical profiling of existing compound data, it is possible to statistically assess fresh compound data in order to facilitate the visualisation and clustering of comparable compounds. This enables the rapid identification of compounds of interest, including those that are already known, bioactive, or novel. This is crucial in the dereplication process of natural products inside a matrix, as it allows for the identification of valuable natural products without the need to isolate compounds within the matrix. This is an invaluable time-saving method in natural product research.

At its core, metabolomics works by acquiring high-resolution mass spectrometry (HRMS) or nuclear

magnetic resonance (NMR) data from biological or environmental samples, followed by the application of statistical algorithms to extract patterns and meaningful correlations. These datasets can be vast and complex, often comprising thousands of features, each representing a unique metabolite or compound ion. Techniques like PCA, Partial Least Squares Discriminant Analysis (PLS-DA), and Hierarchical Cluster Analysis (HCA) reduce this dimensionality and allow researchers to visualise relationships between samples, identify biomarkers, and associate specific metabolites with biological or ecological functions. The level of detail provided by metabolomics includes mass-to-charge ratios (m/z), retention times, and relative abundances, which can be further analysed for structural elucidation and compound annotation. When combined with spectral databases or tools such as molecular networking, metabolomics can reveal not only known compounds but also uncover analogues and novel structures, enhancing both the efficiency and depth of natural product discovery.[73]

1.4 Conclusion

In short, there is a pressing need to discover biologically active natural products from endophytes and microorganisms derived from marine sources to overcome the imminent threat from drug-resistant micro-organisms, as well as the huge challenges posed by cancer and Alzheimer's disease. Highly dynamic environments spur microorganisms to develop complex biosynthetic pathways to generate an abundance of bioactive compounds, which are promising starting points for the development of novel therapeutic agents. Antimicrobial agents remain in high demand for the treatment of drug-resistant microorganisms, with many isolated from endophytes looking promising. In addition, evidence suggests that marine-derived microorganisms could be valuable sources for developing anti-cancer and anti-neurodegenerative agents. Most of the complex biosynthetic pathways would result in small molecules with unique structures and potent bioactivity. Thus, new drug discovery involves identifying lead-like compounds for further development and optimisation. Dereplication is important for differentiating known and new compounds and saving time and resources by avoiding the re-isolation of these known compounds. Hyphenated techniques, such as LC-HRMS, as well as HPLC, support dereplication by identifying and characterising the novel compounds accurately and in detail. Despite the hard work required to isolate the target compounds for further manipulation, recent advances in instrumental analyses using MS, HPLC and NMR coupled with new software have greatly improved the workflow. Natural product chemists are taking advantage of these innovative technologies to tackle biodiversity-related challenges. Molecular networking emerged as a cost- and time-efficient tool that helps visualise the relationship between all molecules, which clinches new drug discoveries and characterisation. Software for structure elucidation has also advanced to aid in phylogenetic and structural data analysis. Specifically, spectral matching using various techniques helps characterise and classify new molecules. HPLC separation analysis provides an extensive purifying technique for isolating pure compounds. The search for natural products continues to delve deeper into endophytes and microorganisms derived from marine sources, and there are promising developments that could have a great impact on the treatment of various diseases, including drug-resistant infections, cancer, and Alzheimer's disease.

Aims and Objectives

Aim: To chemically profile biologically active secondary metabolites derived from plant and marine-organism-derived microbes/fungi.

Objectives:

1. To collect plants and marine invertebrates as source of microorganisms
2. To culture microbes derived from these sources using standard microbiological methods.
3. To isolate microorganisms and perform small scale cultures for bioactivity screening
4. To evaluate bioactivities of extracts using antimicrobial, antibiofilm, and acetylcholinesterase inhibitory assays.
5. To identify fungal strains using 18S rRNA gene sequencing analysis.
6. To isolate and purify extracts using bioassay guided chromatographic techniques.
7. To dereplicate extracts using HR-LC-MS/MS using software-database integrated tool
8. To chemically profile extracts using chemometric software tools
9. To perform structural determinations of biologically active compounds.

Chapter 2: Experimental methods

2.0 Introduction

In this chapter of experimental methods, a series of steps and procedures is outlined, to address the isolation, purification, and characterization of natural bioactive products from endophytic and marine-organism-associated microorganisms. All the required steps and parameters are documented in this section, providing a detailed account of the protocols that underpinned the research. The first section starts on a journey to different ecologically distinct sites: Orman Garden, the soda lakes of Wadi Natrun in Egypt, and the coral reefs of Hurghada on the Red Sea. This part describes the collection and pre-treatment of samples. Then, the sequential approach that led us to isolate endophytic fungi is described, with special emphasis on the media and culture conditions used to enrich their presence. Next, the subsequent steps following sample preparation are presented, involving the extraction techniques used for the crude extracts obtained from the microbial cultures by the abovementioned solvent extraction methods to produce maximum yields of bioactive metabolites. Thereafter, we discuss the initial screening conducted to assess the biological activity of the extracts envisaging antimicrobial, antibiofilm, and acetylcholinesterase inhibition assays. Subsequentially, fractionation and purification of the compounds are discussed, which includes sections on chromatographic techniques such as Thin Layer Chromatography (TLC), Vacuum Liquid Chromatography (VLC), Size Exclusion Chromatography (SEC), and High-Performance Liquid Chromatography (HPLC). The working parameters are detailed for each, with details of every step involved in isolating the compounds in their pure forms. The procedures used for dereplication, and structure elucidation of purified compounds are described, including the use of HMRS, 1D and 2D NMR spectroscopy, and CD spectroscopy. The principles for each technique and how to interpret data arising from each of these techniques are explained. Finally, the bioassays that demonstrated the biological activity used to guide the isolation of the bioactive compounds described. Protocols describing assays against the full range of disease targets are presented in detail, including fungal and bacterial pathogens, biofilm targets, and Alzheimer's disease models. In brief, it forms an overall summary of the approaches to experimental design that were employed during the research. It serves as a guide to carrying out the work again. It also reveals the extent of methodology that the scientific work within this project has seen.

2.1 Sample collection

Samples were collected from Orman Garden, Giza, Wadi El-Natrun depression saline lakes; Al-Hamra and Al-Beida saline (El-Beheira Governorate), and Hurghada coral reefs. Collection permits were obtained from all sampling sites, ensuring full compliance with the Nagoya Protocol. The obtained samples were brought into the laboratory and stored in a fridge at 5°C until microbial cultures and strain separations were performed. Orman Garden and Wadi Natrum samples were identified by Dr Mokhtar from the National Research Centre, Egypt, and Hurghada samples were identified by Dr Mohamed Abdelghani from Aswan University.

Figure 2.1.1. Satellite image of Egypt, outlining the three collection sites. Orman Garden (1), Wadi El Natrun salt lakes (2), and Hurghada coral reefs (3).

2.1.1 Sample collection at Orman Garden

Orman Garden in Giza was chosen as it is an ideal location to explore endophytic natural products due to its rich biodiversity, including a wide variety of native and exotic plant species cultivated over more

than a century. This botanical diversity creates a unique ecological niche for endophytic microorganisms, which are known to produce a vast array of bioactive secondary metabolites.

Plant samples were collected from the outer parts of Orman Garden, Giza **Figure 2.1.1.1**. Coordinates: N 30.02917913076665, E 31.212962871165065. The collected samples were brought into the laboratory, Coded in **Table 2.2.1.1**, photographed in **Table 2.2.2,** and kept in a fridge (5°C), until isolation of microbial strains.

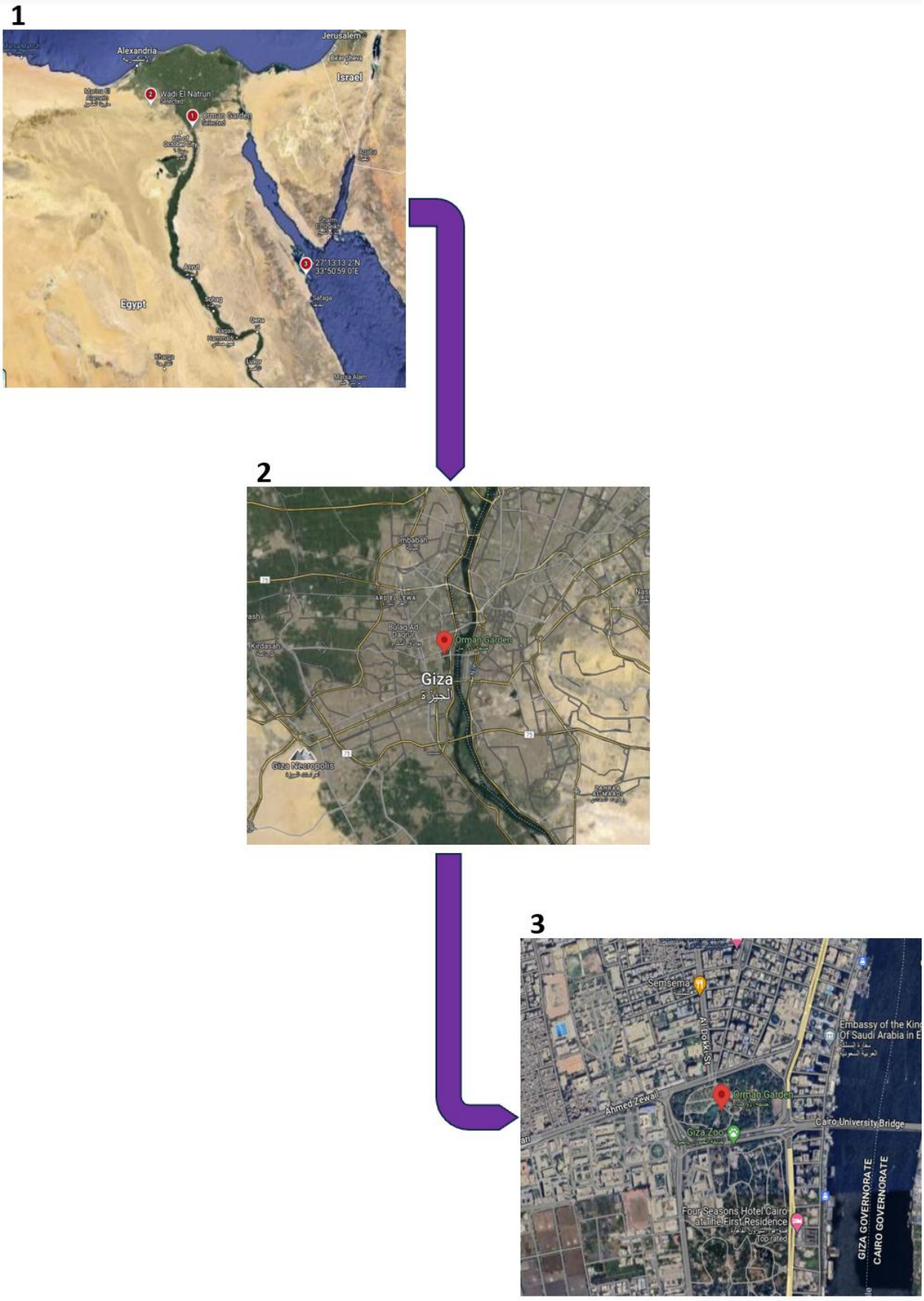

Figure 2.2.1.1. Satellite images of increasing magnification (1 < 2 < 3) of the location of collection site 1, Orman Garden, Giza.

Table 2.2.1. Orman garden sample data.

Plant code	Genus-species	Sample type	Location	Specific location	Morphology
Orm1	*Bauhinia tomentosa*	Plant	Orman garden, Giza	Outside gates	Pic No. 1
Orm2	*Bougainvillea spectabilis*	Plant	Orman garden, Giza	Outside gates	Pic No. 2

Table 2.2.2. Orman garden sample pictures.

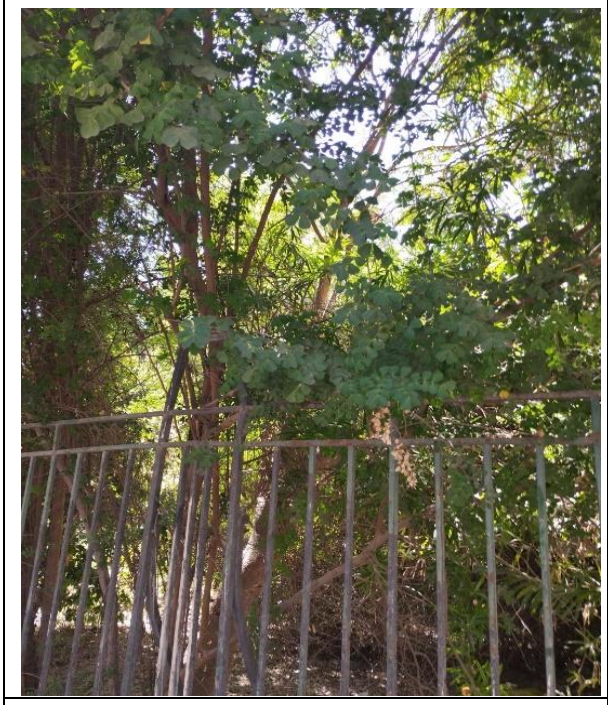	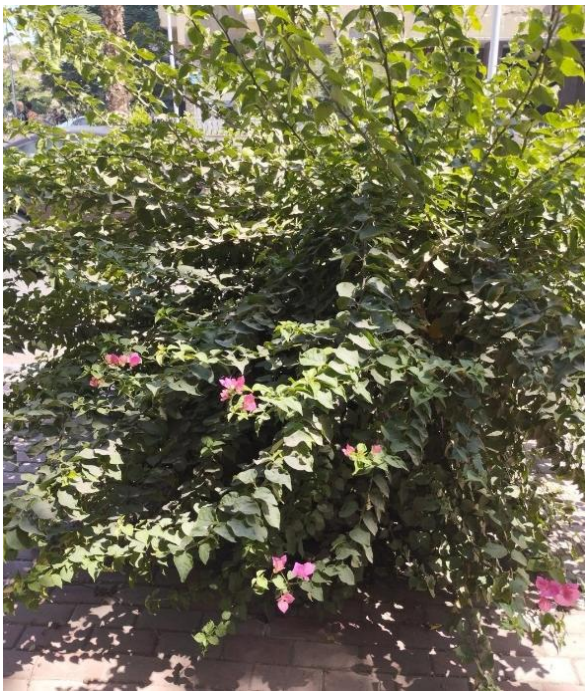
Pic 1 (Orm1)	**Pic 2 (Orm2)**

2.1.2 Sample collection at Wadi El-Natrun salt lakes

Wadi Natrun's salt lakes were chosen as they provide a highly promising environment for discovering novel natural products from extremophilic microorganisms. The region's hypersaline conditions support unique halophilic and halotolerant microbes that have adapted to extreme osmotic stress by producing specialised, potentially bioactive, secondary metabolites. The chemical and microbial diversity of these alkaline salt lakes, combined with their relative underexploration, makes Wadi Natrun an excellent candidate for bioprospecting efforts aimed at finding new bioactive compounds with potential biotechnological or pharmaceutical significance.

Plant samples were collected from two big lakes (Al-Hamra and Al-Beida) of the Wadi El-Natrun depression (El-Beheira Governorate) **Figure 2.1.2.1**. Coordinates: Al-Hamra 30°23'45.1"N 30°19'06.9"E, Al-Beida 30°25'53.4"N 30°14'33.0" E. The collected samples were brought into the laboratory, Coded **Table 2.1.2.1**, photographed **Table 2.1.2.2,** and kept in a fridge (5°C), until isolation of microbial strains.

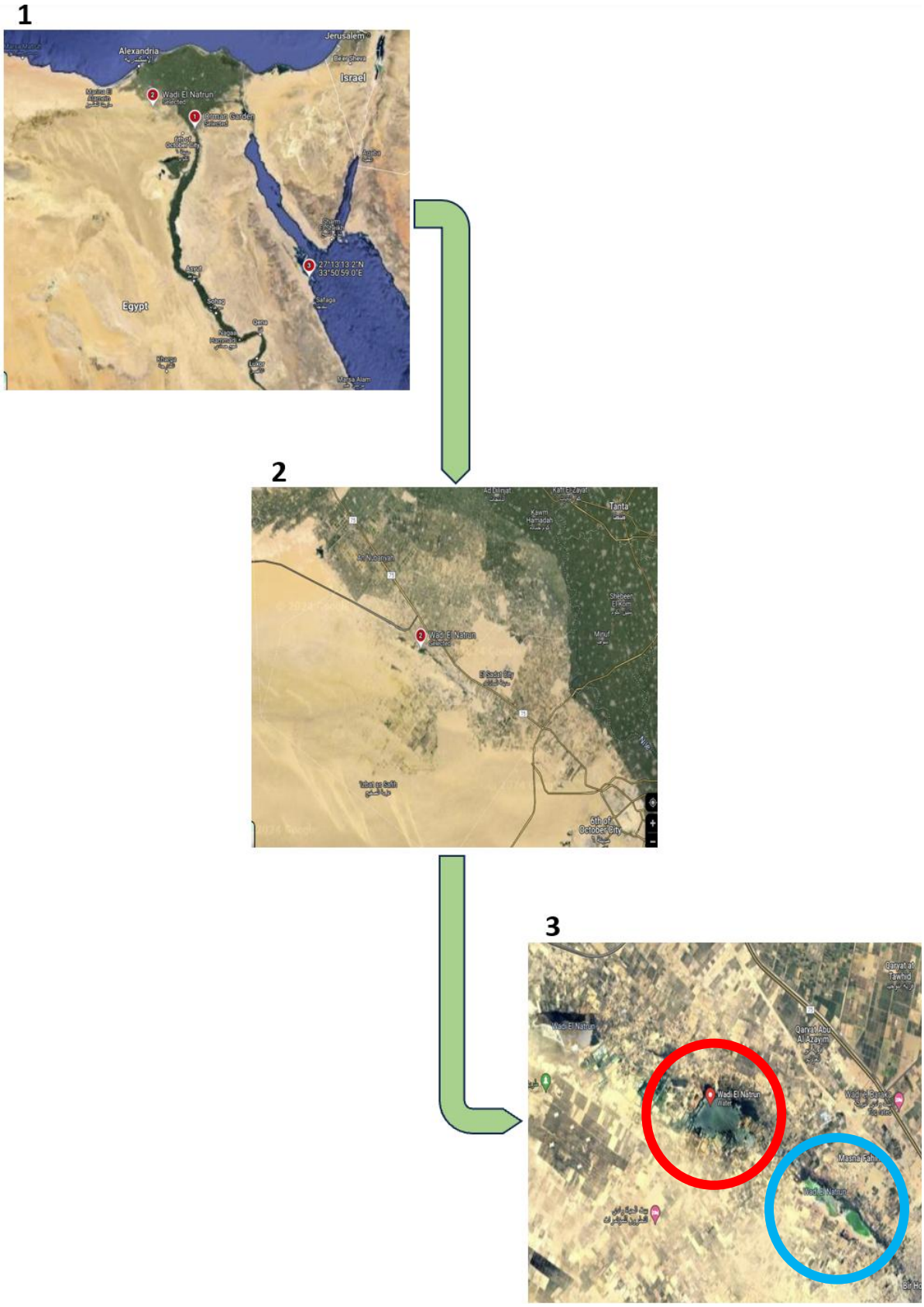

Figure 2.1.2.1. Satellite images of increasing magnification (1 < 2 < 3) of the location of collection site 2, Wadi El Natrun. Al-Beida Lake: red circle, Al-Hamra Lake: blue circle.

Table 2.1.2.1. Wadi El-Natrun sample data.

Plant code	name	Sample type	location	Specific location (Coordinates)	Picture no.
WNS1	*Tamarix nilotica (Ehrenb.)*	plant	Wadi El-Natrun depression (El-Beheira Governorate)	Bani Salama lake (30°25'53.4"N 30°14'33.0"E)	Pic No. 3
WNS2	Unidentified green algae	algae		Bani Salama lake (30°25'53.4"N 30°14'33.0"E)	Pic No. 4
WNS3	*Eleocharis gracilis*	plant		Bani Salama lake (30°25'53.4"N 30°14'33.0"E)	Pic No. 5
WNS4	*Juncus rigidus*	plant		Bani Salama lake (30°25'53.4"N 30°14'33.0"E)	Pic No. 6
WNS5	*Juncus acutus*	plant		Bani Salama lake (30°25'53.4"N 30°14'33.0"E)	Pic No. 7
WNS6		water		Bani Salama lake (30°25'53.4"N 30°14'33.0"E)	Pic No. 8
WNS7	Unidentified Red Algae	algae		Bani Salama lake (30°25'53.4"N 30°14'33.0"E)	Pic No. 9
WNS8	*Cyperus papyrus*	plant		Bani Salama sulphate lake (30°25'53.4"N 30°14'33.0"E)	Pic No. 10
WNS9		water		Bani Salama sulphate lake (30°25'53.4"N 30°14'33.0"E)	Pic No. 11
WNS10	*Phragmites australis*	plant		Bani Salama sulphate lake (30°25'53.4"N 30°14'33.0"E)	Pic No. 12
WNS11	*Cynodon dactylon*	plant		Bani Salama sulphate lake (30°25'53.4"N 30°14'33.0"E)	Pic No. 13
WNS12	*Alhagi graecorum*	plant		Naser region	Pic No. 14
WNS13	*Bassia indica*	plant		Naser region	Pic No. 15
WNS14	*Ficus retusa*	plant		Naser region	Pic No. 16
WNS15	*Salicornia fruticosa*	plant		Hamra lake (30°23'45.1"N 30°19'06.9"E)	Pic No. 17
WNS16		water		Hamra lake (30°23'45.1"N 30°19'06.9"E)	Pic No. 18

WNS17		water		Hamra lake (30°23'45.1"N 30°19'06.9"E)	Pic No. 19

Table 2.1.2.2. Wadi El-Natrun sample pictures.

	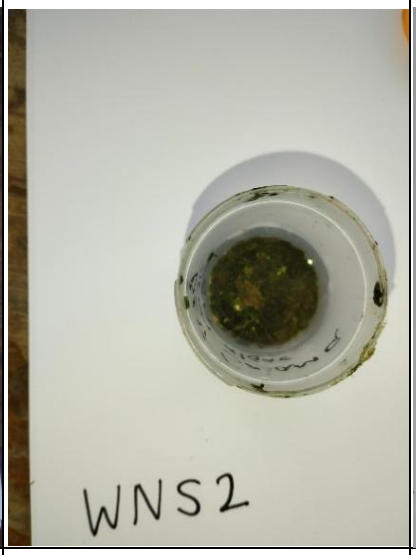	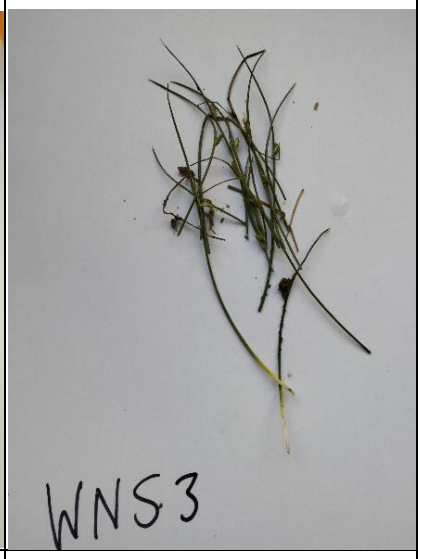
Pic 3 (WNS1)	**Pic 4 (WNS2)**	**Pic 5 (WNS3)**
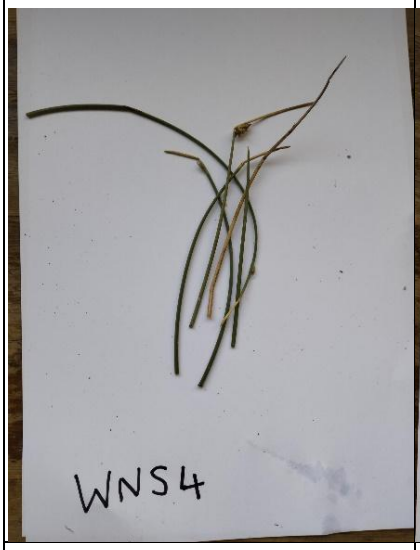		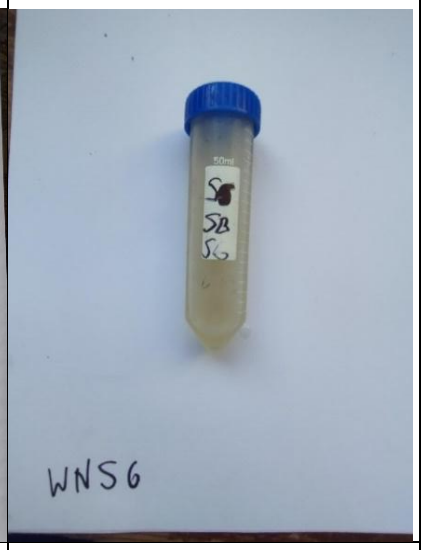
Pic 6 (WNS4)	**Pic 7 (WNS5)**	**Pic 8 (WNS6)**

		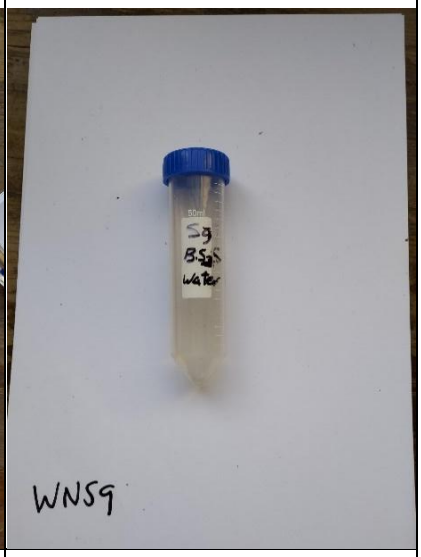
Pic 9 (WNS7)	**Pic 10 (WNS8)**	**Pic 11 (WNS9)**
		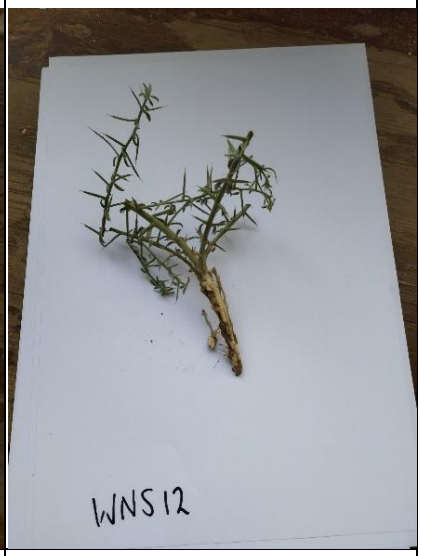
Pic 12 (WNS10)	**Pic 13 (WNS11)**	**Pic 14 (WNS12)**

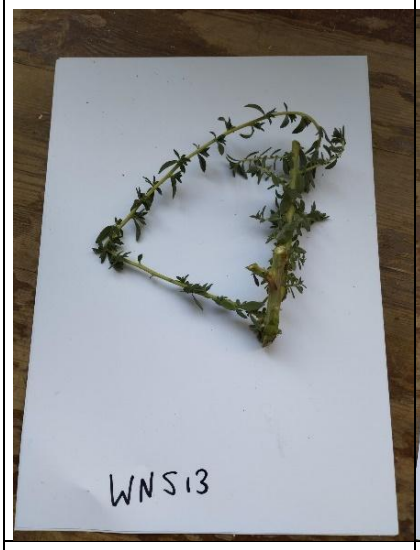

Pic 15. WNS13

Pic 16. WNS14

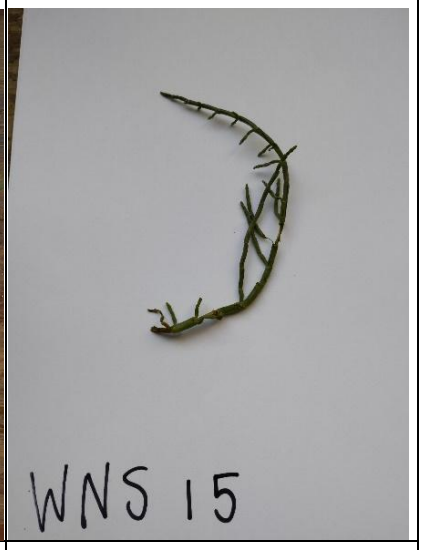

Pic 17. WNS15

Pic 18. WNS16

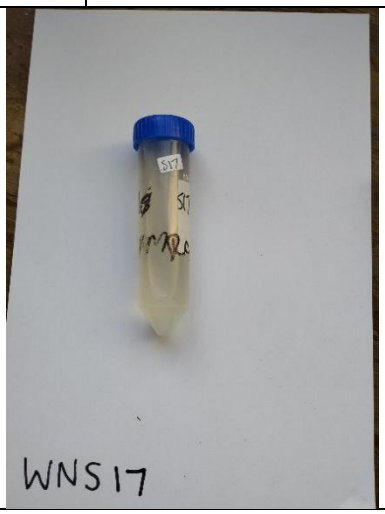

Pic 19. WNS17

2.1.3 Sample collection at Hurghada coral reefs

The coral reefs of Hurghada offer a rich and underexplored source of marine natural products, particularly from symbiotic microorganisms and invertebrates such as sponges, tunicates, and soft corals. These reef ecosystems are highly diverse and competitive, driving the evolution of potent bioactive compounds for defence, communication, and survival. Microbial communities associated with corals and reef organisms, particularly actinomycetes and marine fungi, are known to produce unique secondary metabolites with antibacterial, antifungal, anticancer, and anti-inflammatory properties. Given the ecological complexity and chemical novelty of Red Sea reefs, Hurghada represents a valuable site for marine natural product discovery.

14 marine samples **Figure 2.1.3.1** were collected from Hurghada during fieldwork in September 2023,

using SCUBA equipment. Diving was carried out by Dr Mohamed Abdelghani from Aswan University. We explored southwest to Magawish island reef at 27°11'20.0"N 33°50'53.0" E, between 1 and 5m depth in Hurghada region, Red Sea, Egypt. The samples were 6 marine sponges, 3 algae, 3 soft corals, and 2 sea cucumbers. These samples were collected as, firstly they are not on the endangered list, and secondly because similar invertebrates have been observed to be very rich in diverse natural products. All the samples were frozen in the freezer for investigation analysis, coded in **Table 2.1.3.1**, and photos were taken underwater and at the surface to show the morphology and the surrounding environment **Table 2.1.3.2.**

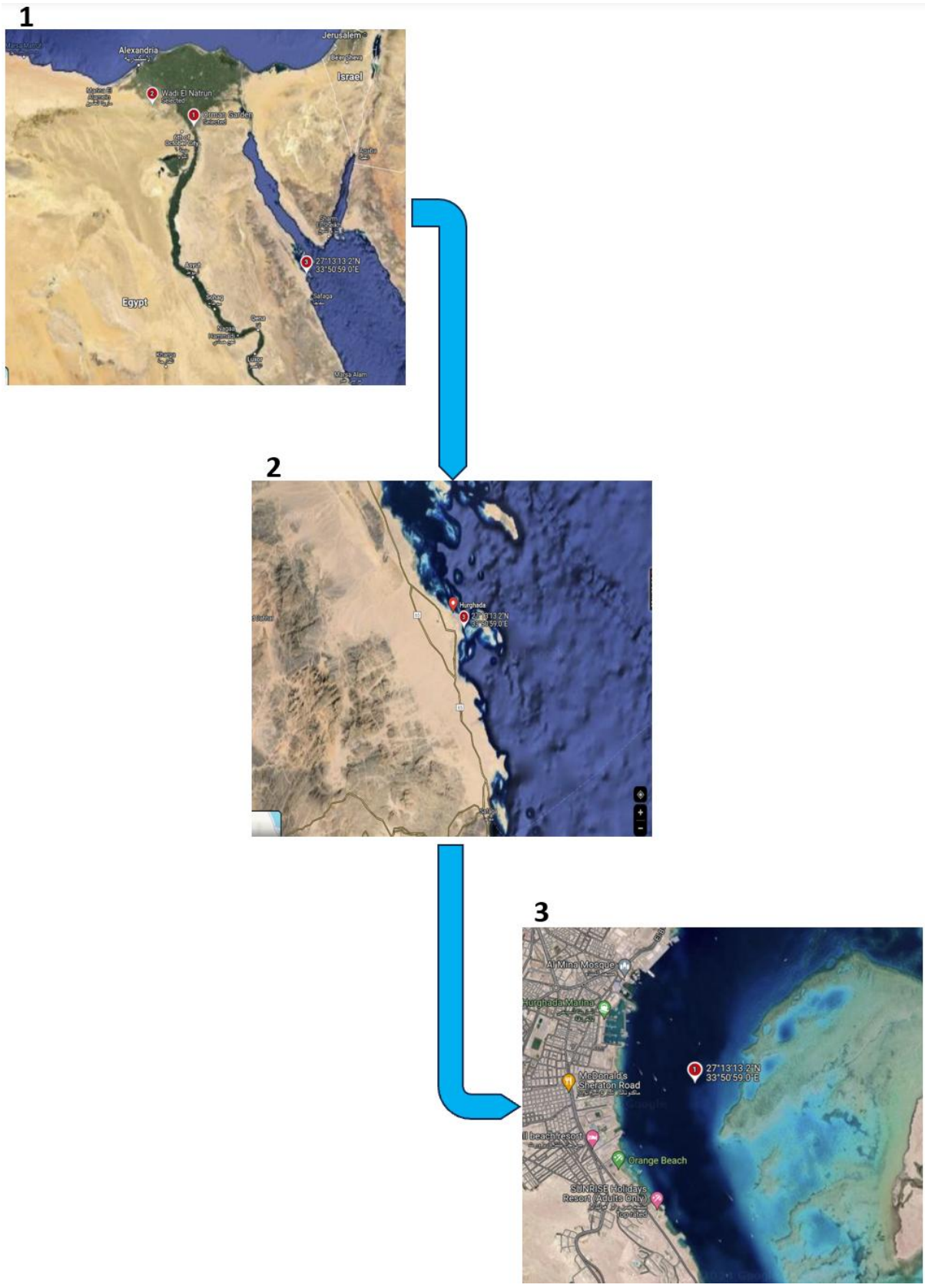

Figure 2.1.3.1. Satellite images of increasing magnification (1 < 2 < 3) of the location of collection site 3, Hurghada coral reefs.

Table 2.1.3.1. Hurghada coral reef sample data.

sp. code	Genus-species	type	site no.	location	Depth (m)	Pictures
HS1	*Actinopyga mauritiana*	sea cucumber	site 1	27°11'20.0"N 33°50'53.0"E	3-5m	Pic no.20
HS2	*Holothuria atra*	sea cucumber	site 1	27°11'20.0"N 33°50'53.0"E	3-5m	Pic no.21
HS3	*Dendronephthya* sp.	Soft coral	site 1	27°11'20.0"N 33°50'53.0"E	3-5m	Pic no.22
HS4	*Caulerpa recemosa*	algae	site 1	27°11'20.0"N 33°50'53.0"E	3-5m	Pic no.23
HS5	*Hemimycal arabica*	sponge	site 1	27°11'20.0"N 33°50'53.0"E	3-5m	Pic no.24
HS6	*Ganonema farinosum*	algae	site 1	27°11'20.0"N 33°50'53.0"E	3-5m	Pic no.25
HS7	*Spongia* sp.	sponge	site 1	27°11'20.0"N 33°50'53.0"E	3-5m	Pic no.26
HS8	*Callyspongia siphonellia*	sponge	site 1	27°11'20.0"N 33°50'53.0"E	3-5m	Pic no.27
HS9	*Dictyoshareia cavernosa*	algae	site 1	27°11'20.0"N 33°50'53.0"E	3-5m	Pic no.28
HS10	*Litophyton arboreum*	soft coral	site 1	27°11'20.0"N 33°50'53.0"E	3-5m	Pic no.29
HS11	*Haliclona* sp.	sponge	site 1	27°11'20.0"N 33°50'53.0"E	3-5m	Pic no.30
HS12	*Crella cyathophora*	sponge	site 1	27°11'20.0"N 33°50'53.0"E	3-5m	Pic no.31
HS13	*Clathria* sp.	sponge	site 1	27°11'20.0"N 33°50'53.0"E	3-5m	Pic no.32
HS14	*Sarcophyton glacum*	soft coral	site 1	27°11'20.0"N 33°50'53.0"E	3-5m	Pic no.33

Table 2.2.3.1. Hurghada coral reef sample codes, taxonomic ID, collection coordinates, and picture codes.

Pic 20 (HS1)

Pic 21 (HS2)

Pic 22 (HS3)

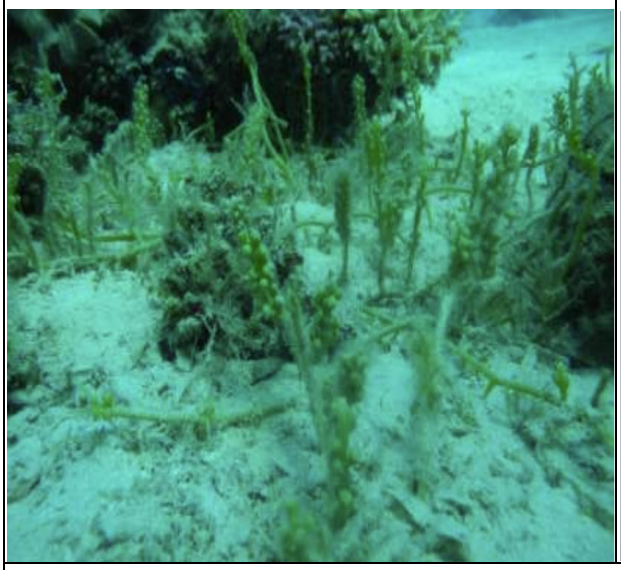

Pic 23 (HS4)

Pic 24 (HS5)

Pic 25 (HS6)

Pic 26 (HS7)

Pic 27 (HS8)

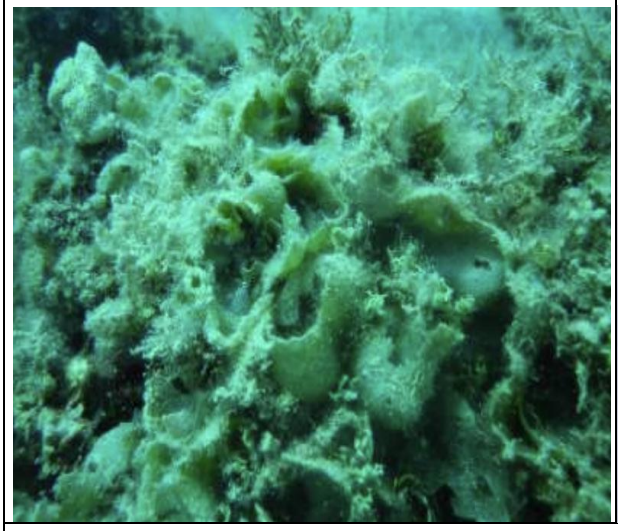

Pic 28 (HS9)

Pic 29 (HS10)

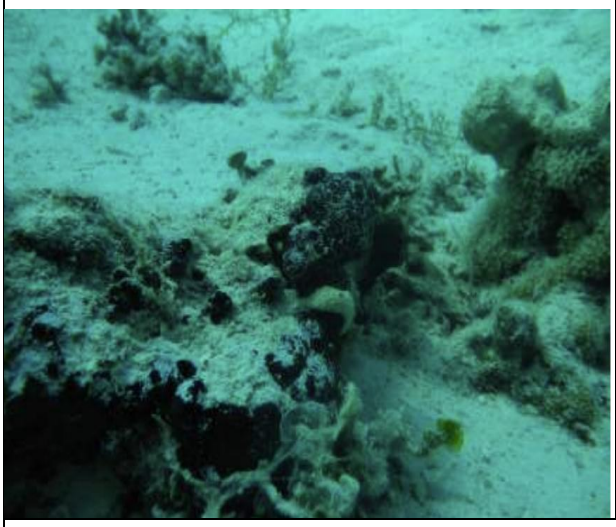

Pic 30 (HS11)

Pic 31 (HS12)

Pic 32 (HS13)

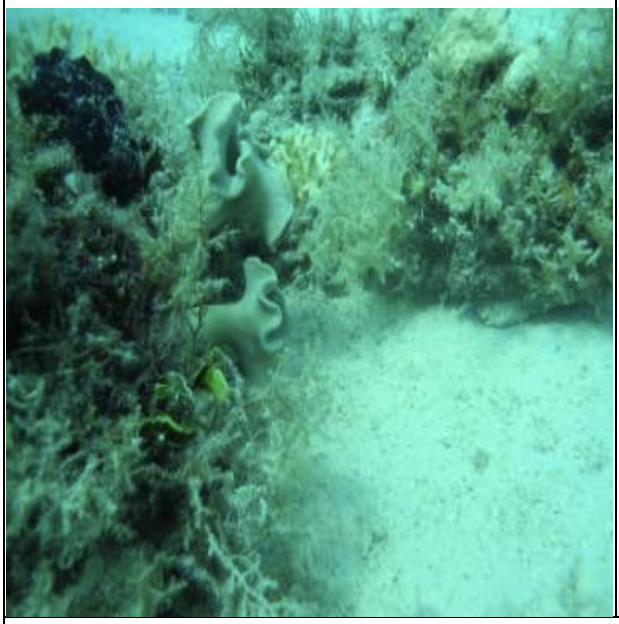

Pic 33 (HS14)

2.2 Isolation and fermentation

2.2.1 Culture media

All culture media were selected to support the growth of the widest possible range of microorganisms.

2.2.1.1 Nutrient agar medium (NA) for bacterial plates:

This medium consists of peptone 5.0 g/L, sodium chloride 8.0 g/L, HM peptone B (beef extract equivalent) 3.0 g/L, Agar No. 2 12.0 g/L, 1.0 L of water pH 7 ± 0.1. The medium was autoclaved at 121 ℃ for 20 minutes before cooling. Inoculation time was 5-7 days at 28°C for plates and slants. Used for all small-scale bacterial strains. The method detailed by Saituo and Nei 1987.[74]

2.2.1.2 Potato dextrose agar (PDA) for fungal plates:

This medium consists of potato extract, 4 g/L, Glucose/dextrose, 20 g/L, Agar, 15.0 g/L, 1 L of distilled water, pH 7 ± 0.1. the medium was autoclaved at 121℃ for 20 minutes before cooling. Inoculation time was for 5-7 days at 28°C for plates and slants. Used for all small-scale fungal strains. The method detailed by Saituo and Nei 1987.[74]

2.2.1.3 Nutrient broth medium (NB) for bacterial small-scale fermentation:

This medium consists of peptone 5.0 g/L, sodium chloride 5.0 g/L, HM peptone B (beef extract equivalent) 1.5 g/L, yeast extract 1.5 g/L, 1.0 L of water pH 7 ± 0.1, with final pH 7.4 ± 0.2 at 25 ℃. The medium was autoclaved at 121 ℃ for 20 minutes before cooling. Inoculation time was 10 days at 28°C for small-scale fermentation. Used for all small-scale bacterial strains. The method detailed by Saituo and Nei 1987.[74]

2.2.1.4 Potato dextrose broth medium (PDB) for fungal small-scale fermentation:

This medium consists of dextrose 20.0 g/L, infusion from potato solids 6.5 g/L, 1 L of water pH 7 ± 0.1, with final pH 5.6 ± 0.2 at 25 ℃. The medium was autoclaved at 121 ℃ for 20 minutes before cooling. Inoculation time was 10 days at 28°C for small-scale fermentation. Used for all small-scale fungal strains. The method detailed by Saituo and Nei 1987.[74]

2.2.1.5 Solid-state rice medium for all large-scale endophyte cultures:

This medium consists of 100 g of rice soaked in 100 mL of distilled water. The medium was autoclaved at 121 ℃ for 20 minutes before cooling. Inoculation time was 15 days at 28°C for large-scale fermentation. Used for all large-scale bacterial/fungal strains. The method detailed by Saituo and Nei 1987.[74]

2.2.2 Organism surface sterilisation and isolation of endophytes from sample cuttings

The process of sample preparation and surface sterilisation was meticulously carried out to ensure the viability and purity of the collected organism samples. Upon collection, samples were sorted, assigned unique codes, and photographed for documentation. Voucher samples were preserved in 100% ethanol to maintain their integrity for further analysis and were stored at the National Research Centre (NRC), Cairo. The samples were processed promptly, ideally on the same day, to minimize

potential contamination and degradation. If processing was delayed, samples were stored at 4°C until the next day. Surface sterilization of the samples involved a series of steps, including washing under running water to remove surface dirt, followed by immersion in 70% ethanol for 30 seconds and subsequent rinsing in sterile water. The samples were then treated with 2% sodium hypochlorite for 30 seconds and rinsed again with sterile water three times to ensure thorough sterilization. To assess the effectiveness of the sterilization procedure, water from the final rinse was inoculated onto potato dextrose and nutrient agar media to check for any microbial growth, confirming the success of the sterilization process. Following sterilization, samples were dried using laminar flow, and small pieces were transferred onto selected isolation medium plates. These plates, containing potato dextrose agar for fungi and nutrient agar for bacteria, were then incubated at room temperature until the growth of endophytic species was observed. Endophytes from Hurghada, Wadi Natrun, and Orman Garden were cultured on potato dextrose agar for fungi and nutrient agar for bacteria. Wadi Natrun and Orman Garden endophytes were incubated with distilled water (however if repeated high saline water would have been used), while Hurghada endophytes were incubated with either 50% sterile artificial seawater (SASW) or 100% SASW to provide ideal growth conditions for various microbial communities in distinct ecological niches. 12 pure microbial strains (8 fungal and 4 bacterial) were isolated from the samples from Orman garden, 29 pure microbial strains were isolated (12 fungal and 17 bacterial) from marine samples of Hurghada, and 46 microbial strains (15 fungal and 31 bacterial) were isolated from samples of Wadi El-Natrun. Samples were sorted, given codes, and photographed.

Figure 2.2.2.1. Initial Petri dishes of Wadi Natrum sample 1 (WNS1) root cuttings. Left: Fungal strains grown on PDA. Right: Bacterial strains grown on NA.

2.2.2.1 Sterile artificial sea water (SASW)

Table 2.2.2.1.1. Components of sterile artificial sea water (SASW), g/L.[75]

NaCl	28.13 g
KCl	0.77 g
$CaCl_2$	1.60 g
$MgCl_2$	4.80 g

$NaHCO_3$	0.11 g
$MgSO_4$	3.50 g
Distilled H_2O	1 L

2.2.3 Small-scale fermentation of microbial strains

Small-scale fermentation was performed in 250 mL flasks using two different media, nutrient broth (bacteria) and potato dextrose broth (fungi), described in section 2.2.1. Two liquid media, medium 1: nutrient agar (28g in 1 L of distilled water, pH 7 ± 0.1). Medium 2: potato dextrose broth (potato extract 4 g, dextrose 20 g in 1 L of distilled water, pH 7 ± 0.1. The flasks were incubated without agitation for 15 days at a temperature of 28°C. After incubation, the cultures were extracted using ethyl acetate, then the extract was evaporated and weighed in preparation for the assessment of biological activity.

2.2.4 Large-scale fermentation of selected microbial strains

All cultures and inoculations were carried out at by myself at the National Research Centre, Cairo, Egypt. Inoculation was carried out in 100 mL of potato dextrose broth media (PDB) for fungi and nutrient broth media (NB) for bacteria for 3 days at 30 °C as seed culture. 5 mL of seed culture was transferred to 20 different 1 L Erlenmeyer flasks comprising 100 g of commercial rice and 100 mL water (0%, 50%, and 100% artificial seawater, dependent on initial growing and isolation conditions). The solid medium was then sterilised in the autoclave for 20 mins at 121 °C, then inoculated with the microbial strains. Incubation of the Erlenmeyer flasks was carried out for 15 days at 28 °C. Subsequently, the mass was extracted using ethyl acetate, followed by purification by filtration and evaporation in vacuo.

2.3 Sample purification

2.3.1 Extraction of bioactive compounds

After the incubation period, the entire fermentation broth was harvested and the mycelia cake separated from the water phase (filtrate), the filtrate was extracted by ethyl acetate, the EtOAc was then evaporated using a rotary evaporator under reduced pressure at 35 °C to dryness.

2.3.2 Modified Kupchan partitioning

A modified technique of Kupchan fractionation[76] was employed for all sample extracts, to fractionate the extract and the metabolites based on solvent polarity. This technique first suspends the total extract in 100% water, before partitioning with DCM separating the aqueous layer (water) from the organic layer (DCM). The organic layer is subsequently dried and then dissolved in methanol/water (9:1), before being partitioned using hexane. The hexane layer is removed to make the FH (hexane) fraction. The methanol/water (9:1) fraction is then phase adjusted to methanol/water (1:1), before

being partitioned with DCM to produce the FD (DCM) and FM (methanol) fractions. The aqueous layer was partitioned with sec-butanol to produce the WW (water) and WB (butanol) fractions (Figure 2.2.5.1). Non-polar (hexane/DCM) fractions often contain terpenoids, fatty acids, and alkaloids. Mid-polar (MeOH) fractions frequently yield flavonoids and phenolics.Polar (BuOH/aqueous) fractions may contain glycosides, saponins, or polar alkaloids.

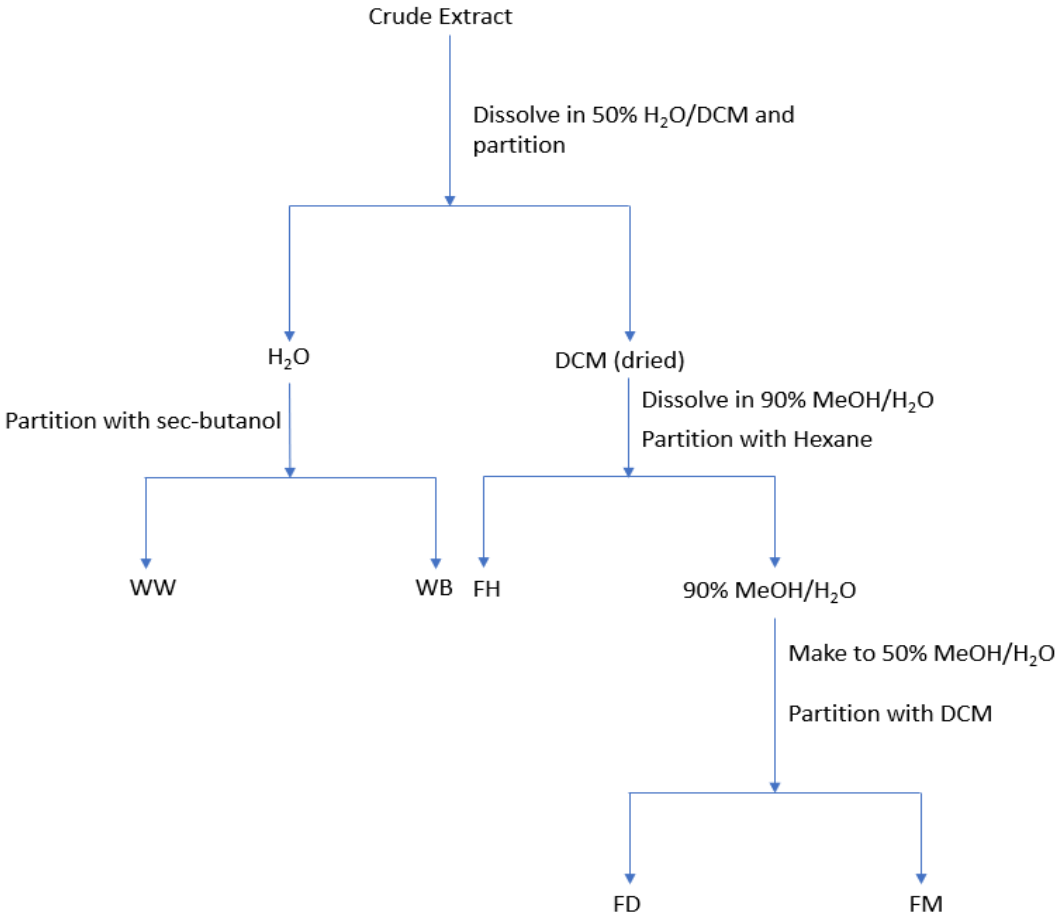

Figure 2.2.5.1. Modified Kupchan Fractionation used on extracts.[76]

2.3.3 Vacuum liquid chromatography (VCL)

VLC was carried out using silica gel 70-230 mesh (Loba Chemie, particle size: d10 75-95 µm, d50 125-150 µm, d50 215-245 µm).[77] Column height 15 cm with a diameter of 4.6 cm. Each polarity step is made up of 100 mL solvent total, with each subsequent fraction increasing in polarity (hexane 100% - methanol 100%).

2.3.4 Size exclusion chromatography (SEC)

Size exclusion chromatography (SEC) was carried out on WNS7(8)F3 and WNS16(8)F2 using a Sephadex LH-20 (Pharmacia) stationary phase, dimensions: height 40 cm, diameter 2 cm. 100% methanol was used for the solvent systems. SEC was carried out on HS4(50)F3 using a Sephadex LH-20 (Pharmacia) stationary phase, dimensions: height 40 cm, diameter 2 cm. Varying ratios of MeOH: DCM and hexane were used for the solvent systems (See Supplementary).

2.3.5 HPLC/UV

Samples were analysed by their UV profiles and compounds were isolated by HPLC using an Agilent 1220 infinity LC, hyphenated to a photodiode array detector (PDA) (columns and conditions given in results).[78] Final purifications were carried out on an Agilent Infinity 1200 HPLC with a photodiode array detector (PDA).

2.4 Identification

2.4.1 Identification of fungi using morphological characteristics

All isolated strains were cultured on potato dextrose agar (PDA) (fungi) or Nutrient agar (bacteria) at 25°C and the main morphological features were examined. A total of 152 different isolates were studied and grouped into seven genera. The following genera were identified: *Aspergillus*, *Chaetomium, Fusarium, Penicillium, Cladosporium, Paecilomyces, and Trichoderma*. For a more accurate determination and results verification molecular identification was acquired.

2.4.2 Genotypic Identification of samples

All fungi were identified using 18S rRNA analysis. Utilising the Qiagen DNeasy Mini Kit procedure[79], fungal DNA was isolated in the lab. The polymerase chain reaction (PCR) was performed on the isolated DNA using the universal primers ITS1 (5'-TCCGTAGGTGAACCTGCG-3') and ITS4 (5'-TCCTCCGCTTATTG ATATGC-3'). Amplified DNA was subjected to DNA sequencing at Macrogen Companies in South Korea, and the results were compared to DNA sequences that were already available in NCBI GenBank*. An accession number was received after the acquired gene sequence was added to the NCBI GenBank database.[80]

2.5 Biological activity

2.5.1 Acetylcholinesterase inhibition

A major target in Alzheimer's disease involves inhibiting the enzyme acetylcholinesterase, as lower

levels of the neurotransmitter acetylcholine are associated with AD. Acetylcholine plays a major role in neuronal messaging, and by inhibiting the enzyme that removes it from the brain, the severity of the symptoms of AD can be reduced. To measure the inhibitory effect of samples, a colorimetric Acetylcholinesterase Inhibitor Screening Kit was used (ab283363, Abcam Discovery Drive, Cambridge Biomedical Campus, Cambridge, CB2 0AX, UK)[81]. Initially, the test samples were dissolved in methanol, which is shown to have the least effect on the enzymes acetylcholinesterase and butyrylcholinesterase according to UM Ghali (2022),[82] and subsequently diluted by a factor of five in the assay buffer. Subsequently, 10 µL of the diluted sample mixtures were added to the microplate. This was followed by 160 µL assay buffer, and finally 10 µL of the diluted acetylcholinesterase enzyme solution. After 15 min of incubation at 25°C, 40 µL of the reaction mixture (10 µL AChE substrate, 5 µL DTNB solution and 25 µL assay buffer) was added. Acetylthiocholine was used as the substrate, and DTNB was used as the indicator. Using a microplate reader, the intensity of the developed colour was measured at 412 nm (S, sample) every 57 seconds for 45 cycles totalling 2565 s or 42 min and 45 s. A control without the inhibitor was measured (EC, enzyme control), and a control with no enzyme or inhibitor was measured (BC, background control). The absorbance of the solvent, methanol, used to dissolve the test inhibitors was measured (SC, solvent control), with the absorbance of Donepezil (1 µM) also measured as a positive control (IC, inhibitor control).[81]

Percentage inhibition was calculated as follows:

$$\%\ \text{Inhibition} = \frac{\text{Slope of EC} - \text{Slope of S}}{\text{Slope of EC}}\ \text{x}\ 100\%$$

2.5.2 Antimicrobial activity

Antimicrobial activity was measured at the Biotechnology Research institute, Egypt. The antimicrobial efficacy of the extracts was evaluated against a range of microbial strains, encompassing Gram-negative bacteria (*Escherichia coli* ATCC 25,922, *Klebsiella pneumoniae*, and *Salmonella typhi*), Gram-positive bacteria (*Staphylococcus aureus* NRRLB-767, *Methicillin-resistant Staphylococcus aureus* (MRSA)), yeast (*Candida albicans* ATCC 10,231), and fungi (*Aspergillus niger* ATCC 10,231).[83] The experiment utilised 96-well flat polystyrene plates. 10 µL of test extracts at a concentration of 250 µg/ml were combined with 80 µl of lysogeny broth (LB broth). Subsequently, 10 µL of bacterial culture suspension in the logarithmic growth phase was added. The plates were incubated overnight at 37 °C. After incubation, the tested extracts exhibited antibacterial activity, as shown by the clearing of the wells. On the other hand, extracts that had no impact on the bacteria caused the growth media in the wells to become opaque. The control group comprised the pathogen with no intervention, with negative controls of ciprofloxacin (antibacterial) and nystatin (antifungal) used. Absorbance was measured 20 hours after the experiment began, at a wavelength of 600 nm using a microplate reader 2100C Rayto Elisa reader rt2100c.[83]

2.5.3 Biofilm inhibition

Biofilm inhibitory activity was measured at Biotechnology Research institute, Egypt. The biofilm inhibitory activity of samples was evaluated using the microtitre plate test (MTP) in 96 well-flat bottom polystyrene titre plates against four clinical pathogens *(E. coli, P. aeruginosa, S. aureus*, and *B. subtilis*).[84] Each well of the 96 well-plate contained 180 µL of lysogeny broth (LB) with the following composition per litre: tryptone 10.0 g, yeast extract 5.0g, NaCl 10.0g. At a pH of 7.2, 10 µL of overnight cultured test bacteria, 10 µL of samples at a concentration of 20 µg mL^{-1}, and the negative control were incubated on a plate for 24 hours at 37 °C. After incubation, the well's contents were extracted, and the floating bacteria were eliminated by rinsing each well with 200 µL of phosphate-buffered saline at pH 7.2. Crystal violet (0.1%, w/v) was added for staining. After 1 hour, the wells were rinsed with 200 µL of distilled water per well, and the plate was left to dry in the laminar flow. 95% ethanol was added to the dried plate, and the optical density (OD) was measured at 570 nm using a microplate reader RT 2100C Rayto Elisa Reader.[84]

2.5.4 Bioassays for the endophytic fungi strains *Aspergillus* ASF and *Aspergillus* ASMN.

Bioassays for the samples *Aspergillus* strain ASF and *Aspergillus* strain ASMN were conducted at the Medina Foundation, Granada, Spain[85] for antibacterial, antifungal, and anticancer assays. For both the antifungal and antibacterial bioassays, various microbes on agar plates were grown with a control plate for each microbe. Amphotericin B and Penicillin G were used as internal positive and negative controls respectively.

2.6 Chemical profiling

2.6.1 LC-HRMS

High-resolution mass spectrometry data, for the sample *Aspergillus* sp. ASMN, was measured at Graz University in Austria on an Agilent MS Q-TOF G6546A mass spectrometer. Parameters for analysis: Gas Temp 280°C, Gas Flow 8 L/min, Nebulizer 30 psig, Sheath Gas Temp 380°C, Sheath Gas Flow 12 arbitrary units. Agilent Infinity Lab Poroshell 120 PN:699675-902 column was used with the solvent system of A (H_2O) and B (ACN 0.1 % formic acid). Flow rate 0.600 mL/min. A gradient of 100% A to 100% B was used from t = 0.00 to t = 12.00 mins, then kept at B 100% until t = 22.00 mins. Data processing was carried out using ACD Labs Spectrus Processor. High-resolution mass spectrometry data, for the sample *Aspergillus* sp. ASF, was measured at Aberdeen University using a Bruker Maxis 2 Q-TOF mass spectrometer. Parameters of analysis using mass spectrometry: capillary voltage 45 V, capillary temperature 320 °C, auxiliary gas flow rate 10−20 arbitrary units, sheath gas flow rate 40−50 arbitrary units, spray voltage 4.5 kV, mass range 100− 2000 amu, resolution 20,000 for MS and 20,000 for MS/MS. Agilent Infinity Lab Poroshell 120 PN:699675-902 column was used with the solvent

system of A (H_2O, 0.1 % formic acid) and B (ACN, 0.1% formic acid). Flow rate 0.400 mL/min. A gradient of 20 % B to 100% B was used from t = 0.00 to t = 10.00 mins, then kept at 100 % until t = 12.00 mins, followed by a gradient of 100% B to 20% B from t = 12.00 to t = 13.00 mins, and then an isocratic system of B 20 % from t = 13.00 to t = 15.00 mins. Data processing was carried out using ACD Labs Spectrus Processor. All other samples were measured at UCLan, on an Agilent 6546 LC/QTOF mass spectrometer. Parameters of analysis: Gas Temperature 325°C, Drying Gas l/min 5.0 l/min, Nebulizer Pressures 20 psi, Capillary Voltage 4000 V, Sheath Gas Temperature 275°C, Sheath Gas Flow 12.0 l/min, Nozzle Voltage 2000 V. A Kinetex® 1.7 µm EVO C18 100 Å LC Column 100 x 2.1 mm S/No. H23-311228 5726-0046 column was used with the solvent system of A (H_2O, 0.1 % formic acid) and B (ACN, 0.1% formic acid). Flow rate 0.400 mL/min. A gradient of 20 % B to 100% B was used from t = 0.00 to t = 10.00 mins, then kept at 100 % until t = 12.00 mins, followed by a gradient of 100% B to 20% B from t = 12.00 to t = 13.00 mins, and then an isocratic system of B 20 % from t = 13.00 to t = 15.00 mins. All reference masses were the same across the board: In the positive mode, reference masses were 121.0508773 and 922.009798, and, in the negative mode, 119.03632 and 966.000725. The instrument software was MassHunter 8.0.0 (Agilent Technologies, Waldbronn, Germany). The mass spectrometry process was conducted using an automated MS/MS mode, which employed tandem mass spectrometry to initially measure precursor peaks and then isolate each peak for subsequent MS/MS analysis. All mass spectrometry data was processed with ACD Labs Spectrus Processor.

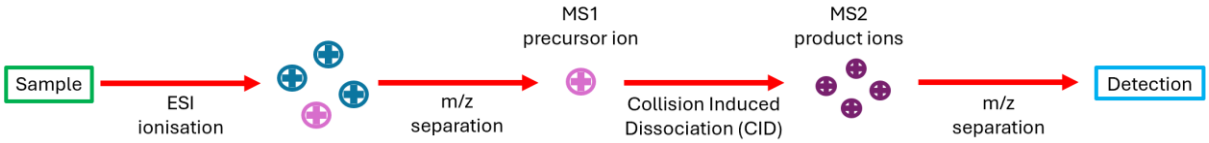

Figure 2.5.5.1. Flow chart displaying the process of tandem MS/MS. Electrospray ionisation (ESI) is first used to convert the molecules into positive molecular ions (MS1), with each individual molecular ion then fragmentated into product ions (MS2) using Collision Induced Dissociation (CID).

2.6.2 Nuclear Magnetic Resonance Spectroscopy

1D and 2D NMR data has been collected at the University of Edinburgh on an 800 MHz Avance III Spectrometer for ^{1}H and 100 MHz for ^{13}C spectra, with a ^{1}H-13C/ 15N/ 2H Bruker CPTCI Cryoprobe. Data has also been collected at UCLan a Bruker AV11 +400MHz, at 400MHz for ^{1}H and 100 MHz for ^{13}C spectra. Both the chemical shift values obtained through the 1D and 2D techniques were referenced to the solvent chemical shift signals (δ_H 3.31 and δ_C 49.00 in CD_3OD). Data processing was carried out on ACD Labs Spectrus Processor.

CHAPTER 3 Results and Discussion – Identification and biological screening

3.0 Introduction

This chapter outlines a comprehensive approach for identifying and biologically evaluating active strains, ensuring accurate classification and robust analysis of their bioactivity. This work presents a solid foundation for the subsequent isolation and characterization of bioactive compounds through the combination of traditional and molecular methods. The first step of the morphological identification was the visual examination of colony characteristics, including colour, texture, growth patterns, and other visible characteristics. Although this approach was used to classify the strains initially, it was complemented by genotypic identification to enhance specificity and resolve any ambiguities that may occur. The genotypic analysis was carried out using 18S rRNA sequencing, which is a widely used molecular technique for identifying eukaryotic microorganisms up to the genus and species level. The sequences obtained were searched against reference databases to confirm the identity of each strain, a crucial step in the taxonomy of microorganisms. The biological evaluation of these strains and their isolated pure compounds is another crucial part of this chapter. The strains were examined for their activity towards different targets such as antibiofilm, antimicrobial and anti-Alzheimer's disease assays. The antibiofilm assays focused on the inhibition of biofilm formation and the disruption of existing biofilms, which are suspected to contribute to persistent infections and antibiotic resistance. The inhibitory activity against a number of pathogenic bacteria and fungi was also assessed to identify strains with broad or narrow antimicrobial activity. Anti-Alzheimer's disease activity was evaluated using enzymatic assays targeting acetylcholinesterase, a key enzyme implicated in the pathophysiology of Alzheimer's disease. Strains demonstrating significant bioactivity in these assays were prioritized for further analysis.

3.1 Identification

3.1.1 Morphological identification of the selected fungi

Preliminary identification based on morphological features identified them as *Aspergillus* sp. and to species level as *A. niger* (Fig 3.1.1.1), A. *terreus* and *A. fumigatus* (Fig 3.1.1.1) *Aspergillus* species exhibit distinct morphologies that aid in initial identification. *Aspergillus niger* forms bold black or dark brown colonies with long, darkening conidiophores and black, biseriate spores.[86] In contrast, *Aspergillus terreus* displays earthy tones (brown, yellow-brown, or orange-brown) in its colonies and produces light brown, single or double-rowed spores on shorter conidiophores. Finally, *Aspergillus fumigatus* is characterized by blue-green to grey-green colonies, short conidiophores with a conical vesicle, and greenish-brown spores arranged in a single row. While colony colour provides a starting point,

definitive identification often necessitates a combination of morphological and molecular techniques.[87]

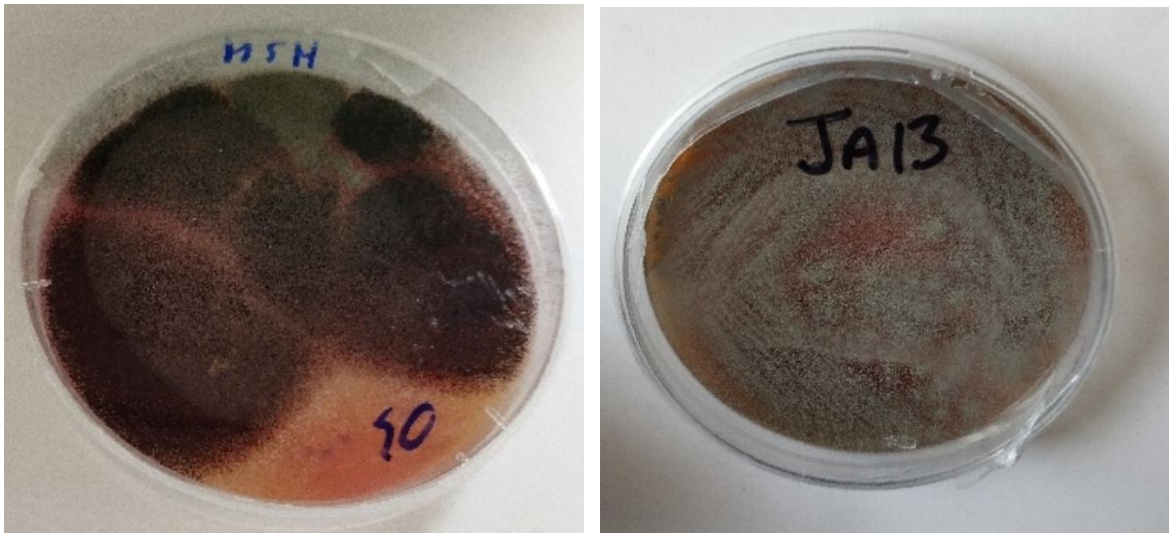

Figure. 3.1.1.1. Left picture: petri dish of original colony of *Aspergillus niger* HS4(50)F3. Right picture: petri dish of isolated *Aspergillus fumigatus* JA13.

3.1.2 Genotypic identification

The genetic identification of the isolated fungi was conducted by employing sequencing techniques targeting the 18 S rRNA gene. The 18S rRNA gene is a highly conserved region of the fungal genome that codes for part of the small ribosomal subunit. The DNA was extracted, amplified, sequenced, and aligned with known sequences stored in the GenBank database using the Basic Local Alignment Search Tool (BLAST). The results obtained demonstrated a high degree of similarity between the obtained sequences of the fungal isolates ASMN, ASF, HS4(50)F3, JA13, WNS7(8)F3, WNS16(8)F2, with a homology, and similarity reached 99.64% for ASMN with *Aspergillus* fumigatus, 100% for ASF with *Aspergillus terreus,* 100% for HS4(50)F3 with *Aspergillus niger*, 100% for JA13 with *Aspergillus* fumigatus, 100% for WNS7(8)F3 with *Aspergillus niger* and 99.82 for WNS16(8)F2 with *Aspergillus* fumigatus. Similarly, the fungal 18S sequences have been archived in GenBank[88] (Table 3.1.2.1). The evolutionary history was deduced by employing the neighbour-joining method, as proposed by Saitou and Nei (1987).[89] The bootstrap test was used to determine the percentage of duplicate trees in which the associated taxa grouped together.[90] These percentages are displayed adjacent to the branches. The illustrated tree has been accurately represented in terms of scale, where the lengths of the branches correlate to the evolutionary distances utilised in the inference of the phylogenetic tree. The Maximum Composite Likelihood technique was employed for determining the evolutionary distances and are in units of the number of base substitutions per site.[91] The current investigation included a total of 20 for ASMN, 20 for ASF, 21 for HS4(50)F3, 21 for JA13 ,21 for WNS7(8)F3 and 15 WNS16(8)F2, for nucleotide sequences. This study included an analysis of the codon positions, which included the first, second, third, and noncoding locations. The paired deletion option was employed to remove all occurrences of ambiguous locations in each pair of sequences. The ultimate dataset comprised a total of 1755 sites. The software MEGAX was utilized to conduct evolutionary analysis.[92]

Table 3.1.2.1. Fungal 18S sequences have been archived in GenBank, with Accession number shown.

Fungal strain	**GenBank Accession number**
Aspergillus sp. ASMN	MN518345
Aspergillus sp. ASF	MN518344
Aspergillus sp. HS4(50)F3	PP861021
Aspergillus sp. JA13	PP861024
Aspergillus sp. WNS7(8)F3	PP861030
Aspergillus sp. WNS16(8)F2	PP861071

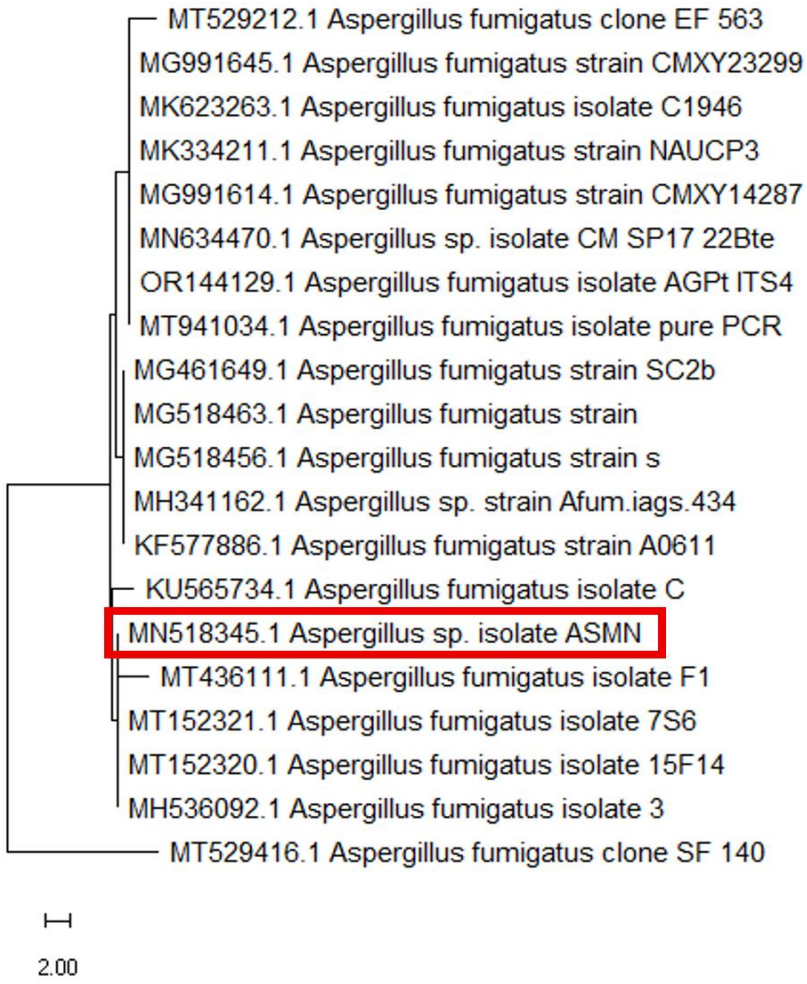

Figure 3.1.2.1. Constructed neighbour-joining phylogenetic tree based on almost complete 18 S rRNA gene sequences (1755 nt), showing the position of for *Aspergillus* sp. ASMN (red box), amongst its phylogenetic neighbours. *Aspergillus fumigatus* clone SF 140 (GenBank accession no. MT529416.1) was used as an outgroup.

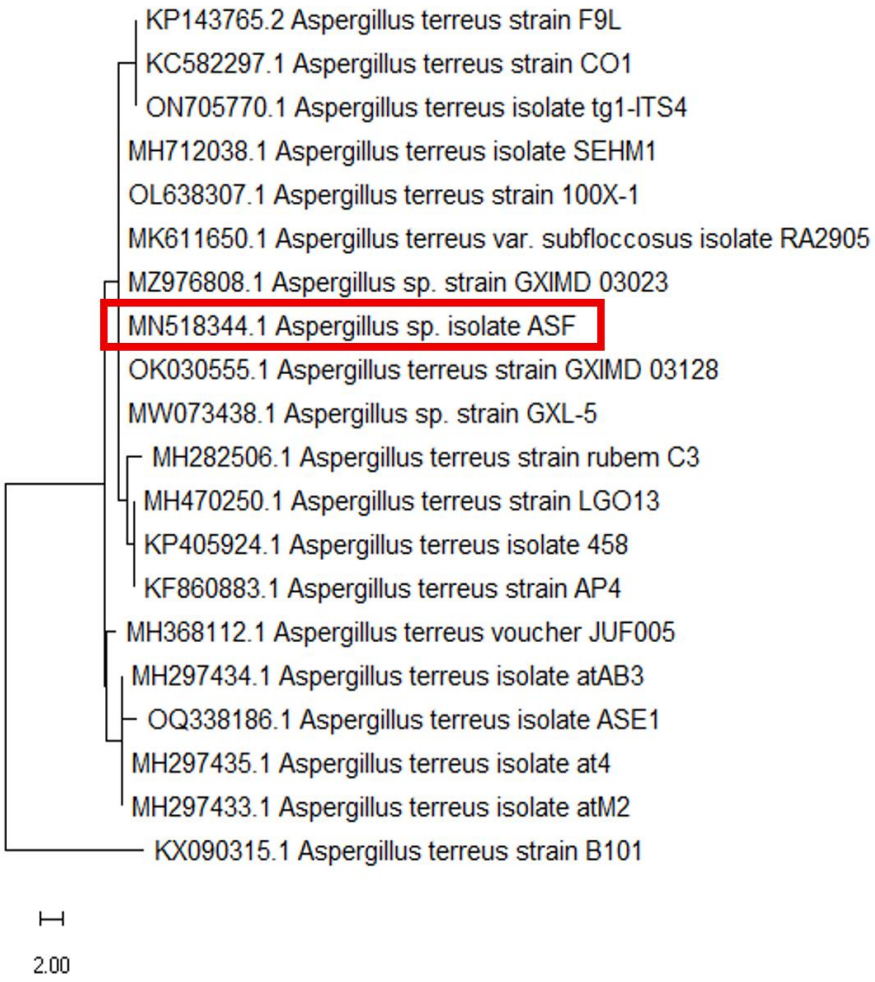

Figure 3.1.2.2. Constructed neighbour-joining phylogenetic tree based on almost complete 18 S rRNA gene sequences (1755 nt), showing the position of for *Aspergillus* sp. ASF (red box) , amongst its phylogenetic neighbours. *Aspergillus terrus* strain B101 (GenBank accession no. KX090315.1) was used as an outgroup.

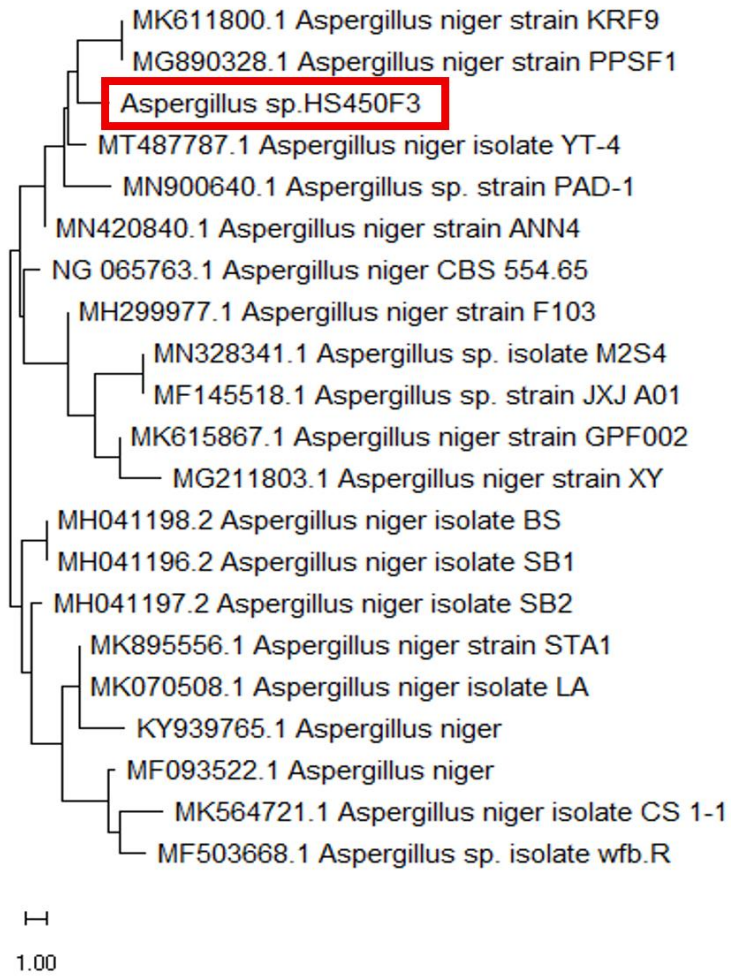

Figure 3.1.2.3. Constructed neighbour-joining phylogenetic tree based on almost complete 18 S rRNA gene sequences (1755 nt), showing the position of for *Aspergillus* sp. HS4(50)F3 (red box), amongst its phylogenetic neighbours.

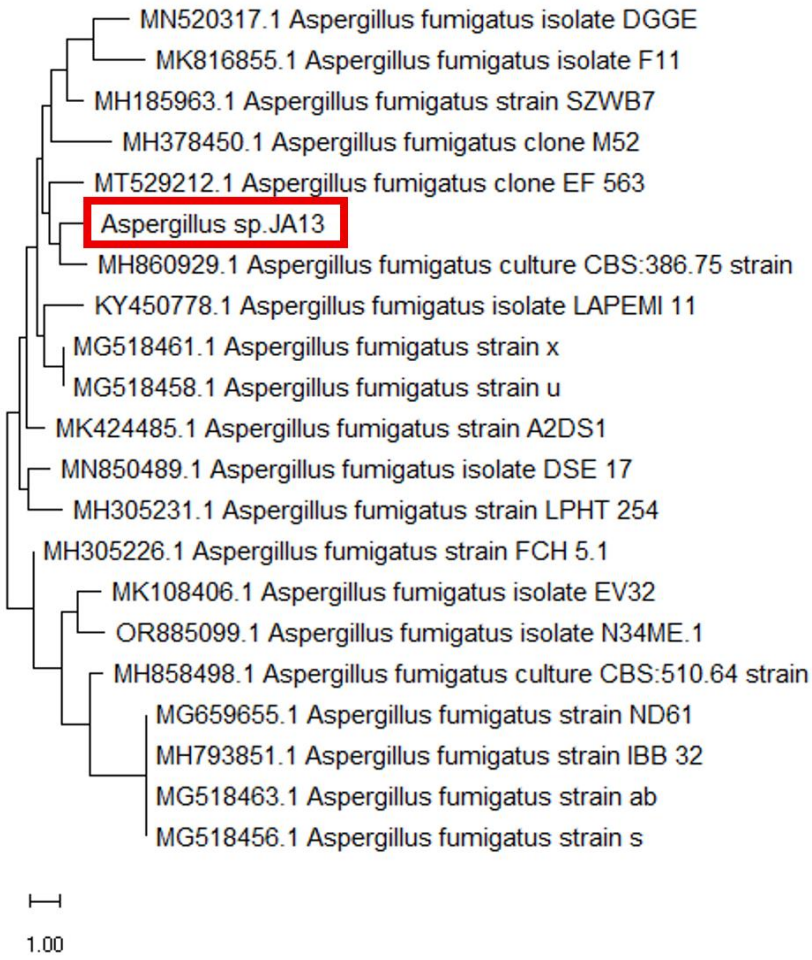

Figure 3.1.2.4. Constructed neighbour-joining phylogenetic tree based on almost complete 18 S rRNA gene sequences (1755 nt), showing the position of for *Aspergillus* sp. JA13 (red box), amongst its phylogenetic neighbours.

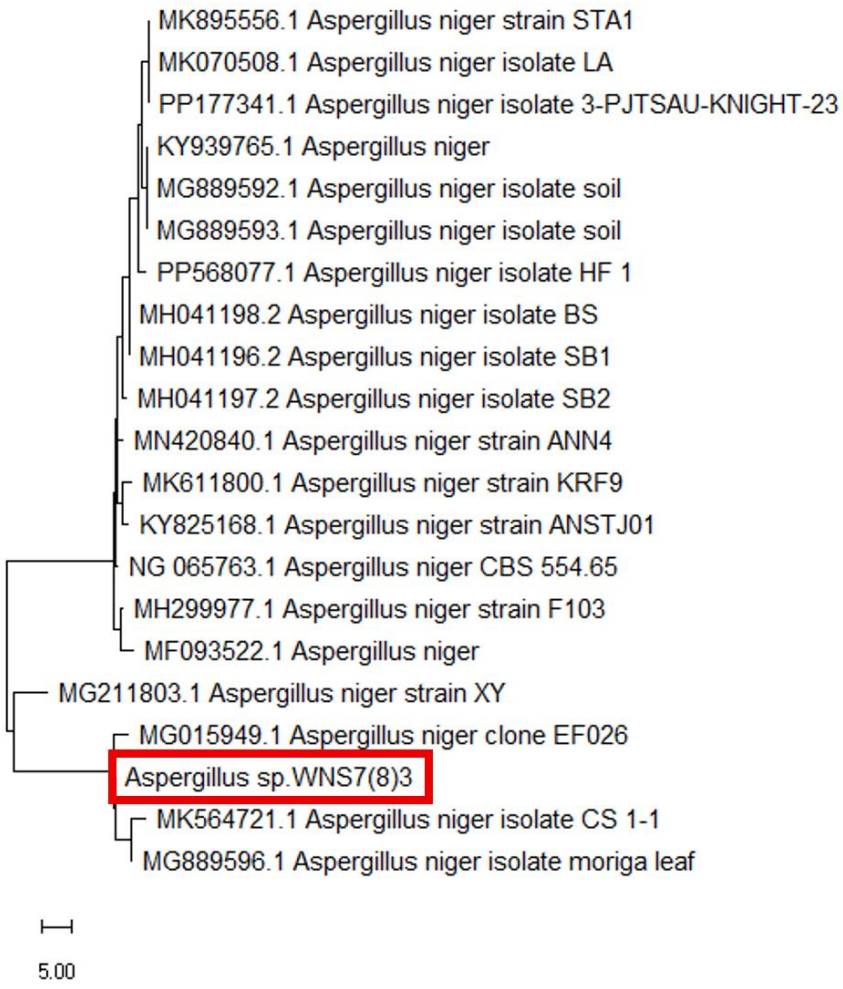

Figure 3.1.2.5. Constructed neighbour-joining phylogenetic tree based on almost complete 18 S rRNA gene sequences (1755 nt), showing the position of for *Aspergillus* sp. WNS7(8)F3 (red box), amongst its phylogenetic neighbours.

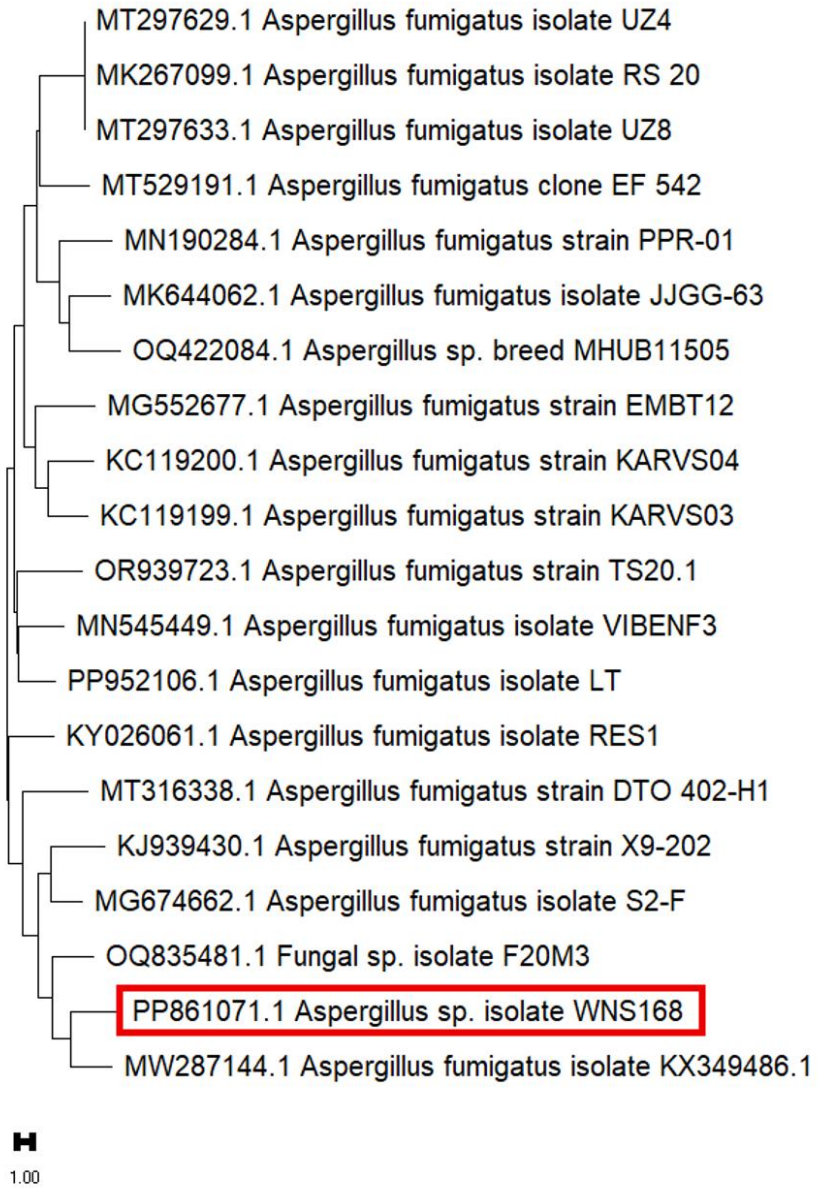

Figure 3.1.2.6. Constructed neighbour-joining phylogenetic tree based on almost complete 18 S rRNA gene sequences (1755 nt), showing the position of for *Aspergillus* sp. WNS16(8)F2 (red box), amongst its phylogenetic neighbours.

3.2 Biological screening of microbial small-scale extracts

3.2.1 Identification of most active strains from all collection sites

In this study 87 endophytic/marine-organism-derived microorganisms have been isolated from 33

plant and marine organism samples, collected from three different Egyptian ecosystems: Orman garden, Wadi El-Natrun salt lakes, and Hurghada coral reefs. The extracts of these microorganisms were screened against one acetylcholinesterase inhibitory, one biofilm and various antibacterial and antifungal bioassays.

The bioassay of crude extracts is essential in the prioritisation of pursuing extracts with a higher probability to yield novel, biologically active compounds. However, the biological evaluation of extracts for bioactivity faces reliability challenges due to false positives (e.g., nonspecific toxicity, assay interference) and false negatives (e.g., low abundance, masking effects). The chemical complexity of crude extracts can cause matrix effects, while concentration variability and compound instability further complicate results. Biological variability (strain differences, culture conditions) and assay-specific issues (e.g., nutrient carryover, cytotoxicity) add to the unpredictability. Mitigation strategies include orthogonal assays, prefractionation, and dereplication to prioritize true bioactive compounds for fractionation.

3.2.1.1 Antibiofilm activity of all microbial strains

Among the 87 microbial strains tested, 72% (63/87) exhibited antibiofilm activity with a percentage inhibition of at least 10%. Furthermore, 25% (22/87) demonstrated biofilm inhibition of 50% or greater, while 9% (8/87) achieved inhibition levels exceeding 80%. The biofilm-forming targets included *Bacillus subtilis*, *Pseudomonas aeruginosa*, *Staphylococcus aureus*, and *Escherichia coli*.

Staphylococcus aureus, *Listeria monocytogenes*, *Bacillus cereus*, and *Escherichia coli* are commonly selected for biofilm inhibition bioassays due to their clinical and industrial relevance as persistent biofilm-forming pathogens. *S. aureus* and *L. monocytogenes* are associated with hospital-acquired infections and foodborne illnesses, respectively, while *B. cereus* and *E. coli* are notorious for their biofilm-related resistance in medical and food-processing environments. These species represent both Gram-positive and Gram-negative bacteria, allowing for broad-spectrum evaluation of natural products' anti-biofilm efficacy. Their well-characterized biofilm mechanisms and standardised in vitro assays make them ideal models for identifying novel biofilm inhibitors with potential therapeutic or industrial applications.

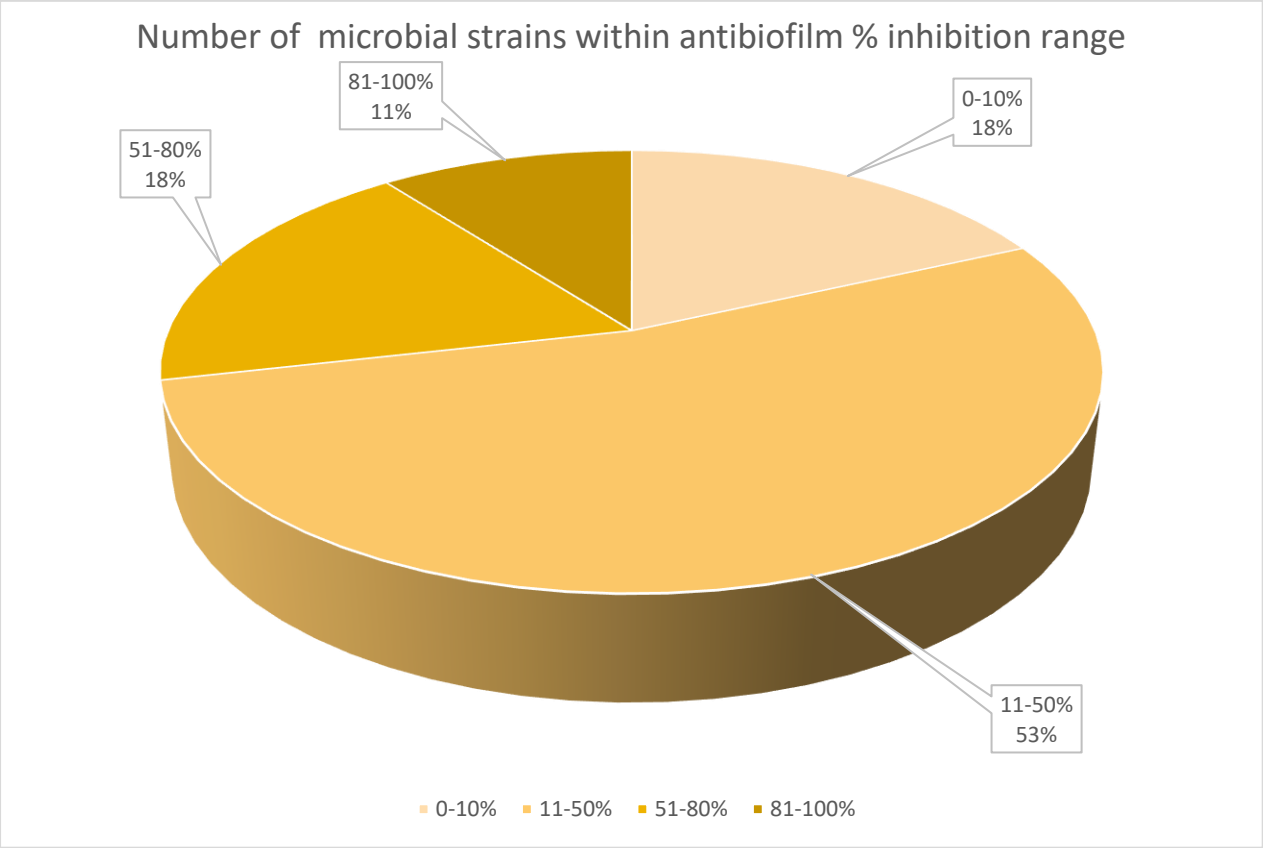

Figure 3.2.1.1.1. Biofilm % inhibition of all crude microbial extracts. % inhibition ranges include: 0 - 10 %, 11 - 50 %, 51 - 80 % and 81 - 100 %.

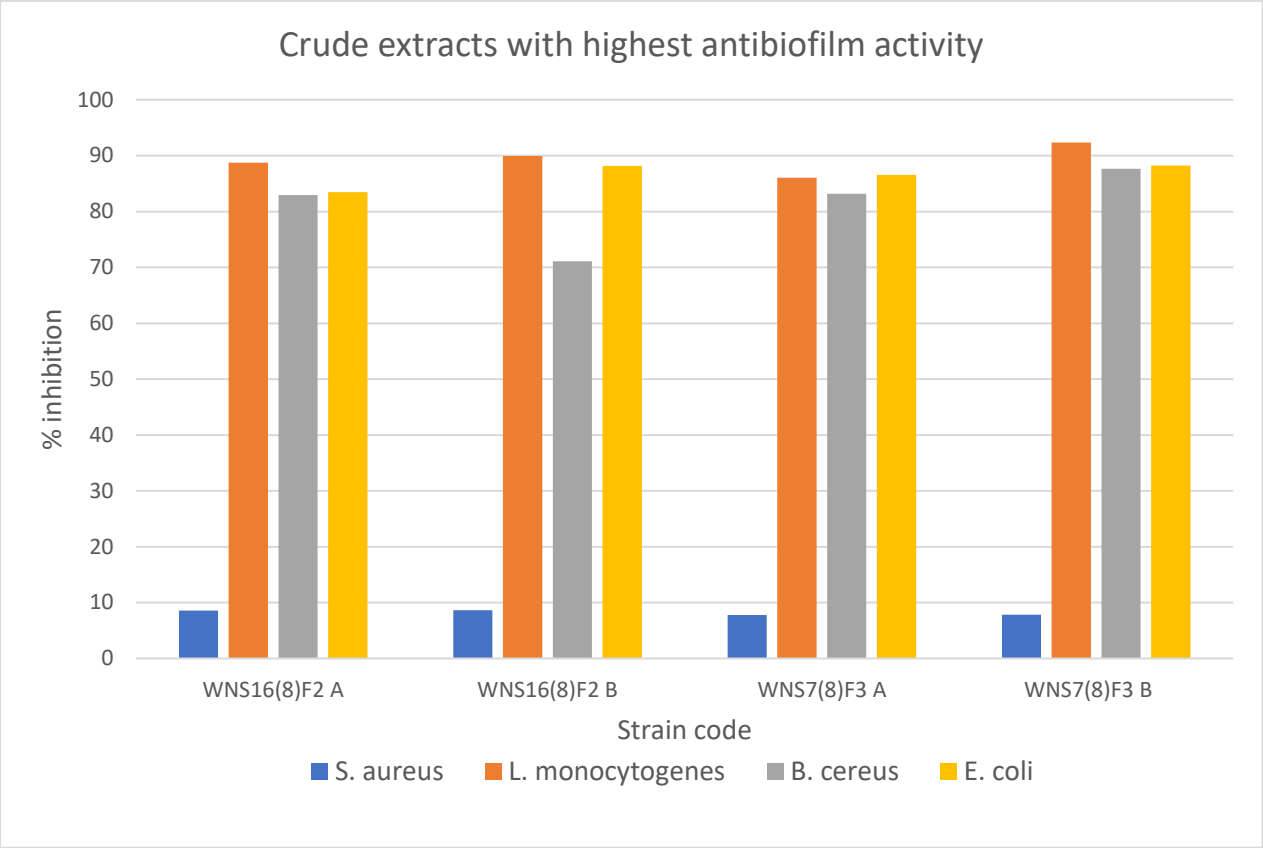

Figure 3.2.1.1.2. Bar chart of microbial strains with the highest antibiofilm activity against various pathogenic targets (WNS16(8)F2 and WNS7(8)F3), chosen for large-scale fermentation and bioassay guided isolation.

3.2.1.1 Antimicrobial activity of all microbial strains

Of the 75 microbial strains isolated from samples collected in Wadi Natrun and Hurghada (excluding Orman Garden samples, as their inhibition zones were measured in millimetres rather than percentage inhibition; data presented in the subsequent section), 97% (73/75) demonstrated antimicrobial activity with a percentage inhibition of at least 10%. Additionally, 55% (41/75) exhibited antimicrobial inhibition of 50% or greater, and 33% (25/75) showed inhibition levels exceeding 80%. The tested antimicrobial targets included *Staphylococcus aureus*, *Escherichia coli*, *Bacillus cereus*, *Listeria monocytogenes*, *Candida albicans*, *Aspergillus niger*, and *Aspergillus flavus* (see bar charts in the section below for further details).

Staphylococcus aureus, *Escherichia coli*, *Bacillus cereus*, *Listeria monocytogenes*, *Candida albicans*, *Aspergillus niger*, and *Aspergillus flavus* were selected for antimicrobial assays due to their broad clinical, industrial, and agricultural significance. *S. aureus* (Gram-positive) and *E. coli* (Gram-negative) are model pathogens for evaluating antibacterial activity, representing common drug-resistant strains. *B. cereus* and *L. monocytogenes* are foodborne pathogens with notable resistance profiles, while *C. albicans* serves as a key fungal pathogen for assessing antifungal properties. *A. niger* and *A. flavus* are included due to their role in spoilage, mycotoxin production, and opportunistic infections, allowing for comprehensive evaluation of natural products against both bacteria and fungi.

Their well-established susceptibility testing protocols and relevance in antimicrobial resistance studies make them ideal for screening bioactive compounds.

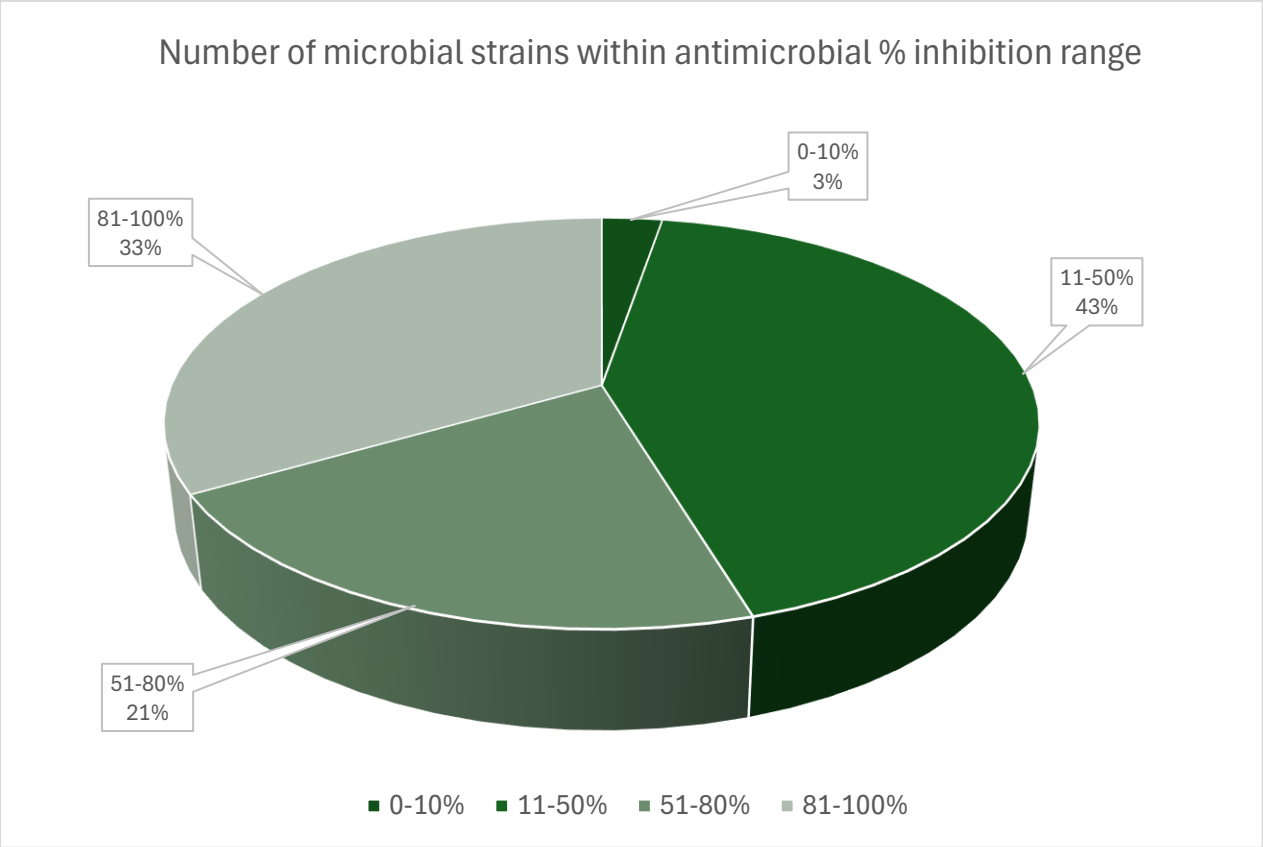

Figure. 3.3.1.1.1. Antimicrobial % inhibition of Wadi Natrun crude microbial extracts. % inhibition ranges include: 0 - 10 %, 11 - 50 %, 51 - 80 % and 81 - 100 %.

3.2.1.2 Acetylcholinesterase inhibition activity of all microbial strains

Of the 87 microbial strains tested, 93% (81/87) demonstrated acetylcholinesterase inhibition activity of at least 10%. Among these, 13% (11/87) exhibited inhibition activity of 50% or greater, while 3% (3/87) achieved inhibition levels exceeding 80%.

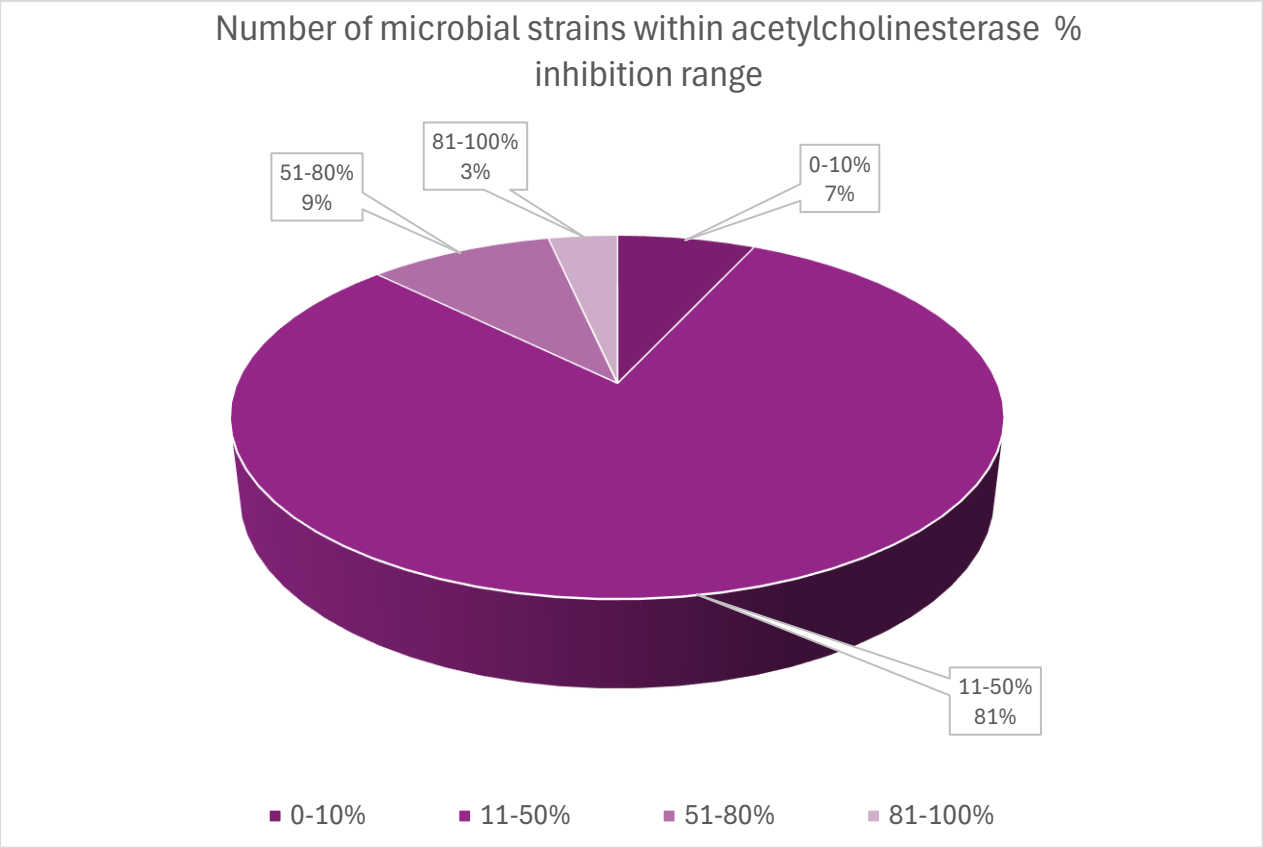

Figure 3.3.1.2.1. Acetylcholinesterase inhibition of all crude microbial extracts. % inhibition ranges include: 0 - 10 %, 11 - 50 %, 51 - 80 % and 81 - 100 %.

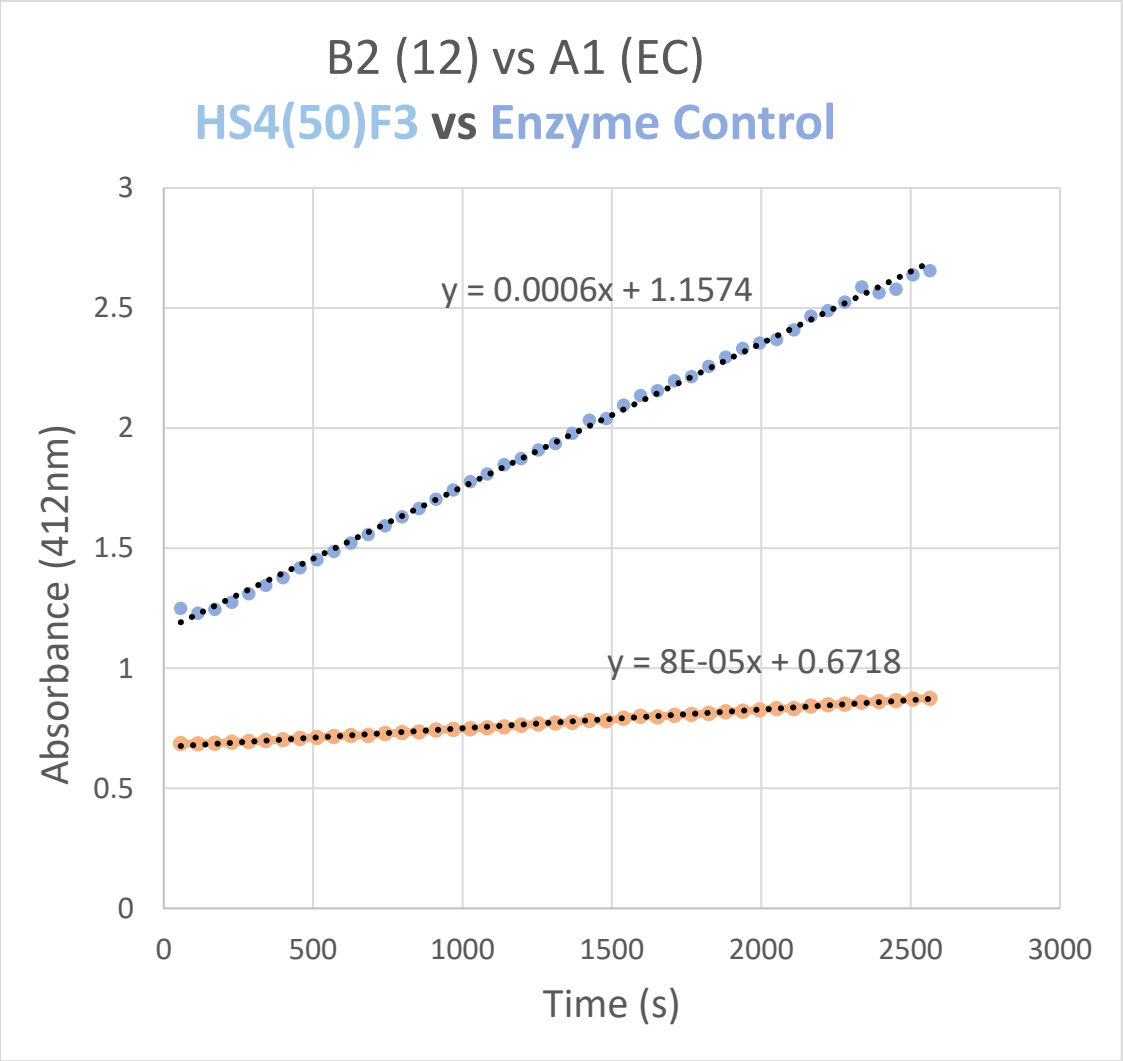

Figure 3.3.1.2.3. Graph of reaction time against UV absorbance at 412nm. Top line on graph is the reaction without an inhibitor present. Bottom line is the reaction with HS4(50)F3 present.

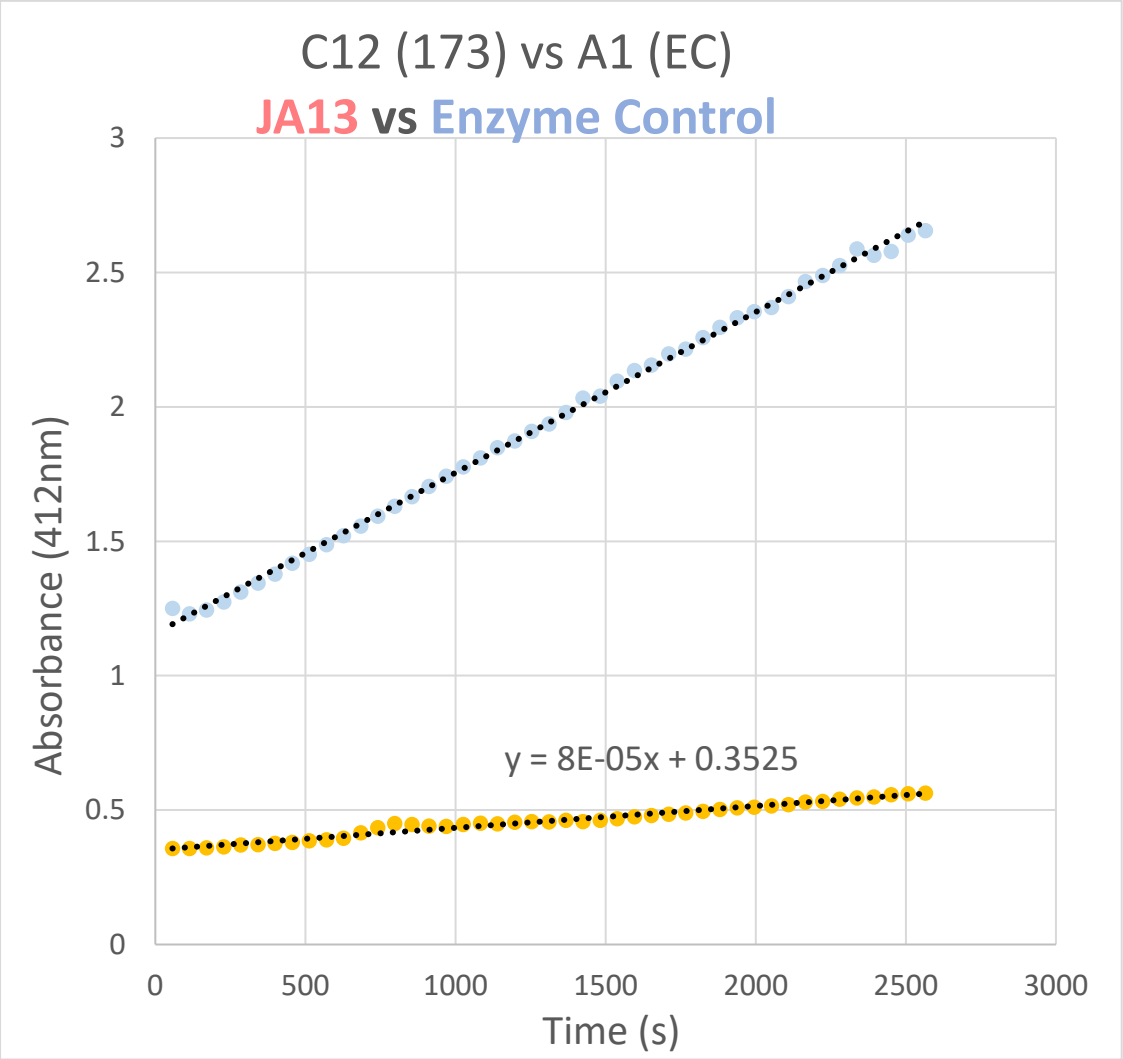

Figure 3.3.1.2.4. Graph of reaction time against UV absorbance at 412nm. Top line on graph is the reaction without an inhibitor present. Bottom line is the reaction with JA13 present.

The acetylcholinesterase inhibitory assay results for HS4(50)F3 (**Figure 3.3.1.2.3.**) and JA13 (**Figure 3.3.1.2.4.**) clearly demonstrate a decreased reaction rate, as illustrated by the bottom lines in comparison to the control (top lines). This reduction in reaction rate highlights the inhibitory activity of the tested samples. Calculation method for percentage inhibition explained in experimental.

3.2.2 Biological evaluation of Orman garden microbial strains

3.2.2.1 Antibiofilm activity of Orman garden microbial strains

From the 12 microbial strains isolated from samples collected in Orman Garden, all strains (100%, 12/12) demonstrated antibiofilm activity with inhibition percentages of at least 10%. Notably, 83% (10/12) of the strains exhibited biofilm inhibition of 50% or higher, and 25% (3/12) showed biofilm inhibition exceeding 80%. The biofilm-forming targets tested included *Bacillus subtilis*, *Pseudomonas*

aeruginosa, *Staphylococcus aureus*, and *Escherichia coli*. Positive control Ciprofloxacin.

The microbial strains with a biofilm percentage inhibition of 80 % ≤ include, JA1, JA2 and JA16.

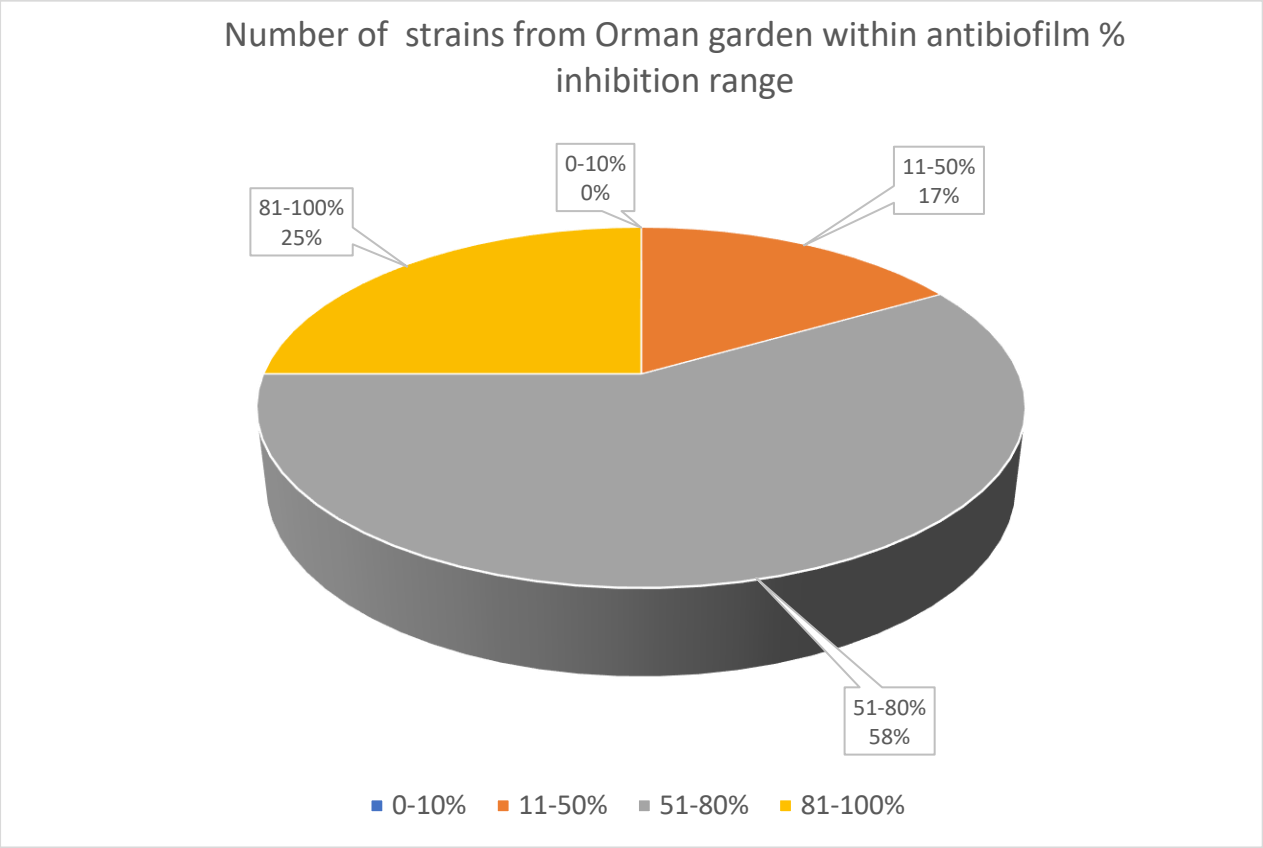

Figure. 3.2.2.1.1. Biofilm % inhibition of Orman garden crude microbial extracts. % inhibition ranges include: 0 - 10 %, 11 - 50 %, 51 - 80 % and 81 - 100 %.

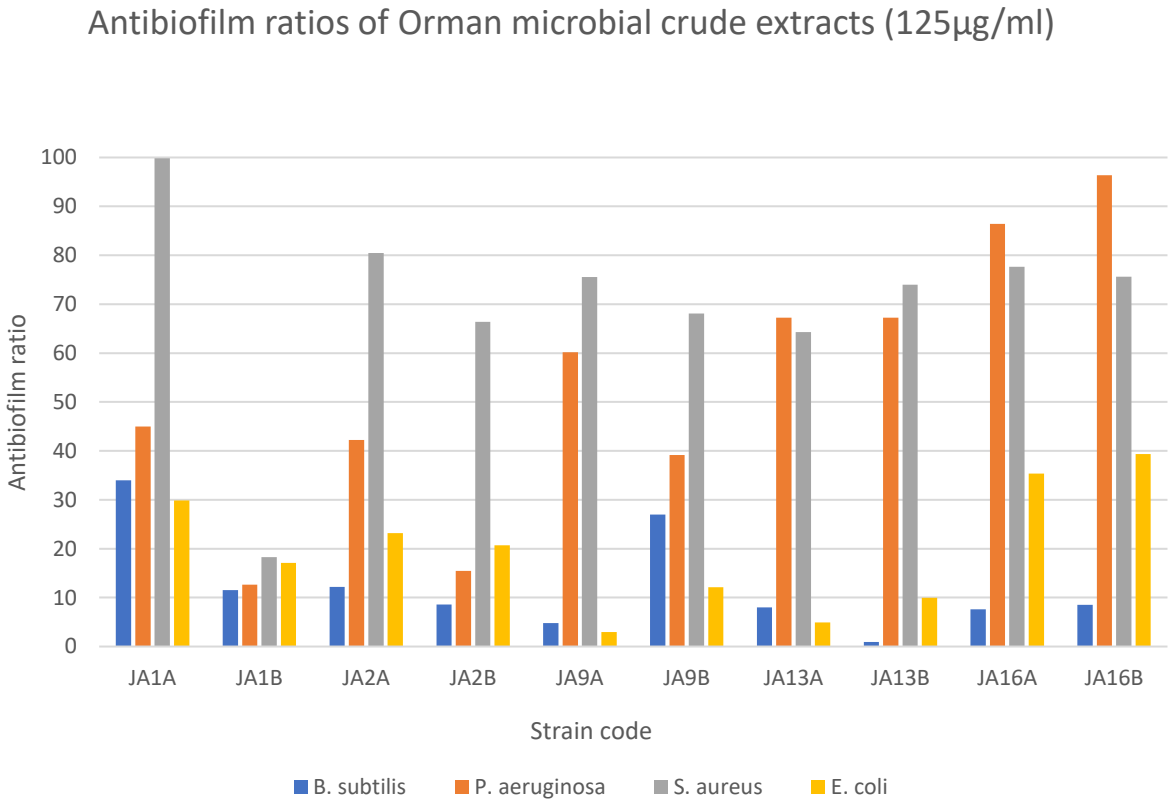

Figure 3.2.2.1.2. Bar chart of Orman garden microbial strains with the highest biofilm inhibitory activity against various pathogenic targets.

3.2.2.2 Antimicrobial activity of Orman garden samples

Of 12 microbial strains retrieved from samples taken from Orman Garden, 42% (5/12) showed antimicrobial activity with inhibition zones of ≥ 2.00 mm. Similarly, 42% (5/12) of the samples had inhibition zones of ≥ 6.00 mm and 33% (4/12) of the samples had inhibition zones of > 12.00 mm. The antimicrobial activity was tested against *Staphylococcus aureus*, *Escherichia coli*, *Bacillus cereus*, *Listeria monocytogenes*, *Candida albicans*, *Aspergillus niger* and *Aspergillus flavus*. The microbial strains with an antimicrobial inhibition zone of > 12.0 mm are JA3, JA7, JA13 and JA16. Positive controls Ciprofloxacin and Nystatin.

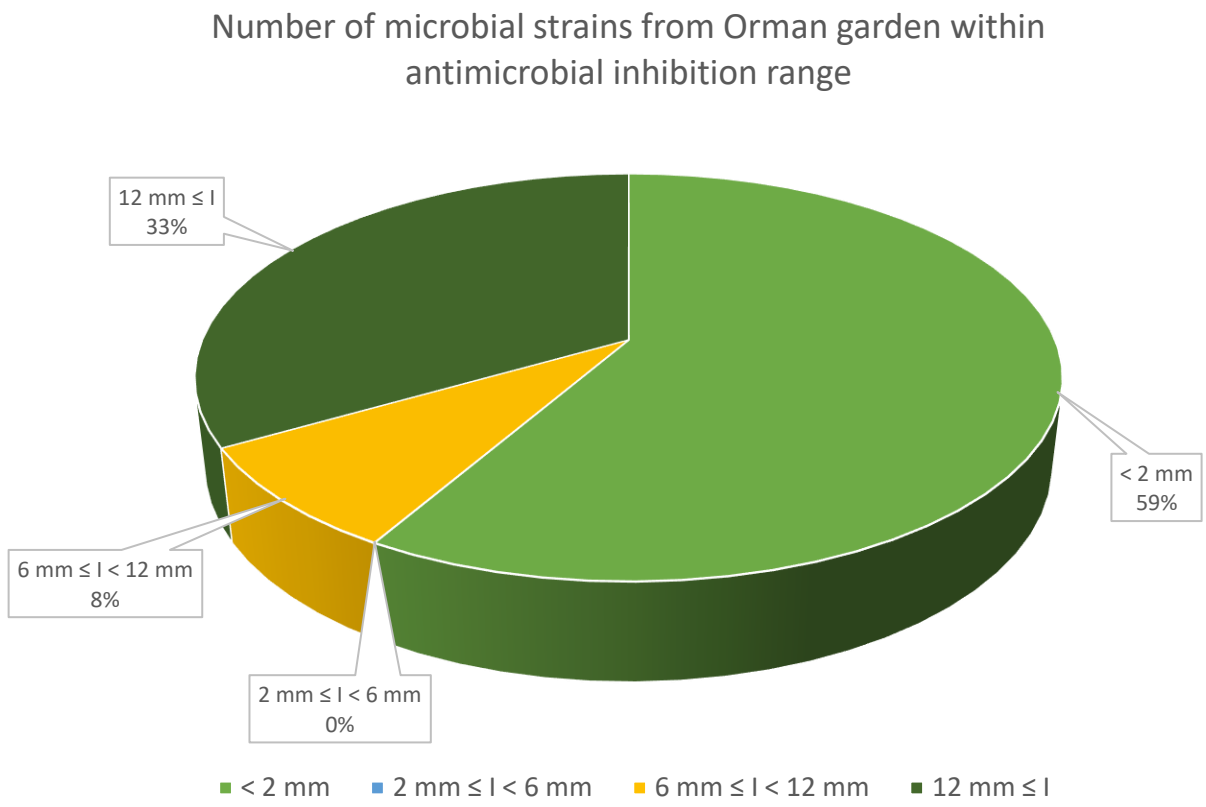

Figure 3.2.2.2.1. Antimicrobial inhibition of Orman garden crude microbial extracts. Inhibition ranges include: < 2.0 mm, 2.0 mm ≤ I < 6.0 mm, 6.0 mm ≤ I < 12.0 mm and 12.0 mm ≤ I (I = inhibition).

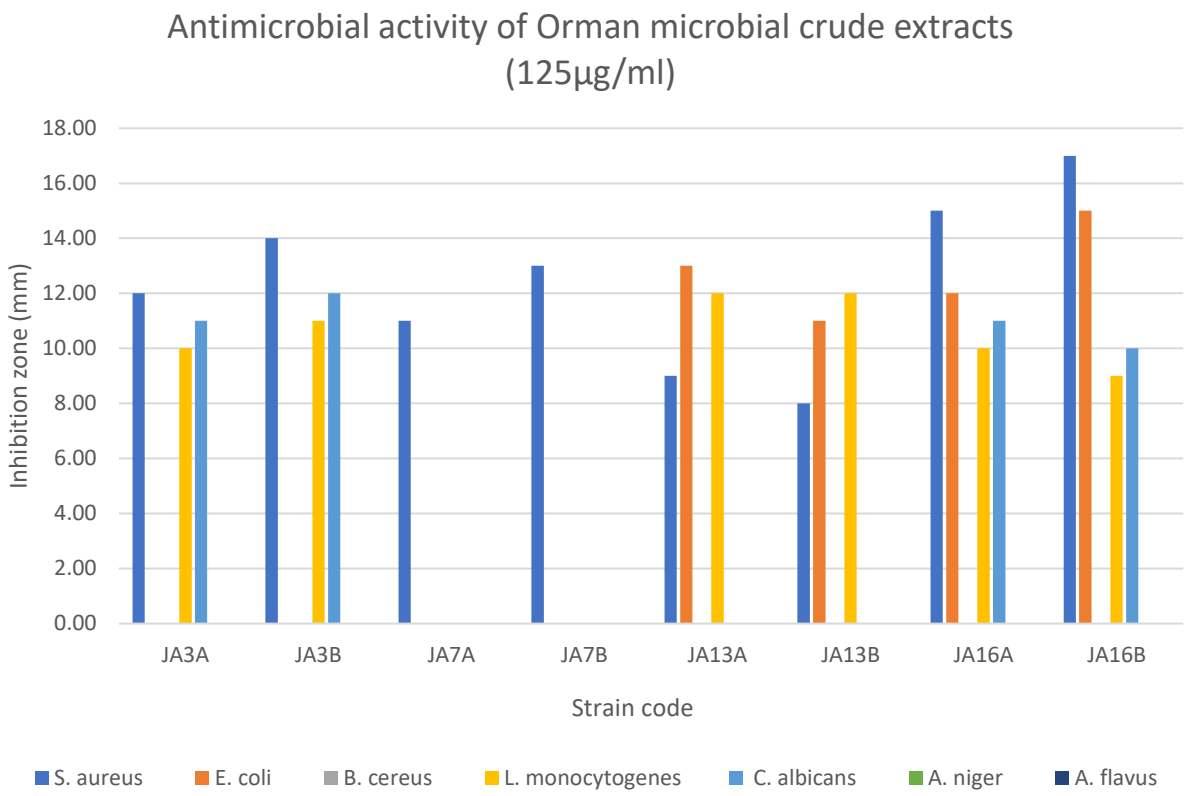

Figure 3.2.2.2.2. Bar chart of Orman garden microbial strains with the highest inhibition zone measurements against various pathogenic targets.

3.2.2.3 Acetylcholinesterase inhibition activity of Orman garden microbial strains

Among the 12 microbial strains isolated from samples collected in Orman Garden, 92% (11/12) exhibited acetylcholinesterase inhibition activity of at least 10%. Of these, 8% (1/12) demonstrated inhibition activity of 50% or greater, with the same strain achieving an inhibition activity exceeding 80%. The strain with acetylcholinesterase inhibition activity exceeding 80% was identified as JA13 (see Fig. G).

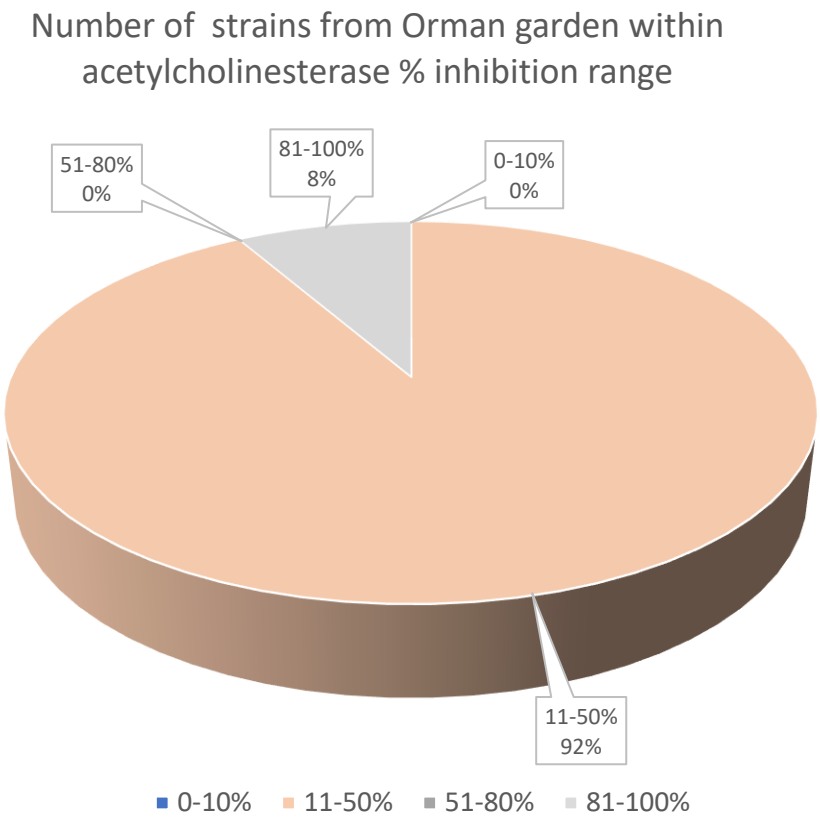

Figure 3.2.2.3.1. Acetylcholinesterase inhibition of Orman garden crude microbial extracts. % inhibition ranges include: 0 - 10 %, 11 - 50 %, 51 - 80 % and 81 - 100 %.

3.2.3 Biological evaluation of Wadi Natrun microbial strains

3.2.3.1 Antibiofilm activity of Wadi Natrun strains

Of the 46 microbial strains isolated from samples collected in Wadi Natrun, 59% (27/46) demonstrated biofilm inhibition activity of at least 10%. Among these, 22% (10/46) exhibited biofilm inhibition of 50% or greater, while 11% (5/46) achieved inhibition levels exceeding 80%. The biofilm-forming targets tested included *Bacillus subtilis*, *Pseudomonas aeruginosa*, *Staphylococcus aureus*, and *Escherichia coli*. The strains with biofilm inhibition activity exceeding 80% were identified as WNS6(5)F1, WNS7(8)F3, WNS11LF1.1, WNS12LF1.1, and WNS16(8)F2. Positive control Ciprofloxacin.

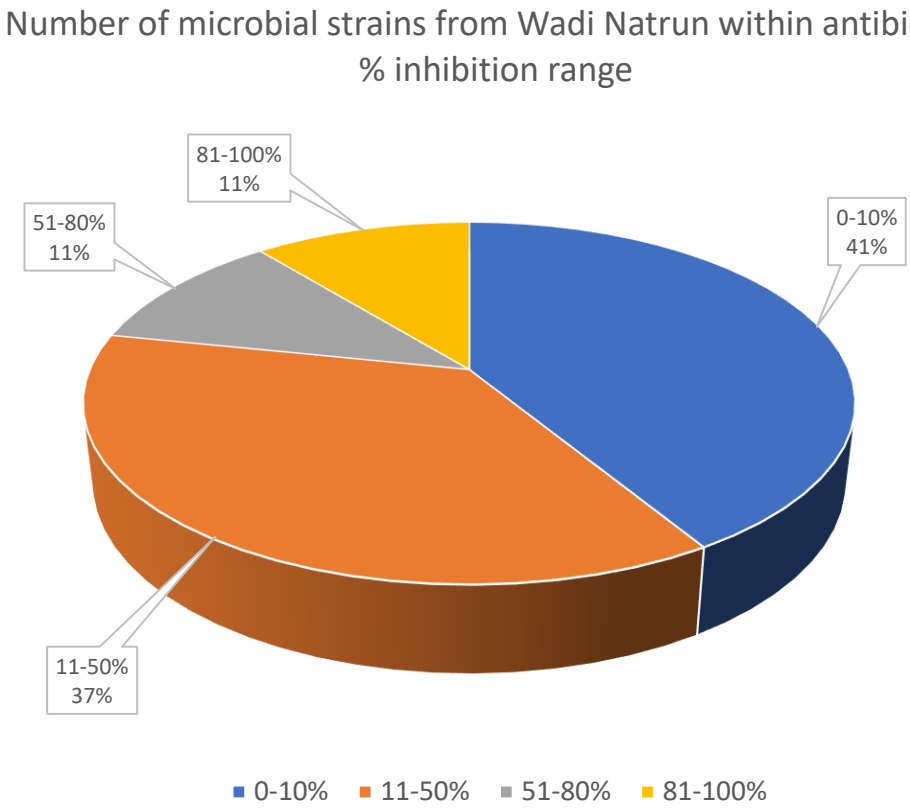

Figure 3.2.3.1.1. Biofilm % inhibition of Wadi Natrun crude microbial extracts. % inhibition ranges include: 0 – 10 %, 11 – 50 %, 51 – 80 % and 81 – 100 %.

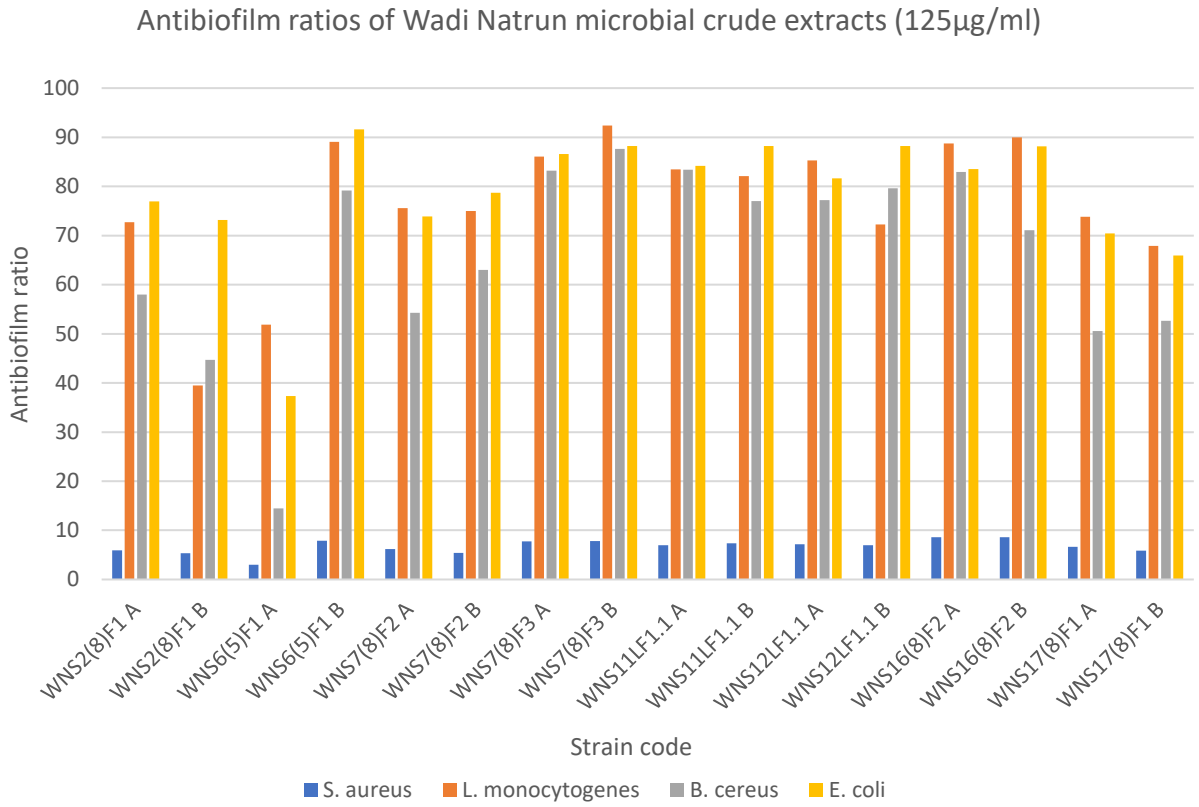

Figure 3.2.3.1.2. Bar chart of Wadi Natrun microbial strains with the highest antibiofilm activities against various pathogenic targets.

3.2.3.2 Antimicrobial activity of Wadi Natrun microbial strains

Among the 46 microbial strains isolated from samples collected in Wadi Natrun, 96% (44/46) exhibited antimicrobial activity with percentage inhibition of at least 10%. Of these, 70% (32/46) demonstrated inhibition levels of 50% or greater, while 52% (24/46) showed inhibition exceeding 80%. The antimicrobial targets tested included *Staphylococcus aureus*, *Escherichia coli*, *Bacillus cereus*, *Listeria monocytogenes*, *Candida albicans*, *Aspergillus niger*, and *Aspergillus flavus*. The strains with the highest antimicrobial percentage inhibition were identified as WNS3RB1.3, WNS3RB2.1, WNS5RB2.1, WNS8LB1.1, WNS8LB2.1, WNS8RB1.2, WNS8RB2.1, WNS10LB2.1, WNS10RB2.2, and WNS14LB1.2. Positive controls Ciprofloxacin and Nystatin.

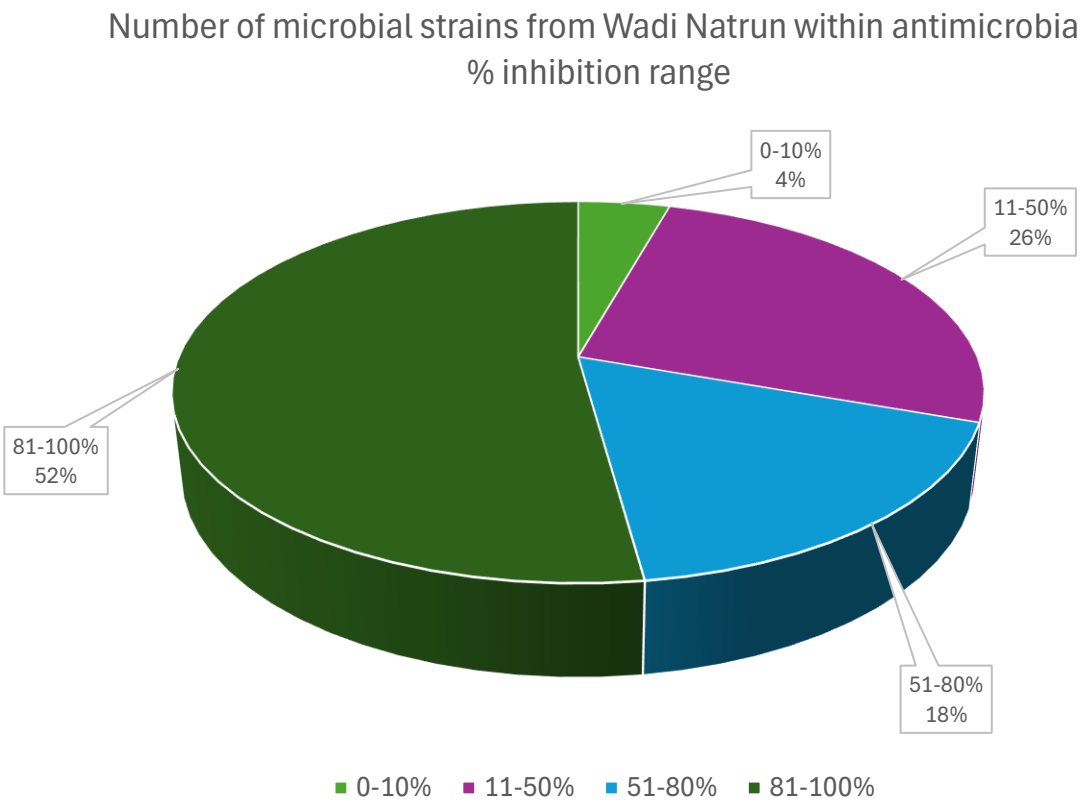

Figure 3.2.3.2.1. Antimicrobial % inhibition of Wadi Natrun crude microbial extracts. % inhibition ranges include: 0 - 10 %, 11 - 50 %, 51 - 80 % and 81 - 100 %.

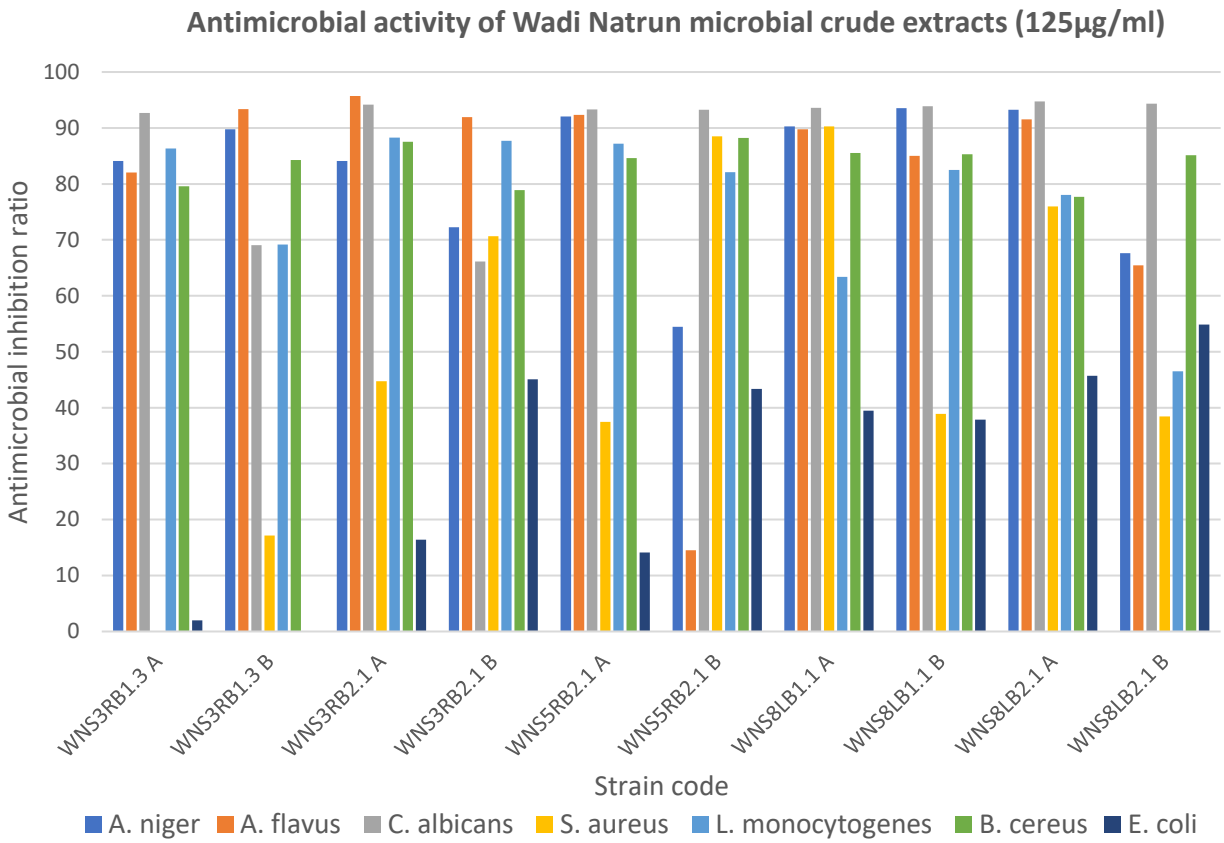

Figure 3.2.3.2.2. Bar chart of Wadi Natrun microbial strains with the highest antimicrobial activities against various pathogenic targets.

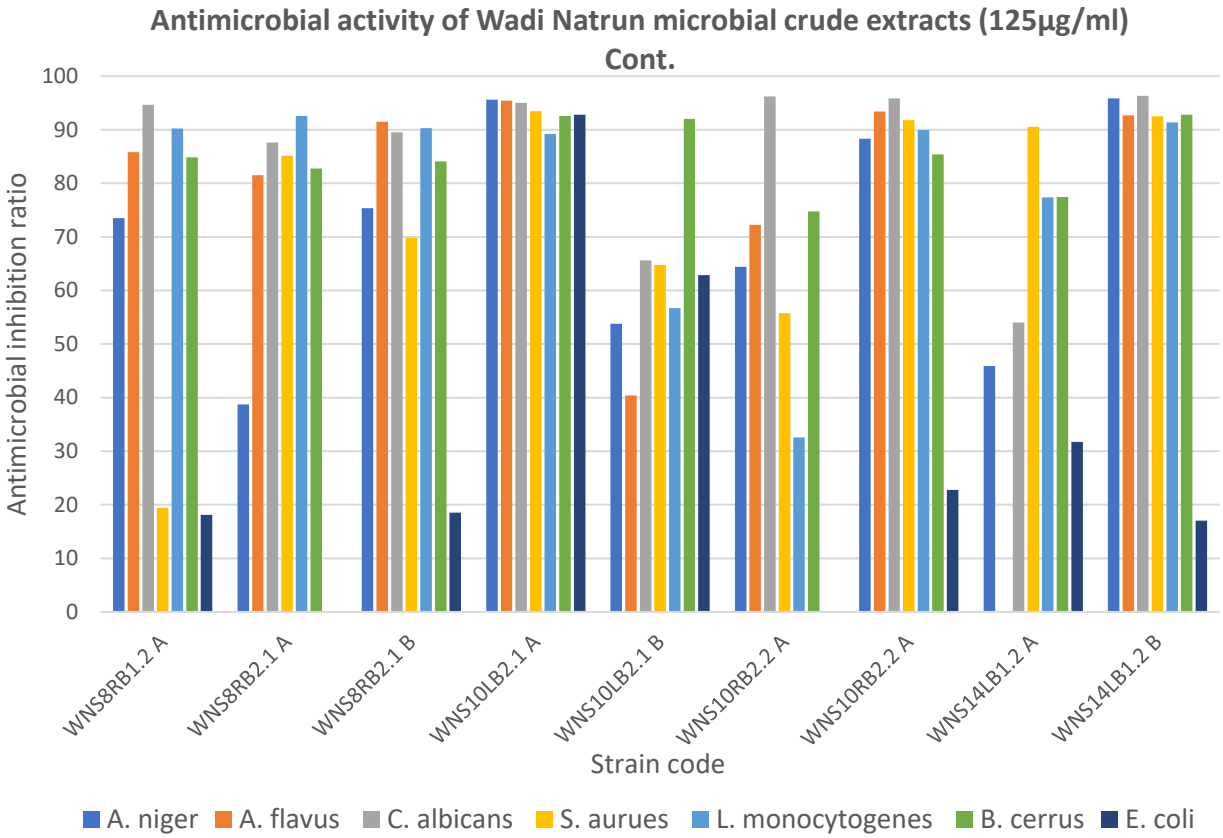

Figure 3.2.3.2.3. Continued bar chart of Wadi Natrun microbial strains with the highest antimicrobial activities against various pathogenic targets.

3.2.3.3 Acetylcholinesterase inhibition activity of Wadi Natrun microbial strains

Among the 46 microbial strains isolated from samples collected in Wadi Natrun, 98% (45/46) exhibited acetylcholinesterase inhibition activity of at least 10%. Of these, 7% (3/46) demonstrated inhibition activity of 50% or greater, while none (0/46) achieved inhibition levels exceeding 80%.

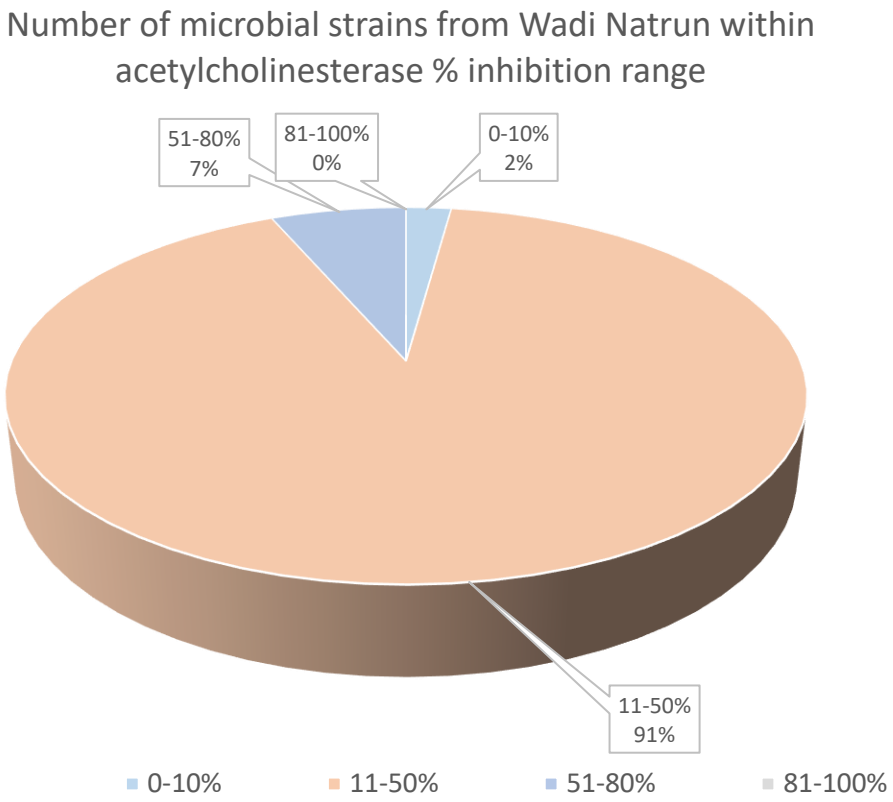

Figure 3.2.3.3.1. Acetylcholinesterase inhibition of Wadi Natrun crude microbial extracts. % inhibition ranges include: 0 - 10 %, 11 - 50 %, 51 - 80 % and 81 - 100 %.

3.2.4 Biological evaluation of Hurghada microbial strains

3.2.4.1 Antibiofilm activity of Hurghada microbial strains

Among the 29 microbial strains isolated from samples collected in Hurghada, 83% (24/29) exhibited antimicrobial activity with a percentage inhibition of at least 10%. However, antibiofilm inhibition was generally lower compared to the Wadi Natrun strains, with none of the strains (0/29) demonstrating antibiofilm activity exceeding 80%. The biofilm-forming targets tested included *Bacillus subtilis*, *Pseudomonas aeruginosa*, *Staphylococcus aureus*, and *Escherichia coli*. Positive control Ciprofloxacin.

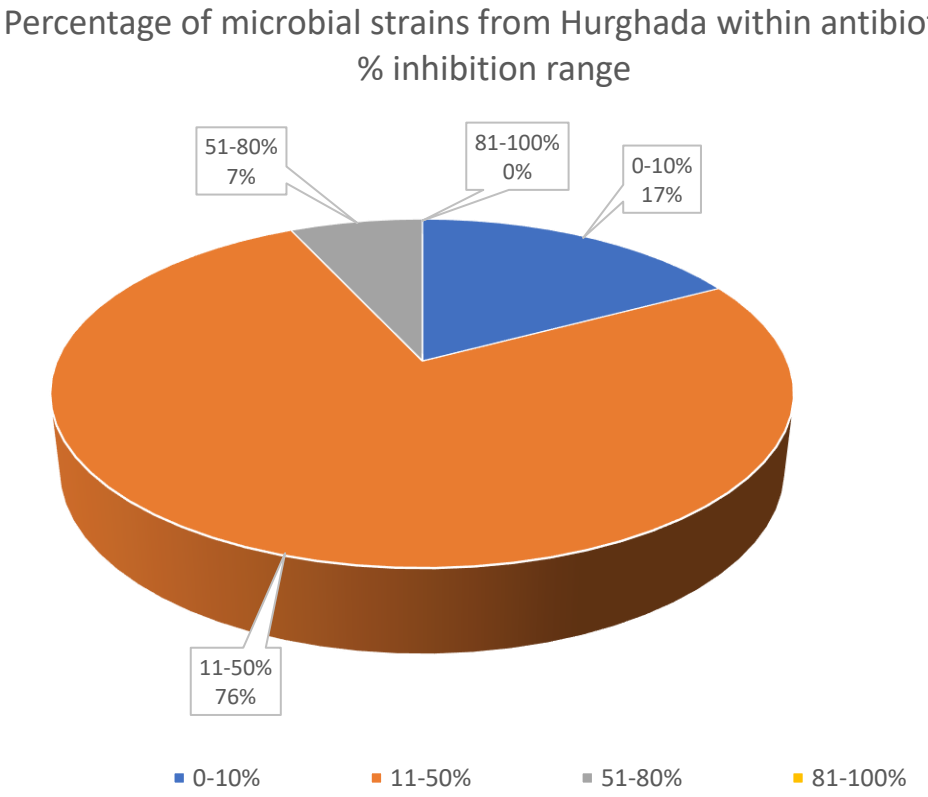

Figure 3.2.4.1.1. Biofilm % inhibition of Hurghada crude microbial extracts. % inhibition ranges include: 0 - 10 %, 11 - 50 %, 51 - 80 % and 81 - 100 %.

3.2.4.2 Antimicrobial activity of Hurghada microbial strains

Among the 29 microbial strains isolated from samples collected in Hurghada, 100% (29/29) exhibited antimicrobial activity with a percentage inhibition of at least 10%. Of these, 31% (9/29) showed antimicrobial inhibition of 50% or greater, and 3% (1/29) demonstrated inhibition exceeding 80%. The antimicrobial targets tested included *Staphylococcus aureus*, *Escherichia coli*, *Bacillus cereus*, *Listeria monocytogenes*, *Candida albicans*, *Aspergillus niger*, and *Aspergillus flavus*. The strain with antimicrobial inhibition exceeding 80% was identified as HS13(50)B3. Positive controls Ciprofloxacin and Nystatin.

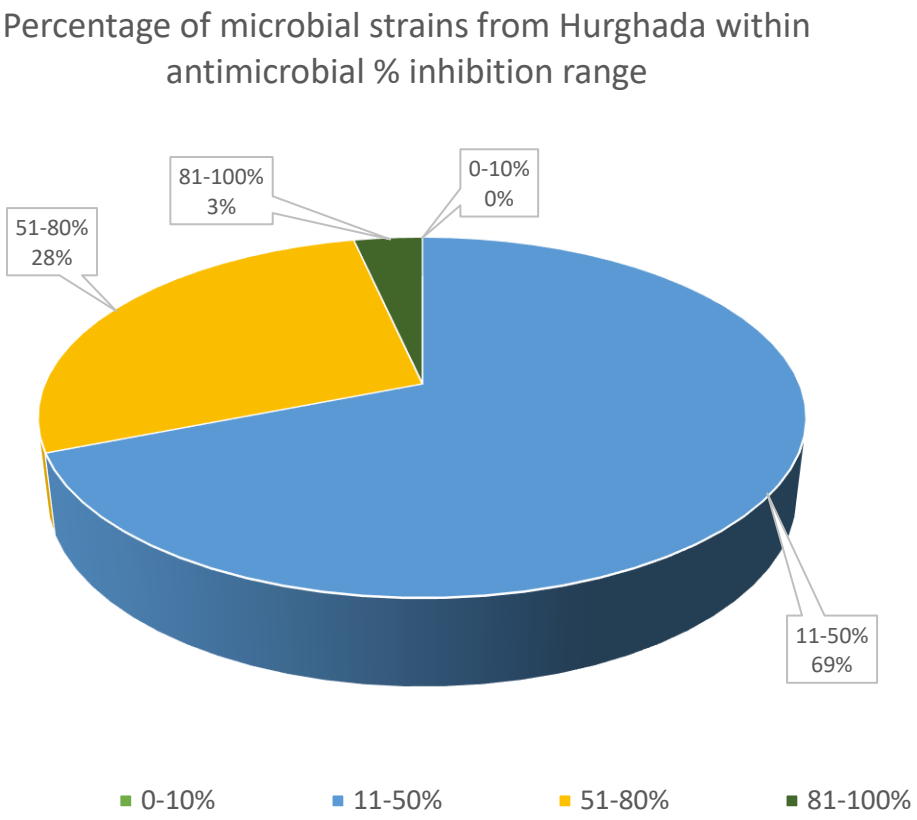

Figure 3.2.4.2.1. Antimicrobial % inhibition of Hughada crude microbial extracts. % inhibition ranges include: 0 - 10 %, 11 - 50 %, 51 - 80 % and 81 - 100 %.

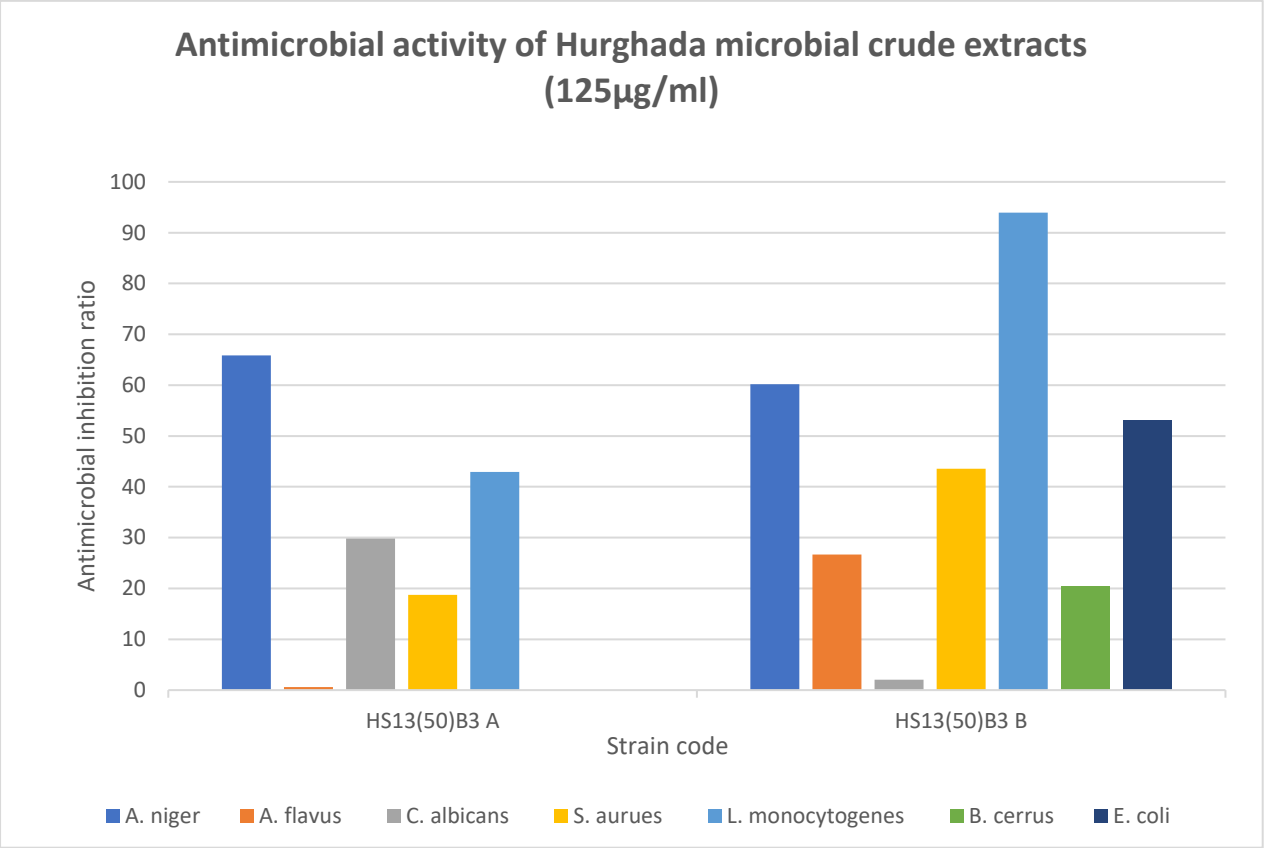

Figure 3.2.4.2.2. Bar chart of Hurghada microbial strain with the highest antimicrobial activities against various pathogenic targets.

3.2.4.3 Acetylcholinesterase inhibition activity of Hurghada microbial strains

Among the 29 microbial strains isolated from samples collected in Hurghada, 83% (24/29) exhibited acetylcholinesterase inhibition activity of at least 10%. Additionally, 24% (7/29) showed inhibition activity of 50% or greater, and 4% (2/46) demonstrated inhibition levels exceeding 80%. The strains with acetylcholinesterase inhibition activity above 80% were identified as HS4(50)F1 and HS4(50)F3.

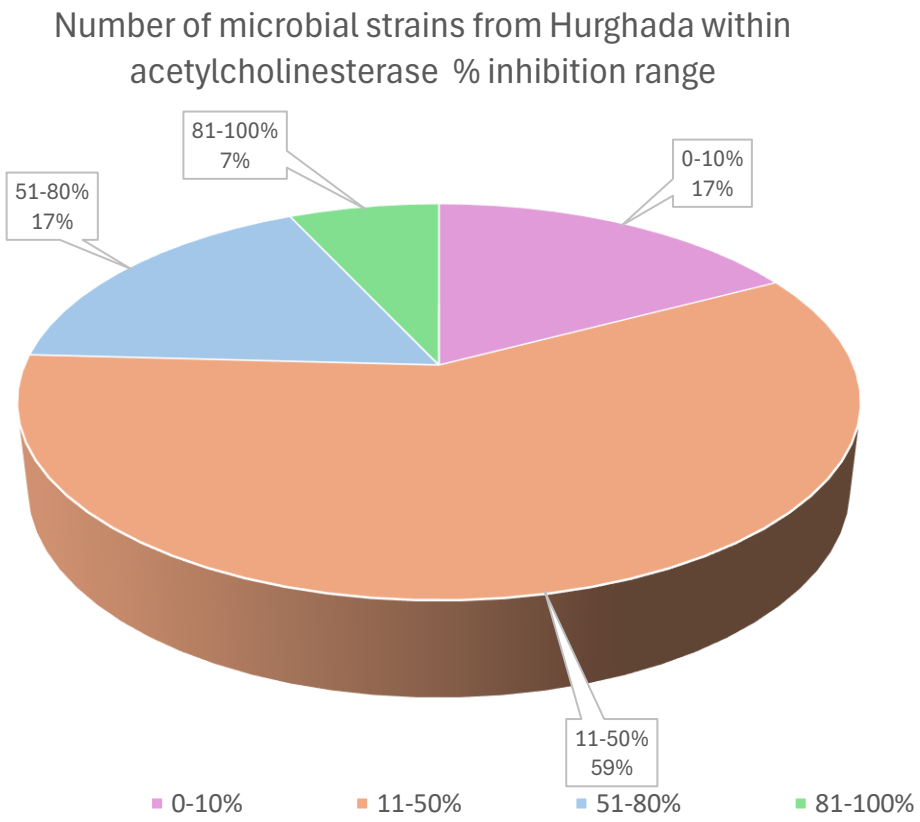

Figure 3.2.4.3.1. Acetylcholinesterase inhibition of Hurghada crude microbial extracts. % inhibition ranges include: 0 - 10 %, 11 - 50 %, 51 - 80 % and 81 - 100 %.

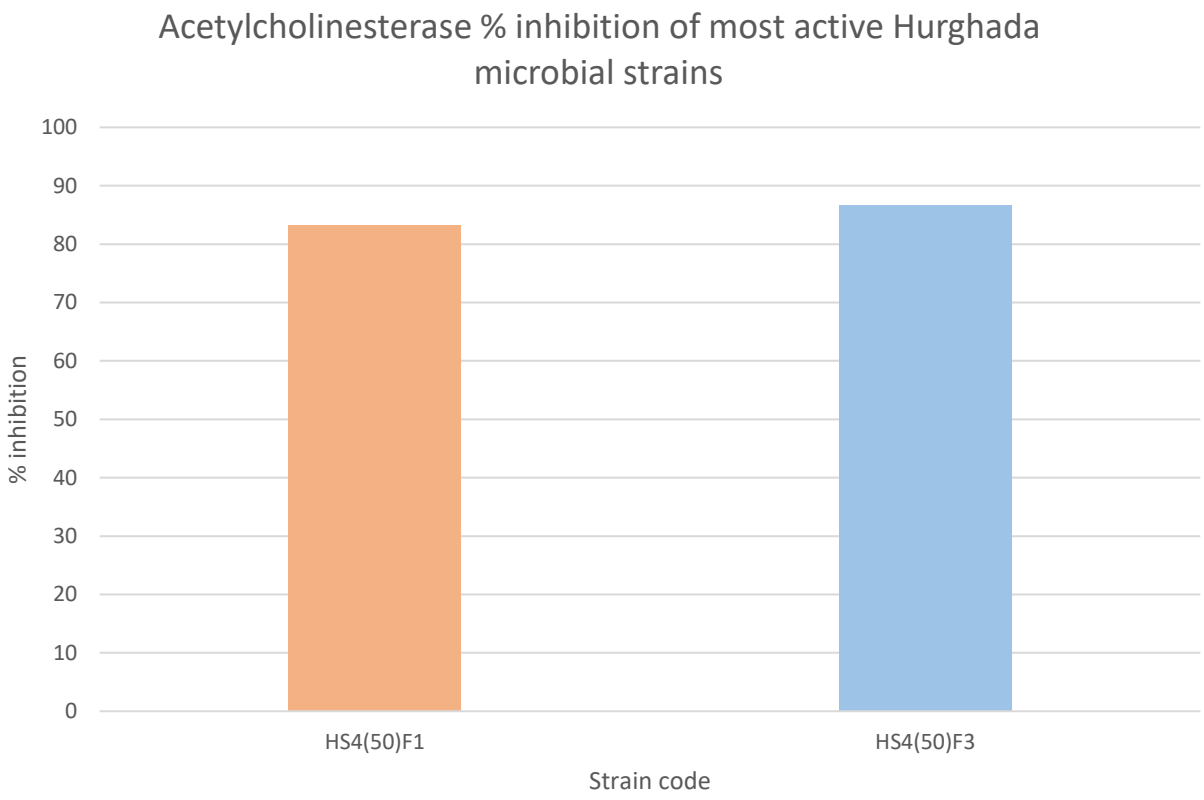

Figure 3.2.4.3.2. Bar chart of Hurghada microbial strains with the highest acetylcholinesterase inhibition activities.

3.3 Identified bioactive microbial strains

3.3.1 *Aspergillus niger*

Aspergillus niger is a filamentous fungus with significant industrial and pharmaceutical importance. This microorganism is found to inhabit a variety of habitats, from soil to decaying vegetation, to being an endophyte. It is used in industry for its extensive enzymatic capability, in the production of enzymes such as amylases, proteases, and lipases, within the food, beverage and textile industries. Within pharmaceuticals, *A. niger* is well known for producing a variety of biologically active secondary metabolites. Research is ongoing into the pharmaceutical potential of *A. niger*, particularly in the field of tackling drug-resistant pathogens, with its prolific production of enzymes and secondary metabolites, making *A. niger* a valuable organism in the search for novel biologically active compounds and potential future therapeutic agents.[93]

A significant number of natural products derived from *A. niger* have demonstrated complex structural diversity, encompassing polyketides, non-ribosomal peptides, terpenoids and alkaloids. These secondary metabolites have shown potent biological activities, including antioxidant, anticancer, antibacterial and antifungal properties. Among the antibacterial compounds, aspergillomarasmin[94] and nigerone[9] have been identified as active against multi-drug-resistant bacteria, such as *Staphylococcus aureus* and *Escherichia coli*. Additionally, *A. niger* produces several antifungal

metabolites, including nigericin[96], which exhibit strong activity against common fungal pathogens like *Candida albicans* and *Aspergillus fumigatus*. Metabolites such as fumonisin B2 have shown antifungal and cytotoxic properties, with fumonisin derivatives currently being explored as anticancer agents.[97] Naphto-γ-pyrones such as aurasperones and asperpyrones (**Figure. 3.3.1.1**) exhibit powerful antioxidant effects and are currently being investigated for their neuroprotective potential.[98] Recent studies have further characterized *A. niger's* secondary metabolites, including ochratoxin A, a nephrotoxic mycotoxin that represents one of its most concerning toxic products.[99] The fungus also produces pyranonigrin A, a terpenoid with notable antioxidant activity, and malformins, cytotoxic peptides that disrupt cellular membranes.[100] These findings complement the known bioactive compounds from A. niger and highlight the need for careful evaluation of both beneficial and toxic metabolites in pharmaceutical applications.[99] These findings highlight the potential of *A. niger* as a valuable source of bioactive secondary metabolites. Continued investigation into their biosynthesis, biological activity, and therapeutic potential may lead to the development of novel drugs to combat global health challenges.

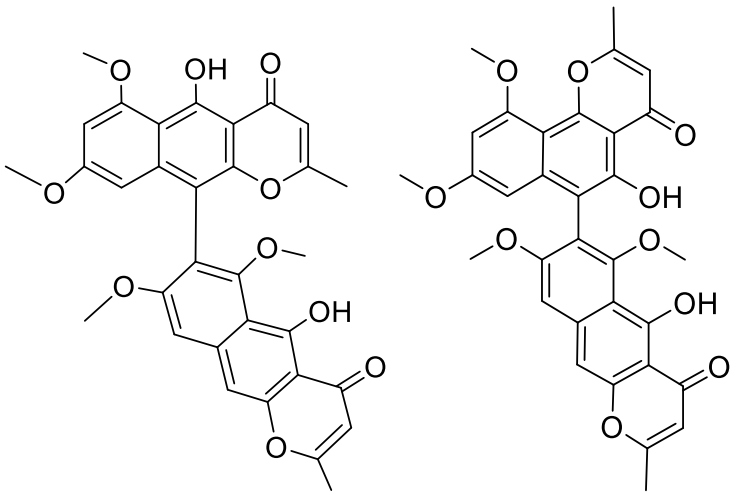

Figure 3.3.1.1. Aurasperone A (left) and Asperpyrone C (right), antioxidants isolated from *Aspergillus niger* strains.

3.3.2 *Aspergillus fumigatus*

Aspergillus fumigatus is a filamentous fungus, commonly located in various habitats, such as soil, decaying organic material, compost and an array of other environments. It is best known for its pathogenic role in invasive aspergillosis in immunocompromised individuals. *A. fumigatus* is thermotolerant, injunction with other adaptive traits for extreme environments, including resilience to oxidative stress, desiccation, and nutrient limitation. This ability to survive, and even thrive, in extreme environmental conditions have provided *A. fumigatus* with a complex secondary metabolome, with a high potential for the discovery of novel, and highly biologically active natural products.[101]

A. fumigatus is well known to produce a variety of natural products high in chemical diversity and potentially high biological activity against various disease targets, including antifungal, antibacterial, anticancer and immunosuppressive targets. It produces polyketides, indole alkaloids, quinazoline alkaloids, pyridine alkaloids and terpenoids. Examples of bioactive secondary metabolites isolated from A. fumigatus include gliotoxin, a well-studied toxin with powerful immunosuppressive and apoptotic effects, while this potent toxicity limits the direct use of gliotoxin in a therapeutic manner,

the mechanism of action provides the understanding required to design novel immunomodulatory agents.[102] Fumitremorgins are indole alkaloids that exhibit strong antitumour activity by inhibiting the breast cancer resistance protein (BCRP), which can reverse drug resistance in cancer therapy.[103] Fumiquinazolines A-F (**Figure. 3.3.2.1**) are alkaloids that have shown to exhibit a range of biological activities, including antifungal and antibacterial activities, and demonstrate cytotoxicity against cancer cell lines.[104] Helvolic acid (**Figure. 3.3.2.1**) is a terpenoid with particularly strong activity against Gram-positive bacteria, with studies ongoing to explore the mechanism of action and its therapeutic potential.[105] Aspyridones (A and B) show antifungal and cytotoxic properties, with high potential for the targeting of fungal infections and specific cancer types.[106] While A. fumigatus has been extensively studied for these compounds, it's worth noting that other Aspergillus species like *A. flavus* produce equally significant metabolites. *A. flavus* is particularly notorious for producing aflatoxins (B_1, B_2, G_1, G_2), some of the most carcinogenic natural compounds known, which contaminate food crops and pose serious health risks.[99] However, A. flavus also produces potentially useful compounds like cyclopiazonic acid (a neurotoxin with possible pharmacological applications) and flavoglaucin, an antioxidant diketopiperazine.[107] The fungus additionally generates aflavinines with insecticidal properties and aspterric acid, a herbicidal meroterpenoid.[100] These findings underscore the immense potential of *Aspergillus fumigatus* as a prolific producer of bioactive secondary metabolites. Ongoing research into the biosynthetic pathways, mechanisms of action, and therapeutic applications of these compounds could pave the way for the development of innovative drugs to address critical global health challenges, including antimicrobial resistance, cancer, and parasitic diseases.

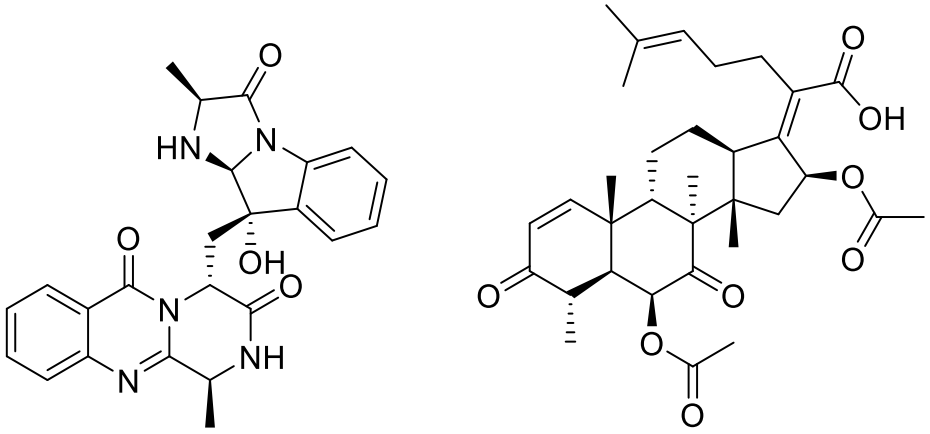

Figure 3.3.2.1. Fumiquinazolines A (left) and Helovic acid (right), isolated from *Aspergillus fumigatus* strains

3.3.3 *Aspergillus terreus*

Aspergillus terreus, a filamentous fungus belonging to the genus Aspergillus, is widely recognized in the field of natural product chemistry for its remarkable biosynthetic potential. This species has emerged as a prolific producer of diverse secondary metabolites, including polyketides, non-ribosomal peptides, and terpenoids, which display a broad spectrum of biological activities. Its metabolic versatility and capacity to generate structurally unique and biologically active compounds make it a valuable organism for biotechnological and pharmaceutical research.[108]

Research on *A. terreus* has uncovered a diverse portfolio of bioactive secondary metabolites. The most

renowned of these is lovastatin (**Figure 3.3.3.1**), a polyketide that inhibits 3-hydroxy-3-methylglutaryl-CoA (HMG-CoA) reductase, a crucial enzyme in cholesterol biosynthesis. Lovastatin was the first statin to be approved for clinical use, revolutionizing the treatment of hypercholesterolemia and the prevention of cardiovascular diseases. Beyond lovastatin, A. terreus produces other significant compounds such as terrein, a molecule with potent antioxidant properties and promising anticancer activity[109], terreic acid, which exhibits robust antimicrobial effects[110], and butyrolactones, a class of metabolites demonstrating antiproliferative activity against cancer cells.[108] These compounds collectively highlight the structural diversity and biological relevance of A. terreus-derived natural products. Recent investigations have expanded our understanding of A. terreus's chemical repertoire to include territrems, tremorgenic neurotoxins that affect mammalian nervous systems, highlighting the need for careful screening of its metabolites.[107] The fungus also produces asterriquinones, which show anticancer activity through kinase inhibition, and additional butyrolactones (**Figure 3.3.3.1**) with anti-inflammatory properties.[100] These discoveries, combined with the known pharmaceutical applications of lovastatin and terrein, demonstrate the dual nature of A. terreus metabolites - containing both valuable therapeutic agents and potentially harmful compounds.[99]

The ongoing exploration of the A. terreus metabolome is yielding new insights into its chemical diversity, providing valuable scaffolds for drug discovery and development. Advances in genomics and metabolic engineering are enhancing our ability to identify and activate silent biosynthetic gene clusters, further expanding the chemical space accessible through A. terreus. This not only facilitates the discovery of novel bioactive compounds but also enables the design and synthesis of analogues with optimized efficacy, safety, and pharmacokinetic profiles. Thus, A. terreus continues to play a pivotal role in advancing natural product-based therapeutics.

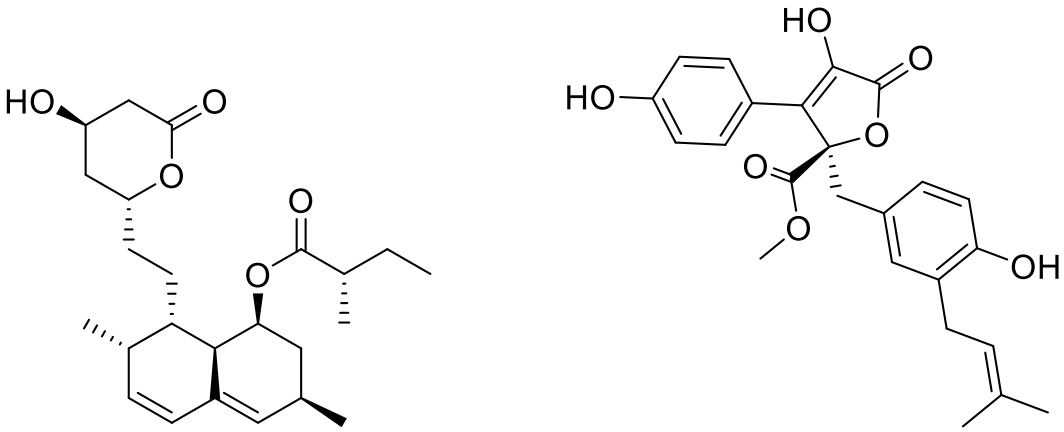

Figure 3.3.3.1. lovastatin (left) and Butyrolactone i (right), isolated from *Aspergillus terrus* strains.

3.4 Conclusion

This chapter describes the successful isolation and biological screening of microbial strains from various Egyptian ecosystems based on a combination of morphological and genotypic approaches for the identification of the strains. High resolution of the taxonomy of the isolated strains was obtained through genotypic identification using 18S rRNA sequencing. This has ensured that a robust

framework for strain identification was obtained from the integration of morphological traits and molecular techniques.

Voucher samples for the host organisms were kept, so that, if required, comparison of metabolite profiles could be carried out using LCMS to further validate the strain's endophytic nature. By extracting metabolites from surface-sterilized organism tissues and the isolated microbe's pure culture, LCMS could identify shared or unique compounds. Differences between inoculated and control organisms would help distinguish true endophytic metabolites from background plant compounds.

The biological evaluation revealed that a significant proportion of these strains exhibited notable bioactivities in multiple assays; these activities include antibiofilm, antimicrobial and anti-Alzheimer's disease activities. This has shown that the identified microbial strains, especially those belonging to the genera *Aspergillus niger* and *Aspergillus fumigatus*, have immense biotechnological potential. The strains had strong inhibitory activities against pathogenic bacteria and fungi, as well as enzymatic targets that are associated with neurodegenerative diseases. Such findings provide a valuable foundation for further investigations into the isolation, purification, and characterization of their bioactive compounds.

Bioassays of a crude extract are a crucial component in natural product discovery, as they provide a direct link between biological activity and the chemical complexity of crude extract sample. Bioassays can also tend to provide a working functional screen, allowing scientists to make important decisions about what to isolate as bioactive while maintaining synergistic effects that may be lost during isolation. One of the main advantages of bioassays is that they can produce a lot of information quickly, they allow the researcher to screen quickly and prioritise extracts with desirable activity, this minimises time wasted on decidedly inert fractions. Bioassays are also valuable because they demonstrate cumulative effects or potential synergistic interactions between compounds that may be lost or missed when testing for activity on purified components of the same sample. In some sense, bioassays of crude extracts can be low-cost, they also allow for high-throughput screening which in some ways gives researchers better access to these techniques as part of early-stage discovery. However, there are disadvantages to bioassays of crude extracts. The bioassay may give a false positive due to nonspecific reactivity from tannins, saponins or other components, or a false negative of a bioassay may occur from the dilution effect or the active constituent may be at a low concentration. The matrix compatibility of crude extracts can hinder some assay endpoints, like the use of absorbance, adjusted analytical markers, and the solubility of compounds can make assay interpretation hard to read. In conclusion, bioassays of crude samples are difficult to ignore when considering exploratory techniques to prospect, as powerful and versatile bioassays lead to valuable leads as well as ecological information on how/if secondary metabolites exert an ecological role.

The ability of the strains that produce bioactive metabolites with high specificity and potency highlights the importance of investigating unique and diverse ecosystems, such as Orman Garden, Wadi Natrun, and Hurghada coral reefs, as sources of new therapeutic agents. This work has provided a strong ground for future studies that aim to exploit the pharmaceutical potential of natural products derived from these strains to address pressing global health issues such as antibiotic resistance, biofilm associated infections, and neurodegenerative diseases.

CHAPTER 4 Results and Discussion - Antibiofilm active samples

4.0 Introduction

Biofilms are complex communities of microorganisms, bacteria or fungi, that attach to surfaces and are surrounded by a protective matrix made of polysaccharides, proteins, and DNA. This structure helps the microorganisms survive by making them resistant to antibiotics, immune responses, and environmental stresses. Biofilms are a significant issue in both medical and industrial fields. They contribute to chronic infections, such as wound infections, cystic fibrosis, and dental caries, as well as biofouling in medical devices and water systems. The formation of biofilms happens in stages, starting with the initial attachment of bacteria. This is followed by the development of microcolonies, maturation into a structured three-dimensional community, and the eventual dispersion of cells to new surfaces.[111]

Because biofilms present challenges, researchers have looked into different compounds that can disrupt their formation or stability. These inhibitors focus on various stages of biofilm development, such as bacterial adhesion, quorum sensing, matrix production, and metabolic pathways. Natural compounds, including D-amino acids and proanthocyanidins from cranberries, interfere with bacterial attachment and the integrity of the matrix. Other agents, like furanones from marine algae and allicin from garlic, disrupt quorum sensing signals, which stops coordinated biofilm growth. Enzymes like DNase I break down extracellular DNA, a vital part of the biofilm matrix. Additionally, synthetic compounds, such as silver nanoparticles, create reactive oxygen species that harm microbial cells. Some antibiotics, like azithromycin, also disrupt biofilms at sub-inhibitory concentrations by affecting bacterial communication instead of killing the cells outright.[111]

Understanding these biofilm inhibitors and how they work is essential for developing new methods to tackle persistent infections and antimicrobial resistance. Future research may look at combining these agents with standard antibiotics or creating new compounds that specifically target biofilm pathways without encouraging resistance. By disrupting biofilms, these inhibitors could improve treatment results in both clinical and industrial settings.[111]

This chapter describes a systematic approach to the isolation, biological assessment, and chemical identification of metabolites from strains showing antibiofilm activity. Antibiofilm compounds are of great interest because they may help in the fight against biofilm-related infections, which are known for their resistance to conventional antimicrobial treatments. This research considers natural products as critical sources in the fight against this global health problem. Strains with significant inhibition of biofilm formation were selected and further studied. The bioassay guided fractionation was the central strategy to isolate active compounds. Chromatographic techniques were used throughout the partitioning process. The initial fractionation was carried out using liquid–liquid partitioning, and the further narrowing of active fractions was achieved through vacuum liquid chromatography and size exclusion chromatography. HPLC was then used for isolating pure compounds. After obtaining pure

compounds, detailed chemical profiling was carried out to determine their structure. High resolution mass spectrometry (HR-MS/MS) was used for the determination of molecular weight and fragmentation which in turn helped in assigning the molecular formulae of the compounds. To complement these findings, Nuclear Magnetic Resonance (NMR) spectroscopy was employed. 1D (1 H and 13 C) and 2D (COSY, HSQC, HMBC and NOESY) NMR experiments were used to determine the compounds' substructures and connectivity. The use of HR-MS/MS and NMR side-by-side allowed for a complete structural characterisation and ensured that the assigned structures are correct. This chapter combines biological evaluation with analytical techniques to illustrate the value of natural product research in managing biomedical problems and the need to explore microbial diversity for new antibiofilm agents.

4.1 Sample selection based on activity

Based on the antimicrobial and antibiofilm screening, the microbial strains *Aspergillus niger* WNS7(50)F3 and *Aspergillus fumigatus* WNS16(50)F2 exhibited the highest antimicrobial and antibiofilm activity against the tested pathogenic microorganisms and were selected for large-scale fermentation and further analysis.

While many of the microbial crude extracts demonstrated exceptionally potent antimicrobial activity, particularly the bacterial strains isolated from Wadi Natrun plants, the microbial mass produced during large-scale fermentation was found to be very low. Bacterial endophytes generate less biomass than fungi because their small cell size and localized growth patterns and different ecological strategies. Bacteria as single-celled organisms (1–5 µm) depend on passive nutrient uptake to colonize discrete areas such as intercellular spaces which restrict their total biomass. The filamentous fungal growth pattern allows them to create extensive hyphal networks which penetrate plant tissues while secreting degradative enzymes and storing energy in durable cell walls to achieve larger biomass accumulation. This necessitated a significant scale-up of fermentation. Consequently, the antifungal strains with antibiofilm activity were prioritized for bioassay-guided isolation over the antimicrobial-active bacterial strains.

4.2 Bioassay guided fractionation of active strains

4.2.1 Fractionation of *Aspergillus niger* WNS7(8)F3 (antibiofilm active)

The crude microbial extracts of *Aspergillus niger* WNS7(8)F3 were first extracted using ethyl acetate, followed by Kupchan fractionation[112], where each microbial crude extract was partitioned into five fractions, Water-water (WW), water-butanol (WB), methanol (FM), DCM (FD) and hexane (FH) (**Figure 4.2.1.1**)

Vacuum liquid chromatography (VLC) was then performed on the WNS7(8)F3 FD fraction (See Supplementary), using silica gel as the stationary phase and varying ratios of n-hexane, DCM and MeOH. No biological evaluation was possible at this time, so WNS7(50)F3 FD was chosen due to this fraction containing a greater mass of components in comparison to the other liquid-liquid extraction (Kupchan) fractions. VLC of WNS7(8)F3 FD formed 24 fractions. Using thin layer chromatography (TLC),

these fractions that were pooled as follows: 1-11, 12, 13, 14, 15, 16-17, 18-20, 21 (See Supplementary).

Size exclusion chromatography (SEC) was then performed on the WNS7(8)F3 FD fractions 13 and 14, pooled from the previous VLC step, due to these fractions containing a greater mass of components in comparison to the other VLC fractions (no biological evaluation available at the time).

For WNS7(8)F3 FD 14, SEC was carried out using a LH-20 Sephadex stationary phase and a 100% MeOH mobile phase. SEC of WNS7(8)F3 FD 14 formed 14 fractions. Using TLC, these fractions were pooled as follows: 1-5, 6-14 (**Figure 4.2.1.1**).

For WNS7(8)F3 FD 13, SEC was carried out using a LH-20 Sephadex stationary phase and a 100% MeOH mobile phase. SEC of WNS7(8)F3 FD 13 formed 24 fractions. Using TLC, these fractions were pooled as follows: 1-3, 4-6, 7-8, 9-10, 11-12, 13-15, 16-24 (**Figure 4.2.1.1**).

SEC was then performed on the WNS7(8)F3 FD 13 s4-6 fraction, pooled from the previous SEC step, due to these fractions containing a greater mass of components in comparison to the other SEC fractions.

For WNS7(8)F3 FD 13 s4-6, SEC was carried out using a LH-20 Sephadex stationary phase and a 100% MeOH mobile phase. SEC of WNS7(8)F3 FD 13 s4-6 formed 44 fractions. Using TLC, these fractions were pooled as follows: A-E, F-X and Y-AR (**Figure 4.2.1.1**).

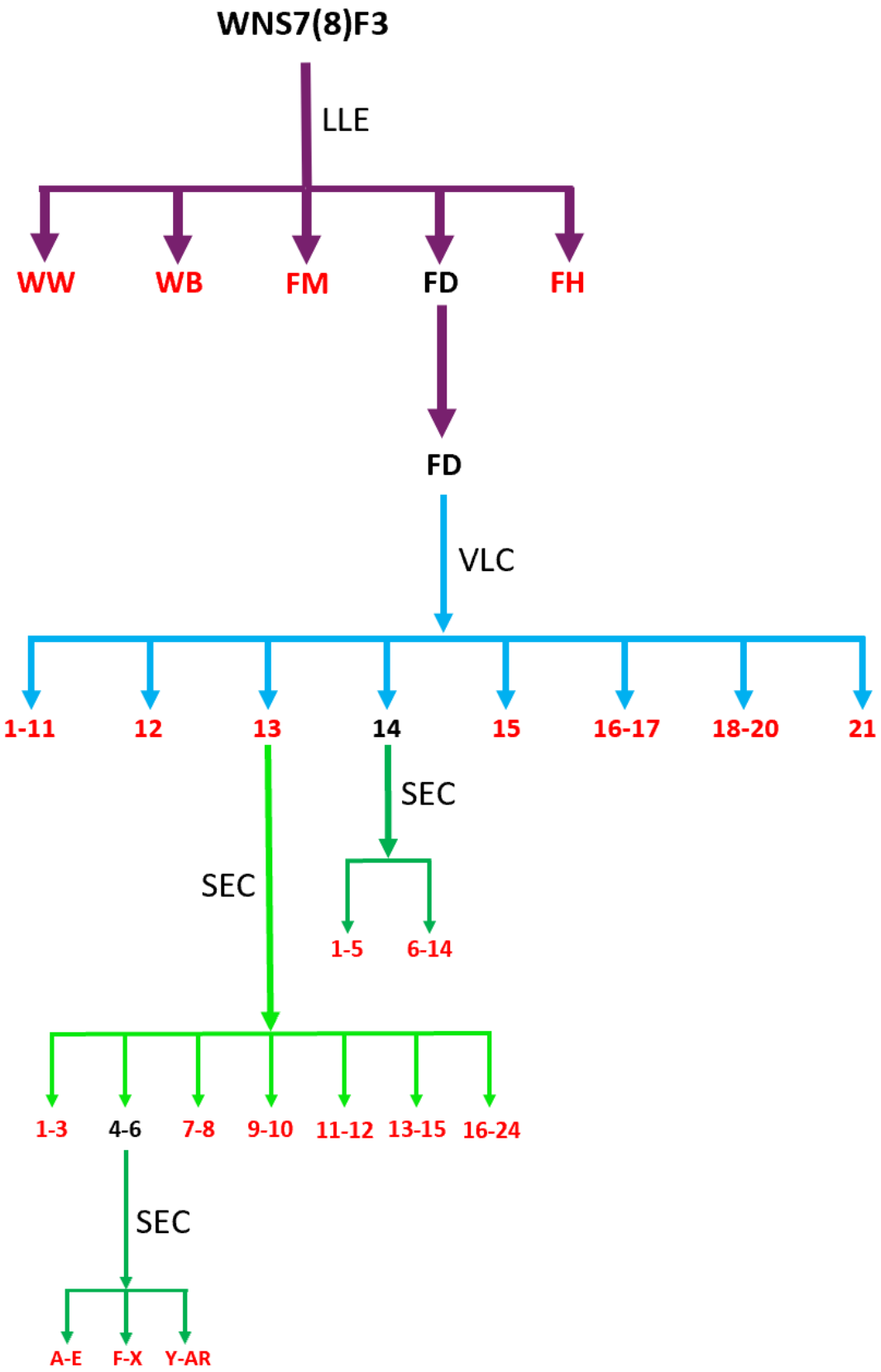

Figure 4.2.1.1. Flowchart of the fractionation of the crude extract of *Aspergillus niger* WNS7(8)F3. All red coloured fractions were further biologically screened against antibiofilm and antimicrobial targets. LLE: Liquid-Liquid Chromatography (Kupchan), VCL: Vacuum Liquid Chromatography, and SEC: Size

Exclusion Chromatography.

4.2.2 Fractionation of *Aspergillus fumigatus* WNS16(8)F2 (antibiofilm active)

The crude microbial extracts of *Aspergillus fumigatus* WNS16(8)F2 were first extracted using ethyl acetate, followed by Kupchan fractionation[112], where each microbial crude extract was partitioned into five fractions, Water-water (WW), water-butanol (WB), methanol (FM), DCM (FD) and hexane (FH) (Fig.) Vacuum liquid chromatography (VLC) was then performed on WNS16(8)F2 fractions WB and FD (Table S.), using silica gel as the stationary phase and varying ratios of n-hexane, DCM and MeOH. WNS16(8)F2 WB and FD were both chosen due to these fractions containing a greater mass of components in comparison to the other liquid-liquid extraction (Kupchan) fractions. VLC of WNS16(8)F2 WB formed 25 fractions. Using TLC, these fractions that were pooled as follows: 1-6, 7, 8, 9, 10, 11, 12, 13, 14, 15, 16-17, 18-19, 20-25 (See Supplementary) (**Figure 4.2.2.1**). VLC of WNS16(8)F2 FD formed 25 fractions. Using TLC, these fractions that were pooled as follows: 1-7, 8, 9, 10-11, 12-13, 14-16, 17-20, 21-25 (**Figure 4.2.2.1**).

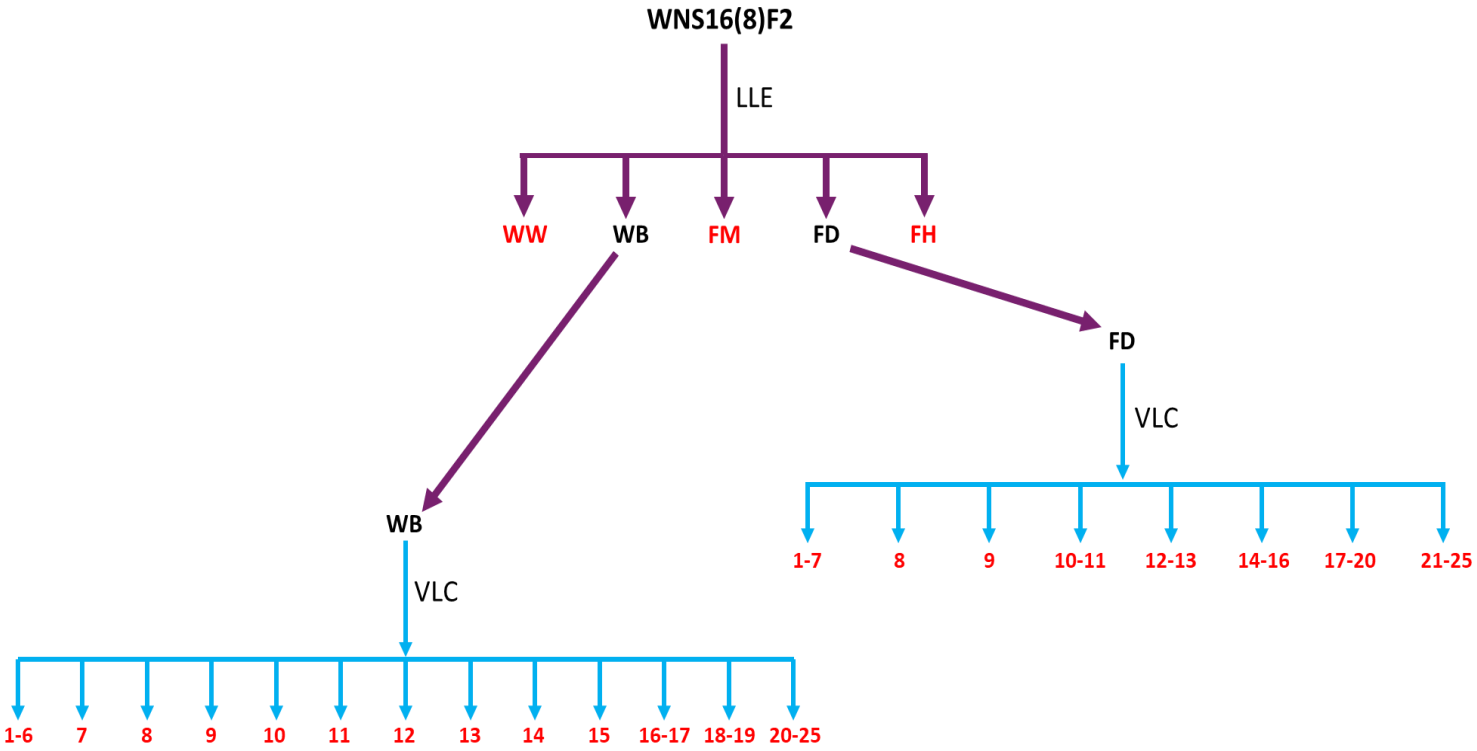

Figure 4.2.2.1. Flowchart of the fractionation of the crude extract of *Aspergillus fumigatus* WNS16(8)F2. All red coloured fractions were further biologically screened against antibiofilm and antimicrobial targets. LLE: Liquid-Liquid Chromatography (Kupchan), and VCL: Vacuum Liquid Chromatography.

4.2.3 Biological evaluation of *Aspergillus niger* WNS7(8)F3 and *Aspergillus fumigatus* WNS16(8)F2 fractions

Fractions from *Aspergillus niger* WNS7(8)F3 and *Aspergillus fumigatus* WNS16(8)F2 were biologically evaluated simultaneously against antibiofilm and antimicrobial targets (Table. S) Biofilm targets include B. subtilis, P. aeruginosa, S. aureus and E. coli. Antimicrobial targets include *E. coli, P. aeruginosa, L. monocytogenes, S. aureus, C. albicans and A. niger.*

Table 4.2.3.1. The % biofilm inhibition of the fractions of WNS7(8)F3 and WNS16(8)F2 with the highest overall antibiofilm and antimicrobial activities.

Fraction	*B. subtilis*	*P. aeruginosa*	*S. aureus*	*E. coli*
WNS7 WW	0.0	0.0	50.2	63.0
WNS7 FD 13 s4-6 ssF-X	26.1	50.2	36.3	73.1
WNS16 WW	64.2	40.3	0.0	75.6
WNS16 FD 13 s9	0.0	50.4	0.0	0.0

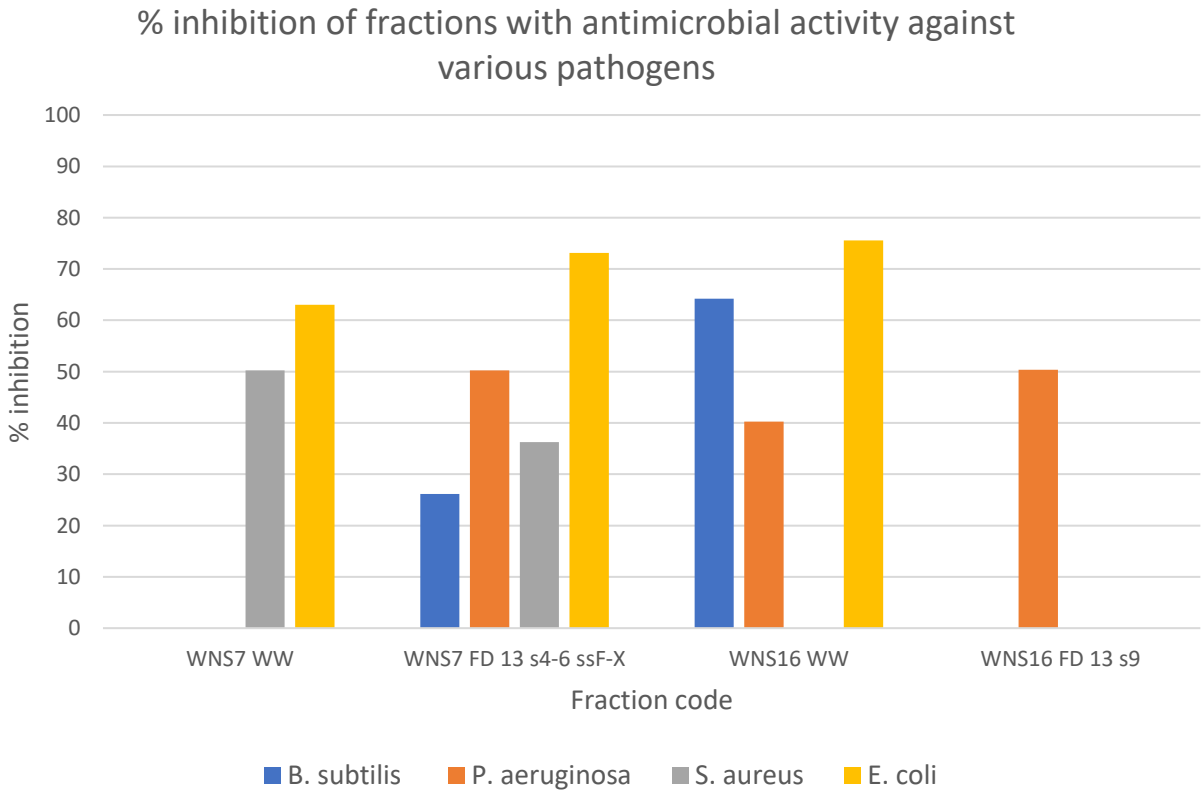

Figure 4.2.3.1. The percentage biofilm inhibition of the fractions of WNS7(8)F3 and WNS16(8)F2 with the highest overall antibiofilm and antimicrobial activities.

Table 4.2.3.2. The % antimicrobial inhibition of the fractions of WNS7(8)F3 and WNS16(8)F2 with the best overall antibiofilm and antimicrobial activities.

Fraction	*E. coli*	*P. aeruginosa*	*L. monocytogenes*	*S. aureus*	*C. albicans*	*A. niger*
WNS7(8)F3 WW	91.7	89.7	8.3	83.5	94.7	86.0
WNS7(8)F3 FD 13 s4-6 ssF-X	93.9	93.4	86.1	89.1	0.0	91.8
WNS16(8)F2 WW	91.5	91.2	85.6	87.4	94.7	89.7
WNS16(8)F2 FD 13 s9	30.3	91.7	62.8	0.0	96.8	0.0

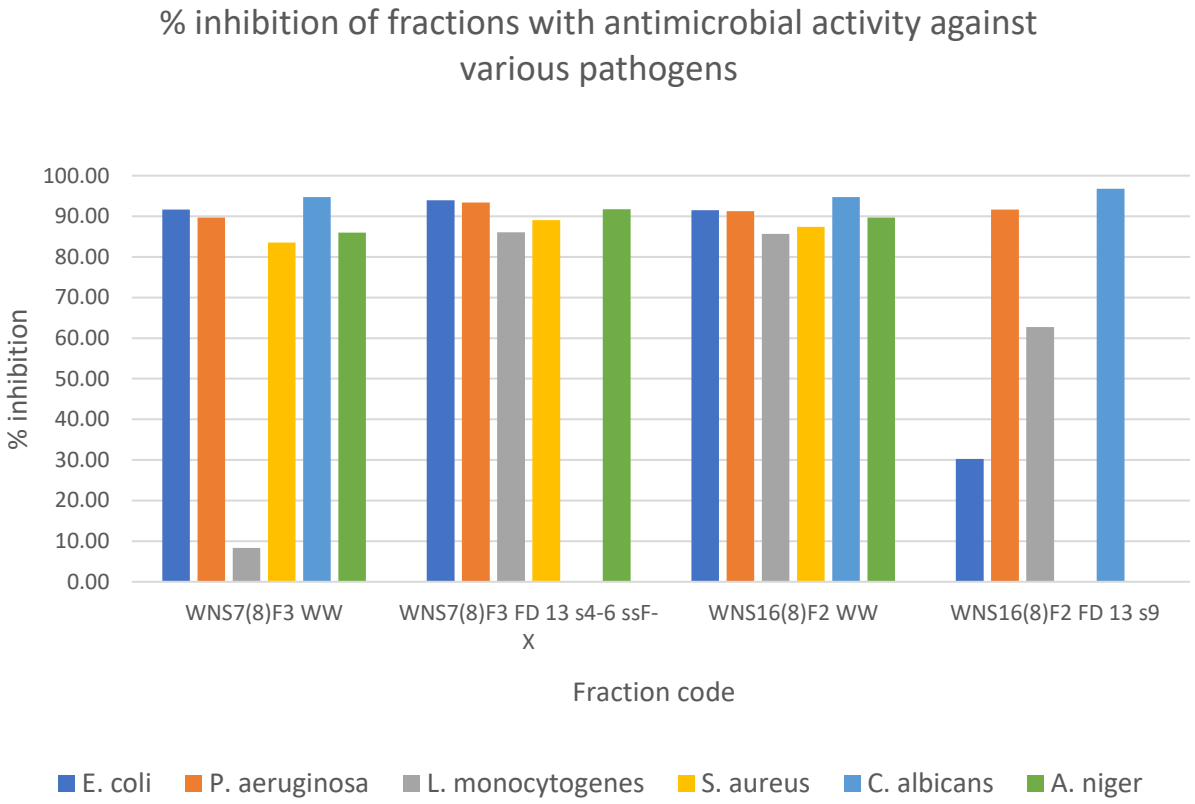

Figure 4.2.3.2. The percentage antimicrobial inhibition of the fractions of WNS7(8)F3 and WNS16(8)F2 with the highest overall antibiofilm and antimicrobial activities.

Following the antibiofilm and antimicrobial evaluation of the fractions, WNS7(8)F3 FD 13 s4-6 ssF-X was chosen for further fractionation. Two SEC columns were run, with the stationary phase LH-20 Sephadex, but two different solvent systems to fractionate the WNS7(8)F3 FD 13 s4-6 ssF-X fraction. The first used DCM:MeOH 50:50 (column D) and the second used ACN:MeOH 50:50 (column A). Column D produced 13 fractions, which were pooled using UV light into the fractions: 1, 2-3, 4-6, 7-8, 9-11, 12, 13 (Fig 3.5.4.3). Column A produced 18 fractions, which were pooled using UV light into the fractions: 1, 2-4, 5-6, 7-9, 10-12, 13-14, 15-17, 18 (**Figure 4.2.3.3.**).

From the ^{1}H NMR data (**Figure 4.2.3.4**) from the fractions produced, it was concluded that the chemistry favoured the fraction Column 1 s9-11 (WNS7(8)F3 FD 13 s4-6 ssF-X cD sss9-11).

HPLC was then performed on this fraction to obtain pure compounds (Fig 3.5.4.5). An Xselect CSH 130 Prep C18 5um 10x250 mm column was used as the stationary phase. The solvent system used was A (100% H_2O + 0.05% TFA) and B (100% MeOH) on an isocratic system of 72% B from t = 0.00 to t = 10.00 mins, followed by gradient system of 72% A to 80% B from t = 10.00 to t = 11.00 mins, and finally an isocratic system of 80% B between t= 11.00 and t = 35.00 mins.

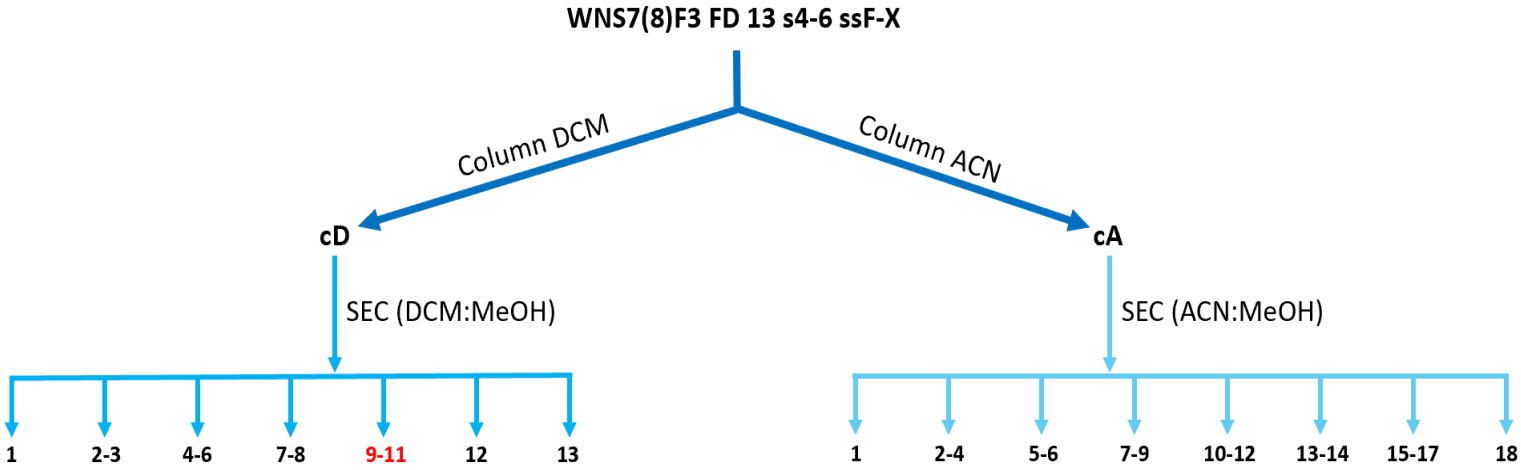

Figure 4.2.3.3. Flow chart of the fractionation of the fraction of *Aspergillus niger* WNS7(8)F3 FD 13 s4-6 ssF-X. The red coloured fraction (cD sss9-11) was further purified using HPLC to produce pure compounds. SEC: Size Exclusion Chromatography.

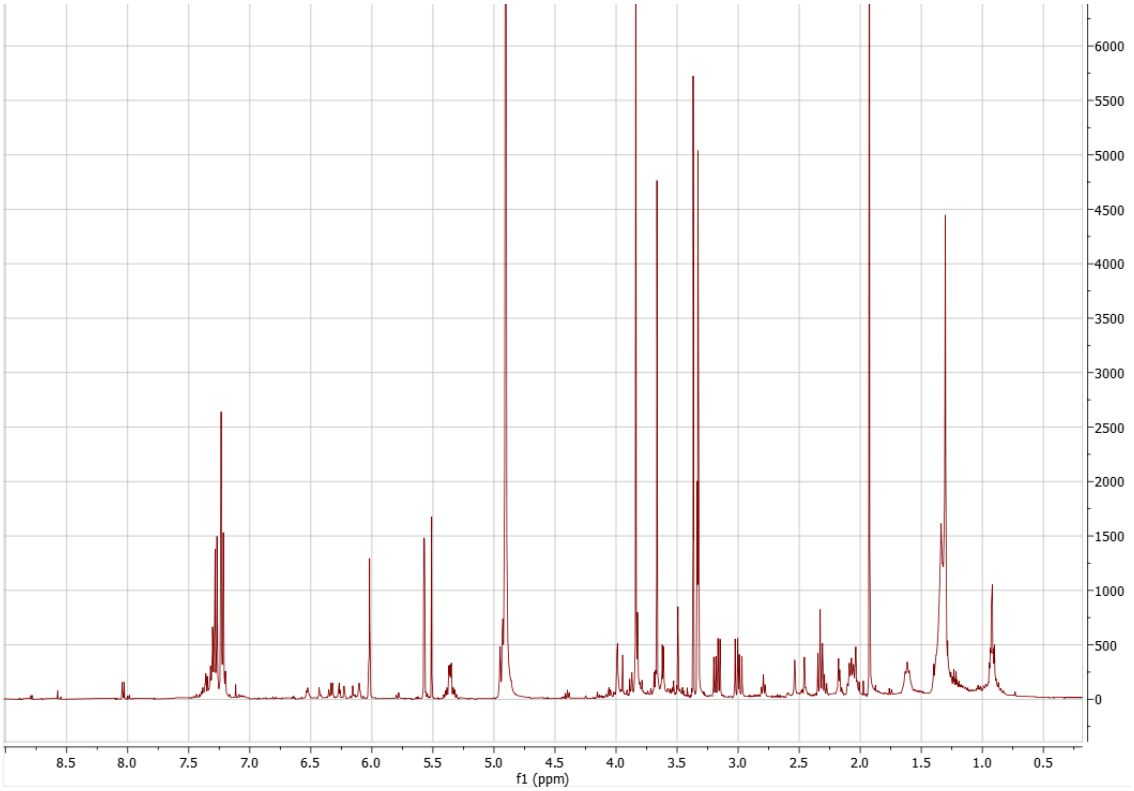

Figure 4.2.3.4. ^{1}H NMR spectra of the fraction WNS7(8)F3 FD 13 s4-6 ssF-X cD sss9-11.

The ^{1}H NMR spectrum of WNS7(8)F3 FD 13 s4-6 ssF-X cD sss9-11 (**Figure 4.2.3.5**) is particularly notable. It shows that several compounds are present in significant quantity and so are ideal for isolation and detailed structural investigation. The presence of unsaturated and aromatic compounds is indicated by signals in the 5.3 to 8.5 ppm region, and highly deshielded protons are indicated by chemical shifts of 8.5 to 8.8 ppm. Moreover, signals found between 3.5 and 4.0 ppm are associated with various methoxy groups, which also indicate the complexity of the compound structures present.

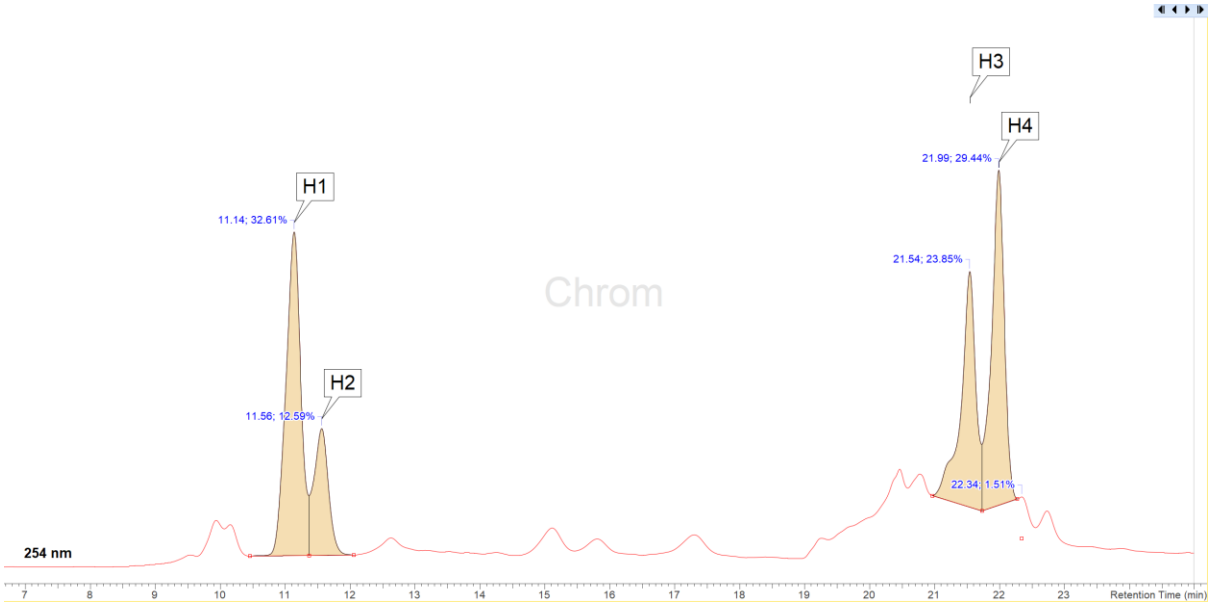

Figure 4.2.3.5. HPLC chromatogram for WNS7(8)F3 FD 13 s4-6 ssF-X sss9-11, absorbance measured at 254 nm. Four pure compounds isolated in total, labelled H1-4.

HPLC peak separation, in this case, was not optimal. In future work this optimisation of peak separation would be pursued fine tuning the mobile phase (solvent ratio, pH, buffers) and column selection (chemistry, particle size, length).

^{1}H NMR of all isolated compounds was conducted, and from this data, three pure compounds were seen to have the most chemical potential, were chosen to be structure elucidated to completion, and pursued for further biological screening. These chosen compounds were WNS7(8)F3 FD 13 s4-6 ssF-X sss9-11 H1 (9.8 mg) 3 (12.1 mg) and 4 (11.3 mg).

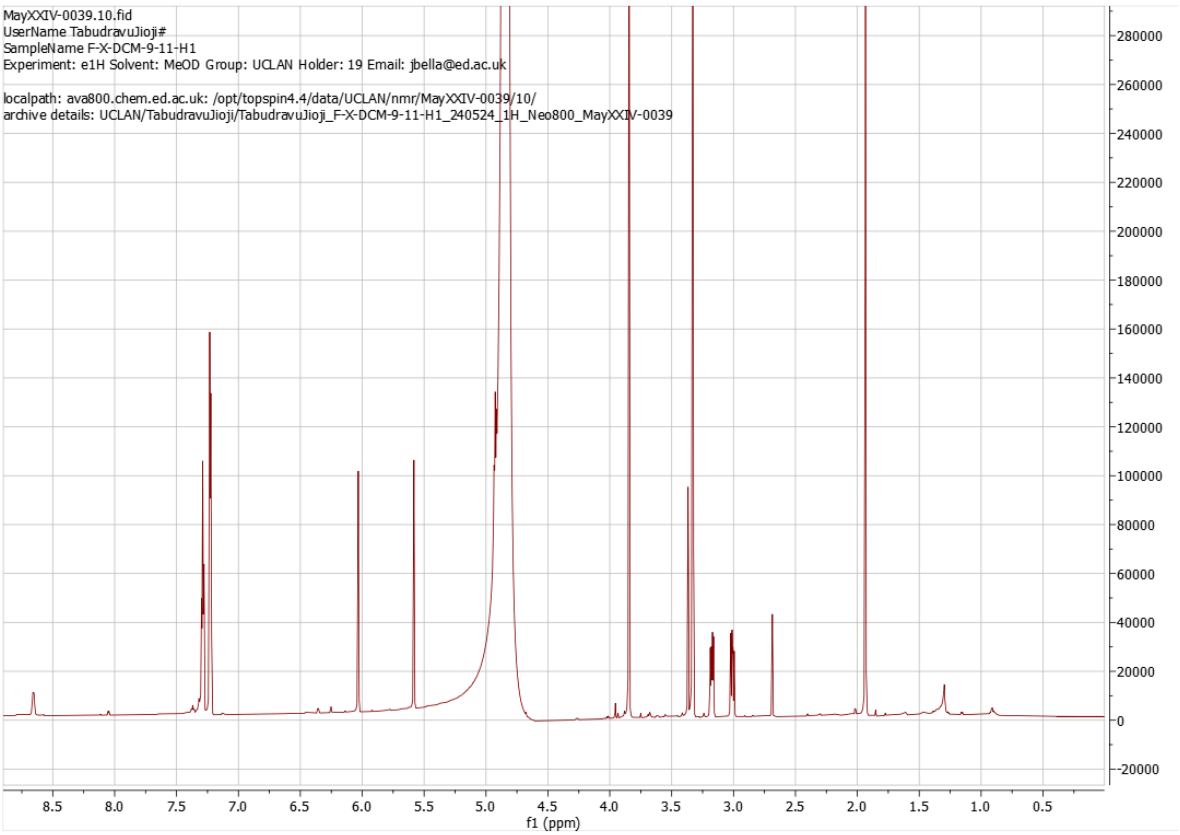

Figure 4.2.3.6. ^{1}H NMR spectra of the pure compound WNS7(8)F3 FD 13 s4-6 ssF-X cD sss9-11 H1.

The H NMR spectrum of WNS7(8)F3 FD 13 s4-6 ssF-X cD sss9-11 H1 (**Figure 4.2.3.6**) is particularly noteworthy, especially since aromatic moieties are indicated by signals observed between 7.0 and 8.7 ppm. Unsaturation is observed by the signals between 5.5 and 6.1 ppm, and signals in the 3.5 to 4.1 ppm range correspond to protons attached to electronegative atoms or functional groups that induce deshielding, which are suggestive of methoxy groups. These features collectively highlight the complexity of the molecule and why it was chosen for further analysis.

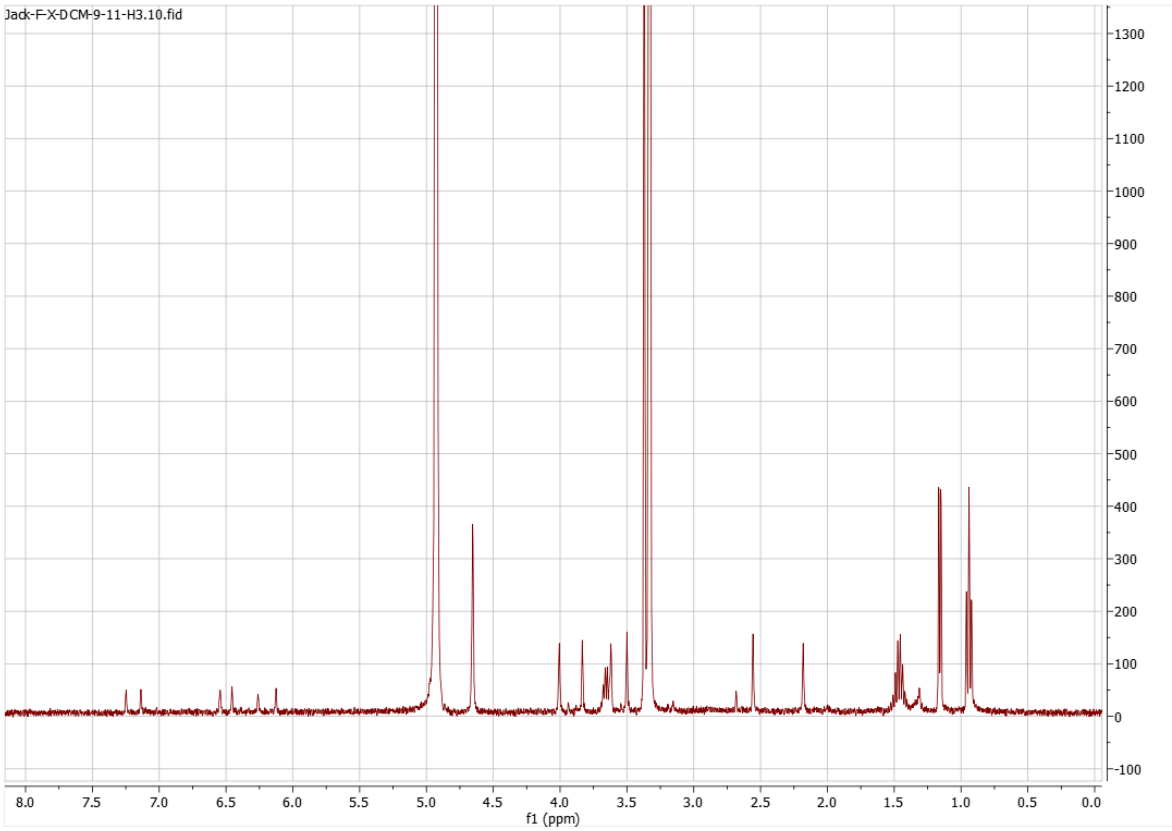

Figure 4.2.3.7. ^{1}H NMR spectra of the pure compound WNS7(8)F3 FD 13 s4-6 ssF-X cD sss9-11 H3.

The ^{1}H NMR spectrum of WNS7(8)F3 FD 13 s4-6 ssF-X cD sss9-11 H3 (**Figure 4.2.3.7**) is particularly noteworthy, especially since aromatic moieties are indicated by signals observed between 6.0 and 7.4 ppm and the signals in the 3.5 to 4.1 ppm range suggest methoxy groups. These features collectively highlight the complexity of the molecule and why it was chosen for further analysis.

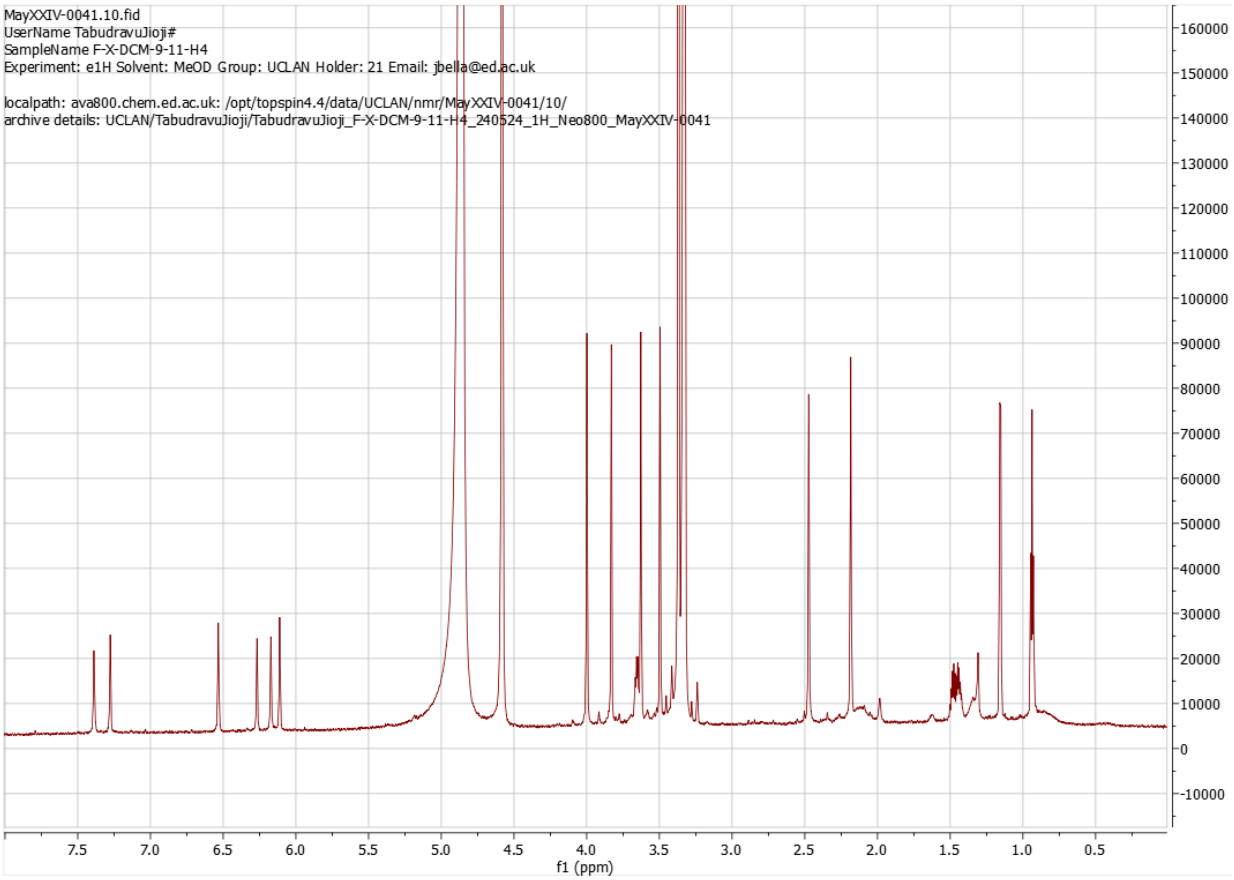

Figure 4.2.3.8. ^{1}H NMR spectra of the pure compound WNS7(8)F3 FD 13 s4-6 ssF-X cD sss9-11 H4.

The ^{1}H NMR spectrum of WNS7(8)F3 FD 13 s4-6 ssF-X cD sss9-11 H4 (**Figure 4.2.3.8**) is especially interesting, simply because aromatic moieties are indicated by signals observed between 6.0 and 7.4 ppm and the signals in the 3.5 to 4.1 ppm range suggest methoxy groups. These features collectively indicate the complexity of the molecule and why it was chosen for further analysis.

4.2.4 Chemical profiling of biofilm inhibitory samples

4.2.4.1 Structure elucidations of *Aspergillus niger* WNS7(8)F3 D 13 s4-6 ssF-X cD sss9-11 H1

The unknown compound WNS7(8)F3 FD 13 s4-6 ssF-X sss9-11 H1 showed a high resolution HRMS of m/z = 288.124 $[M+H]^{+}$, Δ= -0.38 ppm, calculated for molecular formula $C_{16}H_{18}NO_4$ (Figure S5). The molecular formula $C_{16}H_{17}NO_4$ requires nine degrees of unsaturation. The presence of one aromatic benzene ring accounts for four, one pyrone six-membered ring accounts for four, while one carbonyl accounts for another one, which makes a total of nine degrees of unsaturation. Interpretation of ^{1}H NMR, COSY, and HMBC NMR spectra (Figure S1-4) indicated the presence of 5H AB_2C_2 system at 7.22 (1H, dd, *J*= Hz), 7.29 (2H, d, *J*=Hz) and 7.22 (2H, dd, *J*= Hz), indicating the presence of a monosubstituted benzene moiety. The presence of an AC system at 6.03 (1H, s) and 5.58 (1H, s), indicated the presence

of disubstituted pyrone ring moiety. It's ^{13}C NMR showed the presence of six aromatic signals for one aromatic ring and one pyrone, one amide carbonyl signal δ_C 172.06, one methyl signal CH_3 δ_C 21.02, one methylene signal δ_C 37.86, one methine signal CH δ_C 52.78, and one methoxy signal CH_3 δ_C 55.78, and an aromatic carbomethoxy carbon δ_C 171.06. HMBC correlations between C9 and H7, C4 and H8, C8 and H7, and C7 and H8, established the link between the substructures A and B (**Figure 4.2.4.1.1**) Establishing HMBC correlations between fragment C and either fragment A or B proved challenging, as the HMBC correlations observed for fragment C were all internal. However, the link was identified using MS/MS fragmentation data shown in **Figure 4.2.4.1.4**. Analysis using MS, 1D and 2D NMR, and comparison with previously published data confirm the structure of WNS7(8)F3 FD 13 s4-6 ssF-X sss9-11 H1 as Pyrophen.

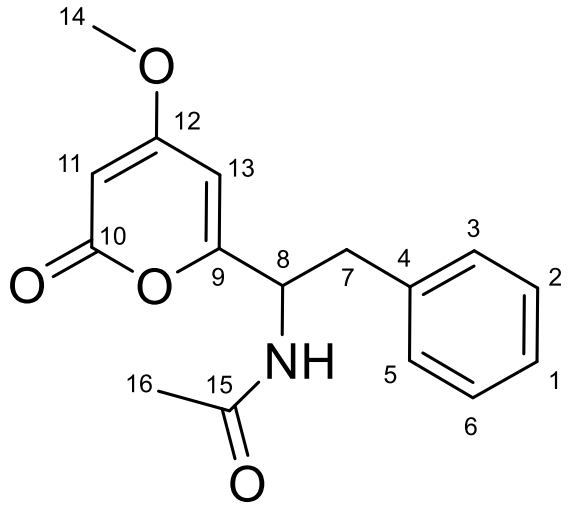

Figure 4.2.4.1.1. Structure of Pyrophen, isolated from the endophytic fungi *Aspergillus niger* WNS7(8)F3. Structure numbered according to Barnes et al 1990.[113]

Table 4.2.4.1.1. NMR Spectroscopic Data for pyrophen in MeOD, alongside literature chemical shifts of pyrophen in DMSO.[113]

Position	**^{13}C Chemical shift (ppm)** [a]	**C-type**	**^{1}H (chemical shift ppm, No. of H, multiplicity, coupling)** [b]	**COSY (^{1}H-^{1}H)**	**HMBC (^{1}H-^{13}C)**	**Literature ^{13}C (DMSO) Chemical shift (ppm)**	**Literature ^{1}H (DMSO) Chemical shift (ppm)**
1	126.6	CH	7.22 (1H, d, J = 6.87 Hz)	2	2, 3	126.5	7.16-7.30
2, 6	128.3	CH_2	7.29 (2H, dd, J = 8.00 Hz)	1, 3	1, 3	128.3	7.16-7.30
3, 5	128.8	C	7.22 (2H, d, J = 6.87 Hz)	2	1, 2, 7	129.0	7.16-7.30
4	136.6	C				137.2	
7	37.7	CH	A: 3.01 (1H, dd, J = 13.54, 8.71 Hz)	8	A: 3, 4, 9 B: 3, 4, 9	37.9	

			B: 3.17 (1H, dd, J = 13.73, 6.99 Hz)				
8	52.8	CH	4.92 (1H, t, J = 1.00 Hz)	7A, 7B	4, 7, 9, 11, 12	52.1	
9	162.9	C				163.2	
10	165.8	C				163.8	
11	100.6	CH	6.03 (1H, s)		8, 9, 12, 13	99.4	5.93
12	171.8	C				169.1	
13	87.7	CH	5.58 (1H, s)		10, 11, 12	88.0	5.43
14	55.8	CH_3	3.84 (3H, s)		12	56.4	3.82
15	172.1	C				170.8	
16	21.0	CH_3	1.93 (3H, s)		15	22.4	1.86

[a] in CD_3OD at 200 MHz

[b] in CD_3OD at 800 MHz

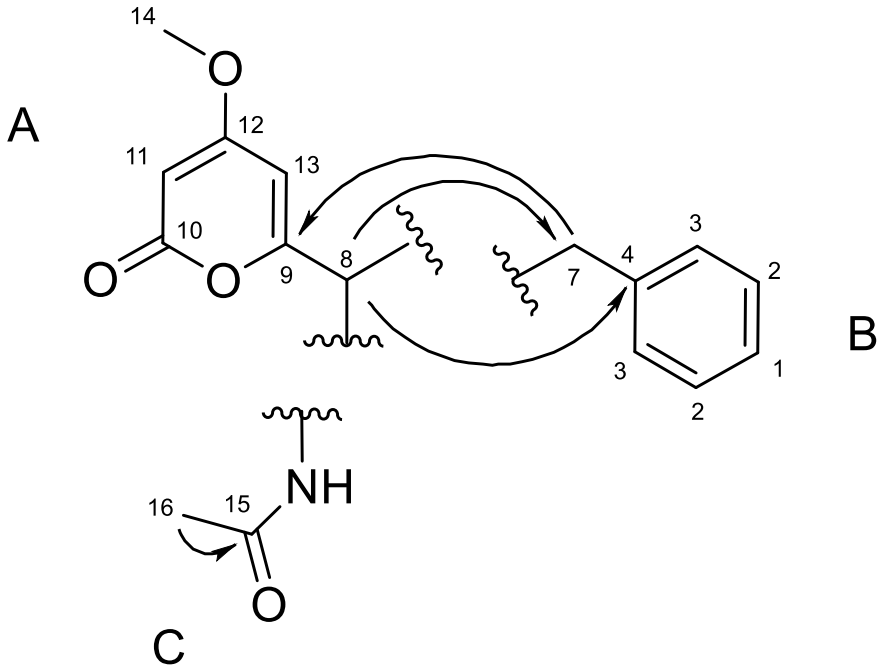

Figure 4.2.4.1.2. Fragments of Pyrophen (A, B and C), constructed and connected through HMBC. Main connections shown.

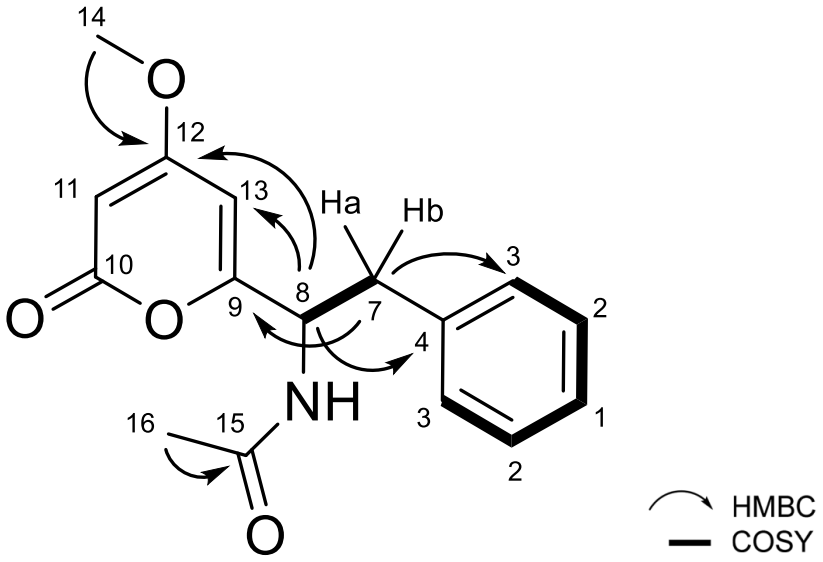

Figure 4.2.4.1.3. Structure of Pyrophen. Arrows show the main HMBC correlations between ^{1}H and ^{13}C atoms used to connect the fragments, and bold bonds show COSY ^{1}H-^{1}H correlations between adjacent hydrogens.

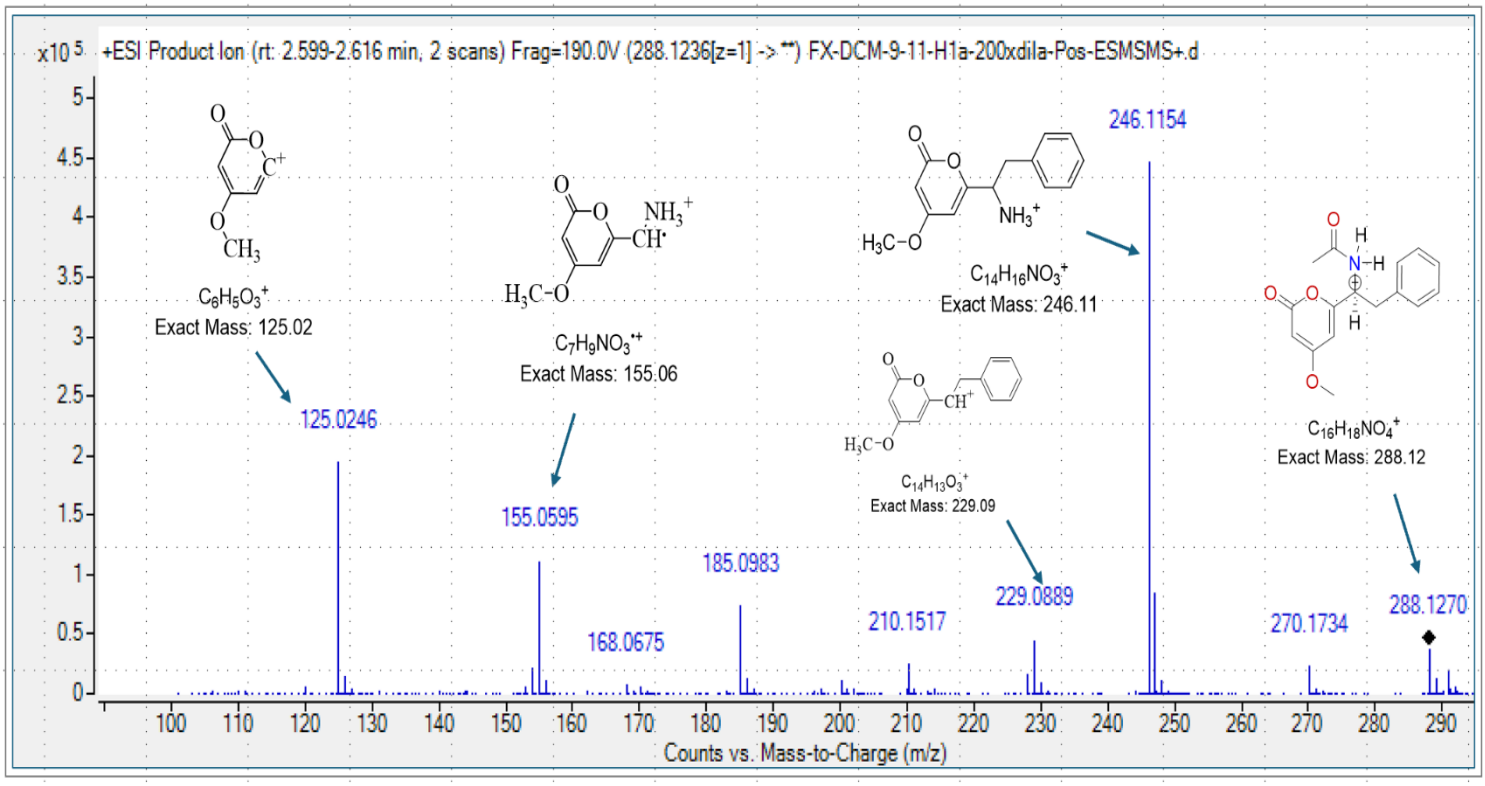

Figure 4.2.4.1.4. Assignment of HR-MS/MS fragments for Pyrophen (WNS7(8)F3 D 13 s4-6 ssF-X cD sss9-11 H1).

4.2.4.2 Structure elucidation of *Aspergillus niger* WNS7(8)F3 D 13 s4-6 ssF-X cD sss9-11 H3

The compound showed a high resolution HRMS of m/z = 571.1680 $[M+H]^+$, Δ = 1.27 ppm, calculated for $C_{32}H_{26}O_{10}$ and requiring 20° of unsaturation. (Figure S12) Interpretation of ^1H, COSY, HSQC and HMBC (Figures S9-11) indicated the presence of seven sp^2 methines, six sp^3 methyls, and fourteen sp^2 quaternary carbons leading to the sub-formula of $C_{28}H_{24}$ suggesting the presence of two exchangeable protons in the structure. The presence of seven sp^2 methines (δ_C 109.7, 106.3, 105.6, , 103.5, 101.6, 96.8, 96.0), six sp^3 methyls (δ_C 60.5, 55.1, 55.1, 54.2, 19.0, 18.9), and fourteen sp^2 quaternaries (δC 168.8, 168.4, 161.9, 160.9, 160.1, 159.1, 156.5, 156.1, 117.1, 108.8, 108.0, 107.6, 105.5, 103.5) plus four missing carbons (not observed in the HMBC spectrum due to desaturation of structure, Figure S11) accounted for fourteen of the twenty double bond equivalents suggesting the presence of six rings to complete the 20° of unsaturation in the structure of this compound. Intensive analysis of 1D and 2D NMR data (**Table 4.2.4.2.1**) enabled the construction of 2 substructures (**Figure 4.2.4.2.1**). Assembling the structural pieces together proved to be a challenge due to the number of possible structures and frameworks.

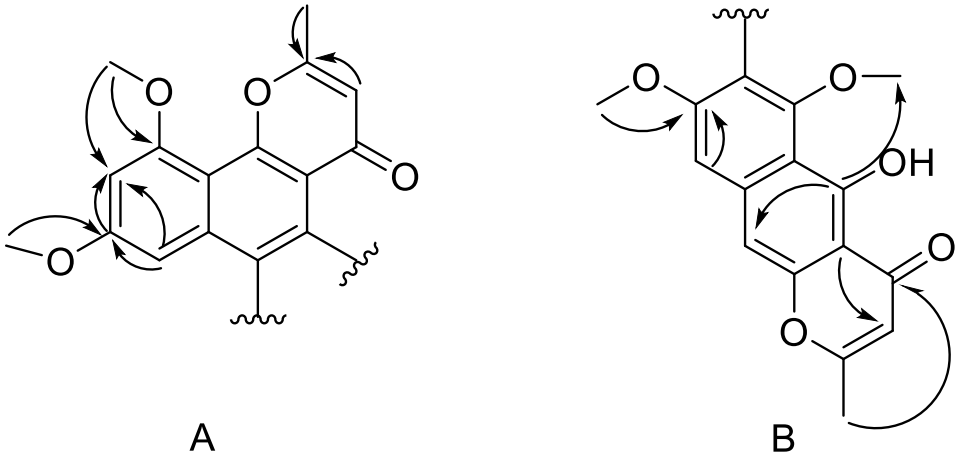

Figure 4.2.4.2.1. Substructures A and B and HMBC correlations for WNS7(8)F3 D 13 s4-6 ssF-X cD sss9-11 H3.

This is mainly due to limited number of observed HMBC correlations which is related to the low number of protons in the molecule (ratio of H: other atoms = 0.6). This type of compound falls within the Crews' rule[114], meaning that the structure is challenging to solve and requires other methods for structural confirmation. Searching the Antimarin database[115] using molecular formula produced seventeen 'hits' from *Aspergillus* sp. with ten structures as most likely candidates. Some of these possible structural frameworks are shown in **Figure 4.2.4.2.2.** Aurasperone A[116], Fonsecinone A[116], Isonigerone[117], Asperpyrone B[118], Asperpyrone C[118] and Rubasperone B[119]. Preliminary analysis of the data (**Table 4.2.4.2.1)** suggest that the compound possibly is Asperpyrone C[118].

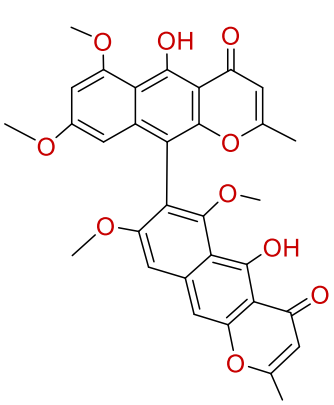

Aurasperone A
[F] *Aspergillus niger*; "Munissi MD"

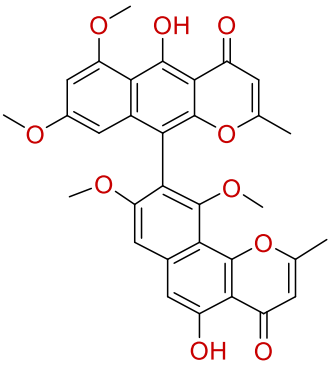

Fonsecinone A
[F] *Aspergillus fonsecaeus*

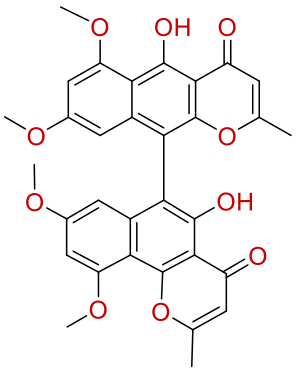

Isonigerone
[F] *Aspergillus niger*

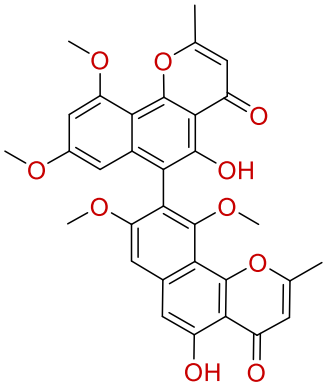

Asperpyrone B
[F] *Aspergillus niger*

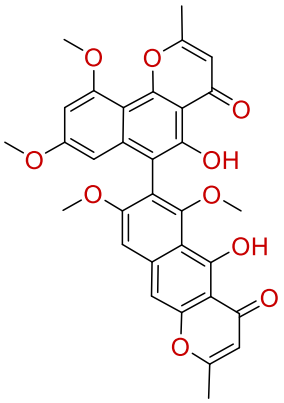

Asperpyrone C
[F] *Aspergillus niger*

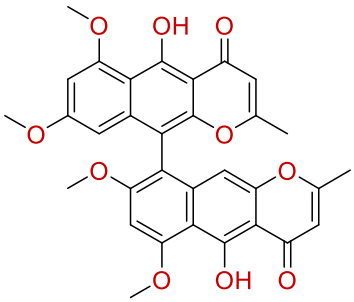

Rubasperone B
[F] *Ascomycota Aspergillus tubingensis*

Figure 4.2.4.2.2. Possible frameworks for WNS7(8)F3 D 13 s4-6 ssF-X cD sss9-11 H3.

To determine the correct structural framework NMR data and HRMS data for this compound were inputted into the ACD/Labs Structure Elucidator[120] and structures calculated using correlation spectroscopy-based generator (CSB) using both standard and "fuzzy" generation mode. Calculation of structures were still on-going when this thesis went into submission and results will be reported later.

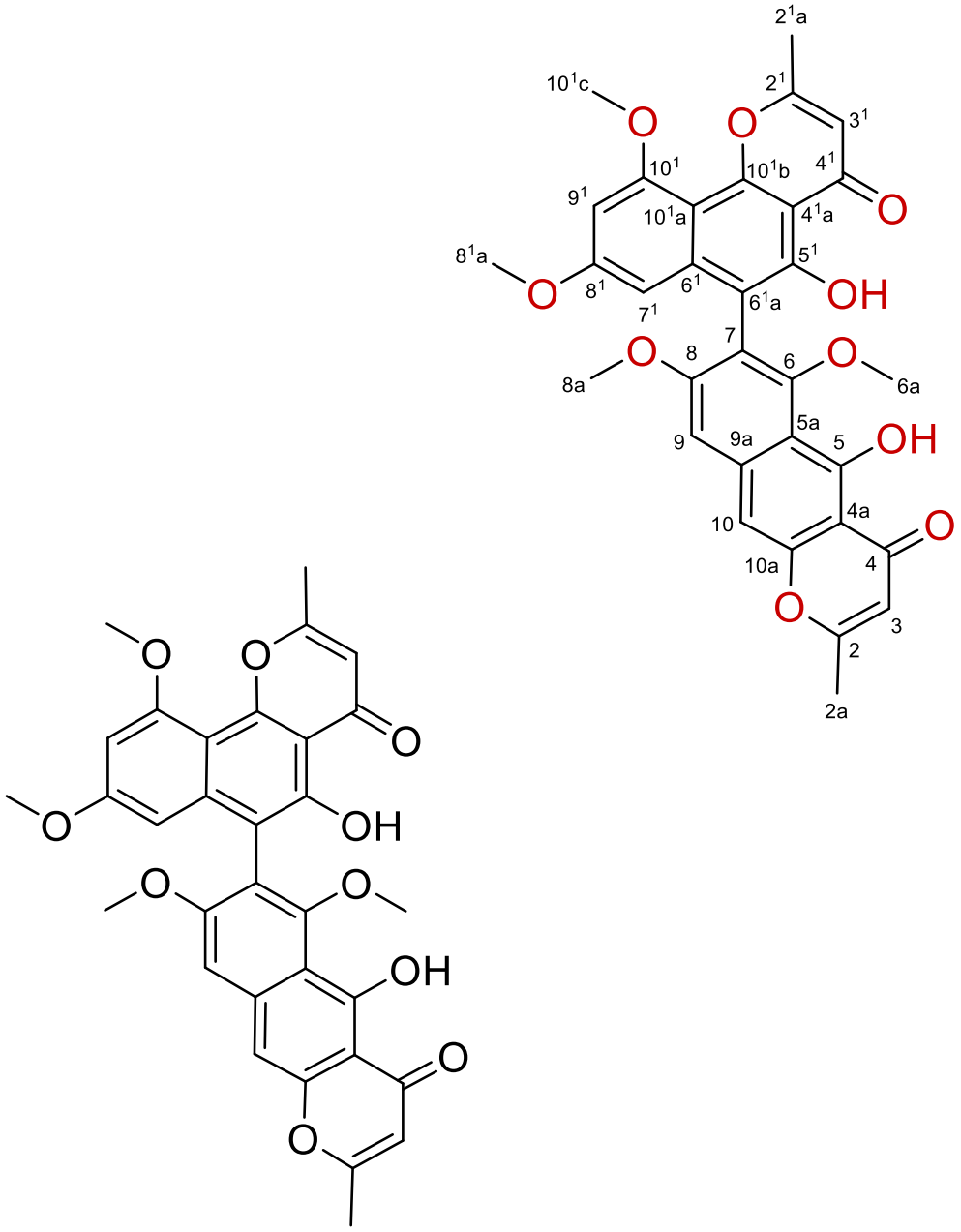

Figure 4.2.4.2.3. Asperpyrone C was seen to be the most likely candidate. Structure numbered according to Abdou et al 2024[121]

Table 4.2.4.2.1. NMR Spectroscopic Data for *Aspergillus niger* WNS7(8)F3 D 13 s4-6 ssF-X cD sss9-11 H3 in MeOD, alongside literature chemical shifts of Asperpyrone C in $CDCl_3$.[118]

Position	^{13}C Chemical shift (ppm)[a]	C-type	^{1}H (chemical shift ppm, No. of H, multiplicity, coupling) [b]	COSY (^{1}H-^{1}H)	HMBC (^{1}H-^{13}C)	Literature ^{13}C ($CDCl_3$) Chemical shift (ppm)	Literature ^{1}H ($CDCl_3$) Chemical shift (ppm)
2a	18.9	CH_3	2.17, 3H, bs		4	20.7	2.17

3	106.34	CH	6.12, 1H, bs			107.4	6.01
4	168.79	C				184.5	
4a	103.50	C				104.6	
5	160.07	C				161.9	
6a	55.08	CH_3	3.83, 3H, bs			62.2	3.62
8	156.48	C				160.2	
8a	60.49	CH_3	3.50, 3H, bs		8	56.1	3.79
9	105.62	CH	7.13, 1H, bs		8	101.7	6.96
10	101.62	CH	6.12, 1H, bs			101.2	7.10
2^1	168.41	C				166.5	
2^1a	18.93	CH_3	2.55, 3H, bs		2^1	20.5	2.52
3^1	109.71	CH	6.45, 1H, bs		2^1	110.2	6.30
7^1	96.04	CH	6.26, 1H, bs		8^1, 8^1a, 9^1	96.6	6.24
8^1	161.92	C				161.4	
8^1a	54.16	CH_3	3.62, 3H, bs		8^1	55.2	3.59
9^1	96.83	CH	6.54, 1H, bs		7^1, 8^1	96.7	6.41
10^1	160.90	C				159.4	
10^1c	55.08	CH_3	4.00, 3H, bs		9^1, 10^1	56.0	3.98

[a] in CD_3OD at 200 MHz

[b] in CD_3OD at 800 MHz

4.2.4.3 Structure elucidation of *Aspergillus niger* WNS7(8)F3 D 13 s4-6 ssF-X cD sss9-11 H4

The compound showed a high resolution HRMS of m/z = 571.1606 $[M+H]^+$, Δ = 1.27 ppm, calculated for $C_{32}H_{26}O_{10}$ and requiring 20° of unsaturation. (Figure S20). This compound is structural isomer of FX-DCM-9-11-H3. Analysis of ^{1}H, HSQC, and HMBC spectrum (Figures S15-18) shows some notable changes in chemical shifts in the aromatic region suggesting a different framework is in place for this compound. This compound has similar complexity to the previous one due to the high number of quaternary carbons and low number of HMBC correlations. Computer assisted structure elucidation using the ACD/Labs Structure Elucidator was performed. All calculations were performed using correlation spectroscopy-based generator (CSB) using both standard and "fuzzy" generation modes. 1D and 2D NMR comprising twelve ^{1}H, twenty-five merged ^{13}C, fifteen NOESY, twelve HSQC, and twenty-two HMBC peaks, plus the molecular formula were inputted to the software and calculations performed using parameters shown **Table 4.2.4.3.1.**. Four hundred and seventy-two structures in total were generated and sorted based on deviations of ^{13}C chemical shifts with those calculated by the Structure Elucidator. The top ten structures (**Table 4.2.4.3.1**) were all below d_A = 3.0 ppm, the cut off point for structures that are often regarded as potentially possible. However, compound sitting at position 1 has the best fit as it has the least d_A value of 1.54 ppm. This compound matches the structure of the known compound Aurasperone A previously reported compound in the literature. [116]

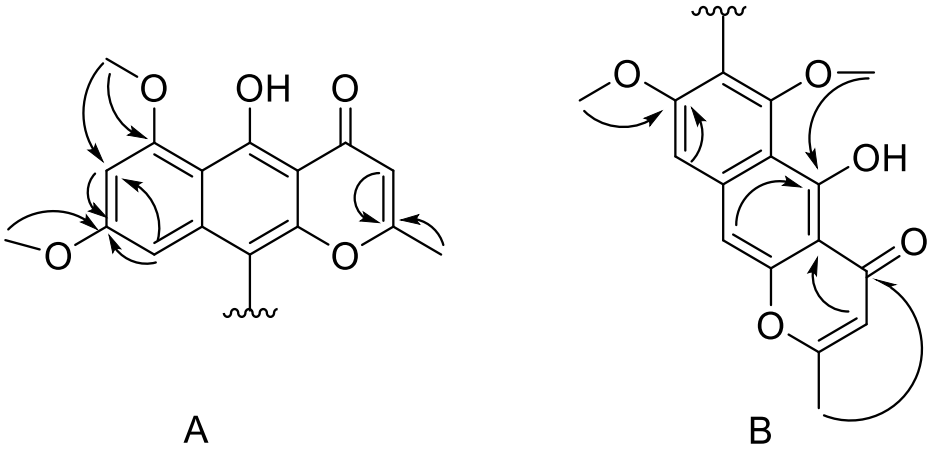

Figure 4.2.4.3.1. Substructures A and B and HMBC correlations.

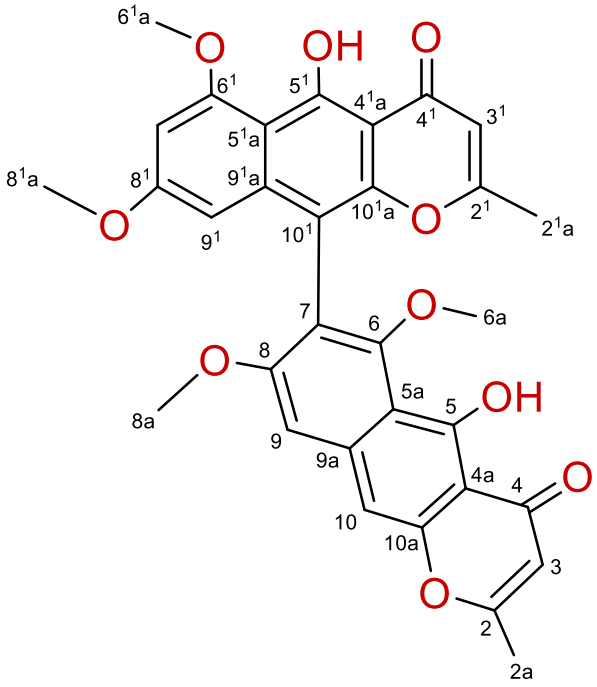

Figure 4.2.4.3.2. Aurasperone A with the structure numbered according to Abdou et al 2024[121]

Table 4.2.4.3.1. NMR Spectroscopic Data for *Aspergillus niger* WNS7(8)F3 D 13 s4-6 ssF-X cD sss9-11 H4 in MeOD, alongside literature chemical shifts for Aurasperone A in DMSO.[121]

Position	^{13}C Chemical shift (ppm)[a]	C-type	^{1}H (chemical shift ppm, No. of H, multiplicity, coupling) [b]	COSY (^{1}H-^{1}H)	HMBC (^{1}H-^{13}C)	^{13}C (DMSO) Chemical shift (ppm)[a]	^{1}H (DMSO) Chemical shift (ppm)[a]
2a	19.00	CH_3	2.18, 3H, s		4	20.1	2.13
3	106.57	CH	6.17, 1H, bs		4a	105.8	6.31
4	168.88	C				183.9	

4a	103.58	C				103.9	
5	160.09	C				160.9	
5a	110.69	C				108.2	
6a	55.10	CH_3	3.82, 3H, s			61.2	3.64
7	110.78	C				117.2	
8	157.75	C				159.8	
8a	61.10	CH_3	3.40, 3H, s		8	61.3	
9	101.76	CH	7.28, 1H, bs		8	103.1	7.39
10	101.68	CH	7.39, 1H, bs			101.4	7.40
2^1	169.27	C				167.9	
2^1a	19.19	CH_3	2.47, 3H, s		2^1	20.2	2.18
3^1	106.41	CH	6.11, 1H, bs		2^1	105.7	6.21
4^1a	104.18	C				103.2	
5^1a	108.09	C				104.9	
6^1	160.92	C				158.6	
6^1a	55.13	CH_3	3.98, 3H, s		6^1, 7^1	55.1	3.84
7^1	96.88	CH	6.53, 1H, bs		8^1, 9^1	96.5	6.15
8^1	161.95	C				159.5	
8^1a	54.21	CH_3	3.63, 3H, s		8^1	50.3	3.95
9^1	96.09	CH	6.27, 1H, bs		7^1, 8^1, 8^1a	96.6	6.58
10^1	105.62	C				110.4	

[a] in CD3OD at 200 MHz

[b] in CD3OD at 800 MHz

Table 4.2.4.3.1. Top ten structural candidates based on deviation of ^{13}C experimental chemical shifts with those calculated by the Structure Elucidator using HOSE code (d_A) algorithm.

1 (ID:846) 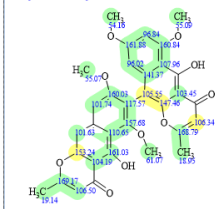	2 (ID:799) 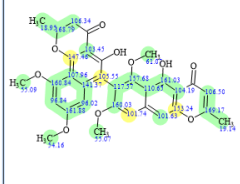	3 (ID:782) 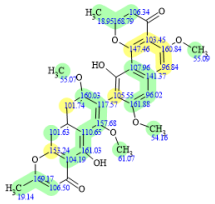	4 (ID:881) 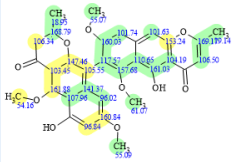	5 (ID:573) 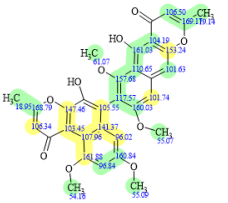
$d_N(^{13}C+^1H)$: 3.685 $d_A(^{13}C)$: 1.561 (v.14.50) $d_N(^{13}C)$: 1.536 PS ID: 3	$d_N(^{13}C+^1H)$: 4.045 $d_A(^{13}C)$: 1.948 (v.14.50) $d_N(^{13}C)$: 1.757 PS ID: 1	$d_N(^{13}C+^1H)$: 4.429 $d_A(^{13}C)$: 2.593 (v.14.50) $d_N(^{13}C)$: 2.220 PS ID: 4	$d_N(^{13}C+^1H)$: 4.690 $d_A(^{13}C)$: 2.700 (v.14.50) $d_N(^{13}C)$: 2.429 PS ID:	$d_N(^{13}C+^1H)$: 5.541 $d_A(^{13}C)$: 2.721 (v.14.50) $d_N(^{13}C)$: 2.751 PS ID:
6 (ID:814) 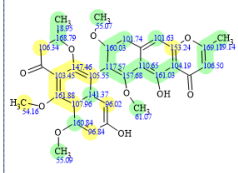	7 (ID:546) 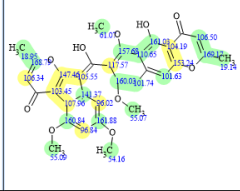	8 (ID:691) 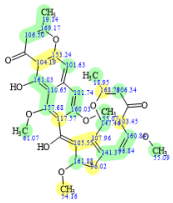	9 (ID:248) 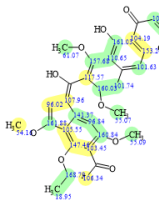	10 (ID:739) 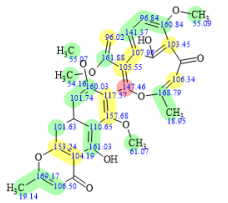
$d_N(^{13}C+^1H)$: 4.616 $d_A(^{13}C)$: 2.739 (v.14.50) $d_N(^{13}C)$: 2.333 PS ID:	$d_N(^{13}C+^1H)$: 5.187 $d_A(^{13}C)$: 2.977 (v.14.50) $d_N(^{13}C)$: 2.823 PS ID:	$d_N(^{13}C+^1H)$: 5.503 $d_A(^{13}C)$: 3.035 (v.14.50) $d_N(^{13}C)$: 3.326 PS ID:	$d_N(^{13}C+^1H)$: 5.856 $d_A(^{13}C)$: 3.045 (v.14.50) $d_N(^{13}C)$: 3.485 PS ID:	$d_N(^{13}C+^1H)$: 5.988 $d_A(^{13}C)$: 3.090 (v.14.50) $d_N(^{13}C)$: 3.652 PS ID:

4.3 Conclusion

This chapter describes the isolation and the characterisation of antibiofilm compounds from two bioactive samples: *Aspergillus niger* WNS7(8)F3 and *Aspergillus fumigatus* WNS16(8)F2. Using bioassay guided fractionation in conjunction with advanced chromatographic techniques (VLC, size exclusion chromatography (SEC), and high-performance liquid chromatography (HPLC)), several bioactive fractions were focused down and purified to the level of structurally diverse, complex compounds.

A combination of high-resolution mass spectrometry (HRMS), 1D and 2D NMR spectroscopy, and MS/MS fragmentation analysis identified the unknown compound *Aspergillus niger* WNS7(8)F3 D 13 s4-6 ssF-X cD sss9-11 H1 as Pyrophen. Nine degrees of unsaturation and the molecular formula $C_{16}H_{17}NO_4$ indicated a monosubstituted benzene ring and a disubstituted lactone moiety. These structural features were also supported by COSY and HMBC correlations. The elucidation of the structure of Pyrophen further shows that combinations of spectral techniques and database comparisons are useful for resolving structural ambiguities.

A high degree of unsaturation and a low proton to carbon ratio made *Aspergillus niger* WNS7(8)F3 D 13 s4-6 ssF-X cD sss9-11 H3 ($C_{32}H_{26}O_{10}$) a highly structurally complex compound. Limited HMBC correlations made it difficult to assemble the structure; however, integration of bioinformatics tools like the Antimarin database and computational analysis via the ACD/Labs Structure Elucidator strongly suggested it to be Asperpyrone C. This assignment was further supported by minimal deviation in 13C chemical shifts (dA < 3.0 ppm).

Aspergillus niger WNS7(8)F3 D 13 s4-6 ssF-X cD sss9-11 H4 was also highly similar to *Aspergillus niger* WNS7(8)F3 D 13 s4-6 ssF-X cD sss9-11 H3 and thus posed similar problems for elucidation. Computational structure generation identified Aurasperone A as the best fitting candidate with a

deviation (dA = 1.54 ppm) indicating strong agreement between experimental and predicted chemical shifts. These findings also illustrate the power of modern computational tools in overcoming challenges posed by complex natural product structures.

The results in this chapter further support the use of natural products as sources of novel antibiofilm agents to help address the problem of biofilm associated infections. Even though, in the literature the isolated compounds have shown no biofilm inhibition, the structural elucidation of compounds such as Pyrophen, Asperpyrone C and Aurasperone A still illustrates the usefulness of combining biological assays with advanced analytical techniques including HRMS, 1D/2D NMR and computational structure prediction. Thus, these results contribute to the growing evidence that natural products are valuable reservoirs of therapeutic agents. In addition, this research opens up new avenues for further investigation of microbial diversity and natural product biosynthesis as sources of new drug candidates. This research also describes a method of bioassay guided fractionation in conjunction with advanced structural elucidation methods to develop novel antibiofilm strategies with potential importance in the fight against antibiotic resistance and the improvement of therapeutic outcomes.

CHAPTER 5 Results and Discussion - Acetylcholinesterase inhibitory active samples

5.0 Introduction

Acetylcholinesterase (AChE) functions as a vital enzyme in the cholinergic nervous system to rapidly break down neurotransmitter acetylcholine (ACh) into choline and acetate at synaptic junctions. The enzyme AChE terminates neuronal signals to maintain proper neuromuscular function and cognitive processes including memory and learning. The inhibition of AChE results in increased ACh levels in synaptic clefts which strengthens cholinergic transmission, and this mechanism is used to treat neurodegenerative diseases including Alzheimer's disease (AD) and myasthenia gravis as well as pesticide and nerve agent toxicity.

Natural products have traditionally provided a vast collection of AChE inhibitors (AChEIs) which include alkaloids such as galantamine and physostigmine alongside terpenoids and flavonoids and phenolic derivatives. The inhibitors show different mechanisms of action (MOA) which include competitive, non-competitive and mixed-type inhibition and they bind to the catalytic active site (CAS) or peripheral anionic site (PAS) of AChE. Some natural AChEIs demonstrate additional therapeutic properties including anti-inflammatory and antioxidant effects and neuroprotective actions which make them suitable for developing multitarget therapeutic approaches in neurodegenerative diseases.

The present work presents a total procedure for the isolation, biological evaluation, and chemical identification of the metabolites produced by microorganisms with potential acetylcholinesterase (AChE) inhibitory activity. The role of bioassay-guided fractionation in conjunction with sophisticated chromatographic techniques in identifying potential bioactive agents is also described. The process begins with the identification and selection of microbial strains that have a strong AChE inhibitory activity, which is very desirable for the treatment of neurodegenerative diseases such as Alzheimer's.

Based on the bioassay data, fractionation procedures were used to increase the concentration of active components and to isolate them. Liquid–liquid partitioning, size-exclusion chromatography, and high-performance liquid chromatography (HPLC) were applied to separate compounds according to their physicochemical properties at different stages of this process. This ultimate step of the process was to obtain pure compounds that could be subjected to chemical analysis. These pure compounds were analysed to determine their structures using very sophisticated analytical methods. High-resolution mass spectrometry (HR-MS/MS) was used for the exact mass measurement and fragmentation which gave information on the molecular formula and structure of the compounds. One-dimensional (1D) and two-dimensional (2D) nuclear magnetic resonance (NMR) spectroscopy, including ^{1}H and ^{13}C NMR, COSY, HSQC, HMBC, and NOESY, was also performed to establish the detailed structural features of the compounds and to confirm the assignments. This chapter also reveals the potential of bioassay-guided approaches combined with modern analytical methods for identifying and characterizing natural products with biological activity. The results obtained in this study not only contribute to the knowledge of AChE inhibitory natural products but also illustrate the effectiveness of systematic approaches in the study of natural products.

5.1 Sample selection based on activity

Based on the acetylcholinesterase inhibition screening, the microbial strains *Aspergillus niger* HS4(50)F3 and *Aspergillus* fumigatus JA13, exhibited the highest acetylcholinesterase inhibition activity, and were selected for large scale fermentation and further analysis.

5.2 Bioassay guided fractionation of active strains

5.2.1 Fractionation and biological evaluation of *Aspergillus niger* HS4(50)F3 and *Aspergillus fumigatus* JA13 (acetylcholinesterase inhibition activity)

The crude microbial extracts of *Aspergillus niger* HS4(50)F3 *Aspergillus fumigatus* JA13 were first extracted using ethyl acetate, followed by Kupchan fractionation[112], where each microbial crude extract was partitioned into five fractions, Water-water (WW), water-butanol (WB), methanol (FM), DCM (FD) and hexane (FH), to form ten Kupchan fractions, five from each extract (Fig.).

A colorimetric acetylcholinesterase inhibitor screening kit was used to measure the % inhibition of all ten Kupchan fractions from both samples. The results showed that the fraction with the highest activity was the HS4(50)F3 fraction (**Table 5.2.1.1**, **Figure 5.2.1.1**).

Table 5.2.1.1. Percentage acetylcholinesterase inhibition of most active Kuphan fractions from *Aspergillus niger* HS4(50)F3 and *Aspergillus fumigatus* JA13 (0.1mg/mL).

Sample fraction	% acetylcholinesterase inhibition
HS4(50)F5 FD	50.0
JA13 WW	43.8

JA13 WB	43.8
JA13 FM	43.8
JA13 FD	37.5

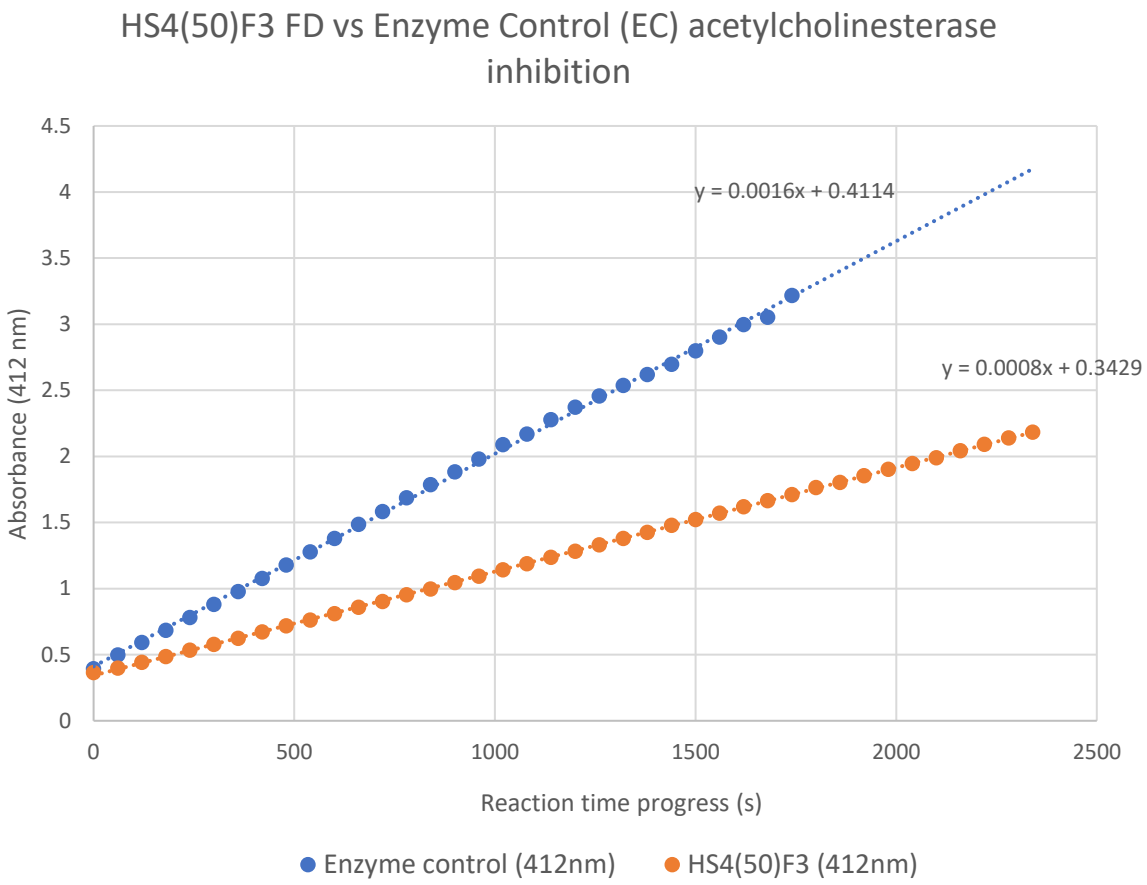

Figure 5.2.1.1. Graph of the relative absorbance at 412 nm of both the Enzyme Control (EC) uninhibited reaction (blue) and the reaction with HS4(50)F3 FD as an inhibitor (orange), clearly showing the slowed reaction rate through the lower gradient of the HS4(50)F3 FD inhibited reaction.

Size exclusion chromatography (SEC) was then performed on the HS4(50)F3 FD fraction. SEC was carried out using a LH-20 Sephadex stationary phase using 5 different columns with varying solvent systems. Column 1 used a MeOH:DCM 50:50 mobile phase, column 2 used a MeOH:ACN 50:50 mobile phase, and columns 3, 4 and 5 used a MeOH:ACN 60:40 mobile phase. Column 1 fractions were pooled as follows: 1-2, 3-4, 5-6, 7, 8-10, 11, 12-14. Column 2 fractions were pooled as follows: 1, 2, 3-4, 5, 6-7, 8-10, 11-12, 13, 14-15, 16-17, 18. Columns 3, 4 and 5 fractions were all added together number wise across the columns, and were pooled as follows: 1-2, 3-4, 5-6, 7-8, 9-10, 11-14, 15-18, 19-23 (**Figure 5.2.1.2**, **Figure 5.2.1.4**). The fractions from columns 3,4 and 5 were screened for acetylcholinesterase inhibition activity, using the same kit as mentioned above. With the fraction HS4(50)F3 FD 345 s11-14 identified as most active (**Table 5.2.1.2**).

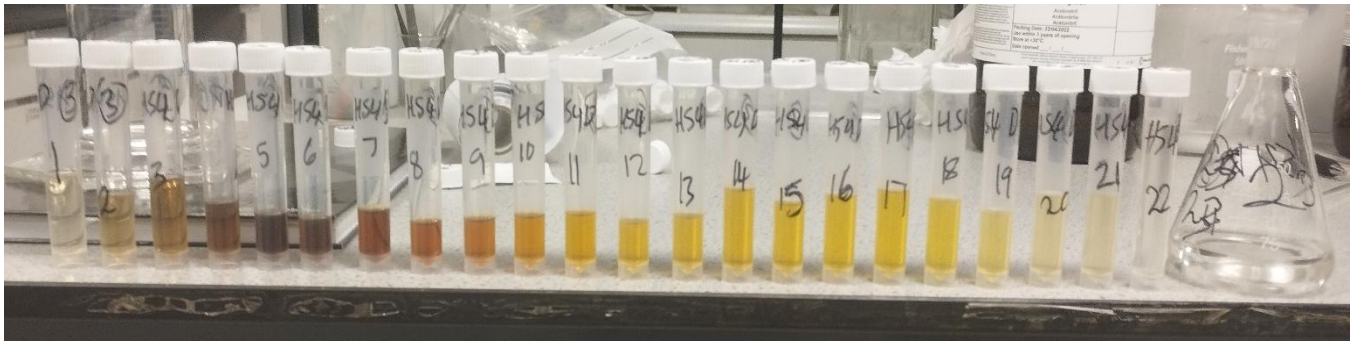

Figure 5.2.1.2. SEC fractions from column 3, numbered 1 to 23.

Table 5.2.1.2. Percentage acetylcholinesterase inhibition of most active Kuphan fractions from the *Aspergillus niger* HS4(50)F3 FD 345 fraction. Fraction HS4(50)F3 FD 345 s11-14 was seen to be the most active.

SEC fraction	% inhibition
5-6	12.5
9-10	12.5
11-14	25
19-23	12.5

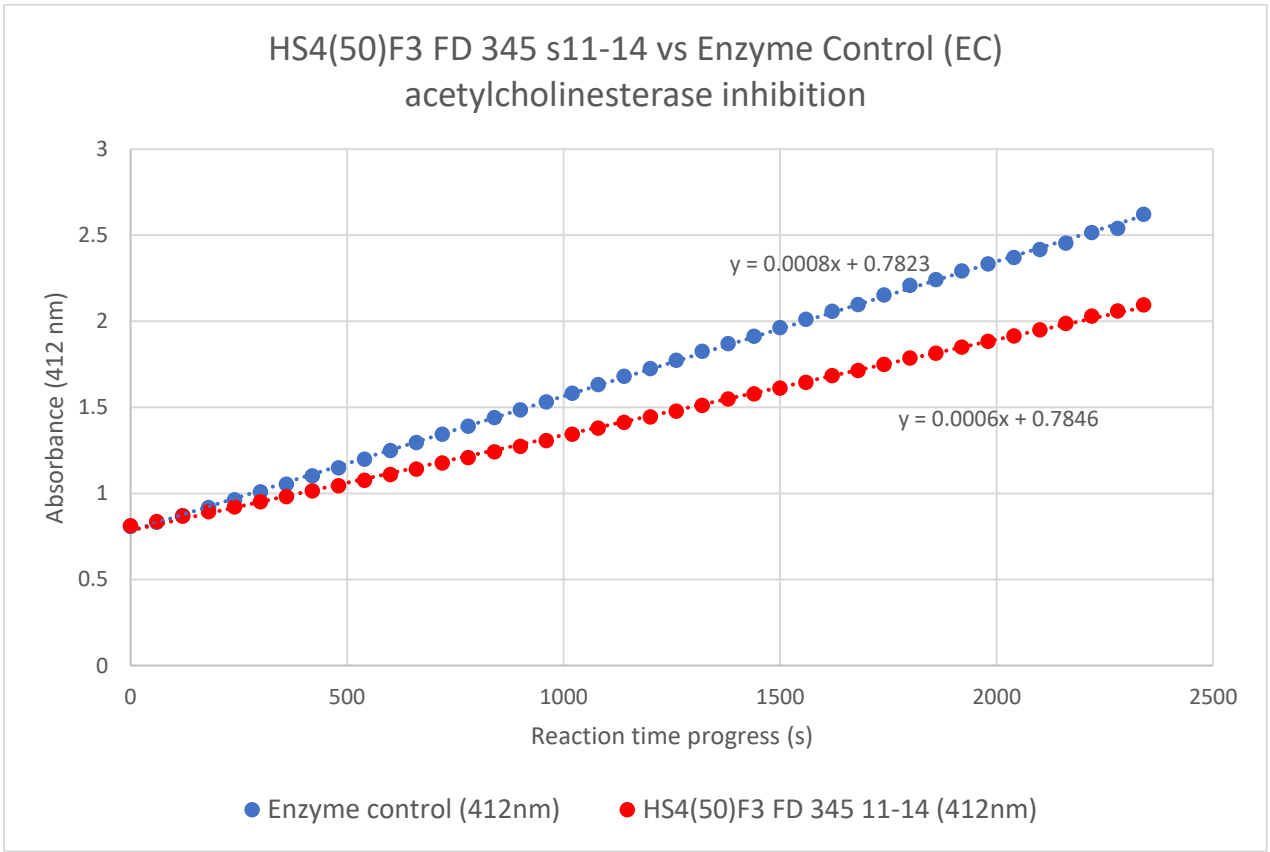

Figure 5.2.1.3. Graph of the relative absorbance at 412 nm of both the Enzyme Control (EC) uninhibited reaction (blue) and the reaction with the fraction HS4(50)F3 FD 345 s11-14 as an inhibitor

(red), clearly showing the slowed reaction rate through the lower gradient of the HS4(50)F3 FD 345 s11-14 inhibited reaction.

For HS4(50)F3 FD 345 s11-14, SEC was carried out using a LH-20 Sephadex stationary phase and a MeOH:ACN 40:60 mobile phase. SEC of HS4(50)F3 FD 345 s11-14 formed 18 fractions. These fractions were pooled as follows: 1-3, 4-8, 9, 10-13 14-15, 16-18 (Fig 3.6.2.1.4).

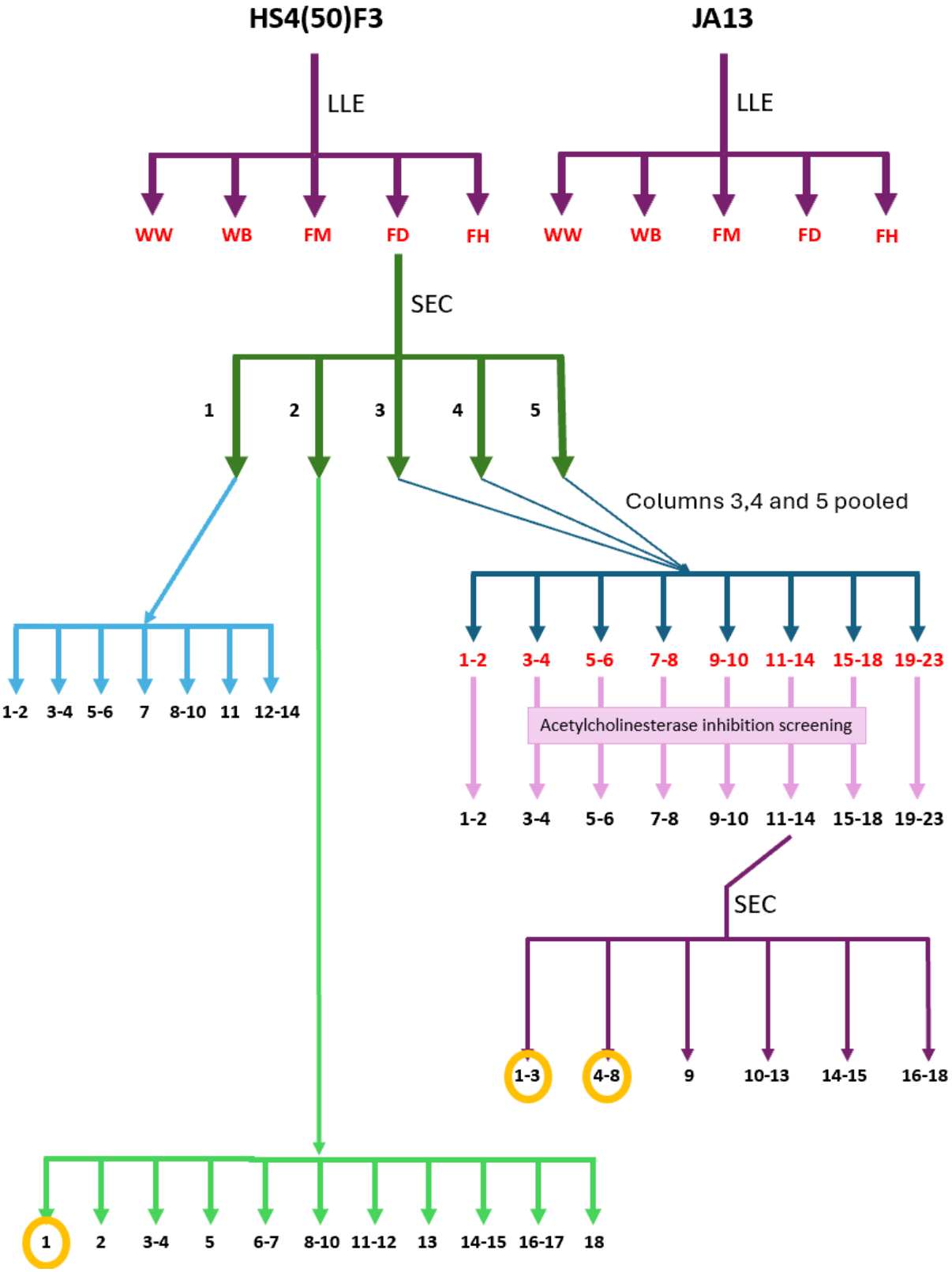

Figure 5.2.1.4. Flow chart of the fractionation of the crude extract of *Aspergillus niger* WNS7(8)F3. All red coloured fractions were further biologically screened against the acetylcholinesterase inhibitory target, and all fractions with an orange circle around are further pursued: HS4(50)F3 FD 2 s1 was pure after SEC, and HS4(50)F3 FD 345 s11-14 ss1-3 and ss4-8 were further purified using HPLC. LLE: Liquid-

Liquid Chromatography (Kupchan), and SEC: Size Exclusion Chromatography.

All fractions were analysed by ^{1}H NMR and fractions ss1-3 and ss4-8 were chosen to be the fractions pursued in further isolation.

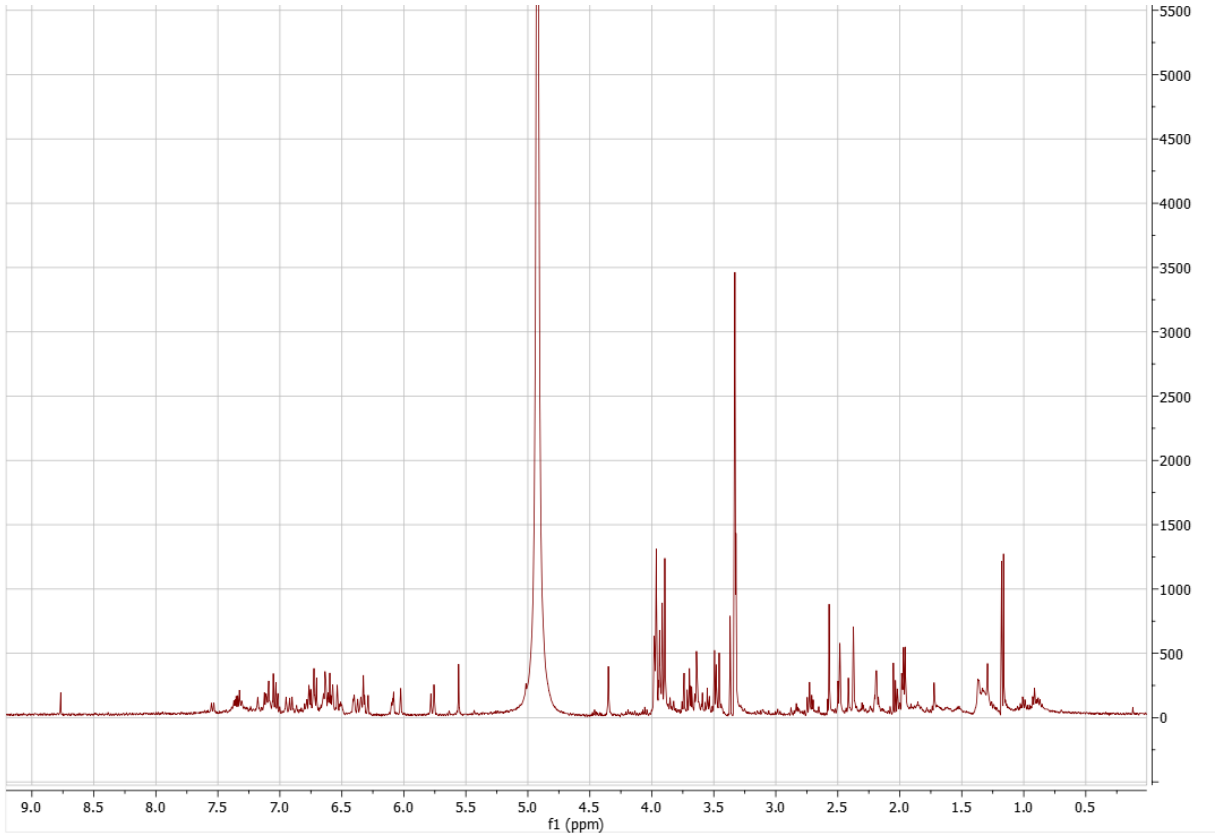

Figure 5.2.1.5. ^{1}H NMR spectra of HS4(50)F3 FD 345 s11-14 ss1-3.

The ^{1}H NMR spectrum of HS4(50)F3 FD 345 s11-14 ss1-3 (**Figure 5.2.1.5**) is noteworthy for several reasons. Firstly, it suggests the presence of multiple compounds in significant quantities, making them viable candidates for isolation and successful structural analysis. The signals observed between 5.5 and 8.0 ppm indicate the presence of unsaturated and/or aromatic compounds, while the chemical shift at approximately 8.8 ppm reveals a highly deshielded proton, further supporting the structural complexity of the sample.

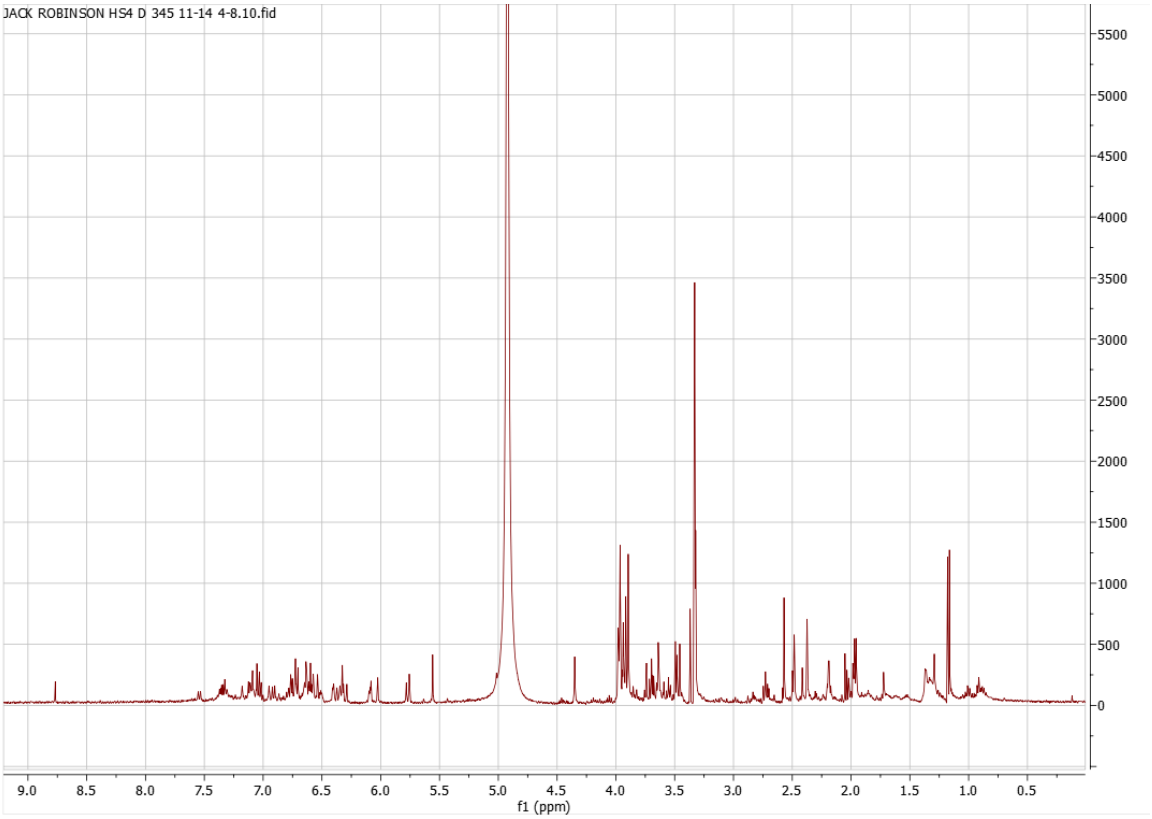

Figure 5.2.1.6. ^{1}H NMR spectra of HS4(50)F3 FD 345 s11-14 ss4-8.

The ^{1}H NMR spectrum of HS4(50)F3 FD 345 s11-14 ss4-8 (**Figure 5.2.1.6**) shares the same qualities as the previously mentioned ss1-3, indicating similar, if not the same compounds found in both fractions. The presence of multiple compounds in significant quantities, indicates the initial value of the fraction. The signals observed between 5.5 and 8.0 ppm indicate the presence of unsaturated and/or aromatic compounds, while the chemical shift at approximately 8.8 ppm reveals a highly deshielded proton, further supporting the structural complexity of the sample.

Reverse phase HPLC was carried out on both the ss1-3 (**Figure 5.2.1.7**) and ss4-8 (**Figure 5.2.1.8**) fractions. Method used for both fractions: An Xselect CSH 130 Prep C18 5um 10x250 mm column was used as the stationary phase. The solvent system used was A (100% H_2O + 0.05% TFA) and B (100% MeOH) on an isocratic system of 72% B from t = 0.00 to t = 10.00 mins, followed by gradient system of 72% A to 80% B from t = 10.00 to t = 11.00 mins, and finally an isocratic system of 80% B between t= 11.00 and t = 35.00 mins.

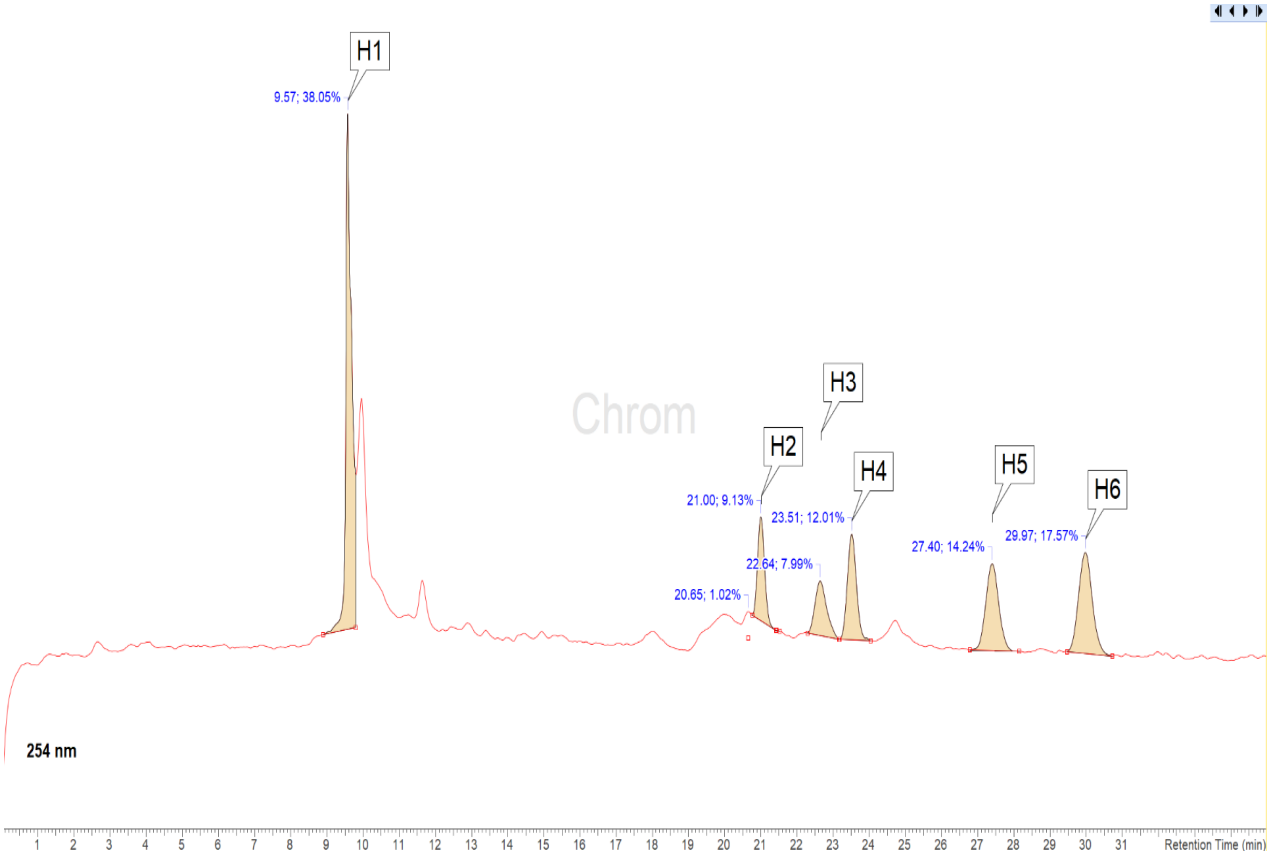

Figure 5.2.1.7. HPLC chromatogram for HS4(50)F3 FD 345 s11-14 ss1-3, absorbance measured at 254 nm. Six pure compounds isolated in total, labelled H1-6.

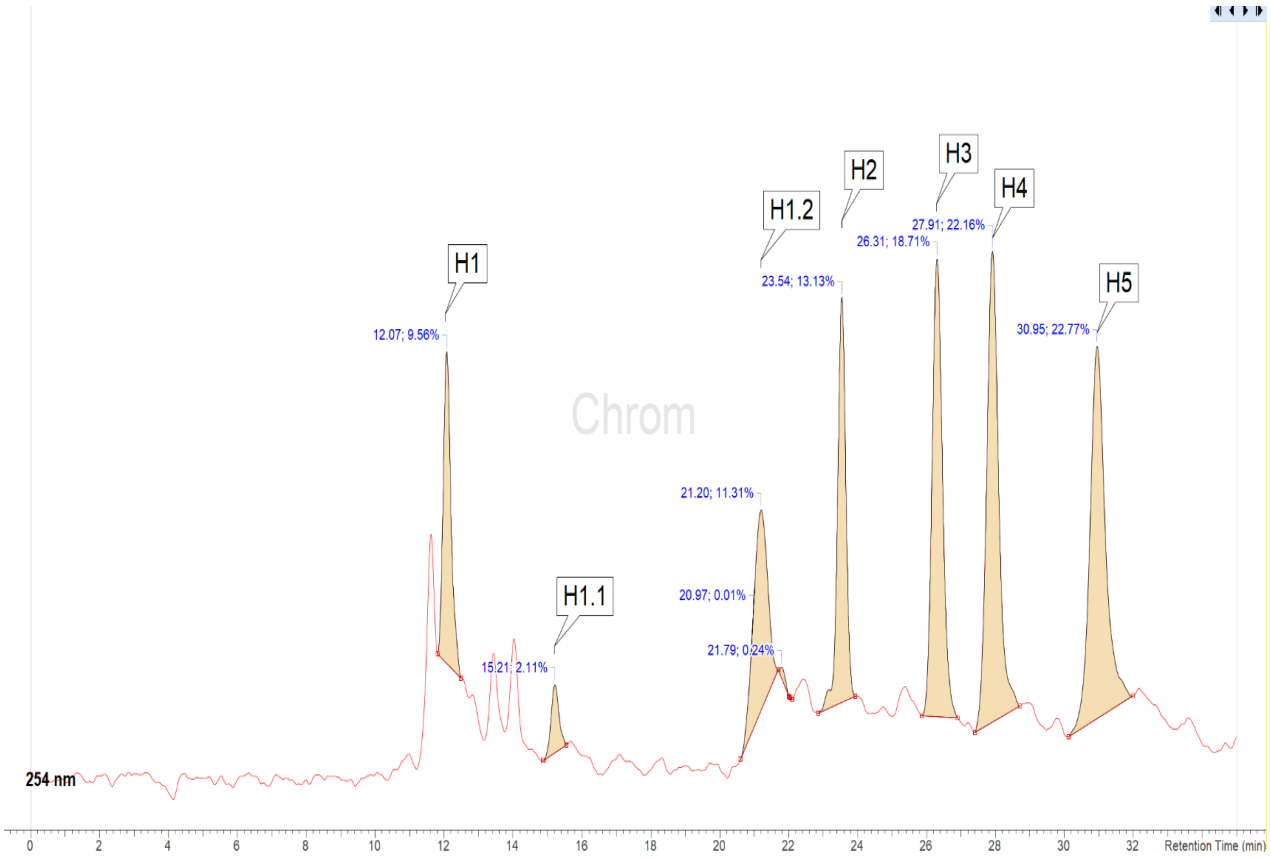

Figure 5.2.1.8. HPLC chromatogram for HS4(50)F3 FD 345 s11-14 ss4-8, absorbance measured at 254 nm. Seven pure compounds isolated in total, labelled H1, 1.1, 1.2, 2, 3, 4, 5.

From the retention times and the UV profiles of the compounds, it was quickly noted that the corresponding numbers for ss1-3 and ss4-8 were the same compounds. However, H6 was not found in ss4-8, and ss4-8 H1.1 and H1.2 were also isolated from ss4-8 and not from ss1-3.

^{1}H NMR of all isolated compounds was conducted, and from this data, two pure compounds were seen to have the most chemical potential, were chosen to be structure elucidated to completion, and pursued for further biological screening. Some of the isolated compounds such as 1, 2, 3, 4 and 5 were seen to be the same compounds and had identical NMR spectra identical MS spectra. These chosen compounds were HS4(50)F3 FD 345 s11-14 ss1-3 H4 (**Figure 5.2.1.9**) and HS4 FD 2 s1 (**Figure 5.2.1.10**).

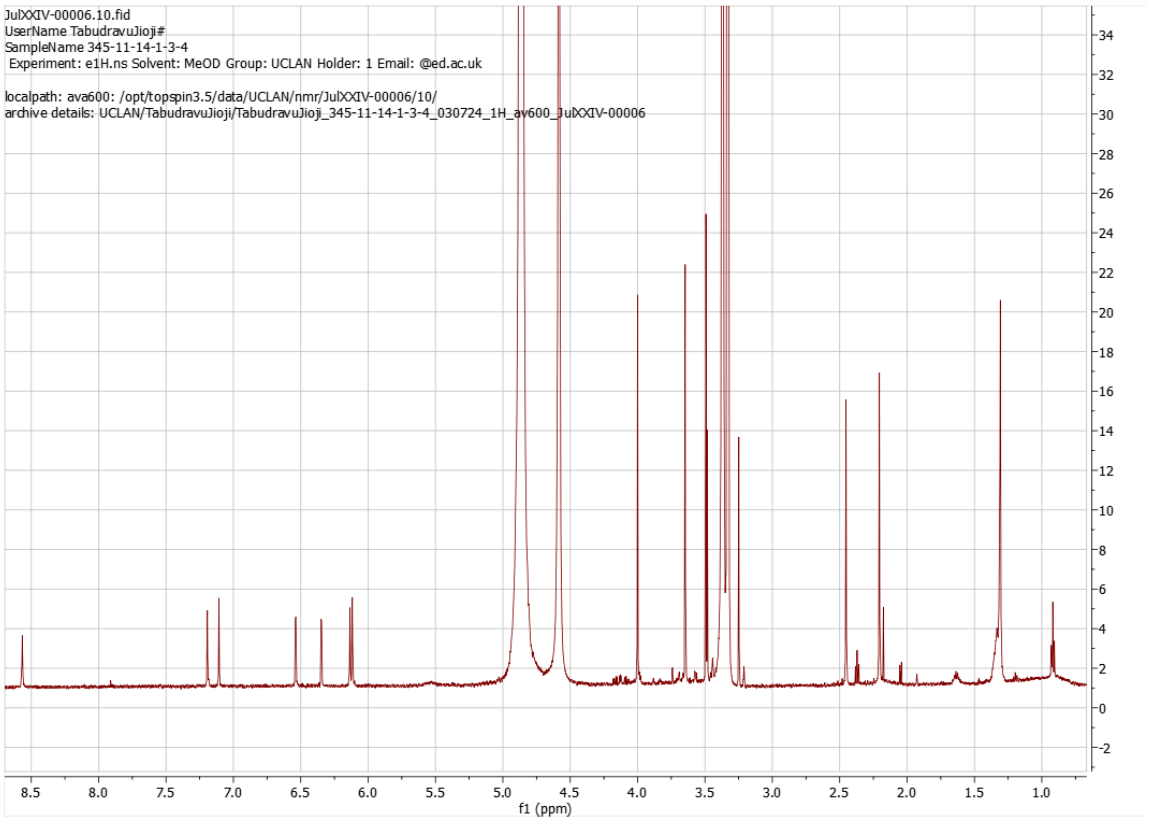

Figure 5.2.1.9. ^{1}H NMR spectra of the pure compound HS4(50)F3 FD 345 s11-14 ss1-3 H4.

The ^{1}H NMR spectrum of HS4(50)F3 FD 345 s11–14 ss1–3 H4 (**Figure 5.2.1.9**) is particularly noteworthy. The spectrum contains sharp peaks, which suggests high purity with only minimal impurities, making the compound suitable for isolation and further structural analysis. Aromatic moieties are indicated by signals observed between 6.0 and 8.7 ppm, and the signals in the 3.5 to 4.0 ppm range suggest the presence of methoxy groups. These features collectively highlight the complexity of the molecule.

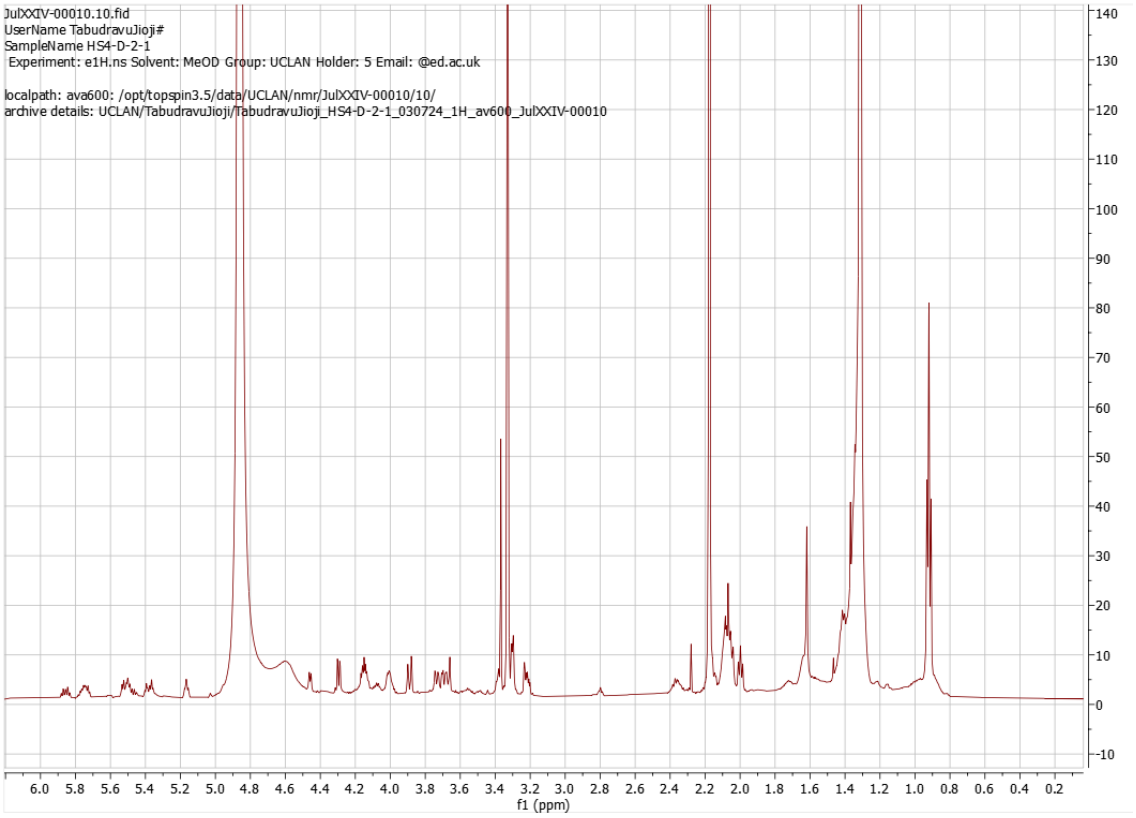

Figure 5.2.1.10. ^{1}H NMR spectra of the pure compound HS4(50)F3 FD 2 s1.

The ^{1}H NMR spectrum of HS4(50)F3 FD 2 s1 (**Figure 5.2.1.10**) has several characteristics that are worth mentioning. First of all, it appears as a pure spectrum with only minimal impurities which make it a good candidate for isolation and for the purpose of structural analysis. The appearance of the signals between 5.0 and 6.0 ppm indicates the presence of unsaturated bonds, and the deshielded methylene protons give signals between 3.5 and 4.0 ppm, which are both an indication of a complex molecular structure.

5.3 Chemical profiling

5.3.1 Structure elucidation of *Aspergillus niger* HS4(50)F3 FD 2 s1

This part of the thesis describes the elucidation of the chemical structure of HS4(50)F3 FD 2 s1 one of the pure compounds isolated from the anti-acetylcholinesterase active fraction described in Chapter 5.

The compound showed a high resolution HRMS of m/z = 524.2860 [M-H]-, Δ = -0.96 ppm, calculated for $C_{27}H_{43}NO_9$ and requiring 7° of unsaturation (See Supplementary). It also displayed HRMS of m/z of 526.3010 (M+H)+, Δ = -0.11 ppm in the positive mode (See Supplementary). Interpretation of ^{1}H, COSY, HSQC and HMBC (Figures S28-32) indicated the presence of seven *sp*2 methines, eight *sp*3 methines, nine *sp*3 methylenes, one *sp*3 methyl, and two *sp*2 quaternary carbons leading to the sub-formula of $C_{27}H_{36}$ suggesting the presence of seven exchangeable protons in the structure. The presence of seven *sp*2 methines (δ_C 133.4, 133.1, 133.1, 129.8, 129.5, 127.5, 123.4), eight *sp*3 methines (δ_C 103.2, 76.5,

76.5, 73.6, 72.6, 71.4, 70.0, 53.2), nine methylenes (δ_C 68.2, 61.2, 39.4, 33.5, 32.4, 31.9, 31.6, 27.7, 24.7), two *sp*2 quaternaries (δ_C 174.1, 135.4) accounted for five of the seven double bond equivalents suggesting the presence of two rings to complete the 7° of unsaturation in the structure of this compound. Intensive analysis of 1D and 2D NMR spectrum enabled the construction of 2 substructures. ^{13}C carbon chemical shift for a protonated carbon (C-1') at dC 103.2 ppm, and δ_H 4.29 ppm is indicative of presence of a glucose unit. COSY and HMBC correlations helped assigned subunits A and B. The unusual ^{13}C chemical shift at δ_C 53.2 ppm for C-19 suggested that this carbon is linked to a nitrogen atom. A COSY correlation of an exchangeable proton at δ_H 7.73 ppm and H-19 suggest the presence of an amide NH adjacent to C-19.

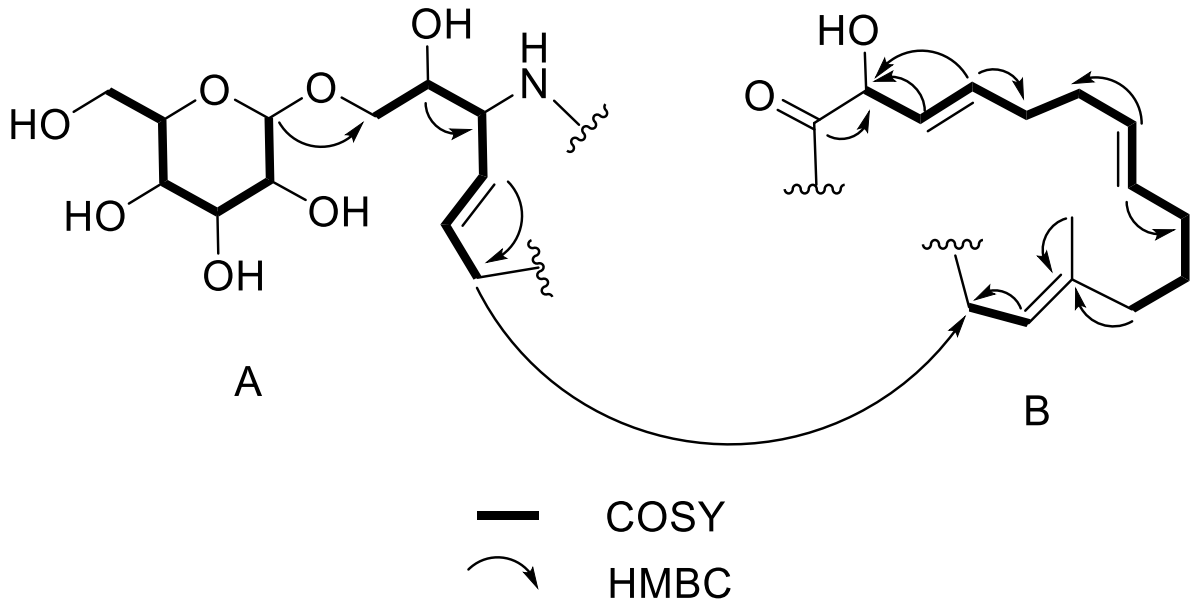

Figure 5.3.1.1. Substructures A and B of *Aspergillus niger* HS4(50)F3 FD 2 s1 with COSY and HMBC correlations.

Long range HMBC correlations and a COSY correlation between H-1 and H-19 linked substructures A to B (**Table 5.3.1.1, Figure 5.3.1.1.**). This is a new compound and the closest similarity to this framework are the vicenistatins isolated from *Streptomyces* sp. HC34[122] (**Figure 5.3.1.3)** which contains amino sugars rather than glucose as in the case of HS4-2-1. Stereochemistry of the three stereocentres (C-3, C19 and C-20) and the sugar unit have not been determined and will be the subject of further studies in order to publish this work in a peer reviewed journal.

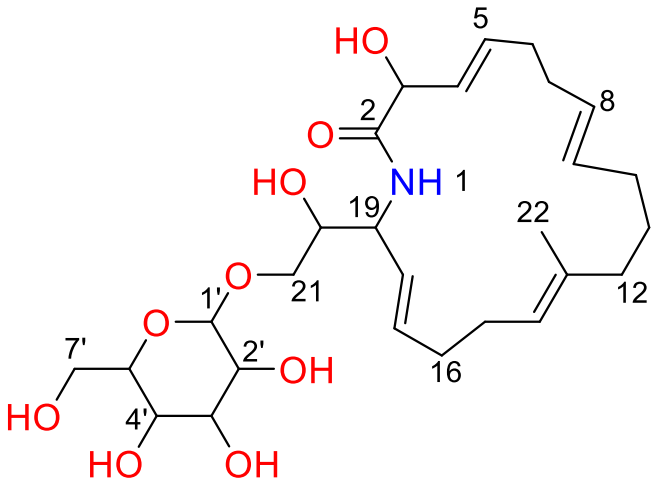

Figure 5.3.1.2. Proposed structure for *Aspergillus niger* HS4(50)F3 FD 2 s1.

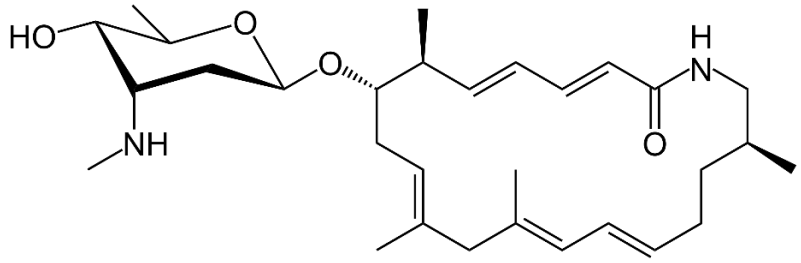

Figure 5.3.1.3. Structure of Vicenistatin.

Table 5.3.1.1. NMR table for *Aspergillus niger* HS4(50)F3 FD 2 s1.

Position	^{13}C Chemical shift (ppm)[a]	C-type	^{1}H (chemical shift ppm, No. of H, multiplicity, coupling)[b]	COSY (^{1}H-^{1}H)	HMBC (^{1}H-^{13}C)
1		NH	7.71, 1H, d, J = 9.1Hz	19	
2	174.07	C			
3	72.58	CH	4.45, 1H, d, J = 6.4Hz	4	2, 4, 5
4	127.51	CH	5.61, 1H, m	3, 5	
5	133.39	CH	5.86, 1H, m	4, 6	3
6	33.45	CH_2	2.35, 2H, bm	5, 7	4, 5, 8
7	32.36	CH_2	2.06, 2H, bm	6, 8	
8	129.48	CH	5.37, 1H, m	7, 9	
9	133.10	CH	0.92, 3H, s	8, 10	
10	31.64	CH_2	1.30, 2H, bm	9, 11	
11	24.66	CH_2	1.63, 1H, m 1.41, 1H, m (overlap with 15)	10, 12	
12	39.42	CH_2	1.99, 2H, t, J = 7.8Hz	11	14
13	135.42	C			
14	123.43	CH	5.16, 1H, t, J = 7.2Hz	15	13, 22
15	27.65	CH_2	1.40, 2H, m (overlap with 11)	14	18
16	31.90	CH_2	2.06, 2H, m		17
17	129.79	CH	5.49, 1H, m		18, 20
18	133.05	CH	5.75, 1H, m		17, 20
19	53.24	CH	4.00, bm	1	
20	71.36	CH	4.15, 1H, m		18
21	68.16	CH_2	A: 4.14, 1H, m B: 3.73, 1H, m		18, 20
22	14.83	CH_3	1.61, 3H, s		
1_1	103.19	CH	4.29, 1H, dd, J = 7.87Hz, 2.13Hz	2_1	21
2_1	73.55	CH	3.21, 1H, m	1_1, 3_1	1_1, 3_1
3_1	76.52	CH	3.38, 1H, bm	2_1, 4_1	4_1
4_1	70.04	CH	3.30, 1H, d, J = 5.6Hz	3_1, 5_1	5_1
5_1	76.52	CH	3.29, 1H, bm	4_1, 6_1	
6_1	61.23	CH_2	A: 3.88, 1H, d, J = 11.8Hz B: 3.68, 1H, dd,	5_1	

			J = 12.0, 4.9Hz		

[a] in CD_3OD at 200 MHz

[b] in CD_3OD at 800 MHz

5.3.2 Structure elucidation of *Aspergillus niger* HS4(50)F3 FD 345 s11-14 ss1-3 H4

The compound showed a high resolution HRMS of m/z = 555.1295 $[M-H]^-$, Δ = -0.31 ppm, calculated for $C_{31}H_{24}O_{10}$ and requiring 20° of unsaturation. (See Supplementary) Interpretation of ^1H, COSY, HSQC and HMBC (Figures S28-31) indicated the presence of seven sp^2 methines, five sp^3 methyls, and eleven sp^2 quaternary carbons leading to the sub-formula of $C_{23}H_{22}$ suggesting the presence of two exchangeable protons (-OHs) in the structure. The presence of seven sp^2 methines (δ_C 106.4, 106.4, 105.1, 103.7, 100.6, 96.9, 96.2), five sp^3 methyls (δ_C 61.1, 55.1, 54.2, 19.2, 19.0), and eleven sp^2 quaternaries (δC 169.1, 169.0, 168.9, 162.0 160.9, 158.3, 153.1, 117.3, 110.2, 108.1, 105.7) plus nine missing carbons (not observed in the HMBC spectrum (Figure S31), accounted for fourteen of the twenty double bond equivalents suggesting the presence of six rings to complete the 20° of unsaturation in the structure of this compound. Dereplication by molecular formula of the Antimarin database[115] showed seven 'hits', all showing compounds previously isolated from *Aspergillus* sp. (**Figure 5.3.2.2**). Preliminary analysis of the data suggests it could be anyone of these compounds, and hence other methods will need to be utilised to confirm the identity of this compound.

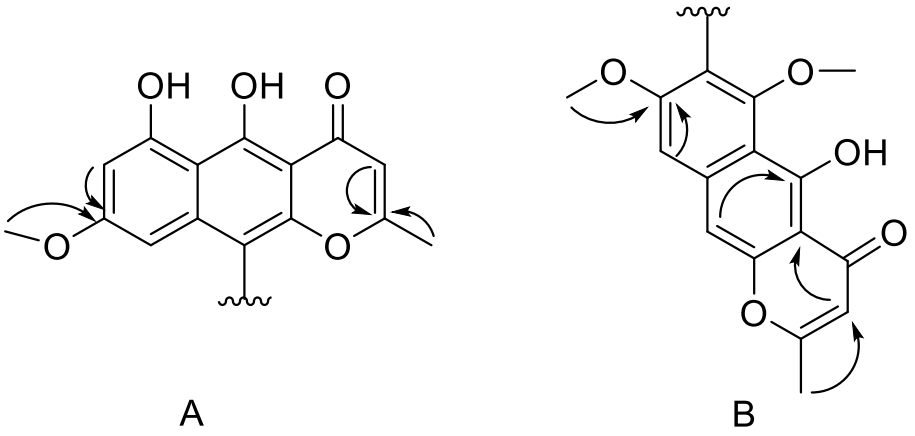

Figure 5.3.2.1. Substructures A and B of *Aspergillus niger* HS4(50)F3 FD 345 s11-14 ss1-3 H4 with main HMBC correlations.

Table 5.3.2.1. NMR table for *Aspergillus niger* HS4(50)F3 FD 345 s11-14 ss1-3 H4 in MeOD, alongside literature chemical shifts of Aurasperone D in DMSO.[121]

Position	^{13}C Chemical shift (ppm)	C-type	^1H (chemical shift ppm, No. of H, multiplicity, coupling)	COSY (^1H-^1H)	HMBC (^1H-^{13}C)	Literature ^{13}C (DMSO) Chemical shift (ppm)	Literature ^1H (DMSO) Chemical shift (ppm)

2	168.9	C				168.5	
2a	19.0	CH_3	2.21, 3H, s		2, 3	20.2	2.40
3	106.4	CH	6.13, 1H, s		2, 4a	105.6	6.21
4a	103.7	C				103.2	
5a	110.2	C				107.6	
7	117.3	C				96.4	6.52
8	158.3	C				157.8	
8a	61.1	CH_3	3.49, 3H, s		8	61.4	3.55
9	105.1	CH	7.11, 1H, s		5a, 7, 10	104.9	7.12
10	100.6	CH	7.19, 1H, s		4a, 5a, 9	115.7	
10a	153.1	C				151.4	
2^1	169.0	C				168.8	
2^1a	19.2	CH_3	2.45, 3H, s		2^1, 3^1	20.1	2.15
3^1	106.4	CH	6.12, 1H, s		4^1a, 5^1a, 7^1	106.7	6.20
4^1a	108.1	C				103.3	
5^1	169.1	C				160.4	
5^1a	105.7	C				108.5	
6^1	162.0	C				160.6	
7^1	96.9	CH	6.54, 1H, d 2.4Hz		5^1a, 8^1	96.7	6.25
8^1	160.9	C				159.5	
8^1a	55.1	CH_3	4.00, 3H, s		8^1	56.1	3.97
9^1	96.2	CH	6.35, 1H, d 2.4Hz			100.4	7.37

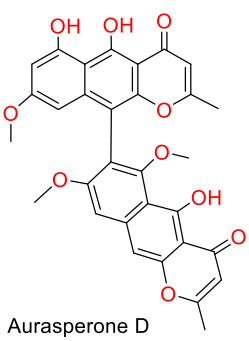

Aurasperone D
F] *Aspergillus niger*

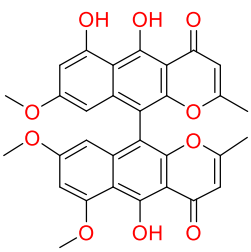

6-O-Demethylnigerone
[F] *Aspergillus niger*

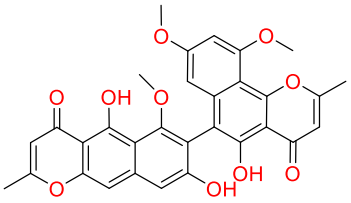

Asperpyrone D
[F] *Aspergillus tubingensis*

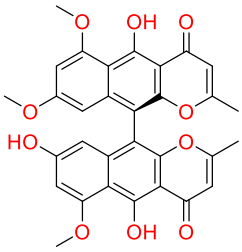

8'-O-demethylnigerone
Ascomycota Aspergillus carbonarius

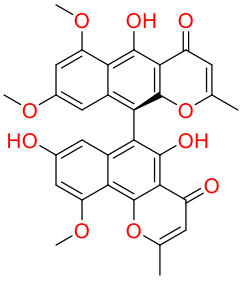

8'-O-demythylisonigerone
Ascomycota Aspergillus carbonarius

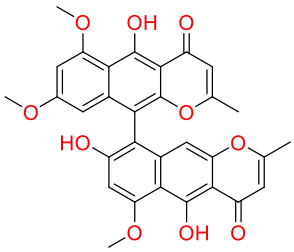

rubasperone A
Ascomycota Aspergillus tubingensis

Figure 5.3.2.2. Structures previously isolated from *Aspergillus* sp with molecular formula $C_{31}H_{24}O_{10}$.

ACD Labs Spectrus Predictor predicted 1H and 13C data for the various potential compounds, and Aurasperone D matched the data the best.

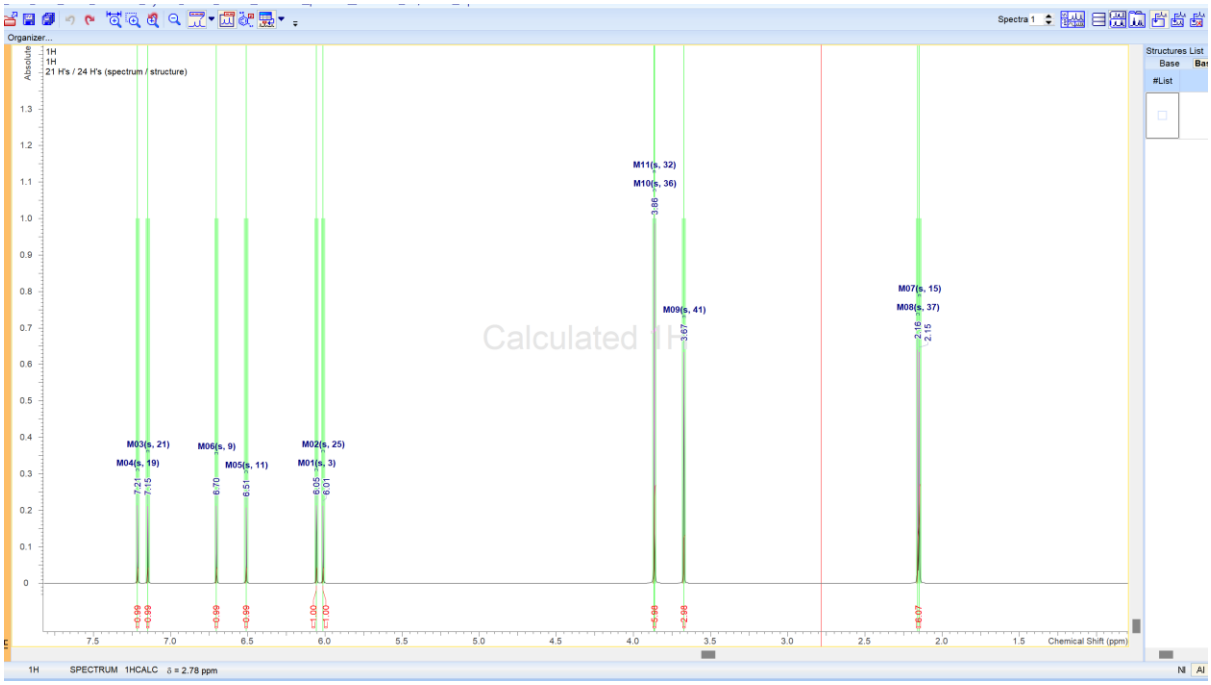

Figure 5.3.2.3. ACD Labs predicted data for Aurasperone D.

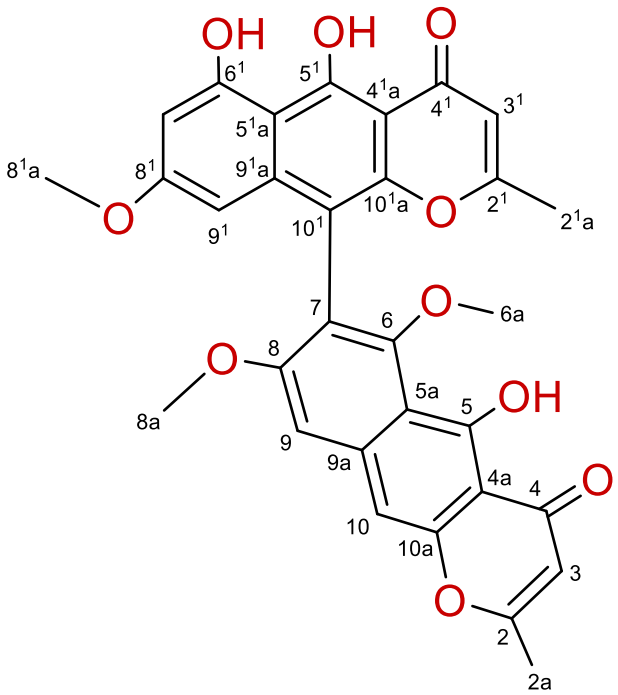

Figure 5.3.2.4. Proposed structure for HS4(50)F3 FD 345 s11-14 ss1-3 H4, Aurasperone D. Structure numbered according to Abdou et al 2024[121]

5.3.3 Conclusion

This chapter describes the isolation and the characterisation of potential acetylcholinesterase inhibitory compounds from two anti-Alzheimer's bioactive samples; *Aspergillus niger* HS4(50)F3 and *Aspergillus fumigatus* JA13. Using bioassay guided fractionation in conjunction with advanced chromatographic techniques (VLC, size exclusion chromatography (SEC), and high-performance liquid chromatography (HPLC) several bioactive fractions were focused down and purified to the level of structurally diverse, complex compounds. This chapter is an example of how advanced spectroscopic techniques and computational tools can be applied in natural product chemistry for the isolation and structural elucidation of two bioactive compounds, HS4(50)F3 FD 2 s1 and HS4(50)F3 FD 345 s11-14 ss1-3 H4 from anti-acetylcholinesterase active fractions. The structure of HS4-2-1 was determined as a novel compound with the molecular formula $C_{27}H_{43}NO_9$, which has a glucose moiety and a nitrogen containing substructure. This compound HS4-2-1 is related to vicenistatins, a class of amino sugar containing natural products and may offer novel biological activity. The stereochemical assignments of its three stereocentres and sugar unit remain unresolved, with CD spectroscopy due to be run; however, this compound can be considered as a promising candidate for the library of bioactive natural products and thus deserves further investigation. The spectroscopic analysis of HS4(50)F3 FD 345 s11-14 ss1-3 H4 gave the molecular formula $C_{31}H_{24}O_{10}$ and a highly unsaturated structure with six rings. Seven potential matches in the Antimarin database were reported by the initial dereplication efforts; Aurasperone D was predicted by computational methods to be the most likely candidate. This compound will also require further experimental validation to confirm its identity. These findings contribute to the ongoing exploration of bioactive natural products and highlight the value of combining traditional spectroscopic methods with modern computational tools to resolve complex

molecular structures. Future work will focus on the stereochemical analysis and biological activity profiling of these compounds and their publication to further understand their chemical and biological potential.

CHAPTER 6: Sample statistical analysis and novelty testing

6.0 Introduction

This chapter describes a two-step statistical analysis method for the metabolomic profiles from various samples based on their mass spectrometry (MS) data. The data processing begins with ACD Labs Spectrus, a powerful software that is used for the pre-treatment and visualization of the MS data. The next step uses the web-based FreeClust platform, which is used for statistical analysis and is employed to cluster the samples based on their MS profiles. This clustering was successful with respect to the sample collection sites, taxonomic classification, and biological activity, thus showing that this two-step process is capable of extracting relevant information from the data. In addition, for better understanding of the metabolites in the samples, AntiMarin (2012) natural product database was used and has been very helpful in identifying how many of the compounds present in the samples are new and how many are known. This step gives useful information that assists in selecting samples for further analysis and isolation based on the percentage novelty of samples. The novelty percentage is particularly useful for choosing the samples that are most likely to contain new natural products and in the early stages of natural product research and drug discovery.

6.1 Statistical analysis

6.1.1 Introduction

High performance liquid chromatography coupled to high resolution mass spectrometry (HPLC-HRMS) are tandem techniques used in analysing complex samples which include food, environmental matrices, biological fluids and natural products. LC-MS allows for the identification of the trace component, qualitative and quantitative analysis of compounds in the mixtures, and the metabolite fingerprinting.[123] The LC-MS technology has been developed and improved for higher sensitivity, robustness, automation, and data acquisition rates over the last quarter century, which makes it possible to analyse large numbers of samples and collect large data sets per analysis.[124]

Therefore, to manage these datasets, various software tools have been developed for the preprocessing tasks like peak picking and chromatogram deconvolution. There is, however, proprietary software that is offered by instrument vendors and which comes with data acquisition and processing capabilities; however, such software is limited to certain data formats.[125] Expert users can use XCMS or MZmine 3 for common uni-directional processing, while ACD/Spectrus is a multifunctional platform that is compatible with various analytical techniques and formats of vendor data. Nevertheless, most of the software suites are capable of solving only part of the processing problem, which means that there is always half of the workflow performed on a different software platform with respect to the other half.[126]

Natural product research is still hampered by the challenge of dereplication hence there are software

platforms such as the Global Natural Product Social Molecular Network (GNPS), which is a commonly used platform that uses raw or preprocessed MS/MS data. ACD Labs also has dereplication tools in spectral database searches. The analysis of the LC-MS data for comparative processing of the chromatograms, metabolite pattern identification, and sample classification involves the use of different techniques such as chromatogram cross-comparison, and data clustering. Preprocessing can be performed with XCMS and MZmine 2,[127] while more elaborate statistical analysis like PCA is only available in MetaboAnalyst which is suitable for users with prior knowledge of the tool.[128]

In addition to ACD Labs Spectrus and FreeClust, several other methodologies have been developed to address the complexity of LC-MS data processing in natural product research. Notably, software platforms such as MetaboAnalyst, MS-DIAL, and OpenMS offer comprehensive solutions for statistical analysis, metabolite annotation, and visualization of complex datasets. These tools contribute significantly to enhancing workflow efficiency and data interpretation. For instance, MetaboAnalyst facilitates advanced multivariate statistical analyses including PCA, PLS-DA, and hierarchical clustering, supporting more informed biological conclusions. MS-DIAL provides an open-source platform for untargeted metabolomics and lipidomics with capabilities for deconvolution, alignment, and identification using in-house or public MS/MS libraries. Similarly, OpenMS is a flexible and extensible framework designed for high-throughput LC-MS data analysis and integrates well with other bioinformatics tools. These complementary platforms not only expand the capabilities beyond vendor-restricted software but also highlight the importance of interoperability and open formats in analytical workflows. The integration of FreeClust into this ecosystem thus represents a valuable advancement, offering an accessible, user-friendly clustering approach that enhances comparative analysis and facilitates the interpretation of complex chromatographic datasets within a single coherent framework.[128]

To meet the challenges of the natural product discovery workflow, ACD Labs Spectrus[120] was used to combine data analysis and place all analytical data in a single software platform. The data mining process is divided into two steps. The first step uses IntelliXtract, an add-in tool integrated in ACD Labs Spectrus, and the second step uses FreeClust[129], an open source, web based clustering tool developed in the R language. The results are more easily interpretable because of the simplified comparison of data sets and streamlined results analysis enabled by the FreeClust flexible interface.

6.1.2 Methods

6.1.2.1 LCMS Separation.

The analyses were carried out at UCLan with an Agilent 6546 UHD series LC/QTOF mass spectrometer under the following conditions: Resolution (FWHM): up to 60,000 at m/z 922 (full width at half maximum), Gas temperature was set at 325°C, drying gas was set at 5.0 L/min, nebulizer pressure was set at 20 psi, capillary voltage was set at 4000 V, sheath gas temperature was set at 275°C, sheath gas flow was set at 12.0 L/min and nozzle voltage was set at 2000 V. The chromatographic separation was done on a Kinetex® 1.7 µm EVO C18 100 Å LC column (100 × 2.1 mm, S/No. H23-311228 5726-0046), column temperature was set at 40°C, with binary mobile phase of solvent A: H2O with 0.1% formic acid and solvent B: ACN with 0.1% formic acid. Injection volume was 4 µL. The flow rate was

kept constant at 0.400 mL/min, with the following gradient elution: From t = 0. 00 to 10.00 mins, 20% B to 100% B. From t = 10.00 to 12.00 mins isocratic system of 100% B. From t = 12.00 to 13.00 mins, 100% B to 20% B. Finally, from t = 13.00 to 15.00 mins, an isocratic system of 20% B. The equilibrium time between each injection was 10.0 mins. The instrument was operated in the automated positive MS mode, detecting precursor ions. The following reference masses were used for calibration: 121.0508773 (Purine, low ,ass reference) and 922.009798 (Hexakis, HP-921, high mass reference) in positive mode. The data acquisition was performed using Agilent MassHunter version 8.0.0 (Agilent Technologies, Waldbronn, Germany)[130], while all the mass spectrometry data were processed using ACD Labs Spectrus Processor[120] on a Dell personal computer with an 11th Gen Intel Core i7-11800H CPU with a clock speed of 2.30 GHz. The IntelliXtract (IX) add-in tool was employed with the following CODA settings: True Peak Signal-to Noise (S/N) Threshold was kept at 100 and the profile data was converted to centroid using Savitsky-Golay method, FFT shape was fixed, and the data analysis region was selected from a retention time (Rt) of 2 to 26 mins. FreeClust settings: Rescale data: log10(x), Convert missing values to zero, Hierarchical clustering, Dissimilarity measure: Euclidean, Linkage method: Average, Number of dendrogram branches to cut: 10.

6.1.2.2 Preparation of microbial samples.

Solid phase extraction (SPE) was done on each microbial sample using a SPE C18-E Phenomenex cartridge (Strata C18-E, 55um, 70 Å). The cartridge was first washed with distilled water to remove sugars and then washed column was further eluted with 25% aqueous methanol and absolute methanol to give two fractions. The 25% methanol fraction had little metabolite content, while the majority of the metabolites were found in the 100% methanol fraction. Therefore, only the 100% methanol fractions were used for the analysis. All the samples were diluted to a final concentration of 0.01 mg/mL before subjecting them to MS analysis.

6.1.3 Results and discussion

6.1.3.1 Introduction

In order to perform the comparative metabolite profiling of large sets of LC-ESI-MS chromatograms, a two-step data mining workflow was used[131]. The chromatogram processing software ACD Labs IntelliXtract was used for data mining and the clustering and visualization of the data was done using FreeClust. ACD/IX incorporates a generic component detection algorithm, CODA (COmponent Detection Algorithm), for removing noise and background interferences in mass spectra, to make data analysis easier. This gives a comprehensive chromatogram deconvolution which enables the identification of trace compounds and those that are present in the same peak. The peaks in a chromatogram are characterized by their retention time (Rt) and mass to charge ratio (m/z) of the ions and these are provided as inputs (Rt-m/z) for further processing. The web-based application, FreeClust, was developed using the R programming language and the Shiny[132] package. This independent platform operates separately from the ACD Labs software suite and offers an interactive, freely accessible environment for the statistical evaluation and visualization of large datasets.

The two-step workflow of IntelliXtract followed by FreeClust was applied to the LC-HRMS data of 81 microbial samples from three collection sites, Orman Garden, Wadi Natrun salt lakes and Hurghada coral reefs. The top ten largest peak areas were chosen from each microbial sample, and assembled into a matrix table in Excel, with rows representing samples and columns representing a molecular mass of a molecule at a specific retention time (Rt-m/z). All the spectral data that is important for interpretation such as isotopes, $^{12}C/^{13}C$ ratios, adduct ions, multimers, neutral losses, fragment ions and $[M+H]^+$ or $[M-H]^-$ ion assignments are obtained using ACD Labs IntelliXtract (ACD/IX) and all these data are put into the input values. This process creates an input list for each of the individual chromatograms. Then the comparative metabolite profiling add-in tool is used to analyse the mass and retention time (metabolites) across the samples and generate a single master list of features. A table of components is produced as shown below outlining the area under the curve (AUC) of compounds identified in every chromatogram. The results are then processed using FreeClust, an online tool for clustering and visualization of data that is available for public use. The output of Excel spreadsheet is saved as text file and then imported into FreeClust. FreeClust provides several clustering options for the data such as hierarchical clustering and sparse hierarchical clustering. Outliers are detected with the help of histograms which help the users to choose the right clustering method. Furthermore, the importance score of each metabolite in the dataset is computed to give a measure of its importance in the clustering process. The results are presented by dendrograms and heatmaps using a colour-coded system which shows the ion intensity in each sample to facilitate easy visualisation of the analysed data.

Heatmaps and dendrograms are used to present the results of data analysis in order to effectively visualize feature values. In the heatmap, metabolite abundances are represented using a colour gradient based on the visible light spectrum (**Figure 6.1.4.2**). Metabolites with higher abundances are depicted in shades closer to the red end of the spectrum, while those with lower intensities are shown in shades nearer to the blue end. There is an interactive plotting feature which enables one to select individual values within the heatmap and also there is a zoom in tool that enables one to view the details of large data sets (See Supplementary). A dendrogram which is shown next to the heatmap on the left presents the clustering of samples. Different colours can be used to distinguish between different clusters and there is an option to select the number of clusters to define based on the analysis being conducted. This combination of heatmaps and dendrograms thus enables a better and easy understanding of the results.

6.1.4 Results

Only the top ten most abundant metabolites from each microbial strain are considered in the comparison analysis, due to the large variability of samples. To identify the same compound across different samples, a set of criteria was established. If the UV profiles of the compounds from each sample matched, the following conditions were applied: the maximum allowable fluctuation in retention time (Rt) was ±0.1 minutes from the midrange of the retention times, and the maximum allowable fluctuation in the m/z value was ±0.0015 from the midrange of the m/z values.

The strategy of comparing only the top ten most abundant metabolites from each microbial strain using UV profiles, retention time (Rt), and accurate mass (m/z) tolerances is a practical and efficient approach for preliminary identification of shared compounds across different species. By applying

strict criteria, such as UV spectral matching, a ±0.1 minute window for Rt, and a ±0.0015 m/z tolerance, this method offers a relatively robust way to detect overlapping metabolites in complex datasets while managing variability across samples. It is particularly useful in high-throughput studies, where prioritizing dominant features helps streamline analysis. However, this approach has limitations. Restricting the comparison to the top metabolites may lead to false negatives by excluding lower-abundance, yet biologically relevant, compounds. Additionally, the lack of MS/MS fragmentation data increases the risk of false positives, especially in distinguishing between isomers or closely related analogues with similar UV and mass characteristics. Moreover, minor variations in chromatographic conditions can affect retention time alignment across runs. Therefore, while this strategy serves as a valuable screening tool for detecting potentially shared metabolites, it should ideally be complemented by confirmatory techniques such as MS/MS spectral comparison, molecular networking, or co-injection with reference standards to establish structural identity with greater certainty.

For this statistical analysis, microbial strains, represented by rows on the heatmap, were categorized based on their biological activity, microbial taxonomic group, collection site and sample source/host (**Figure 6.1.4.2 and 6.1.4.3**). Strains were considered to have antibacterial activity if they inhibited 80% or more of the growth of a pathogenic bacterial species, Wadi Natrun and Hurghada strains, or over 7.0 mm of inhibition for Orman Garden strains, (24 out of 81 strains), represented on heatmap rows by [AMb]. Strains were considered to have antifungal activity if they inhibited 80% or more of the growth of a pathogenic fungal species (23 out of 81 strains), represented on heatmap rows by [AMf]. Strains were considered to have antibiofilm activity if they inhibited 70% or more of biofilm formation (8 out of 81 strains), represented on heatmap rows by [AB]. Strains were considered to have Anti Alzheimer's activity if they inhibited 50% or more of acetylcholinesterase activity (10 out of 81 strains), represented on heatmap rows by [Alz].

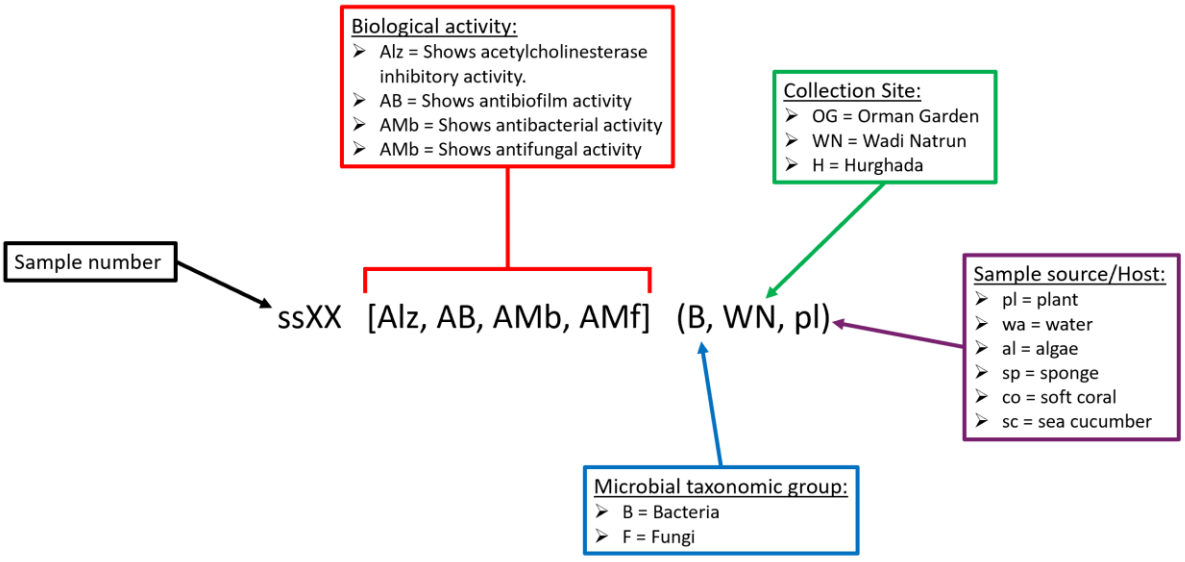

Figure 6.1.4.1. Key illustrating the labelling system used for strain names in the rows of the heatmap.

The dendrogram and 2D heatmap are both shown in Fig 2. **Cluster 1** comprises a single fungal strain collected from Orman Garden. **Cluster 2** includes five fungal strains sourced from Orman Garden and Wadi Natrun. Among these, three strains exhibit antibacterial activity: two through direct inhibition of pathogenic bacterial species and one via antibiofilm activity. This highlights the clustering of strains with antibacterial properties. Additionally, two metabolites are consistently detected across all strains within this cluster. **Cluster 3** contains nine microbial strains, encompassing both bacterial and fungal types. Of these, eight were isolated from plants, all originating from either Orman Garden or Wadi Natrun, demonstrating clustering based on symbiotic host similarities. Three metabolites are shared across all strains within this cluster. **Cluster 4** consists of eight microbial strains, seven of which are fungal and one bacterial. Seven strains were isolated from Hurghada, while one was collected from Wadi Natrun. Metabolomic analysis reveals clustering based on both geographic origin and organism type, with Hurghada strains forming a distinct group and fungal strains clustering separately from the bacterial strain. Three metabolites are common to all strains in this cluster. **Cluster 5** comprises twenty microbial strains, all collected from Hurghada, emphasizing the shared metabolomic profiles of strains from a single collection site. Notably, six of the ten strains exhibiting significant inhibitory activity against the Alzheimer's acetylcholinesterase target are found in this cluster, suggesting a potential correlation between the metabolites present and activity against this disease target. **Cluster 6** includes three strains, two of which are fungal strains collected from Wadi Natrun that exhibit antibiofilm activity. This cluster reflects the potential clustering of strains based on both collection site and antibiofilm activity. Six metabolites are consistently detected across all strains in this cluster. **Cluster 7** comprises thirteen strains, all isolated from Wadi Natrun. Of these, twelve are bacterial, illustrating the clustering of bacterial strains. All thirteen strains display antibacterial activity: twelve through direct inhibition of pathogenic bacterial strains and one via antibiofilm activity. Furthermore, twelve strains exhibit antifungal activity against various pathogenic fungal species, highlighting clustering based on antifungal properties. One metabolite is consistently detected across all strains in this cluster. **Cluster 8** contains twenty strains, all collected from Wadi Natrun, strongly demonstrating clustering driven by a single collection site. **Cluster 9** consists of a single bacterial strain isolated from Hurghada. **Cluster 10** is represented by a single fungal strain collected from Wadi Natrun. At this time no molecule can be distinctively identified.

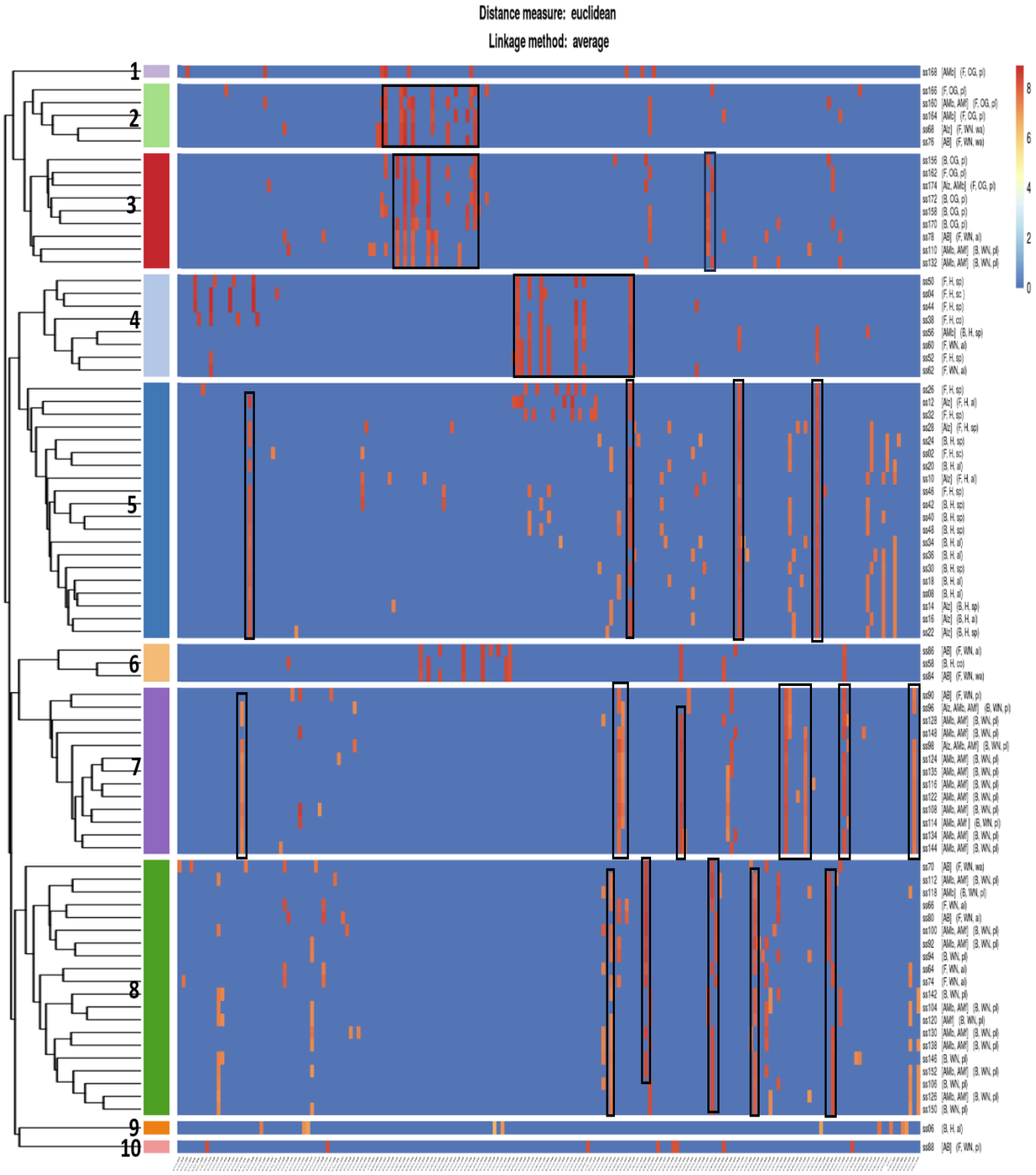

Figure 6.1.4.2. Dendrogram and 2D heatmap showing the metabolite profile of 81 microbial samples compared to each other. The dendrogram is placed on the left-hand side of the heatmap with clusters differentiated by unique colours. The intensity of the colour of individual cells in the heatmap represents the abundance of the molecular ions. The y-axis (right side of the heatmap) shows the sample identities, and the x-axis represents features which include Retention Time (RT) and m/z value of the compounds. Notable metabolite patterns within specific clusters are outlined in black frames.

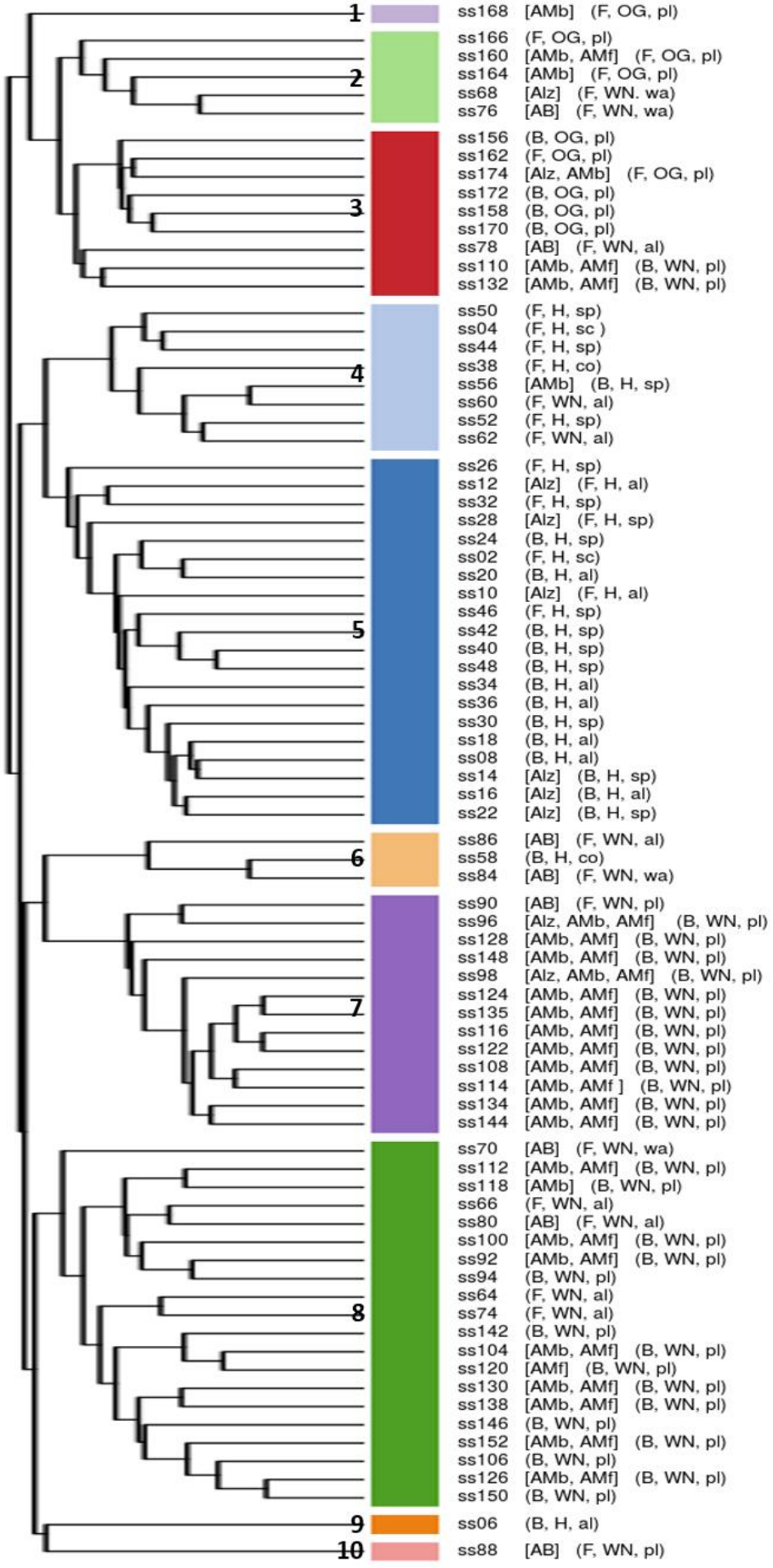
1
ss168 [AMb] (F, OG, pl)
2
ss166 (F, OG, pl)
ss160 [AMb, AMf] (F, OG, pl)
ss164 [AMb] (F, OG, pl)
ss68 [Alz] (F, WN. wa)
ss76 [AB] (F, WN, wa)
3
ss156 (B, OG, pl)
ss162 (F, OG, pl)
ss174 [Alz, AMb] (F, OG, pl)
ss172 (B, OG, pl)
ss158 (B, OG, pl)
ss170 (B, OG, pl)
ss78 [AB] (F, WN, al)
ss110 [AMb, AMf] (B, WN, pl)
ss132 [AMb, AMf] (B, WN, pl)
4
ss50 (F, H, sp)
ss04 (F, H, sc)
ss44 (F, H, sp)
ss38 (F, H, co)
ss56 [AMb] (B, H, sp)
ss60 (F, WN, al)
ss52 (F, H, sp)
ss62 (F, WN, al)
5
ss26 (F, H, sp)
ss12 [Alz] (F, H, al)
ss32 (F, H, sp)
ss28 [Alz] (F, H, sp)
ss24 (B, H, sp)
ss02 (F, H, sc)
ss20 (B, H, al)
ss10 [Alz] (F, H, al)
ss46 (F, H, sp)
ss42 (B, H, sp)
ss40 (B, H, sp)
ss48 (B, H, sp)
ss34 (B, H, al)
ss36 (B, H, al)
ss30 (B, H, sp)
ss18 (B, H, al)
ss08 (B, H, al)
ss14 [Alz] (B, H, sp)
ss16 [Alz] (B, H, al)
ss22 [Alz] (B, H, sp)
6
ss86 [AB] (F, WN, al)
ss58 (B, H, co)
ss84 [AB] (F, WN, wa)
7
ss90 [AB] (F, WN, pl)
ss96 [Alz, AMb, AMf] (B, WN, pl)
ss128 [AMb, AMf] (B, WN, pl)
ss148 [AMb, AMf] (B, WN, pl)
ss98 [Alz, AMb, AMf] (B, WN, pl)
ss124 [AMb, AMf] (B, WN, pl)
ss135 [AMb, AMf] (B, WN, pl)
ss116 [AMb, AMf] (B, WN, pl)
ss122 [AMb, AMf] (B, WN, pl)
ss108 [AMb, AMf] (B, WN, pl)
ss114 [AMb, AMf] (B, WN, pl)
ss134 [AMb, AMf] (B, WN, pl)
ss144 [AMb, AMf] (B, WN, pl)
8
ss70 [AB] (F, WN, wa)
ss112 [AMb, AMf] (B, WN, pl)
ss118 [AMb] (B, WN, pl)
ss66 (F, WN, al)
ss80 [AB] (F, WN, al)
ss100 [AMb, AMf] (B, WN, pl)
ss92 [AMb, AMf] (B, WN, pl)
ss94 (B, WN, pl)
ss64 (F, WN, al)
ss74 (F, WN, al)
ss142 (B, WN, pl)
ss104 [AMb, AMf] (B, WN, pl)
ss120 [AMf] (B, WN, pl)
ss130 [AMb, AMf] (B, WN, pl)
ss138 [AMb, AMf] (B, WN, pl)
ss146 (B, WN, pl)
ss152 [AMb, AMf] (B, WN, pl)
ss106 (B, WN, pl)
ss126 [AMb, AMf] (B, WN, pl)
ss150 (B, WN, pl)
9
ss06 (B, H, al)
10
ss88 [AB] (F, WN, pl)

Figure 6.1.4.3. Zoomed-in dendrogram of the group of data sets obtained from the comparative metabolite profiling of 81 symbiotic microbial samples. Clusters are highlighted by different colours.

6.1.5 Conclusion

The two-step workflow which includes ACD/Labs IntelliXtract and FreeClust has been demonstrated to be a useful method for the analysis of metabolite profiling data and subsequent statistical analysis. This approach successfully clustered microbial strains based on their collection sites and taxonomic groups, as well as potentially based on their strain source/host and associated biological activities. The findings of this study thus demonstrate the potential of this workflow in identifying significant trends within large datasets and, as such, it is highly beneficial in prioritising samples for further investigation. Beyond microbial metabolomics, this workflow can also be applied to a wide range of natural product research contexts, including plant, marine, and endophytic sources, where chemical diversity is high and dereplication is essential. Furthermore, it can aid in chemotaxonomic studies, ecological metabolomics, and comparative analyses of biosynthetic expression under varied environmental conditions. With further integration into high-throughput pipelines, this strategy also holds potential for industrial-scale screening, metabolite fingerprinting for quality control, and bioprospecting in underexplored environments. Through the optimisation and simplification of the analysis and selection process, this workflow therefore presents a versatile and effective strategy for enhancing efficiency across multiple dimensions of the natural product drug discovery process and beyond.

6.2 Sample novelty testing using the AntiMarin database

6.2.1 Introduction

The process of taking a natural product through the process of identification, isolation, structural determination and biological testing to become a drug is a very complicated and time-consuming process. All these steps have to be carried out before the preclinical studies can be initiated and include the isolation, structural analysis and the bioactivity testing. It takes about 10-12 years for a drug to be developed from the initial research to market launch. By the early 2000s, the cost of this process had already exceeded $1 billion, and this was not only because of the enormous effort that went into the work and the use of advanced techniques but also because more than 90% of the clinical trials failed.[133]

Natural products chemistry researchers are mainly involved in the initial stage of this challenging process. Nevertheless, time and project resources may be considerably misused if the end result is the rediscovery of previously known compounds. To this end, the technique of dereplication was introduced. Dereplication is the process of identifying new metabolites from the already known metabolites. The identification of novel compounds is usually performed in the first place by preparing a crude extract and then subjecting it to mass spectrometry (MS) and in most cases combined with high performance liquid chromatography (HPLC). The obtained data is usually matched by hand to the database to search for the corresponding fragments. However, this approach has certain drawbacks; it is rather conventional and rather dependent on the human work and therefore rather

time consuming. In order to enhance the process of dereplication, several chemists have developed software that help in the process to enhance and simplify the process.[134]

The software used for the optimization of the dereplication process are different types of HRMS analysis software such as MZMine 3, Agilent MassHunter, ACD Lab Spectrus and Global Natural Products Social (GNPS). These tools employ peak picking algorithms that work to analyse the LC-MS data and output a list of features, which include the peaks with their mass and retention time for each compound and the proposed molecular formulae. GNPS has an inbuilt natural product database and it has an inbuilt tool that screens MS/MS fragmentation patterns of compounds to identify if they are known compounds and then it clusters the compounds identified into networks where the carbon skeleton of the compounds in each cluster is closely related. The other software listed does not, however, they are all compatible with external databases that the data can still be screened to identify if it is a known compound or not.[135] The GNPS database is a high-quality, community-driven platform that supports metabolite identification through MS/MS spectral matching and molecular networking. It offers a large and growing collection of publicly shared spectra, making it a valuable tool for dereplication and comparative metabolomics in natural product research. However, its spectral coverage is still incomplete and biased toward well-studied compounds, meaning novel or rare metabolites may go unidentified. While false positives can occur, especially without additional data, GNPS remains one of the most effective resources for rapid annotation and discovery when used alongside complementary analytical techniques.[135]

This analysis shows how the preprocessed MS data and ACD/IX software can be used with natural product database search engines like AntiMarin to prioritise crude samples after they have been processed through the database. Therefore, it is possible to determine the percentage novelty of compounds in a mixture as an additional parameter to base the choice of samples for isolation. It can be used in conjunction with other important prioritization strategies, for instance bioassay-guided prioritization and NMR analysis to enhance the confidence of sample selection (Fig. 3.7.2.1). There is a great potential of this extra layer of certainty to help in reducing the bottleneck usually experienced in sample prioritization in natural product-based drug discovery enhancing efficiency and productivity.

6.2.2 Methods

This section explains the application of ACD labs Spectrus with the built-in tool IntelliXtract 1.0 (IX) along with the AntiMarin database in estimating the percentage of novel compounds as compared to the known compounds. Four samples were selected for the validation of this approach. The bioactive antibiofilm samples WNS16(8)F2 (84) (Fig. 3.7.3.3), WNS16(8)F2 (86) (Fig. 3.7.3.4) isolated from Wadi Natrun salt lakes and the bioactive acetylcholinesterase inhibitory samples HS4(50)F3 (12) (Fig. 3.7.3.2) and JA13 (174) (Fig. 3.7.3.5), obtained from the Red sea and Orman garden respectively. First, the extract was separated into two fractions namely the 100% MeOH fraction and 25% MeOH aqueous fraction through SPE. It was also observed that the majority of the potential 'drug-like' molecules were in the SPE-100 fractions and not in the SPE-25 fractions, therefore only the SPE-100 fractions were used in the analysis while the SPE-25 were not used.

After the initial SPE and LC-MS operations, the data were analysed as described below using the IX software that is incorporated in the ACD Labs Spectrus (See S77 for settings), which provided a list of

the compounds identified based on the MS adducts and fragmentations. The database AntiMarin was used to create a more selective database by searching for the term '*Aspergillus*' in the note search tool. This was done because all the samples in question were identified to be in the *Aspergillus* genus. These compound lists were then searched in this new *Aspergillus* database and the number of the known and unknown compounds was recorded.

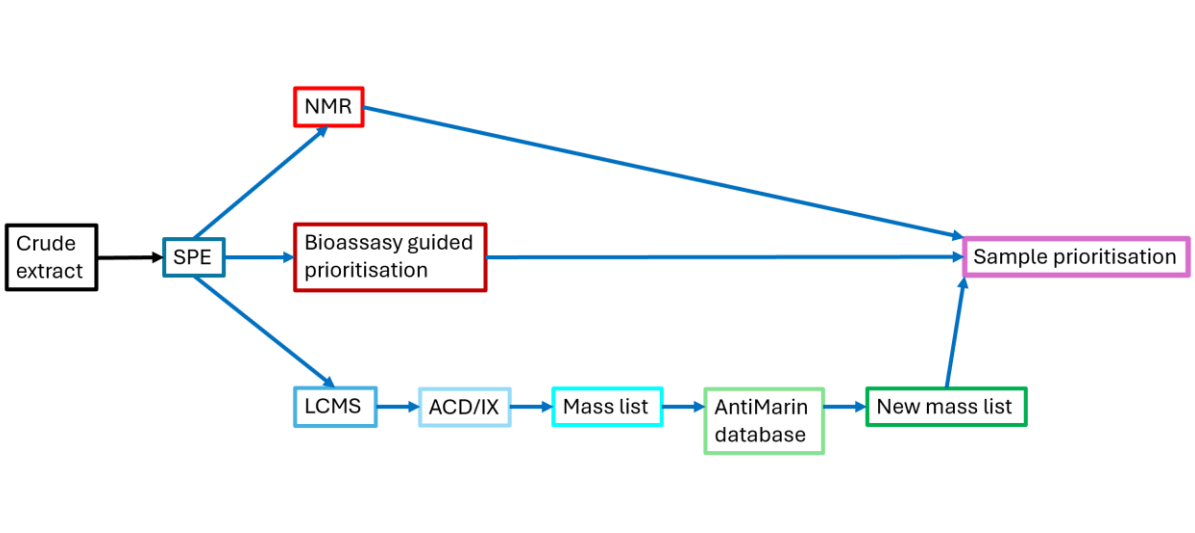

Figure 6.2.2.1. Flowchart of the process used to prioritise crude samples, during the dereplication of natural products.

6.2.3 Results

From this combined MS data analysis and database searching, sample 86 (Fig. 3.7.3.4) was seen to have the higher novelty percentage, 94.9% and thus would be the chosen sample if prioritising through this method. The second sample chosen would be sample 84 (Fig. 3.7.3.3), with a 91.9% novelty percentage, followed by sample 12 (Fig. 3.7.3.2), with an 84.5% novelty percentage, and finally sample 174 (Fig. 3.7.3.5), with a 71.3% novelty percentage. This method, used in tandem with bioassay-guided prioritization and NMR analysis prioritisation, adds an extra level of certainty to the prioritising process, demonstrating the potential value in this two-step workflow.

The reliability of the method's novelty testing using ACD Labs Spectrus and the AntiMarin database is corroborated with its high-throughput efficiency, targeted database scouting, and alignment with traditional techniques such as bioassay-guided prioritization and NMR. Its potency in novelty detection is underscored with high percentages such as 94.9% for Sample 86 and the scatter plot visuals showing clear divides. Nevertheless, the method's reliability is limited by the AntiMarin database's coverage. Gaps in comprehensive data could result in misclassification. In addition, the interpretation of MS data and possible bias stemming from the sample prep (e.g., only looking at SPE-100 fractions) could skew findings. Increasing reliability could stem from broadening database search parameters to include GNPS, and cross-corroborative NMR or synthetic standard analyses, as well as applying consistent analytical benchmarks. Even with these factors to consider, the method provides

an ideal starting point for dereplication when paired with other techniques and can be improved through repetitive refinement and validation. Natural product drug discovery could benefit from benchmarking these methods against other workflows focused on dereplication.

Table 6.2.3.1. Percentage novelty of the four samples analysed through Intelliextract and Antimarin database.

Sample	Total compounds identified by IX	Unidentified	Identified	Percentage Novelty
12	103	87	16	84.5
84	62	57	5	91.9
86	79	75	4	94.9
174	80	57	23	71.3

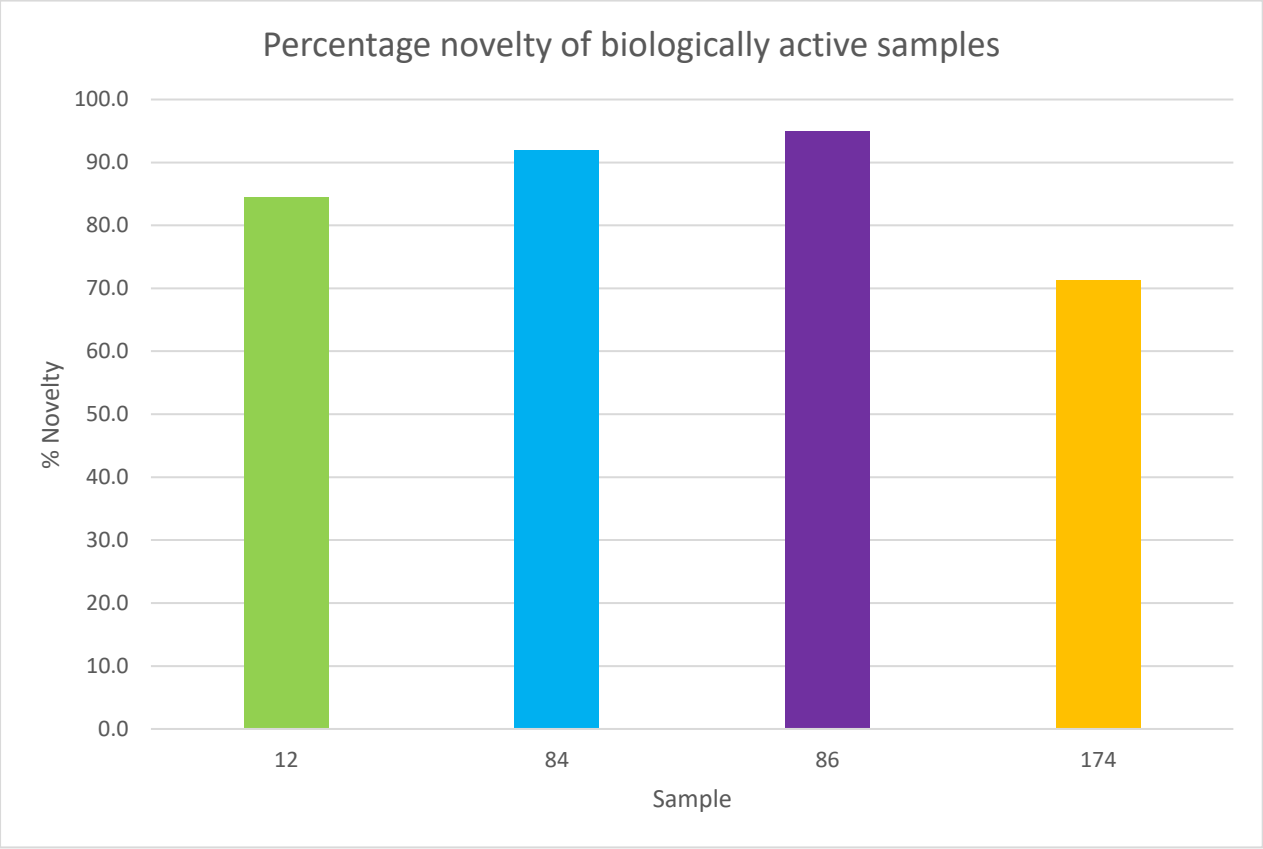

Figure 6.2.3.1. Percentage novelty of the 4 samples analysed through IntelliXtract and Antimarin database.

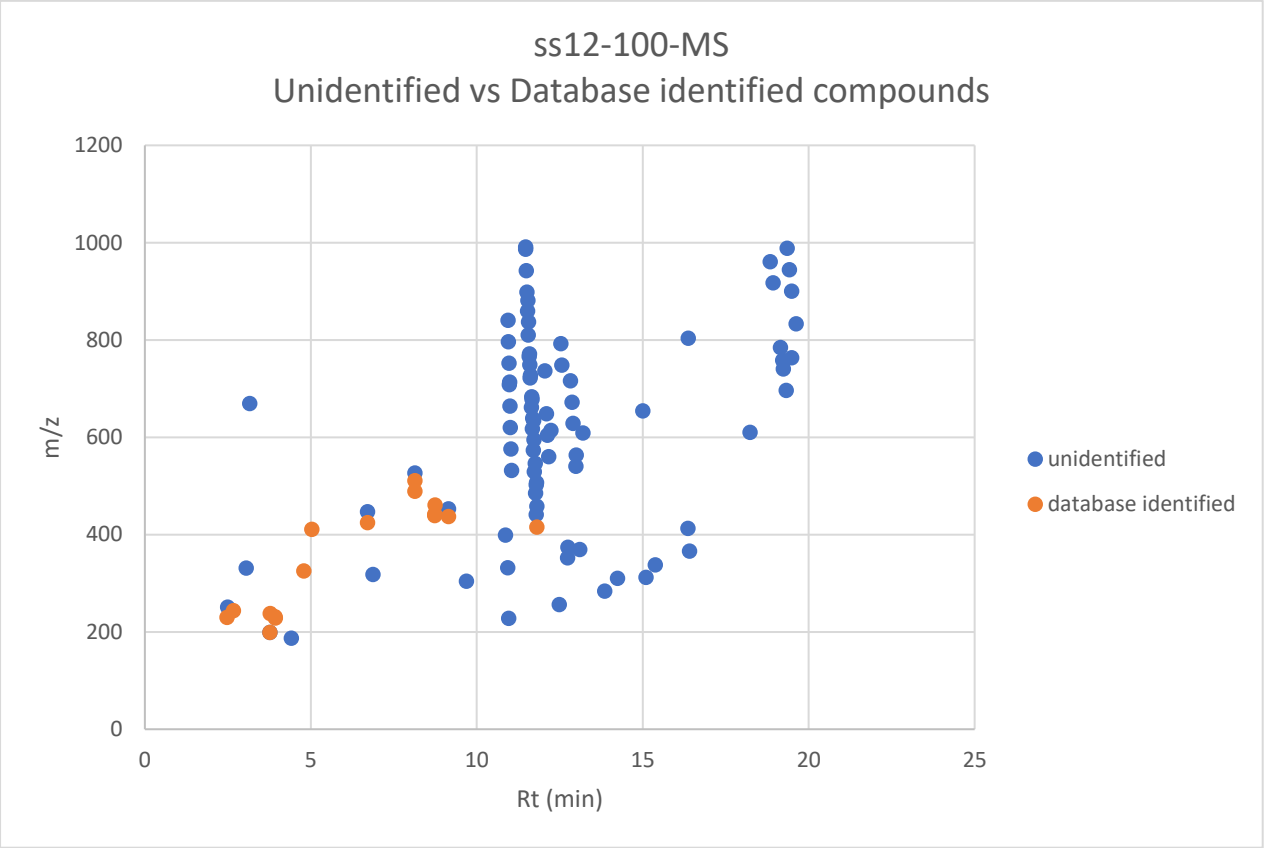

Figure 6.2.3.2. A scatter plot showing the retention times (Rt) and m/z values for compounds in the HS4(50)F3 (12) sample. Blue dots represent unidentified compounds, while orange dots correspond to compounds identified in the database.

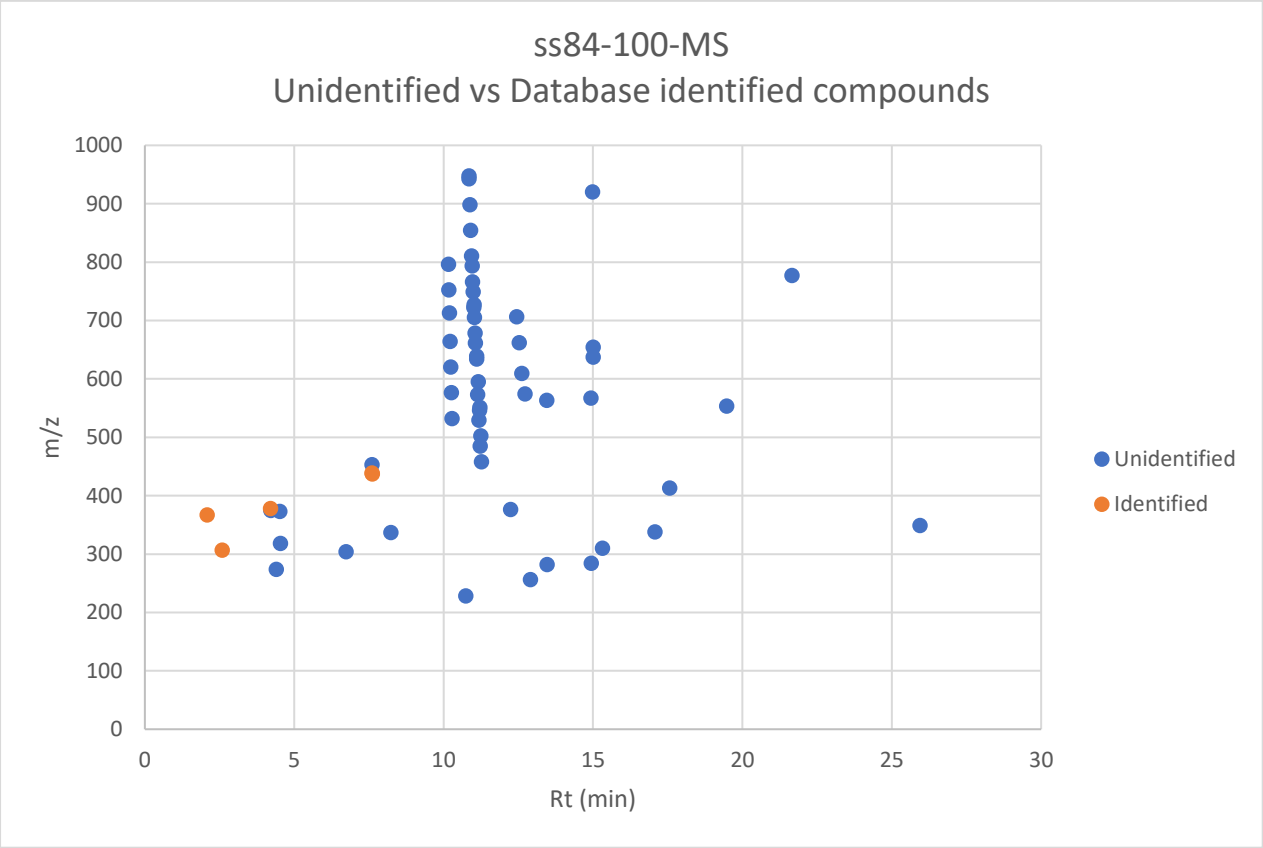

Figure 6.2.3.3. A scatter plot showing the retention times (Rt) and m/z values for compounds in the WNS16(8)F2 (84) sample. Blue dots represent unidentified compounds, while orange dots correspond to compounds identified in the database.

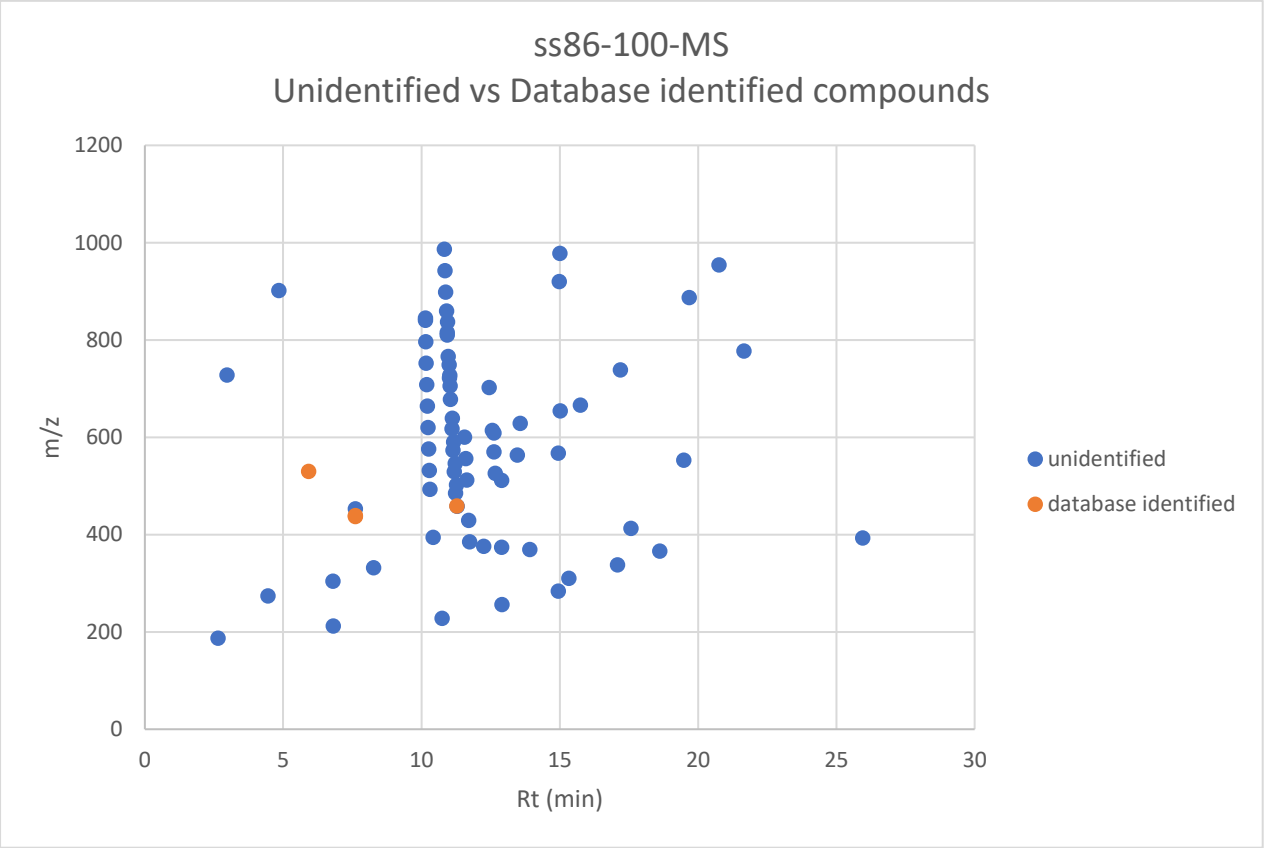

Figure 6.2.3.4. A scatter plot showing the retention times (Rt) and m/z values for compounds in the WNS7(8)F3 (86) sample. Blue dots represent unidentified compounds, while orange dots correspond to compounds identified in the database.

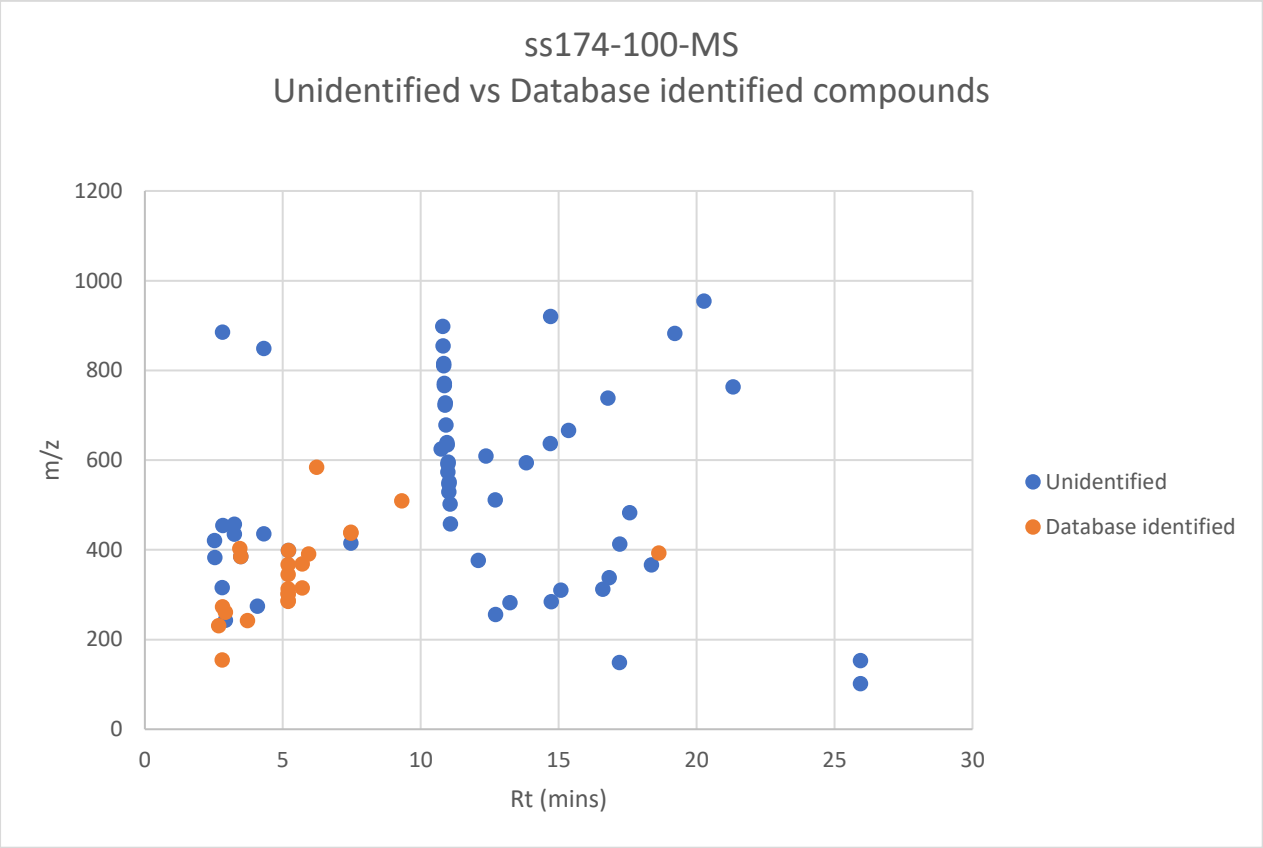

Figure 6.2.3.5. A scatter plot showing the retention times (Rt) and m/z values for compounds in the JA13 (174) sample. Blue dots represent unidentified compounds, while orange dots correspond to compounds identified in the database.

6.2.4 Conclusion

The integration of dereplication tools such as ACD Labs Spectrus and the AntiMarin database has been an effective strategy for the purpose of novelty of natural product samples. This approach combines advanced LC-MS data processing with targeted database searches to enable the estimation of the percentage of novel compounds within complex mixtures. This has resulted in the identification of the potential of this method to streamline sample prioritization for natural product drug discovery.

Out of the samples analysed, Sample 86 had the highest novelty percentage of 94.9%, Sample 84 of 91.9%, Sample 12 of 84.5%, and Sample 174 of 71.3%. Thus, the findings of this study show that the novelty assessment can be a useful additional parameter for sorting crude extracts, consistent with traditional bioassay-guided and NMR-based approaches to sorting them.

However, in LC-MS-based dereplication studies, the presence of polyethylene glycols (PEGs) as systemic contaminants can significantly impact data interpretation, particularly when assessing compound novelty. These polymer-based impurities appear as characteristic peaks spaced 44 mass units apart (e.g., m/z 441, 485, 529), typically with sodium or potassium adducts, and consistently elute at fixed retention times across samples. Their origin traces to ubiquitous plastic labware like tubes, SPE cartridges, and vial septa, as well as solvent impurities and laboratory environmental contamination. When these PEG-related peaks are inadvertently included in novelty calculations, they

artificially inflate the percentage of "unknown" compounds, leading to potentially misleading conclusions about sample composition. To address this issue in future work, several preventative measures should be implemented: First, minimizing plastic contact by using glass vials with PTFE-lined caps and metal/glass syringes for all sample handling steps. Second, maintaining rigorous LC-MS system hygiene through regular ion source cleaning and use of fresh, high-purity solvents stored in glass containers. Third, incorporating systematic data processing controls, including blank subtraction protocols and automated detection of 44-Da-spaced mass clusters using software like MZmine or XCMS. Additionally, to ensure accurate novelty assessment, researchers should cross-validate MS findings with orthogonal techniques such as NMR and implement exclusion lists for known contaminants during database searches. By implementing these measures, studies can more reliably distinguish true novel compounds from methodological artifacts, thereby producing more accurate assessments of sample novelty and avoiding the pitfalls of contamination-induced overestimation. Transparent reporting of these quality control measures in methods sections will further strengthen the validity of future dereplication studies.

Even with the unreliability of the method, this multi-faceted workflow is a significant improvement in efficiency and decision making in the early stages of drug discovery that minimises the chance of finding out a compound is already known and thus wasting time and resources. Thus, percentage novelty calculations can assist researchers in making more informed decisions when selecting samples, which in turn can enhance the efficiency of natural product-based drug development pipelines.

CHAPTER 7 Isolation and chemical profiling of *Neovasinin B* from *Aspergillus fumigatus* strain ASMN.

7.0 Introduction

The fungal strain *Aspergillus sp.* strain ASMN is an endophyte of the Middle Eastern plant, *Fagonia arabica*. The host plant is known to have medicinal properties, including treatment of stomatitis and has noted deobstruent action so may be used in blood purification.[136] It is also known to treat skin disorders, tumours, neck swelling and small pox,[137] with diuretic activity found within the dried aerial parts of the plant.[138] Endophytes are known to produce bioactive metabolites similar to those of their host plants, though this is not a universal rule. A well-documented example is the anticancer drug Taxol (paclitaxel), originally isolated from the bark of Taxus (yew) trees. Later, certain endophytic fungi, such as *Pestalotiopsis microspora* and others, were discovered to also synthesise Taxol. While this discovery demonstrated the potential for fungal-derived Taxol, industrial-scale production still primarily relies on plant cell culture or semi-synthesis from yew precursors due to higher yields. However, research continues into optimizing fungal fermentation as a more sustainable alternative.[139] In addition, The genus *Aspergillus* is renowned for its exceptional chemical diversity, producing a wide array of secondary metabolites with pharmaceutical potential. A prominent example is lovastatin, a cholesterol-lowering drug originally isolated from *Aspergillus terreus*. Lovastatin was the first statin approved for clinical use and works by inhibiting HMG-CoA reductase, a key enzyme in cholesterol biosynthesis. Today, industrial production of lovastatin relies heavily on optimized strains of *A. terreus* through submerged fermentation, highlighting the importance of fungi in large-scale drug manufacturing.[140]. This chapter describes the isolation and structural characterisation of natural products isolated from *Aspergillus sp.* strain ASMN using chromatographic and spectroscopic techniques. Various methods, including liquid-liquid extraction, size exclusion chromatography (SEC), and high-performance liquid chromatography (HPLC) were optimized to isolate bioactive compounds. High resolution mass spectrometry (HR-MS/MS) with fragmentation analysis and 1D and 2D NMR spectroscopy (1H, 13C, COSY, HSQC, HMBC, NOESY) were used for the structural elucidation. This workflow assisted in identifying and characterising the novel natural product *'neovasinin B'*.

7.1 Isolation of *neovasinin B* from *Aspergillus* sp. strain ASMN

Separation of ASMN-BT (culture and isolation in experimental) was carried out using SPE was carried out on the DCM fraction, using a SPE C18-E Phenomenex cartridge (Strata C18-E, 55um, 70 Å) before HPLC. SPE was performed by dissolving the sample in 60% methanol and 40% water the cartridge is equilibrated and conditioned with the same ratio of methanol and water to wet the sorbent. The sample loading solution was placed through the SPE cartridge at 60% MeOH/40% H_2O with the compounds soluble in this 60% MeOH/H_2O solution collected below to make up a 60% MeOH fraction. 100% MeOH was then used to attempt to dissolve the remaining insoluble compounds in the sample and was washed through the sorbent. This formed another fraction of compound soluble in 100% methanol. The remaining compounds that were insoluble in 100% methanol were then placed in another fraction, labelled insoluble in 100% methanol. These fractions were then rotary evaporated

and dried further with air to produce 3 fractions of dry extract. Fraction 60% methanol, fraction 100% methanol and fraction insoluble in methanol were all analysed by ^{1}H NMR and HPLC-UV/Vis and it was decided the 60% methanol fraction was the only one worth pursuing in terms of natural product content, as the other fractions were seen to have featureless spectra. To purify the butanol fraction a HPLC Sunfire C18 OBD 5µm 10 x 250 mm column was used. The solvent system used was A (100% H_2O + 0.05% TFA) and B (100% CH_3CN) on an isocratic system of 85% A and 15% B from t = 0.00 to t = 20.00 mins followed by a gradient of 15% B to 100% B between t= 20.00and t = 25.00 mins, then kept at 100% B until t = 30.00 mins.

7.2 Structure elucidation

Neovasinin B showed a HRESIMS with m/z = 227.09 $[M+H]^+$, Δ = 1.10 ppm, with molecular formula $C_{11}H_{14}O_5$. requiring five degrees of unsaturation. ^{13}C data shows five sp^2 carbons: δ_C 166.72, 163.22, 157.25, 108.33, 98.60 accounting for 3 degrees of unsaturation suggesting the presence of two rings in the structure of figure 7.2.1. Interpretation of ^{1}H NMR, COSY, edited HMQC and HMBC NMR spectra identified 11 carbon resonances, including five sp²-hybridized carbons (δC 166.72, 163.22, 157.25, 108.33, 98.60), accounting for three degrees of unsaturation and suggesting a bicyclic system. Key structural fragments were assembled using HMBC correlations. The pyran-2-one core was established by correlations from the methyl singlet H_9 (δH 1.91) to the carbonyl carbon C_1 (δC 166.72) and the olefinic carbons C_2 (δC 98.60) and C_3 (δC 163.22). Additionally, the H_7 (δH 3.66, q) and H_8 (δH 1.23, d) spin system in the COSY spectrum, along with HMBC correlations from H_8 to C_6 (δC 68.46) and C_7 (δC 77.52), confirmed a 2,3-dihydrofuran ring fused to the pyranone. The side-chain assignments were determined by HMBC correlations from the methylene protons H_{10} (δH 4.49/4.54) to C_5 (δC 157.25), C_6, and C_7, positioning an –OCH_2– group at C_6, while the singlet methyl H_{11} (δH 1.35) correlated with C_5, C_6, and C_7, confirming a gem-dimethyl substitution on the dihydrofuran ring.

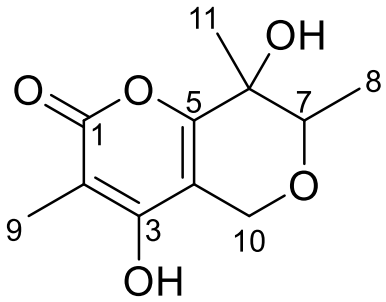

Figure 7.2.1. Structure of *Neovasinin B*, isolated from the endophytic fungi *Aspergillus sp.* strain ASMN.

Table 7.2.1. NMR Spectroscopic Data for *neoviasinin B*.

Position	^{13}C Chemical shift (ppm)[a]	C-type	^{1}H (chemical shift ppm, No. of H, multiplicity, coupling)[b]	COSY (^{1}H-^{1}H)	HMBC (^{1}H-^{13}C)
1	166.72	C			
2	98.60	C			
3	163.22	C			
4	108.33	C			
5	157.25	C			
6	68.46	C			
7	77.52	CH	H_7: 3.66 (q, J = 7.0, 6.4 Hz, 1H)	8	
8	12.98	CH_3	H_8: 1.23 (d, 6.4 Hz, 3H)	6	6, 7
9	7.33	CH_3	H_9: 1.91 (s, 1H)		1, 2, 3
10	61.97	CH_2	(H_{10a} /H $_{10b}$): 4.49/4.54 (dd, J = 17 Hz, 2H)	10a/10b	5, 4, 7
11	18.39	CH_3	H_{11}: 1.35 (s, 1H)		5, 6, 7

a 100 MHZ in CD_3OD

b 400 MHz in CD_3OD

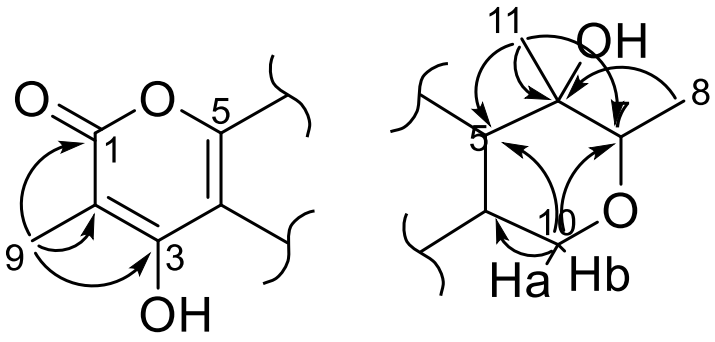

Figure 7.2.2. Fragments constructed and connected through HMBC. Main connections shown.

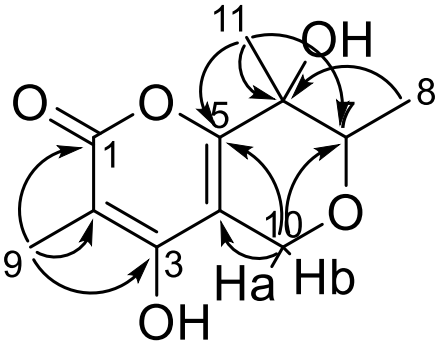

Figure 7.2.3. Structure of *neovasinin B*. Arrows show HMBC correlations between ^{1}H and ^{13}C atoms.

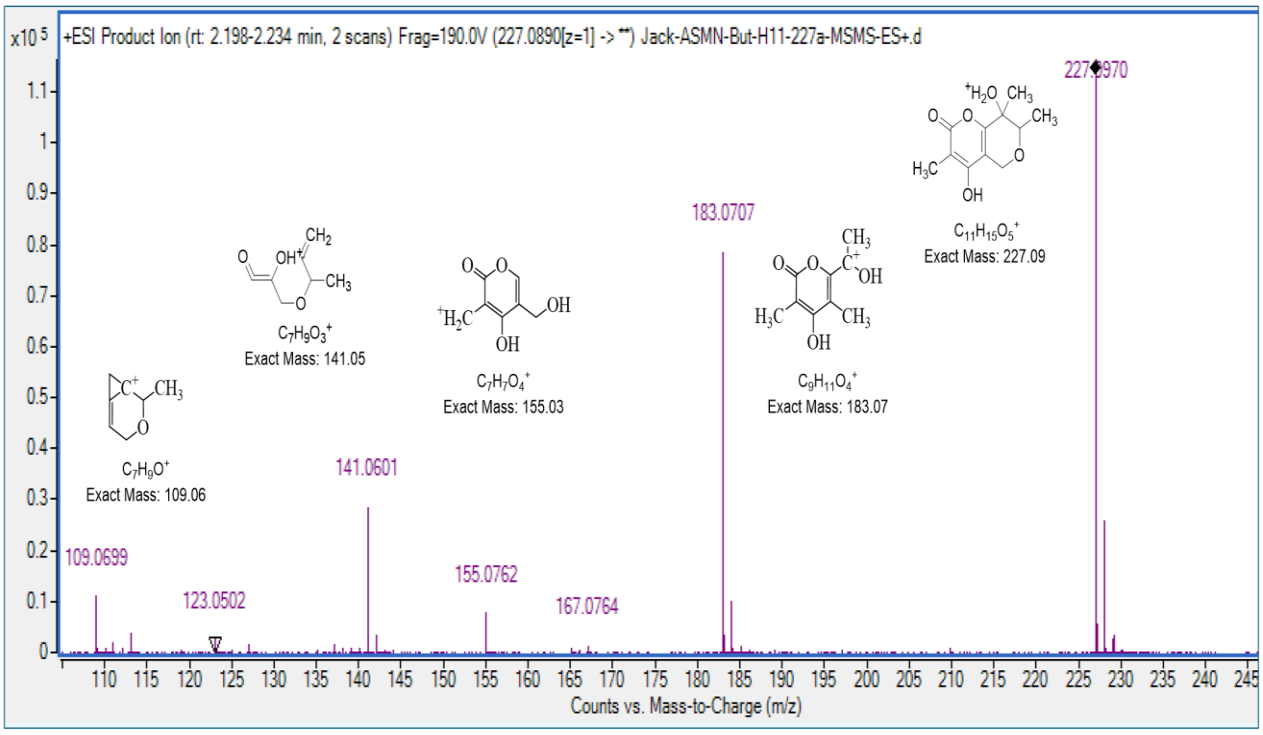

Figure 7.2.3. Assignment of HR-MS/MS fragments for ASMN-BT-H11.

7.2.1 Computer Assisted Structure elucidation (CASE)

To confirm the structure of *neovasinin B*, data analysis was performed using Computer Assisted Structure Elucidation (CASE) using ACD/LABS Structure Elucidator. 1D and 2D NMR, and the molecular formula were entered to the software and calculations performed (calculations performed by Jioji Tabudravu, supervisor, see appendix). Calculation follows a define sequence starting by checking data for consistencies followed by building molecular connectivity diagrams (**Figure 7.2.1.1**). If no contradictions are identified at this stage, the calculation proceeds and all the possible structural isomers within generally defined parameters are generated. In this case 1,001,584 structures were generated, and 98 structures were stored as meeting the minimum requirements set by the software (see supplementary). These 98 structures were then sorted depending on how close the chemical shifts were to the ^{13}C carbon experimental data using two algorithms: HOSE Code and Neural Network. The HOSE (Hierarchically Ordered Spherical Environment) code predicts NMR chemical shifts by analysing a carbon atom's immediate chemical environment, including its bonds and neighbouring atoms, then comparing this to a database of known structures with similar environments to generate predicted shift values. Neural networks take a machine learning approach, training on vast datasets of known chemical shifts to recognize complex patterns and relationships between molecular features and NMR signals, allowing them to make increasingly accurate shift predictions. Both methods serve as powerful tools for structural verification, with the HOSE code excelling at matching known structural motifs while neural networks can handle more novel or complex molecular environments, together providing complementary approaches for validating proposed structures through

comparison of predicted versus experimental NMR data. HOSE code-based predictions were performed using a depth of 5, balancing specificity and computational coverage of atom environments. The chemical shift tolerance was set at ±1.5 ppm for ^{13}C NMR and ±0.2 ppm for ^{1}H NMR data, allowing for precise correlation between experimental and predicted shifts. Neural network predictions were enabled alongside HOSE codes to enhance prediction accuracy, particularly in regions with atypical electronic or stereochemical features. Stereochemical information was incorporated into the analysis where available, especially when NOESY or ROESY data supported spatial correlations. Additionally, the dereplication module was enabled using an internal compound database to filter out known scaffolds early in the process. Structure proposals were further refined using HMBC, COSY, and HSQC correlation data, and candidate structures were ranked based on overall spectral consistency, shift prediction quality, and structural feasibility. This configuration provided a robust platform for high-confidence structural assignment of natural products in the study. The top four structures are shown in **Table 7.2.1.1**.

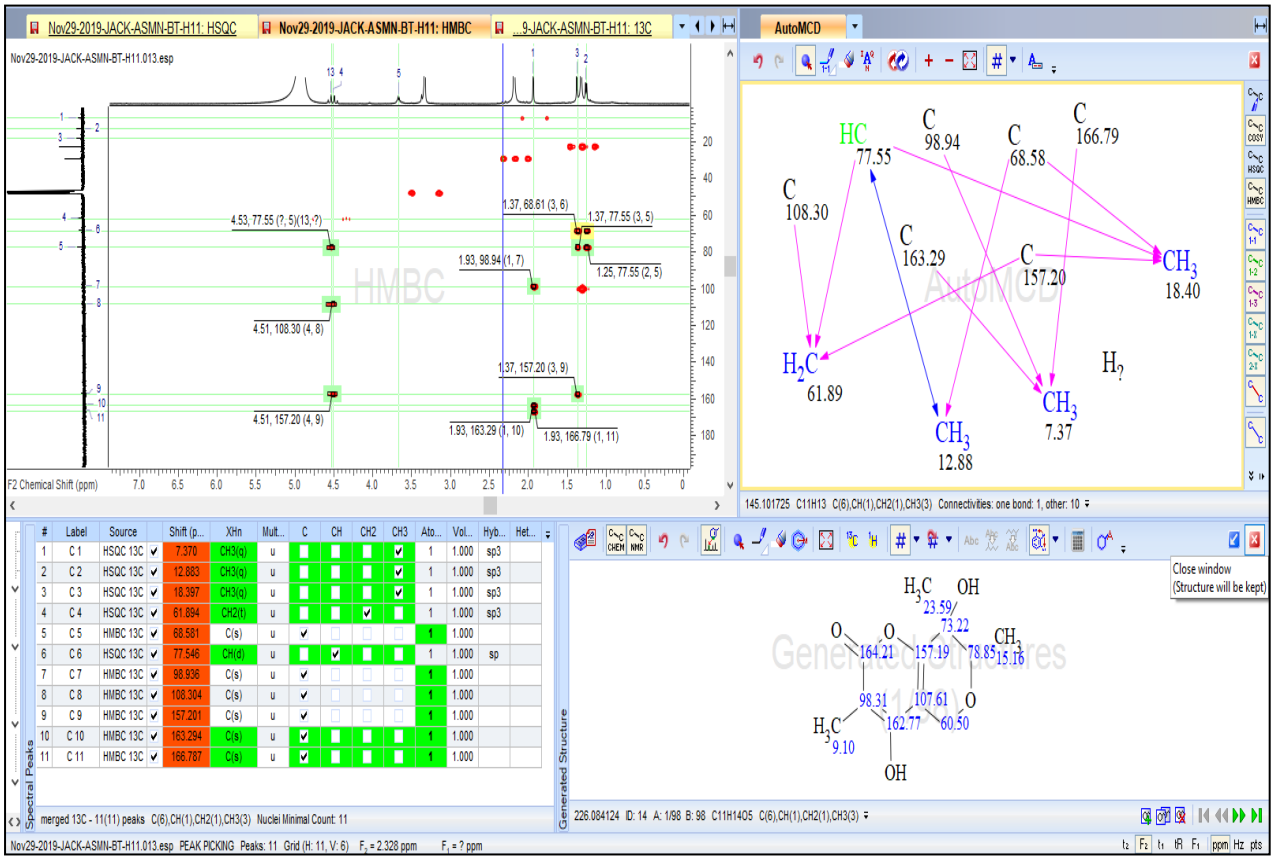

Figure 7.2.1.1. Screenshot of the ACD/Labs Structure Elucidator showing HMBC, and the overall ^{13}C data entry, molecular connectivity diagrams, and one of the calculated structures.

Table 7.2.1.1. Top 4 candidates where the proposed structure occupies the top two positions. Candidates 3 and 4 are structural isomers of the proposed structure. Chemical shifts shown are predicted chemical shifts based on the HOSE code algorithm. The values shown at the bottom are the overall differences between the experimental and the calculated chemical shifts based on Hose code (d_A) and Neural Network (d_N).

1 (ID:14)	2 (ID:58)	3 (ID:28)	4 (ID:52)
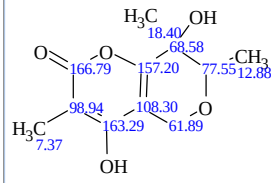	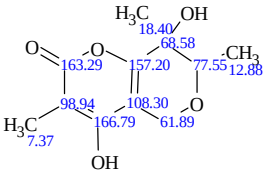	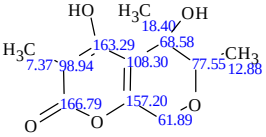	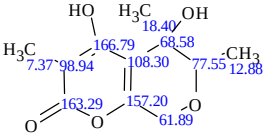
$d_N(^{13}C)$: 2.234 $d_A(^{13}C)$: 1.906 (v.14.50) $d_N(^{13}C+^{1}H)$: 3.130	$d_N(^{13}C)$: 2.038 $d_A(^{13}C)$: 2.073 (v.14.50) $d_N(^{13}C+^{1}H)$: 2.935	$d_N(^{13}C)$: 2.319 $d_A(^{13}C)$: 2.079 (v.14.50) $d_N(^{13}C+^{1}H)$: 3.542	$d_N(^{13}C)$: 2.692 $d_A(^{13}C)$: 2.579 (v.14.50) $d_N(^{13}C+^{1}H)$: 3.915

Differences in ^{13}C chemical shifts can be visualised by plotting the ^{13}C experimental vs Predicted chemical shifts. The data fit extremely well with a coefficient of determination, R^2, value of 0.9988 (**Figure 7.2.1.2**), indicating that the data is close enough to be a structural match, and further confirming the elucidated structure to be correct.

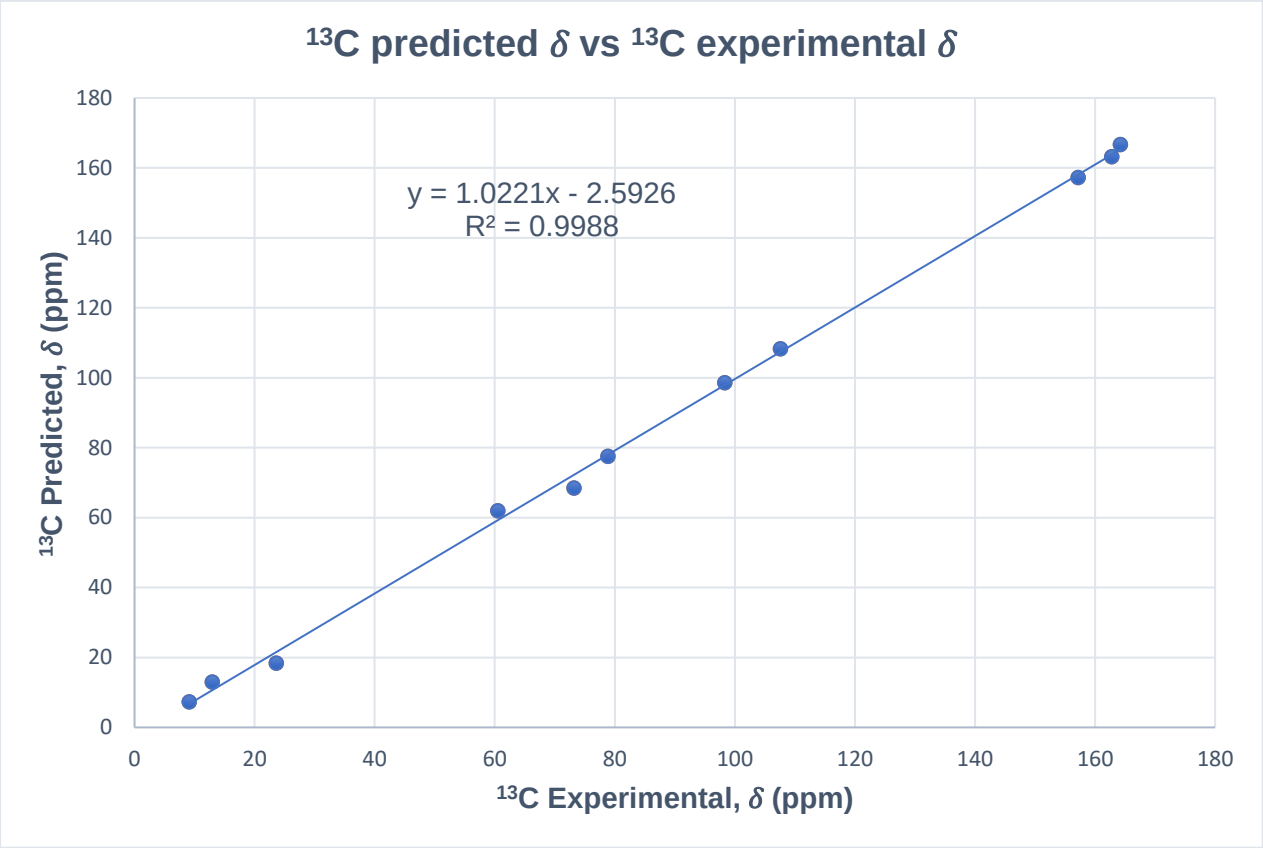

Figure 7.2.1.2. Experimental vs predicted 13C NMR data for *ASMN* compound 1.

The Antimarin database (version 2011) contains 15,831 exclusive masses and 35,850 molecular structures. The structure could not be found in the natural product database, however, the closest structural match is a fungal metabolite called neovasinin (**Figure 7.2.1.3**), isolated from the endophytic fungus *Neocosmospora vasinfecta* E.F. Smith (*Neocosmospora vasinfecta* NHL2298), found in many soils in South Africa. Neovasinin is a phytotoxin that is responsible for the rotting of fruit and roots, seedling damping off and is even phytotoxic against one of the host plants of this fungus, soybean. [141]

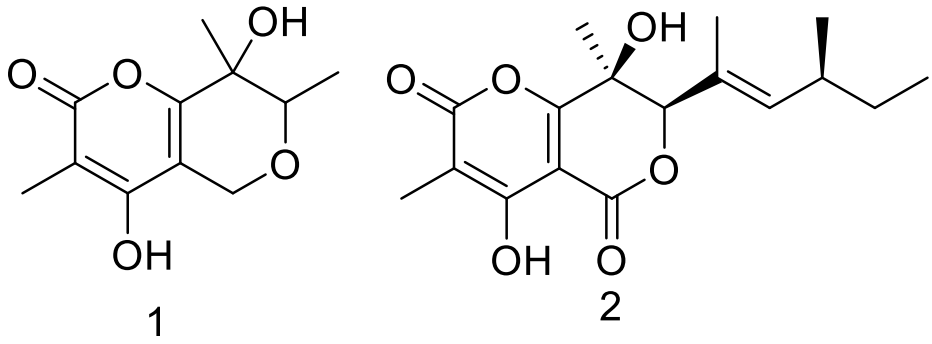

Figure 7.2.1.3. Structure of *neovasinin B* (1) and neovasinin (2)., with CD spectroscopy still ongoing to determine absolute stereochemistry.

7.3 Conclusion

This chapter describes the isolation, purification and the molecular structure of a new natural product, neovasinin B from the culture supernatant of *Aspergillus* sp. strain ASMN, which is a fungus that lives inside the soil of *Fagonia arabica*, a plant that is used medicinally. The activity of *F. arabica* and the great variety of the secondary metabolites produced by *Aspergillus* genus suggest that this symbiotic relationship may be a good source of useful compounds. A well-established method which involves liquid-liquid extraction, size exclusion chromatography (SEC), solid phase extraction (SPE) and high-performance liquid chromatography (HPLC) was used to obtain pure *neovasinin B*. From the HRESIMS and 1D and 2D NMR spectroscopic analysis, the molecular structure of *neovasinin B* was determined as a 3,5,6-trisubstituted 4-hydroxy-2H-pyran-2-one. The structure of *neovasinin B* was also supported by computer assisted structure elucidation (CASE), which, based on the experimental data, recognised *neovasinin B* as a new compound not present in the Antimarin, PubChem, or ChemSpider databases. *Neovasinin B* has a similar structure to neovasinin, a phytotoxin produced by *Neocosmospora*, which shows the diversity of fungal metabolites in regards to their function and structure. The present study on the isolation and identification of neovasinin B is a good example of the unexploited chemical potential of fungal endophytes and the importance of considering these fungi as a source of new bioactive agents. The discovered knowledge on the fungal secondary metabolism contributes to the development of further investigations of neovasinin B's activity and its uses.

CHAPTER 8 Isolation and chemical profiling of natural products from the endophytic fungi *Aspergillus* sp. strain ASF

8.0 Introduction

The endophytic fungal strain *Aspergillus* sp. ASF was isolated from the medicinal plant *Alhagi maurorum* (Leguminosae family), commonly known as "camelthorn," which thrives in arid Middle Eastern regions. This plant has been extensively utilised in traditional medicine systems across Southwest Asia and North Africa, where it is employed as a polyherbal remedy for diverse pathological conditions.[142] Ethnopharmacological records indicate its use in treating inflammatory disorders (rheumatism), neurological ailments (migraine), dermatological manifestations (warts), and hemorrhoidal disease, primarily attributed to its multifaceted pharmacologic activities as a purgative, diaphoretic, expectorant, and diuretic agent. Despite its widespread traditional use, modern scientific validation of *A. maurorum*'s therapeutic potential remains surprisingly limited. Current phytochemical investigations have identified flavonoids, alkaloids, and phenolic compounds as major constituents, but comprehensive metabolomic profiling and mechanistic pharmacological studies are conspicuously absent from the literature. This significant knowledge gap presents a compelling opportunity for systematic investigation of both the plant's native phytochemistry and the metabolic repertoire of its associated endophytes. The ecological symbiosis between medicinal plants and endophytic fungi has emerged as a particularly rich source of novel bioactive metabolites. Endophytes like *Aspergillus* sp. ASF have evolved sophisticated biosynthetic pathways that often produce structural analogues or functional mimics of host plant metabolites, a phenomenon potentially resulting from horizontal gene transfer or co-evolutionary adaptation.[142] As endophytic fungi are known to biosynthesise metabolites structurally and functionally analogous to those of their host plants, *Aspergillus* sp. ASF represents a promising source of pharmacologically relevant compounds. The Aspergillus genus is particularly notable for its exceptional chemical diversity, producing a wide array of secondary metabolites with demonstrated biological activities. In this study, we successfully isolated and characterized five distinct metabolites from *Aspergillus* sp. ASF. Notably, fraction ASF DCM FW 3 was found to contain two additional compounds; however, their complete isolation proved challenging due to substantial differences in relative abundance. This investigation contributes to the growing body of knowledge regarding the biosynthetic potential of endophytic fungi and their role in drug discovery.

8.1 Isolation of natural products from *Aspergillus sp.* strain ASF

Crude extract of *Aspergillus ASF* (isolation and growth conditions described in experimental) was partitioned using the Kupchan method described before, with resulting fractions analysed by ^{1}H NMR. The five fractions: WW (water fraction), WB (butanol fraction), FD (DCM fraction), FH (hexane fraction) and FM (methanol fraction) before further separation of constituent compounds by reversed phase HPLC system.

For the WW fraction a HPLC reversed phase column of Xselect CSH 130 prep 5 µm 10 x 250 mm was used using a solvent system, at t = 0.00 mins of A H_2O (0.05% TFA) 60.0% and B MeOH 40.0%, with a gradient until t = 10.00 mins to A H_2O (0.05% TFA) 0.0% and B MeOH 100.0%, then kept at 100% B

until t = 25.0 mins. This gave 4 isolated compounds, ASF DCM WW 1, 2, 3 and 4. However, only WW 3 was isolated in an amount enough for efficient analysis, structure determination and bioassay testing. For ASF DCM WW 3: 4.2 mg isolated in total.

For the WB fraction a HPLC a Luna C18(2) 100Å 5 µm 10 x 250 mm was used using a solvent system, at t = 0.00 mins of A H_2O (0.05% TFA) 70.0% and B ACN 30.0%, with a gradient until t = 15.00 mins to H_2O (0.05% TFA) 0.0% and ACN 100.0%, then kept at 100% B until t = 25.0 mins. This gave 6 isolated compounds, ASF DCM WB 1, 2, 3, 4, 5 and 6. However, only WB 4 was isolated in an amount enough for efficient analysis, structure determination and bioassay testing. For ASF DCM WB 4: 2.1 mg isolated in total.

For the FD fraction a HPLC a Luna C18(2) 100 Å 5 µm 10 x 250 mm, using a solvent system, at t = 0.00 mins of A H_2O (0.05% TFA) 40.0% and B MeOH 60.0%, with a gradient until t = 10.00 mins to A H_2O (0.05% TFA) 0.0% and B MeOH 100.0%, then kept at 100% B until t = 25.0 mins. This gave 6 isolated compounds, ASF DCM FD 1, 2, 3, 4, 5 and 6. However, only FD 4 and FD 5 were isolated in an amount enough for efficient analysis, structure determination and bioassay testing. FD 1 was noted to be largely impure, and FD 6 peak seems to disappear after a couple of HPLC runs. For ASF DCM FD 4: 2.0 mg and for ASF DCM FD 5: 2.2 mg isolated in total.

For the FH fraction, tell-tale plasticizer contaminant peaks were present within the ^{1}H NMR spectra, sharp aromatic peaks and long unbranched aliphatic chains were present, and therefore this fraction was not pursued for compound isolation and determination.

For the FM fraction a HPLC reverse phase column of Xselect CSH 130 prep 5 µm 10 x 250 mm, using a solvent system, at t = 0.00 mins of A H_2O (0.05% TFA) 50.0% and B MeOH 50.0%, with a gradient until t = 15.00 mins to H_2O (0.05% TFA) 0.0% and MeOH 100.0%, then kept at 100% B until t = 25.0 mins. This gave 6 isolated compounds, ASF DCM FM 1, 2, 3, 4, 5 and 6. However, FM 2 and FM 4 were not isolated in an amount enough for efficient analysis, structure determination and bioassay testing. For ASF DCM FM 1: 4.7 mg, for FM 3: 1.6 mg, for FM 5: 3.7 mg, and for FM 6: 1.0 mg isolated in total.

8.2 Structure elucidation of natural products from *Aspergillus sp.* strain ASF

ASF DCM FM 1 (1) showed a high resolution HRMS of m/z = 357.0688 $[M+H]^+$, Δ= -0.11 ppm, calculated for molecular formula $C_{19}H_{17}O_7$. The molecular formula $C_{19}H_{16}O_6$ requires twelve degrees of unsaturation, the presence of two aromatic rings accounts for eight while one carbonyl and two olefinic carbons account for another two, which makes a total of ten degrees of unsaturation, suggesting the presence of two rings in the structure. Interpretation of ^{1}H NMR, COSY, edited HMQC and HMBC NMR spectra indicated the presence of 4H AA'BB' system at 7.61 (2H, d, *J*=8.7 Hz) and 6.89 (2H, d, *J*=8.8Hz), indicating the presence of a para-disubstituted benzene moiety. Another 4H A_2B_2 at 6.66 (2H, d, *J*=9.0 Hz) and 6.53 (2H, d, 8.1Hz), indicated the presence of another para-disubstituted benzene moiety. It's ^{13}C NMR showed the presence of ten aromatic signals for two aromatic rings, one ester carbonyl δ_C 170.16, one olefinic carbon signal δ_C 127.82, one sp^3 CH_2 δ_C 38.09 and a carbomethoxy carbon δ_C 52.37. Through database dereplication one of the rings, predicted by the

degrees of unsaturation, was suggested to instead be a carbonyl group (C9) unseen by HMBC, due to the unsaturation of bonds near the carbonyl carbon.

ASF DCM FM 3 (2) showed a high resolution HRMS of m/z = 441.1543 $[M+H]^+$, Δ= 0.2ppm, calculated for molecular formula $C_{24}H_{25}O_8$. The molecular formula $C_{24}H_{24}O_8$ requires thirteen degrees of unsaturation, the presence of two aromatic rings accounts for eight while one carbonyl and two olefinic carbons account for another two, which makes a total of ten degrees of unsaturation, suggesting the presence of three rings in the structure. Interpretation of ^{1}H NMR, COSY, edited HMQC and HMBC NMR spectra indicated the presence of 4H A_2B_2 system at 7.55 (2H, d, *J*=8.2 Hz) and 6.89 (2H, d, *J*=9.2Hz), indicating the presence of a para-disubstituted benzene moiety. Another benzene was observed, 3H ABC trisubstituted benzene moiety with two adjacent carbons harbouring hydrogens with a doublet of doublet peak at 6.53 (1H, dd, J=7.9, 1.5Hz) and a doublet at 6.50 (1H, d, J=7.6Hz) and with one isolated Hydrogen causing a doublet at 6.41 (1H, d, 2.4Hz). It's ^{13}C NMR showed the presence of ten aromatic signals for two aromatic rings, one ester carbonyl δ_C 170.13, one olefinic carbon signal δ_C 127.93, one sp^3 CH_2 δ_C 36.70 and a carbomethoxy carbon δ_C 50.39. HMBC analysis indicate carbons at δ_C 76.60 (C22) and 67.63 (C21) are coupled to the protons at δ_H 2.49/2.82 (H20), 1.27 (H23) and 1.17 (H24). Similarly, carbon δ_C 124.77 (C18) being coupled to δ_H 2.49/2.82 (H20) and 3.66 (H21), indicating the side chain observed on 2 (Figure 3.2.1). Through database dereplication one of the rings, predicted by the degrees of unsaturation, was suggested to instead be a carbonyl group (C9) unseen by HMBC.

ASF DCM FM 5 (3) showed a high resolution HRMS of m/z = 425.1593 $[M+H]^+$, Δ= 0.4ppm, ASF DCM WB 4 (3) showed a high resolution HRMS of m/z = 425.1600 $[M+H]^+$, Δ = -1.1ppm, mSigma = 5.6, calculated for molecular formula $C_{24}H_{25}O_7$. The molecular formula $C_{24}H_{24}O_7$ requires thirteen degrees of unsaturation, the presence of two aromatic rings accounts for eight while one carbonyl and four olefinic carbons account for another three, which makes a total of eleven degrees of unsaturation, suggesting the presence of two rings in the structure. Interpretation of ^{1}H NMR, COSY, edited HMQC and HMBC NMR spectra indicated the presence of 4H A_2B_2 system at 7.58 (2H, d, *J*=8.4 Hz) and 6.87 (2H, d, *J*=8.8Hz), indicating the presence of a para-disubstituted benzene moiety. Another benzene was observed, 3H ABC trisubstituted benzene moiety with two adjacent carbons harbouring hydrogens with a doublet of doublet peak at 6.54 (1H, dd, J=7.9, 1.9Hz) and a doublet at 6.50 (1H, d, J=7.6Hz) and with one isolated Hydrogen causing a doublet at 6.41 (1H, d, 2.7Hz).). It's ^{13}C NMR showed the presence of ten aromatic signals for two aromatic rings, one ester carbonyl δ_C 170.24, one olefinic carbon signal δ_C 127.93, one sp^3 CH_2 δ_C 38.16 and a carbomethoxy carbon δ_C 50.17. HMBC analysis indicate carbons at δ_C 131.68 (C22) and 122.19 (C21) are coupled to the protons at δ_H 3.07 (H20), 1.66 (H23) and 1.56 (H24). Similarly, carbon δ_C 127.11 (C18) being coupled to δ_H 3.07 (H20) and 5.06 (H21), indicating the side chain observed on 3 (Figure 3.2.1). Through database dereplication one of the rings, predicted by the degrees of unsaturation, was suggested to instead be a carbonyl group (C9) unseen by HMBC.

ASF DCM FW 3 (4) showed a high resolution HRMS of m/z = 425.1594 $[M+H]^+$, Δ = 0.1ppm, calculated for molecular formula $C_{24}H_{25}O_8$. The molecular formula $C_{24}H_{24}O_7$ requires thirteen degrees of

unsaturation, the presence of two aromatic rings accounts for eight while one carbonyl and two olefinic carbons account for another two, which makes a total of ten degrees of unsaturation, suggesting the presence of three rings in the structure. Interpretation of ^{1}H NMR, COSY, edited HMQC and HMBC NMR spectra indicated the presence of 4H A_2B_2 system at 7.57 (2H, d, *J*=8.4 Hz) and 6.91 (2H, d, *J*=8.6Hz), indicating the presence of a para-disubstituted benzene. Another benzene was observed, 3H ABC trisubstituted benzene moiety with two adjacent carbons harbouring hydrogens with a doublet of doublet peak at 6.52 (1H, dd, J=8.2, 1.4Hz) and a doublet at 6.44 (1H, d, J=8.4Hz) and with one isolated Hydrogen causing a doublet at 6.47 (1H, d, 2.2Hz). It's ^{13}C NMR showed the presence of ten aromatic signals for two aromatic rings, one ester carbonyl δ_C 169.60, one olefinic carbon signal δ_C 128.05, one sp^3 CH_2 δ_C 38.15 and a carbomethoxy carbon δ_C 52.40. HMBC analysis indicate carbons at δ_C 70.15 (C22) and 32.36 (C21) are coupled to the protons at δ_H 2.42/2.50 (H20), 1.21 (H23) and 1.26 (H24). Similarly, carbon δ_C 120.08 (C18) being coupled to δ_H 2.42/2.50 (H20) and 1.74 (H21), indicating the ring structure observed on 4 (Figure 3.2.1). Through database dereplication one of the rings, predicted by the degrees of unsaturation, was suggested to instead be a carbonyl group (C9) unseen by HMBC.

ASF DCM FW 3 (5) showed a high resolution HRMS of m/z= 443.1701 $[M+H]^+$, Δ = 0.0ppm, calculated for molecular formula $C_{24}H_{27}O_8$. Molecular formula $C_{24}H_{26}O_8$ requires twelve degrees of unsaturation, the presence of two aromatic rings accounts for eight while one carbonyl and two olefinic carbons account for another two, which makes a total of ten degrees of unsaturation, suggesting the presence of two rings in the structure. Interpretation of ^{1}H NMR, COSY, edited HMQC and HMBC NMR spectra indicated the presence of 4H A_2B_2 system at 7.57 (2H, d, *J* = 8.4 Hz) and 6.91 (2H, d, *J*=8.6Hz), indicating the presence of a para-disubstituted benzene Another benzene was observed, 3H ABC trisubstituted benzene moiety with two adjacent carbons harbouring hydrogens with a doublet of doublet peak at 6.52 (1H, dd, J = 8.2, 1.4 Hz) and a doublet at 6.44 (1H, d, J = 8.4 Hz) and with one isolated Hydrogen causing a doublet at 6.47 (1H, d, 2.2 Hz). It's ^{13}C NMR showed the presence of ten aromatic signals for two aromatic rings, one ester carbonyl δ_C 169.60, one olefinic carbon signal δ_C 128.05, one sp^3 CH_2 δ_C 38.15 and a carbomethoxy carbon δ_C 52.40. HMBC analysis indicate carbons at δ_C 70.16 (C22) and 43.21 (C21) are coupled to the protons at δ_H 2.58 (H20), 1.20 (H23) and 1.26 (H24). Similarly, carbon δ_C 120.08 (C18) being coupled to δ_H 2.58 (H20) and 1.55 (H21), indicating the side chain observed on 5 (Figure 3.2.1). Through database dereplication one of the rings, predicted by the degrees of unsaturation, was suggested to instead be a carbonyl group (C9) unseen by HMBC.

Through use of Antimarin and Reaxys databases, compound 1 was deduced to be the known compound, butyrolactone ii, IUPAC name methyl 4-hydroxy-3-(4-hydroxyphenyl)-2-[(4-hydroxyphenyl)methyl]-5-oxo-furan-2-carboxylate. Other isolated compounds include: butyrolactone iii (2), butyrolactone i, (3), Aspernolide A (4) and Aspernolide B (5). The other isolated natural products are all analogues of (1). Number 2-5 (Figure 3.2.1) have identical chemical backbones, except for an extra functional chain, bonded to the phenol group (14-19) attached at carbon 18.

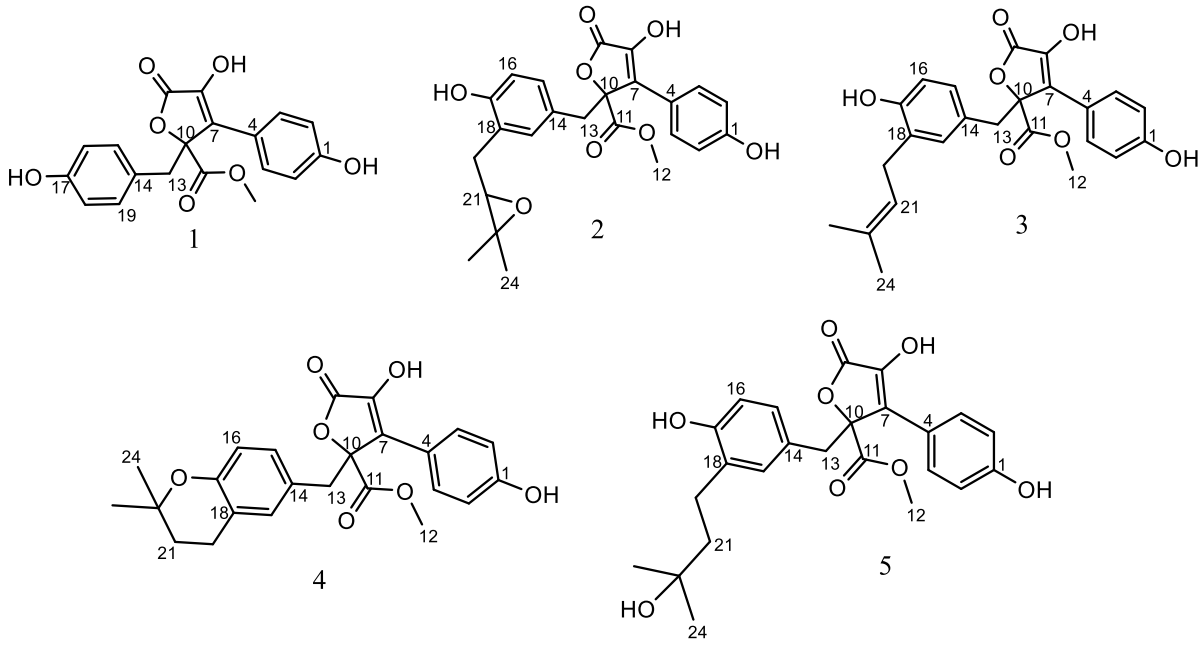

Figure 8.2.1. Natural products isolated and identified from the endophytic fungi, *Aspergillus sp.* strain *ASF*. All compounds already known. Butyrolactone ii (1), butyrolactone iii (2), butyrolactone i (3), Aspernolide A (4) and Aspernolide B (5).

Table 8.2.1. NMR table used in the structure elucidation of ASF DCM FM 1, alongside 13C and 1H chemical shifts in literature of butyrolactone ii in acetone-d6.[143]

Position	^{13}C Chemical shift (ppm)[a]	C-type	^{1}H (chemical shift ppm, No. of H, multiplicity, coupling)[b]	COSY (^{1}H-^{1}H)	HMBC (^{1}H-^{13}C)	Literature ^{13}C (acetone-d6) Chemical shift (ppm)	Literature ^{1}H (acetone-d6) Chemical shift (ppm)
1	158.05	C				158.91	
2, 6	115.27	CH	$H_{2,6}$: 6.89, 2H, d, 8.8	3,5	1	116.66	6.98
3, 5	129.04	CH	$H_{3,5}$: 7.61, 2H, d, 8.7	2,6	2, 4, 7	132.33	7.66
4	128.99	C				130.12	
7	127.82	C				128.06	
10	84.92	C				85.97	
11	170.16	C				170.94	
12	52.37	CH_3	H_{10}: 3.80, 3H, s		11	53.79	3.76
13	38.09	CH2	H_{11}: 3.48, 2H, s		7, 10, 14, 15	39.18	3.40
14	123.83	C				124.89	
15, 19	131.15	CH	$H_{15,19'}$: 6.66, 2H, d, 9.0	16,18	13, 16, 17	139.28	6.69
16, 18	114.22	CH	H_{16}: 6.53, 2H, d, 8.1	15,19	14, 15, 17	115.47	6.59
17	156.18	C				156.18 157.38	

[a] 200 MHZ in CD_3OD

[b] 800 MHz in CD_3OD

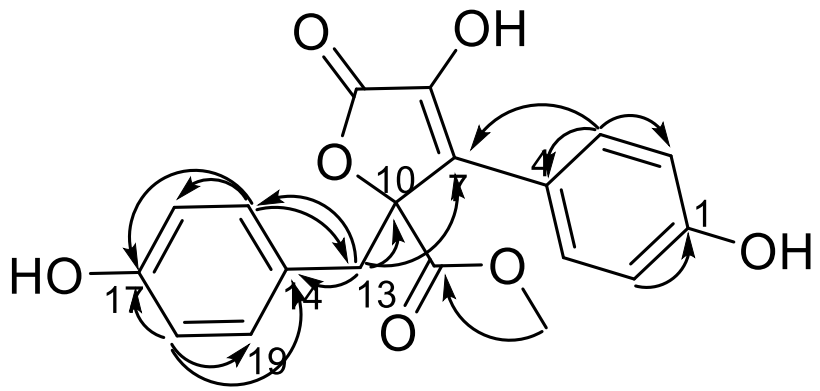

Figure 8.2.2. HMBC correlations of ASF DCM FM 1, butyrolactone ii.

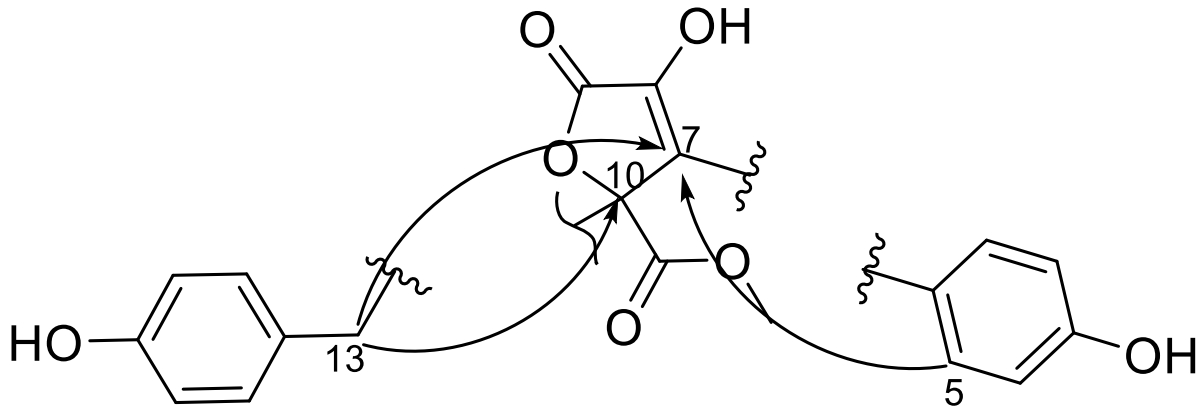

Figure 8.2.3. Fragments constructed and connected through HMBC. Main connections shown.

Table 8.2.2. Table comparing NMR chemical shifts (^{13}C 150 MHz and ^{1}H 800MHz) of ASF DCM FM1. Butyrolactone ii (1), ASF DCM FM 3 Butyrolactone iii (2), ASF DCM FM5 Butyrolactone I (3), in CD_3OD. Alongside literature chemical shfts of Butyrolactone iii (2)[144] and Butyrolactone i (3)[145], in $CDCl_3$.

Position	**δ_C, compound 1, Butyrolactone ii**	**δ_H (J in Hz)**	**δ_C, compound 2, Butyrolactone iii**	**δ_H (J in Hz)**	Literature ^{13}C Butyrolactone iii ($CDCl3$) Chemical shift (ppm)	Literature ^{1}H Butyrolactone iii $CDCl3$) Chemical shift (ppm)	**δ_C, compound 3, Butyrolactone i (FM fraction)**	**δ_H (J in Hz)**	Literature ^{13}C Aspernolide B ($CDCl_3$) Chemical shift (ppm)	Literature ^{1}H Aspernolide A ($CDCl_3$) Chemical shift (ppm)
1	158.1		158.1		157.9		157.9		157.5	
2, 6	115.3	$H_{2,6}$: 6.89, 2H, d, 8.7Hz	113.9	$H_{2,6}$: 6.89, 2H, d, J=9.2Hz	115.6	6.9	115.3	$H_{2,6}$: 6.87, 2H, d, J=8.8Hz	115.0	6.85
3, 5	129.0	$H_{3,5}$: 7.61, 2H, d, 8.7Hz	127.9	$H_{3,5}$: 7.55, 2H, d, J=8.2Hz	128.8	7.5	128.8	$H_{3,5}$: 7.58, 2H, d, J=8.4Hz	129.2	7.54
4	129.0		128.9		121.1		129.0		121.8	
7	127.8		127.9		127.7		127.9		128.2	
10	84.9		85.4		84.8		86.14		85.7	
11	170.2		170.1		169.7		170.2		170.1	
12	52.4	H_{10}: 3.80, 3H, s	50.4	H_{12}: 3.79, 3H, s	53.5	3.8	52.2	H_{12}: 3.79, 3H, s	53.3	3.74
13	38.1	H_{11}: 3.48, 2H, s	36.7	H_{13}: 3.44, 2H, s	38.1	3.4	38.2	H_{13}: 3.42, 2H, s	38.4	3.43
14	123.8		131.6		119.6		131.0		128.1	
15	131.2	$H_{15,19'}$: 6.66, 2H, d, 9.0Hz	127.6	H_{15}: 6.53, 1H, dd, J=7.9, 1.5Hz	128.8	6.6	128.1	H_{15}: 6.54, 1H, dd, J=7.9, 1.9Hz	128.9	6.54
16	114.2	$H_{16,18}$: 6.53, 2H, d, 8.1Hz	114.4	H_{16}: 6.47, 1H, d, J=8.5Hz	114.1	6.5	113.8	H_{16}: 6.50, 1H, d, J=7.6Hz	114.4	6.49
17	156.2		152.1		151.7		153.7		153.4	
18			124.8		124.3		127.1		124.0	

19			129.7	H_{19}: 6.48, 1H, d, J=2.4Hz	131.6	6.6	130.7	H_{19}: 6.41, 1H, d, J=1.1Hz	131.8	6.40
20			29.1	H_{20a}: 2.61, 1H, dd, J=17.5, 4.6Hz H_{20b}: 2.49, 1H, dd, J=16.8, 7.5Hz	31.0	3.0	27.3	H_{20}: 3.07, 2H, d, 8.2	23.2	2.53
21			67.6	H_{19}: 3.66, 1H, t, J=5.6Hz	68.7	3,8	122.2	H_{21}: 5.06, 1H, t, 7.5	40.0	1.54
22			76.6		77.0		131.7		75.4	
23			23.0	H_{23}: 1.27, 3H, s	25.7	1.1	24.6	H_{23}: 1.66, 3H, s	24.9	1.12
24			18.0	H_{24}: 1.17, 3H, s	20.1	1.1	16.4	H_{24}: 1.56, 3H, s	24.0	1.12

Table 8.2.3. Table comparing NMR chemical shifts (^{13}C 150 MHz and ^{1}H 800MHz) of Aspernolide A (4) and Aspernolide B (5), in CD_3OD. Alongside literature chemical shifts of Aspernolide A (4)[145] and Aspernolide B (5)[145], in CD_3OD

Position	**δ_C, compound 4, Aspernolide A**	**δ_H (J in Hz)**	Literature ^{13}C Aspernolide A ($CDCl_3$) Chemical shift (ppm)	Literature ^{1}H Aspernolide A ($CDCl_3$) Chemical shift (ppm)	**δ_C, compound 5, Aspernolide B**	**δ_H (J in Hz)**	Literature ^{13}C Aspernolide B ($CDCl_3$) Chemical shift (ppm)	Literature ^{1}H Aspernolide A ($CDCl_3$) Chemical shift (ppm)
1	157.9		156.4		157.9		157.5	
2, 6	115.3	$H_{2,6}$: 6.91, 2H, d, J=8.6Hz	115.9	6.86	115.3	$H_{2,6}$: 6.89, 2H, d, J=8.6Hz	115.6	6.87
3, 5	131.3	$H_{3,5}$: 7.57, 2H, d, J=8.9Hz	129.5	7.56	131.3	$H_{3,5}$: 7.57, 2H, d, J=8.8Hz	129.1	7.55
4	131.5		122.2		131.5		121.6	
7	128.1		128..8		128.1		128.3	
10	85.4		86.1		85.4		86.1	
11	169.6		169.6		170.2		170.1	
12	52.4	H_{12}: 3.81, 3H, s	53.4	3.72	52.4	H_{12}: 3.81, 3H, s	53.5	3.76
13	38.2	H_{13}: 3.45, 2H, s	38.6	3.39	38.2	H_{13}: 3.45, 2H, s	38.3	
14	131.6		123.5		131.6		128.1	
15	128.9	H_{15}: 6.52, 1H, dd, J=8.2, 1.4Hz	129.0	6.47	128.9	H_{15}: 6.52, 1H, dd, J=8.2, 1.4Hz	128.6	6.55
16	116.0	H_{16}: 6.44, 1H, d, J=8.4Hz	116.6	6.47	116.0	H_{16}: 6.44, 1H, d, J=8.4Hz	114.6	6.52
17	153.8		152.9		153.8		153.2	
18	120.1		120.3		120.1		120.3	
19	131.5	H_{19}: 6.47, 1H, d, J=2.2Hz	131.4	6.53	131.5	H_{19}: 6.47, 1H, d, J=2.2Hz	131.4	6.41
20	24.3	H_{20a}: 2.50, 1H, d, J=5.2Hz H_{20b}: 2.42, 1H, d, J=5.3Hz	22.1	2.53	32.4	J=H_{20}: 2.58, 1H, t, 7.1Hz	24.2	2.37
21	32.4	H_{21}:	32.5	1.66	43.3	1.55,	43.2	1.53

		1.74, 1H, t, J=6.8Hz				2H, t, J=7.2Hz		
22	70.2		74.2		70.2		70.8	
23	27.6	H_{23}: 1.21, 3H, s	26.6	1.21	27.6	1.20, 3H, s	28.4	1.20
24	25.5	H_{24}: 1.26, 3H, s	26.6	1.21	25.6	1.26, 3H, s	28.5	1.21

8.2.1 Bioassays

Bioassays have been run for compounds butyrolactone ii (1), butyrolactone iii (2), butyrolactone i (3) (from FM fraction) and butyrolactone i (3) (from WB fraction), Aspernolide A (4) and Aspernolide B (5) at Medina Foundation, Granada, Spain, to check for antimicrobial activity (fungi, viral and bacterial targets). Unfortunately, all these compounds did not show observable activity against these targets.

8.3 Conclusion

Isolation and chemical profiling of natural products from the endophytic fungus *Aspergillus* sp. strain ASF revealed it as a rich source of bioactive compounds. The study used *Alhagi maurorum* as the host plant and shows that endophytes and their host plants have a significant number of medicinally relevant metabolites in common. Five natural products were isolated, identified and characterized using HPLC, NMR spectroscopy and HRMS. These are butyrolactone II, III, I, Aspernolide A and Aspernolide B which are butyrolactone with diverse structures and different functional groups, which are of significant pharmacological interest. From the available literature, the butyrolactone derivative, butyrolactones I–III, Aspernolide A, and Aspernolide B exhibit a diverse array of biologically significant activities, making them promising candidates for further pharmacological investigation. These compounds demonstrate antibacterial, antifungal, antiviral, and cytotoxic properties, with notable efficacy against drug-resistant pathogens such as MRSA and Candida albicans, as well as selective activity against cancer cell lines, including HeLa, MCF-7, and HepG2. Their mechanisms of action involve topoisomerase II inhibition, ROS induction, NF-κB suppression, and quorum sensing disruption, highlighting their potential as anti-infective and anticancer agents. Additionally, Aspernolide A and B exhibit antimalarial and α-glucosidase inhibitory effects, suggesting applications in antiparasitic and antidiabetic therapies. The structure-activity relationships (SAR) of these molecules reveal that the γ-butyrolactone core is critical for bioactivity, while modifications such as epoxy groups and alkyl side chains enhance their potency and selectivity. Given their broad-spectrum bioactivities and unique mechanisms, these natural products warrant further exploration for drug development, particularly in addressing emerging challenges in antimicrobial resistance and oncology. Future studies should focus on synthetic optimization, in vivo efficacy, and mechanistic elucidation to fully harness their therapeutic potential. The butyrolactone II, III, I, Aspernolide A and Aspernolide B identified in this study show that the Aspergillus genus is rich in producing chemically diverse and biologically active secondary metabolites. However, some compounds could not be isolated because they are present in small amounts or are contaminated, which is a problem. This study has laid a good ground for the future exploration of *Aspergillus* metabolites and the next step should be to develop better methods of extraction and purification, increase the yield and do more bioassays to find out how best these compounds can be used as therapeutic agents. In conclusion, this chapter presents a new approach of using endophytic fungi for natural product research, especially from fungi from plants known to be medicinal, and in doing so

adds to the existing initiatives in developing new drugs from natural sources.

CHAPTER 9: Final discussion

This thesis, entitled *"Chemical Profiling of Endophytic and Marine-Organism-Derived Microorganisms from Diverse Egyptian Ecosystems"*, presents a comprehensive investigation into the chemical diversity and bioactivity of fungal-derived natural products across three interrelated research projects. The first project employed a bioassay-guided fractionation and metabolomic profiling approach to isolate bioactive compounds from endophytic and marine-derived fungal samples. Four fungal extracts demonstrated significant antibiofilm and acetylcholinesterase inhibitory activities. Notably, pure compounds were successfully isolated from strains WNS7(8)F3 (biofilm inhibition) and HS4(50)F3 (acetylcholinesterase inhibition), both identified as *Aspergillus niger*. Statistical metabolomic analysis using ACD/Labs Spectrus and FreeClust revealed hierarchical clustering patterns linked to sample origin, taxonomy, and bioactivity. Dereplication against the AntiMarin database indicated the presence of several potentially novel compounds within these samples.

The second project focused on the isolation and structural elucidation of neovasinin B, a previously underexplored metabolite from *Aspergillus fumigatus* ASMN, highlighting the chemical potential of under-investigated fungal species. The third project led to the identification of five compounds—Butyrolactones I, II, and III, as well as Aspernolide A and Aspernolide B—from *Aspergillus terreus* ASF, further contributing to the pool of structurally diverse and biologically relevant natural products. Together, these studies underscore the remarkable metabolic capacity of fungi from Egyptian terrestrial and marine ecosystems and support their continued exploration for novel bioactive compounds.

9.0 Conclusion

The overarching aim of this research was to chemically profile biologically active secondary metabolites derived from plant- and marine-organism-associated microbes and fungi. This aim was successfully achieved through the systematic completion of nine specific objectives. (1) A diverse collection of plants and marine invertebrates was gathered, ensuring a wide pool of microbial diversity for downstream investigations. (2) Microorganisms associated with these samples were cultured using standard microbiological techniques, resulting in a robust collection of isolates. (3) Small-scale culturing of these isolates enabled the preparation of crude extracts for bioactivity screening. (4) The bioactivities of these extracts were systematically evaluated using antimicrobial, antibiofilm, and acetylcholinesterase inhibitory assays, revealing several promising candidates for further analysis. (5) Bioactive fungal strains were identified through 18S rRNA gene sequencing, ensuring precise taxonomic classification. (6) Active extracts were fractionated and purified using bioassay-guided chromatographic techniques, leading to the isolation of individual bioactive compounds. (7) Dereplication of these extracts was performed using HR-LC-MS/MS combined with advanced software-database tools, effectively minimizing redundancy in compound identification. (8) Chemometric tools were employed to provide detailed chemical profiling of the extracts, offering valuable insights into their metabolomic composition. (9) The structures of biologically active

compounds were elucidated using spectroscopic techniques such as NMR and MS, confirming their novelty and bioactivity. By accomplishing these objectives, this research has significantly contributed to the discovery and characterisation of secondary metabolites from underexplored microbial sources. These findings underscore the chemical and biological potential of these metabolites and establish a strong foundation for their future exploration in pharmaceutical and biotechnological applications. In conclusion, this work shows that bioassay guided fractionation, metabolomic profiling and chemical characterisation are useful in selecting fungal samples for further investigation. The high frequency of novel compounds detected also emphasises the richness of fungal metabolites for drug discovery. In this regard, this thesis has laid a very good ground for future natural product research in Egypt and recommends the use of advanced dereplication technologies, in depth investigation of promising samples and optimal bioactivity to release other potential in this area.

9.1 Future work

Based on the findings of this study, future work will focus on several key areas to advance the natural product discovery pipeline. One priority will be the incorporation of molecular networking, a powerful MS/MS-based clustering approach that enables the visualisation of structural relationships between compounds. By grouping metabolites into molecular families based on fragmentation similarity, this method improves dereplication by helping to distinguish known compounds from potentially novel analogues. It also leverages built-in spectral libraries for rapid annotation, facilitating the prioritisation of new chemical entities for further study. This approach will be applied in future analyses of complex natural product mixtures to enhance the efficiency and depth of metabolomic investigations. Additionally, the stereochemical configuration of certain compounds identified in this study, such as HS4(50)F3-2-s1 and the ASMN compound, remains unresolved. Due to time constraints, full stereochemical elucidation was not completed, but ongoing work will address this using circular dichroism (CD) spectroscopy, polarimetry, and related techniques to better understand their structure–activity relationships. The study also revealed several purified compounds that have yet to undergo biological evaluation. Future investigations will assess their antimicrobial, antibiofilm, acetylcholinesterase inhibitory, and cytotoxic activities to explore their therapeutic potential. Altogether, these next steps will significantly contribute to natural product chemistry by refining dereplication strategies, completing structural elucidation, and expanding bioactivity profiling—ultimately aiding the discovery of novel bioactive compounds for drug development.

10. References

(1) Dias, D. A.; Urban, S.; Roessner, U. A Historical Overview of Natural Products in Drug Discovery. *Metabolites* **2012**, *2* (2), 303–336. https://doi.org/10.3390/metabo2020303.

(2) Newman, D. J.; Cragg, G. M. Natural Products as Sources of New Drugs over the Nearly Four Decades from 01/1981 to 09/2019. *J. Nat. Prod.* **2020**, *83* (3), 770–803. https://doi.org/10.1021/acs.jnatprod.9b01285.

(3) *Current and Future Treatments in Alzheimer Disease: An Update - Konstantina G Yiannopoulou, Sokratis G Papageorgiou, 2020*. https://journals.sagepub.com/doi/full/10.1177/1179573520907397 (accessed 2024-02-16).

(4) Sung, H.; Ferlay, J.; Siegel, R. L.; Laversanne, M.; Soerjomataram, I.; Jemal, A.; Bray, F. Global Cancer Statistics 2020: GLOBOCAN Estimates of Incidence and Mortality Worldwide for 36 Cancers in 185 Countries. *CA. Cancer J. Clin.* **2021**, *71* (3), 209–249. https://doi.org/10.3322/caac.21660.

(5) Rossiter, S. E.; Fletcher, M. H.; Wuest, W. M. Natural Products as Platforms To Overcome Antibiotic Resistance. *Chem. Rev.* **2017**, *117* (19), 12415–12474. https://doi.org/10.1021/acs.chemrev.7b00283.

(6) Strobel, G.; Daisy, B. Bioprospecting for Microbial Endophytes and Their Natural Products. *Microbiol. Mol. Biol. Rev. MMBR* **2003**, *67* (4), 491–502. https://doi.org/10.1128/MMBR.67.4.491-502.2003.

(7) Khan, A. L.; Hussain, J.; Al-Harrasi, A.; Al-Rawahi, A.; Lee, I.-J. Endophytic Fungi: Resource for Gibberellins and Crop Abiotic Stress Resistance. *Crit. Rev. Biotechnol.* **2015**, *35* (1), 62–74. https://doi.org/10.3109/07388551.2013.800018.

(8) Schulz, B.; Boyle, C.; Draeger, S.; Römmert, A.-K.; Krohn, K. Endophytic Fungi: A Source of Novel Biologically Active Secondary Metabolites* *Paper Presented at the British Mycological Society Symposium on Fungal Bioactive Compounds, Held at the University of Wales Swansea on 22–27 April 2001. *Mycol. Res.* **2002**, *106* (9), 996–1004. https://doi.org/10.1017/S0953756202006342.

(9) Porras-Alfaro, A.; Bayman, P. Hidden Fungi, Emergent Properties: Endophytes and Microbiomes. *Annu. Rev. Phytopathol.* **2011**, *49* (1), 291–315. https://doi.org/10.1146/annurev-phyto-080508-081831.

(10) Mp, S.; Je, J.; Sf, B. Cytoskyrins and Cytosporones Produced by Cytospora Sp. CR200: Taxonomy, Fermentation and Biological Activities. *PubMed* **2007**.

(11) E, P.-M.; Ma, S.-B.; E, S.; E, G.-D.; Nc, S.-G.; Ma, M.-R.; Ej, C.; J, V.; Ál, C.; C, S.-T. The Nurr7 Agonist Cytosporone B Differentially Regulates Inflammatory Responses in Human Polarized Macrophages. *PubMed*.

(12) Nakayama, J.; Uemura, Y.; Nishiguchi, K.; Yoshimura, N.; Igarashi, Y.; Sonomoto, K. Ambuic Acid Inhibits the Biosynthesis of Cyclic Peptide Quormones in Gram-Positive Bacteria. *Antimicrob.*

Agents Chemother. **2009**, *53* (2), 580–586. https://doi.org/10.1128/AAC.00995-08.

(13) R, K.; J, C. Codinaeopsin, an Antimalarial Fungal Polyketide. *PubMed* **2008**.

(14) *Fusaricidin A, a New Depsipeptide Antibiotic Produced by* Bacillus polymyxa *KT-8*. https://www.jstage.jst.go.jp/article/antibiotics1968/49/2/49_2_129/_article/-char/ja/ (accessed 2024-06-07).

(15) Qin, S.; Xing, K.; Jiang, J.-H.; Xu, L.-H.; Li, W.-J. Biodiversity, Bioactive Natural Products and Biotechnological Potential of Plant-Associated Endophytic Actinobacteria. *Appl. Microbiol. Biotechnol.* **2011**, *89* (3), 457–473. https://doi.org/10.1007/s00253-010-2923-6.

(16) Bushley, K. E.; Raja, R.; Jaiswal, P.; Cumbie, J. S.; Nonogaki, M.; Boyd, A. E.; Owensby, C. A.; Knaus, B. J.; Elser, J.; Miller, D.; Di, Y.; McPhail, K. L.; Spatafora, J. W. The Genome of Tolypocladium Inflatum: Evolution, Organization, and Expression of the Cyclosporin Biosynthetic Gene Cluster. *PLOS Genet.* **2013**, *9* (6), e1003496. https://doi.org/10.1371/journal.pgen.1003496.

(17) Salehi, B.; Selamoglu, Z.; S. Mileski, K.; Pezzani, R.; Redaelli, M.; C. Cho, W.; Kobarfard, F.; Rajabi, S.; Martorell, M.; Kumar, P.; Martins, N.; Subhra Santra, T.; Sharifi-Rad, J. Liposomal Cytarabine as Cancer Therapy: From Chemistry to Medicine. *Biomolecules* **2019**, *9* (12), 773. https://doi.org/10.3390/biom9120773.

(18) De Souza, M. V. N. (+)-Discodermolide: A Marine Natural Product Against Cancer. *Sci. World J.* **2004**, *4* (1), 297813. https://doi.org/10.1100/tsw.2004.96.

(19) Ganjoo, K. N.; Patel, S. Trabectedin: An Anticancer Drug from the Sea. *Expert Opin. Pharmacother.* **2009**, *10* (16), 2735–2743. https://doi.org/10.1517/14656560903277236.

(20) Chen, C.; Imamura, N.; Nishijima, M.; Adachi, K.; Sakai, M.; Sano, H. Halymecins, New Antimicroalgal Substances Produced by Fungi Isolated from Marine Algae. *J. Antibiot. (Tokyo)* **1996**, *49* (10), 998–1005. https://doi.org/10.7164/antibiotics.49.998.

(21) Saleem, M.; Ali, M. S.; Hussain, S.; Jabbar, A.; Ashraf, M.; Lee, Y. S. Marine Natural Products of Fungal Origin. *Nat. Prod. Rep.* **2007**, *24* (5), 1142–1152. https://doi.org/10.1039/B607254M.

(22) Rateb, M. E.; Ebel, R. Secondary Metabolites of Fungi from Marine Habitats. *Nat. Prod. Rep.* **2011**, *28* (2), 290–344. https://doi.org/10.1039/c0np00061b.

(23) Aly, A. H.; Debbab, A.; Proksch, P. Fifty Years of Drug Discovery from Fungi. *Fungal Divers.* **2011**, *50* (1), 3–19. https://doi.org/10.1007/s13225-011-0116-y.

(24) *Biomolecules | Free Full-Text | Bioactive Compounds: Natural Defense Against Cancer?* https://www.mdpi.com/2218-273X/9/12/758 (accessed 2024-02-16).

(25) Bhadresha, K. P.; Jain, N. K.; Rawal, R. M. Assessing the Protective Effect of Moringa Oleifera Extract against Bone Metastasis: An In Vitro Simulated Digestion Approach. *Nutr. Cancer* **2022**, *74* (3), 1023–1036. https://doi.org/10.1080/01635581.2021.1933099.

(26) Garcia-Oliveira, P.; Otero, P.; Pereira, A. G.; Chamorro, F.; Carpena, M.; Echave, J.; Fraga-Corral, M.; Simal-Gandara, J.; Prieto, M. A. Status and Challenges of Plant-Anticancer Compounds in Cancer Treatment. *Pharmaceuticals* **2021**, *14* (2), 157. https://doi.org/10.3390/ph14020157.

(27) Saville, M. W.; Lietzau, J.; Pluda, J. M.; Feuerstein, I.; Odom, J.; Wilson, W. H.; Humphrey, R. W.;

Feigal, E.; Steinberg, S. M.; Broder, S. Treatment of HIV-Associated Kaposi's Sarcoma with Paclitaxel. *Lancet Lond. Engl.* **1995**, *346* (8966), 26–28. https://doi.org/10.1016/s0140-6736(95)92654-2.

(28) Wani, M. C.; Taylor, H. L.; Wall, M. E.; Coggon, P.; McPhail, A. T. Plant Antitumor Agents. VI. The Isolation and Structure of Taxol, a Novel Antileukemic and Antitumor Agent from Taxus Brevifolia. *J. Am. Chem. Soc.* **1971**, *93* (9), 2325–2327. https://doi.org/10.1021/ja00738a045.

(29) *Semi-Synthesis of Paclitaxel Analogues - ProQuest*. https://www.proquest.com/openview/b396b00138a93eee0688af2a0c8cf7a1/1?pq-origsite=gscholar&cbl=51922&diss=y (accessed 2025-05-28).

(30) Stierle, A.; Strobel, G.; Stierle, D. Taxol and Taxane Production by Taxomyces Andreanae, an Endophytic Fungus of Pacific Yew. *Science* **1993**, *260* (5105), 214–216. https://doi.org/10.1126/science.8097061.

(31) Wall, M. E.; Wani, M. C.; Cook, C. E.; Palmer, K. H.; McPhail, A. T.; Sim, G. A. *Plant Antitumor Agents. I. The Isolation and Structure of Camptothecin, a Novel Alkaloidal Leukemia and Tumor Inhibitor from Camptotheca acuminata1,2*. ACS Publications. https://doi.org/10.1021/ja00968a057.

(32) Natarajan, S.; Pucker, B.; Srivastava, S. Genomic and Transcriptomic Analysis of Camptothecin Producing Novel Fungal Endophyte: Alternaria Burnsii NCIM 1409. *Sci. Rep.* **2023**, *13* (1), 14614. https://doi.org/10.1038/s41598-023-41738-6.

(33) Uma Shaanker, R.; Ramesha, B. T.; Ravikanth, G.; Gunaga, R.; Vasudeva, R.; Ganeshaiah, K. N. Chemical Profiling of Nothapodytes Nimmoniana for Camptothecin, an Important Anticancer Alkaloid: Towards the Development of a Sustainable Production System. In *Bioactive Molecules and Medicinal Plants*; Ramawat, K. G., Merillon, J. M., Eds.; Springer: Berlin, Heidelberg, 2008; pp 197–213. https://doi.org/10.1007/978-3-540-74603-4_10.

(34) Kousar, R.; Naeem, M.; Jamaludin, M. I.; Arshad, A.; Shamsuri, A. N.; Ansari, N.; Akhtar, S.; Hazafa, A.; Uddin, J.; Khan, A.; Al-Harrasi, A. Exploring the Anticancer Activities of Novel Bioactive Compounds Derived from Endophytic Fungi: Mechanisms of Action, Current Challenges and Future Perspectives. *Am. J. Cancer Res.* **2022**, *12* (7), 2897–2919.

(35) *Antimicrobial resistance*. https://www.who.int/news-room/fact-sheets/detail/antimicrobial-resistance (accessed 2024-03-07).

(36) *Bioactive Natural Compounds from the Plant Endophytic Fungi Pesta...: Ingenta Connect*. https://www.ingentaconnect.com/content/ben/mrmc/2012/00000012/00000013/art00006 (accessed 2024-03-07).

(37) *Hirsutellide A, a New Antimycobacterial Cyclohexadepsipeptide from the Entomopathogenic Fungus Hirsutella kobayasii | Journal of Natural Products*. https://pubs.acs.org/doi/abs/10.1021/np020055+ (accessed 2024-03-07).

(38) *Marine Drugs | Free Full-Text | Bioactive Compounds Produced by Strains of Penicillium and Talaromyces of Marine Origin*. https://www.mdpi.com/1660-3397/14/2/37 (accessed 2024-03-07).

(39) Ibraheem, W.; Chaar, C.; Camiade, E.; Hervé, V.; Fouquenet, D.; Roux, A.-E.; Si-Tahar, M.; Ahmed, E.; Thibonnet, J.; Thiery, E.; Petrignet, J. Synthesis, Antibacterial and Cytotoxic Evaluation of Cytosporone E and Analogs. *J. Mol. Struct.* **2022**, *1252*, 132135. https://doi.org/10.1016/j.molstruc.2021.132135.

(40) Bondi, M. W.; Edmonds, E. C.; Salmon, D. P. Alzheimer's Disease: Past, Present, and Future. *J. Int. Neuropsychol. Soc.* **2017**, *23* (9–10), 818–831. https://doi.org/10.1017/S135561771700100X.

(41) Khan, S.; Barve, K. H.; Kumar, M. S. Recent Advancements in Pathogenesis, Diagnostics and Treatment of Alzheimer's Disease. *Curr. Neuropharmacol.* **2020**, *18* (11), 1106–1125. https://doi.org/10.2174/1570159X18666200528142429.

(42) *Memantine hydrochloride | Drugs | BNF content published by NICE*. https://bnf.nice.org.uk/drugs/memantine-hydrochloride/ (accessed 2024-06-12).

(43) *Donepezil: a medicine to treat some types of dementia*. nhs.uk. https://www.nhs.uk/medicines/donepezil/ (accessed 2024-06-12).

(44) *Rivastigmine | Drugs | BNF content published by NICE*. https://bnf.nice.org.uk/drugs/rivastigmine/ (accessed 2024-06-12).

(45) *Tacrine*. https://go.drugbank.com/drugs/DB00382 (accessed 2024-06-12).

(46) Wang, Z.; Ma, Z.; Wang, L.; Tang, C.; Hu, Z.; Chou, G.; Li, W. Active Anti-Acetylcholinesterase Component of Secondary Metabolites Produced by the Endophytic Fungi of Huperzia Serrata. *Electron. J. Biotechnol.* **2015**, *18* (6), 399–405. https://doi.org/10.1016/j.ejbt.2015.08.005.

(47) Piemontese, L. New Approaches for Prevention and Treatment of Alzheimer's Disease: A Fascinating Challenge. *Neural Regen. Res.* **2017**, *12* (3), 405–406. https://doi.org/10.4103/1673-5374.202942.

(48) Sabbagh, M. N.; Hendrix, S.; Harrison, J. E. FDA Position Statement "Early Alzheimer's Disease: Developing Drugs for Treatment, Guidance for Industry." *Alzheimers Dement. Transl. Res. Clin. Interv.* **2019**, *5*, 13–19. https://doi.org/10.1016/j.trci.2018.11.004.

(49) Cummings, J.; Lee, G.; Ritter, A.; Sabbagh, M.; Zhong, K. Alzheimer's Disease Drug Development Pipeline: 2019. *Alzheimers Dement. Transl. Res. Clin. Interv.* **2019**, *5*, 272–293. https://doi.org/10.1016/j.trci.2019.05.008.

(50) Zhu, J.; Wang, Z.; Song, L.; Fu, W.; Liu, L. Anti-Alzheimer's Natural Products Derived from Plant Endophytic Fungi. *Molecules* **2023**, *28* (5), 2259. https://doi.org/10.3390/molecules28052259.

(51) *Natural Products Isolation | SpringerLink*. https://link.springer.com/book/10.1007/978-1-61779-624-1 (accessed 2024-03-01).

(52) Zhang, Q.-W.; Lin, L.-G.; Ye, W.-C. Techniques for Extraction and Isolation of Natural Products: A Comprehensive Review. *Chin. Med.* **2018**, *13* (1), 20. https://doi.org/10.1186/s13020-018-0177-x.

(53) *Kjer, 2009 Methods For Isolation of Marine-Derived Endophytic Fungi and Their Bioactive Secondary Products | PDF | Chromatography | High Performance Liquid Chromatography*. Scribd. https://www.scribd.com/document/282369174/Kjer-2009-Methods-for-Isolation-of-

Marine-Derived-Endophytic-Fungi-and-Their-Bioactive-Secondary-Products (accessed 2024-02-23).

(54) Striegel, A. M. Size-Exclusion Chromatography: A Twenty-First Century Perspective. *Chromatographia* **2022**, *85* (4), 10.1007/s10337-022-04143–1. https://doi.org/10.1007/s10337-022-04143-1.

(55) van Santen, J. A.; Jacob, G.; Singh, A. L.; Aniebok, V.; Balunas, M. J.; Bunsko, D.; Neto, F. C.; Castaño-Espriu, L.; Chang, C.; Clark, T. N.; Cleary Little, J. L.; Delgadillo, D. A.; Dorrestein, P. C.; Duncan, K. R.; Egan, J. M.; Galey, M. M.; Haeckl, F. P. J.; Hua, A.; Hughes, A. H.; Iskakova, D.; Khadilkar, A.; Lee, J.-H.; Lee, S.; LeGrow, N.; Liu, D. Y.; Macho, J. M.; McCaughey, C. S.; Medema, M. H.; Neupane, R. P.; O'Donnell, T. J.; Paula, J. S.; Sanchez, L. M.; Shaikh, A. F.; Soldatou, S.; Terlouw, B. R.; Tran, T. A.; Valentine, M.; van der Hooft, J. J. J.; Vo, D. A.; Wang, M.; Wilson, D.; Zink, K. E.; Linington, R. G. The Natural Products Atlas: An Open Access Knowledge Base for Microbial Natural Products Discovery. *ACS Cent. Sci.* **2019**, *5* (11), 1824–1833. https://doi.org/10.1021/acscentsci.9b00806.

(56) A, G. The Impact of Natural Products upon Modern Drug Discovery. *PubMed*.

(57) Feher, M.; Schmidt, J. M. Property Distributions: Differences between Drugs, Natural Products, and Molecules from Combinatorial Chemistry. *J. Chem. Inf. Comput. Sci.* **2003**, *43* (1), 218–227. https://doi.org/10.1021/ci0200467.

(58) Urbain, A.; Simões-Pires, C. Thin-Layer Chromatography for the Detection and Analysis of Bioactive Natural Products. **2020**, 1–29. https://doi.org/10.1002/9780470027318.a9907.pub2.

(59) Neuss, N.; Miller, R. D.; Affolder, C. A.; Nakatsukasa, W.; Mabe, J.; Huckstep, L. L.; De Higuera, N. L.; Hunt, A. H.; Occolowitz, J. L.; Gilliam, J. H. High Performance Liquid Chromatography (HPLC.) of Natural Products. III [1]. Isolation of New Tripeptides from the Fermentation Broth of P. Chrysogenum. *Helv. Chim. Acta* **1980**, *63* (5), 1119–1129. https://doi.org/10.1002/hlca.19800630503.

(60) Sawikowska, A.; Piasecka, A.; Kachlicki, P.; Krajewski, P. Separation of Chromatographic Co-Eluted Compounds by Clustering and by Functional Data Analysis. *Metabolites* **2021**, *11* (4), 214. https://doi.org/10.3390/metabo11040214.

(61) Kimura, M.; Rodriguez-Amaya, D. B. A Scheme for Obtaining Standards and HPLC Quantification of Leafy Vegetable Carotenoids. *Food Chem.* **2002**, *78* (3), 389–398. https://doi.org/10.1016/S0308-8146(02)00203-0.

(62) Wolfender, J.-L. HPLC in Natural Product Analysis: The Detection Issue. *Planta Med.* **2009**, *75* (7), 719–734. https://doi.org/10.1055/s-0028-1088393.

(63) Avery, V. M.; Camp, D.; Carroll, A. R.; Jenkins, I. D.; Quinn, R. J. 3.07 - The Identification of Bioactive Natural Products by High Throughput Screening (HTS). In *Comprehensive Natural Products II*; Liu, H.-W. (Ben), Mander, L., Eds.; Elsevier: Oxford, 2010; pp 177–203. https://doi.org/10.1016/B978-008045382-8.00062-9.

(64) *Identification and characterization of molecular targets of natural products by mass spectrometry - Cheng - 2010 - Mass Spectrometry Reviews - Wiley Online Library*. https://analyticalsciencejournals.onlinelibrary.wiley.com/doi/full/10.1002/mas.20235

(accessed 2024-02-28).

(65) Bross-Walch, N.; Kühn, T.; Moskau, D.; Zerbe, O. Strategies and Tools for Structure Determination of Natural Products Using Modern Methods of NMR Spectroscopy. *Chem. Biodivers.* **2005**, *2* (2), 147–177. https://doi.org/10.1002/cbdv.200590000.

(66) *Determination of the absolute configuration of natural products - ScienceDirect*. https://www.sciencedirect.com/science/article/abs/pii/S1875536413600163 (accessed 2024-02-28).

(67) Halabalaki, M.; Vougogiannopoulou, K.; Mikros, E.; Skaltsounis, A. L. Recent Advances and New Strategies in the NMR-Based Identification of Natural Products. *Curr. Opin. Biotechnol.* **2014**, *25*, 1–7. https://doi.org/10.1016/j.copbio.2013.08.005.

(68) Sorokina, M.; Steinbeck, C. Review on Natural Products Databases: Where to Find Data in 2020. *J. Cheminformatics* **2020**, *12* (1), 20. https://doi.org/10.1186/s13321-020-00424-9.

(69) Elyashberg, M.; Argyropoulos, D. Computer Assisted Structure Elucidation (CASE): Current and Future Perspectives. *Magn. Reson. Chem.* **2021**, *59* (7), 669–690. https://doi.org/10.1002/mrc.5115.

(70) Watrous, J.; Roach, P.; Alexandrov, T.; Heath, B. S.; Yang, J. Y.; Kersten, R. D.; van der Voort, M.; Pogliano, K.; Gross, H.; Raaijmakers, J. M.; Moore, B. S.; Laskin, J.; Bandeira, N.; Dorrestein, P. C. Mass Spectral Molecular Networking of Living Microbial Colonies. *Proc. Natl. Acad. Sci.* **2012**, *109* (26), E1743–E1752. https://doi.org/10.1073/pnas.1203689109.

(71) Yang, J. Y.; Sanchez, L. M.; Rath, C. M.; Liu, X.; Boudreau, P. D.; Bruns, N.; Glukhov, E.; Wodtke, A.; de Felicio, R.; Fenner, A.; Wong, W. R.; Linington, R. G.; Zhang, L.; Debonsi, H. M.; Gerwick, W. H.; Dorrestein, P. C. Molecular Networking as a Dereplication Strategy. *J. Nat. Prod.* **2013**, *76* (9), 1686–1699. https://doi.org/10.1021/np400413s.

(72) Quinn, R. A.; Nothias, L.-F.; Vining, O.; Meehan, M.; Esquenazi, E.; Dorrestein, P. C. Molecular Networking As a Drug Discovery, Drug Metabolism, and Precision Medicine Strategy.

(73) Wenderski, T. A.; Stratton, C. F.; Bauer, R. A.; Kopp, F.; Tan, D. S. Principal Component Analysis as a Tool for Library Design: A Case Study Investigating Natural Products, Brand-Name Drugs, Natural Product-like Libraries, and Drug-like Libraries. *Methods Mol. Biol. Clifton NJ* **2015**, *1263*, 225–242. https://doi.org/10.1007/978-1-4939-2269-7_18.

(74) Beever, R. E.; Bollard, E. G. The Nature of the Stimulation of Fungal Growth by Potato Extract. *Microbiology* **1970**, *60* (2), 273–279. https://doi.org/10.1099/00221287-60-2-273.

(75) DSMZ_Medium243.Pdf. https://www.dsmz.de/microorganisms/medium/pdf/DSMZ_Medium243.pdf (accessed 2024-07-21).

(76) Tedesco, P.; Maida, I.; Palma Esposito, F.; Tortorella, E.; Subko, K.; Ezeofor, C. C.; Zhang, Y.; Tabudravu, J.; Jaspars, M.; Fani, R.; De Pascale, D. Antimicrobial Activity of Monoramnholipids Produced by Bacterial Strains Isolated from the Ross Sea (Antarctica). *Mar. Drugs* **2016**, *14* (5), 83. https://doi.org/10.3390/md14050083.

(77) *112926-00-8 CAS | SILICA GEL 70-230 MESH | Column & Thin Layer Chromatographic Reagent |*

Article No. 05699. https://www.lobachemie.com/Column-Thin-layer-Chromatographic-Reagent-5699A/SILICA-GEL-70-230-MESH-CASNO-112926-00-8.aspx (accessed 2024-10-16).

(78) 5991-1023EN.Pdf. https://www.agilent.com/cs/library/applications/5991-1023EN.pdf (accessed 2024-10-16).

(79) *Real-Time PCR Kits | qPCR Enzymes & Kits | QIAGEN*. https://www.qiagen.com/us/product-categories/discovery-and-translational-research/pcr-qpcr-dpcr/real-time-pcr-enzymes-and-kits?cmpid=PC_PCR_PCR_pcr-traffic_1120_SEA_GA&gad_source=1&gclid=Cj0KCQjwyL24BhCtARIsALo0fSBt4-gHTm_vqT15uY4MaZ7J2z4xewmUh-xiQEf72YhxTEvizaZnaBkaAmqEEALw_wcB (accessed 2024-10-16).

(80) *GenBank Overview*. https://www.ncbi.nlm.nih.gov/genbank/ (accessed 2024-10-16).

(81) *Acetylcholinesterase Inhibitor Screening Kit (Colorimetric) (ab283363) | Abcam*. https://www.abcam.com/products/assay-kits/acetylcholinesterase-inhibitor-screening-kit-colorimetric-ab283363.html (accessed 2024-02-28).

(82) Rethinking Common Solvents in Butyrylcholinesterase Activity Assays. *Inorg. Chem. Commun.* **2022**, *143*, 109796. https://doi.org/10.1016/j.inoche.2022.109796.

(83) Kokoska, L.; Polesny, Z.; Rada, V.; Nepovim, A.; Vanek, T. Screening of Some Siberian Medicinal Plants for Antimicrobial Activity. *J. Ethnopharmacol.* **2002**, *82* (1), 51–53. https://doi.org/10.1016/s0378-8741(02)00143-5.

(84) Christensen, G. D.; Simpson, W. A.; Younger, J. J.; Baddour, L. M.; Barrett, F. F.; Melton, D. M.; Beachey, E. H. Adherence of Coagulase-Negative Staphylococci to Plastic Tissue Culture Plates: A Quantitative Model for the Adherence of Staphylococci to Medical Devices. *J. Clin. Microbiol.* **1985**, *22* (6), 996–1006.

(85) *Fundación MEDINA | Our mission on drug discovery and pharma research*. https://www.medinadiscovery.com/ (accessed 2024-10-16).

(86) Tsang, C.-C.; Tang, J. Y. M.; Lau, S. K. P.; Woo, P. C. Y. Taxonomy and Evolution of Aspergillus, Penicillium and Talaromyces in the Omics Era - Past, Present and Future. *Comput. Struct. Biotechnol. J.* **2018**, *16*, 197–210. https://doi.org/10.1016/j.csbj.2018.05.003.

(87) Kozakiewicz, Z. Aspergillus Toxins and Taxonomy. In *The Genus Aspergillus: From Taxonomy and Genetics to Industrial Application*; Powell, K. A., Renwick, A., Peberdy, J. F., Eds.; Springer US: Boston, MA, 1994; pp 303–311. https://doi.org/10.1007/978-1-4899-0981-7_23.

(88) *Index of /genbank*. https://ftp.ncbi.nih.gov/genbank/ (accessed 2025-01-04).

(89) Saitou, N.; Nei, M. The Neighbor-Joining Method: A New Method for Reconstructing Phylogenetic Trees. *Mol. Biol. Evol.* **1987**, *4* (4), 406–425. https://doi.org/10.1093/oxfordjournals.molbev.a040454.

(90) Felsenstein, J. CONFIDENCE LIMITS ON PHYLOGENIES: AN APPROACH USING THE BOOTSTRAP. *Evol. Int. J. Org. Evol.* **1985**, *39* (4), 783–791. https://doi.org/10.1111/j.1558-5646.1985.tb00420.x.

(91) Tamura, K.; Nei, M.; Kumar, S. Prospects for Inferring Very Large Phylogenies by Using the

Neighbor-Joining Method. *Proc. Natl. Acad. Sci. U. S. A.* **2004**, *101* (30), 11030–11035. https://doi.org/10.1073/pnas.0404206101.

(92) Kumar, S.; Stecher, G.; Li, M.; Knyaz, C.; Tamura, K. MEGA X: Molecular Evolutionary Genetics Analysis across Computing Platforms. *Mol. Biol. Evol.* **2018**, *35* (6), 1547–1549. https://doi.org/10.1093/molbev/msy096.

(93) Nielsen, K. F.; Mogensen, J. M.; Johansen, M.; Larsen, T. O.; Frisvad, J. C. Review of Secondary Metabolites and Mycotoxins from the Aspergillus Niger Group. *Anal. Bioanal. Chem.* **2009**, *395* (5), 1225–1242. https://doi.org/10.1007/s00216-009-3081-5.

(94) Lewis, K. The Science of Antibiotic Discovery. *Cell* **2020**, *181* (1), 29–45. https://doi.org/10.1016/j.cell.2020.02.056.

(95) Lima, M. A. S.; Oliveira, M. da C. F. de; Pimenta, A. T. Á.; Uchôa, P. K. S. *Aspergillus Niger*: A Hundred Years of Contribution to the Natural Products Chemistry. *J. Braz. Chem. Soc.* **2019**, *30*, 2029–2059. https://doi.org/10.21577/0103-5053.20190080.

(96) Kumar Sahu, A.; S. Said, M.; Hingamire, T.; Gaur, M.; Khan, A.; Shanmugam, D.; T. Barvkar, V.; S. Dharne, M.; A. Bharde, A.; G. Dastager, S. Approach to Nigericin Derivatives and Their Therapeutic Potential. *RSC Adv.* **2020**, *10* (70), 43085–43091. https://doi.org/10.1039/D0RA05137C.

(97) Frisvad, J. C.; Smedsgaard, J.; Samson, R. A.; Larsen, T. O.; Thrane, U. Fumonisin B2 Production by Aspergillus Niger. *J. Agric. Food Chem.* **2007**, *55* (23), 9727–9732. https://doi.org/10.1021/jf0718906.

(98) El Awady, M. E.; Boulis, A. G.; Attia, A. R.; Shaaban, M. Dimeric Naphtho-γ-Pyrones and Further Diverse Bioactive Metabolites from the Marine-Derived Aspergillus Flavus Af/MMA 2018. *Egypt. Pharm. J.* **2019**, *18* (3), 245. https://doi.org/10.4103/epj.epj_11_19.

(99) Youssef, F. S.; Singab, A. N. B. An Updated Review on the Secondary Metabolites and Biological Activities of Aspergillus Ruber and Aspergillus Flavus and Exploring the Cytotoxic Potential of Their Isolated Compounds Using Virtual Screening. *Evid.-Based Complement. Altern. Med. ECAM* **2021**, *2021*, 8860784. https://doi.org/10.1155/2021/8860784.

(100) *Fungal secondary metabolism: regulation, function and drug discovery | Nature Reviews Microbiology*. https://www.nature.com/articles/s41579-018-0121-1 (accessed 2025-06-24).

(101) Frisvad, J. C.; Rank, C.; Nielsen, K. F.; Larsen, T. O. Metabolomics of *Aspergillus Fumigatus*. *Med. Mycol.* **2009**, *47* (s1), S53–S71. https://doi.org/10.1080/13693780802307720.

(102) Sutton, P.; Newcombe, N. R.; Waring, P.; Müllbacher, A. In Vivo Immunosuppressive Activity of Gliotoxin, a Metabolite Produced by Human Pathogenic Fungi. *Infect. Immun.* **1994**, *62* (4), 1192–1198. https://doi.org/10.1128/iai.62.4.1192-1198.1994.

(103) Abraham, W.-R. Fumitremorgins and Relatives - From Tremorgenic Compounds to Valuable Anti-Cancer Drugs. *Curr. Med. Chem.* **2018**, *25* (2), 123–140. https://doi.org/10.2174/0929867324666170724103410.

(104) *Antitumor Activity of Quinazolinone Alkaloids Inspired by Marine Natural Products*. https://www.mdpi.com/1660-3397/16/8/261 (accessed 2024-12-03).

(105) *Chemical Constituents and Bioactivities of the Plant-Derived Fungus Aspergillus fumigatus*. https://www.mdpi.com/1420-3049/29/3/649 (accessed 2024-12-03).

(106) Hashem, A. H.; Attia, M. S.; Kandil, E. K.; Fawzi, M. M.; Abdelrahman, A. S.; Khader, M. S.; Khodaira, M. A.; Emam, A. E.; Goma, M. A.; Abdelaziz, A. M. Bioactive Compounds and Biomedical Applications of Endophytic Fungi: A Recent Review. *Microb. Cell Factories* **2023**, *22* (1), 107. https://doi.org/10.1186/s12934-023-02118-x.

(107) Frisvad, J. C.; Larsen, T. O.; de Vries, R.; Meijer, M.; Houbraken, J.; Cabañes, F. J.; Ehrlich, K.; Samson, R. A. Secondary Metabolite Profiling, Growth Profiles and Other Tools for Species Recognition and Important Aspergillus Mycotoxins. *Stud. Mycol.* **2007**, *59*, 31–37. https://doi.org/10.3114/sim.2007.59.04.

(108) Amr, K.; Ibrahim, N.; Elissawy, A. M.; Singab, A. N. B. Unearthing the Fungal Endophyte Aspergillus Terreus for Chemodiversity and Medicinal Prospects: A Comprehensive Review. *Fungal Biol. Biotechnol.* **2023**, *10* (1), 6. https://doi.org/10.1186/s40694-023-00153-2.

(109) *A Focused Review of the Pharmacological Potentials of Terrein as an Anticancer Agent - Jyoti Goutam, Gunjan Sharma, Vandana Yadav, Gauri Pathak, Ravindra Nath Kharwar, Divakar Sharma, 2023*. https://journals.sagepub.com/doi/full/10.1177/1934578X231174128 (accessed 2024-12-10).

(110) Olesen, S. H.; Ingles, D. J.; Yang, Y.; Schönbrunn, E. Differential Antibacterial Properties of the MurA Inhibitors Terreic Acid and Fosfomycin. *J. Basic Microbiol.* **2014**, *54* (4), 322–326. https://doi.org/10.1002/jobm.201200617.

(111) Shree, P.; Singh, C. K.; Sodhi, K. K.; Surya, J. N.; Singh, D. K. Biofilms: Understanding the Structure and Contribution towards Bacterial Resistance in Antibiotics. *Med. Microecol.* **2023**, *16*, 100084. https://doi.org/10.1016/j.medmic.2023.100084.

(112) Novera. *The Art and Science of Natural Products Purification: Basic Preparative Phytochemistry for Plant Scientists Participants*; 2016.

(113) Barnes, C. L.; Steiner, J. R.; Torres, E.; Pacheco, R.; Marquez, H. Structure and Absolute Configuration of Pyrophen, a Novel Pryrone Derivative of L-Phenylalanine from Aspergillus Niger. *Int. J. Pept. Protein Res.* **1990**, *36* (3), 292–296. https://doi.org/10.1111/j.1399-3011.1990.tb00981.x.

(114) Senior, M. M.; Williamson, R. T.; Martin, G. E. Using HMBC and ADEQUATE NMR Data to Define and Differentiate Long-Range Coupling Pathways: Is the Crews Rule Obsolete? *J. Nat. Prod.* **2013**, *76* (11), 2088–2093. https://doi.org/10.1021/np400562u.

(115) *MarinLit - A database of the marine natural products literature*. https://marinlit.rsc.org/ (accessed 2025-01-19).

(116) Priestap, H. A. New Naphthopyrones from Aspergillus Fonsecaeus. *Tetrahedron* **1984**, *40* (19), 3617–3624. https://doi.org/10.1016/S0040-4020(01)88792-5.

(117) P. Gorst-Allman, D.; S. Stern, P.; J. Rabie, C. Structural Elucidation of the Nigerones, Four New Naphthopyrones from Cultures of Aspergillus Niger. *J. Chem. Soc. Perkin 1* **1980**, *0* (0), 2474–2479. https://doi.org/10.1039/P19800002474.

(118) *New Dimeric Naphthopyrones from Aspergillus niger | Journal of Natural Products*. https://pubs.acs.org/doi/full/10.1021/np020174p?casa_token=g6xbs5Nj0EYAAAAA%3AX1UYTJu7iHvt044jPsZZy1XKuUJ0kqfALFEoPxWwyR19xY2DoHTIyRkp_TKHWPxORG-D1zi0f32QQGc (accessed 2025-01-19).

(119) *Cytotoxic Naphtho-γ-pyrones from the Mangrove Endophytic Fungus Aspergillus tubingensis (GX1-5E) - Huang - 2011 - Helvetica Chimica Acta - Wiley Online Library*. https://onlinelibrary.wiley.com/doi/abs/10.1002/hlca.201100050?casa_token=3U6gDVLOaiAAAAAA%3A3w-bawjm3pq3z6_l208XFlUGpNqFg9EgTpk3xTohXiDuChY7YZDpeb0VusmG7rnjCXNLTcOSEsqgww (accessed 2025-01-23).

(120) *Software for NMR, Chromatography, MS & more | Spectrus Processor*. ACD/Labs. https://www.acdlabs.com/products/spectrus-platform/spectrus-processor/ (accessed 2025-01-03).

(121) (PDF) Bioactive Metabolites of Aspergillus Neoniger, an Endophyte of the Medicinal Plant Ficus Carica. *ResearchGate* **2024**. https://doi.org/10.36468/pharmaceutical-sciences.755.

(122) Matsushima, Y.; Nakayama, T.; Fujita, M.; Bhandari, R.; Eguchi, T.; Shindo, K.; Kakinuma, K. Isolation and Structure Elucidation of Vicenistatin M, and Importance of the Vicenisamine Aminosugar for Exerting Cytotoxicity of Vicenistatin. *J. Antibiot. (Tokyo)* **2001**, *54* (3), 211–219. https://doi.org/10.7164/antibiotics.54.211.

(123) Dettmer, K.; Aronov, P. A.; Hammock, B. D. Mass Spectrometry-Based Metabolomics. *Mass Spectrom. Rev.* **2007**, *26* (1), 51–78. https://doi.org/10.1002/mas.20108.

(124) Puyana, M.; Pawlik, J.; Blum, J.; Fenical, W. Metabolite Variability in Caribbean Sponges of the Genus Aplysina. *Rev. Bras. Farmacogn.* **2015**, *25* (6), 592–599. https://doi.org/10.1016/j.bjp.2015.08.002.

(125) Chervin, J.; Stierhof, M.; Tong, M. H.; Peace, D.; Hansen, K. Ø.; Urgast, D. S.; Andersen, J. H.; Yu, Y.; Ebel, R.; Kyeremeh, K.; Paget, V.; Cimpan, G.; Wyk, A. V.; Deng, H.; Jaspars, M.; Tabudravu, J. N. Targeted Dereplication of Microbial Natural Products by High-Resolution MS and Predicted LC Retention Time. *J. Nat. Prod.* **2017**, *80* (5), 1370–1377. https://doi.org/10.1021/acs.jnatprod.6b01035.

(126) *MZmine 2 Data-Preprocessing To Enhance Molecular Networking Reliability | Analytical Chemistry*. https://pubs.acs.org/doi/full/10.1021/acs.analchem.7b01563?casa_token=6bjYbFbKvT8AAAAA%3AyTRMRzif0X6bv6I17dG4OL2LpNLr4hwZ_S3xo39bp1AKE5zd5h6vqqua28xBR2ZXOJ9YLF7I3UugBKs (accessed 2025-01-03).

(127) Wolfender, J.-L.; Marti, G.; Thomas, A.; Bertrand, S. Current Approaches and Challenges for the Metabolite Profiling of Complex Natural Extracts. *J. Chromatogr. A* **2015**, *1382*, 136–164. https://doi.org/10.1016/j.chroma.2014.10.091.

(128) Xia, J.; Sinelnikov, I. V.; Han, B.; Wishart, D. S. MetaboAnalyst 3.0--Making Metabolomics More Meaningful. *Nucleic Acids Res.* **2015**, *43* (W1), W251-257. https://doi.org/10.1093/nar/gkv380.

(129) *FreeClust*. https://macdobry.shinyapps.io/free-clust/ (accessed 2025-01-03).

(130) *ICP-MS software, ICP-QQQ software, ICP-MS MassHunter | Agilent*. https://www.agilent.com/en/product/atomic-spectroscopy/inductively-coupled-plasma-mass-spectrometry-icp-ms/icp-ms-software/icp-ms-masshunter-software (accessed 2025-01-03).

(131) Božičević, A.; Dobrzyński, M.; De Bie, H.; Gafner, F.; Garo, E.; Hamburger, M. Automated Comparative Metabolite Profiling of Large LC-ESIMS Data Sets in an ACD/MS Workbook Suite Add-in, and Data Clustering on a New Open-Source Web Platform FreeClust. *Anal. Chem.* **2017**, *89* (23), 12682–12689. https://doi.org/10.1021/acs.analchem.7b02221.

(132) Oksanen, J.; Simpson, G. L.; Blanchet, F. G.; Kindt, R.; Legendre, P.; Minchin, P. R.; O'Hara, R. B.; Solymos, P.; Stevens, M. H. H.; Szoecs, E.; Wagner, H.; Barbour, M.; Bedward, M.; Bolker, B.; Borcard, D.; Carvalho, G.; Chirico, M.; De Caceres, M.; Durand, S.; Evangelista, H. B. A.; FitzJohn, R.; Friendly, M.; Furneaux, B.; Hannigan, G.; Hill, M. O.; Lahti, L.; McGlinn, D.; Ouellette, M.-H.; Ribeiro Cunha, E.; Smith, T.; Stier, A.; Ter Braak, C. J. F.; Weedon, J. Vegan: Community Ecology Package, 2001, 2.6-8. https://doi.org/10.32614/CRAN.package.vegan.

(133) *Drugs: From Discovery to Approval, 3rd Edition | Wiley*. Wiley.com. https://www.wiley.com/en-us/Drugs%3A+From+Discovery+to+Approval%2C+3rd+Edition-p-9781118907276 (accessed 2024-11-29).

(134) *Handbook of Marine Natural Products*.

(135) Pluskal, T.; Castillo, S.; Villar-Briones, A.; Oresic, M. MZmine 2: Modular Framework for Processing, Visualizing, and Analyzing Mass Spectrometry-Based Molecular Profile Data. *BMC Bioinformatics* **2010**, *11*, 395. https://doi.org/10.1186/1471-2105-11-395.

(136) *Medicinal Herbal: A Textbook for Medical Students and Doctors*; Hamdard Foundation Pakistan, 1996.

(137) Kanwal, I.; Fatima, N.; Wazir, A.; Khan, M.; Zaheer, M.; Masroor, D.; Syed, S. Fagonia Arabica Linn, a Miraculous Medicinal Plant with Diminutive Scientific Data but Hefty Potential Fagonia Arabica Linn, a Miraculous Medicinal Plant with Diminutive Scientific Data but Hefty Potential A B S T R A C T. **2021**.

(138) Farheen, R.; Mahmood, I.; Parveen, R. REVIEW ON MEDICINAL AND BIOACTIVE ROLE OF GENUS FAGONIA. *FUUAST J. Biol.* **2017**, *7* (1), 33–36.

(139) Qiao, W.; Tang, T.; Ling, F. Comparative Transcriptome Analysis of a Taxol-Producing Endophytic Fungus, Aspergillus Aculeatinus Tax-6, and Its Mutant Strain. *Sci. Rep.* **2020**, *10* (1), 10558. https://doi.org/10.1038/s41598-020-67614-1.

(140) *Lovastatin Monograph for Professionals - Drugs.com*. https://www.drugs.com/monograph/lovastatin.html (accessed 2023-05-24).

(141) Nakajima, H.; Nishimura, K.; Hamasaki, T.; Kimura, Y.; Udagawa, S. Structure of Neovasinin, a New Metabolite Produced by the Fungus, Neocosmospora Vasinfecta E.F. Smith, and Its Biological Activity to Lettuce Seedlings. *Agric. Biol. Chem.* **1987**, *51* (10), 2831–2833. https://doi.org/10.1080/00021369.1987.10868449.

(142) Ahmad, N.; Bibi, Y.; Saboon; Raza, I.; Zahara, K.; idrees, S.; Khalid, N.; Bashir, T.; Tabassum, S.; Mudrikah. Traditional Uses and Pharmacological Properties of Alhagi Maurorum: A Review.

Asian Pac. J. Trop. Dis. **2015**, *5* (11), 856–861. https://doi.org/10.1016/S2222-1808(15)60945-8.

(143) Dewi, R. T.; Tachibana, S.; Darmawan, A. Effect on α-Glucosidase Inhibition and Antioxidant Activities of Butyrolactone Derivatives from Aspergillus Terreus MC751. *Med. Chem. Res.* **2013**, *23* (1), 454–460. https://doi.org/10.1007/s00044-013-0659-4.

(144) Rao, K. V.; Sadhukhan, A. K.; Veerender, M.; Ravikumar, V.; Mohan, E. V. S.; Dhanvantri, S. D.; Sitaramkumar, M.; Moses Babu, J.; Vyas, K.; Om Reddy, G. Butyrolactones from Aspergillus Terreus. *Chem. Pharm. Bull. (Tokyo)* **2000**, *48* (4), 559–562. https://doi.org/10.1248/cpb.48.559.

(145) Parvatkar, R. R.; D'Souza, C.; Tripathi, A.; Naik, C. G. Aspernolides A and B, Butenolides from a Marine-Derived Fungus *Aspergillus Terreus*. *Phytochemistry* **2009**, *70* (1), 128–132. https://doi.org/10.1016/j.phytochem.2008.10.017.

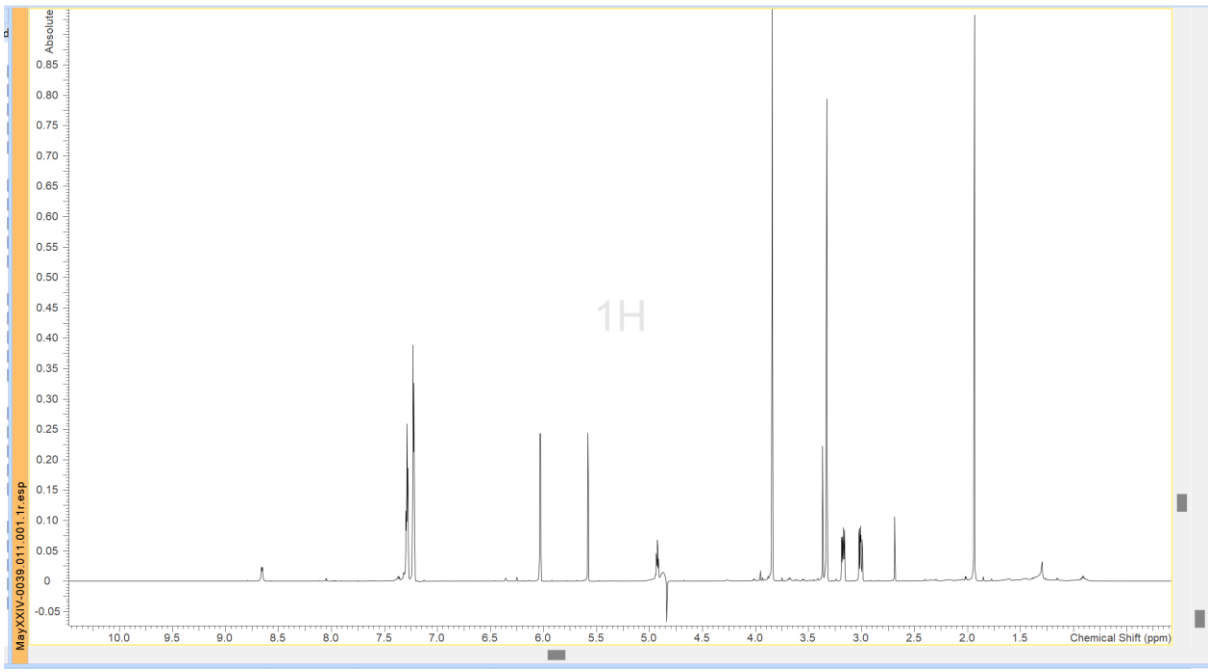

Figure S1. ^{1}H NMR for WNS7(8)F3 D 13 s4-6 ssF-X cD sss9-11 H1.

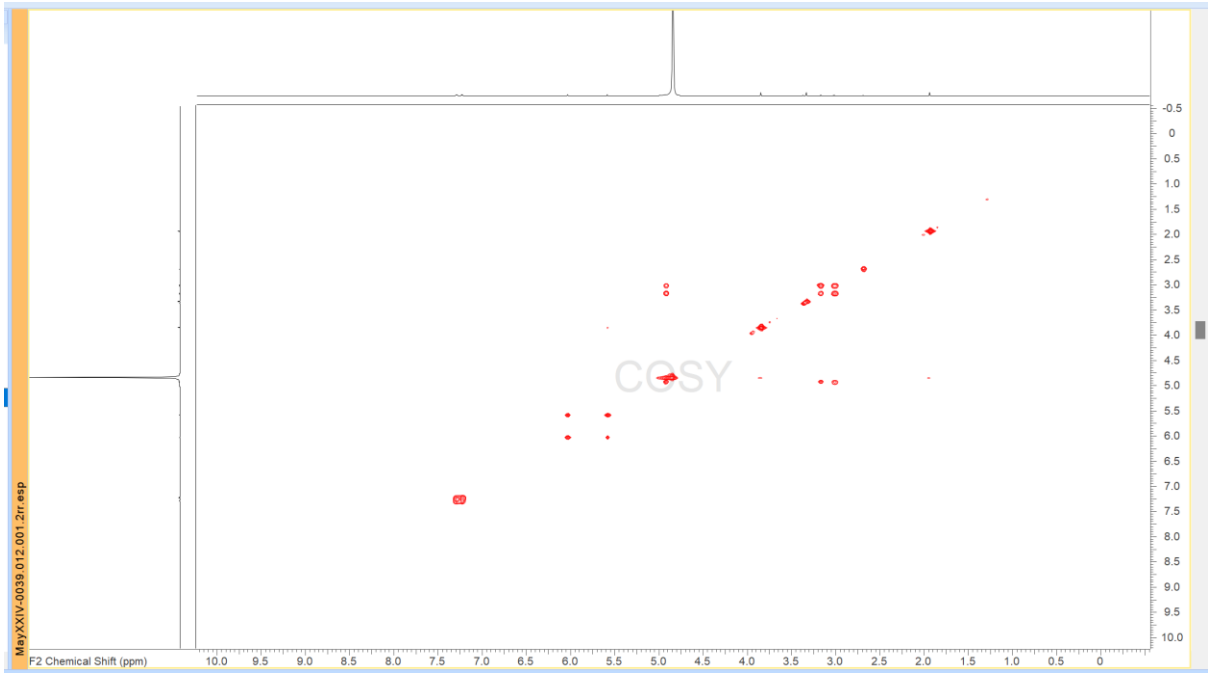

Figure S2. COSY NMR for WNS7(8)F3 D 13 s4-6 ssF-X cD sss9-11 H1.

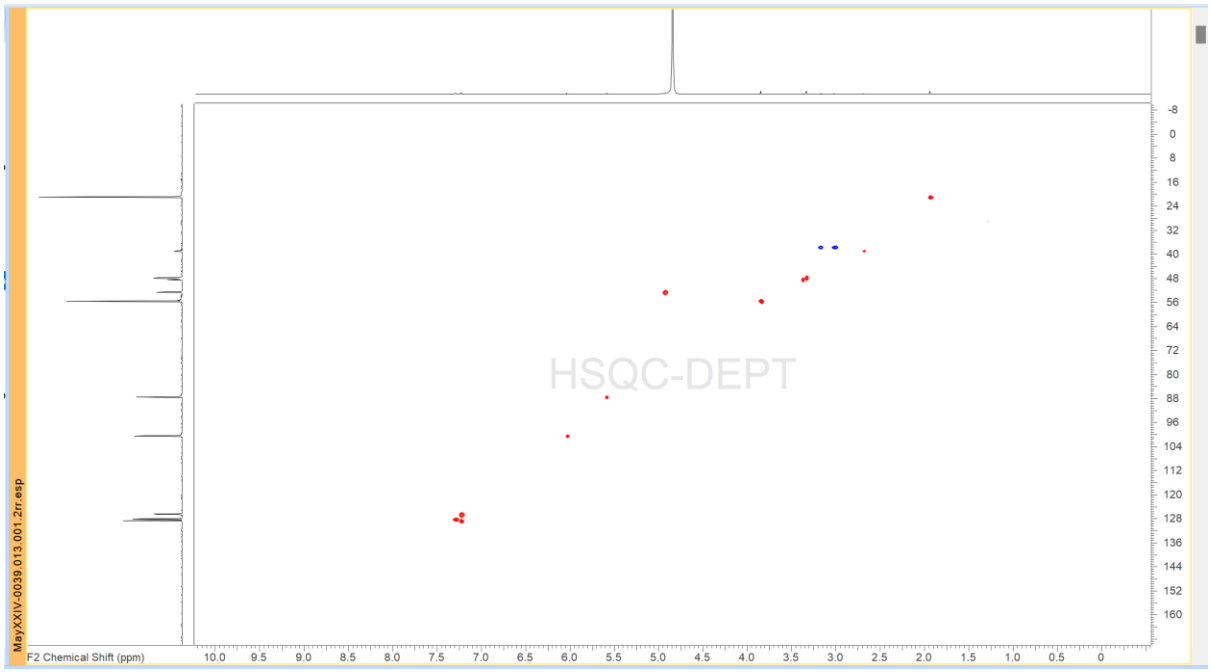

Figure S3. HSQC NMR for WNS7(8)F3 D 13 s4-6 ssF-X cD sss9-11 H1.

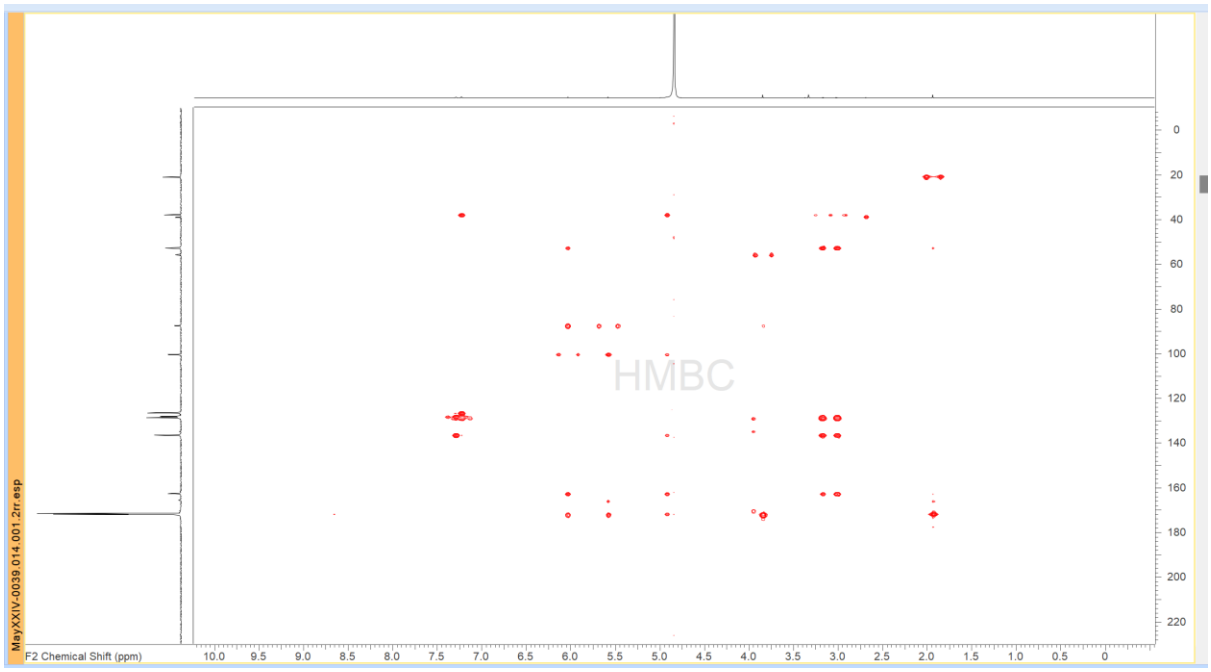

Figure S4. HMBC NMR for WNS7(8)F3 D 13 s4-6 ssF-X cD sss9-11 H1.

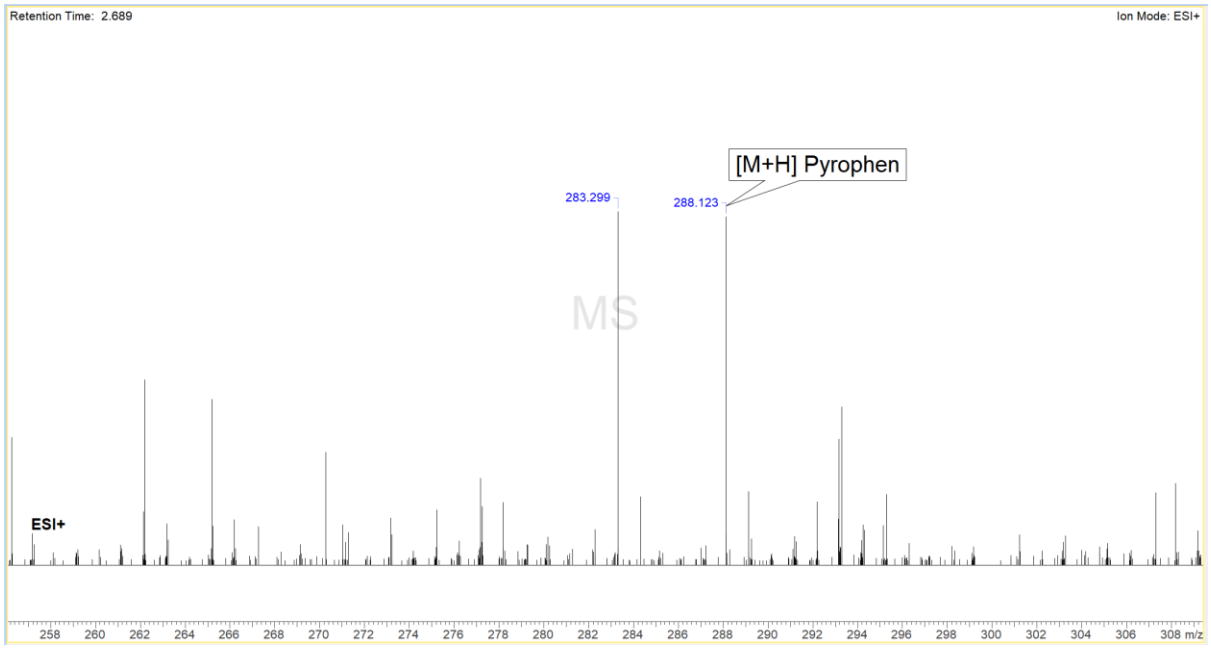

Figure S5. HR-MS/MS for WNS7(8)F3 D 13 s4-6 ssF-X cD sss9-11 H1.

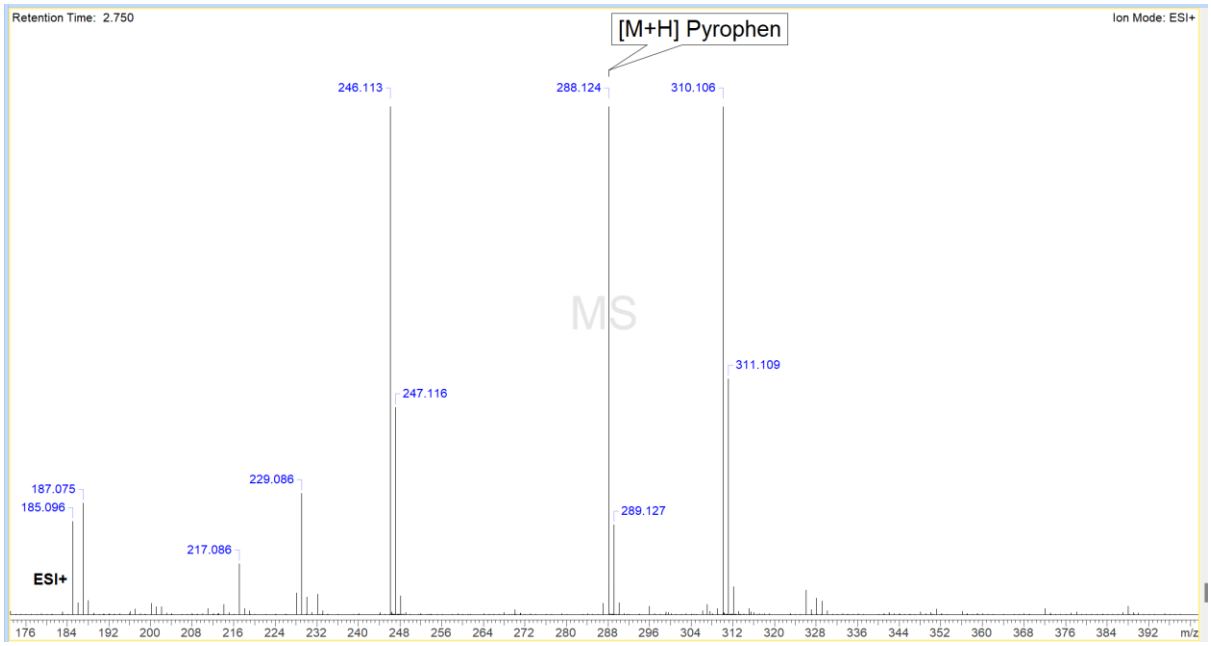

Figure S6. HR-MS/MS for WNS7(8)F3 D 13 s4-6 ssF-X sss9-11 showing H1.

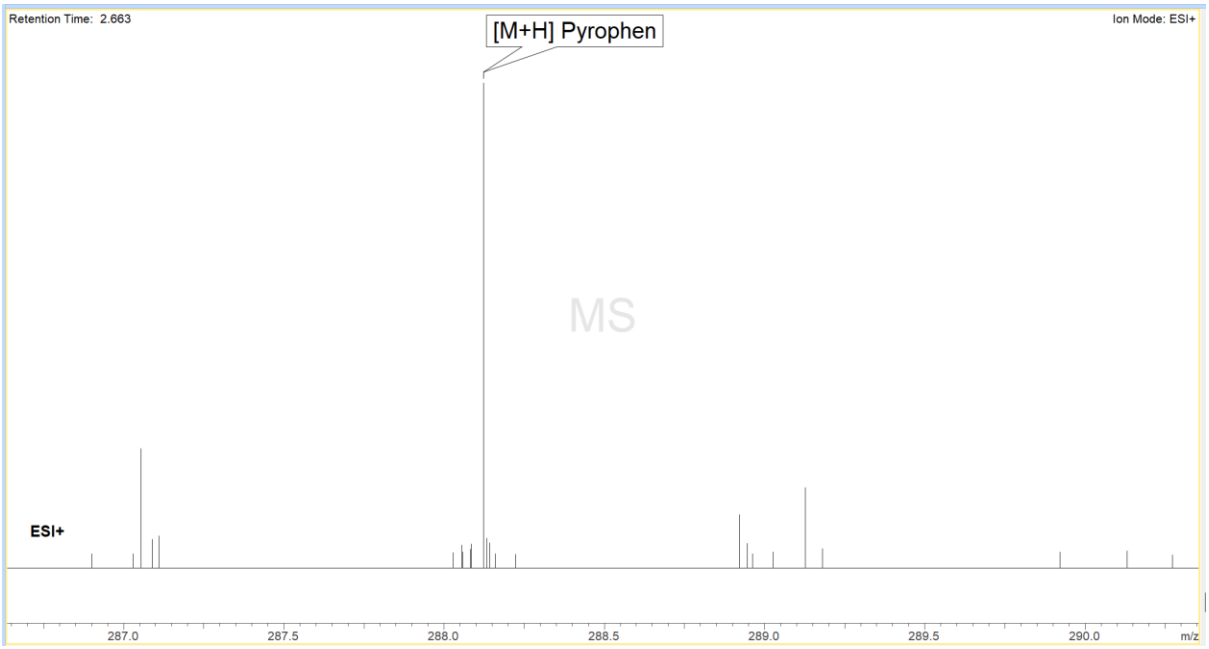

Figure S7. HR-MS/MS for WNS7(8)F3 D 13 s4-6 ssF-X showing H1.

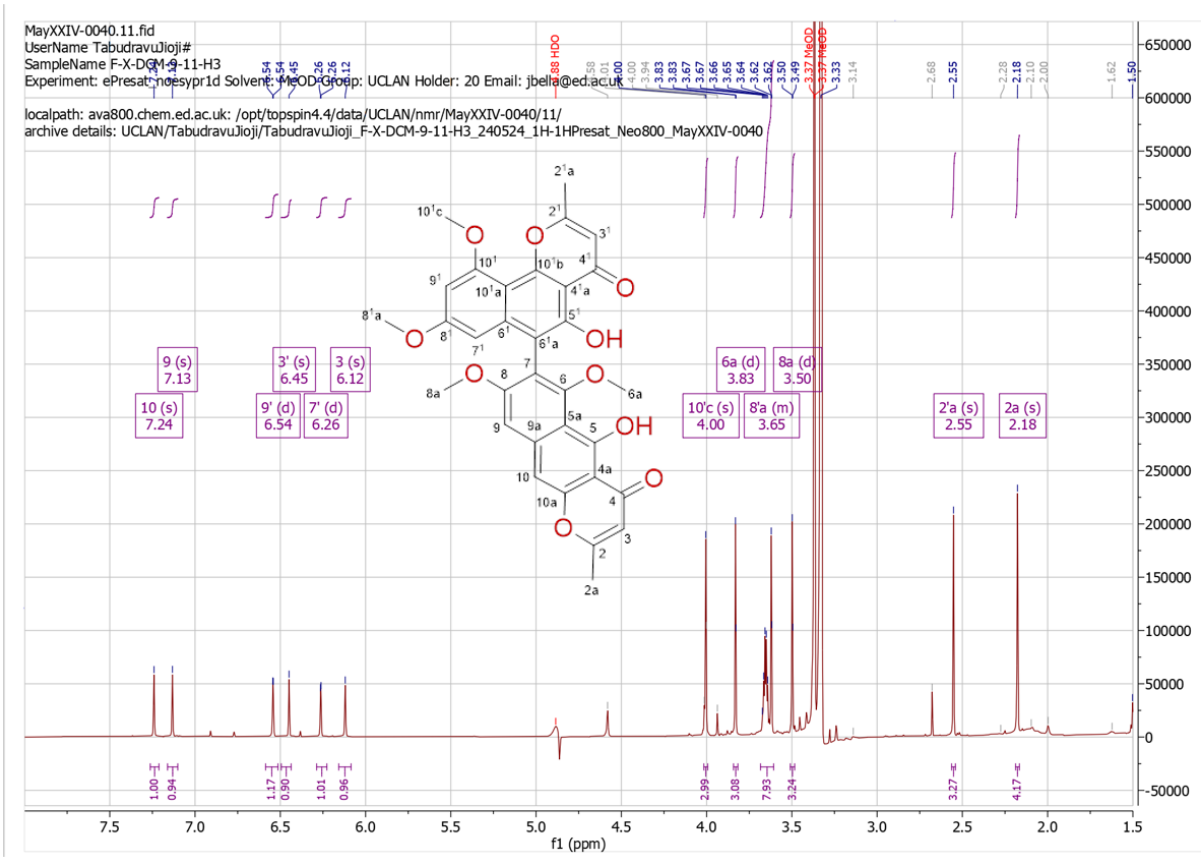

Figure S8. ^{1}H NMR for WNS7(8)F3 D 13 s4-6 ssF-X cD sss9-11 H3.

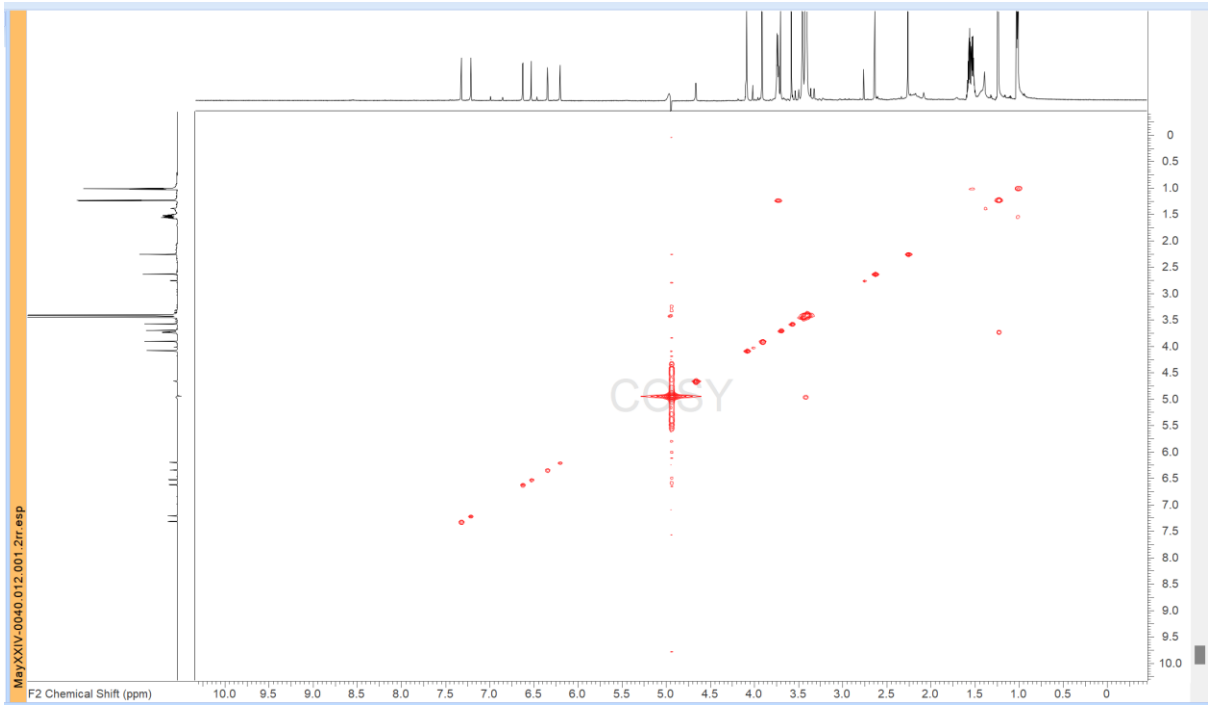

Figure S9. COSY NMR for WNS7(8)F3 D 13 s4-6 ssF-X cD sss9-11 H3.

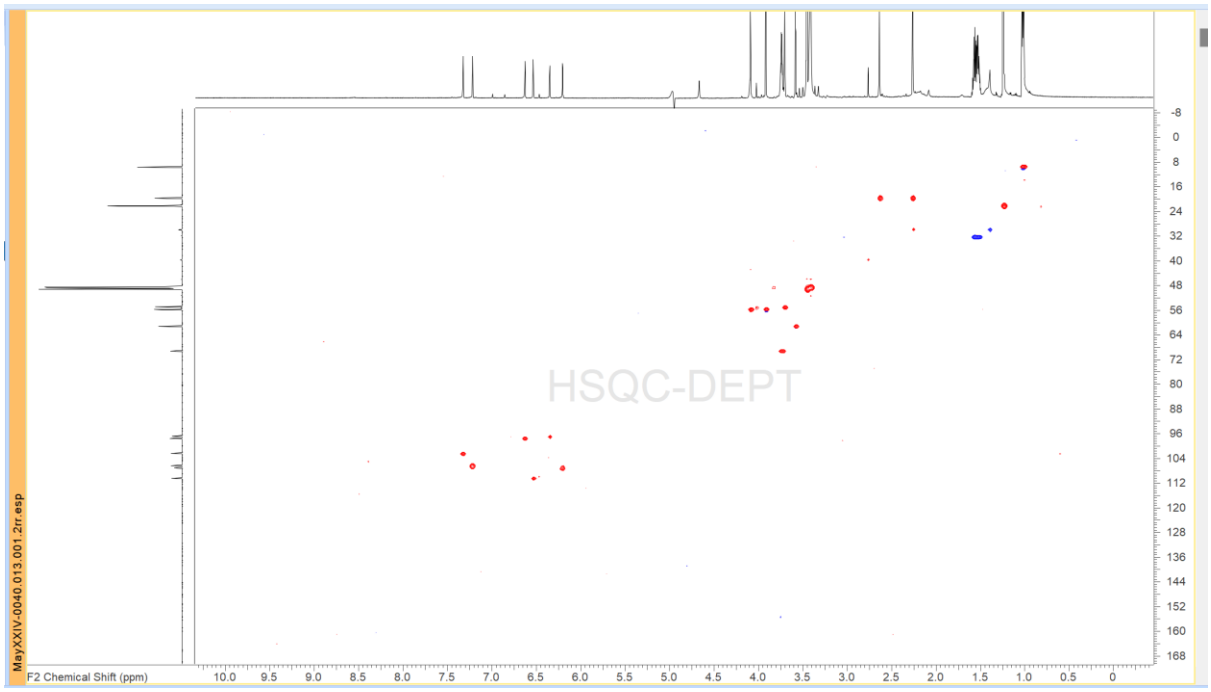

Figure S10. HSQC NMR for WNS7(8)F3 D 13 s4-6 ssF-X cD sss9-11 H3.

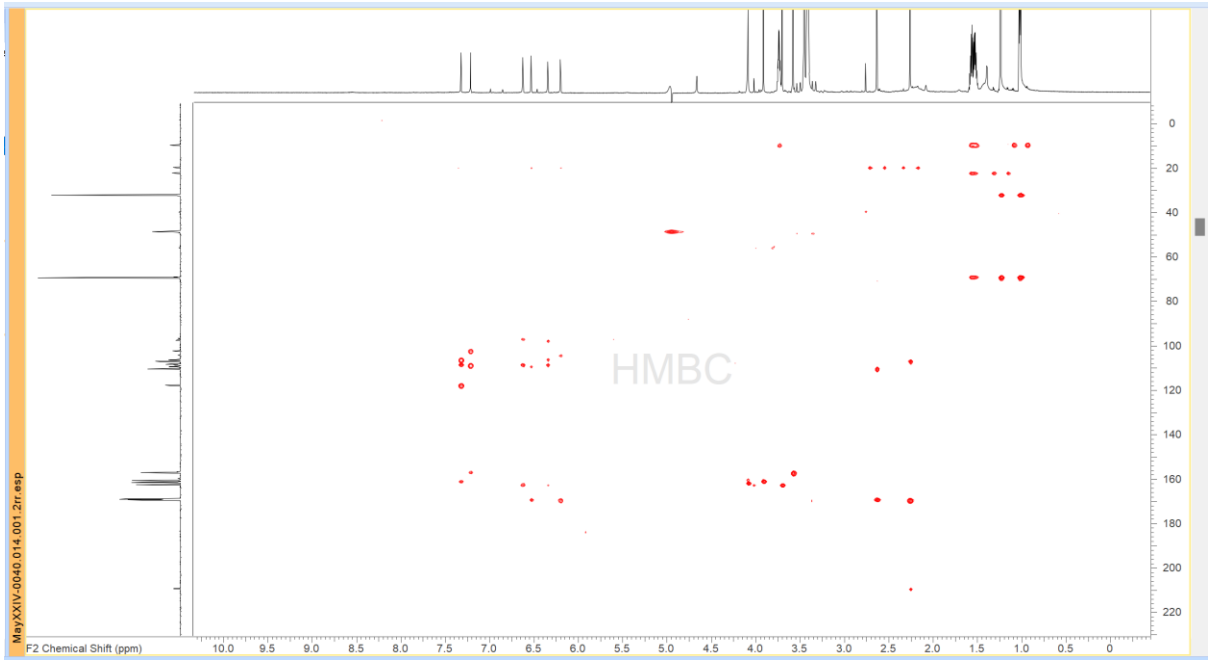

Figure S11. HMBC NMR for WNS7(8)F3 D 13 s4-6 ssF-X cD sss9-11 H3.

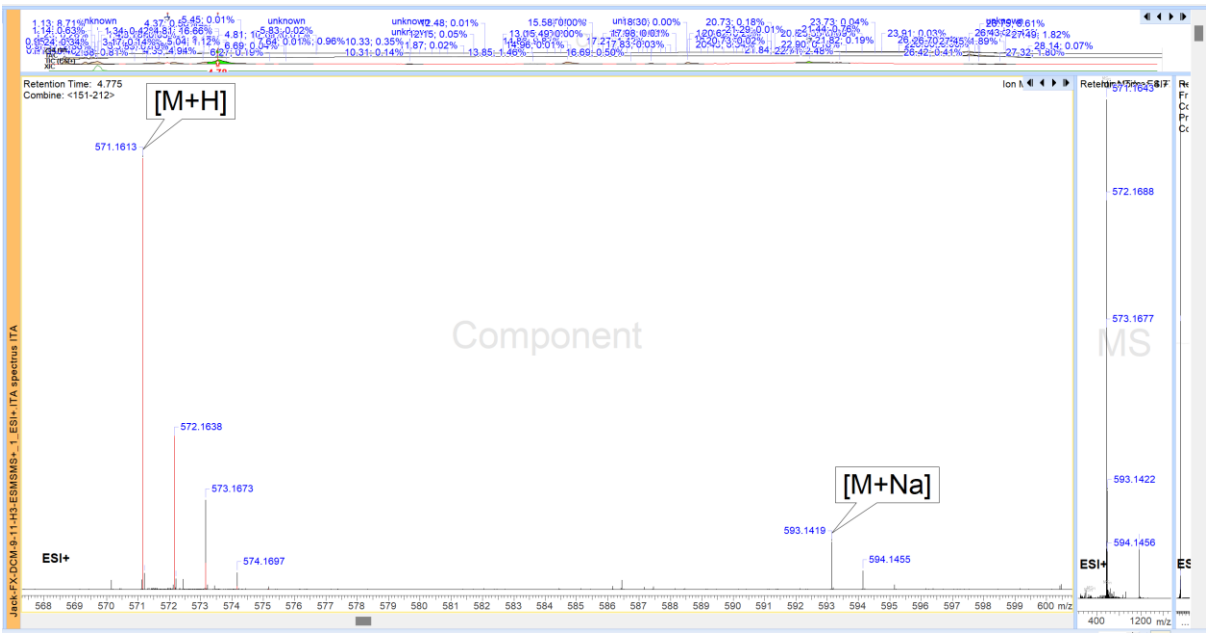

Figure S12. HR-MS/MS for WNS7(8)F3 D 13 s4-6 ssF-X cD sss9-11 H3.

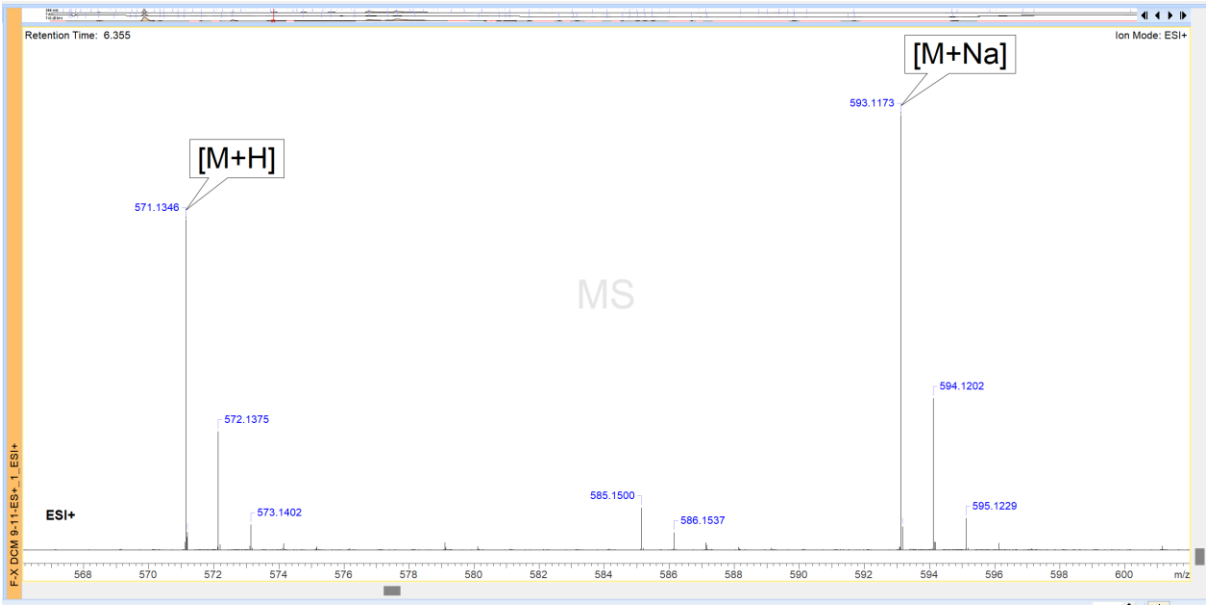

Figure S13. HR-MS/MS for WNS7(8)F3 D 13 s4-6 ssF-X cD sss9-11 showing H3.

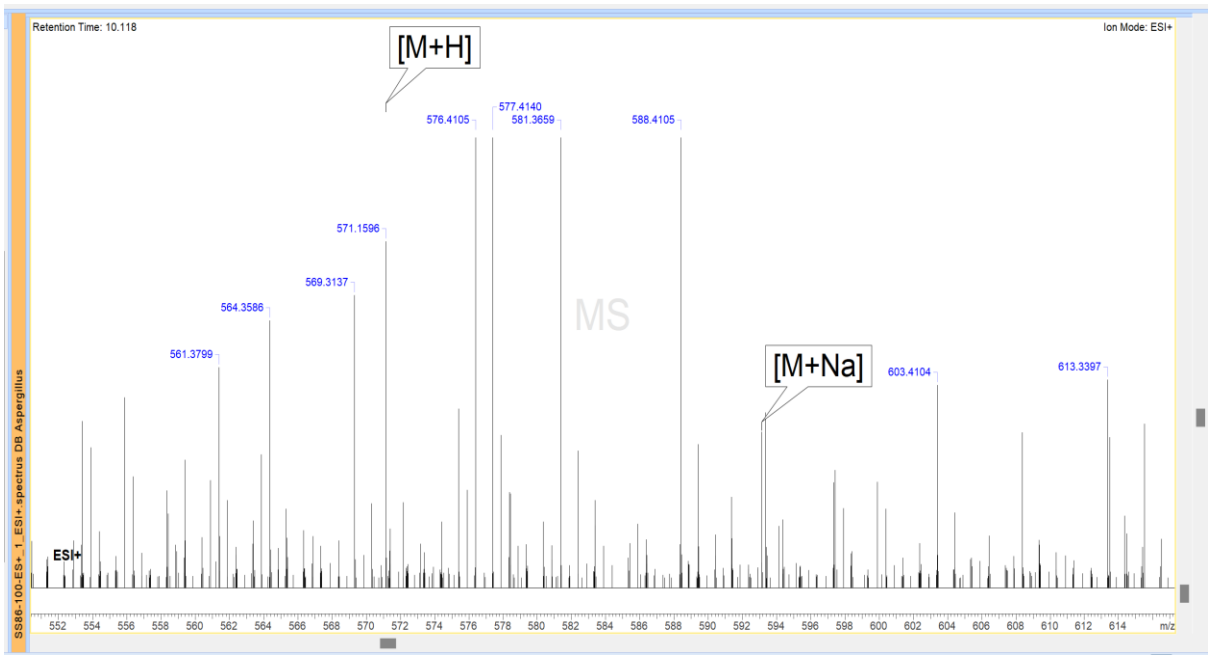

Figure S14. HR-MS/MS for WNS7(8)F3 SPE100 showing H3.

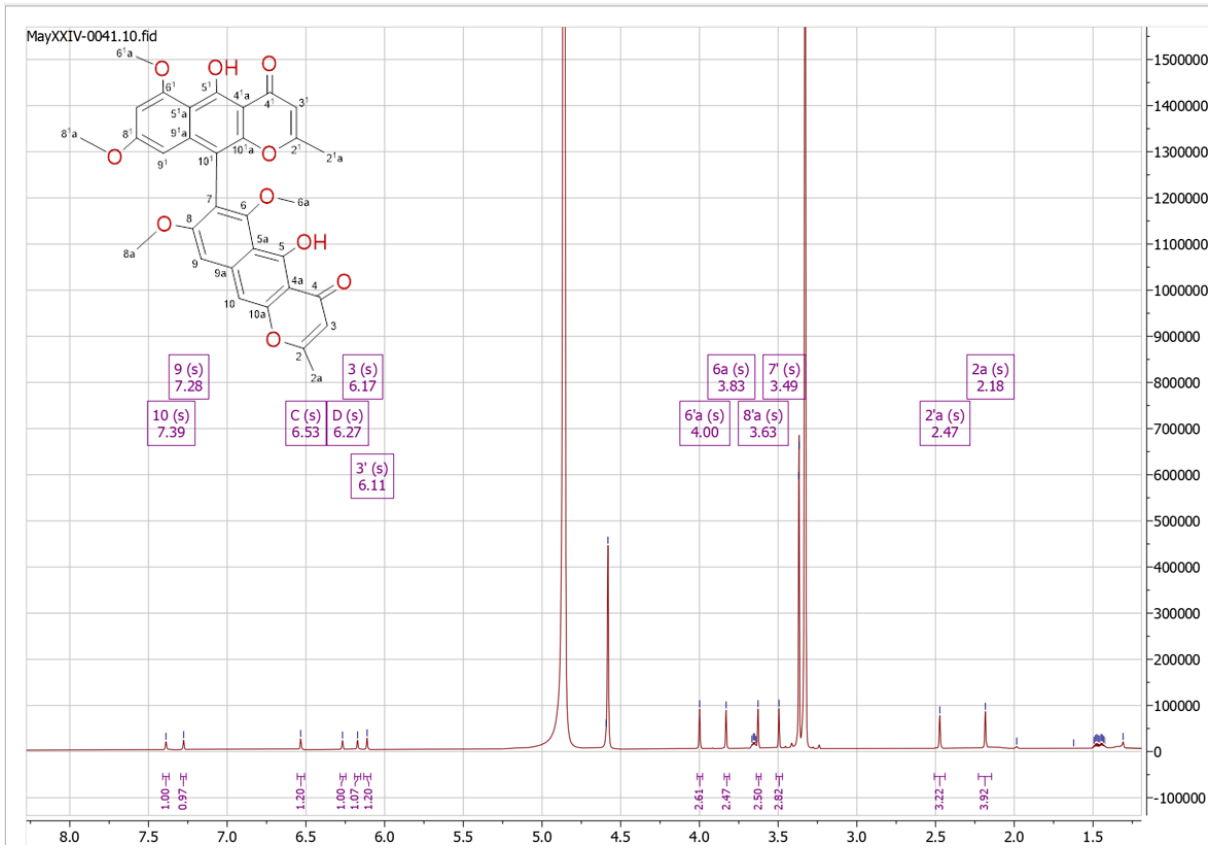

Figure S15. ^{1}H NMR for WNS7(8)F3 D 13 s4-6 ssF-X cD sss9-11 H4.

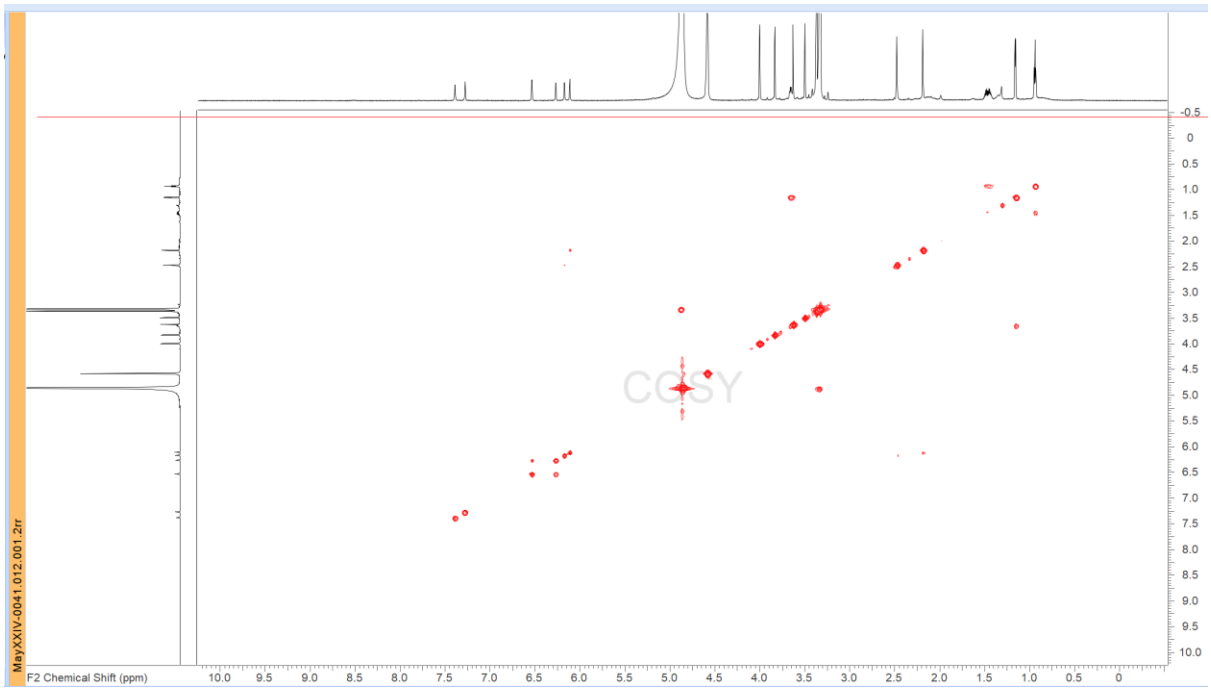

Figure S16. COSY NMR for WNS7(8)F3 D 13 s4-6 ssF-X cD sss9-11 H4.

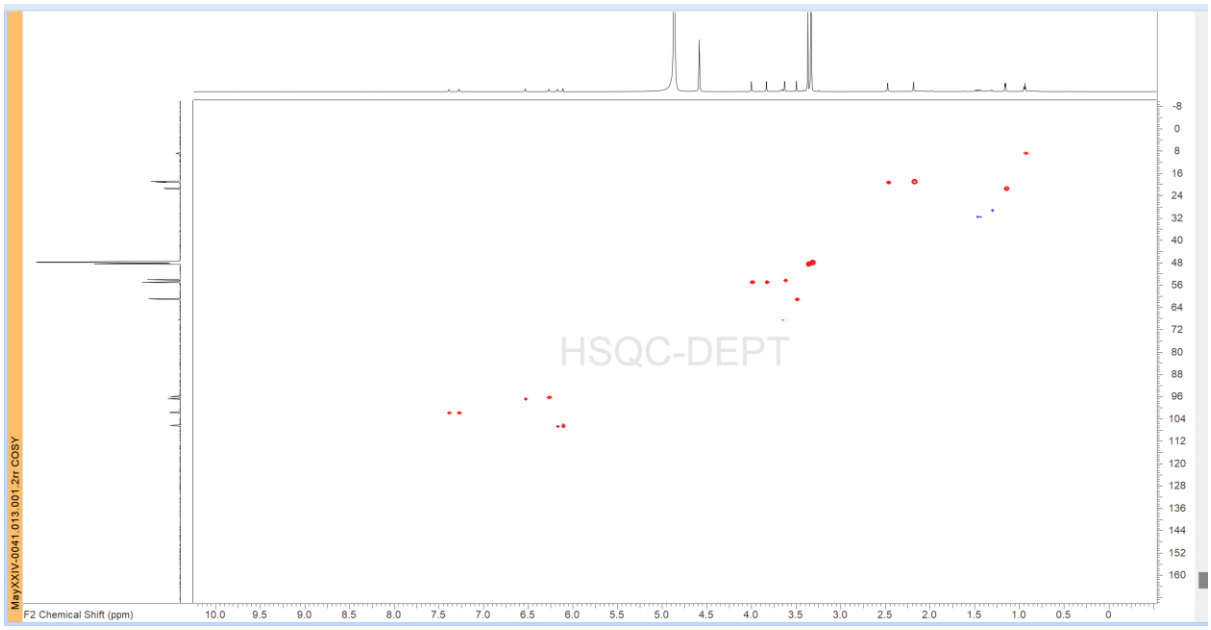

Figure S17. HSQC NMR for WNS7(8)F3 D 13 s4-6 ssF-X cD sss9-11 H4.

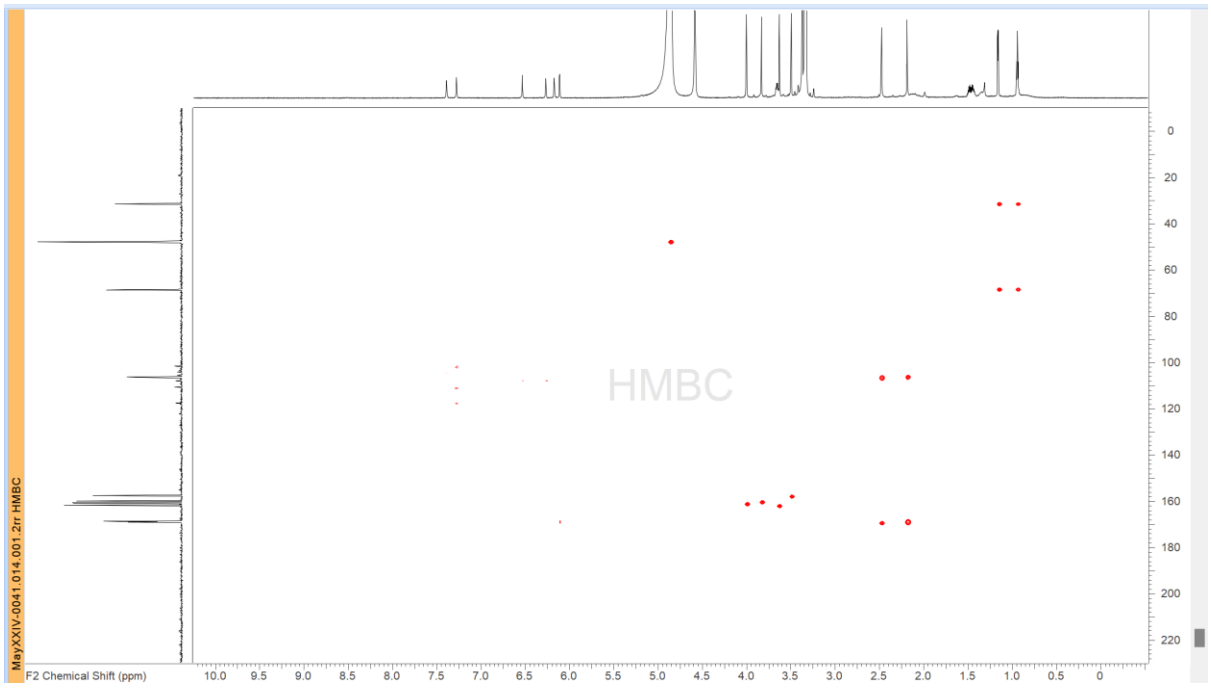

Figure S18. HMBC NMR for WNS7(8)F3 D 13 s4-6 ssF-X cD sss9-11 H4.

Figure S19. NOSEY NMR for WNS7(8)F3 D 13 s4-6 ssF-X cD sss9-11 H4.

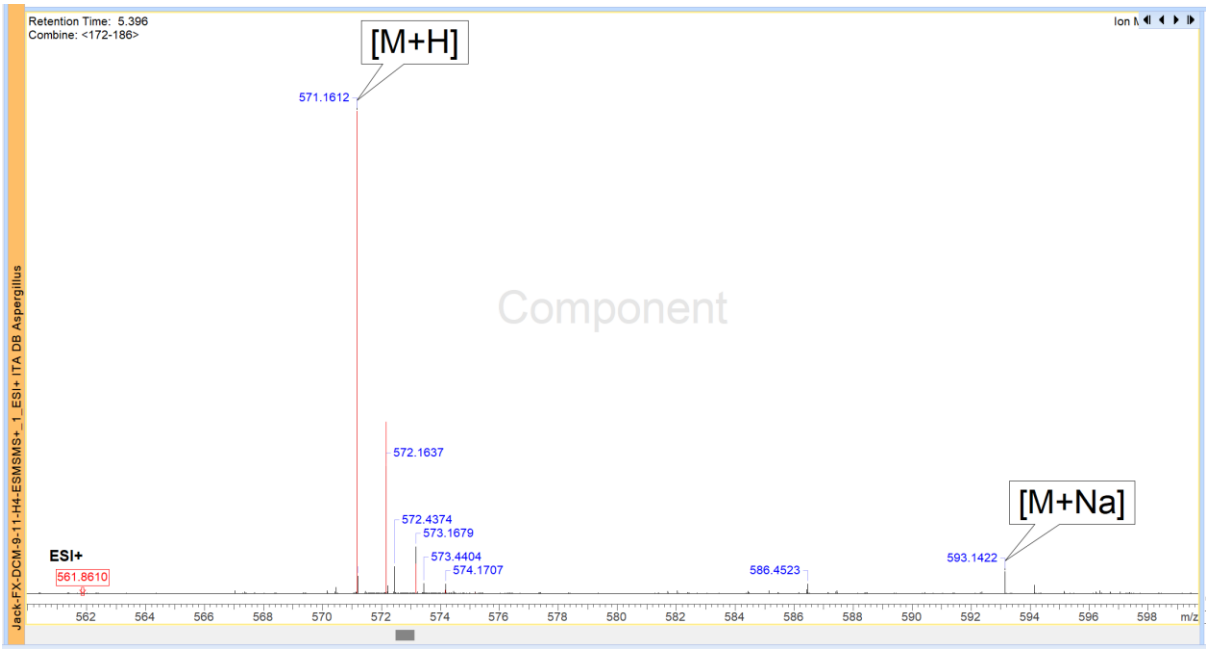

Figure S20. HR-MS/MS for WNS7(8)F3 FD 13 s4-6 ssF-X sss9-11 H4.

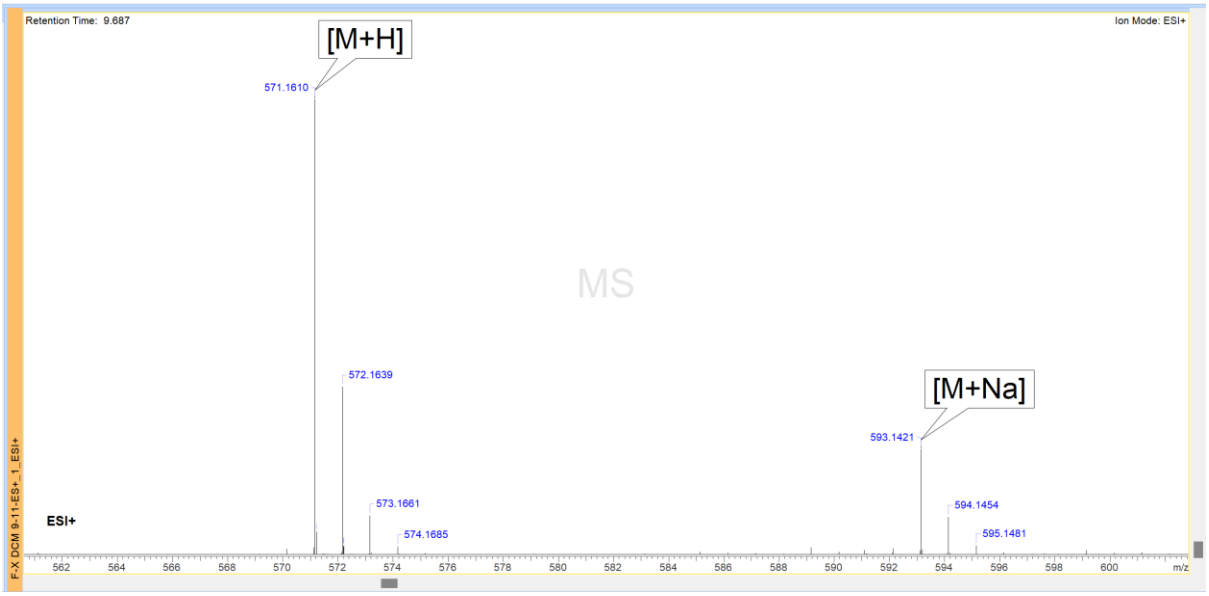

Figure S21 . HR-MS/MS for WNS7(8)F3 FD 13 s4-6 ssF-X sss9-11 showing H4.

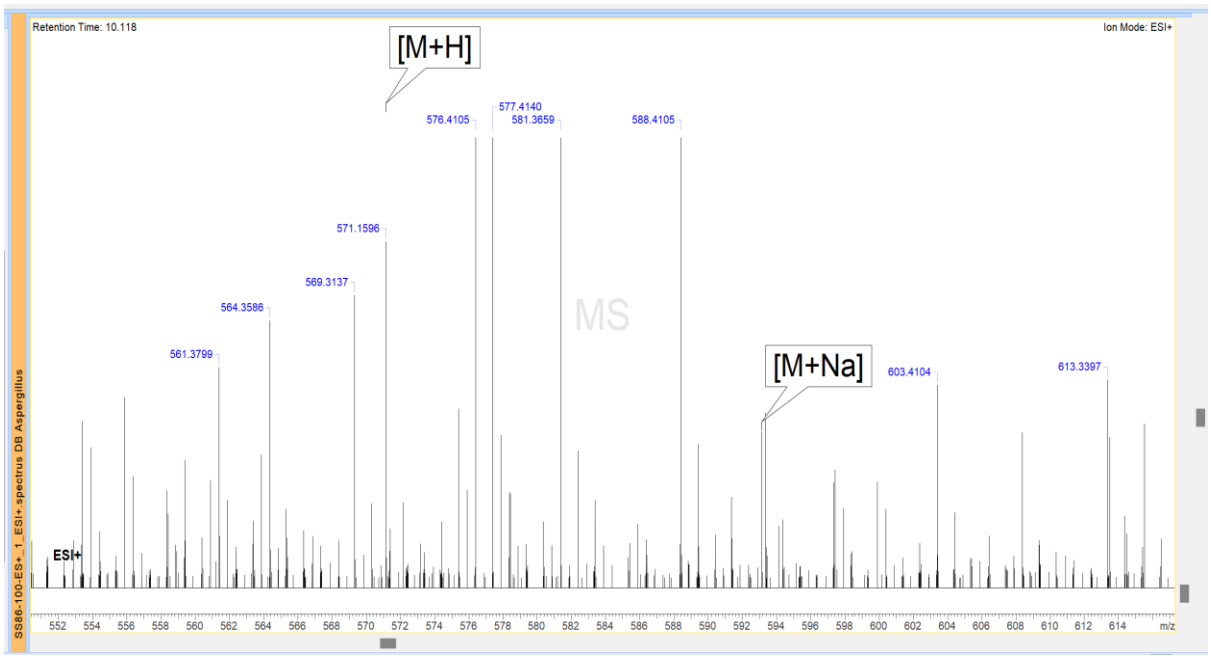

Figure S22 . HR-MS/MS for WNS7(8)F3 SPE100 showing H4.

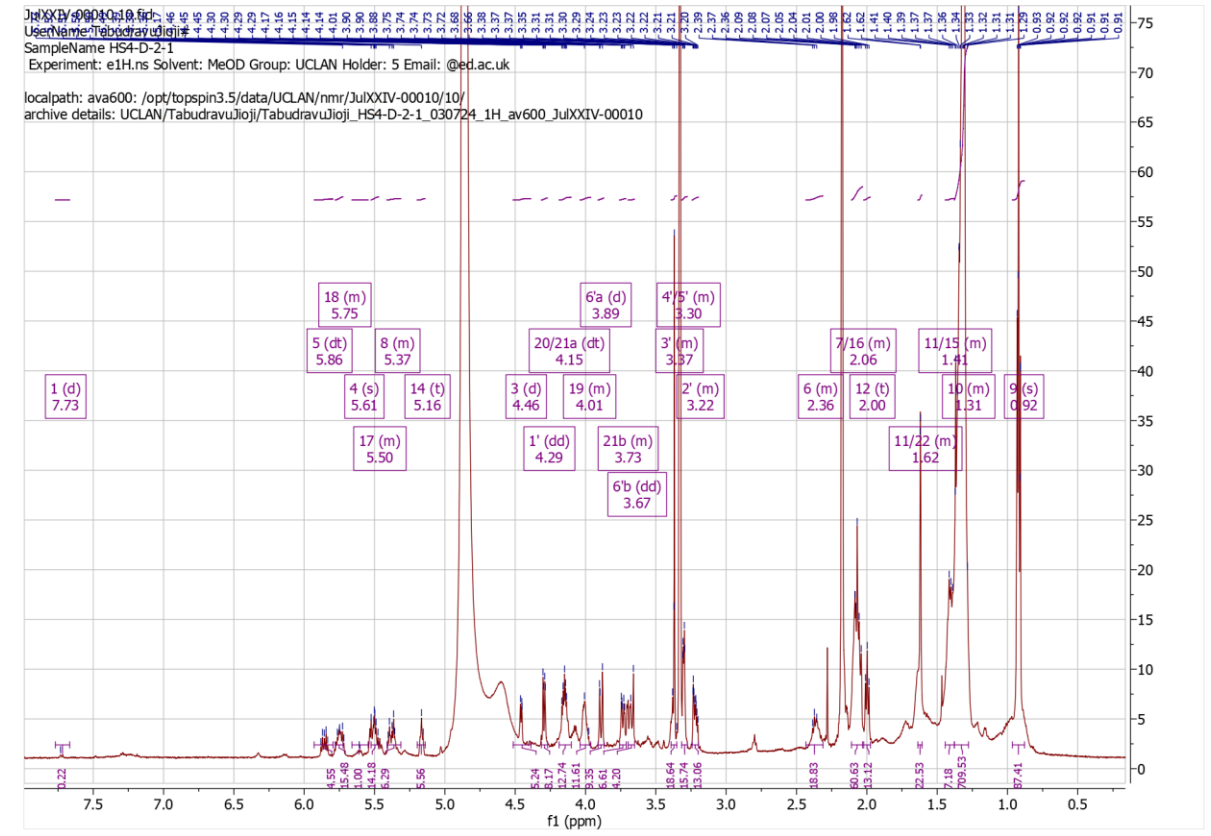

Figure S23. ^{1}H NMR spectra for HS4(50)F3 FD 2 s1.

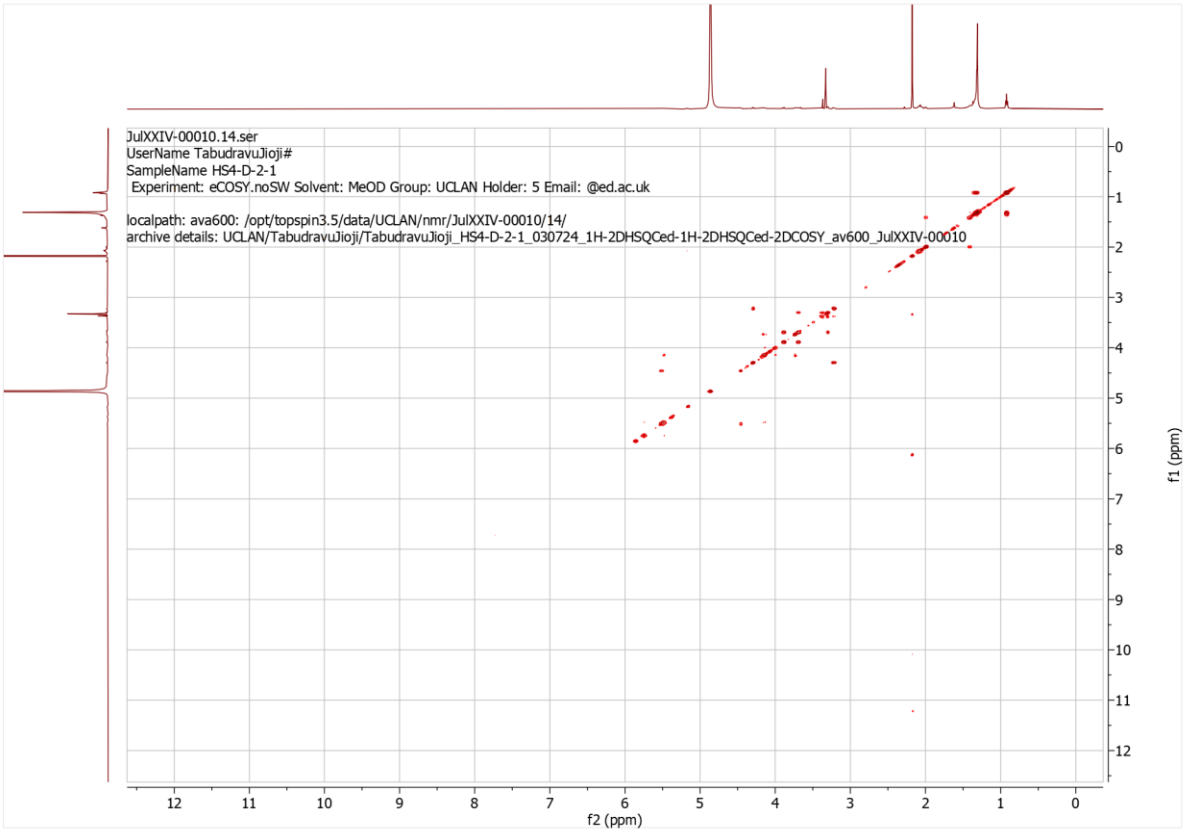

Figure S24. COSY NMR spectra for HS4(50)F3 FD 2 s1.

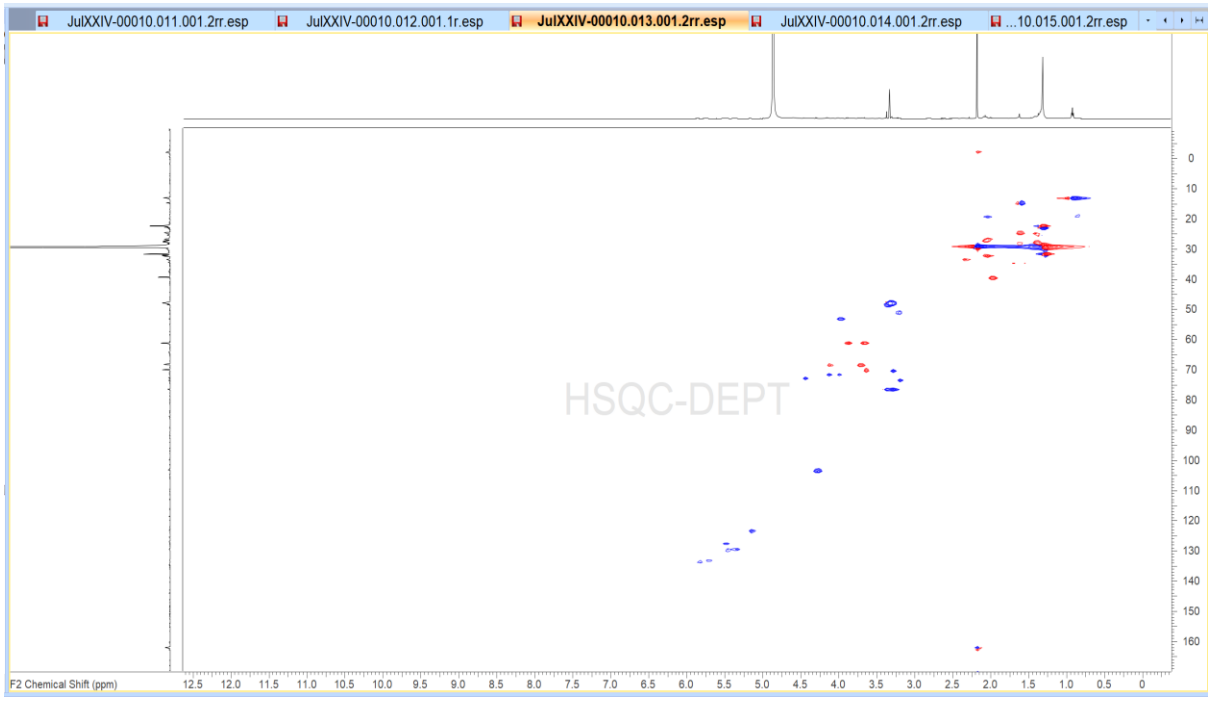

Figure S25. HSQC NMR spectra for HS4(50)F3 FD 2 s1.

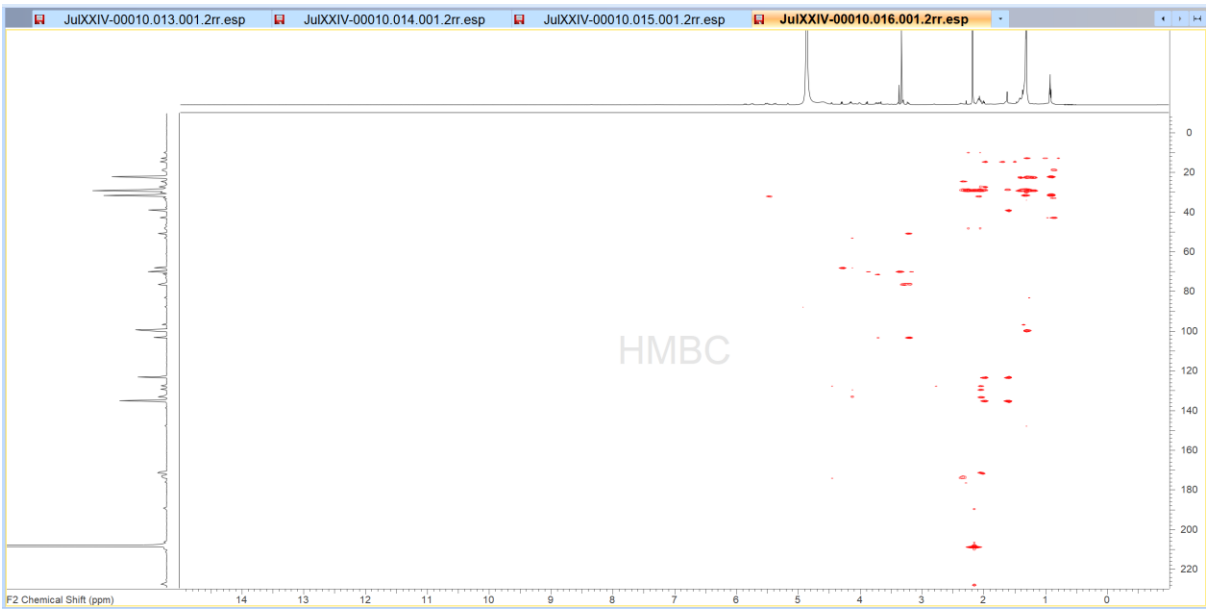

Figure S26. HMBC NMR spectra for HS4(50)F3 FD 2 s1.

Figure S27. NOSEY NMR spectra for HS4(50)F3 FD 2 s1.

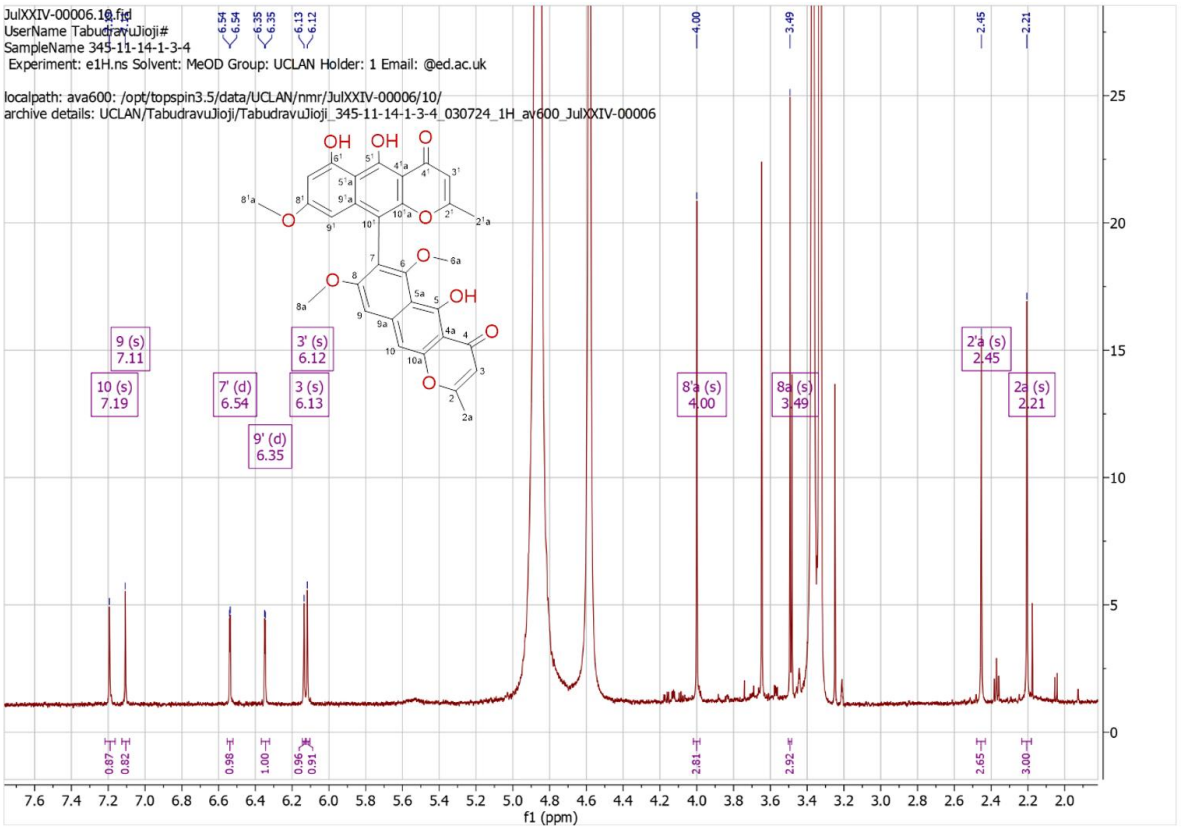

Figure S28 . ^{1}H NMR spectra for HS4(50)F3 FD 345 s11-14 ss1-3 H4.

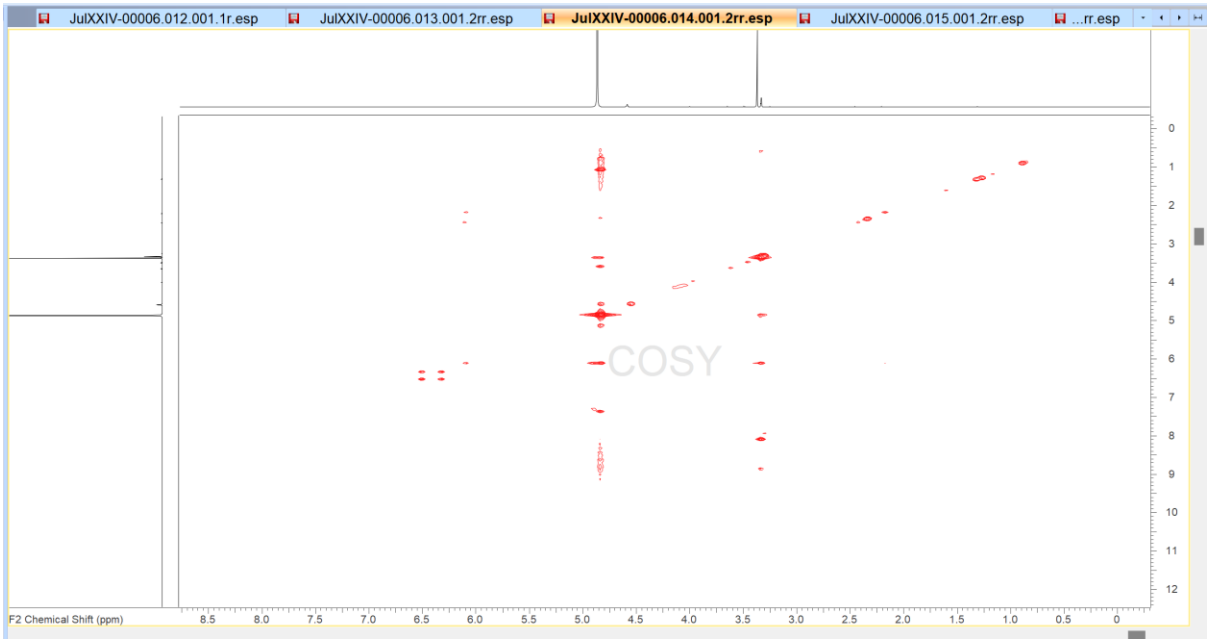

Figure S29. COSY NMR spectra for HS4(50)F3 FD 345 s11-14 ss1-3 H4.

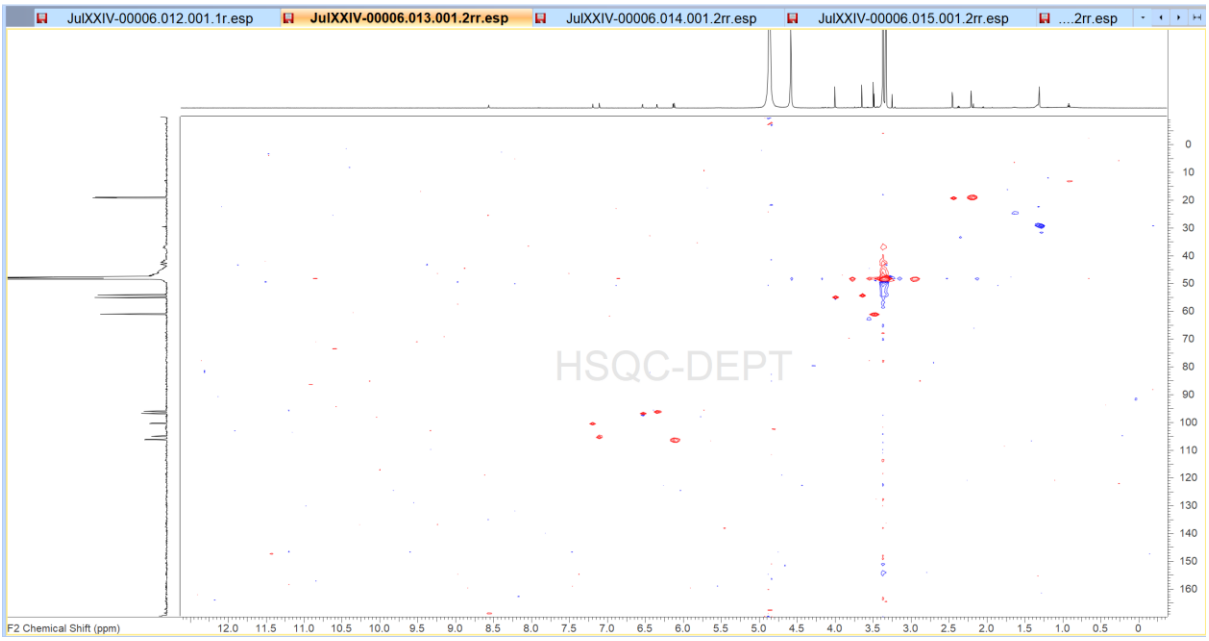

Figure S30. HSQC NMR spectra for HS4(50)F3 FD 345 s11-14 ss1-3 H4.

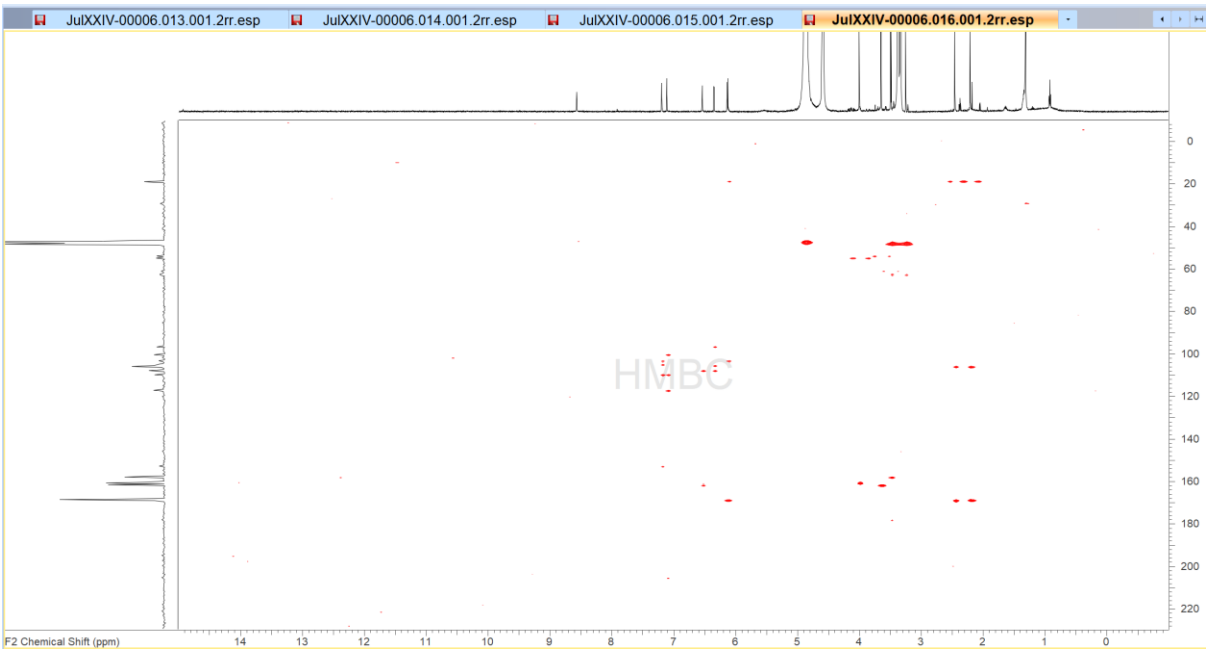

Figure S31. HMBC NMR spectra for HS4(50)F3 FD 345 s11-14 ss1-3 H4.

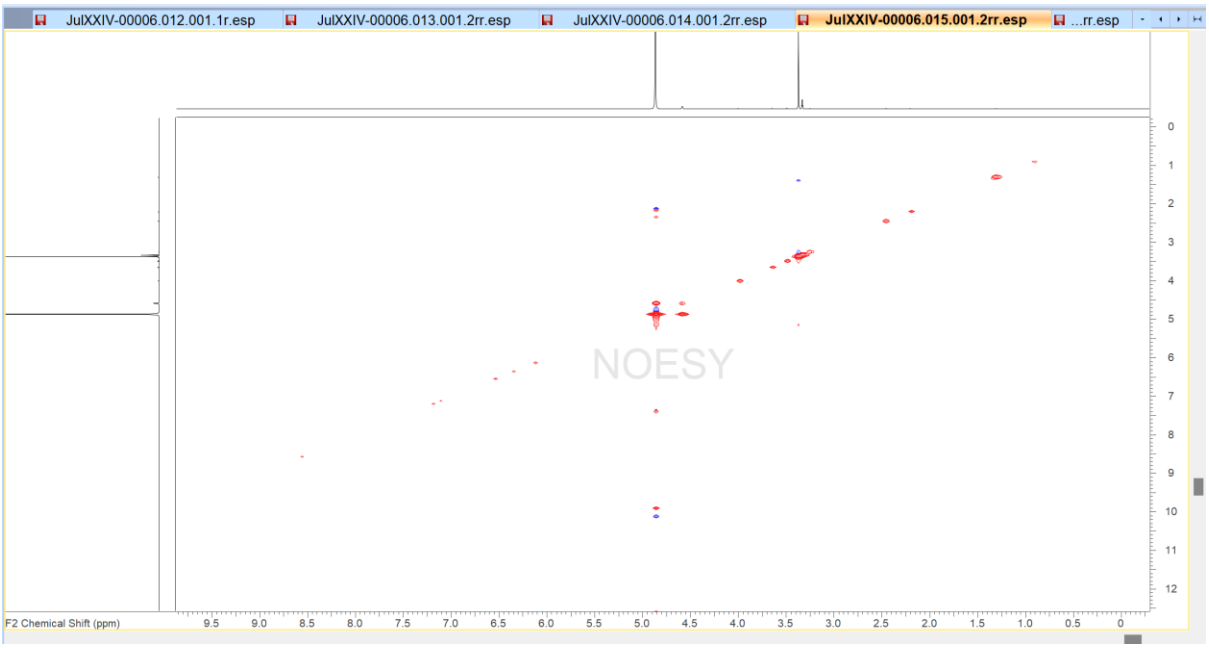

Figure S32 NOSEY NMR spectra for HS4(50)F3 FD 345 s11-14 ss1-3 H4.

Table S1. Antimicrobial bioassay results for crude samples (Part 1).

Sample number codes	Sample code	Inhibition ratio (%)						
		Pathogenic fungi			Pathogenic bacteria			
		A. niger	A. flavus	C. albican	S. aurues	L. monocytogenes	B. cerrus	E. coli

				s				
1	HS1(50)F1	0.0000	40.3127	14.3300	0.0000	3.0906	0.0000	0.0000
2	HS1(50)F1	55.4990	0.0000	14.1439	55.1850	0.0000	0.0000	17.5802
3	HS1(100)F2	0.0000	25.4929	20.7816	5.4579	17.7265	0.0000	0.0000
4	HS1(100)F2	0.0000	5.0306	0.0000	0.0000	0.0000	0.0000	0.0000
5	HS4(50)B2	0.0000	0.0000	0.0000	42.2074	0.0000	0.0000	0.0000
6	HS4(50)B2	33.1214	58.6676	45.5335	81.6252	0.0000	0.0000	0.0000
7	HS4(50)B5	46.5353	15.4317	0.0000	13.2808	0.0000	0.0000	0.0000
8	HS4(50)B5	0.0000	0.0000	0.0000	0.0000	0.0000	24.1949	0.0000
9	HS4(50)F1	0.0636	25.5608	32.2581	8.9145	2.4512	0.0000	16.9712
10	HS4(50)F1	38.9065	37.5255	0.0000	43.7235	9.6980	3.7159	22.8177
11	HS4(50)F3	0.0000	0.0000	0.0000	47.7259	0.0000	0.0000	5.5623
12	HS4(50)F3	0.0000	0.0000	0.0000	0.0000	0.0000	0.0000	0.0000
13	HS5(50)B1	0.0000	0.0000	0.0000	0.0000	0.0000	0.0000	0.0000
14	HS5(50)B1	0.0000	0.0000	0.0000	48.6962	0.0000	0.0000	0.0000
15	HS6(100)B1	38.5251	75.8668	0.0000	15.6458	18.8988	0.0000	0.0000
16	HS6(100)B1	0.0000	0.0000	0.0000	0.0000	2.9130	18.4145	0.0000
17	HS6(100)B2	0.0000	36.7777	0.0000	17.2226	0.0000	0.0000	0.0000
18	HS6(100)B2	0.0000	0.0000	0.0000	0.0000	0.0000	0.0000	0.0000
19	HS6(100)B3	0.0000	0.0000	0.0000	0.0000	0.0000	11.3955	0.0000
20	HS6(100)B3	0.0000	0.0000	0.0000	0.0000	0.0000	0.0000	0.0000
21	HS7(100)B1	0.0000	0.0000	0.0000	0.0000	14.4227	0.0000	0.0000
22	HS7(100)B1	0.0000	0.0000	0.0000	0.0000	0.0000	0.0000	1.5022
23	HS7(100)B2	0.0000	11.4888	0.0000	17.3438	13.8188	0.0000	17.0524
24	HS7(100)B2	0.0000	0.0000	0.0000	0.0000	9.8046	0.0000	0.0000

25	HS7(50)F4	0.0000	0.0000	0.0000	0.0000	6.2167	0.0000	0.0000
26	HS7(50)F4	46.6624	0.0000	0.0000	34.3238	8.8810	8.0925	0.0000
27	HS7(100)F5	0.0000	6.8661	0.0000	59.3087	25.3286	0.0000	0.0000
28	HS7(100)F5	0.0000	0.0000	0.0000	0.0000	0.0000	0.0000	17.0930
29	HS8(50)B1	6.9294	0.0000	0.0000	47.4227	31.6519	16.2675	34.0235
30	HS8(50)B1	0.0000	41.4684	0.0000	25.4700	59.6803	9.9917	39.1393
31	HS8(50)F1	0.0000	0.0000	0.0000	8.4294	0.0000	0.0000	12.4239
32	HS8(50)F1	0.0000	0.0000	0.0000	0.0000	13.0018	0.0000	19.2854
33	HS9(50)B1	0.0000	0.0000	0.0000	54.6392	0.0000	0.0000	0.0000
34	HS9(50)B1	0.0000	0.0000	0.0000	0.0000	22.6288	0.0000	0.7714
35	HS9(50)B3	59.3134	0.0000	0.0000	0.0000	7.9218	0.0000	1.1368
36	HS9(50)B3	0.0000	12.6445	0.0000	38.3869	5.7904	0.0000	0.0000
37	HS10(50)F1	36.4908	0.0000	42.9901	8.6719	5.3996	0.0000	11.2058
38	HS10(50)F1	21.4240	39.4290	0.0000	0.0000	31.9716	0.0000	34.7950
39	HS11(50)B2	47.7432	0.0000	0.0000	53.1837	25.8970	0.0000	0.0000
40	HS11(50)B2	8.3280	35.1462	0.0000	34.8090	13.5346	0.0000	0.0000
41	HS11(50)B3	0.0000	0.0000	0.0000	0.0000	0.0000	0.0000	0.0000
42	HS11(50)B3	64.1449	50.7138	14.8883	0.0000	30.0533	7.6796	28.9484
43	HS11(100)F1	10.8074	12.6445	12.2829	0.0000	10.9414	0.0000	25.8628
44	HS11(100)F1	0.0000	0.0000	0.0000	0.0000	0.0000	0.0000	0.0000
45	HS11(100)F2	0.0000	0.0000	0.0000	0.0000	10.7993	0.0000	0.0000
46	HS11(100)F2	0.0000	0.0000	0.0000	0.0000	0.0000	0.0000	0.0000
47	HS12(50)B1	0.0000	10.8770	0.0000	0.0000	3.8721	0.0000	0.0000
48	HS12(50)B1	0.0000	0.0000	0.0000	0.0000	0.0000	0.0000	0.0000
49	HS12(100)F1	0.0000	0.0000	0.2481	0.0000	0.0000	0.0000	0.0000

50	HS12(100)F1	0.0000	0.0000	0.0000	0.0000	7.8153	0.0000	0.0000
51	HS12(50)F2	0.0000	0.0000	0.0000	0.0000	19.5027	0.0000	0.0000
52	HS12(50)F2	0.0000	0.0000	0.0000	0.0000	0.0000	0.0000	0.0000
53	HS13(50)B2	22.1233	28.4160	27.4814	11.9466	26.2877	0.0000	0.0000
54	HS13(50)B2	0.0000	33.5146	32.3821	9.5209	19.0764	1.8993	26.3500
55	HS13(50)B3	65.8614	0.6118	29.8387	18.7386	42.9485	0.0000	0.0000
56	HS13(50)B3	60.2034	26.6485	2.0471	43.5415	93.9254	20.3138	53.1060
57	HS14(50)B1	0.0000	2.1754	10.9181	0.0000	44.5826	8.7531	38.9363
58	HS14(50)B1	18.6904	8.7016	45.0372	0.0000	48.9165	0.0000	19.9756
59	WNS2(3)F2	0.0000	0.0000	0.0000	0.0000	0.0000	0.0000	0.0000
60	WNS2(3)F2	0.0000	0.0000	0.0000	0.0000	0.0000	0.0000	0.0000
61	WNS7(3)F1	0.0000	0.0000	0.0000	0.0000	0.0000	0.0000	2.9233
62	WNS7(3)F1	14.2403	0.0000	17.7419	22.1953	36.7318	34.2692	11.8961
63	WNS2(3)F1	0.0000	0.0000	0.0000	0.0000	0.0000	4.1288	0.0000
64	WNS2(3)F1	0.0000	0.0000	0.0000	0.0000	0.0000	0.0000	8.0390
65	WNS2(3)F3	40.3051	6.6621	27.2333	0.0000	14.0320	0.0000	0.0000
66	WNS2(3)F3	0.0000	0.0000	20.5955	0.0000	11.5808	22.0479	0.0000
67	WNS17(5)F1	0.0000	3.1271	25.8685	0.0000	0.0000	0.0000	0.0000
68	WNS17(5)F1	0.0000	0.0000	0.0000	0.0000	19.6803	15.1941	0.0000
69	WNS6(5)F1	35.5372	19.3066	6.9479	7.3984	0.0000	0.0000	13.1953
70	WNS6(5)F1	0.0000	0.0000	0.0000	6.0643	19.9290	0.0000	0.0000
71	WNS6(5)F1	0.0000	0.0000	0.0000	0.0000	0.0000	0.0000	0.0000
72	WNS6(5)F1	0.0000	0.0000	0.0000	0.0000	0.0000	0.0000	39.0987
73	WNS7(8)F1	0.0000	0.0000	0.0000	0.0000	0.0000	0.0000	0.0000
74	WNS7(8)F1	0.0000	0.0000	0.0000	0.0000	0.0000	0.0000	10.3126

75	WNS17(8)F1	0.0000	0.0000	0.0000	0.0000	1.9183	0.0000	9.6224
76	WNS17(8)F1	0.0000	0.0000	15.0744	0.0000	0.0000	0.0000	0.0000
77	WNS2(8)F1	43.4838	2.9912	44.2928	23.6507	29.3428	19.0751	37.6370
78	WNS2(8)F1	0.0000	0.0000	0.0000	0.0000	0.0000	0.0000	0.0000
79	WNS7(8)F2	13.6682	0.0000	15.2605	0.0000	16.6252	0.0000	38.1648
80	WNS7(8)F2	0.0000	25.4929	0.0000	0.0000	0.0000	0.0000	49.0865
81	WNS7(8)F2	0.0000	0.0000	0.0000	0.0000	0.0000	71.5111	0.0000
82	WNS7(8)F2	0.0000	0.0000	0.0000	0.0000	22.8774	0.0000	0.0000
83	WNS16(8)F2	0.0000	20.1903	0.0000	39.5391	41.2433	0.0000	0.0000
84	WNS16(8)F2	0.0000	11.9646	0.0000	34.1419	38.5435	0.0000	0.0000
85	WNS7(8)F3	0.0000	0.0000	0.0000	0.0000	9.9822	0.0000	0.0000
86	WNS7(8)F3	0.0000	40.0408	0.0000	0.0000	0.0000	0.0000	0.0000
87	WNS11LF1.1	0.0000	7.2060	0.0000	10.4306	0.0000	0.0000	0.0000
88	WNS11LF1.1	0.0000	8.1577	0.0000	0.0000	56.6963	0.0000	3.0045
89	WNS12LF1.1	0.0000	0.0000	0.0000	0.0000	0.0000	0.0000	1.3804
90	WNS12LF1.1	0.0000	0.0000	0.0000	0.0000	0.0000	0.0000	0.0000
91	Unknown	0.0000	0.0000	0.0000	0.0000	18.7567	0.0000	0.0000
Cip		-	-	-	98.1632	-	-	99.2302
Nys		97.3690	98.3002	97.0025	-	-		-

Table S1. Antimicrobial bioassay results for crude samples (Part 2).

Sample numb	**Sample codes**	**Inhibition ratio (%)**						
		Pathogenic Fungi			**Pathogenic bacteria**			
		Aspergillus flavus	**Aspergillus niger**	**Candida albica**	**Bacillus cereus**	**Listeria monocytogenes**	**Staphylococcus aureus**	**Escherichia coli**

er codes				ns				
92	WNS1LB1.1	95.1882	91.2960	93.6971	87.7751	37.4249	0.0000	76.4635
93	WNS1LB1.1	38.3633	76.3804	65.0131	79.6367	0.0000	9.5176	2.2933
94	WNS3LB1.2	0.0000	0.0000	56.7552	1.7115	24.5497	0.0000	0.0000
95	WNS3RB1.1	86.0229	57.0169	55.8506	88.0894	30.8873	4.5632	9.7767
96	WNS3RB1.1	91.6203	23.3512	94.5142	84.5616	0.0000	0.0000	0.0000
97	WNS3RB1.3	82.0295	84.0874	92.6758	79.5669	86.3242	0.0000	1.9916
98	WNS3RB1.3	93.3879	89.7623	69.0400	84.2473	69.1795	17.1447	0.0000
99	WNS3RB2.1	95.7119	84.0874	94.1932	87.5306	88.2588	44.7197	16.4152
100	WNS3RB2.1	91.9149	72.2776	66.1220	78.9032	87.7252	70.6649	45.0815
101	WNS3RB2.1	48.8380	58.6656	63.4666	53.8247	26.2842	22.6858	0.0000
103	WNS3RB2.2	96.1375	74.1948	94.1056	93.5732	88.3923	93.3507	60.3500
104	WNS3RB2.2	36.2029	54.2178	70.1780	67.6912	65.7105	48.3703	15.8117
105	WNS4LB1.2	41.6367	19.6702	55.3837	67.4467	0.0000	0.0000	7.4231
106	WNS4LB1.2	26.7758	55.0997	61.2197	58.9242	32.3549	0.0000	0.0000
107	WNS4LB2.1	44.0262	27.5307	95.3020	86.8669	54.5030	10.9518	0.0000
108	WNS4RB2.1	95.0900	92.4080	94.6017	92.7698	91.5277	88.4615	40.4345
109	WNS4RB1.1	78.5925	77.2239	74.0006	42.3332	36.8913	14.6023	0.0000
110	WNS4RB1.1	95.4173	89.6856	95.1561	91.7569	91.7278	93.1551	35.3048
111	WNS4RB1.2	0.0000	54.0644	54.3041	49.1093	74.0494	56.7797	0.0000
112	WNS4RB1.2	0.0000	66.9862	61.0155	82.9899	45.9640	80.7040	43.2710
113	WNS4RB2.1	72.9624	66.0276	66.7056	76.3185	43.0287	53.8462	55.7634
114	WNS4RB2.1	93.6498	93.0598	93.6971	93.7827	87.4583	92.0469	48.4007
115	WNS5LB1.1	88.5434	91.9862	95.0394	88.5784	86.9246	92.3077	48.8835
116	WNS5LB1.1	71.2602	67.9448	86.5188	77.3315	66.2442	32.2034	29.2698

117	WNS5LB2.1	36.0720	52.1472	79.6032	44.0796	0.0000	0.0000	0.0000
118	WNS5LB2.1	0.0000	0.0000	53.5746	23.4370	0.0000	10.9518	0.0000
119	WNS5RB1.1	0.0000	10.0844	41.9025	28.3269	0.0000	0.0000	0.0000
120	WNS5RB1.1	0.0000	52.4540	60.8987	76.6329	37.9586	9.5176	0.0000
121	WNS5RB2.1	92.3404	92.0245	93.2886	84.5966	87.1915	37.4837	14.1219
122	WNS5RB2.1	14.5336	54.4479	93.2302	88.2291	82.1214	88.5267	43.3313
123	WNS8LB1.1	89.7545	90.2991	93.5804	85.5047	63.3756	90.2868	39.4689
124	WNS8LB1.1	85.0409	93.5583	93.8722	85.2951	82.5217	38.9179	37.8395
125	WNS8LB1.2	68.2160	65.7209	71.2285	71.8477	40.1601	48.1095	24.1400
126	WNS8LB1.2	69.9509	87.4617	81.7625	82.1167	66.0440	67.7314	0.0000
127	WNS8LB2.1	91.5548	93.2515	94.7476	77.6808	78.0520	75.9452	45.6850
128	WNS8LB2.1	65.4337	67.6380	94.3391	85.1554	46.4977	38.4615	54.8582
129	WNS8LB2.2	83.3715	82.8604	91.5961	76.2138	77.7852	0.0000	0.0000
130	WNS8LB2.2	69.6563	79.9847	33.9364	57.7366	0.0000	39.7001	9.1129
131	WNS8RB1.1	79.3781	69.0951	83.0172	73.3846	64.7765	23.0117	-16.6566
132	WNS8RB1.2	85.8265	73.5046	94.6892	84.8760	90.2602	19.4263	18.1050
133	WNS8RB2.1	81.5057	38.7270	87.5985	82.7803	92.5951	85.1369	0.0000
134	WNS8RB2.1	91.5221	75.3451	89.4952	84.0727	90.3269	69.8175	18.5275
135	WNS8RB2.2	94.2390	94.8236	94.8351	85.4349	80.7872	91.2647	22.2088
136	WNS8RB2.2	0.0000	52.0322	69.4193	78.2745	64.1761	59.9739	6.6385
137	WNS10LB1.1	82.9460	78.8727	72.6291	76.7377	38.3589	44.2634	1.9312
138	WNS10LB1.1	74.2390	74.5015	82.9880	74.1530	63.0420	61.5385	7.9662
139	WNS10LB2.1	95.4173	95.6288	95.0102	92.5603	89.1928	93.4811	92.8183
140	WNS10LB2.1	40.3928	53.7960	65.5967	92.0014	56.7045	64.7979	62.8847
141	WNS10LB2.2	28.7725	0.0000	22.4686	0.0000	45.2969	0.0000	0.0000

142	WNS10LB 2.2	61.6367	28.3359	48.52 64	24.799 2	8.2055	0.0000	0.0000
143	WNS10RB 2.2	72.2422	64.4172	96.20 66	74.746 8	32.5550	55.7366	0.0000
144	WNS10RB 2.2	93.3879	88.3052	95.82 73	85.399 9	89.9266	91.7862	22.7520
145	WNS14LB 1.1	39.5417	40.5675	60.25 68	75.026 2	33.8893	0.0000	38.6240
146	WNS14LB 1.1	0.0000	7.5920	39.24 72	54.243 8	40.8939	4.7588	0.0000
147	WNS14LB 1.2	0.0000	45.8972	54.01 23	77.436 3	77.3849	90.5476	31.7441
148	WNS14LB 1.2	92.6678	95.8589	96.35 25	92.804 8	91.3943	92.5033	17.0187
149	WNS14BB 1.1	0.0000	0.0000	41.58 16	59.238 6	38.4923	34.4198	9.0525
150	WNS14BB 1.1	38.7561	9.2025	44.93 73	66.957 7	48.0987	34.1591	17.0791
151	WNS15LB 2.1	96.5957	94.6702	96.58 59	94.656 0	92.6618	84.2894	0.0000
152	WNS15LB 2.1	48.3797	0.0000	20.86 37	34.963 3	41.0274	7.8227	0.0000
154	WNS3RB2. 1	51.0966	18.9801	0.000 0	12.329 7	0.0000	0.0000	0.0000
Cip		-	-	-	-	-	98.9540	99.0235
Nys		98.236	98.2531	97.91 20	-	-	-	-

10.0.1 Table S2. Antibiofilm activity of crude samples.

Samples number code	Samples code	Biofilm inhibition ratio (%)			
		Staphylococcus aureus	Listeria monocytogenes	Bacillus cereus	Escherichia coli
1	HS1(50)F1	1.3390	15.7630	0.0000	0.0000
2	HS1(50)F1	1.4493	11.7056	0.0000	0.0000
3	HS1(100)F2	2.2869	25.0987	0.0000	0.0000
4	HS1(100)F2	0.0000	0.0000	0.0000	0.0000
5	HS4(50)B2	0.0000	0.0000	0.0000	0.0000
6	HS4(50)B2	0.0000	24.3447	0.0000	0.0000
7	HS4(50)B5	0.0000	2.0467	0.0000	0.0000
8	HS4(50)B5	0.0000	2.1544	0.0000	0.0000
9	HS4(50)F1	0.7121	18.3124	0.0000	0.0000
10	HS4(50)F1	0.8927	34.2908	0.0000	8.9934
11	HS4(50)F3	1.7553	23.2675	0.0000	12.9280
12	HS4(50)F3	2.6128	0.0000	0.0000	11.2417
13	HS5(50)B1	0.0000	10.2334	0.0000	0.0000
14	HS5(50)B1	3.1344	32.6391	0.0000	0.0000
15	HS6(100)B1	0.0000	0.0000	0.0000	0.0000
16	HS6(100)B1	0.0000	5.0628	0.0000	9.1467
17	HS6(100)B2	0.0000	22.6212	0.0000	0.0000
18	HS6(100)B2	0.0000	0.0000	0.0000	0.0000
19	HS6(100)B3	0.0000	0.0000	0.0000	0.0000
20	HS6(100)B3	0.0000	0.3591	0.0000	0.0000
21	HS7(100)B1	0.0000	1.3285	0.0000	0.0000
22	HS7(100)B1	0.0000	13.2855	0.0000	34.6449
23	HS7(100)B2	2.5476	35.9785	18.9577	34.5938
24	HS7(100)B2	0.0000	24.8474	0.0000	54.9310
25	HS7(50)F4	0.0000	25.3501	0.0000	0.0000
26	HS7(50)F4	0.7773	13.1418	0.0000	0.0000
27	HS7(100)F5	0.0000	0.0000	0.0000	12.5192
28	HS7(100)F5	0.0000	8.2585	0.0000	0.0000
29	HS8(50)B1	0.4614	42.1544	4.0391	31.6811
30	HS8(50)B1	1.4443	40.5027	1.3681	29.0240
31	HS8(50)F1	0.0000	0.0000	0.0000	0.0000
32	HS8(50)F1	2.6730	15.4399	0.0000	0.0000
33	HS9(50)B1	0.0000	0.0000	0.0000	20.1329
34	HS9(50)B1	0.1254	0.0000	0.0000	13.8477
35	HS9(50)B3	0.0000	21.4004	0.0000	0.0000
36	HS9(50)B3	0.0000	24.2370	0.0000	0.0000
37	HS10(50)F1	1.2939	38.4201	0.0000	12.6214
38	HS10(50)F1	1.0682	27.0377	0.0000	20.8482

39	HS11(50)B2	0.0000	0.0000	0.0000	0.0000
40	HS11(50)B2	0.0000	0.0000	0.0000	0.0000
41	HS11(50)B3	0.0000	20.5745	0.0000	0.0000
42	HS11(50)B3	1.9007	33.7522	0.0000	13.7455
43	HS11(100)F1	1.7001	2.5494	0.7818	4.6500
44	HS11(100)F1	0.0000	40.2154	0.0000	28.2575
45	HS11(100)F2	2.1163	36.8761	0.0000	30.5059
46	HS11(100)F2	0.0000	21.4722	0.0000	0.0000
47	HS12(50)B1	0.3511	13.0341	0.0000	0.0000
48	HS12(50)B1	0.0000	0.0000	0.0000	0.0000
49	HS12(100)F1	-1.2939	28.4381	0.0000	0.0000
50	HS12(100)F1	0.0000	27.2890	0.0000	13.5411
51	HS12(50)F2	0.1404	7.5404	0.0000	16.9136
52	HS12(50)F2	0.0000	23.3393	0.0000	15.3296
53	HS13(50)B2	1.8104	32.9264	0.0000	14.7164
54	HS13(50)B2	0.4413	34.5422	0.0000	24.5784
55	HS13(50)B3	2.1163	39.8923	0.0000	31.0169
56	HS13(50)B3	3.1043	46.9659	0.0000	37.4042
57	HS14(50)B1	1.4042	42.1903	0.0000	28.1042
58	HS14(50)B1	4.6138	69.1562	2.7362	43.6382
59	WNS2(3)F2	2.9238	30.7361	2.3453	33.8784
60	WNS2(3)F2	2.4173	39.0305	0.6515	50.8942
61	WNS7(3)F1	1.9308	25.3501	0.0000	40.7256
62	WNS7(3)F1	2.0010	49.4794	10.0977	37.4042
63	WNS2(3)F1	0.0000	40.4668	4.2345	29.3817
64	WNS2(3)F1	0.0000	18.8510	0.0000	20.5927
65	WNS2(3)F3	0.8927	39.3178	0.0000	32.5498
66	WNS2(3)F3	0.0000	19.7127	0.0000	19.9285
67	WNS17(5)F1	0.0000	20.6822	0.0000	15.4829
68	WNS17(5)F1	3.2849	54.4704	16.6775	23.3010
69	WNS6(5)F1	2.9840	51.8492	14.4625	37.3020
70	WNS6(5)F1	7.9087	89.0844	79.1531	91.6198
71	WNS6(5)F1	0.0000	43.9138	8.6645	15.5851
72	WNS6(5)F1	0.0000	0.0000	0.0000	20.1840
73	WNS7(8)F1	1.5145	12.5314	0.0000	28.4619
74	WNS7(8)F1	0.0000	10.1257	0.0000	0.0000
75	WNS17(8)F1	6.6349	73.7882	50.5537	70.4139
76	WNS17(8)F1	5.8676	67.8636	52.6384	65.9172
77	WNS2(8)F1	5.9478	72.6750	57.9805	76.9545
78	WNS2(8)F1	5.3561	39.4614	44.6906	73.1732
79	WNS7(8)F2	5.2658	69.0485	0.0000	69.5963
80	WNS7(8)F2	6.1685	71.8133	46.8404	68.8809
81	WNS7(8)F2	6.1936	75.5835	54.2671	73.8886
82	WNS7(8)F2	5.4213	75.0090	62.9967	78.6919

83	WNS16(8)F2	8.6058	88.7253	82.9316	83.4951
84	WNS16(8)F2	8.6209	89.9461	71.0749	88.1451
85	WNS7(8)F3	7.7783	86.0682	83.1922	86.5611
86	WNS7(8)F3	7.8435	92.3519	87.6221	88.1962
87	WNS11LF1.1	6.9509	83.4470	83.3876	84.1594
88	WNS11LF1.1	7.3320	82.0826	77.0033	88.1962
89	WNS12LF1.1	7.1815	85.2783	77.1987	81.6045
90	WNS12LF1.1	6.9809	72.2442	79.6091	88.1962
92	WNS1LB1.1	0.0000	35.5982	38.8133	4.6796
93	WNS1LB1.1	0.0000	61.1521	0.0000	40.5565
94	WNS3LB1.2	0.0000	0.0000	6.9917	0.0000
95	WNS3RB1.1	0.0000	0.0000	0.0000	0.0000
96	WNS3RB1.1	0.0000	0.0000	0.0000	24.7470
97	WNS3RB1.3	18.2790	0.0000	0.0000	18.4654
98	WNS3RB1.3	12.9877	17.7622	0.0000	0.0000
99	WNS3RB2.1	22.4479	5.5022	0.0000	0.0000
100	WNS3RB2.1	0.0000	13.8848	7.1051	3.3727
101	WNS3RB2.1	0.0000	26.5510	40.1738	0.0000
103	WNS3RB2.2	0.0000	20.1994	0.0000	29.6374
104	WNS3RB2.2	42.0096	33.4564	38.7377	29.7218
105	WNS4LB1.2	0.0000	0.0000	0.0000	0.0000
106	WNS4LB1.2	0.0000	0.0000	0.0000	0.0000
107	WNS4LB2.1	0.0000	0.0000	0.0000	0.0000
108	WNS4RB2.1	0.0000	0.0000	0.0000	0.0000
109	WNS4RB1.1	0.0000	0.0000	0.0000	0.0000
110	WNS4RB1.1	0.0000	0.0000	0.0000	0.0000
111	WNS4RB1.2	0.0000	0.0000	0.0000	0.0000
112	WNS4RB1.2	0.0000	0.0000	0.0000	0.0000
113	WNS4RB2.1	0.0000	0.0000	0.0000	0.0000
114	WNS4RB2.1	0.0000	0.0000	0.0000	0.0000
115	WNS5LB1.1	0.0000	0.0000	0.0000	0.0000
116	WNS5LB1.1	0.0000	12.6292	0.0000	0.0000
117	WNS5LB2.1	0.0000	29.2097	0.0000	0.0000
118	WNS5LB2.1	0.0000	0.0000	14.8148	9.9916
119	WNS5RB1.1	0.0000	1.8095	0.0000	32.8415
120	WNS5RB1.1	0.0000	41.9867	0.0000	27.3187
121	WNS5RB2.1	0.0000	32.8287	0.0000	0.0000
122	WNS5RB2.1	0.0000	0.0000	0.0000	49.5363
123	WNS8LB1.1	0.0000	0.0000	0.0000	11.8887
124	WNS8LB1.1	0.0000	0.0000	0.0000	16.3153
125	WNS8LB1.2	0.9621	0.0000	13.8322	0.0000
126	WNS8LB1.2	9.1395	0.0000	0.0000	14.7133
127	WNS8LB2.1	0.0000	0.0000	41.1943	11.8465
128	WNS8LB2.1	0.0000	20.9380	24.9811	20.6155

129	WNS8LB2.2	0.0000	0.0000	0.0000	0.0000
130	WNS8LB2.2	0.0000	0.0000	0.0000	0.0000
131	WNS8RB1.1	0.0000	0.0000	0.0000	0.0000
132	WNS8RB1.2	0.0000	0.0000	0.0000	0.0000
133	WNS8RB2.1	0.0000	0.0000	0.0000	0.0000
134	WNS8RB2.1	0.0000	0.0000	0.0000	0.0000
135	WNS8RB2.2	0.0000	0.0000	0.0000	0.0000
136	WNS8RB2.2	0.0000	0.0000	0.0000	0.0000
137	WNS10LB1.1	0.0000	0.0000	0.0000	0.0000
138	WNS10LB1.1	0.0000	0.0000	0.0000	0.0000
139	WNS10LB2.1	0.0000	0.0000	0.0000	0.0000
140	WNS10LB2.1	0.0000	0.0000	0.0000	0.0000
141	WNS10LB2.2	0.0000	0.0000	0.0000	0.0000
142	WNS10LB2.2	0.0000	0.0000	0.0000	0.0000
143	WNS10RB2.2	0.0000	0.0000	0.0000	0.0000
144	WNS10RB2.2	0.0000	0.0000	0.0000	0.0000
145	WNS14LB1.1	0.0000	0.0000	0.0000	0.0000
146	WNS14LB1.1	0.0000	0.0000	0.0000	0.0000
147	WNS14LB1.2	0.0000	0.0000	0.0000	0.0000
148	WNS14LB1.2	0.0000	0.0000	0.0000	0.0000
149	WNS14BB1.1	0.0000	0.0000	0.0000	0.0000
150	WNS14BB1.1	0.0000	0.0000	0.0000	0.0000
151	WNS15LB2.1	0.0000	0.0000	0.0000	4.2159
152	WNS15LB2.1	0.0000	0.0000	0.0000	0.0000
154	WNS3RB2.1	56.8680	39.6972	12.5094	15.5143

Table S3. Antimicrobial bioassay results of fractions from WNS7(8)F3 and WNS16(8)F2.

Sample number	Sample name	*E. coli*	*P. auerginosa*	*L. momocytogens*	*S. aureus*	*C. albicans*	*A. niger*
1	WNS7(8)F3 FH	0	86.92307692	0	0	0	88.15920398
2	WNS7(8)F3 WW	91.67741935	89.69230769	8.309859155	83.52272727	94.69879518	85.97014925
3	WNS7(8)F3 FM	85.61290323	78.30769231	80.91549296	72.04545455	89.67871486	77.21393035
4	WNS7(8)F3 WB	15.87096774	0	18.66197183	0	51.56626506	12.23880597
5	WNS7(8)F3 FD 1-11	26.19354839	86.38461538	24.36619718	23.06818182	30.562249	89.15422886
6	WNS7(8)F3 FD 12	6.064516129	87.84615385	0	0	56.90763052	89.85074627
7	WNS7(8)F3 FD 15	0	68.23076923	0	0	0.923694779	0
8	WNS7(8)F3 FD 16-17	0	0	0	0	30	0
9	WNS7(8)F3 FD 18-20	25.48387097	77.46153846	33.38028169	82.5	57.59036145	79.80099502
10	WNS7(8)F3 FD 21	16.58064516	86	21.76056338	87.95454545	60.88353414	88.35820896
11	WNS7(8)F3 FD 14 S1-5	38.38709677	89.38461538	24.71830986	0	57.63052209	0
12	WNS7(8)F3 FD 14 S6-14	92.19354839	93.30769231	87.53521127	87.61363636	94.97991968	89.15422886
13	WNS7(8)F3 FD 13 S1-3	20.58064516	68.30769231	0	0	49.67871486	90.14925373
14	WNS7(8)F3 FD 13 S7-8	0	4.692307692	0	0	0	0
15	WNS7(8)F3 FD 13 S9-10	10.90322581	31.07692308	0	47.95454545	29.63855422	87.36318408
16	WNS7(8	36.64	48.846153	7.183098592	0	0	90.646766

	)F3 FD 13 S11-12	516129	85				17
17	WNS7(8)F3 FD 13 S13-15	14.903225 81	0.153846154	5.704225352	0	36.26506024	73.03482587
18	WNS7(8)F3 FD 13 S16-24	42	76.23076923	0	89.09090909	76.2248996	89.25373134
19	WNS7(8)F3 FD 13 S456A-E	92.516129 03	90.38461538	82.11267606	85.79545455	94.81927711	88.45771144
20	WNS7(8)F3 FD 13 S456F-X	93.935483 87	93.38461538	86.05633803	89.09090909	0	91.74129353
21	WNS7(8)F3 FD 13 S456Y-AR	35.677419 35	82.38461538	-29.57746479	0	48.6746988	91.54228856
22	WNS16(8)F2 FH	0	87.23076923	18.8028169	0	27.91164659	92.73631841
23	WNS16(8)F2 WW	91.483870 97	91.23076923	85.63380282	87.38636364	94.73895582	89.65174129
24	WNS16(8)F2 FM	61.741935 48	42.07692308	48.73239437	28.40909091	79.55823293	52.43781095
25	WNS16(8)F2 FD 1-7	0	88.15384615	17.11267606	63.97727273	18.63453815	81.29353234
26	WNS16(8)F2 FD 8	79.677419 35	0	79.08450704	0	27.14859438	0
27	WNS16(8)F2 FD 9	30.258064 52	91.69230769	62.74647887	0	96.78714859	0
28	WNS16(8)F2 FD 10-11	0	0	0	0	0	0
29	WNS16(8)F2 FD 12-13	0.129032258	84	24.50704225	0	45.42168675	88.05970149
30	WNS16(8)F2 FD 14-16	7.483870968	78.30769231	5.281690141	0	46.02409639	0
31	WNS16(	8.645	84.846153	0	0	46.465863	0

	8)F2 FD 17-20	16129	85			45	
32	WNS16(8)F2 FD 21-25	15.096774 19	86.23076923	10.63380282	0	31.64658635	92.33830846
33	WNS16(8)F2 WB 1-6	0	27.84615385	0	0	52.28915663	60.49751244
34	WNS16(8)F2 WB 7	28.967741 94	76.61538462	29.36619718	0	80	83.08457711
35	WNS16(8)F2 WB 8	0	31.84615385	0	0	61.40562249	0
36	WNS16(8)F2 WB 9	22.709677 42	49.53846154	0	37.38636364	46.66666667	37.11442786
37	WNS16(8)F2 WB 10	21.161290 32	63.38461538	0	38.06818182	74.41767068	37.71144279
38	WNS16(8)F2 WB 11	21.354838 71	78.53846154	22.67605634	39.09090909	57.91164659	79.80099502
39	WNS16(8)F2 WB 12	49.032258 06	71.30769231	31.76056338	70.34090909	39.91967871	63.38308458
40	WNS16(8)F2 WB 13	40	81.15384615	34.29577465	13.06818182	69.31726908	74.92537313
41	WNS16(8)F2 WB 14	26.645161 29	40.76923077	44.43661972	70.45454545	70.96385542	83.38308458
42	WNS16(8)F2 WB 15	41.354838 71	81.46153846	53.16901408	61.93181818	64.73895582	84.67661692
43	WNS16(8)F2 WB 16-17	18.580645 16	52.53846154	19.22535211	4.659090909	57.95180723	4.676616915
44	WNS16(8)F2 WB 18-19	0	27.46153846	5.14084507	0	44.57831325	63.48258706
45	WNS16(8)F2 WB 20-25	7.5483870 97	52.15384615	23.02816901	0	55.943775 1	1.492537313

Table S4. Solvent fractions used in the VLC of WNS7(50)F3 FD.

Fraction number	n-Hexane %	DCM %
1	100	0
2	90	10
3	80	20
4	70	30
5	60	40
6	50	50
7	40	60
8	30	70
9	20	80
10	10	90
11	0	100
	MeOH %	DCM %
12	10	90
13	20	80
14	30	70
15	40	60
16	50	50
17	60	40
18	70	30
19	80	20
20	90	10
21	100	0

Table S5. Solvent fractions used in the VLC of WNS16(8)F2 WB.

Fraction number	n-Hexane %	DCM %
1	100	0
2	75	25
3	50	50
4	25	75
5	0	100
	MeOH %	DCM %
6	5	95
7	10	90
8	15	85
9	20	80
10	25	75
11	30	70
12	35	65
13	40	60
14	45	55
15	50	50
16	55	45
17	60	40
18	65	35

19	70	30
20	75	25
21	80	20
22	85	15
23	90	10
24	95	5
25	100	0

Table S6. Solvent fractions used in the VLC of WNS16(8)F2 FD.

Fraction number	n-Hexane %	DCM %
1	100	0
2	75	25
3	50	50
4	25	75
5	0	100
	MeOH %	DCM %
6	5	95
7	10	90
8	15	85
9	20	80
10	25	75
11	30	70
12	35	65
13	40	60
14	45	55
15	50	50
16	55	45
17	60	40
18	65	35
19	70	30
20	75	25
21	80	20
22	85	15
23	90	10
24	95	5
25	100	0

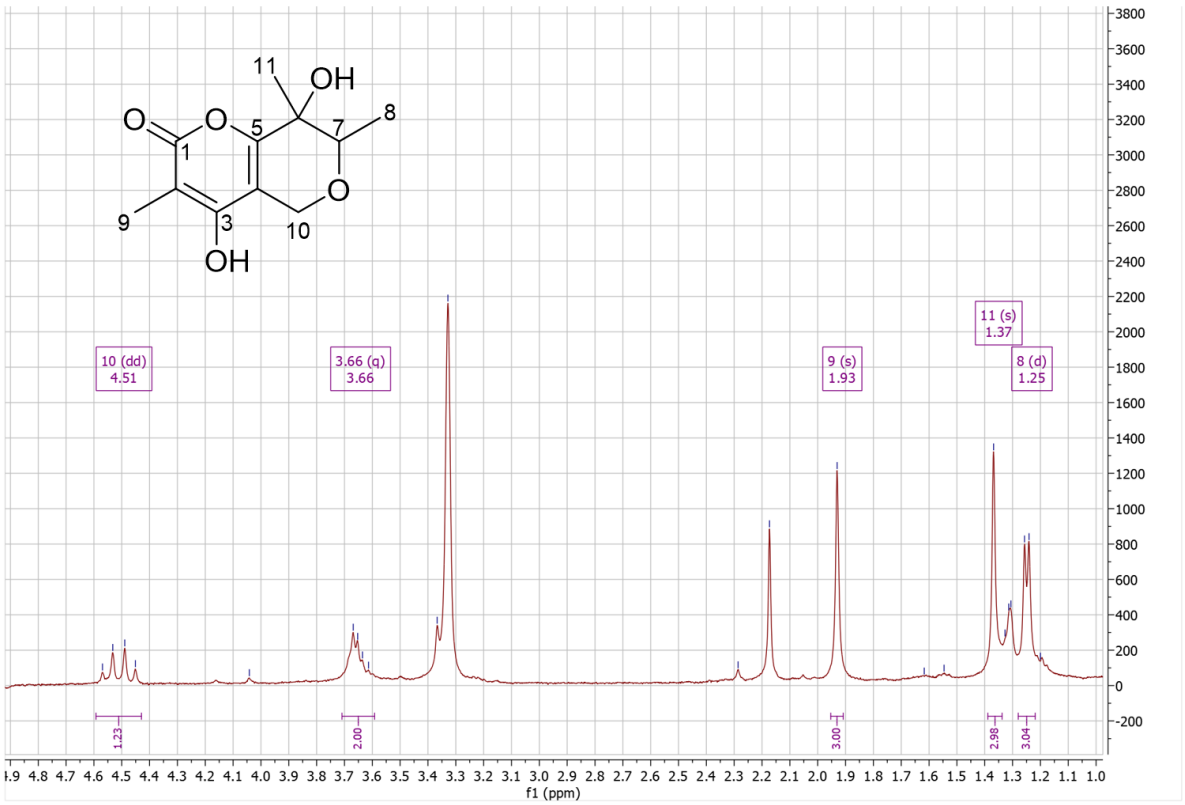

Figure S33. ^{1}H NMR spectrum (400 MHz, CD3OD) for *ASMN*-BT-H11.

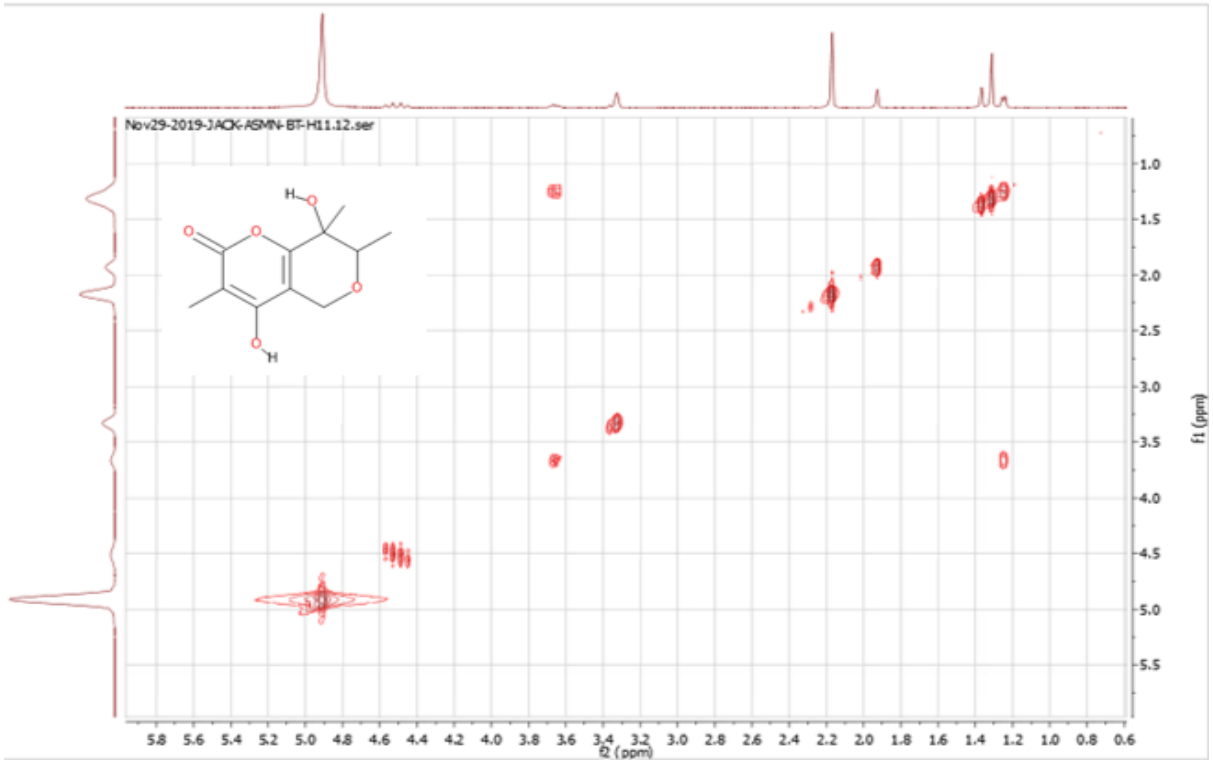

Figure s34. COSY NMR (600 MHz/100 MHz, CD3OD) spectrum of *ASMN*-BT-H11.

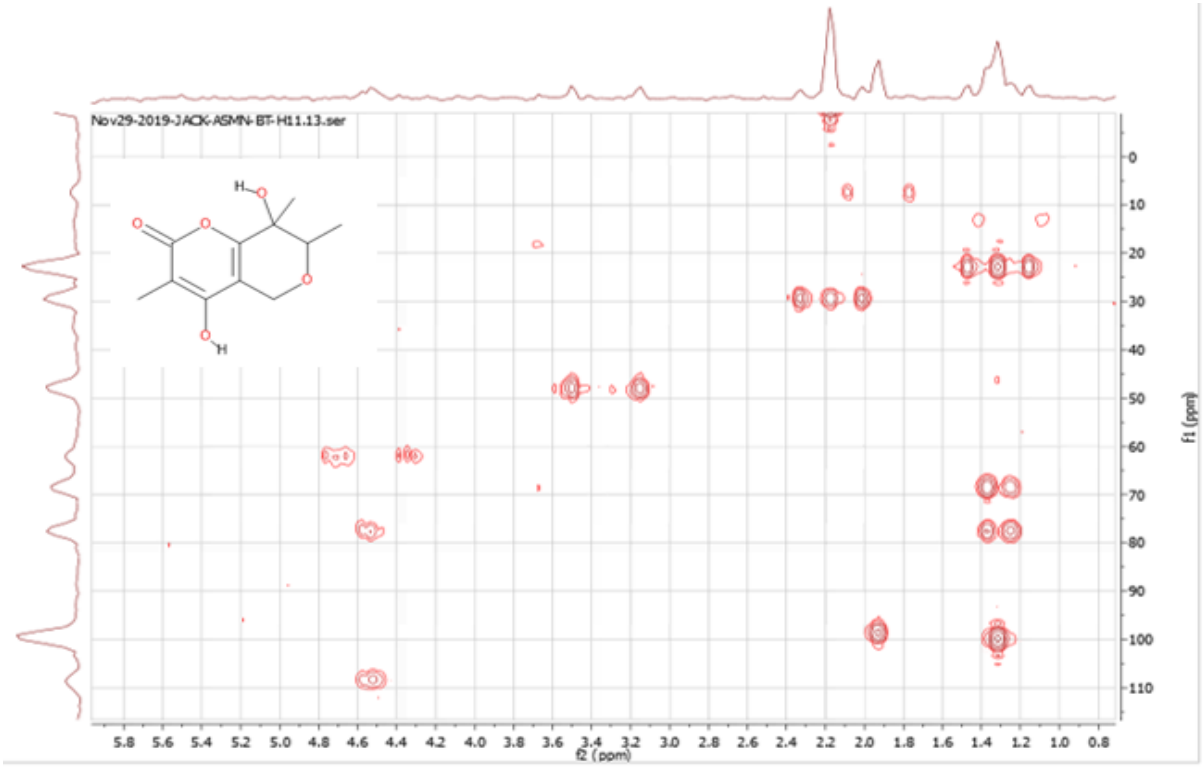

Figure S35. HMBC NMR (400 MHz/100 MHz, CD3OD) spectrum of *ASMN*-BT-H11.

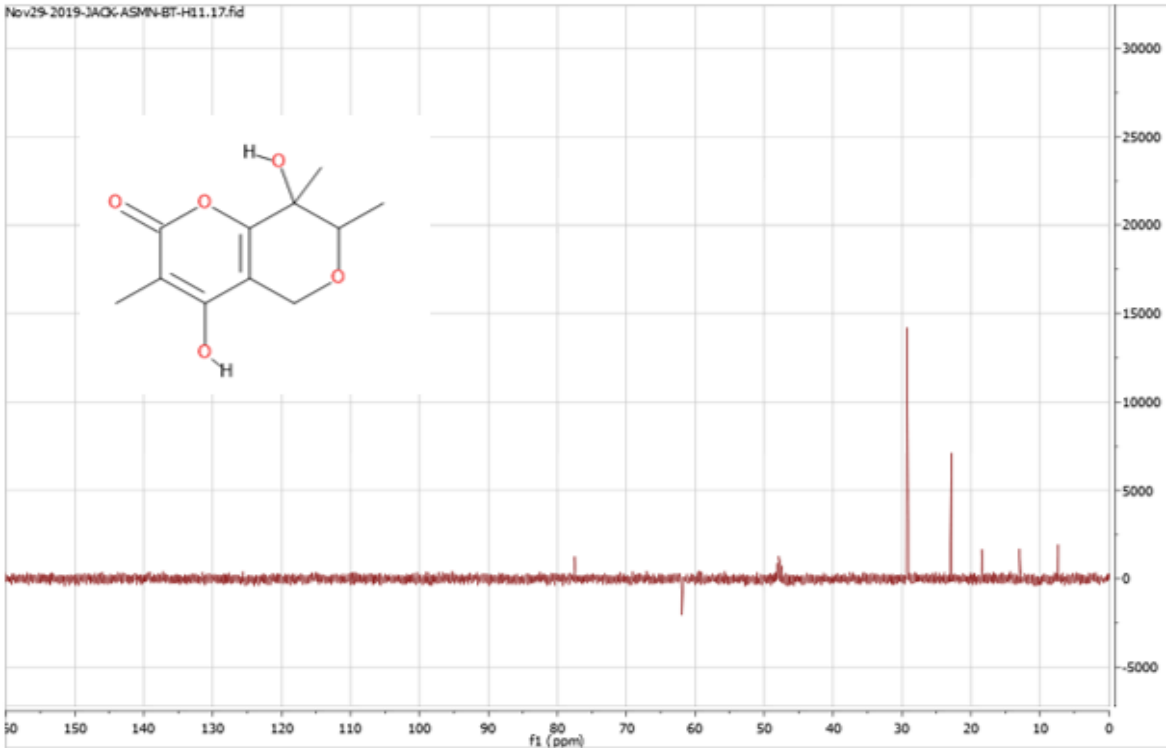

Figure S36. ^{13}C NMR (600 MHz/100 MHz, CD3OD) spectrum of *ASMN*-BT-H11.

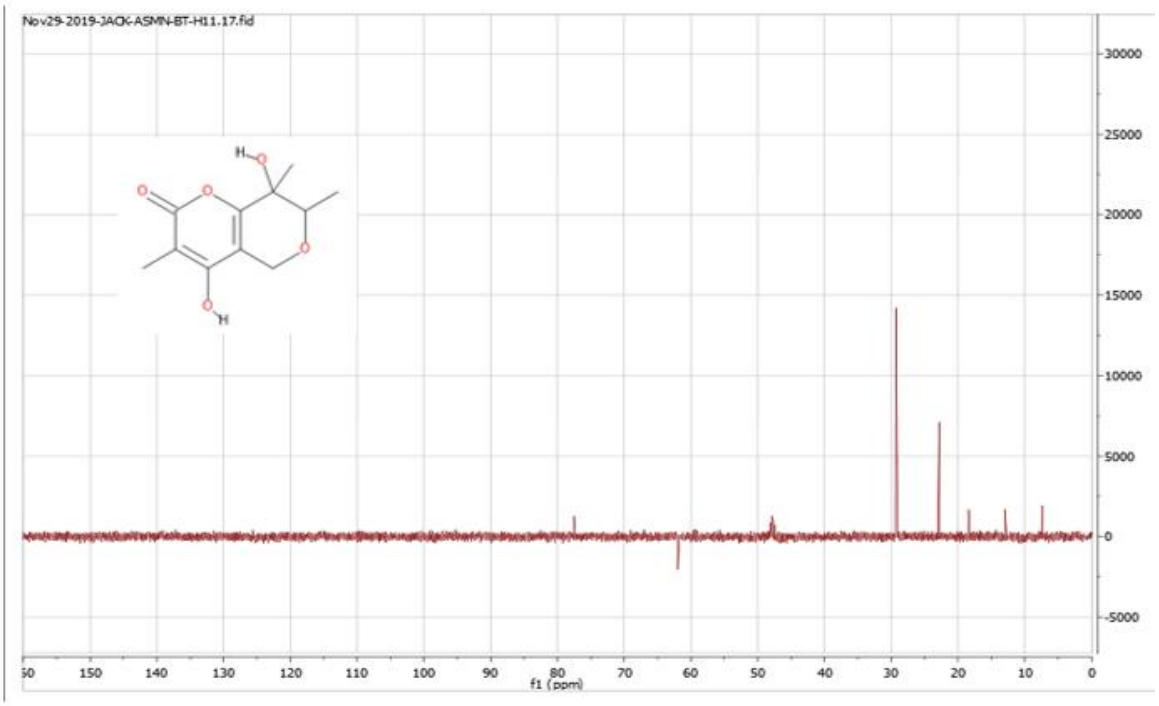

Figure S37. DEPT90 NMR (100 MHz, CD3OD) spectrum of ASMN-BT-H11.

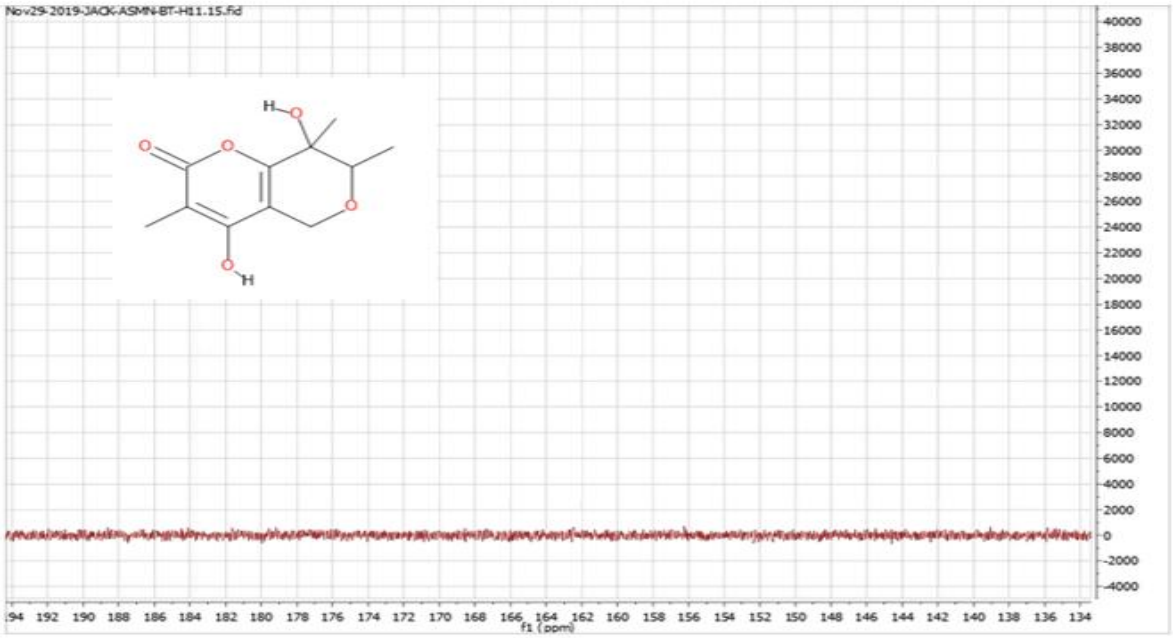

Figure S38. DEPT135 NMR (100 MHz, CD3OD) spectrum of *ASMN*-BT-H11.

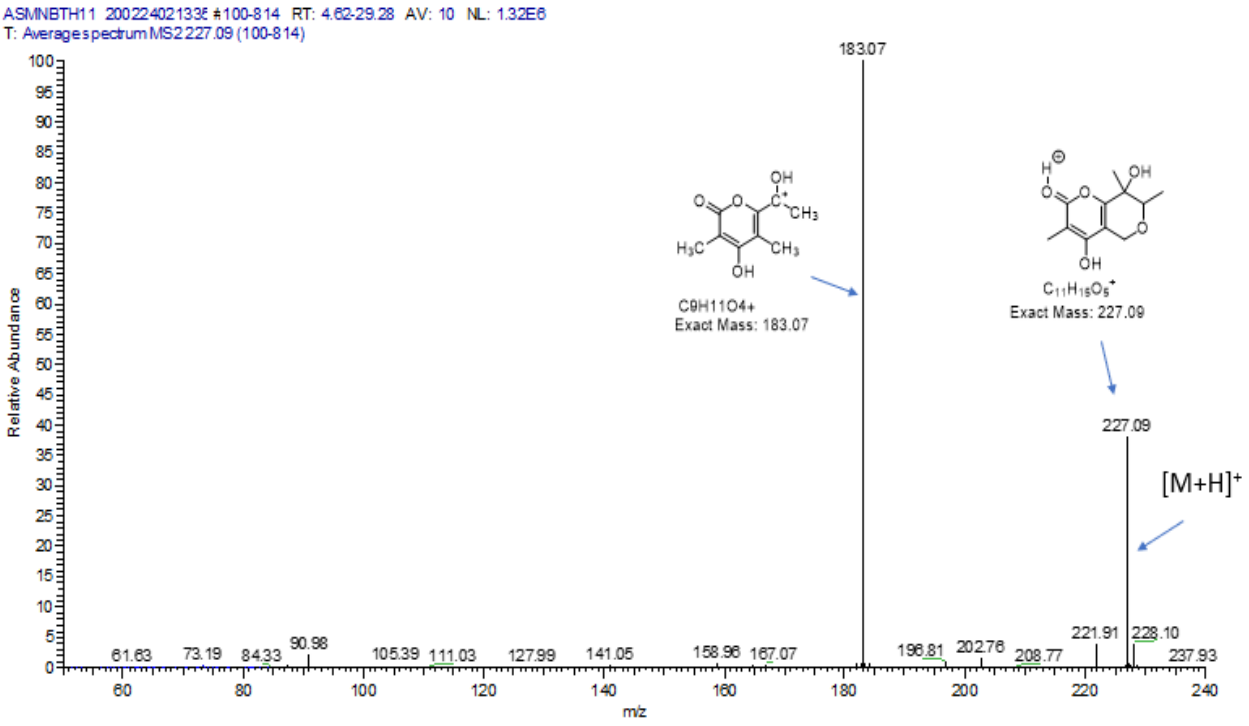

Figure S39. HR-MS/MS data of ASMN-BT-H11.

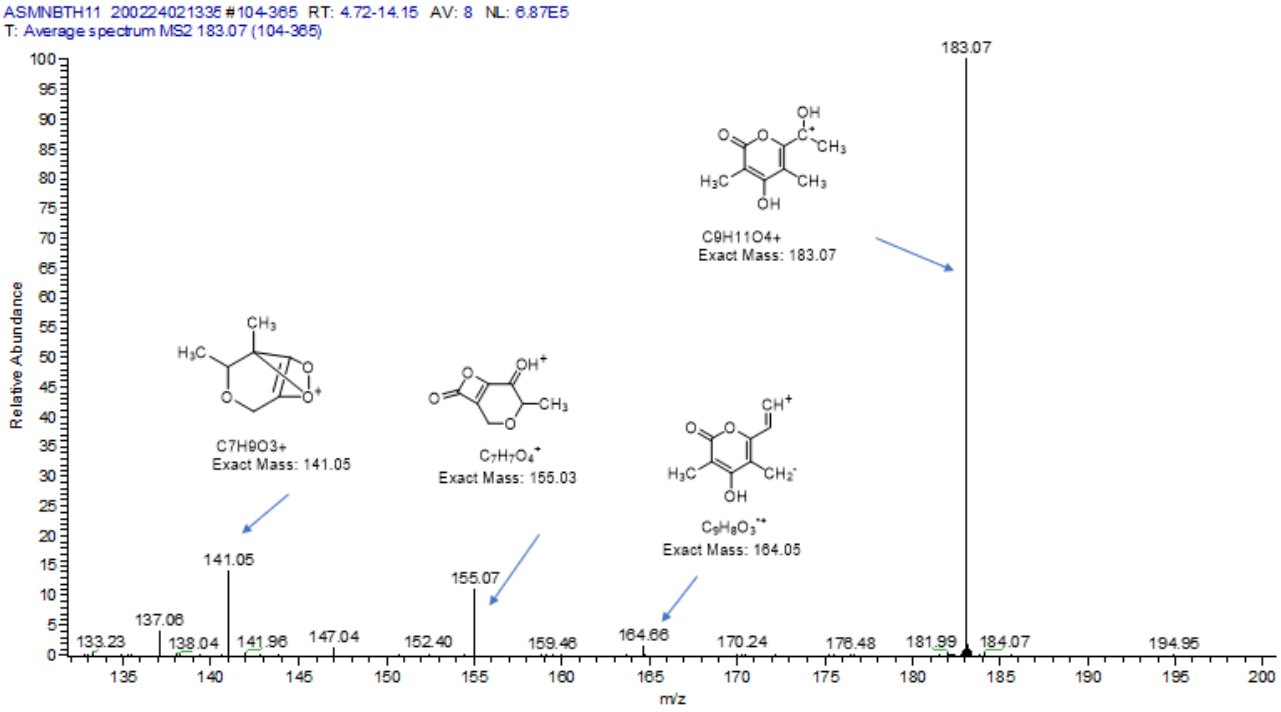

Figure S40. HR-MS/MS data of ASMN-BT-H11.

Table S7. HRESIMS: 227.09 $[M + H]^+$. From the HRESIMS data, three molecular formulas were predicted.

m/z	Theoretical Mass Composition (amu)	Delta (ppm)	Molecular Formula
227.09	227.09	-0.24 9.5	$C_{12}H_{11}ON_4$
	227.09	**1.10 4.5**	**$C_{11}H_{15}O_5$**
	227.09	1.11 10.0	$C_{11}H_{15}O_5$

ASMN Structure Elucidation Calculations

Computer assisted structure elucidation

Elucidation Protocol

Start: Search Structures by 13C NMR 04/30/2020
13:56:17 Search by CNMR options:
Clear Generated Molecules List = Yes
Maximum Average Deviation = 2.0000 ppm
Keep Molecules with Number of CNMR Shifts Less than in Query = Yes
Minimum Possible Tolerance for All Atoms (no less than) = 20.00
Maximum Possible Tolerance for All Atoms (no more than) = 20.00
Process subspectra search in E:\BACKUP _HARD DRIVE\PHAMASEA\ACDLABS\PUBCHEM DB\PUBCHEM_COMPOUNDS_01A_V12_CALC_CH_COMPACTED_I.SED
11 structure(s) have been found by NMR spectra and added to Generated Structures
Process subspectra search in E:\BACKUP _HARD DRIVE\PHAMASEA\ACDLABS\PUBCHEM DB\PUBCHEM_COMPOUNDS_04A_V12_CALC_CH_COMPACTED_I.SED
15 structure(s) have been found by NMR spectra and added to Generated Structures
Process subspectra search in E:\BACKUP _HARD DRIVE\PHAMASEA\ACDLABS\PUBCHEM DB\PUBCHEM_COMPOUNDS_05C_V12_CALC_CH_COMPACTED_I.SED
0 structure(s) have been found by NMR spectra and added to Generated Structures
Process subspectra search in E:\BACKUP _HARD DRIVE\PHAMASEA\ACDLABS\PUBCHEM DB\PUBCHEM_COMPOUNDS_02A_V12_CALC_CH_COMPACTED_I.SED
8 structure(s) have been found by NMR spectra and added to Generated Structures
Process subspectra search in E:\BACKUP _HARD DRIVE\PHAMASEA\ACDLABS\PUBCHEM DB\PUBCHEM_COMPOUNDS_03A_V12_CALC_CH_COMPACTED_I.SED
2 structure(s) have been found by NMR spectra and added to Generated Structures
Process subspectra search in E:\BACKUP _HARD DRIVE\PHAMASEA\ACDLABS\PUBCHEM DB\PUBCHEM_COMPOUNDS_02B_V12_CALC_CH_COMPACTED_I.SED
8 structure(s) have been found by NMR spectra and added to Generated Structures
Process subspectra search in E:\BACKUP _HARD DRIVE\PHAMASEA\ACDLABS\PUBCHEM DB\PUBCHEM_COMPOUNDS_03B_V12_CALC_CH_COMPACTED_I.SED
21 structure(s) have been found by NMR spectra and added to Generated Structures
Process subspectra search in E:\BACKUP _HARD DRIVE\PHAMASEA\ACDLABS\PUBCHEM DB\PUBCHEM_COMPOUNDS_05A_V12_CALC_CH_COMPACTED_I.SED
16 structure(s) have been found by NMR spectra and added to Generated Structures
Process subspectra search in E:\BACKUP _HARD DRIVE\PHAMASEA\ACDLABS\PUBCHEM DB\PUBCHEM_COMPOUNDS_04B_V12_CALC_CH_COMPACTED_I.SED
8 structure(s) have been found by NMR spectra and added to Generated Structures
Process subspectra search in E:\BACKUP _HARD DRIVE\PHAMASEA\ACDLABS\PUBCHEM DB\PUBCHEM_COMPOUNDS_01B_V12_CALC_CH_COMPACTED_I.SED
6 structure(s) have been found by NMR spectra and added to Generated Structures
Process subspectra search in E:\BACKUP _HARD DRIVE\PHAMASEA\ACDLABS\PUBCHEM DB\PUBCHEM_COMPOUNDS_05B_V12_CALC_CH_COMPACTED_I.SED
3 structure(s) have been found by NMR spectra and added to Generated Structures Finish: Search Structures by 13C NMR 04/30/2020 13:56:41

Start: Create MCDs for Correlation Spectroscopy Based Generator 04/30/2020 14:01:52 Options:
Clear Existing MCDs = Yes
Minimum CNMR Assignment Error = 1.50
Set Atom Properties From CNMR Data = Yes
Set Atom Properties From HNMR Data = Yes
Allow SPQ Carbons = Yes

1 MCD has been created from MF: C11H14O5

Finish: Create MCDs for Correlation Spectroscopy Based Generator 04/30/2020 14:01:52

Start: Check MCDs 04/30/2020
14:01:58 Check MCDs options:
Delete "Bad" MCDs from List A = No
Automatically Resolve Contradictions = Yes
2D NMR Spectral Data Must Contain Connectivities = Real spectrum
Increase Connectivity Length when Merging Connectivities = No
Allow Bonds between Heteroatoms = No
Allow Bonds between Heteroatoms of the Same Atom Type = No
Use NMR Shifts Correlation Table = 2
Maximum bond multiplicity = 3
Check MCD #1 (ID = 1)

Stage 1
Visible non-standard connectivities were not detected.
Stage 2
Atoms with non-standard connectivities were not detected.
Stage 3
Contradictions in 2D NMR data were not detected.
Evident bonds were not detected during analysis of existing correlations.

Check MCD #1 (ID = 1) passed all tests
Finish: Check MCDs 04/30/2020 14:01:59

Start: Structure Generation 04/30/2020 14:02:04
Correlation Spectroscopy Based Structure Generator options:
Keep Generated Molecules = Yes
Clear Generated Molecules List Before Generation = No
Add Structures Already Existing in Generated Molecules List = No
Transfer Spectra to Generated Structures = Yes
Use Assignment when Removing Duplicates = Yes
Allow Filter during Generation = Yes
Use Only 1000 First MCD(s)
Allow "Fuzzy" Generation = Yes
"Fuzzy" Generation Options were Determined Automatically
2D NMR Spectral Data Must Contain Connectivities = Real spectrum
Increase Connectivity Length when Merging Connectivities = No
Allow Bonds between Heteroatoms = No
Allow Bonds between Heteroatoms of the Same Atom Type = No
Use NMR Shifts Correlation Table = 2
Maximum bond multiplicity = 3
MCD #1 (ID = 1): (1001584/0) structures have been generated and (98/0) structures stored
1001584 structure(s) have been generated by Correlation Spectroscopy Based Generator and 98 structure(s) have been stored.
Generation time: 5 m 30 s (Check: 0 s, Generation: 5 m 29 s 352 ms)
No (from No) connectivities have been extended during generation
Finish: Structure Generation 04/30/2020 14:07:3

1 (ID:46) 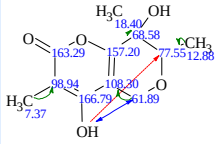	2 (ID:12) 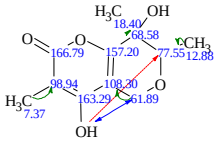	3 (ID:25) 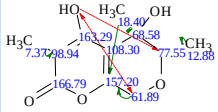	4 (ID:75) 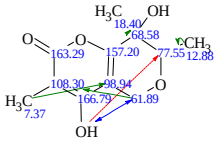	5 (ID:48) 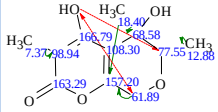
$d_N(^{13}C)$: 2.038	$d_N(^{13}C)$: 2.234	$d_N(^{13}C)$: 2.319	$d_N(^{13}C)$: 2.590	$d_N(^{13}C)$: 2.692
6 (ID:70) 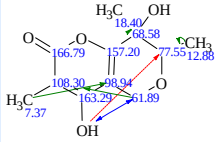	7 (ID:76) 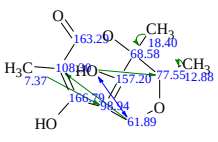	8 (ID:11) 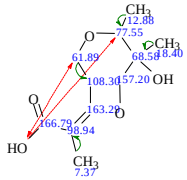	9 (ID:34) 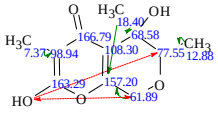	10 (ID:42) 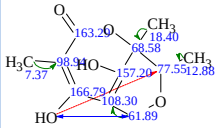
$d_N(^{13}C)$: 2.786	$d_N(^{13}C)$: 3.484	$d_N(^{13}C)$: 3.629	$d_N(^{13}C)$: 3.643	$d_N(^{13}C)$: 3.651
11 (ID:19) 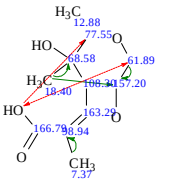	12 (ID:96) 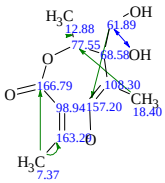	13 (ID:33) 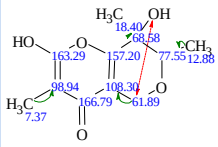	14 (ID:52) 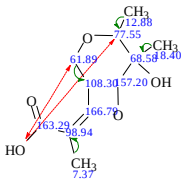	15 (ID:38) 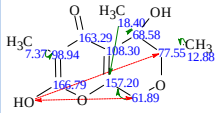
$d_N(^{13}C)$: 4.098	$d_N(^{13}C)$: 4.178	$d_N(^{13}C)$: 4.181	$d_N(^{13}C)$: 4.264	$d_N(^{13}C)$: 4.279
16 (ID:30) 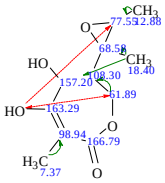	17 (ID:40) 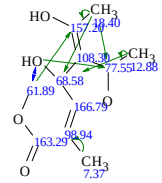	18 (ID:6) 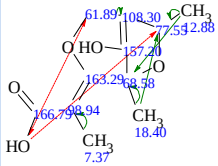	19 (ID:8) 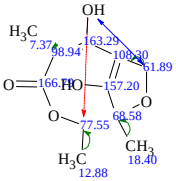	20 (ID:41) 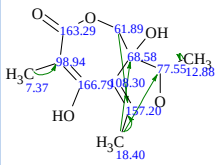
$d_N(^{13}C)$: 4.341	$d_N(^{13}C)$: 4.401	$d_N(^{13}C)$: 4.467	$d_N(^{13}C)$: 4.624	$d_N(^{13}C)$: 4.682
21 (ID:21) 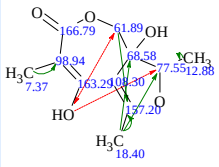	22 (ID:60) 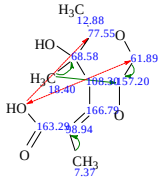	23 (ID:37) 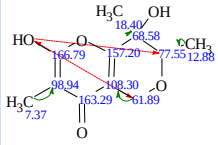	24 (ID:65) 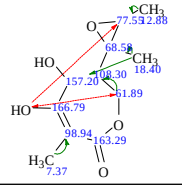	25 (ID:28) 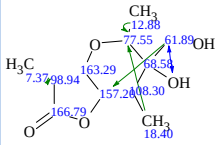
$d_N(^{13}C)$: 4.682	$d_N(^{13}C)$: 4.733	$d_N(^{13}C)$: 4.816	$d_N(^{13}C)$: 4.832	$d_N(^{13}C)$: 4.840

26 (ID:43) 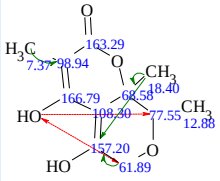	27 (ID:22) 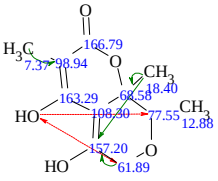	28 (ID:54) 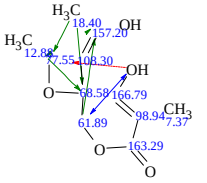	29 (ID:45) 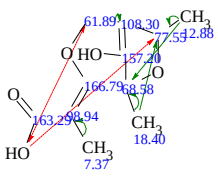	30 (ID:47) 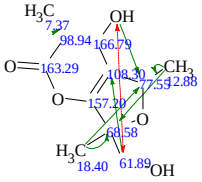
$d_N(^{13}C)$: 4.888	$d_N(^{13}C)$: 4.888	$d_N(^{13}C)$: 4.893	$d_N(^{13}C)$: 4.930	$d_N(^{13}C)$: 4.960
31 (ID:71) 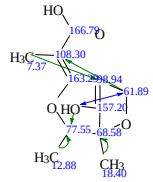	32 (ID:49) 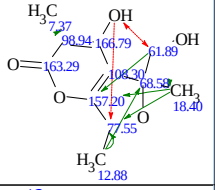	33 (ID:84) 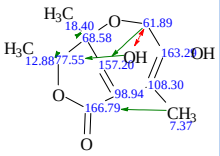	34 (ID:68) 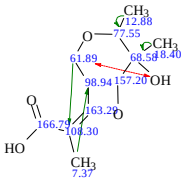	35 (ID:53) 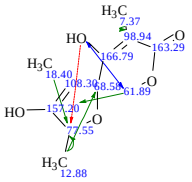
$d_N(^{13}C)$: 5.143	$d_N(^{13}C)$: 5.152	$d_N(^{13}C)$: 5.197	$d_N(^{13}C)$: 5.222	$d_N(^{13}C)$: 5.258
36 (ID:16) 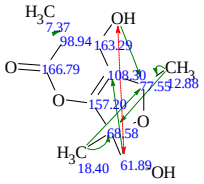	37 (ID:85) 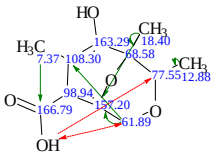	38 (ID:2) 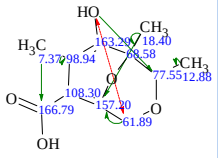	39 (ID:20) 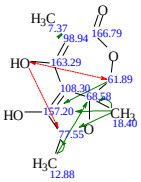	40 (ID:64) 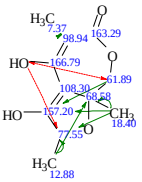
$d_N(^{13}C)$: 5.289	$d_N(^{13}C)$: 5.380	$d_N(^{13}C)$: 5.380	$d_N(^{13}C)$: 5.386	$d_N(^{13}C)$: 5.386
41 (ID:39) 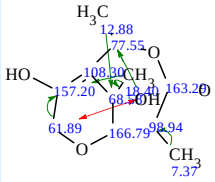	42 (ID:24) 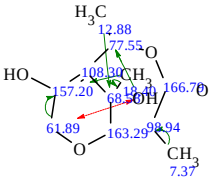	43 (ID:62) 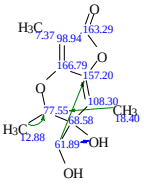	44 (ID:94) 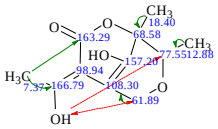	
$d_N(^{13}C)$: 5.446	$d_N(^{13}C)$: 5.446	$d_N(^{13}C)$: 5.475	$d_N(^{13}C)$: 5.497	

1 (ID:14)	2 (ID:58) The Best Structure	3 (ID:28)	4 (ID:52)	5 (ID:33)
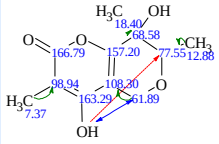	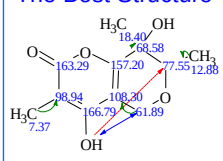	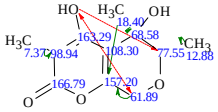	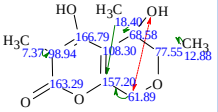	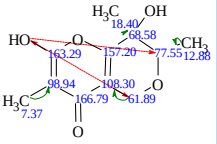
$d_A(^{13}C)$: 1.906 (v.14.50) $d_N(^{13}C)$: 2.234	$d_A(^{13}C)$: 2.073 (v.14.50) $d_N(^{13}C)$: 2.038	$d_A(^{13}C)$: 2.079 (v.14.50) $d_N(^{13}C)$: 2.319	$d_A(^{13}C)$: 2.579 (v.14.50) $d_N(^{13}C)$: 2.692	$d_A(^{13}C)$: 3.356 (v.14.50) $d_N(^{13}C)$: 4.181
6 (ID:34)	7 (ID:70)	8 (ID:38)	9 (ID:75)	10 (ID:76)
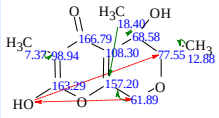	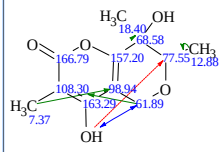	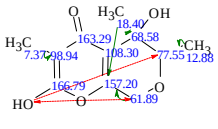	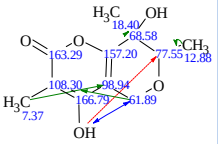	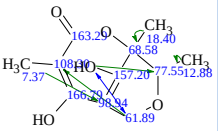
$d_A(^{13}C)$: 3.447 (v.14.50) $d_N(^{13}C)$: 3.643	$d_A(^{13}C)$: 3.483 (v.14.50) $d_N(^{13}C)$: 2.786	$d_A(^{13}C)$: 3.641 (v.14.50) $d_N(^{13}C)$: 4.279	$d_A(^{13}C)$: 3.650 (v.14.50) $d_N(^{13}C)$: 2.590	$d_A(^{13}C)$: 3.805 (v.14.50) $d_N(^{13}C)$: 3.484
11 (ID:40)	12 (ID:37)	13 (ID:53)	14 (ID:31)	15 (ID:59)
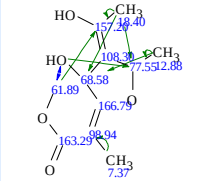	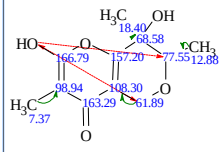	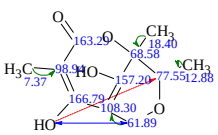	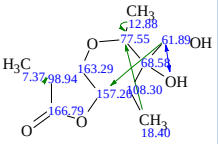	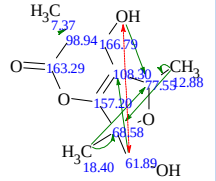
$d_A(^{13}C)$: 3.835 (v.14.50) $d_N(^{13}C)$: 4.401	$d_A(^{13}C)$: 3.865 (v.14.50) $d_N(^{13}C)$: 4.816	$d_A(^{13}C)$: 4.077 (v.14.50) $d_N(^{13}C)$: 3.651	$d_A(^{13}C)$: 4.127 (v.14.50) $d_N(^{13}C)$: 4.840	$d_A(^{13}C)$: 4.233 (v.14.50) $d_N(^{13}C)$: 4.960
16 (ID:71)	17 (ID:1)	18 (ID:61)	19 (ID:21)	20 (ID:84)
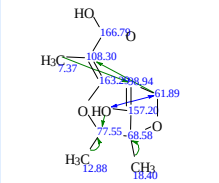	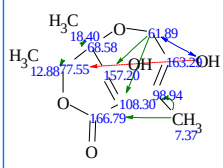	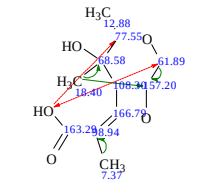	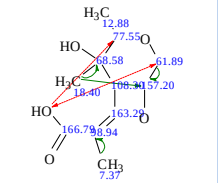	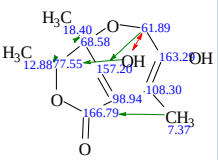
$d_A(^{13}C)$: 4.258 (v.14.50) $d_N(^{13}C)$: 5.143	$d_A(^{13}C)$: 4.396 (v.14.50) $d_N(^{13}C)$: 5.587	$d_A(^{13}C)$: 4.421 (v.14.50) $d_N(^{13}C)$: 4.733	$d_A(^{13}C)$: 4.421 (v.14.50) $d_N(^{13}C)$: 4.098	$d_A(^{13}C)$: 4.478 (v.14.50) $d_N(^{13}C)$: 5.197
21 (ID:54)	22 (ID:13)	23 (ID:16)	24 (ID:64)	25 (ID:77)
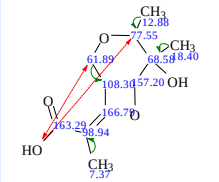	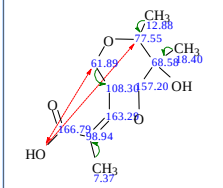	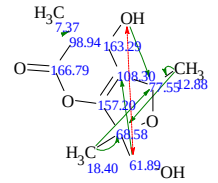	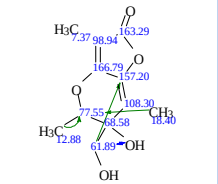	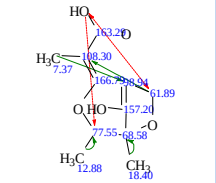
$d_A(^{13}C)$: 4.493 (v.14.50) $d_N(^{13}C)$: 4.264	$d_A(^{13}C)$: 4.493 (v.14.50) $d_N(^{13}C)$: 3.629	$d_A(^{13}C)$: 4.709 (v.14.50) $d_N(^{13}C)$: 5.289	$d_A(^{13}C)$: 4.762 (v.14.50) $d_N(^{13}C)$: 5.475	$d_A(^{13}C)$: 4.893 (v.14.50) $d_N(^{13}C)$: 5.778

26 (ID:10)	27 (ID:23)	28 (ID:42)	29 (ID:65)	30 (ID:15)
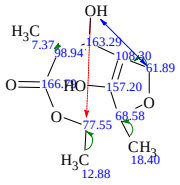	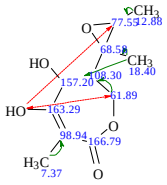	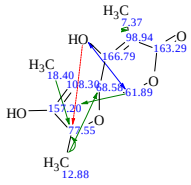	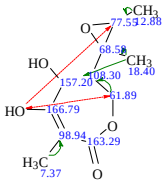	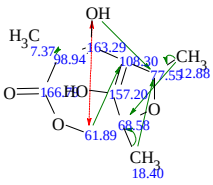
$d_A(^{13}C)$: 4.934 (v.14.50) $d_N(^{13}C)$: 4.624	$d_A(^{13}C)$: 4.952 (v.14.50) $d_N(^{13}C)$: 4.341	$d_A(^{13}C)$: 4.959 (v.14.50) $d_N(^{13}C)$: 5.258	$d_A(^{13}C)$: 4.993 (v.14.50) $d_N(^{13}C)$: 4.832	$d_A(^{13}C)$: 5.025 (v.14.50) $d_N(^{13}C)$: 5.544
31 (ID:49)	32 (ID:4)	33 (ID:30)	34 (ID:83)	35 (ID:25)
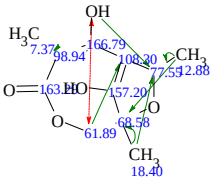	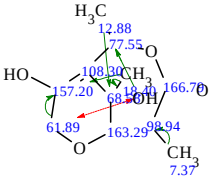	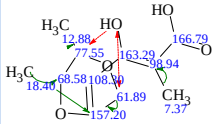	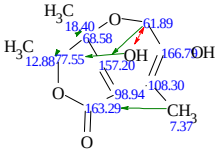	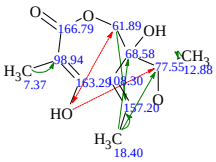
$d_A(^{13}C)$: 5.025 (v.14.50) $d_N(^{13}C)$: 5.544	$d_A(^{13}C)$: 5.091 (v.14.50) $d_N(^{13}C)$: 5.446	$d_A(^{13}C)$: 5.098 (v.14.50) $d_N(^{13}C)$: 5.992	$d_A(^{13}C)$: 5.113 (v.14.50) $d_N(^{13}C)$: 5.759	$d_A(^{13}C)$: 5.173 (v.14.50) $d_N(^{13}C)$: 4.682
36 (ID:51)	37 (ID:39)	38 (ID:9)	39 (ID:90)	40 (ID:94)
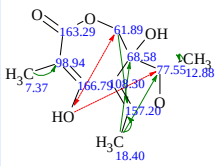	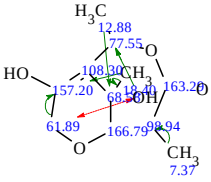	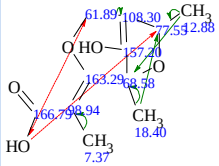	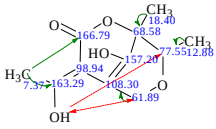	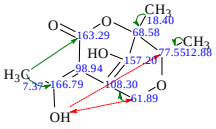
$d_A(^{13}C)$: 5.173 (v.14.50) $d_N(^{13}C)$: 4.682	$d_A(^{13}C)$: 5.207 (v.14.50) $d_N(^{13}C)$: 5.446	$d_A(^{13}C)$: 5.228 (v.14.50) $d_N(^{13}C)$: 4.467	$d_A(^{13}C)$: 5.264 (v.14.50) $d_N(^{13}C)$: 5.920	$d_A(^{13}C)$: 5.264 (v.14.50) $d_N(^{13}C)$: 5.497
41 (ID:36)	42 (ID:98)	43 (ID:73)	44 (ID:68)	45 (ID:48)
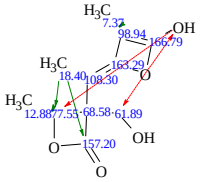	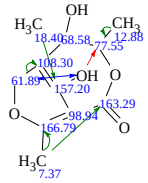	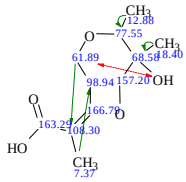	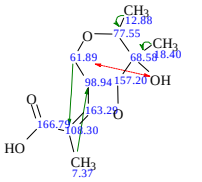	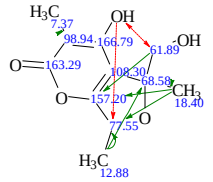
$d_A(^{13}C)$: 5.321 (v.14.50) $d_N(^{13}C)$: 5.855	$d_A(^{13}C)$: 5.410 (v.14.50) $d_N(^{13}C)$: 5.925	$d_A(^{13}C)$: 5.440 (v.14.50) $d_N(^{13}C)$: 5.857	$d_A(^{13}C)$: 5.440 (v.14.50) $d_N(^{13}C)$: 5.222	$d_A(^{13}C)$: 5.451 (v.14.50) $d_N(^{13}C)$: 5.152
46 (ID:97)	47 (ID:5)	48 (ID:56)	49 (ID:66)	50 (ID:89)
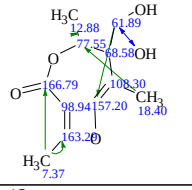	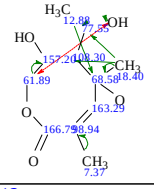	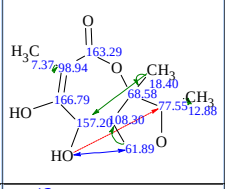	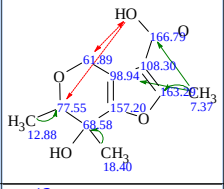	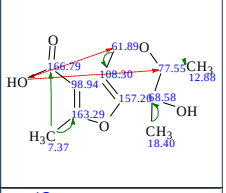
$d_A(^{13}C)$: 5.472 (v.14.50) $d_N(^{13}C)$: 4.178	$d_A(^{13}C)$: 5.477 (v.14.50) $d_N(^{13}C)$: 6.650	$d_A(^{13}C)$: 5.584 (v.14.50) $d_N(^{13}C)$: 5.683	$d_A(^{13}C)$: 5.621 (v.14.50) $d_N(^{13}C)$: 5.830	$d_A(^{13}C)$: 5.621 (v.14.50) $d_N(^{13}C)$: 5.830

51 (ID:26) 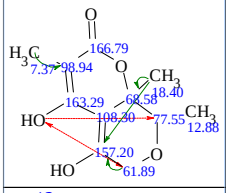	52 (ID:57) 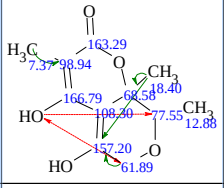	53 (ID:69) 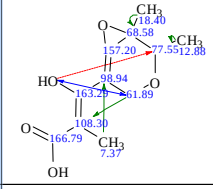	54 (ID:74) 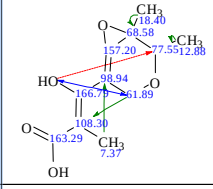	55 (ID:43) 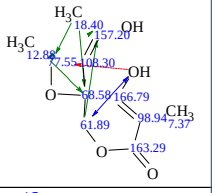
$d_A(^{13}C)$: 5.635 (v.14.50) $d_N(^{13}C)$: 4.888	$d_A(^{13}C)$: 5.635 (v.14.50) $d_N(^{13}C)$: 4.888	$d_A(^{13}C)$: 5.646 (v.14.50) $d_N(^{13}C)$: 7.882	$d_A(^{13}C)$: 5.646 (v.14.50) $d_N(^{13}C)$: 7.882	$d_A(^{13}C)$: 5.690 (v.14.50) $d_N(^{13}C)$: 4.893
56 (ID:63) 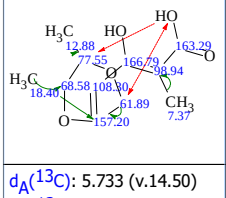	57 (ID:27) 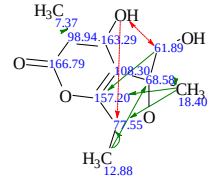	58 (ID:92) 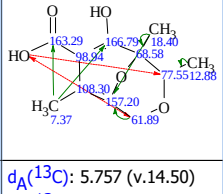	59 (ID:88) 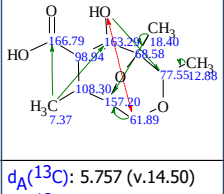	60 (ID:46) 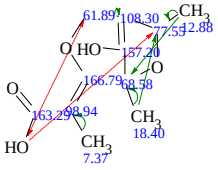
$d_A(^{13}C)$: 5.733 (v.14.50) $d_N(^{13}C)$: 6.627	$d_A(^{13}C)$: 5.745 (v.14.50) $d_N(^{13}C)$: 5.562	$d_A(^{13}C)$: 5.757 (v.14.50) $d_N(^{13}C)$: 6.345	$d_A(^{13}C)$: 5.757 (v.14.50) $d_N(^{13}C)$: 5.710	$d_A(^{13}C)$: 5.858 (v.14.50) $d_N(^{13}C)$: 4.930
61 (ID:95) 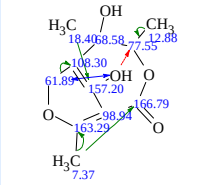	62 (ID:24) 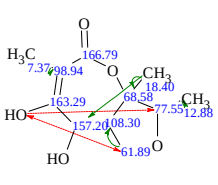	63 (ID:32) 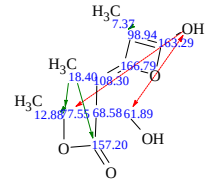	64 (ID:2) 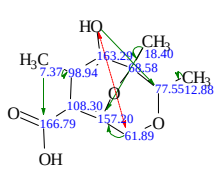	65 (ID:85) 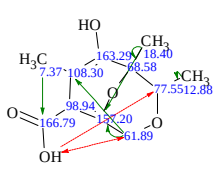
$d_A(^{13}C)$: 5.905 (v.14.50) $d_N(^{13}C)$: 5.703	$d_A(^{13}C)$: 5.936 (v.14.50) $d_N(^{13}C)$: 5.717	$d_A(^{13}C)$: 5.956 (v.14.50) $d_N(^{13}C)$: 5.855	$d_A(^{13}C)$: 5.979 (v.14.50) $d_N(^{13}C)$: 5.380	$d_A(^{13}C)$: 5.979 (v.14.50) $d_N(^{13}C)$: 5.380
66 (ID:11) 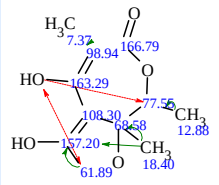	67 (ID:96) 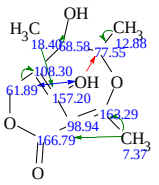	68 (ID:44) 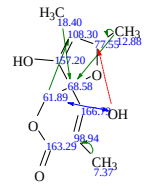	69 (ID:41) 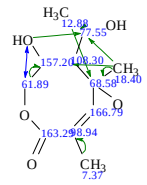	70 (ID:20) 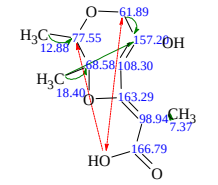
$d_A(^{13}C)$: 5.982 (v.14.50) $d_N(^{13}C)$: 6.009	$d_A(^{13}C)$: 5.982 (v.14.50) $d_N(^{13}C)$: 6.693	$d_A(^{13}C)$: 5.992 (v.14.50) $d_N(^{13}C)$: 7.092	$d_A(^{13}C)$: 6.052 (v.14.50) $d_N(^{13}C)$: 7.285	$d_A(^{13}C)$: 6.068 (v.14.50) $d_N(^{13}C)$: 6.044
71 (ID:3) 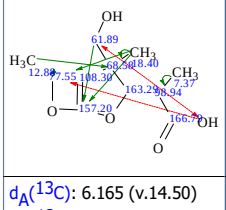	72 (ID:45) 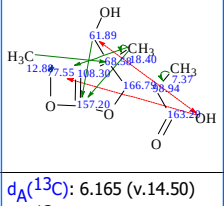	73 (ID:87) 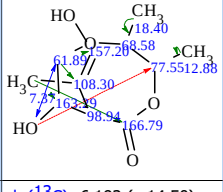	74 (ID:86) 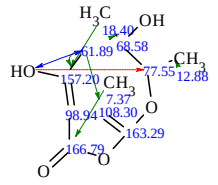	75 (ID:93) 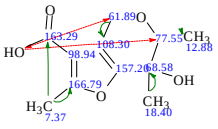
$d_A(^{13}C)$: 6.165 (v.14.50) $d_N(^{13}C)$: 6.793	$d_A(^{13}C)$: 6.165 (v.14.50) $d_N(^{13}C)$: 6.793	$d_A(^{13}C)$: 6.192 (v.14.50) $d_N(^{13}C)$: 5.870	$d_A(^{13}C)$: 6.252 (v.14.50) $d_N(^{13}C)$: 6.253	$d_A(^{13}C)$: 6.256 (v.14.50) $d_N(^{13}C)$: 6.465

76 (ID:67) 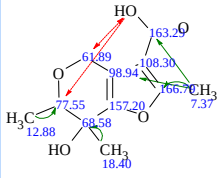 $d_A(^{13}C)$: 6.256 (v.14.50) $d_N(^{13}C)$: 6.465	77 (ID:72) 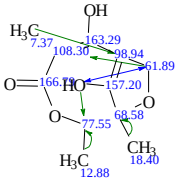 $d_A(^{13}C)$: 6.302 (v.14.50) $d_N(^{13}C)$: 6.022	78 (ID:78) 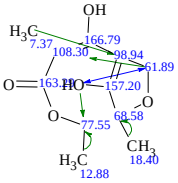 $d_A(^{13}C)$: 6.302 (v.14.50) $d_N(^{13}C)$: 6.022	79 (ID:55) 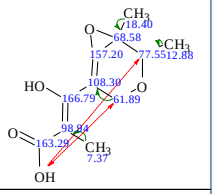 $d_A(^{13}C)$: 6.347 (v.14.50) $d_N(^{13}C)$: 7.975	80 (ID:17) 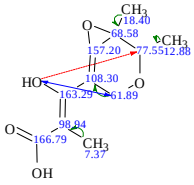 $d_A(^{13}C)$ $d_N(^{13}C)$: 7.975
81 (ID:50) 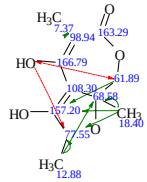 $d_A(^{13}C)$: 6.397 (v.14.50) $d_N(^{13}C)$: 5.386	82 (ID:22) 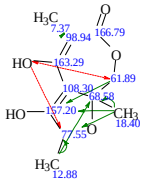 $d_A(^{13}C)$: 6.397 (v.14.50) $d_N(^{13}C)$: 5.386	83 (ID:29) 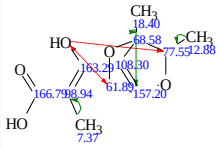 $d_A(^{13}C)$: 6.471 (v.14.50) $d_N(^{13}C)$: 6.656	84 (ID:7) 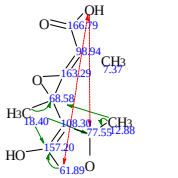 $d_A(^{13}C)$: 6.544 (v.14.50) $d_N(^{13}C)$: 5.884	85 (ID:80) 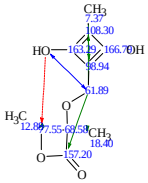 $d_A(^{13}C)$ $d_N(^{13}C)$: 6.131
86 (ID:19) 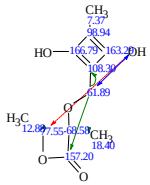 $d_A(^{13}C)$: 6.637 (v.14.50) $d_N(^{13}C)$: 6.131	87 (ID:35) 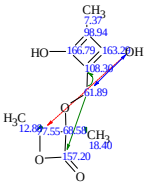 $d_A(^{13}C)$: 6.637 (v.14.50) $d_N(^{13}C)$: 6.131	88 (ID:79) 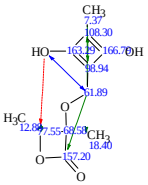 $d_A(^{13}C)$: 6.637 (v.14.50) $d_N(^{13}C)$: 6.131	89 (ID:60) 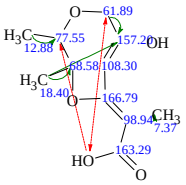 $d_A(^{13}C)$: 6.703 (v.14.50) $d_N(^{13}C)$: 6.679	90 (ID:62) 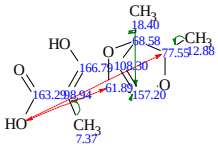 $d_A(^{13}C)$ $d_N(^{13}C)$: 7.291
91 (ID:12) 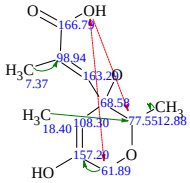 $d_A(^{13}C)$: 7.137 (v.14.50) $d_N(^{13}C)$: 6.466	92 (ID:18) 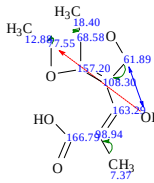 $d_A(^{13}C)$: 7.413 (v.14.50) $d_N(^{13}C)$: 7.862	93 (ID:82) 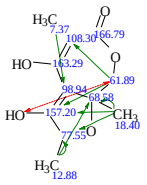 $d_A(^{13}C)$: 7.522 (v.14.50) $d_N(^{13}C)$: 6.466	94 (ID:6) 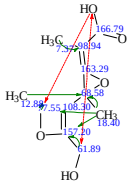 $d_A(^{13}C)$: 7.711 (v.14.50) $d_N(^{13}C)$: 6.458	95 (ID:8) 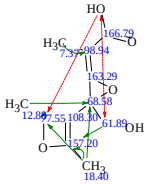 $d_A(^{13}C)$ $d_N(^{13}C)$: 5.588
96 (ID:81) 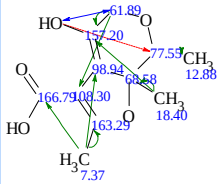 $d_A(^{13}C)$: 8.259 (v.14.50) $d_N(^{13}C)$: 7.622	97 (ID:91) 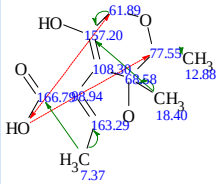 $d_A(^{13}C)$: 8.259 (v.14.50) $d_N(^{13}C)$: 7.622	98 (ID:47) 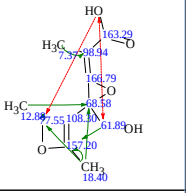 $d_A(^{13}C)$: 8.592 (v.14.50) $d_N(^{13}C)$: 6.223		

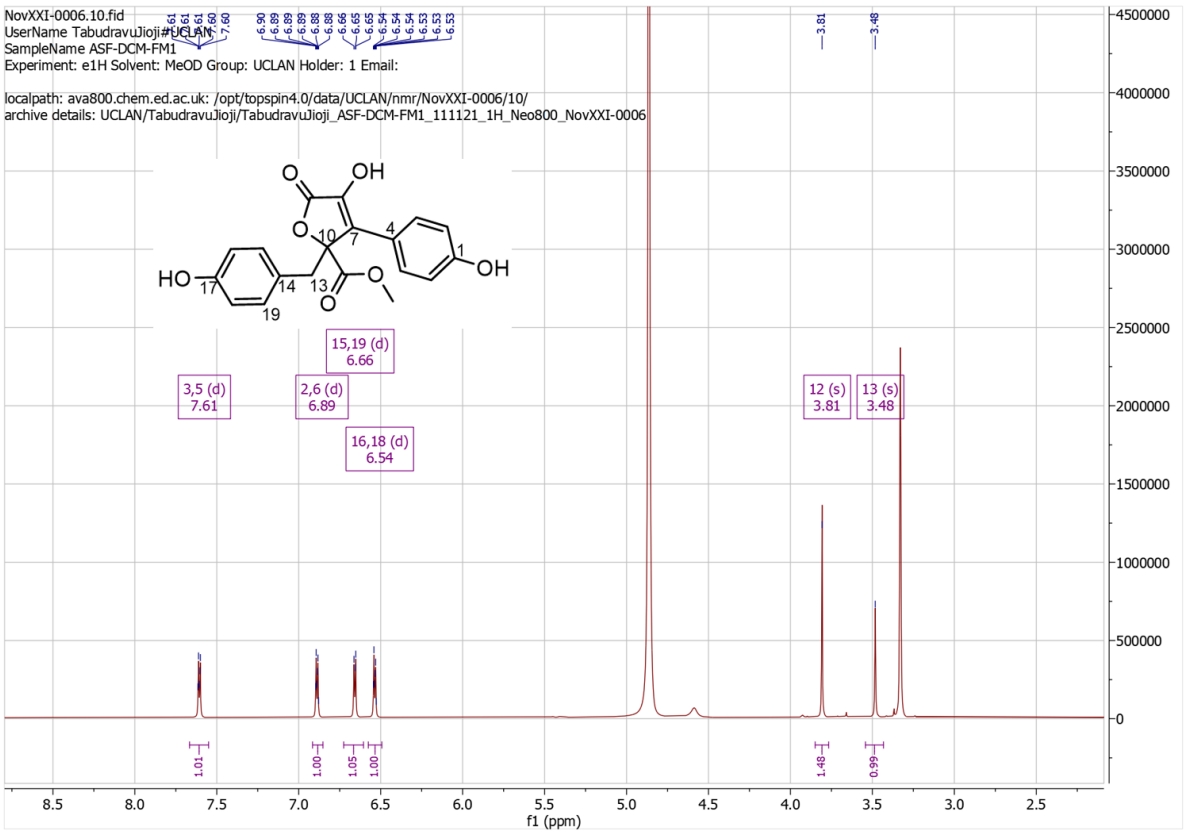

Figure S41. ^{1}H NMR spectrum of ASF DCM FM 1, butyrolactone ii in CD3OD.

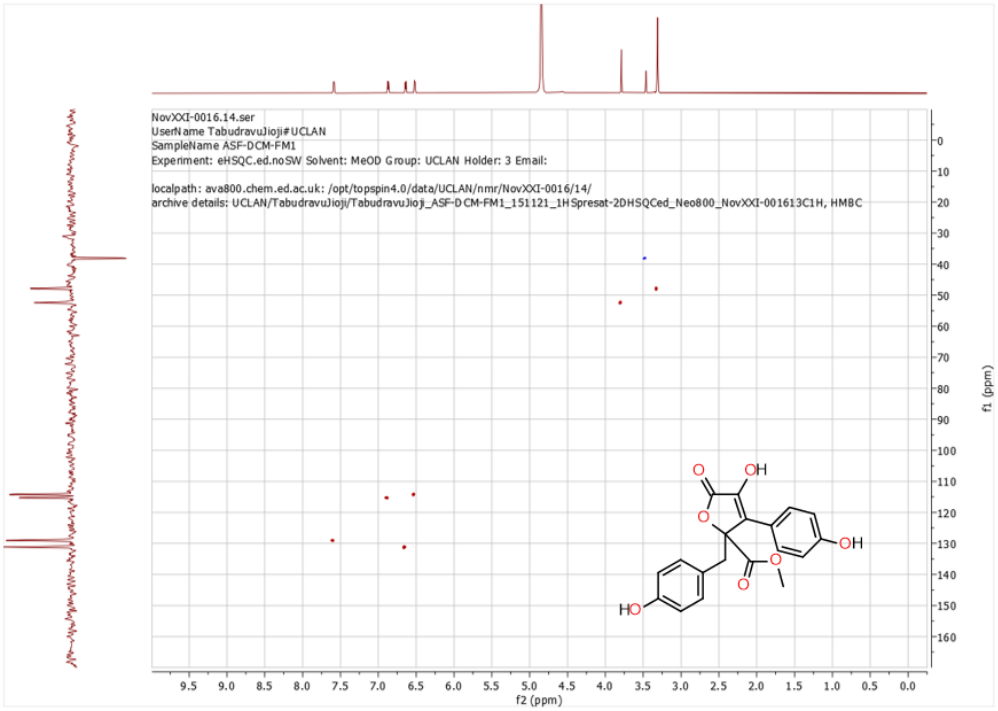

Figure S42. HSQC NMR spectrum of ASF DCM FM 1, butyrolactone ii in CD3OD.

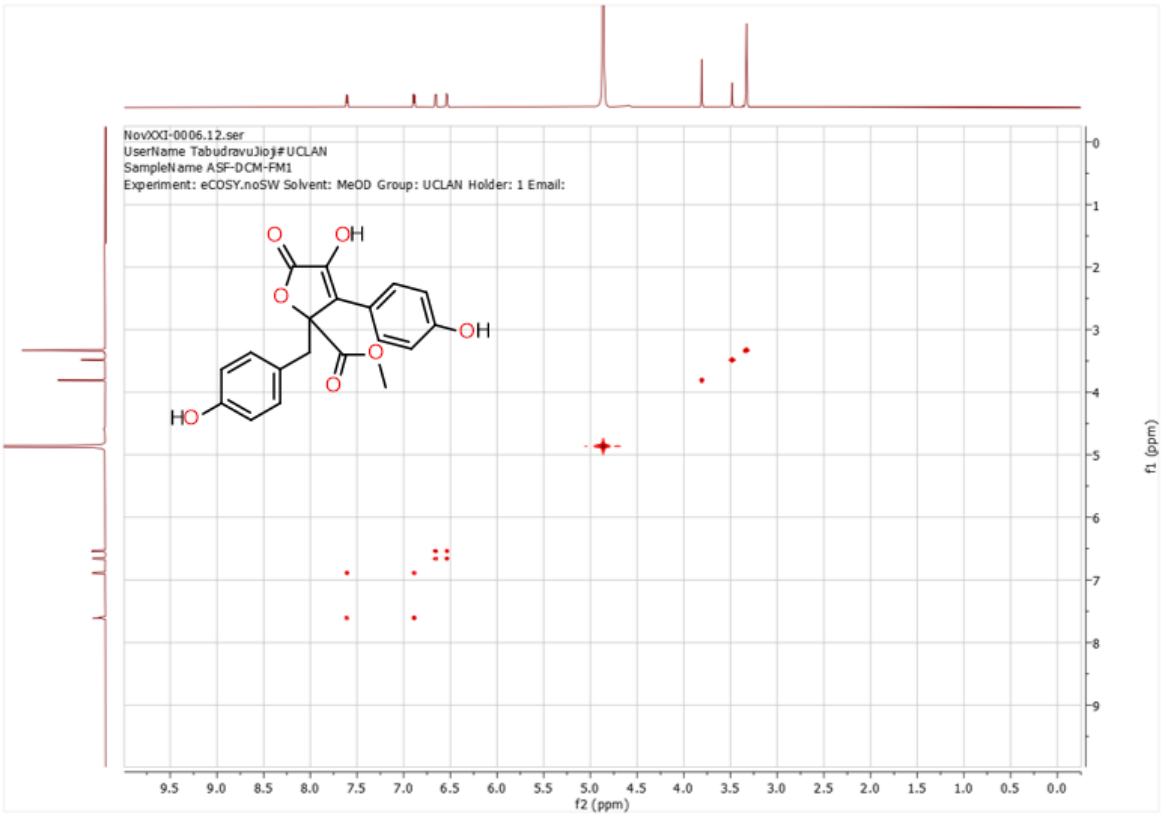

Figure S43. ^{1}H-^{1}H COSY NMR spectrum of ASF DCM FM 1, butyrolactone ii in CD3OD.

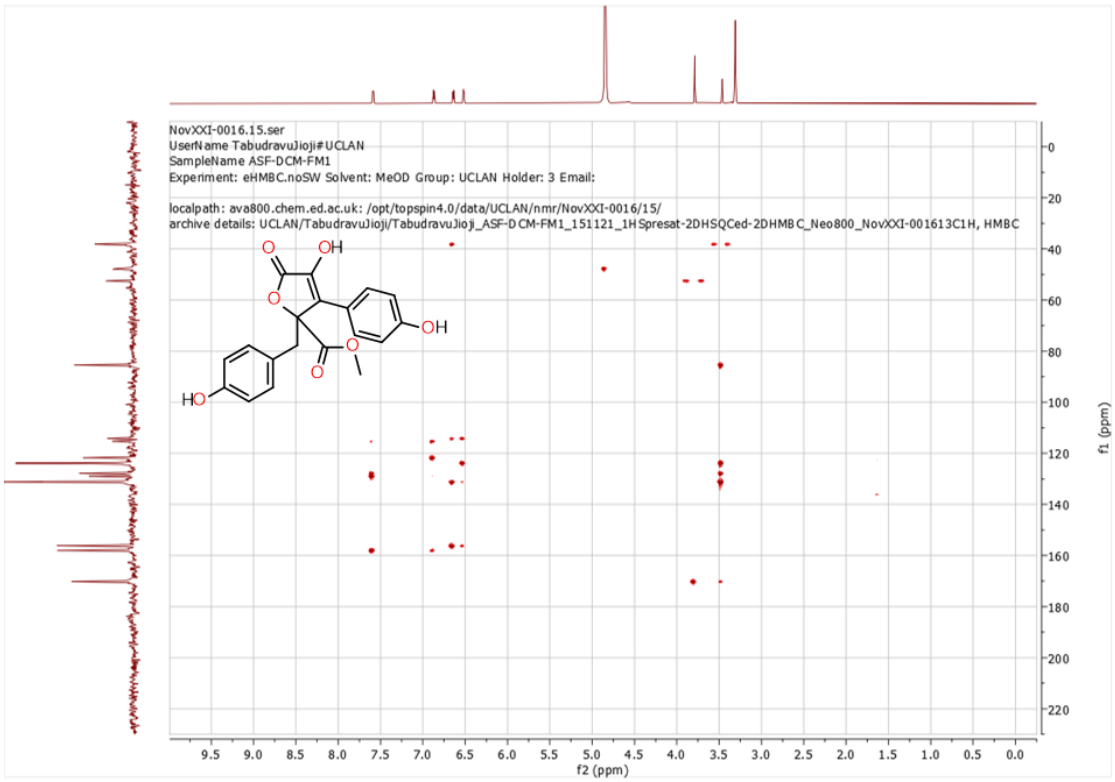

Figure S44. HMBC NMR spectrum of ASF DCM FM 1, butyrolactone ii in CD3OD.

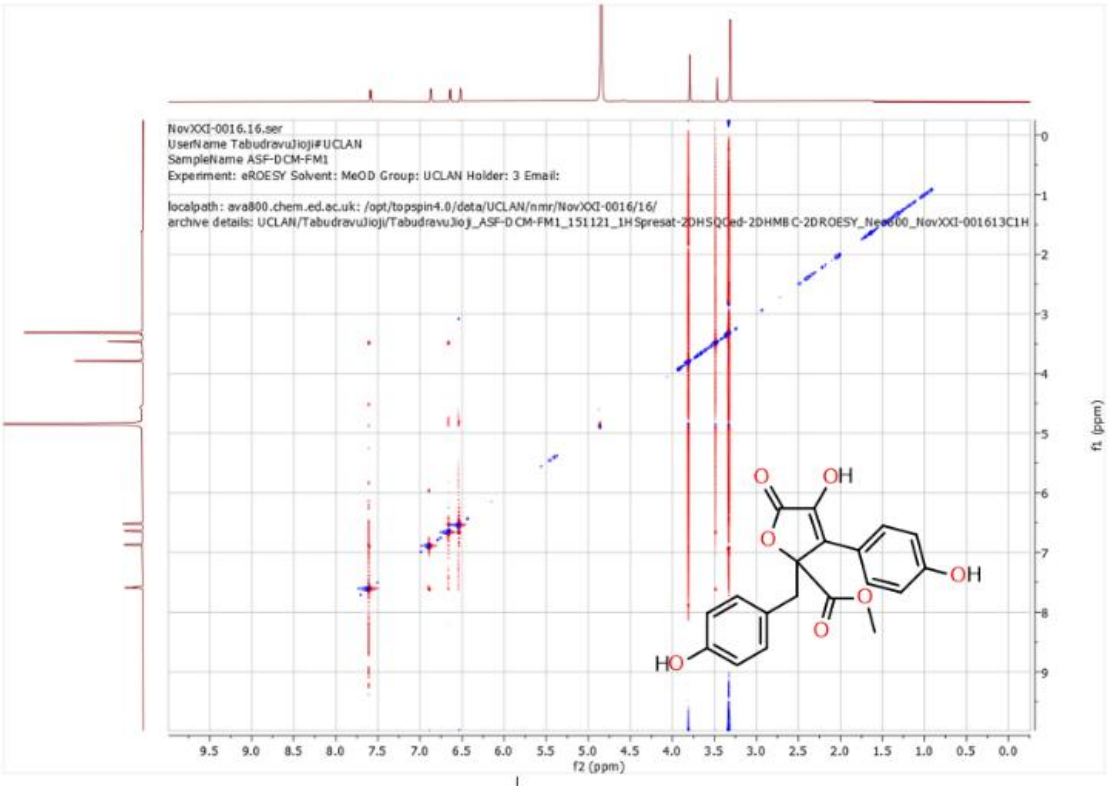

Figure S45. ROSEY NMR spectrum of ASF DCM FM 1 in CD3OD.

Table S8. NMR table used in the structure elucidation of ASF DCM FM 1, butyrolactone ii.
a 100 MHZ in CD_3OD
b 400 MHz in CD_3OD

Position	^{13}C Chemical shift (ppm)[a]	C-type	^{1}H (chemical shift ppm, No. of H, multiplicity, coupling)[b]	COSY (^{1}H-^{1}H)	HMBC (^{1}H-^{13}C)
1	158.05	C			
2, 6	115.27	CH	$H_{2,6}$: 6.89, 2H, d, 8.8	3,5	C1
3, 5	129.04	CH	$H_{3,5}$: 7.61, 2H, d, 8.7	2,6	C2, C4, C7
4	128.99	C			
7	127.82	C			
10	84.92	C			
11	170.16	C			
12	52.37	CH_3	H_{10}: 3.80, 3H, s		C11
13	38.09	CH2	H_{11}: 3.48, 2H, s		C7, C10, C14, C15
14	123.83	C			
15, 19	131.15	CH	$H_{15,19'}$: 6.66, 2H, d, 9.0	16,18	C13, C16, C17
16, 18	114.22	CH	H_{16}: 6.53, 2H, d, 8.1	15,19	C14, C15, C17
17	156.18	C			

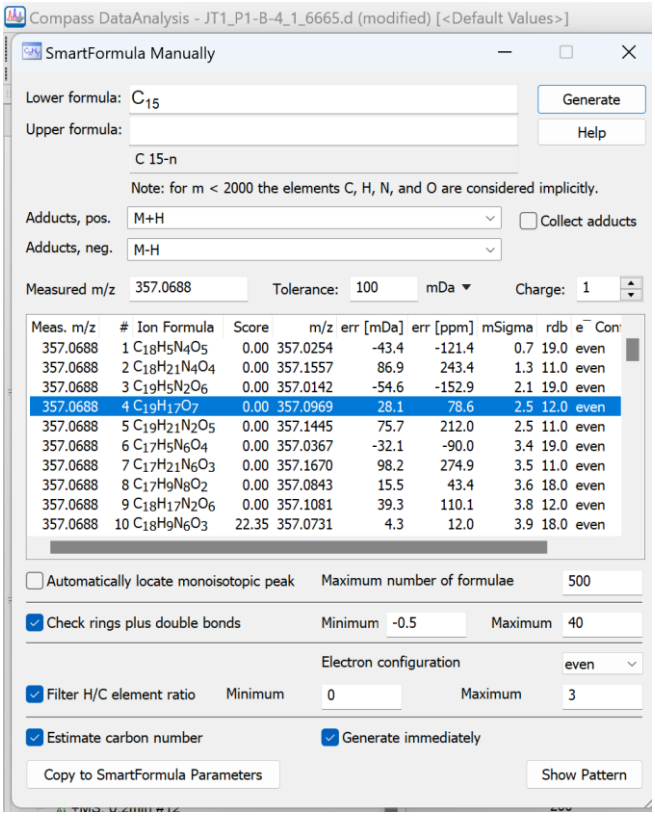

Figure S46. HRMS for ASF DCM FM 1, butyrolactone II.

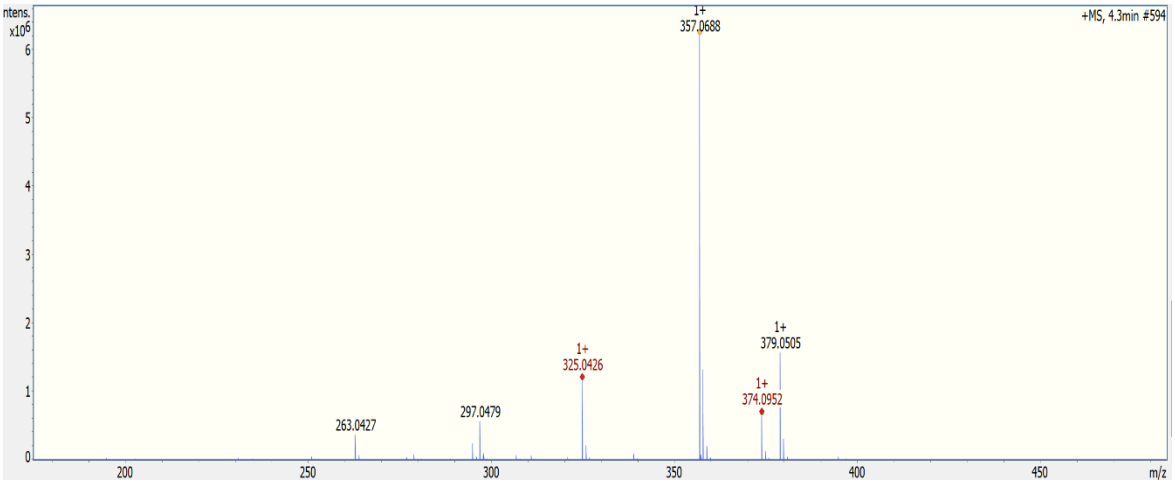

Figure S47 HRMS data of ASF FM 1, butyrolactone II.

From HRMS data:

$(M+H)^+$ = 357.0688, Δ= 78.6ppm, mSigma 2.5, rdb: 12.0

Therefore, $(M+H)^+$ molecular formula: $C_{19}H_{17}O_7$

Compound molecular formula: $C_{19}H_{16}O_6$

Utilising Antimarin database with molecular formula $C_{19}H_{16}O_6$ yields Butyrolactone ii.

Ref: Nittta et al. 1983, chem, pharm, Bull, 31, 1528

Previously isolated from: *Aspergillus terrus.*

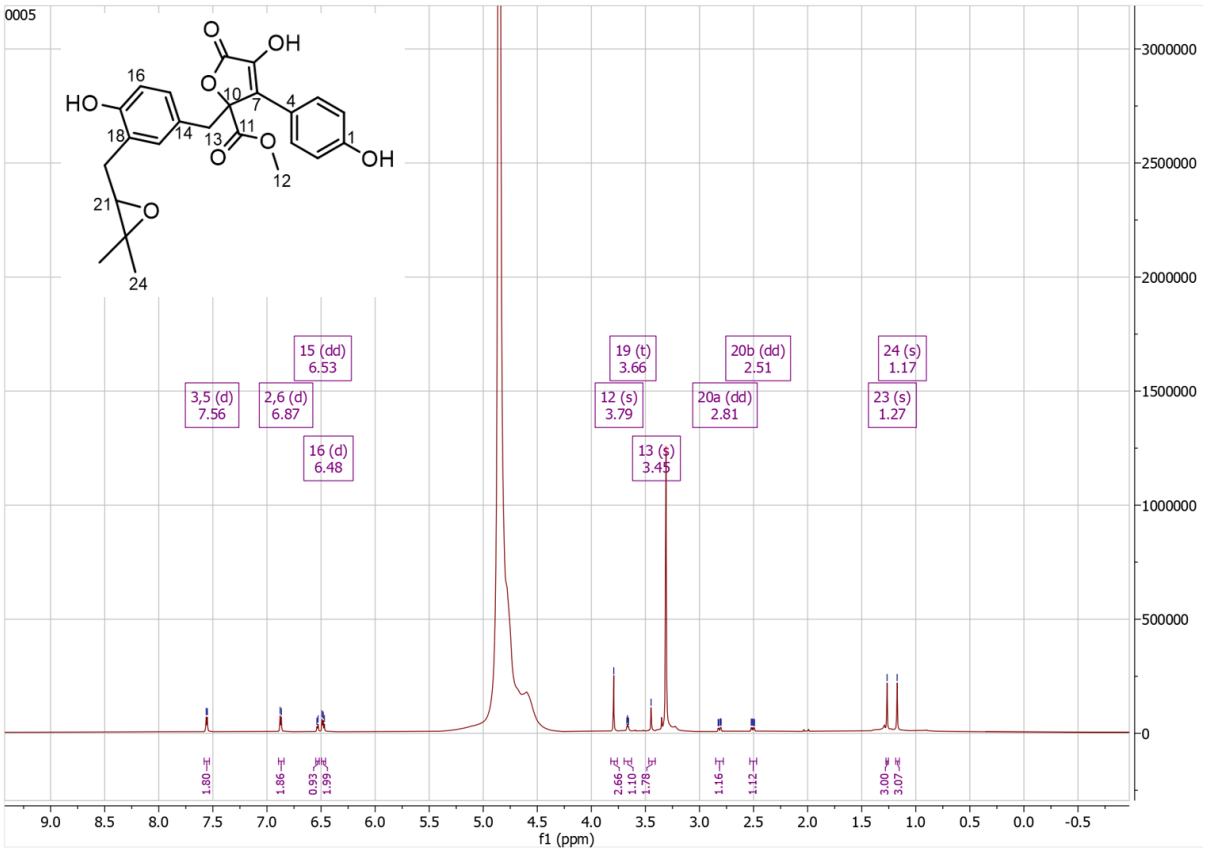

Figure S48. ^{1}H NMR spectrum of ASF DCM FM 3, Butyrolactone iii in CD_3OD.

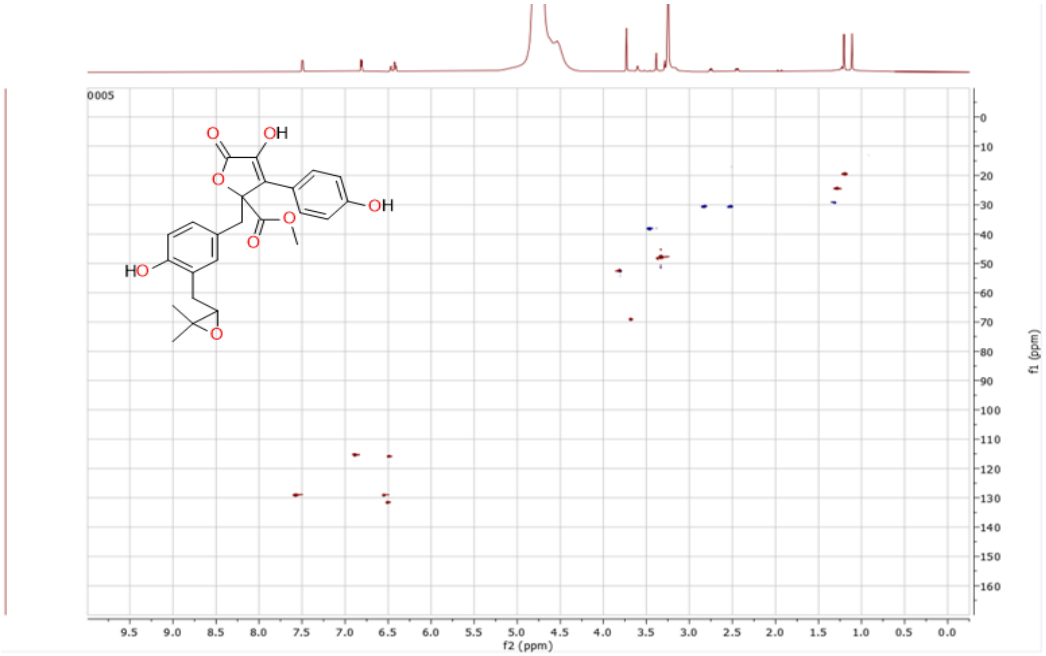

Figure S49. ^{1}H-^{1}H COSY NMR spectrum of ASF DCM FM 3, Butyrolactone iii in CD_3OD.

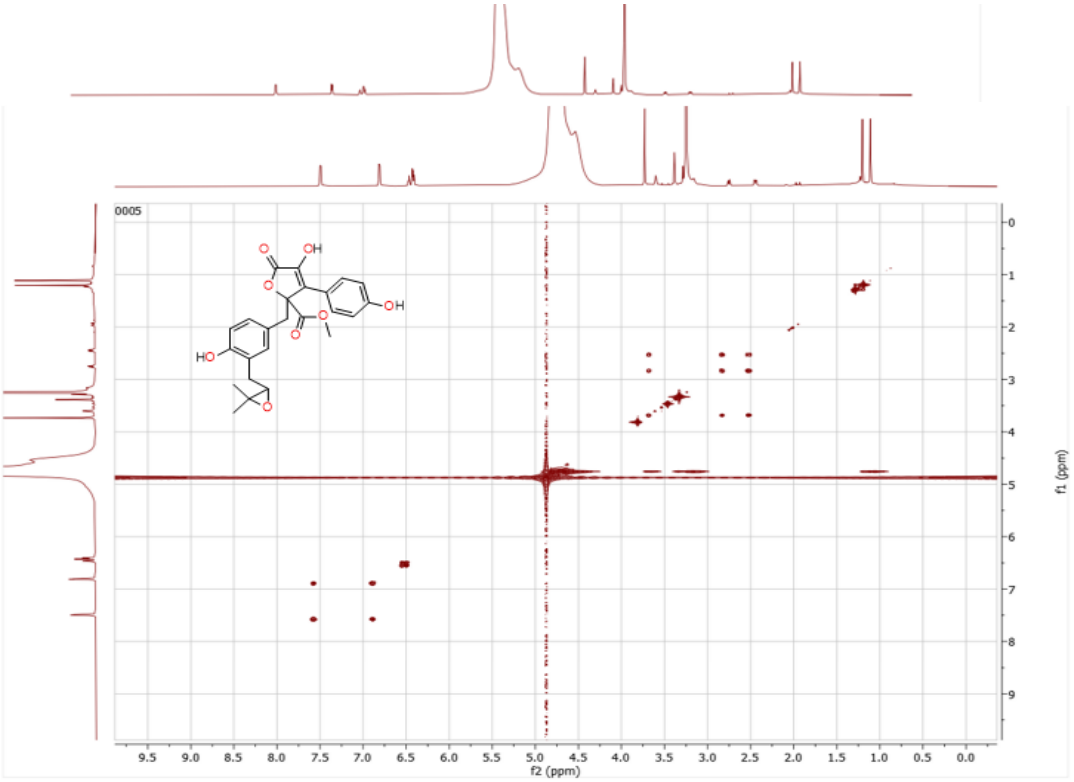

Figure S50. HSQC NMR spectrum of ASF DCM FM 3, Butyrolactone iii in CD_3OD.

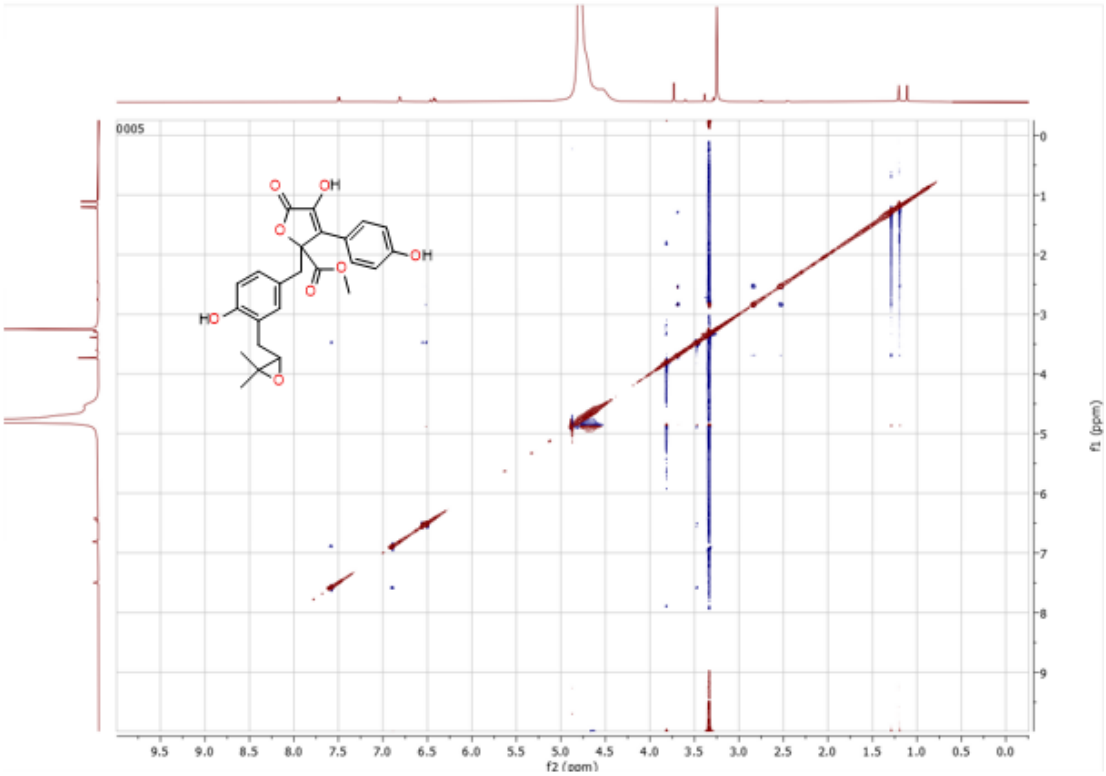

Figure S51. HMBC NMR spectrum of ASF DCM FM 3, Butyrolactone iii in CD_3OD.

Figure S52. ROSEY NMR spectrum of ASF DCM FM 3, Butyrolactone iii in CD_3OD.

Position	δ_C, compound 2, Butyrolactone iii [a]	C-type	^1H (chemical shift ppm, No. of H, multiplicity, coupling)[b]	COSY (^1H-^1H)	HMBC (^1H-^{13}C)
1	158.05	C			
2, 6	113.86	CH	$H_{2,6}$: 6.89, 2H, d, J=9.2Hz	3,5	C1
3, 5	127.89	CH	$H_{3,5}$: 7.55, 2H, d, J=8.2Hz	2,6	C2, C4, C7
4	128.94	C			
7	127.93	C			
10	85.39	C			
11	170.13	C			
12	50.39	CH_3	H_{12}: 3.79, 3H, s		C11
13	36.70	CH_2	H_{13}: 3.44, 2H, s		C7, C10, C14, C15
14	131.57	C			
15	127.57	CH	H_{15}: 6.53, 1H, dd, J=7.9, 1.5Hz	16	C13, C16, C17
16	114.39	CH	H_{16}: 6.47, 1H, d, J=8.5Hz	15	C14, C15, C17
17	152.08	C			
18	124.77	C			
19	129.72	CH	H_{19}: 6.48, 1H, d, J=2.4Hz		C14, C15, C17, C18
20	29.14	CH	H_{20a}: 2.82, 1H, dd, J=17.5, 4.6Hz H_{20b}: 2.49, 1H, dd, J=16.8, 7.5Hz	21	C17, C18, C21
21	67.63	CH	H_{19}: 3.66, 1H, t, J=5.6Hz	20	C18, C20, C22, C23, C24
22	76.60				
23	22.98	CH_3	H_{23}: 1.27, 3H, s		C21, C22, C24
24	17.89	CH_3	H_{24}: 1.17, 3H, s		C21, C22, C23

Table S9. NMR table used in the structure elucidation of ASF DCM FM 3, butyrolactone iii.

a 100 MHZ in CD_3OD

b 400 MHz in CD_3OD

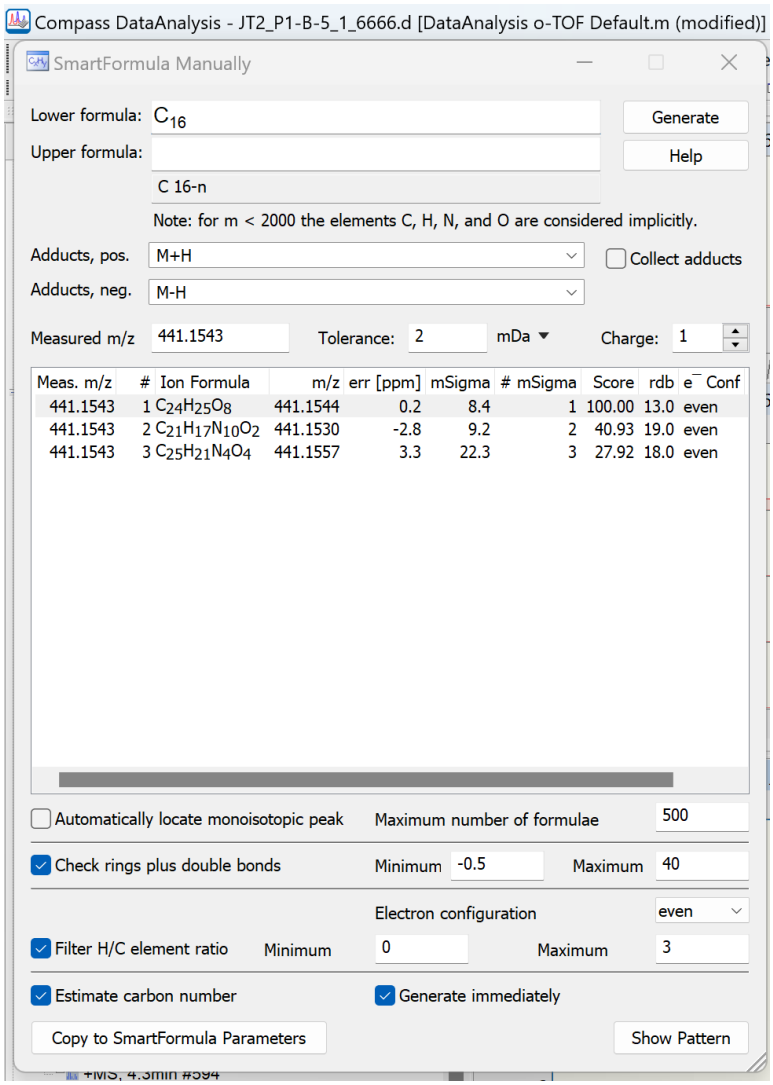

Figure S53. HRMS data formula predictor for ASF DCM FM 3, Butyrolactone III.

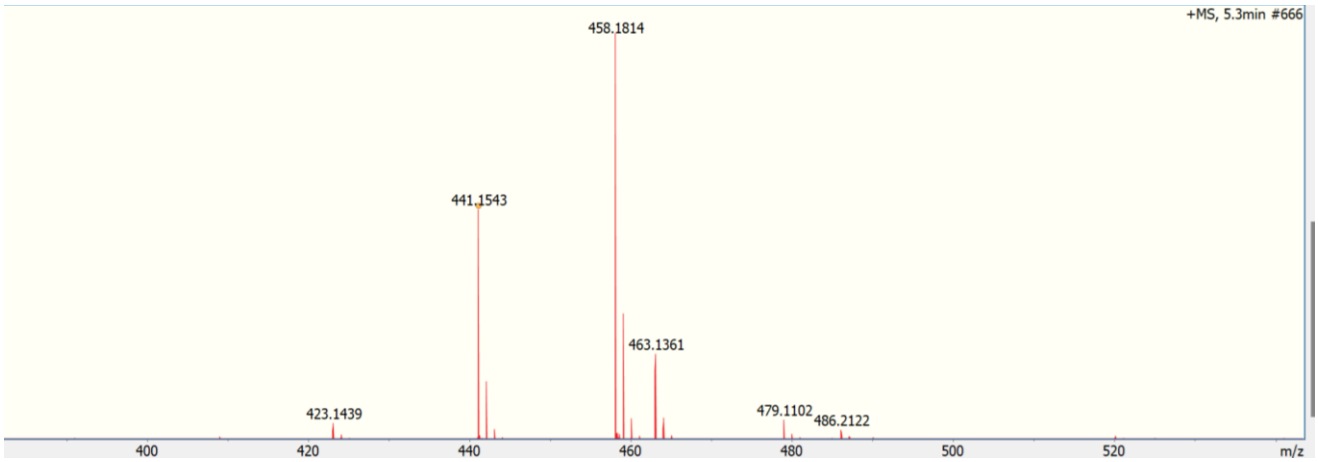

Figure S54. HRMS data for ASF DCM FM 3,Butyrolactone III.

HRMS data:

$(M+H)^+$ = 441.1532, Δ= 2.8ppm, RDB = 13.0

Therefore, $(M+H)^+$ molecular formula: $C_{24}H_{25}O_6$

Compound molecular formula: $C_{24}H_{24}O_6$

Utilising Antimarin database with molecular formula $C_{24}H_{24}O_6$ yields Butyrolactone iii.

Ref: Nittta et al. 1983, chem, pharm, Bull, 31, 1528

Previously isolated from: *Aspergillus terrus.*

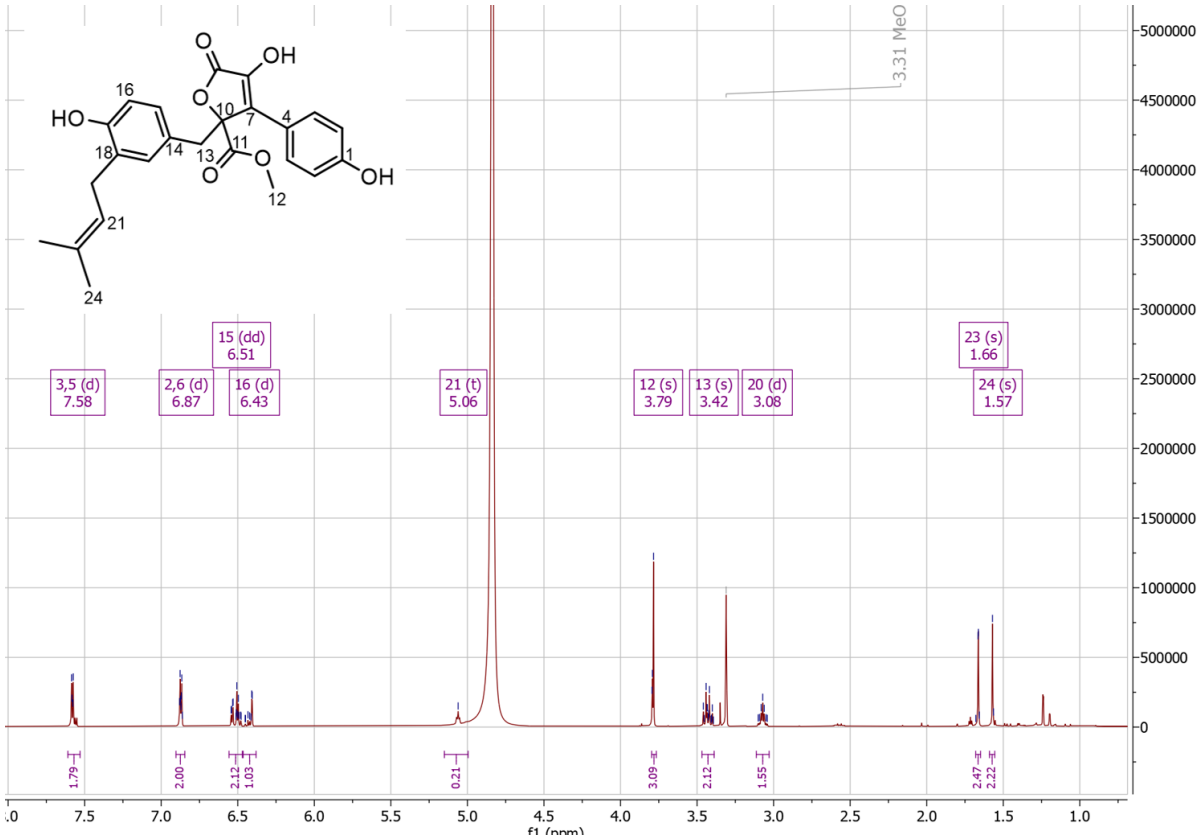

Figure S55. ^{1}H NMR spectrum of ASF DCM FM 5, Butyrolactone i in CD_3OD.

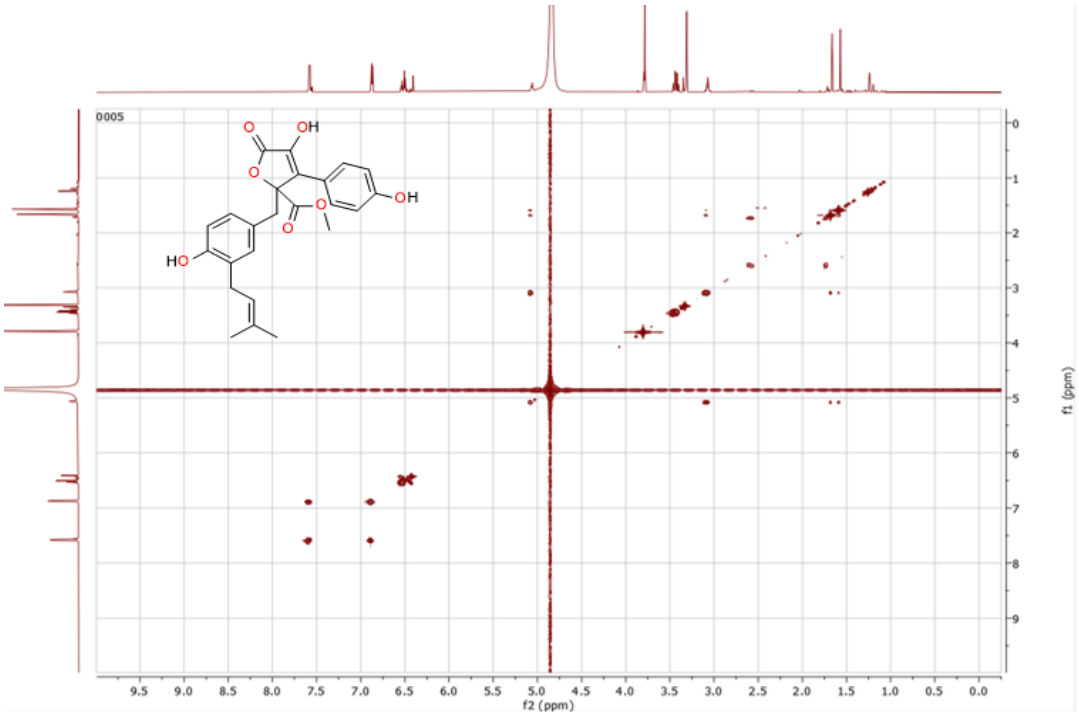

Figure S56. ^{1}H-^{1}H COSY NMR spectrum of ASF DCM FM 3, Butyrolactone iii in CD_3OD.

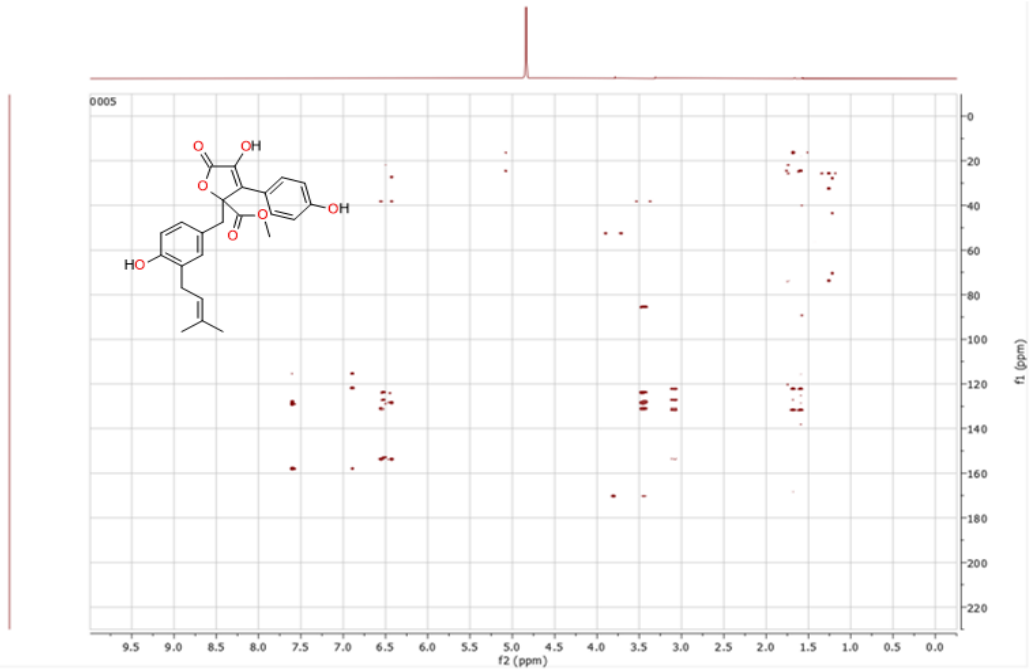

Figure S57. HMBC NMR spectrum of ASF DCM FM 5, Butyrolactone i in CD_3OD.

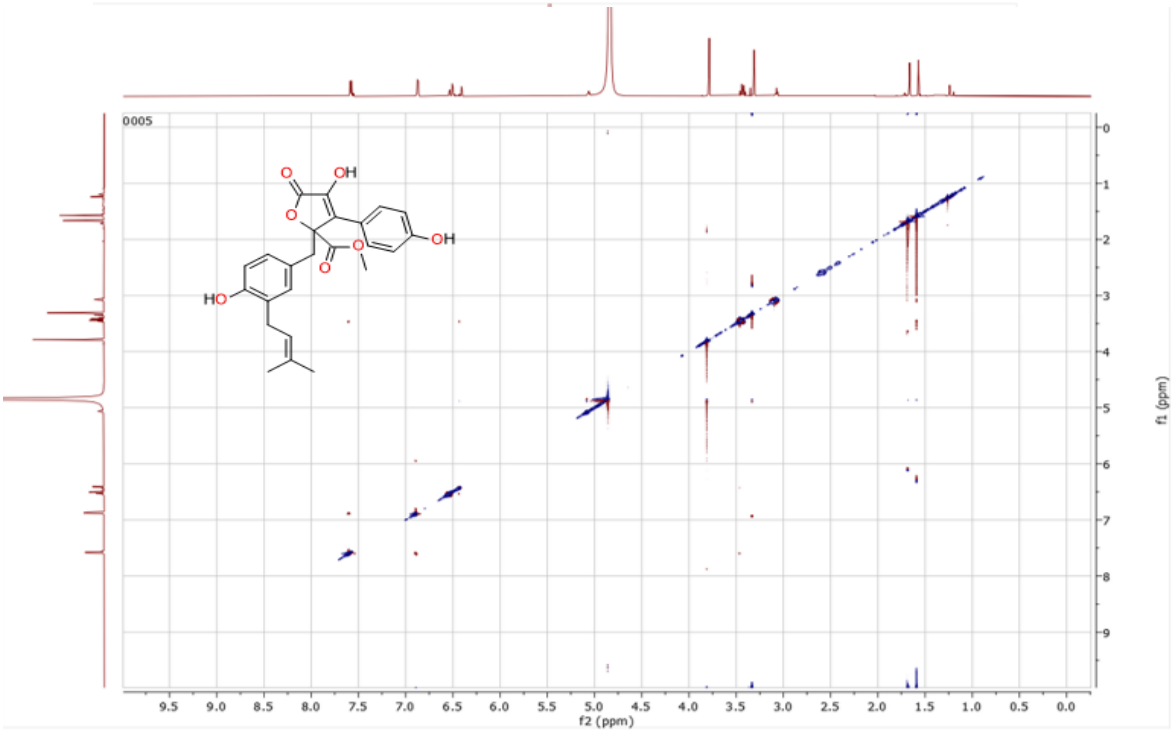

Figure S58. ROSEY NMR spectrum of ASF DCM FM 5, Butyrolactone i in CD_3OD.

Table S10. NMR table used in the structure elucidation of ASF DCM FM 5, butyrolactone i.

a 100 MHZ in CD_3OD

b 400 MHz in CD_3OD

Position	**δ_C, compound 3, Butyrolactone i (FM fraction)[a]**	**C-type**	**^1H (chemical shift ppm, No. of H, multiplicity, coupling)[b]**	**COSY (^1H-^1H)**	**HMBC (^1H-^{13}C)**
1	157.94	C			
2, 6	115.27	CH	$H_{2,6}$: 6.87, 2H, d, J=8.8Hz	3,5	C1
3, 5	128.81	CH	$H_{3,5}$: 7.58, 2H, d, J=8.4Hz	2,6	C2, C4, C7
4	128.99	C			
7	127.93	C			
10	86.14	C			
11	170.24	C			
12	52.17	CH_3	H_{12}: 3.79, 3H, s		C11
13	38.16	CH_2	H_{13}: 3.42, 2H, s		C7, C10, C14, C15
14	130.98	C			
15	128.11	CH	H_{15}: 6.54, 1H, dd, J=7.9, 1.9Hz	16	C13, C16, C17
16	113.75	CH	H_{16}: 6.50, 1H, d, J=7.6Hz	15	C14, C15, C17
17	153.72	C			
18	127.11	C			
19	130.74	CH	H_{19}: 6.41, 1H, d, J=1.1Hz		C14, C17, C18, C20
20	27.25	CH	H_{20}: 3.07, 2H, d, 8.2	20	C17, C18, C21
21	122.19	CH	H_{21}: 5.06, 1H, t, 7.5	21	C18, C20, C22, C23
22	131.68				
23	24.56	CH_3	H_{23}: 1.66, 3H, s		C21, C22
24	16.35	CH_3	H_{24}: 1.56, 3H, s		C21, C22, C23

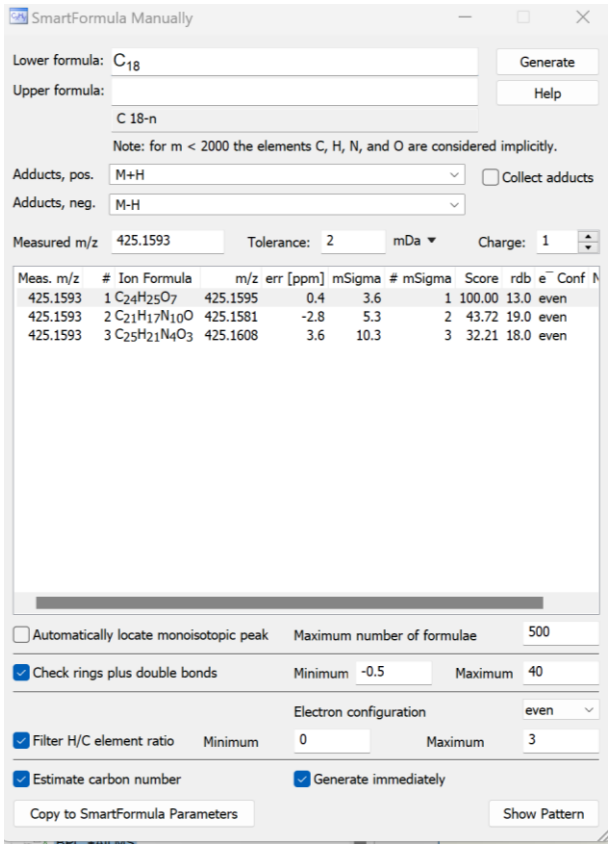

Figure S59. HRMS data of ASF DCM FM 5, butyrolactone i.

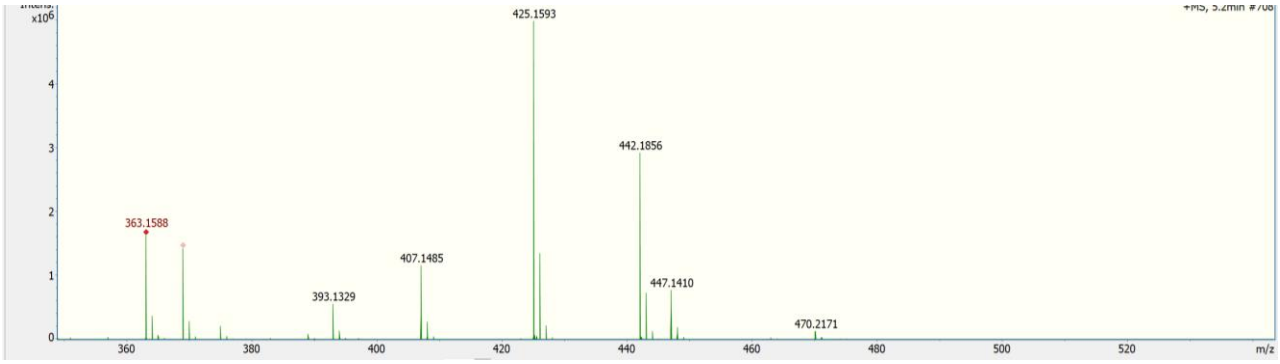

Figure S60. HRMS data of ASF DCM FM 5, butyrolactone i.

Table S10. Structure elucidation through 1D and 2D NMR of ASF DCM FM 3, Butyrolactone iii.

Position	δ_C, compound 4, Aspernolide A [a]	C-type	^1H (chemical shift ppm, No. of H, multiplicity, coupling)[b]	COSY (^1H-^1H)	HMBC (^1H-^{13}C)
1	157.94	C			
2, 6	115.33	CH	$H_{2,6}$: 6.87, 2H, d, J=8.8Hz	3,5	C1
3, 5	131.33	CH	$H_{3,5}$: 7.58, 2H, d, J=8.4Hz	2,6	C2, C4, C7
4	131.45	C			
7	128.05	C			
10	85.39	C			
11	169.60	C			
12	52.40	CH_3	H_{12}: 3.79, 3H, s		C11
13	38.15	CH_2	H_{13}: 3.42, 2H, s		C7, C10, C14, C15
14	131.57	C			
15	128.89	CH	H_{15}: 6.54, 1H, dd, J=7.9, 1.9Hz	16	C13, C16, C17
16	116.04	CH	H_{16}: 6.50, 1H, d, J=7.6Hz	15	C14, C15, C17
17	153.83	C			
18	120.08	C			
19	131.50	CH	H_{19}: 6.41, 1H, d, J=1.1Hz		C14, C17, C18, C20
20	24.32	CH	H_{20}: 3.07, 2H, d, 8.2	21	C17, C18, C21
21	32.36	CH	H_{21}: 5.06, 1H, t, 7.5	20	C18, C20, C22, C23
22	70.15				
23	27.62	CH_3	H_{23}: 1.66, 3H, s		C21, C22, C24
24	25.51	CH_3	H_{24}: 1.56, 3H, s		C21, C22, C23

From HRMS data:

$(M+H)^+$ = 425.1593, Δ = 0.4ppm, mSigma = 3.6, rbd: 13.0

Therefore, $(M+H)^+$ molecular formula: $C_{24}H_{25}O_7$

Compound molecular formula: $C_{24}H_{24}O_7$

Utilising Reaxys database with molecular formula $C_{24}H_{24}O_7$ yields Butyrolactone i.

Ref: Nittta et al. 1983, chem, pharm, Bull, 31, 1528

Previously isolated from: *Aspergillus terrus.*

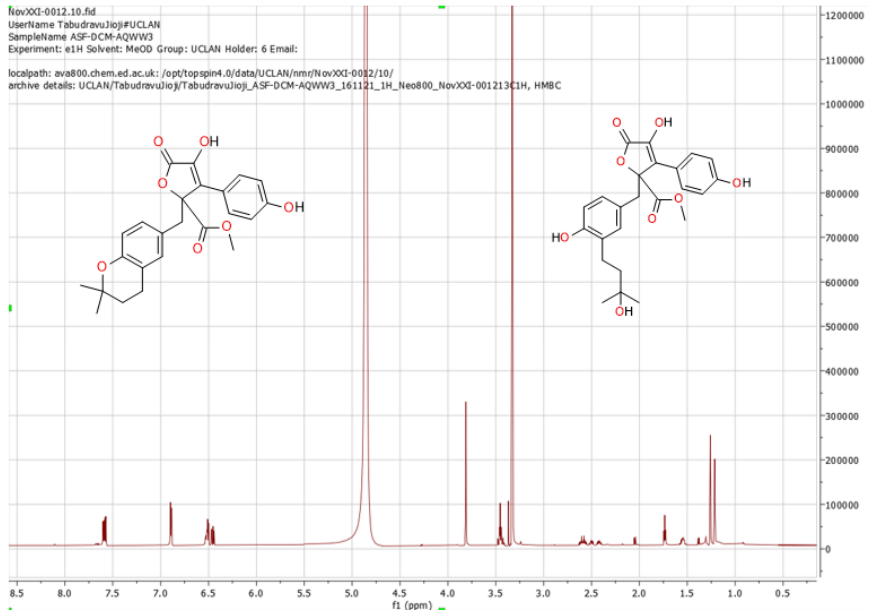

Figure S61. ^{1}H NMR spectrum of ASF DCM AQWW 3, Aspernolide A and Aspernolide B in CD_3OD.

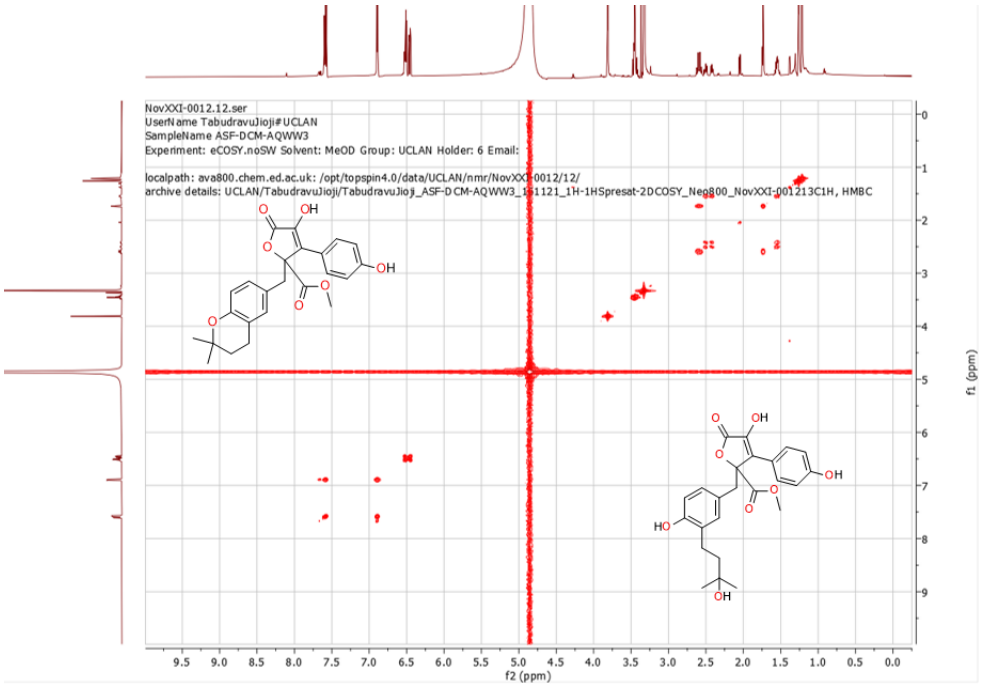

Figure S62. ^{1}H-^{1}H COSY NMR spectrum of ASF DCM AQWW 3, Aspernolide A and Aspernolide B in CD_3OD.

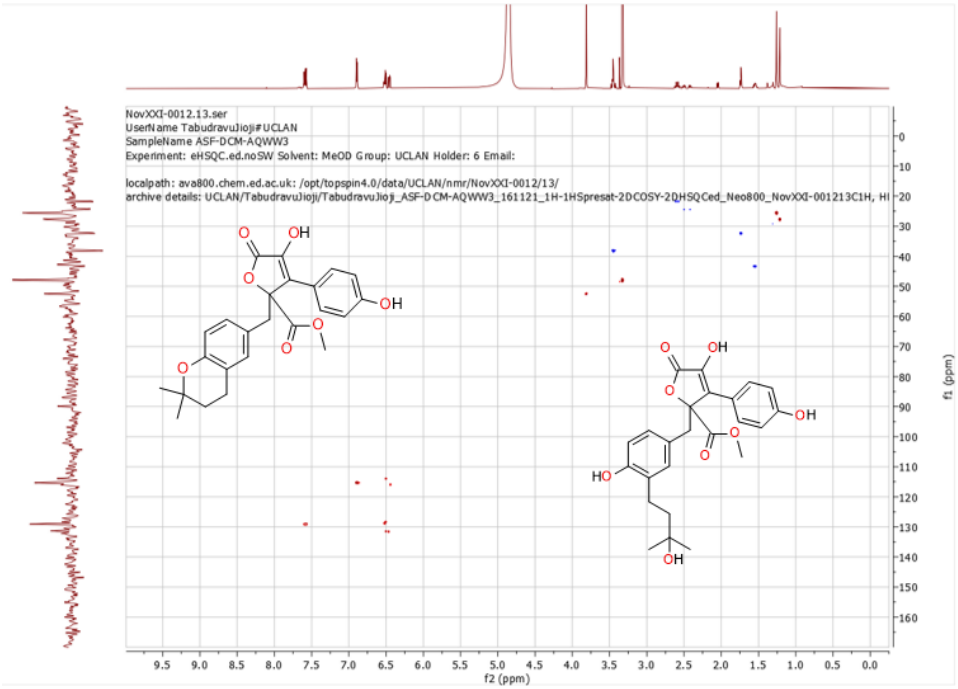

Figure S 63. HSQC NMR spectrum of ASF DCM AQWW 3, Aspernolide A and Aspernolide B in CD_3OD.

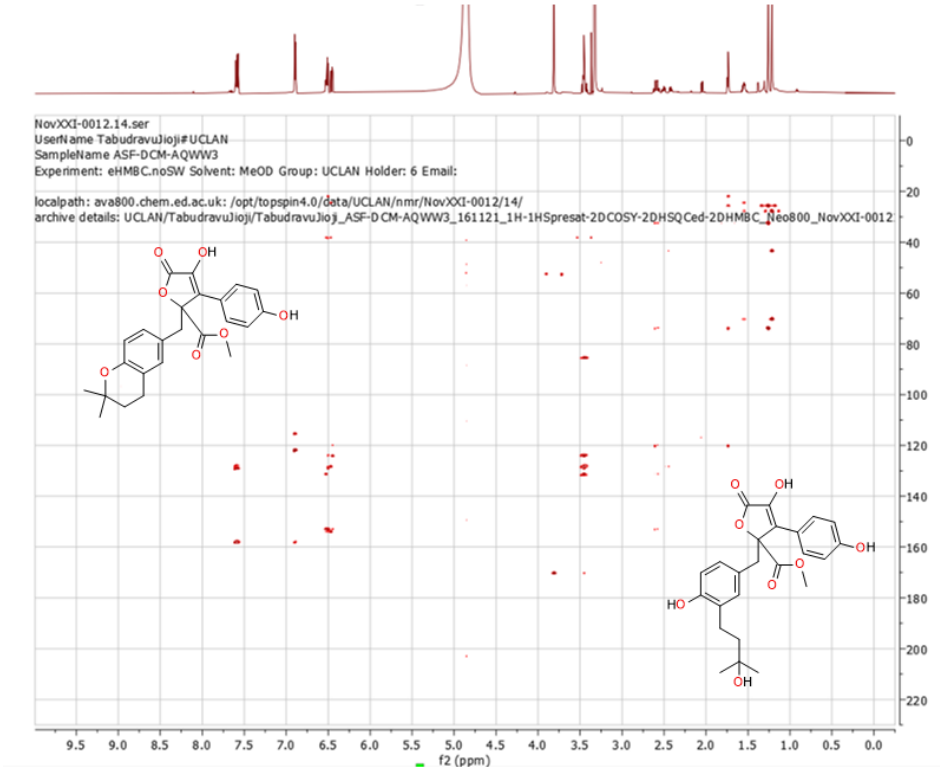

Figure S64. HMBC NMR spectrum of ASF DCM AQWW 3, Aspernolide A and Aspernolide B in CD_3OD.

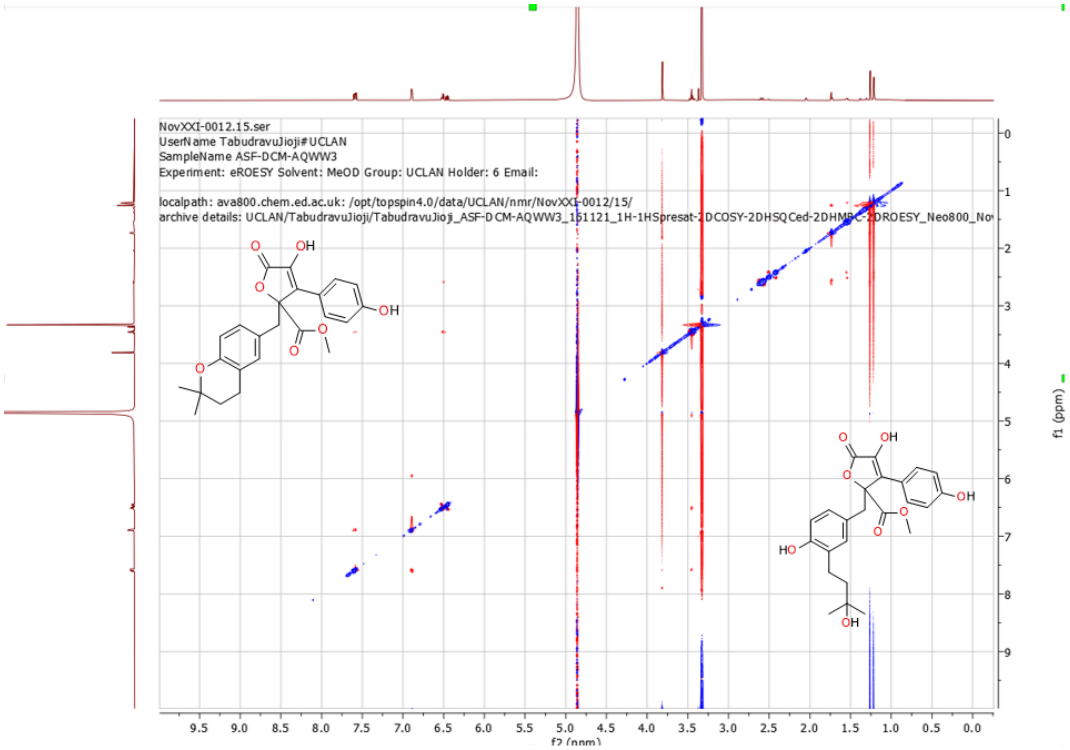

Figure S 65. ROSEY NMR spectrum of ASF AQWW 3, Aspernolide A and Aspernolide B in CD_3OD.

Table S11. NMR table used in the structure elucidation of ASF DCM FM 5, butyrolactone i.

a 100 MHZ in CD_3OD

b 400 MHz in CD_3OD

Position	δ_C, compound 4, Aspernolide A [a]	C-type	^1H (chemical shift ppm, No. of H, multiplicity, coupling)[b]	COSY (^1H-^1H)	HMBC (^1H-^{13}C)
1	157.94	C			
2, 6	115.33	CH	$H_{2,6}$: 6.87, 2H, d, J=8.8Hz	3,5	C1
3, 5	131.33	CH	$H_{3,5}$: 7.58, 2H, d, J=8.4Hz	2,6	C2, C4, C7
4	131.45	C			
7	128.05	C			
10	85.39	C			
11	169.60	C			
12	52.40	CH_3	H_{12}: 3.79, 3H, s		C11
13	38.15	CH_2	H_{13}: 3.42, 2H, s		C7, C10, C14, C15
14	131.57	C			
15	128.89	CH	H_{15}: 6.54, 1H, dd, J=7.9, 1.9Hz	16	C13, C16, C17
16	116.04	CH	H_{16}: 6.50, 1H, d, J=7.6Hz	15	C14, C15, C17
17	153.83	C			
18	120.08	C			
19	131.50	CH	H_{19}: 6.41, 1H, d, J=1.1Hz		C14, C17, C18, C20
20	24.32	CH	H_{20}: 3.07, 2H, d, 8.2	21	C17, C18, C21
21	32.36	CH	H_{21}: 5.06, 1H, t, 7.5	20	C18, C20, C22, C23
22	70.15				
23	27.62	CH_3	H_{23}: 1.66, 3H, s		C21, C22, C24
24	25.51	CH_3	H_{24}: 1.56, 3H, s		C21, C22, C23

Aspernolide A

From HRMS data:

$(M+H)^+$ = 425.1595, Δ = -1.2ppm, mSigma = n.a

Therefore, $(M+H)^+$ molecular formula: $C_{24}H_{25}O_7$

Compound molecular formula: $C_{24}H_{24}O_7$

Utilising Antimarin database with molecular formula $C_{24}H_{24}O_6$ yields Aspernolide A.

Ref: Nittta et al. 1983, chem, pharm, Bull, 31, 1528

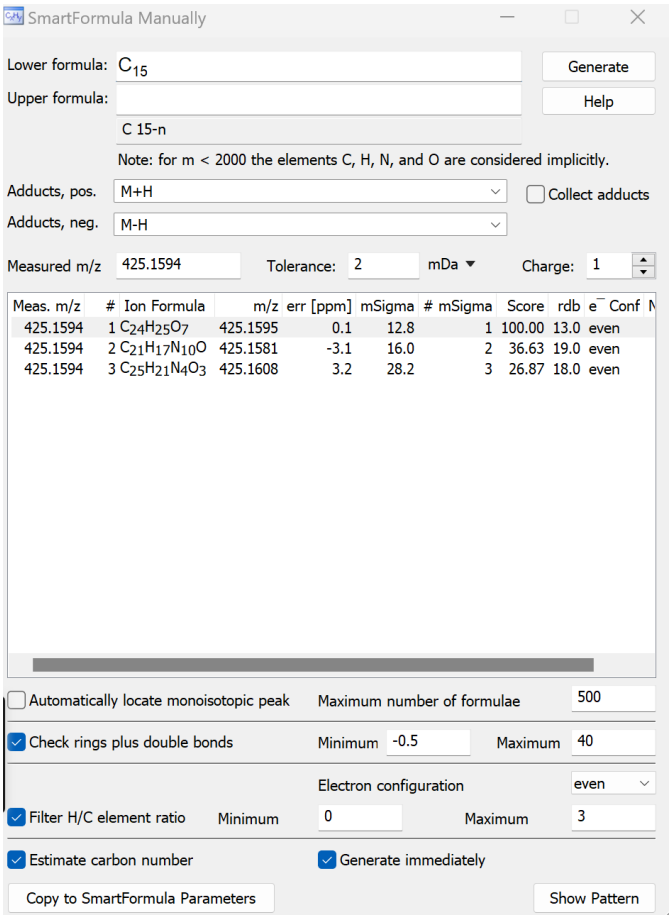

Figure S66. HRMS formula predictor from $[M+H]^+$ ion for Aspernolide A (ASF FW 3).

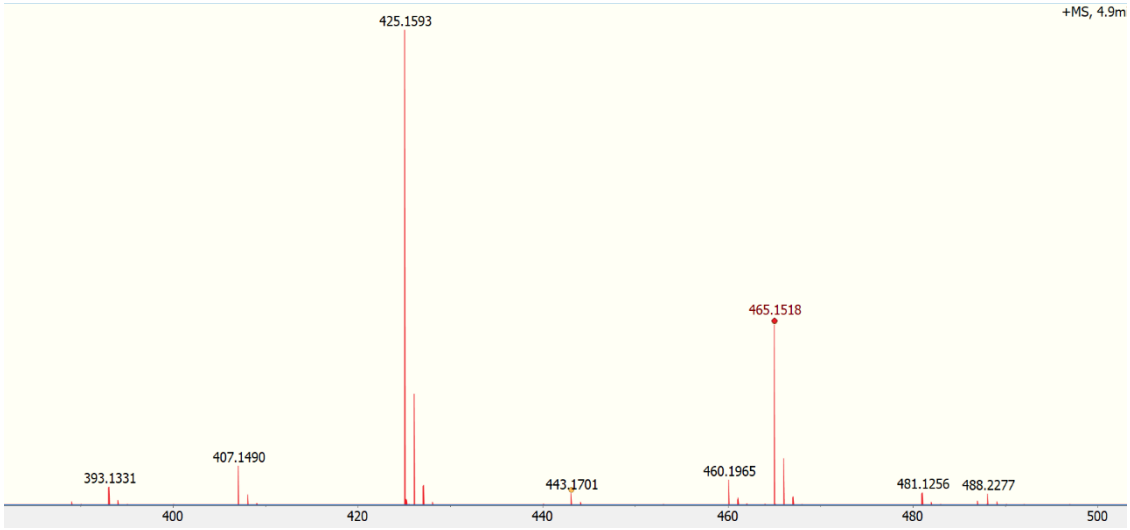

Figure S67. HRMS data for Aspernolide A (ASF WW 3).

Aspernolide B

From HRMS data:

$(M+H)^+$ = 443.1701, Δ= -0.0ppm, mSigma = 4.5

Therefore, $(M+H)^+$ molecular formula: $C_{24}H_{27}O_8$

Compound molecular formula: $C_{24}H_{26}O_8$

Utilising Antimarin database with molecular formula $C_{24}H_{26}O_8$ yields Aspernolide B.

Ref: Nittta et al. 1983, chem, pharm, Bull, 31, 1528

Previously isolated from: *Aspergillus terrus.*

Position	**δ_C, compound 5, Aspernolide B**	**C-type**	**^1H (chemical shift ppm, No. of H, multiplicity, coupling)[b]**	**COSY (^1H-^1H)**	**HMBC (^1H-^{13}C)**
1	157.94	C			
2, 6	115.33	CH	$H_{2,6}$: 6.89, 2H, d, J=8.6Hz	3,5	C1
3, 5	131.33	CH	$H_{3,5}$: 7.57, 2H, d, J=8.8Hz	2,6	C2, C4, C7
4	131.45	C			
7	128.05	C			
10	85.39	C			
11	170.24	C			
12	52.40	CH_3	H_{12}: 3.81, 3H, s		C11
13	38.15	CH_2	H_{13}: 3.45, 2H, s		C7, C10, C14, C15
14	131.57	C			
15	128.89	CH	H_{15}: 6.52, 1H, dd, J=8.2, 1.4Hz	16	C13, C16, C17
16	116.04	CH	H_{16}: 6.44, 1H, d, J=8.4Hz	15	C14, C15, C17
17	153.83	C			
18	120.08	C			
19	131.50	CH	H_{19}: 6.47, 1H, d, J=2.2Hz		C14, C17, C18, C20
20	32.36	CH	J=H_{20}: 2.58, 1H, t, 7.1Hz	21	C17, C18, C21
21	43.26	CH	1.55, 2H, t, J=7.2Hz	20	C18, C20, C22, C23

22	70.16				
23	27.60	CH_3	1.20, 3H, s		C21, C22, C24
24	25.55	CH_3	1.26, 3H, s		C21, C22, C23

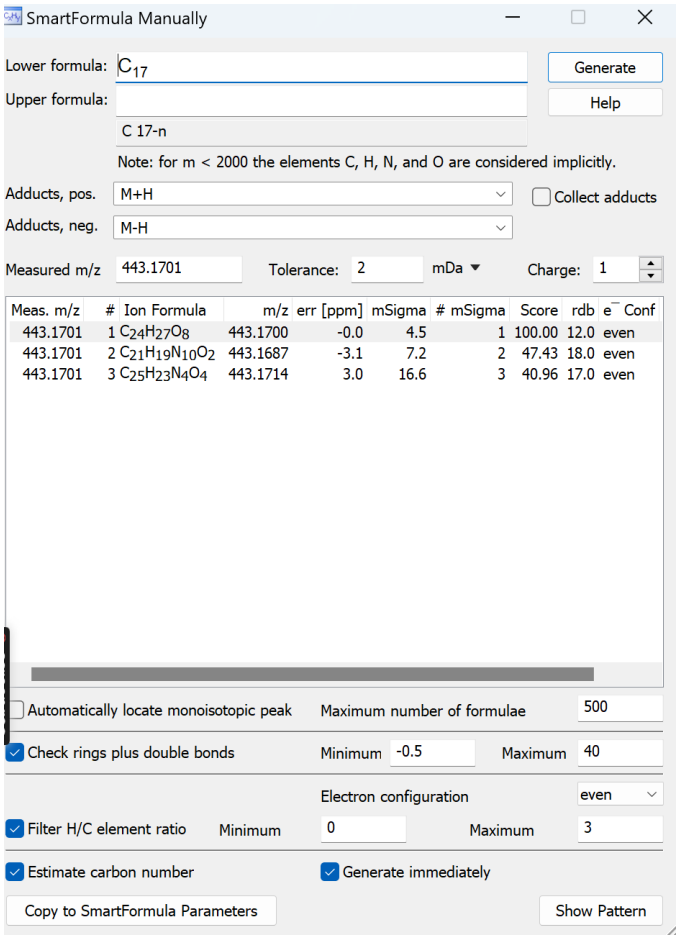

Figure S68. HRMS formula predictor from $[M+H]^+$ ion for Aspernolide B (ASF WW 3).

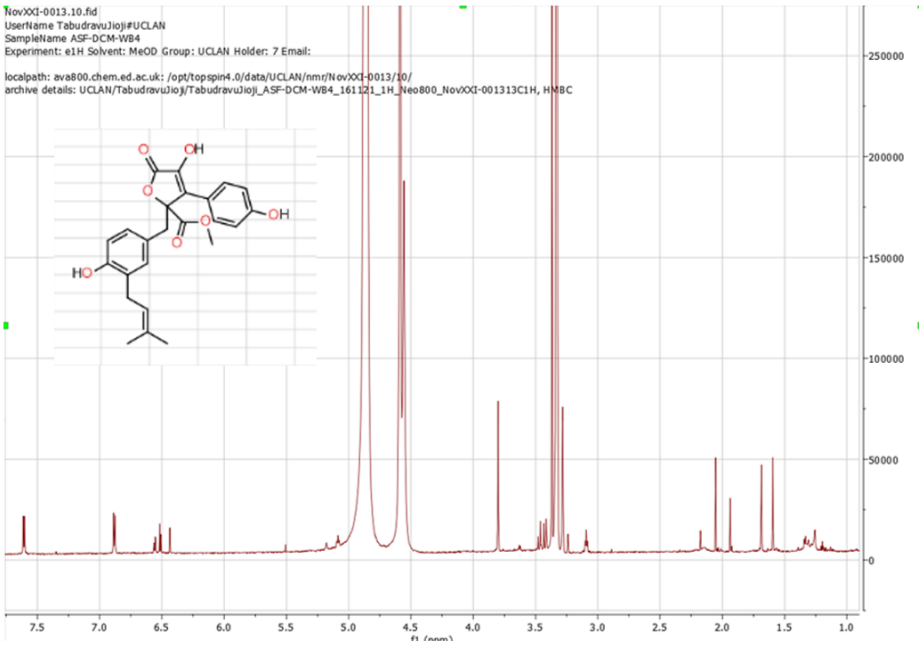

Figure S69. ^{1}H NMR spectrum of ASF DCM WB 4, Butyrolactone I in CD_3OD.

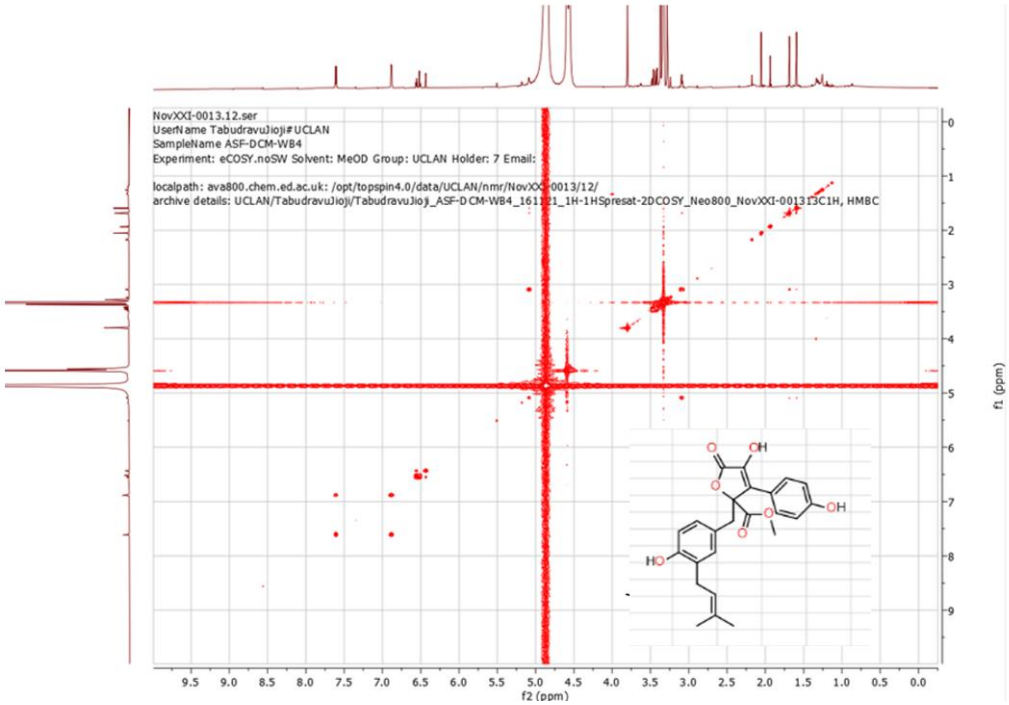

Figure S70 ^{1}H-^{1}H COSY NMR spectrum of ASF DCM WB 4, butyrolactone I in CD_3OD.

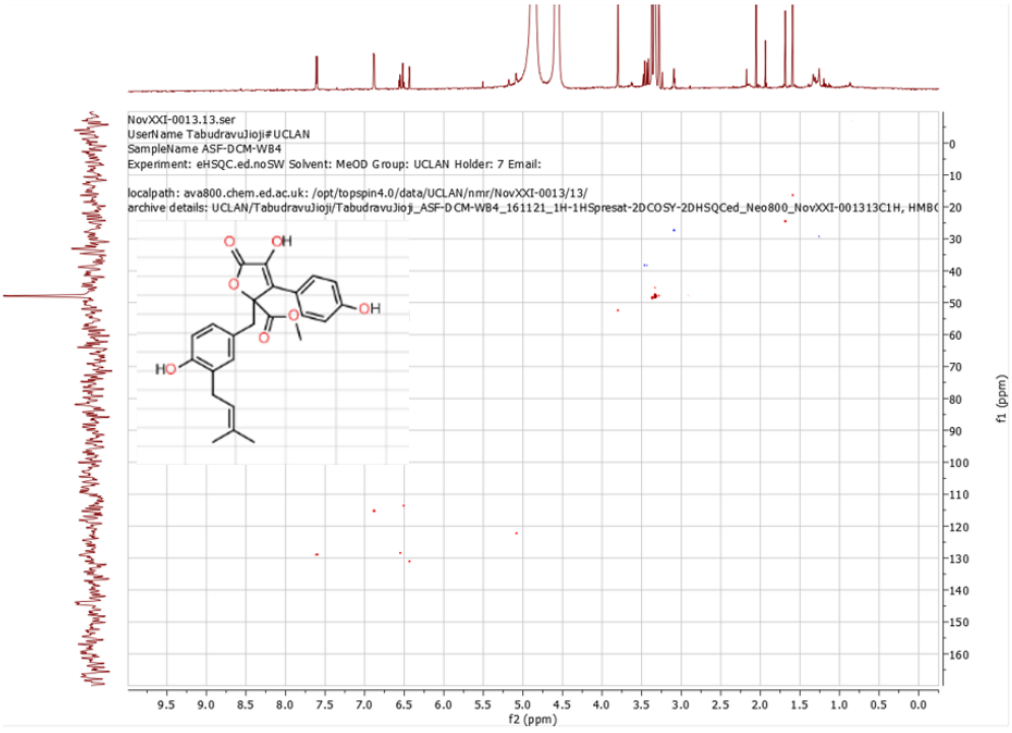

Figure S71. HSQC NMR spectrum of ASF DCM WB 4, Butyrolactone I in CD_3OD.

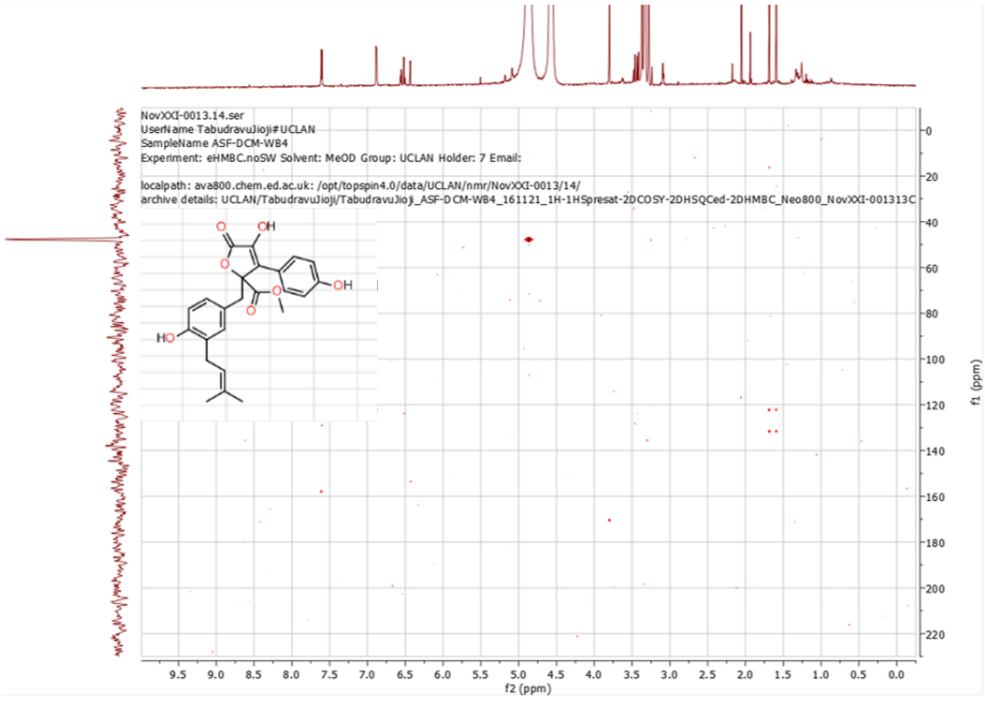

Figure S72. HMBC NMR spectrum of ASF DCM WB 4, Butyrolactone I in CD_3OD.

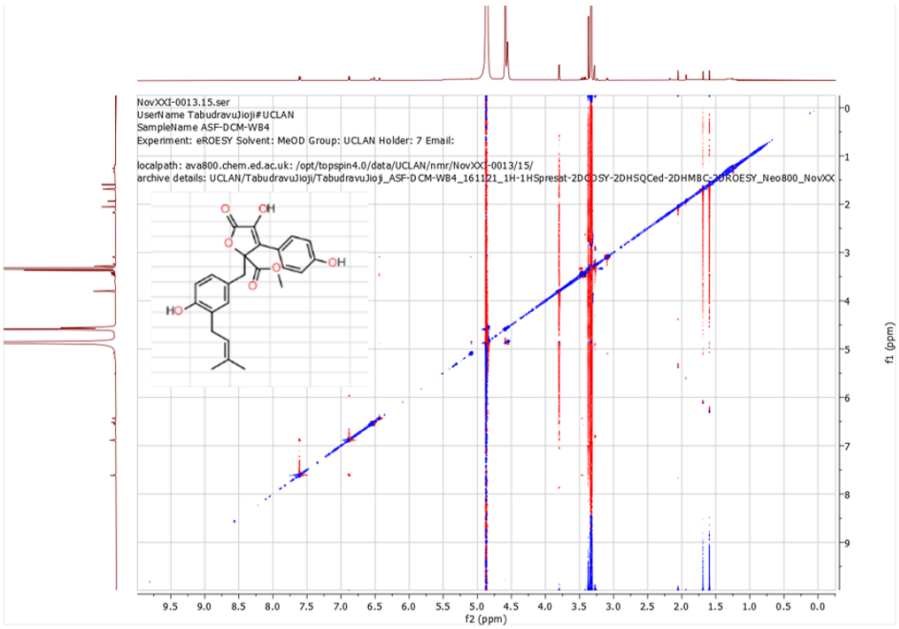

Figure S73. ROSEY NMR spectrum of ASF DCM WB 4, Butyrolactone I in CD_3OD.

Position	δ_C, compound 3, butyrolactone I [a]	C-type	^1H (chemical shift ppm, No. of H, multiplicity, coupling)[b]	COSY (^1H-^1H)	HMBC (^1H-^{13}C)
1	157.82	C			
2, 6	115.16	CH	$H_{2,6}$: 6.88, 2H, d, J=9.6Hz	3,5	C1
3, 5	128.87	CH	$H_{3,5}$: 7.60, 2H, d, J=8.7Hz	2,6	C2, C4, C7
4	128.99	C			
7	128.28	C			
10	85.39	C			
11	171.48	C			
12	52.40	CH_3	H_{12}: 3.80, 3H, s		C11
13	38.16	CH_2	H_{13a}: 3.43, 1H, s H_{13b}: 3.46, 1H, s		C7, C10, C14, C15
14	127.35	C			
15	128.34	CH	H_{15}: 6.55, 2H, dd, J=8.2, 2.4Hz	16	C13, C16, C17
16	113.75	CH	H_{16}: 6.51, 1H, d, J=8.3Hz	15	C14, C15, C17
17	153.83	C			
18	123.83	C			
19	130.98	CH	H_{19}: 6.43, 1H, d J=1.6Hz		C14, C17, C18, C20
20	27.27	CH	H_{20}: 3.09, 2H, t, 6.7	21	C17, C18, C21
21	122.19	CH	H_{21}: 5.08, 1H, t, 7.5	20	C18, C20, C22, C23
22	131.57				
23	24.45	CH_3	H_{23}: 1.68, 3H, s		C21, C22
24	16.37	CH_3	H_{24}: 1.59, 3H, s		C21, C22, C23

Table S12. NMR table used in the structure elucidation of ASF DCM FM 5, butyrolactone i.

a 100 MHZ in CD_3OD

b 400 MHz in CD_3OD

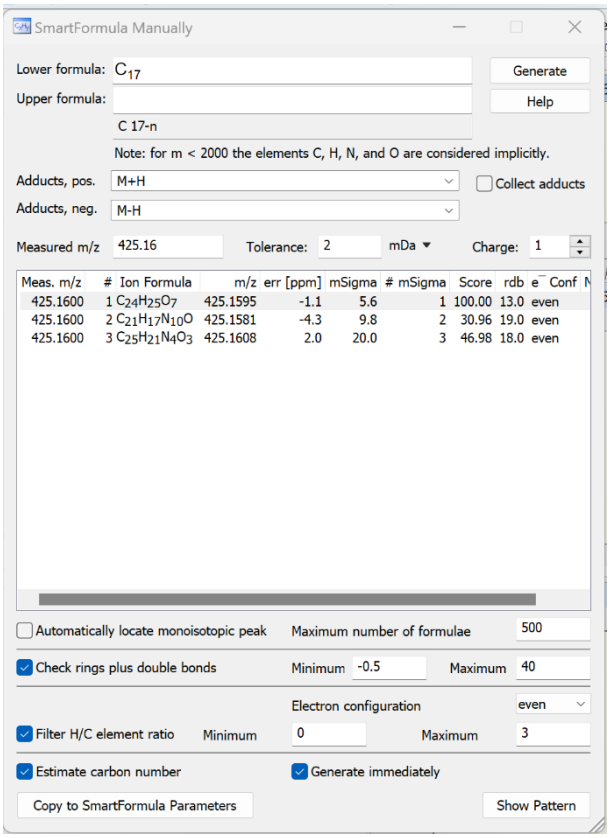

Figure S74. HRMS formula predictor from $[M+H]^+$ ion for ASF DCM WB 4, butyrolactone I.

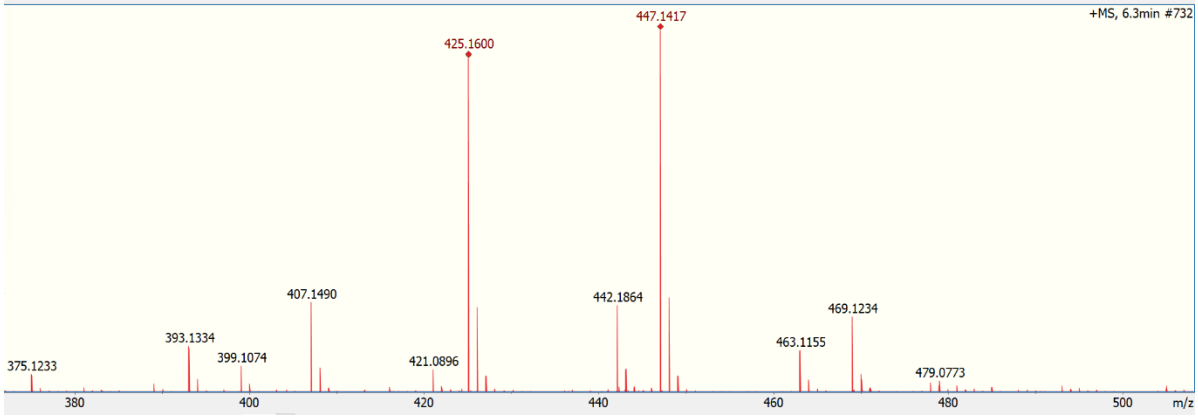

Figure S75. HRMS data of ASF DCM WB 4, butyrolactone I.

From HRMS data:

$(M+H)^+$ = 425.1595, Δ= -1.1ppm, mSigma = 5.6

Therefore, $(M+H)^+$ molecular formula: $C_{24}H_{25}O_7$

Compound molecular formula: $C_{24}H_{24}O_7$

Utilising Antimarin database with molecular formula $C_{24}H_{24}O_7$ yields butyrolactone I.

Ref: Nittta et al. 1983, chem, pharm, Bull, 31, 1528

Previously isolated from: *Aspergillus terrus.*

Table S13. Table comparing NMR chemical shifts (^{13}C and ^{1}H) of butyrolactone ii (1), butyrolactone i (3) (from FM fraction) and butyrolactone i (3) (from WB fraction). ^{13}C 150MHz, ^{1}H 800MHz, CD_3OD.

Position	δ_C, compound 1, Butyrolactone ii	δ_H (J in Hz)	δ_C, compound 3, Butyrolactone i (FM fraction)	δ_H (J in Hz)	δ_C, compound 3, Butyrolactone i (WB fraction)	δ_H (J in Hz)
1	158.05		157.94		157.82	
2, 6	115.27	$H_{2,6}$: 6.89, 2H, d, 8.7	115.27	$H_{2,6}$: 6.87, 2H, d, J=8.8Hz	115.16	$H_{2,6}$: 6.88, 2H, d, J=9.6Hz
3, 5	129.04	$H_{3,5}$: 7.61, 2H, d, 8.7	128.81	$H_{3,5}$: 7.58, 2H, d, J=8.4Hz	128.87	$H_{3,5}$: 7.60, 2H, d, J=8.7Hz
4	128.99		128.99		128.99	
7	127.82		127.93		128.28	
10	84.92		86.14		85.39	
11	170.16		170.24		171.48	
12	52.37	H_{10}: 3.80, 3H, s	52.17	H_{12}: 3.79, 3H, s	52.40	H_{12}: 3.80, 3H, s
13	38.09	H_{11}: 3.48, 2H, s	38.16	H_{13}: 3.42, 2H, s	38.16	H_{13a}: 3.43, 1H, s H_{13b}: 3.46, 1H, s
14	123.83		130.98		127.35	
15	131.15	$H_{15,19'}$: 6.66, 2H, d, 9.0	128.11	H_{15}: 6.54, 1H, dd, J=7.9, 1.9Hz	128.34	H_{15}: 6.55, 2H, dd, J=8.2, 2.4Hz
16	114.22	H_{16}: 6.53, 2H, d, 8.1	113.75	H_{16}: 6.50, 1H, d, J=7.6Hz	113.75	H_{16}: 6.51, 1H, d, J=8.3Hz
17	156.18		153.72		153.83	
18			127.11		123.83	
19			130.74	H_{19}: 6.41, 1H, d, J=1.1Hz	130.98	H_{19}: 6.43, 1H, d J=1.6Hz
20			27.25	H_{20}: 3.07, 2H, d, 8.2	27.27	H_{20}: 3.09, 2H, t, 6.7
21			122.19	H_{21}: 5.06, 1H, t, 7.5	122.19	H_{21}: 5.08, 1H, t, 7.5
22			131.68		131.57	
23			24.56	H_{23}: 1.66, 3H, s	24.45	H_{23}: 1.68, 3H, s
24			16.35	H_{24}: 1.56, 3H, s	16.37	H_{24}: 1.59, 3H, s

Table S14. Table comparing NMR chemical shifts (^{13}C and ^{1}H) of butyrolactone iii (2), Aspernolide A (4) and Aspernolide B (5). ^{13}C 150MHz, ^{1}H 800MHz, CD_3OD.

Position	δ_C, compound 2, Butyrolactone iii	δ_H (J in Hz)	δ_C, compound 4, Aspernolide A	δ_H (J in Hz)	δ_C, compound 5, Aspernolide B	δ_H (J in Hz)
1	158.05		157.94		157.94	
2, 6	113.86	$H_{2,6}$: 6.89, 2H, d, J=9.2Hz	115.33	$H_{2,6}$: 6.91, 2H, d, J=8.6Hz	115.33	$H_{2,6}$: 6.89, 2H, d, J=8.6Hz
3, 5	127.89	$H_{3,5}$: 7.55, 2H, d, J=8.2Hz	131.33	$H_{3,5}$: 7.57, 2H, d, J=8.9Hz	131.33	7.57, 2H, d, J=8.8Hz
4	128.94		131.45		131.45	
7	127.93		128.05		128.05	
10	85.39		85.39		85.39	
11	170.13		169.60		170.24	
12	50.39	H_{12}: 3.79, 3H, s	52.40	H_{12}: 3.81, 3H, s	52.40	H_{12}: 3.81, 3H, s
13	36.70	H_{13}: 3.44, 2H, s	38.15	H_{13}: 3.45, 2H, s	38.15	H_{13}: 3.45, 2H, s
14	131.57		131.57		131.57	
15	127.57	H_{15}: 6.53, 1H, dd, J=7.9, 1.5Hz	128.89	H_{15}: 6.52, 1H, dd, J=8.2, 1.3Hz	128.89	H_{15}: 6.52, 1H, dd, J=8.2, 1.4Hz
16	114.39	H_{16}: 6.47, 1H, d, J=8.5Hz	116.04	H_{16}: 6.44, 1H, d, J=8.4Hz	116.04	H_{16}: 6.44, 1H, d, J=8.4Hz
17	152.08		153.83		153.83	
18	124.77		120.08		120.08	
19	129.72	H_{19}: 6.48, 1H, d, J=2.4Hz	131.50	H_{19}: 6.47, 1H, d, J=2.2Hz	131.50	H_{19}: 6.47, 1H, d, J=2.2Hz
20	29.14	H_{20a}: 2.61, 1H, dd, J=17.5, 4.6Hz H_{20b}: 2.49, 1H, dd, J=16.8, 7.5Hz	24.32	H_{20a}: 2.50, 1H, d, J=5.2Hz H_{20b}: 2.42, 1H, d, J=5.3Hz	32.36	J=H_{20}: 2.58, 1H, t, 7.1
21	67.63	H_{19}: 3.66, 1H, t, J=5.6Hz	32.36	H_{21}: 1.74, 1H, t, J=6.8Hz	43.26	1.55, 2H, t, J=7.2Hz
22	76.60		70.15		70.16	
23	22.98	H_{23}: 1.27, 3H, s	27.62	H_{23}: 1.21, 3H, s	27.60	1.20, 3H, s
24	17.89	H_{24}: 1.17, 3H, s	25.51	H_{24}: 1.26, 3H, s	25.55	1.26, 3H, s

Example of the output of the acetylcholinesterase inhibition bioassay

Table 15. Time vs Absorption of sample 3, microplate position F1.

Cycle	Time (s)	Absorption (412nm)
1	57	1.229
2	114	1.253
3	171	1.278

4	228	1.307
5	285	1.339
6	342	1.367
7	399	1.396
8	456	1.429
9	513	1.458
10	570	1.482
11	627	1.514
12	684	1.554
13	741	1.572
14	798	1.609
15	855	1.638
16	912	1.673
17	969	1.699
18	1026	1.737
19	1083	1.768
20	1140	1.806
21	1197	1.841
22	1254	1.857
23	1311	1.883
24	1368	1.926
25	1425	1.959
26	1482	1.976
27	1539	2.031
28	1596	2.044
29	1653	2.101
30	1710	2.108
31	1767	2.141
32	1824	2.164
33	1881	2.203
34	1938	2.221
35	1995	2.242
36	2052	2.274
37	2109	2.285
38	2166	2.347
39	2223	2.39
40	2280	2.417
41	2337	2.418
42	2394	2.427
43	2451	2.589
44	2508	2.493
45	2565	2.529

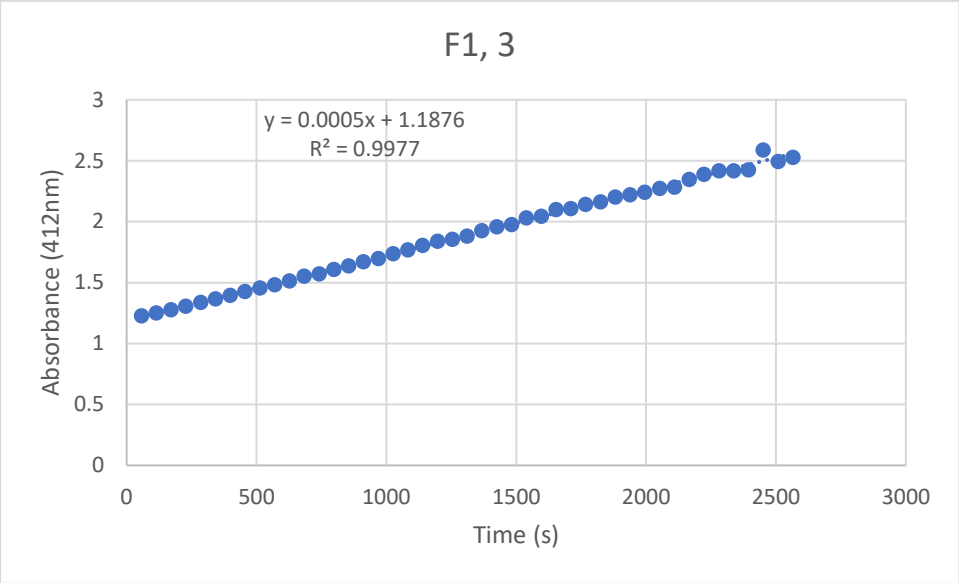

Figure 76. Graph of time vs absorbance of sample 3, microplate position F1, gradient = 0.0005.

Statistical Analysis

Example of part of the data table for statistical analysis.

Table. Excel spreadsheet of data used for FreeClust analysis (table 1).

Rt / Mass	Rt = 2.1 m/z = 309.1204	Rt = 2.6 m/z = 343.1304	Rt = 2.8, m/z = 885.3087	Rt = 3.1, m/z = 289.0941	Rt = 3.1, m/z = 669.4039	Rt = 3.2, m/z = 669.4282	Rt = 3.2, m/z = 669.4065	Rt = 3.3, m/z = 555.201
ss02 (F, H, sc)								
ss04 (F, H, sc)					3.81E+08			
ss06 (B, H, al)								
ss08 (B, H, al)								
ss10 [Alz] (F, H, al)								
ss12 [Alz] (F, H, al)								
ss14 [Alz] (B, H,								

sp)								
ss16 [Alz] (B, H, al)								
ss18 (B, H, al)								
ss20 (B, H, al)								
ss22 [Alz] (B, H, sp)								
ss24 (B, H, sp)								
ss26 (F, H, sp)							1.29E+08	